Cranfield UNIVERSITY

EPSRC
Engineering and Physical Sciences Research Council

Microarray Ltd

CRANFIELD UNIVERSITY

INSTITUTE OF BIOSCIENCE AND TECHNOLOGY

Ph.D. THESIS

Academic Years 2001-2004

DAVINIA DORITA GORNALL

STUDIES TOWARDS THE EXPLOITATION OF SONOCHEMICALLY FORMED MICROELECTRODE ARRAYS FOR THE DEVELOPMENT OF ELECTROCHEMICAL SENSORS

Supervisor: Professor Séamus P. J. Higson

December 2004

This thesis is submitted in partial fulfilment of the requirements for the degree of Doctor of Philosophy

For my parents, Dorita and John.

Acknowledgements

In the preparation of this thesis I would firstly like to thank my supervisor, Professor Séamus Higson, without whose support and advice, this thesis would never have been possible.

I gratefully recognise the Engineering and Physical Research Council and Microarray Limited for providing the funding for this project. Thanks also to Mark Thompson of Microarray Limited for his additional support.

I would also like to thank my colleagues both from Manchester and Silsoe namely, Andrew Barton, Frank Davis, Karen Law, Tony McGurk, Daniel Mills, Jeanette Pritchard, William Roberts, Rachael Warrington and especially, Emma Lawrence.

For their technical assistance with AFM and SEM respectively, I thank Robert Jones at Lancaster University and Colin Matthews at Cranfield University.

Rebecca Hutchinson, Katherine Granger and Monique Kalsi all played a big part in my early university days and their friendship and support is still appreciated more than they know. A special thank you must also go to all the girls from back home for always being there to provide some light relief from my studies!

My family, particularly my sister, Serena, and my parents, to whom this thesis is dedicated. I love you dearly, thank you.

Final thanks must be given to my dearest Stuart who has been there for me throughout. Not only has he had to read this thesis several times over, but he has also had to put up with me throughout the entire writing of it. Stuart, you know how much it has meant to me. All my love and thank you.

Declaration

This is a declaration to certify that no portion of the work referred to in this thesis has been submitted in support of an application for another degree or qualification of this or any other university, or institute of learning.

Davinia Dorita Gornall

December 2004

Abstract

Microelectrodes offer a number of advantages for exploitation as electrochemical sensors such as imparting stir-independence to sensor responses and allowing lower limits of detection to be minimised. Microelectrode arrays offer an attractive route for increasing the current responses of microelectrodes, whilst still retaining their advantageous properties. Despite this, no commercial sensors, to date, have successfully employed microelectrode arrays, largely due to conventional fabrication routes proving too costly to be economically viable for the production of disposable sensing devices. Previous work carried out by this research group has described a novel and patented procedure for the fabrication of microelectrode arrays via the sonochemical ablation of insulating polymer films electrochemically deposited upon conductive surfaces. This format lends itself to mass fabrication due to the simplicity and inexpensiveness of the approach.

This thesis describes work focussed towards the optimisation of each of the individual components involved in the formation of sonochemically fabricated microelectrode arrays. In particular, factors and techniques that may facilitate the commercial exploitation and mass fabrication of such arrays as generic sensing templates are described.

Screen printed carbon has been investigated for its suitability as a host electrode. The comparative use of a number of possible activation methods to increase amperometric current responses at such electrodes is also described. Homogeneous poly(*o*-phenylenediamine) films of ~40 nm thickness formed at the surfaces of screen printed carbon electrodes via the anodic electropolymerisation of *o*-phenylenediamine are shown to serve as effective diffusional barriers, thus insulating the underlying carbon electrodes. Microelectrode arrays formed by the sonochemical ablation of such films to expose microscopic areas of the underlying conductive substrates are seen to possess electrode element populations of ~7.3 x 10^4 cm^{-2}. Over 400 such sensors are shown to be able to be fabricated simultaneously with reproducibility of responses <4% relative standard deviation.

Amperometric and cyclic voltammetric characterisations of the thus produced microelectrode arrays performed in model redox systems are shown to agree with accepted theoretical microelectrode behaviour, demonstrating sigmoidal shaped voltammograms, fluctuations in steady-state current responses of <10% with convection, scan rate independence and fast attainment (<20 seconds) of steady-state responses.

Arrays of this type are also demonstrated to be suitable for exploitation within aqueous chlorine sensing devices, offering detection limits of <0.005 mg/l free chlorine, representing an order of magnitude lower than those obtainable via contemporary optical wet chemistry based approaches. In order to demonstrate further the applicability of this approach to the mass fabrication of disposable devices, methods for the deposition of a chemical modifying layer are also investigated, to avoid the need for additional reagents.

CONTENTS

LIST OF FIGURES AND TABLES

FIGURES

TABLES

NOMENCLATURE

A	geometric electrode area
A_a	electroactive electrode area
A_f	frequency factor
AFM	atomic force microscopy
A_{mono}	area of monomer unit
Ag/AgCl	silver/silver chloride
aq	solution phase/aqueous
atm	atmospheres
$[C]_o$	surface concentration of electroactive species
$[C]_\infty$	bulk concentration of electroactive species
CE	counter electrode
C_d	double layer capacitance
Cl_2	molecular chlorine
ClO^-	hypochlorite ion
Cl^-	chloride ion
d	thickness of polymer film
d_c	centre-centre spacing of electrodes within an array
D	diffusion coefficient
2,3-DAP	2,3-diaminophenazine
DPD	N,N-diethyl-*p*-phenylenediamine
poly(DVB/EVB)	poly(divinylbenzene/ethyl vinylbenzene)
E	applied potential
E_e	equilibrium potential
E_F	Fermi level
E_{pa}	anodic peak potential
E_{pc}	cathodic peak potential
E^Θ	potential under standard conditions of temperature and concentration
E_1	potential value where no electroactive species reacts
E_2	potential value where all the species that reach the electrode react

ΔE_p	voltammetric peak potential separations
ESI-ITMS	electrospray ionisation-ion trap mass spectroscopy
EQCM	electrochemical quartz crystal microbalance
F	Faraday constant (9.6×10^4 C mol^{-1})
f	transducer operating frequency
FACTS	free available chlorine test with syringaldazine
FEG-SEM	field emission gun scanning electron microscopy
FT-NMR	Fourier transform nuclear magnetic resonance
Fc	ferrocene
$Fc(CO_2H)^{3+/2+}$	ferrocenemonocarboxylic acid reversible redox species
$Fe(CN)_6^{3-/4-}$	ferricyanide reversible redox species
Fe	iron
GOD	glucose oxidase
G	Gibbs free energy
G_{ox}	free energy change of reactant
G_{red}	free energy change of product
G^{Φ}	transition state
ΔG^{Φ}_{red}	Gibbs free energy of activation for reduction
h	depth of microelectrode recess
H_2O_2	hydrogen peroxide
$HClO^-$	hypochlorous acid
i	net observed current
i_L	limiting current
i_a	anodic current
i_c	cathodic current
$i_{c,p}$	capacitative current for a planar electrode
ic,m	capacitative current for a microelectrode
i_o	standard exchange current
i_p	peak current
i_{pa}	peak anodic current
i_{pc}	peak cathodic current
IHP	inner helmholtz plane

I_2	iodine
I^-	iodide ion
J	diffusional flux of a species
KI	potassium iodide
k_d	mass transfer coefficient
k_{ox}	heterogeneous rate constant for oxidative electron transfer reaction
k_{red}	heterogeneous rate constant for reductive electron transfer reaction
$k_{ox}[R]_o$	flux of reduced material to electrode
$k_{red}[O]_o$	flux of oxidised material to electrode
LCD	liquid crystal display
m	metal electrode
M_d	depth of a single polymer monolayer
M_n	total number of polymer monolayers deposited
MDL	method detection limit
MIPS	molecularly imprinted polymers
n	number of electrons transferred
NaOCl	sodium hypochlorite
NCl_3	nitrogen trichloride
NH_3	ammonia
NH_2Cl	monochloramine
$NHCl_2$	dichloramine
OHP	outer helmholtz plane
*o*PD	*o*-phenylenediamine
P_A	ambient pressure
P_W	wave amplitude
PANI	polyaniline
PAO	*N*-phenylarsine
PPD	poly(*o*-phenylenediamine)
ppb	parts per billion
ppm	parts per million
Q_{ox}	charge passed by one electron
Q_{tot}	total charge passed during an electropolymerisation

q	disc density
q^m	charge density at electrode
q^s	charge density in solution
R	molar gas constant (8.31 J K^{-1} mol^{-1})
R_s	electrical resistance of intervening solution
$Ru(NH_3)_6^{3+/2+}$	hexaammineruthenium reversible redox species
r_i	radius of insulator surrounding disc
r	radius of sphere
r_{disc}	radius of disc
$r_{hemisphere}$	radius of hemisphere
RDE	rotating disk electrode
RRDE	rotating ring disk electrode
RE	reference electrode
RSD	relative standard deviation
SCE	saturated calomel electrode
SHE	standard hydrogen electrode
S/N ratio	signal-to-noise ratio
T	absolute temperature (in Kelvins)
t	time
U_{tot}	total number of monomer units deposited
U_{mono}	number of monomer units per monolayer
ULR-DPD	ultra low range *N*,*N*-diethyl-*p*-phenylenediamine
UV-VIS	ultraviolet-visible spectroscopy
USEPA	United States Environmental Protection Agency
v	velocity of sound
v_s	sweep rate
v_x	velocity of solution
WE	working electrode
XPS	X-ray photoelectron spectroscopy
α	transfer coefficient
β	electrode dimension
γ_s	Stokes radii

δ	diffusion layer thickness
η	overpotential
λ	wavelength

CHAPTER 1

RATIONALE FOR RESEARCH PROGRAMME

The primary focus of this research programme is to develop a simple-to-use, disposable sensor for the rapid determination of chlorine in aqueous media, utilising a novel sonochemical microelectrode fabrication technique, and to prove its applicability to production on a mass scale.

The need to analyse chemical species in increasingly complex systems has bought a rapid expansion in the use of analytical tools. However, many of these analytical methods depend on highly skilled staff, cumbersome sample pre-treatment regimes and expensive dedicated equipment. Chemical sensors have been shown to offer alternative methods for detection, being capable of satisfying the increasing demand for precise analytical information at lower cost via devices that require relatively simple instrumentation and little, if any, pre-treatment of the sample (Galan-Vidal *et al.*, 1995). Sensor technology is still a rapidly evolving and ever expanding field and many chemical sensors for various applications have been proposed over the last twenty years. Specifically, there have been impressive advances in the biomedical, industrial and environmental fields (Alvarez-Icaza & Bilitewski, 1993).

However, this sizable effort does not correspond to the scarce commercial implementation of these devices. Most sensors have been designed for very specific applications and show practical constraints such as reliability, response time and cost – problems which, if solved, would allow greater practical expansion in the field. The main requirements for an applicable sensor are good precision, a broad dynamic range in the area of the interesting concentration values, a fast response and a good specificity for the analyte to be analysed. Furthermore, for disposable sensors, a low unit price is often required. Another common problem involves removing the fluctuations in sensor responses that are sometimes experienced with variations in convection caused by variable flow or stirring/agitation within an analyte sample matrix.

Current strategies have been devoted to the development of microelectrode array based sensors. Microelectrodes have several properties which make them attractive as the active element in a sensor for the determination of a species in, for example,

flowing water streams. Specifically, there is a high steady-state rate of diffusion to microelectrodes which leads to an enhancement of the current response. This leads to enhanced sensitivity, and independence from the effects of convectional mass transport and therefore solution flow-rate (Wightman, 1981). However, individual microelectrodes offer very small responses and one approach for overcoming this problem is to use many microelectrodes connected together in the form of an array to allow a larger cumulative response to be measured. Despite this, no commercial chemical sensors, to date, have successfully employed microelectrode arrays, largely due to the cost of conventional fabrication routes such as photolithography or laser ablation, since these have not proved commercially viable for disposable sensor devices.

Previous work by this research group (Myler, 2000) has provided a novel and patented (Higson, 1996) procedure for the fabrication of microelectrodes, involving the sonochemical ablation of thin poly-*o*-phenylenediamine film coatings that insulate planar electrode surfaces. This format lends itself to mass fabrication due to the simplicity and inexpensiveness of the approach. Microarray Limited was formed in 1999 under the UMIST Ventures Limited arm, in order to exploit the commercial potential of this new technology. Microarray believes that an ideal initial application to launch this technology is in the measurement of aqueous chlorine solutions and provided CASE sponsorship of the EPSRC studentship which funded this PhD programme of research.

Chlorine is a powerful oxidising agent that is used widely as a disinfectant in the treatment of industrial, recreational and drinking water. A variety of industrial processes are heavily dependant on the use of chlorine because of its potency and effectiveness as a germicide, and it is essential that individual users and companies are able to measure chlorine to determine if adequate levels for disinfection are present. However, in addition to its benefits, chlorine does have some adverse effects and the presence of excessive amounts of chlorine may be detrimental to human health and aquatic life.

Concern over the environmental and health effects of chlorination have led to a number of laws and legislations regarding its determination (European Economic Community, 1998; US Environmental Protection Agency, 2000). Therefore, accurate, sensitive and simple procedures are required for the monitoring of chlorine by users and regulatory agents in order to assure compliance with regulations. For example, EU law (European Economic Community, 1978) mandates that in fish bearing fresh water, chlorine levels have to be regularly monitored since fish (particularly salmon and trout) are very sensitive to low chlorine levels. The Environment Agency in the UK and the other EU states are currently unable to meet this legislated monitoring requirement as there is no field instrument presently capable of measuring such low levels of chlorine, and as a result, the Environment Agency are sponsoring the development of the Microarray instrument. It can be seen then that the scope for chlorine analysis is vast and it is estimated that over 20 million chlorine tests are being undertaken across the globe each day (Hall & Hyde, 1992).

The analytical methods presently recommended for the measurement of chlorine utilise wet chemistry colour mixing and matching techniques. This can easily lead to limitations, such as poor accuracy and a limited range of response due to variations in colour change. The method also requires skilled operators for use, the equipment is cumbersome and sampling is time consuming (Gordon *et al.*, 1992). ***A technique which would permit easy, rapid, accurate and qualitative analysis of chlorine for both free and total solutions over a wide detection range would clearly be advantageous.*** Microarray Limited is focusing towards the development of the next generation of portable analysers, based on the arrangement of disposable microelectrode array based sensor strips which will be used in conjunction with a hand-held instrument. This technique allows for greater sensitivity and precision, it may also be selective for both free and total chlorine levels simultaneously and would require minimal handling and training for use. It is envisaged that the device will be capable of producing readings with accuracy approximately 10 times greater than current state-of-the-art testing methods, for the equivalent cost. It would also provide an 'on-the-spot' result within seconds rather than minutes and would avoid

the damaging environmental impact caused by the widespread use of carcinogenic chemicals utilised within conventional colourimetric tests.

This research programme has been structured to sequentially meet each of the intermediary stages in the development of a sonochemically fabricated microarray shown in Figure 1.1.

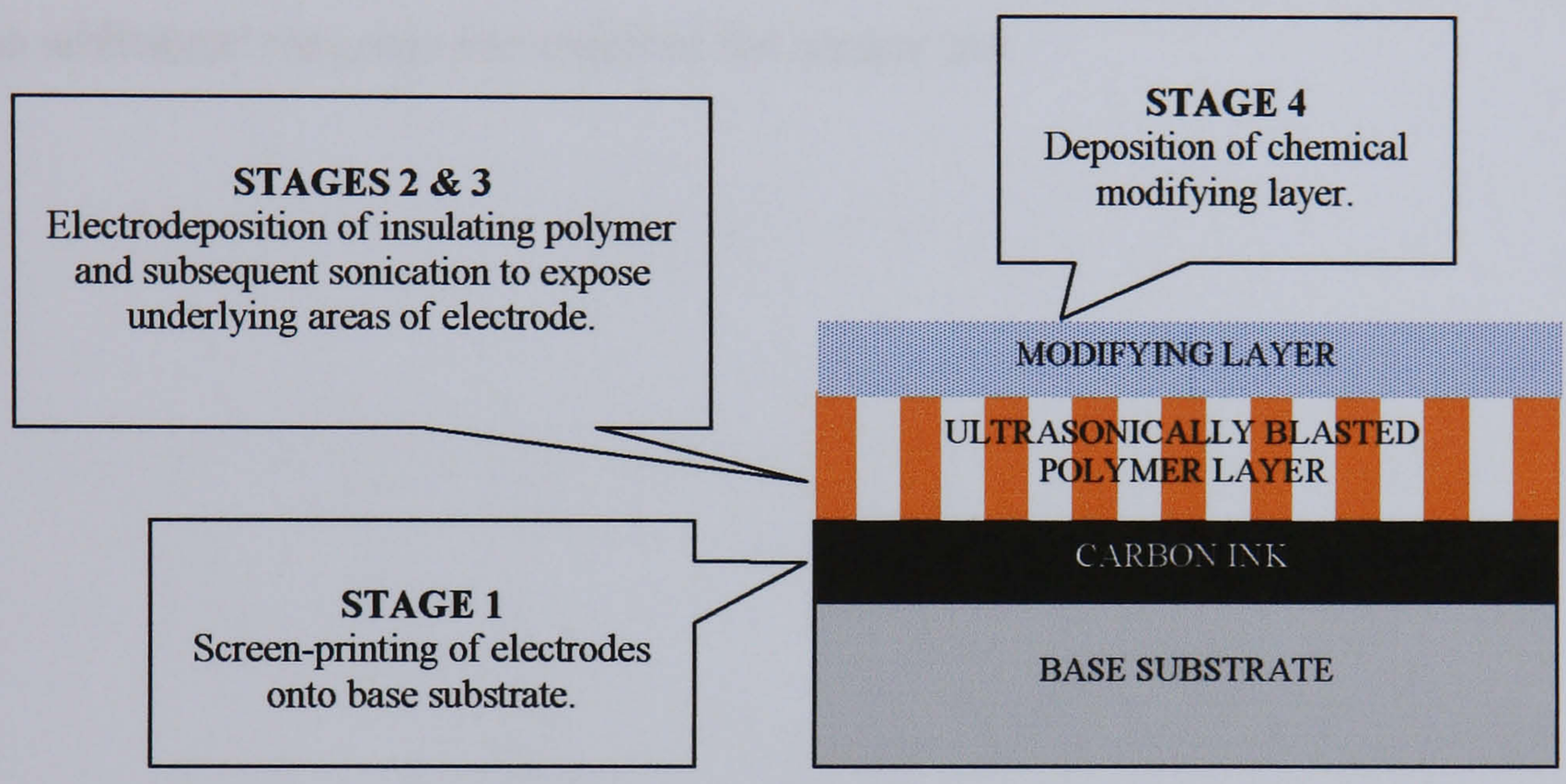

Figure 1.1 Processes involved in the sonochemical fabrication of microarrays.

It is the optimisation of each of these fabrication stages, and the interrogation of the fabricated sensor to chlorine solutions, that forms the basis of the objectives of this project, namely to;

- Examine the use of commercially available carbon inks screen-printed onto polycarbonate based substrates as suitable hosts for the fabrication of microelectrode arrays.

- Optimise the formation of electropolymerised films in terms of repeatability and scale-up fabrication, and investigate their insulating properties to aqueous chlorine/redox probes.

- Reproducibly fabricate microelectrode arrays via the optimisation and investigation of ultrasound conditions.

- Prove the applicability of microelectrodes to amperometric aqueous chlorine measurement by interrogation with standard chlorine/redox probes.

- Develop a chemical modifying layer and investigate deposition techniques so that no additional reagents are required for sensor use.

CHAPTER 2

INTRODUCTION AND LITERATURE REVIEW

2.1 CHEMICAL SENSORS IN CONTEXT

There has for many years been a worldwide effort towards the development of analytical devices that can be used for the detection, quantification and monitoring of specific chemical species of scientific importance. The majority of these approaches, such as high performance liquid chromatography and mass spectroscopy, generally incur high production and running costs, are confined to laboratory use due to their cumbersome size, and often require highly skilled staff for their operation. In contrast, miniaturised chemical sensors offer possibilities for providing measurements that previously could not be determined, within a relatively rapid time scale, at lower cost levels and with simplicity that would not be achievable with other more traditional techniques. Sensors may also be used as screening tools to eliminate the analysis of non-critical samples, thus reducing the number of analyses required by these more sophisticated and expensive laboratory analytical approaches.

It is not surprising in this context that over the past 20 years or so, research and development in the field of sensor science has expanded exponentially in terms of financial investment, number of papers published, and the number of active researchers worldwide. However, the development of chemical sensors is still an open field and further research needs to be performed before many of these devices become commercialised. An ideal sensor should be able to be inserted into a matrix containing the species to be detected and would display the result of the chemical analysis within a few seconds with a high degree of precision and sensitivity. No sampling, dilution or reagent addition would ideally be required, and changes in the analyte concentration or activity would be displayed in real time. This has been exemplified by the Medisense® (ExacTech™) glucose sensor designed for use by diabetics. The success of this biosensor has largely yet been equalled in the *chemical* sensor field. In fact, probably the only commercial chemical sensor of this type to have reached a similar level of commercial success is the pH electrode. This is mainly due to many chemical sensors failing to satisfy a number of key performance criteria resulting from the lack of novel and financially viable ways to fabricate sensors so that they may indeed meet these criteria on a mass production scale.

Traditional sensor manufacturing companies have tended to be small entities in terms of personnel and financial power, specialising in a few (usually hand-made) products, with low turnover and high profit margins (Diamond, 1998). It follows therefore that if a low cost and highly reproducible fabrication method of chemical sensor production for multiple applications could be achieved, the current commercial market for chemical sensors could be revolutionised, unravelling new markets aimed at non-expert users that would make investment in this area extremely attractive.

2.1.1 Definition of a chemical sensor

Sensors can be categorised into two general groups. There are *physical* sensors, which are sensitive to such physical responses as temperature, pressure, magnetic field, and force, and these do not have a chemical interface. Then, there are *chemical* sensors which rely on a particular chemical reaction for their response.

A chemical sensor may be defined as ***a device which responds to a particular analyte in a selective way through a chemical reaction and can be used for the qualitative or quantitative determination of the analyte*** (Cattrall, 1997). There are two parts to a chemical sensor; the region where the selective chemistry takes place, and the transducer. The chemical reaction produces a signal such as a colour change, the emission of fluorescent light, a change in the electrical potential at a surface, a flow of electrons, the production of heat, or a change in the oscillator frequency of a crystal. The transducer responds to this signal and translates the magnitude of the signal into a measure of the amount of the analyte under investigation.

Chemical sensors are commonly sub-categorised into the following groups; electrochemical (Fiaccabrino & Koudelka-Hep, 1998), optical (Peterson *et al.*, 1980), mass sensitive (Guilbault, 1983) or heat sensitive (Mosbach & Danielsson, 1981), according to their transducer type. Electrochemical devices currently constitute the largest group of chemical sensors, with approximately 50% of sensor literature being

devoted to this topic (Janata *et al.*, 1998). There are differing modes of operation for electrochemical sensors, in particular; (a) the measurement of the equilibrium potential of an indicator electrode under effectively zero-current conditions – a *potentiometric* mode, (b) the measurement of the concentration of charge which is obtained through the measurement of solution resistance – a *conductrimetric* mode or (c) the measurement of current that is passed when a fixed potential is applied to an electrode, causing the species being determined to react – an *amperometric* mode. Each mode has relative advantages which can be useful depending on the intended application of the device. For example, potentiometric sensors have the advantage of not destructing or consuming any of the analyte since no current flows, and are largely stir independent in their behaviour. This contrasts with amperometric sensors in which the response behaviour is normally strongly dependant on the stir rate and does involve some consumption of the analyte.

Amperometric transduction however, does generally represent the most robust of the electrochemical techniques. Amperometric sensors often possess the ability under favourable conditions to detect concentrations in the range of 10^{-8} to 10^{-9} M (Turner, 1989). For this reason they have become one of the most highly developed classes of sensors, and at the time of writing account for the largest share of the chemical and biosensor markets (Janata, 2001).

2.1.2 Electrochemical amperometric based sensors

Amperometry (or voltammetry) involves the measurement of the current flowing in an electrochemical cell as a function of the applied potential. Many species undergo oxidation or reduction at a potential which is characteristic of the particular species. If the potential is fixed at the value appropriate to the reduction or oxidation of the species being determined, the amount of current which flows can be directly related to the concentration of the species which is being detected at the working electrode. Amperometric sensors are used in this mode.

A useful example of an amperometric based sensor is the so called '*Clark electrode*' first developed in 1962 by Leyland Clark. The device was designed to measure glucose levels present in tissue and blood samples, and was a combination of the amperometric oxygen electrode (described by Clark in his definitive paper published in 1956) serving as a transducer, and the enzyme, glucose oxidase (GOD) as the recognition entity. The electrode worked on the basic principle that glucose (the analyte) can be enzymatically oxidised with the consumption of oxygen (the co-reactant). The glucose oxidase was entrapped immediately in front of a platinum electrode surface by a highly oxygen-permeable membrane. Glucose is oxidised to gluconic acid (Equation 2.1) and the cathodic current resulting from the oxygen reduction (Equation 2.2) relates to the decrease in substrate concentration and produces a quantifiable electrical signal via amperometric transduction.

$$\beta.D.glucose + O_2 \xrightarrow{GOD} gluconolactone + H_2O_2 \qquad (2.1)$$

$$\tfrac{1}{2}O_2 + 2H^+ + 2e^- \xrightarrow{-700\,mV\,(vs.\,Ag/AgCl)} H_2O \qquad (2.2)$$

In 1967, Updike and Hicks further developed the Clark enzyme electrode by immobilising glucose oxidase in a polyacrylamide gel at the surface of an oxygen electrode, thus enhancing the operational stability of the enzyme. Work in this area continued and in 1972 Reitnauer demonstrated the successful application of an enzyme electrode in a prototype blood glucose analyser.

The original oxygen detection approach of Clark was found to be susceptible to signal drift due to fluctuations in the ambient environmental oxygen levels. Thus, Clark (1970) modified his original design, utilising the alternative electrochemical detection of hydrogen peroxide by reversing the polarity of the working electrode. Unfortunately, many additional electro-active species present in blood (e.g. ascorbic acid and uric acid) were also found to be oxidised at this high over-potential, thus giving rise to erroneous responses. The Yellow Springs Instrument Company (YSI, Ohio, USA) incorporated a novel perm-selective barrier to the Clark enzyme electrode to exclude these interferents. A schematic representation of this electrode is shown in Figure 2.1.

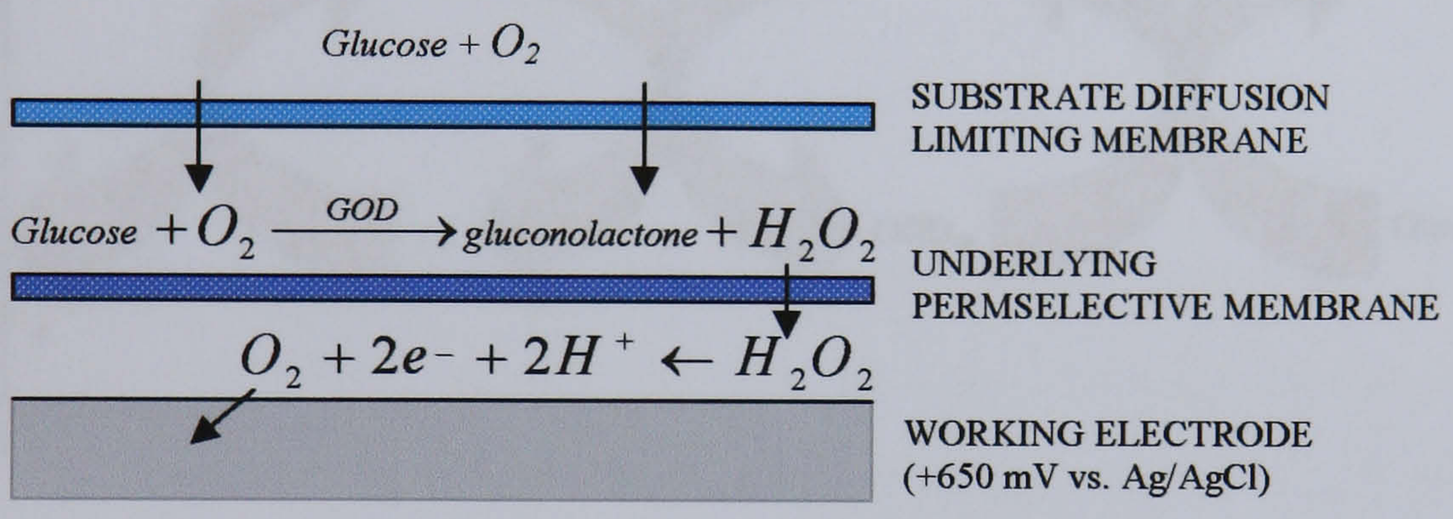

Figure 2.1 Schematic of the enzyme membrane laminate.

This work was commercialised in 1974 with the launch of the YSI 23A glucose analyser with updated versions of the instrument still in use today. Many other instruments based on this principle have also been built by competitor manufacturers.

Despite the success of the YSI 23A, it was realised that a device that would allow diabetics to monitor their own blood glucose levels easily and in their own home would be highly advantageous. This led to the next real milestone, the development of the Medisense® (ExacTech™) blood glucose analyser. It resulted from a 1984 paper describing the use of ferrocene and its derivatives as an immobilised mediator for use with oxidoreductases in the construction of inexpensive enzyme electrodes (Cass *et al.*, 1984). This sensor again utilised the enzymatic oxidation of glucose, but the mediator, ferrocene, now acted as the electron acceptor in place of molecular oxygen, as shown in Figure 2.2. Ferrocene is an iron-containing bi-pentyl carbon

ring compound that may be easily and reversibly oxidised or reduced between the Fc/Fc^+ redox states. Once the ferrocene is reduced by the enzyme, glucose oxidase, it may be re-oxidised by the electrode, thus removing the electron it acquired from the reduced form of the enzyme. The mediator can once more acquire an electron from another enzyme molecule and in this way can constantly shuttle charge from the enzyme to the working electrode. The mediator is not consumed in the process but rather is constantly re-cycled, ready for further use.

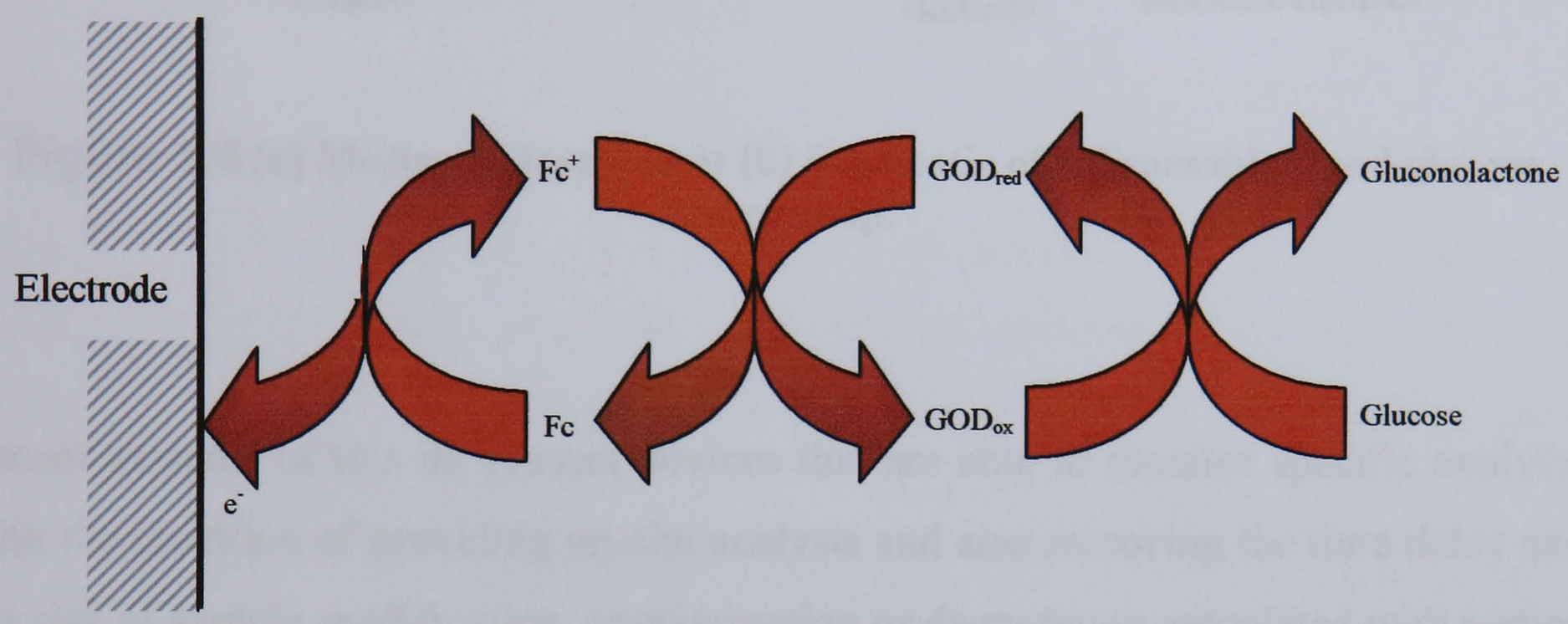

Figure 2.2 Reaction scheme in the ferrocene mediated glucose sensor.

The Medisense® blood glucose sensor is one of the best known (and arguably the most successful) portable analysers to have reached commercialisation. It complies with the idealised specification of a chemical sensor i.e. it is specific, rapid, offers a cost effective analytical approach and can be employed with minimal sample treatment. The sensor utilises a disposable strip based on screen-printing technology, in conjunction with a small potentiostat with a liquid crystal display (LCD) (Figure 2.3). The strip plugs into the instrument and a drop of blood is deposited upon the sensor tip thus bridging the working, reference and counter electrodes. This completes the circuit allowing for a steady-state potential to be applied across the electrodes and initiates a 20 second countdown on the LCD, during which time the current is recorded. This current is then referred to a calibration curve in the electronic memory of the instrument with the resultant concentration of glucose being displayed on the LCD.

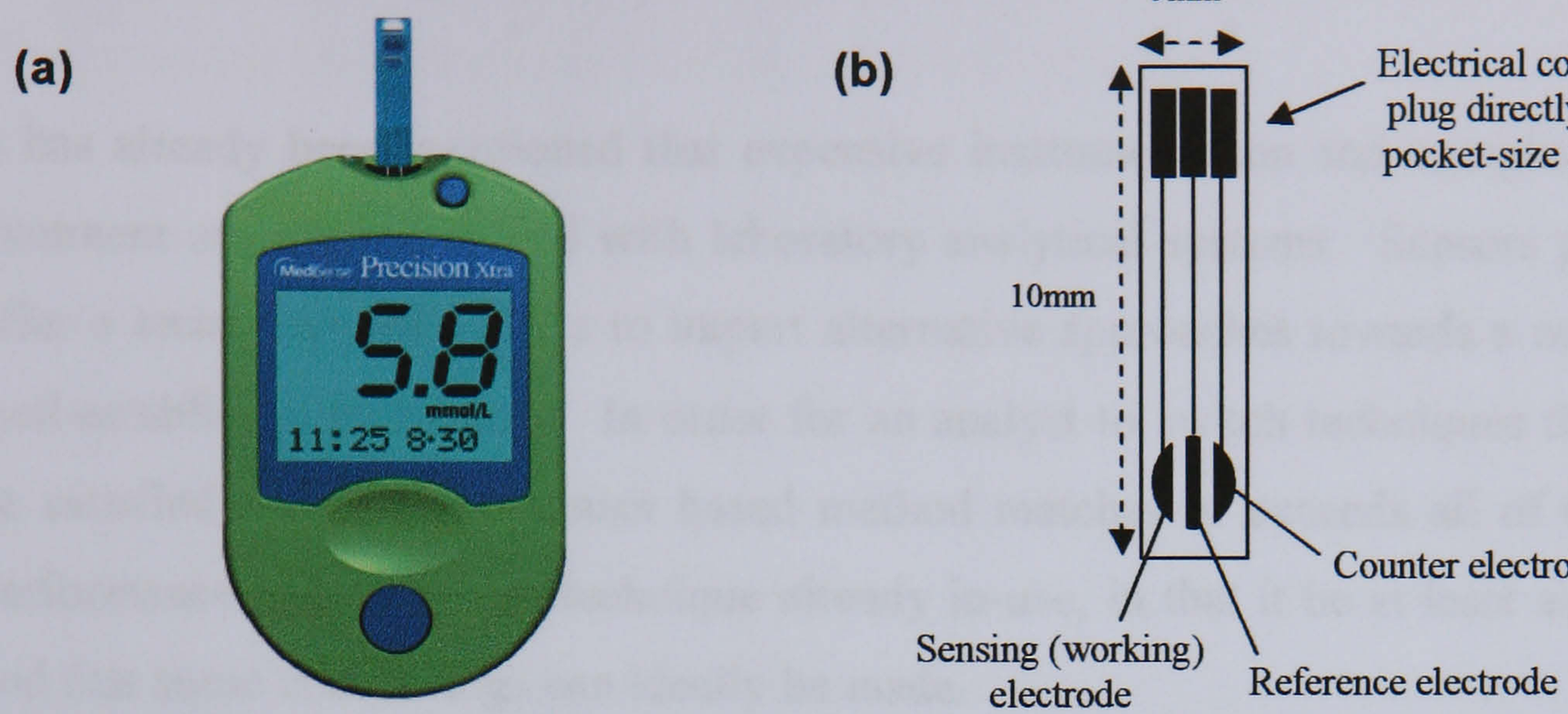

Figure 2.3 (a) Medisense instrument (b) Schematic of a disposable blood-glucose sensor strip.

Sensor systems of this ilk present devices that are able to monitor specific analytes with the intention of providing on-site analysis and also removing the time delay and the risk of sample modification, contamination or degradation associated with testing at a centralized laboratory. These rapid, accurate and simple methods for the determination of indictor species enable potentially critical incidents to be identified and limit their impact by allowing rapid decisions to be made and the correct response taken.

2.1.3 Scope of amperometric sensors in chlorine determination

It has already been mentioned that expensive instrumentation and complex sample treatment are often involved with laboratory analytical systems. Sensors primarily offer a technology that seeks to impart alternative approaches towards a number of well-established techniques. In order for an analyst to switch techniques they must be satisfied that the new sensor based method matches or exceeds all of the main performance criteria of the technique already in-use, in that it be at least as reliable and that some cost savings can ideally be made.

It is principally these hurdles which have previously hampered the widespread application of sensing devices. In an effort to overcome these difficulties, there have been a number of notable advances in the field of chemical sensors as specifically applied to the biomedical, industrial (food and pharmaceutical) and environmental fields (Alvarez-Icaza & Bilitewski, 1993). The changing geo-political situation has also impacted upon the applications of sensors and sensing systems. There is also a growth of literature describing sensors for security and defence applications aimed mainly at the detection and prevention of possible terrorist activities and the detection of illicit substances in general (Koochaki *et al.*, 1995).

In particular, the scope for sensor use within the area of environmental monitoring has received much attention in recent years (Bilitewski & Turner, 2000). Environmental sensing and monitoring is the subject of several general reviews covering both gaseous (Seiyama *et al.*, 1994) and aqueous (Dietrich *et al.*, 1996) media. Recent legislation has opened up huge potential markets in this area by becoming ever more stringent, demanding the determination of contaminants at lower and more precise levels (European Economic Community, 1978). Water analysis as legislation demands requires the determination of global parameters that indicate the water quality and suitability for human consumption, or alternatively, for discharge into the environment. The only successful (and the only commercialised) amperometric chemical sensor for use in environmental monitoring is the dissolved oxygen probe (used as a measure of biochemical oxygen demand). The probe is

successful simply because it provides a competitive advantage (the time of analysis) when compared with the traditional analytical procedures.

Therefore an obvious area where specific sensors could find a 'niche' market for application is in the analysis of such environmental samples, where contemporary analysis procedures could be surpassed with the use of a chemical sensor. One such application is for the determination of chlorine in aqueous solutions. The most commonly used assay for chlorine determination is based on the original method proposed by Palin (1957) in which N,N-diethyl-*p*-phenylenediamine (DPD) is oxidised by chlorine to give an intense red colouration with an absorbance maximum at 516 nm which can be measured spectrophotometrically. Chlorine which has not reacted with any other species is termed 'free chlorine' (present either as dissolved Cl_2, $HClO^-$ or ClO^-). However, chlorine may also react with compounds present in natural waters to give derivatives, such as the chloramines (termed 'combined chlorine'). Each of these chlorine species has different disinfecting properties, with free chlorine being the preferred chemical state. For this reason, there has been a considerable effort to develop assays that specifically detect free chlorine. The Palin based test kit only tests for specific species and hence different tests have to be performed for both free and 'total' (free plus combined) chlorine. Because of the experimental difficulties associated with the field determination of chlorine species in this way, most of the rapid test kits use packages containing pre-measured quantities of reagents. However, addition of these reagents can add errors to the analyses coupled with the fact that the sample volume is also critical to the determination. Electrochemical amperometric sensors may therefore permit an alternative to these cumbersome techniques.

Amperometric methods for the determination of chlorine have been extensively utilised in two ways, firstly as an end point detection technique for titrations (Jensen & Johnson, 1990) and also as a direct measure of chlorine concentration (Moorow & Roop, 1975). In the latter case, the original sensors used consisted of an electrode of an inert material with the potential simply being controlled by dissolution of a copper counter electrode. Not surprisingly, this technique proved

unreliable since the measured currents depended upon the mass-transfer coefficient established at the electrode surface by hydrodynamics prevailing in the measurement cell. Although the consumption of a very small quantity of the analyte may not have significantly affected the bulk analyte concentration, solute diffusion gradients were created, which imparted an unwanted stir-dependant response (explained further in Section 2.4). It is worth noting here that the use of microelectrode arrays can prevent convective effects such as stirring from influencing the mass flow at the working electrode.

The long-term stability of the electrode surface was another drawback. This problem is related to the kinetics of chlorine reduction which occurs as a fast reversible reaction on clean surfaces, but becomes irreversible when the electrode surface becomes contaminated (Moorow & Roop, 1975). This problem can be overcome by designing low cost disposable sensors which do not require a long lifetime or good reproducibility over time (i.e. a 'one-shot' device). These requirements can also permit simplification of some aspects of the realisation technology (e.g. screen-printed electrodes) in terms of lowered costs and minimised critical parameters.

2.1.4 Factors affecting sensor performance

Despite the vast research effort that is presently being focused on developing sensors for new applications, comparatively few have yet reached commercial success. This is largely due to many sensors failing to reach important performance criteria (Higson, 2003). The success of a sensor system in meeting these criteria can be analytically evaluated via quantifiable measures such as precision, accuracy, working concentration range, selectivity and response time. Longevity, robustness, and financial viability are also important considerations in sensor design.

The *precision* is a measure of how repeatable the results of an analysis are, in other words, how closely the replicate measurements lie to each other. The precision can be found by considering the spread of the readings. Ideally, if an analysis were to include 10 replicate measurements, the same result would be recorded each time. This should also be true for sensors created from different production batches (i.e. the reproducibility). However, every measurement will invariably have some degree of uncertainty. The precision of a sensor can be aided by assuring a constant flux of electroactive species to the electrode. This may be achieved by using controlled convective flow over the electrode (e.g. a hydrodynamic electrode) or by creating a sufficiently high concentration gradient, as microelectrodes frequently experience.

The *accuracy* describes how close the measured value is to the true or accepted value, although this may in practice be hard to determine. The accuracy may never be determined exactly since this would assume that the true value was already known with an absolute certainty. For this reason, the accuracy of the data may be described in terms of the error in the reading and is often quoted in comparison to a standard method of detection for a particular analyte.

The *working concentration range* takes into consideration both the upper and lower detection limits of a sensor. Any sensor must be capable of working within the required analyte concentration range for its desired application(s). The method

detection limit (MDL) is therefore a useful tool to determine the applicability of analytical methods. In general terms, the MDL is a measurement of how low a given method can practically measure, in other words, the lowest concentration below which the test will fail to recognise the presence of an analyte. This can be greatly influenced by the signal-to-noise ratio (S/N ratio).

When determining the concentration range over which a sensor may operate, the *linearity* of the method may also be established. Increasing the linearity of a sensor concentration range can be extremely helpful in producing a more accurate device. The *sensitivity* (i.e. how close in magnitude two readings may be and still be distinguished from each other) of an analytical test can also be determined from investigations of the linearity by calculating the slope of the calibration curve. This relates to the change in signal per unit change in concentration. The signal output should be proportional, or bear a simple mathematical relationship, to the amount of species present in the sample. However, this is becoming less important with the advent of in-device electronics and integration of complex signal processing options that are capable of recording calibration curves with more complex profiles.

The *selectivity* (or *specificity*) of a sensor indicates its ability to differentiate between separate and different components present within a sample mixture. The acceptable characteristics of a sensor are often a function of the application. Hence, a sensor that performs well for monitoring a particular analyte in a given situation may be totally unsuitable for monitoring the same analyte in a different matrix. Factors that contribute to the suitability of a device for a particular assay may include physical parameters such as temperature, pH or pressure, as well as chemical interferences arising from the chemical matrices. Without adequate selectivity, the user cannot relate the signal obtained to the target species concentration with any confidence. The quest for better selectivity remains the cornerstone for chemical sensing research. For chemical sensors, it follows the route of selective matrices (Janata *et al.*, 1998) and can result from the applied potential or the choice of electrode material. Selectivity can also be derived from the dynamic behaviour of the sensors by the use of microelectrode arrays.

The *response time* of a sensor is often of great importance in many applications. Response times can vary from a few milliseconds up to several minutes, but are usually required to be less than 60 seconds. Slow response times often arise from, for example, multiple sensing membranes or sluggish exchange kinetics, and can seriously limit the scope of possible application as well as preventing use in real-time monitoring situations. The response time may also be affected by the thickness and permeability of any membranes, the level of analyte concentration, the temperature of solution, stirring effects and the geometries of the sensing element.

The *stability* of the sensor is also an important consideration. This can be considered in terms of the electrode ageing to; i) storage conditions or, ii) continuous (in-line) monitoring situations. Fouling or leaching onto the electrode surface could become a problem in the latter case with an inevitable signal drift or diminution in performance with time. Alternatively, if a disposable sensor is used, the working lifetime is less critical and any problems with sensor stability would be due to storage issues and the effect that these may have on the sensor before it is actually used for its required operation. For example, non-biological sensors are inherently more robust than those which incorporate enzymes because they are less sensitive to high temperature humidity storage conditions, or life-time issues.

2.2 DYNAMIC ELECTROCHEMISTRY

The principles of electrochemistry are fundamental to electrochemical sensor applications. In the context of electrode processes, which are heterogeneous in nature, dynamic electrochemistry deals with the study of charge transfer processes at the electrode/solution interface, either in equilibrium at the interface, or under partial or total kinetic control. Consider a metallic electrode, *m*, placed into a source of electrons (e.g. a solution phase, *aq*). A transfer of charge (electrons) takes place across the electrode/solution interface. An example of this is shown in Equation 2.3:

$$Fe^{3+}{}_{(aq)} + e^{-}{}_{(m)} \Leftrightarrow Fe^{2+}{}_{(aq)} \tag{2.3}$$

As this reaction gradually moves towards equilibrium, the transfer of electrons across the electrode/solution interface produces a net charge separation between the two phases, thereby creating a potential difference. An electrochemical cell can be operated under conditions where a current flows by applying a potential to the cell which is different in value to the equilibrium potential. The resultant current induces the exchange of electrons between the electrode and the molecules in solution (altering the oxidation state of the molecule) and *electrolysis* occurs. The transfer of electrons can occur in either direction; a molecule in solution may accept an electron from the electrode and become *reduced* (Equation 2.4), or a molecule may donate an electron to the electrode and become *oxidised* (Equation 2.5):

$$Fe^{3+}{}_{(aq)} + e^{-}{}_{(m)} \rightarrow Fe^{2+}{}_{(aq)} \tag{2.4}$$

$$Fe^{2+}{}_{(aq)} \rightarrow Fe^{3+}{}_{(aq)} + e^{-}{}_{(m)} \tag{2.5}$$

For the reductive electrolysis of Fe^{3+}, the act of passing a current through the cell converts Fe^{3+} to Fe^{2+} at the electrode/solution interface, with the result that the concentration of Fe^{3+} at the electrode is no longer the same as that in the bulk. This is because typically, the rate of depletion through electrolysis is faster than the speed

at which reactant may be replenished by diffusion from the bulk solution to the interfacial region.

It follows that the observed electrolytic current may be dependant on either; the transport of reactants to, or products from, the electrode surface (*rate-determining mass transport*) – this is discussed in Section 2.4, or the rate of the heterogeneous electron transfer (*rate-determining electrode kinetics*). A comprehensive review of the latter has been given by Bard & Faulker (2001), with relevant aspects summarised below.

2.2.1 Rate of electron transfer

The electrode kinetics for any electrolytic reaction can be controlled by the potential. Consider the general reaction shown in Equation 2.6 which represents in the simplest case that most charge transfer processes involve the transfer of electrons. The oxidised species, O, and the reduced species, R, are both soluble in solution and O receives n electrons in order to be transformed into R.

$$O_{(aq)} + ne^{-}{}_{(m)} \underset{k_{ox}}{\overset{k_{red}}{\rightleftharpoons}} R_{(aq)} \tag{2.6}$$

The electrons in the conducting electrode have a maximum energy which is distributed around the Fermi level (the energy of the highest occupied orbital). It is only around this level of energy that electrons can be supplied or received. Hence, the Fermi level, E_F, can be externally influenced by application of a voltage which either supplies electrons to, or removes electrons from, the conductor. For a reduction, the electrons in the electrode must have a minimum amount of energy in order to be transferred from the electrode to the receptor orbital in O; for oxidation, the energy of the electrons in the donor orbital of R must be equal to or higher than the electrode's Fermi level in order to be transferred to the electrode.

In order to study this relationship, the potential dependence of the heterogeneous rate constant for the electron transfer reaction must be quantified. It is assumed in Equation 2.6, that there are arbitrary quantities of O and R present in the solution and that k_{red} and k_{ox} describe the first order heterogeneous rate constants for the forward (reductive) and reverse (oxidative) electron transfer reactions respectively.

The reductive and oxidative components of Equation 2.6 can be predicted by Equations 2.7 and 2.8 respectively;

$$i_a = FAk_{ox}[R]_o \tag{2.7}$$

$$i_c = -FAk_{red}[O]_o \tag{2.8}$$

where $k_{red}[O]_o$ and $k_{ox}[R]_o$ are the respective fluxes of material to the electrode surface, F is the Faraday constant (9.6×10^4 Cmol^{-1}) , A is the electrode area (in cm^2) and i_a and i_c are the oxidative (anodic) and reductive (cathodic) currents respectively.

The net current flowing, i, is:

$$i = i_a + i_c \tag{2.9}$$

Therefore by substituting Equations 2.7 and 2.8 into the above we get:

$$i = FA(k_{ox}[R]_o - k_{red}[O]_o) \tag{2.10}$$

It should be noted here that the fluxes $k_{ox}[\mathrm{R}]_o$ and $k_{red}[\mathrm{O}]_o$ are only balanced (Equation 2.11) when Equation 2.6 is at equilibrium, hence, current flow has ceased.

$$k_{red}[O]_o = k_{ox}[R]_o \tag{2.11}$$

Electron transfer reactions can be described using the transition state model (Figure 2.4). This model views the reaction as occurring via a path that involves the reactants [$O_{(aq)} + e^-_{(m)}$] overcoming an energy barrier (the summit of which is termed the transition state, G^{Φ}) *en route* to becoming products, $R_{(aq)}$. Transition state theory, a detailed description of which is given by Cox (1994), predicts the rate of the reduction reaction, k_{red}, to be:

$$k_{red} = Af \exp\left(\frac{-\Delta G^{\Phi}_{red}}{RT}\right) \qquad (2.12)$$

where ΔG^{Φ}_{red} is the Gibbs free energy of activation for reduction, R is the molar gas constant (8.31 J K^{-1} mol^{-1}), T is the absolute temperature (in Kelvins) and Af is a 'frequency factor', which accounts for the rate of collision of the electroactive molecule with the electrode surface.

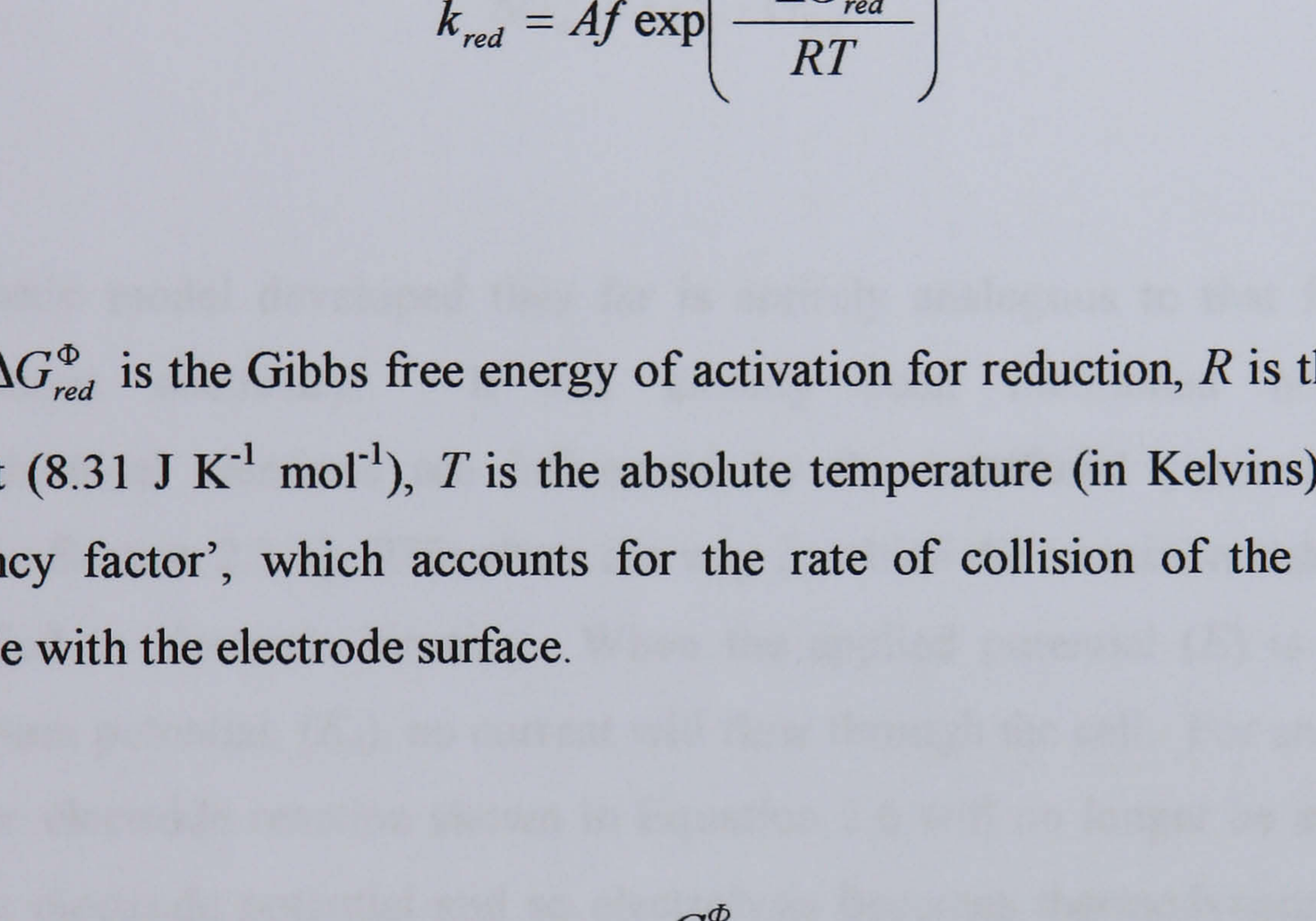

Figure 2.4 **Free energy plot for a simple one electron reduction of a species $O_{(aq)}$.**

For a fixed temperature and pressure, the activation free energies for the reductive and oxidative reactions are given by Equations 2.13 and 2.14 respectively where G_{ox} and G_{red} are the free energy changes of the reactant and the product respectively.

$$\Delta G_{red}^{\Phi} = G^{\Phi} - G_{ox} \tag{2.13}$$

$$\Delta G_{ox}^{\Phi} = G^{\Phi} - G_{red} \tag{2.14}$$

The kinetic model developed thus far is entirely analogous to that familiar from homogenous chemistry. It has already been mentioned however, that electrochemical reactions are influenced by the interfacial potential (explained further in Section 2.3.1). This alters the way in which the transition state theory may be applied to electrode kinetics. When the applied potential (E) is equal to the equilibrium potential, (E_e), no current will flow through the cell. For any other value of E, the electrode reaction shown in Equation 2.6 will no longer be at equilibrium with the electrode potential and so electrolysis becomes thermodynamically viable. Whether or not any current flows will depend on the kinetics of the particular electrode reaction under investigation. It follows that for electrolysis to occur, a potential different in value to that of E_e for the reaction in question must be applied to the working electrode in order to 'drive' or initiate the electrode reaction. The deviation of E from the equilibrium potential is given the term 'overpotential' (η) and is shown in Equation 2.15.

$$\eta = E - E_e \tag{2.15}$$

So far, the description of interfacial rates has been restricted to the consideration of a process (specifically Equation 2.6) occurring at one electrode/electrolyte interface. For experimental purposes it is much more desirable to know how k_{red} (and k_{ox}) depend on the over-potential applied to a cell of two (or three) electrodes. Fundamental work in electrode kinetics by Butler (1924) and Volmer (1930) has been combined to form the Butler-Volmer equation (2.16) which predicts how the observed current, i, varies as a function of the overpotential and the transfer coefficient, α. If the solution under investigation is well stirred, the surface concentrations of the reactants will be equal to their bulk values i.e. ($[R]_o = [R]_\infty$ and $[O]_o = [O]_\infty$).

$$i = i_o\left(\exp\left\{\frac{(1-\alpha)F\eta}{RT}\right\} - \exp\left\{\frac{-\alpha F\eta}{RT}\right\}\right) \qquad (2.16)$$

Whether a particular system is reversible or irreversible depends on whether i_o (the standard exchange current) is 'small' or 'large'. These are relative terms and signify the time-scale of the electrode kinetics relative to the transport of material in and out of the interfacial region (this will become further apparent in Section 2.4). For processes that have a small value of i_o, i.e. irreversible processes, values of α can be found experimentally by Tafel analysis (Tafel, 1905) which involves plotting $\ln(i)$ against E. The quantity of i_o can also be estimated via Tafel plots. A model as to the origin of reversible and irreversible electrode processes at the molecular level, according to whether fast or slow electrode kinetics operate, has been reported by Marcus (1963), but is beyond the scope of this thesis.

2.2.2 Electrode/solution interface

The region between the electrode and solution where electrode reactions actually occur and where the greatest potential differences across the electrical circuit appear is referred to as the interfacial region. The structure of this region can also control the rate at which electron transfer occurs.

We can consider an inert metal electrode simply as a source of electrons. Depending on the applied potential, a net charge will appear at the surface which will attract charge of opposite polarity. This charge separation means that there is a capacitative charge associated with the interfacial region, often referred to as the electrolyte double layer due to the charge separation on either side of the electrode/solution contact plane.

A number of models have been proposed which aim to establish the nature of the processes at the solid/liquid interface, all of which assume that no faradaic processes (electron transfer reactions) occur at the electrode. Initially, Helmholtz (1853) proposed a simple model based on the idea that a metal electrode possesses a charge density (q^m) which arises from an excess (q^mnegative) or deficiency (q^mpositive) of electrons at the electrode surface. In order for the interface as a whole to maintain electrical neutrality, the charge on the electrode must be matched in solution by an equal but opposite charge (q^s):

$$q^m = -q^s \tag{2.17}$$

This charge arises from the redistribution of electrolyte ions at the interface and/or the re-orientation of dipoles in solvent molecules. The driving force for the re-distribution is electrostatic. A potential difference results across the interface, creating an electric field gradient across the charge separation layer. Ions are attracted or repelled electrostatically within the solution layer close to the electrode surface, and an excess of either anions or cations is built up. The attracted ion is able to approach the electrode to a distance limited by the solvation shell of the ion, and it

is assumed that a monolayer of solvation exists between the ion and the electrode. The plane drawn through the centre of these ions at a minimum distance from the electrode surface is called the Outer Helmholtz Plane (OHP). In the Helmholtz model the excess charge on the metal is completely balanced in solution by ions situated at the OHP and the potential drop across the interface occurs totally over the region between the metal surface and the OHP. The potential drop between these two layers is linear.

Helmholtz's model was improved by Gouy (1910) and Chapman (1913) who concluded that the excess charge density in solution is not exclusively situated at the OHP. This occurs since the electrostatic attraction forces attracting or repelling ions from the electrode are counteracted by Brownian motion in solution which tends to disperse the excess ions. The Gouy-Chapman model used point charges to represent the ions and proposed that the charge density in solution is contained within a single 'diffuse layer' close to the electrode surface. In this diffuse layer the net charge density decreases with distance away from the phase boundary. The potential drop across this diffuse layer is then mainly concentrated in the region closest to the electrode surface, but some charge is now held further away from the electrode than the OHP.

In 1924, Stern combined the Helmholtz and Gouy-Chapman models by assuming that the ions have a minimum distance of approach (OHP), as well as accepting the idea that Brownian motion in solution creates a diffuse layer. In terms of the potential drop across the interface, a sharp drop exists between the electrode and OHP beyond which the potential gradually falls to a value characteristic of the bulk electrolyte.

The electrode/electrolyte interface model was further modified in 1947 by Grahame. A schematic representation of his model is shown in Figure 2.5:

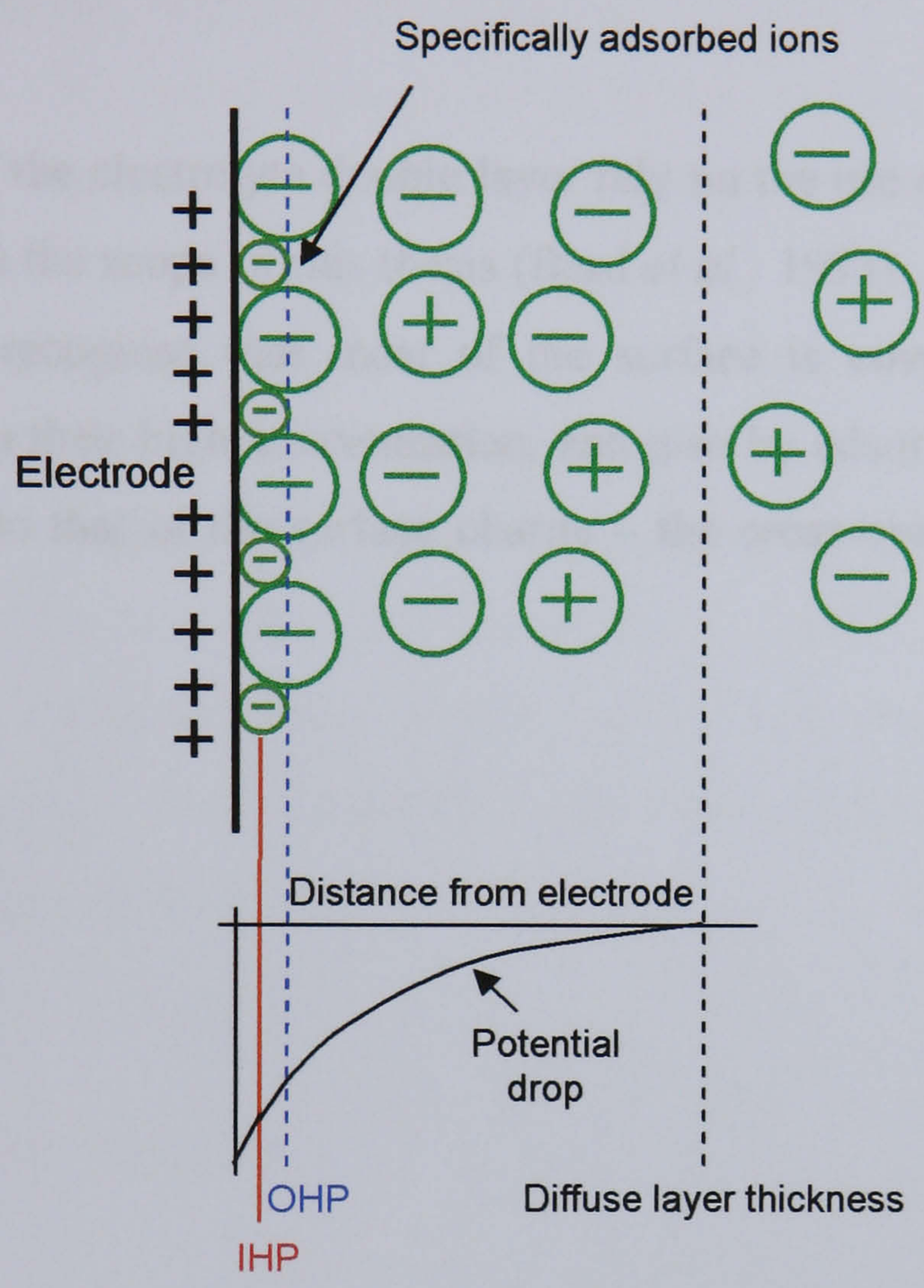

Figure 2.5 Schematic picture of the Grahame model of the electrical double layer. IHP is the inner Helmholtz plane and OHP is the outer Helmholtz plane.

Grahame proposed that although the zone closest to the electrode is mainly occupied by solvent molecules, it may be possible for some ionic or uncharged species to penetrate into this region. This could occur if the ion possessed no solvation shell, or if the solvation shell was lost when the ion approached the electrode. In this case ions are directly in contact with the electrode and are said to be 'specifically adsorbed'. The adsorption is termed 'specific' since the interaction occurs only for certain ions or molecules and is often unrelated to the charge on the ion. For example, it is possible for negatively charged ions to adsorb onto an electrode surface that already carries a negative charge density. A new (closer) plane of minimum approach was therefore added to the model termed the Inner Helmholtz

Plane (IHP). The IHP is defined as the axis through the centre of these specifically adsorbed species. The general effect of specific adsorption is to reduce the charge density needed in solution, between the 'double layer', to compensate for the charge on the electrode.

Modern views of the electrolyte double layer rely on the use of statistical mechanics which are outside the scope of this thesis (Bard *et al.*, 1993). However, it should be noted that they recognise that most of the surface is covered by polar solvent molecules, due to their high concentration, and also by adsorbed electrolyte ions of charge opposite to that of the surface charge – the cross-over point is the point of zero charge.

2.3 VOLTAMMETRY

Voltammetric analysis can provide remarkably detailed information about the mechanism of a cell reaction of interest (Brett & Brett, 1998). Voltammetric sensors function by measuring the current response as a function of applied potential (or the potential response as a function of applied current). This section will describe a general overview of instrumentation and experimental set-up required for the voltammetric analysis of sensors. The basic principles of some relevant steady-state techniques and a description of their use in analysing electroactive species in solution will also be explained. As the sensor being developed in this thesis is amperometrically interrogated (i.e. a fixed potential is applied and the resulting current is recorded), a special case of voltammetry, chronoamperometry (current change over time), will also be discussed.

2.3.1 Cells and electrodes

Experimental assemblies consist of a vessel of variable geometry (the electrochemical cell) in which at least two independent electrodes are immersed in a conducting phase, usually a solution, and are linked through the solution and through external connectors so as to form an electrical circuit. One of the electrodes is termed the *working electrode* and this is where the reaction of interest occurs. The second is a *reference electrode*, which provides a stable and fixed potential so that when a voltage is applied between the two electrodes, the drop in potential between the working electrode and the solution, $\Phi_m - \Phi_s$, is precisely defined. Complementary oxidation or reduction reactions occur at each electrode, consuming electrons at one electrode and supplying them at the other, so that the overall chemical reaction does not involve any net consumption of electrons.

The simple two-electrode arrangement described above is perfectly acceptable for the measurement of current/voltage curves where only a tiny current is passed (e.g. microelectrodes). However, for larger electrodes, a difficulty arises, and is explained below.

Consider a potential, E, applied between a large working electrode and a reference electrode, and assume that a finite current is flowing between them. In this situation, E could be calculated using Equation 2.18:

$$E = (\Phi_m - \Phi_s) + iR + (\Phi_s - \Phi_{REF}) \qquad (2.18)$$

Notice that E is split into three terms. The first of these, $(\Phi_m\text{-}\Phi_s)$, is the driving force for electrolysis at the working electrode/solution interface. The second term, iR, describes the voltage drop in solution due to passage of current, i, between the two electrodes (where R is the electrical resistance of the intervening solution). The third term, $(\Phi_s\text{-}\Phi_{REF})$ is the potential drop at the reference electrode/solution interface and is fixed by the chemical composition of the chosen reference solution. For small electrodes the iR term can be neglected and as $(\Phi_s\text{-}\Phi_{REF})$ is fixed, changes in the applied potential, E, are directly reflected in the driving force, $(\Phi_m\text{-}\Phi_s)$. Therefore the current can be measured meaningfully with two electrodes. However, with larger electrodes, iR is no longer negligible and so changes in the applied potential are not confined to changes in the driving force. The passage of large currents through the reference electrode can also change its composition and so the potential drop will no longer be fixed.

This problem can be overcome by the use of a three electrode arrangement in which a third *counter (secondary or auxiliary) electrode* is introduced. This third electrode acts to donate or accept electrons as required in the system. The potential imposed at the working electrode (the polarising potential) is set with respect to the reference electrode using a *potentiostat*. The potentiostat maintains the potential across the electrodes - irrespective of the current drawn by the circuit. This ensures that current only flows between the working and counter electrodes. Current is further prevented

from flowing through the reference electrode since the metal/solution interface of this electrode is designed to have extremely high electrical impedance.

The working electrode must be a good electron conductor (if it is to be used under non-equilibrium conditions) and therefore is often a precious inert metal such as platinum or gold, although more recently glassy carbon or carbon pastes have been used due to their relative ease of production and low cost. Usually it is also important that the electrode material is inert in the region of potential in which the electroanalytical determination is carried out. The potential range is determined by one or more of; solvent decomposition (i.e. oxidation or reduction of the solvent), decomposition of the supporting electrolyte, electrode dissolution, redox potential of the species under investigation, and/or the formation of a layer of insulating/semi-conducting substance on its surface.

The standard hydrogen electrode (SHE) is the reference electrode used for the calculation of standard electrode potentials. However, it is not convenient to use on a day-to-day basis (due to its size) and so reference electrodes for electrochemical analyses are commonly the silver/silver chloride electrode (Ag/AgCl) or the saturated calomel electrode (SCE). Ideally a reference electrode should be completely non-polarisable, i.e. no current should flow across the interface between the electrode and the solution, irrespective of the current which flows through the cell. Reference electrodes are chosen due to their stable electrical double layer properties (See Section 2.2.2.). Hence, they are able to maintain a stable potential difference that may be referred to. For this reason, electrochemical potentials are normally quoted versus, or with respect to, the reference electrode. It should be noted here that the reference electrode tip should be located close to the working electrode surface, so that voltage drop due to the resistance of the solution (iR) is minimised.

The counter electrode should ideally be at least 5-10 times larger in size than the working electrode so as not to limit the rate of the electrochemical reaction occurring at the working electrode surface. In some cases it is necessary to ensure that the

reaction products from the auxiliary electrode cannot reach the working electrode. In these cases, a two-compartment cell is employed using, for example, a glass frit separator.

The conductivity of the solution should also be sufficient to allow for the flow of current across the solvent. The inclusion of ionic supporting electrolytes (such as sodium or potassium chloride) can, in addition to pH buffering, increase the conductivity of the solution.

2.3.2 Linear sweep and cyclic voltammetry

Linear sweep voltammetry and cyclic voltammetry are both dynamic electrochemical techniques since they involve the variation of an applied (polarising) potential. The resultant current is monitored throughout the potential sweep with respect to the applied potential. If the current is plotted with respect to the potential, the resulting current-potential profile is known as a voltammogram. Linear sweep and cyclic voltammetry is easy to perform and can provide quick and useful information about an electrochemical system under investigation. Naturally, potential sweep techniques can also give quantitative information, since the currents obtained are directly proportional to the analyte concentration.

Consider the reversible reaction of A (the electroactive analyte present in the solution) being reduced to B (the product) via a simple one electron process;

$$A_{(aq)} + e^{-}{}_{(m)} \underset{k_{ox}}{\overset{k_{red}}{\rightleftharpoons}} B_{(aq)} \qquad (2.19)$$

The potential of the working electrode is swept in a negative direction from a value, E_1, at which A cannot undergo reduction, to a potential, E_2, where the electron transfer is driven rapidly. This is *linear sweep voltammetry*, the potential sweep profile of which can be seen in Figure 2.6.

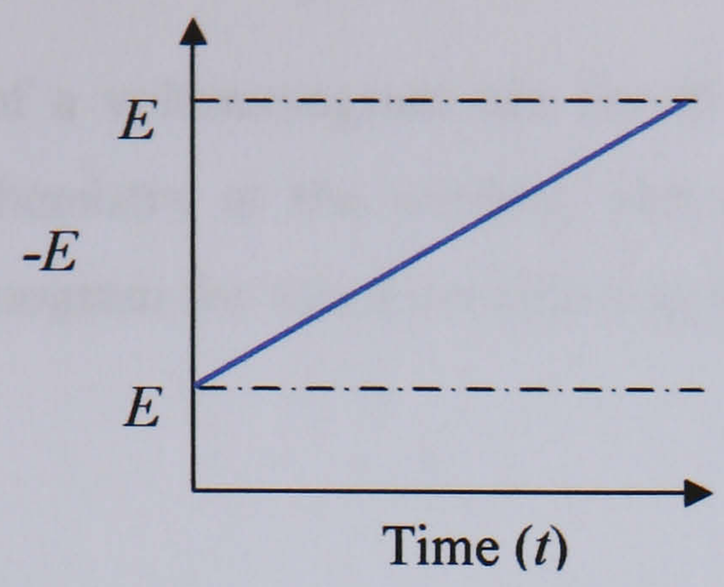

Figure 2.6 **Potential sweep profile of a linear voltammogram.**

The applied potential E is a function of the speed at which the potential is swept, v_s, and the time of the sweep, t:

$$E(t) = E_1 - v_s t \tag{2.20}$$

The sweep rate, v_s, is of extreme importance and typically varies between 1 mVs^{-1} and 1 Vs^{-1}, although much higher sweep rates are routinely found. As the sweep rate is increased, the time-scale of the experiment becomes smaller so that eventually, equilibrium is not reached at the electrode surface and kinetic effects begin to appear.

If the direction of the potential ramp is then reversed at the end of the sweep until the original starting potential (or another end point) is reached once more (Figure 2.7), the technique is known as *cyclic voltammetry*. The potential cycle may be repeated several times if desired.

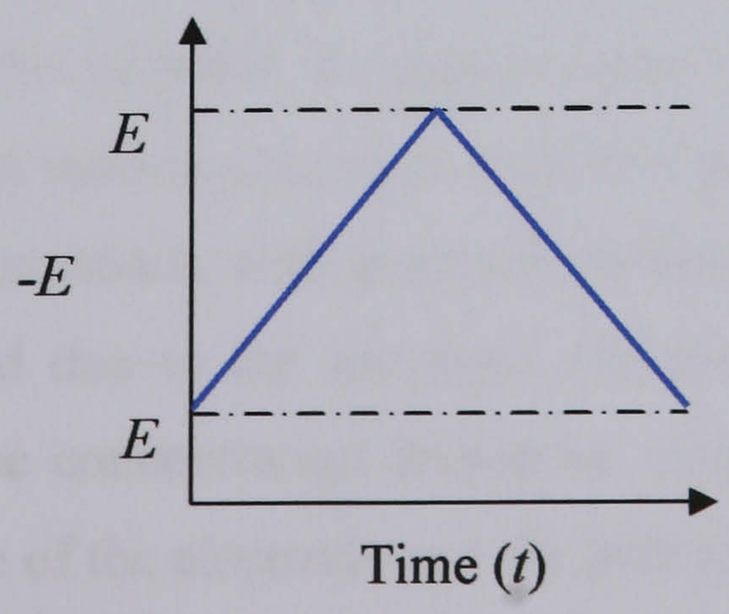

Figure 2.7 **Potential sweep profile of a cyclic voltammogram.**

The shape and nature of a voltammogram can reveal a great deal of information relating to the electrochemistry at the working electrode. Figure 2.8 shows an idealised cyclic voltammogram for the reversible couple, *A/B*, depicted in Equation 2.19:

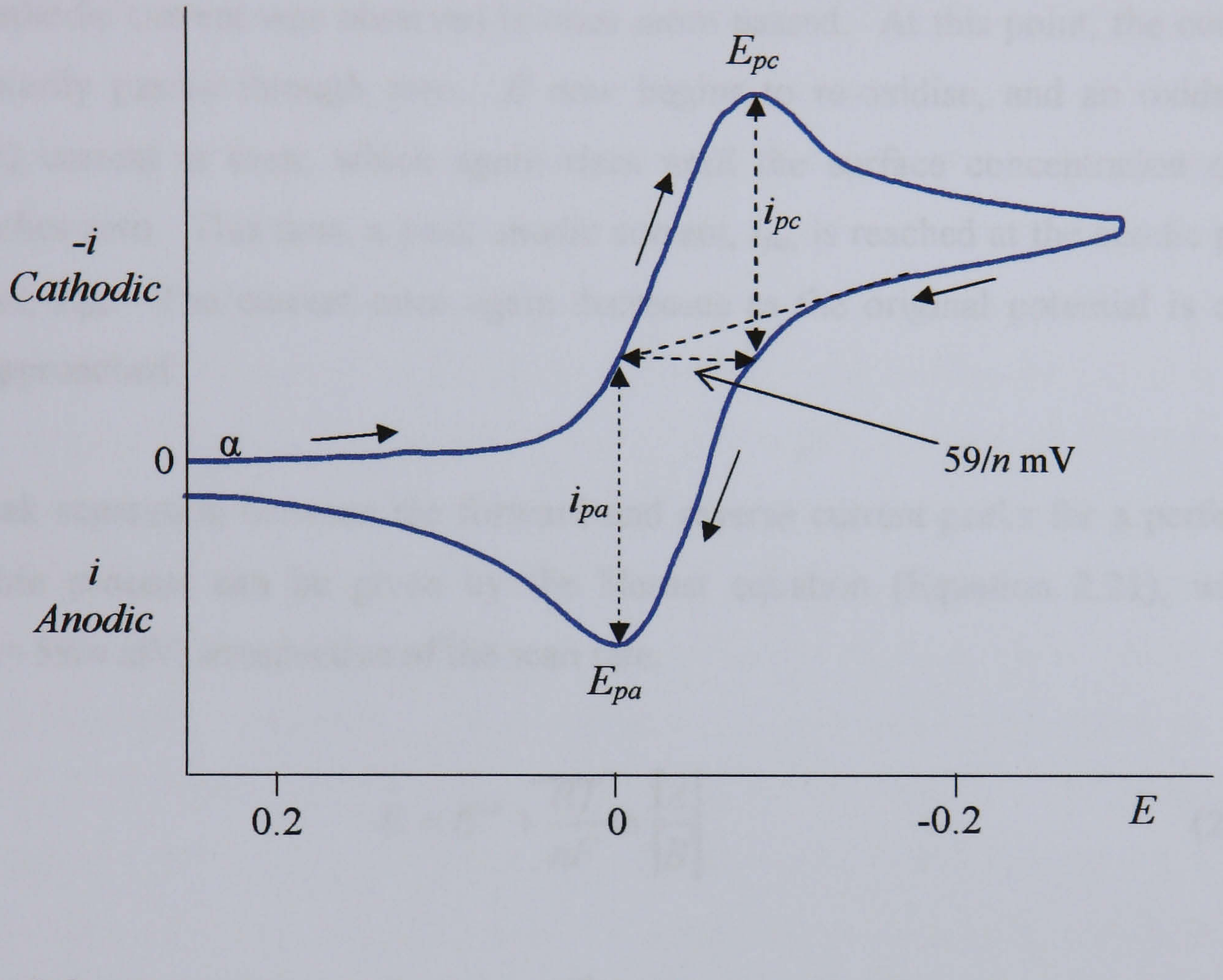

Figure 2.8 Idealised cyclic voltammogram for a reversible electron transfer reaction.

Initially, at point α, no current is passed since the applied potential is insufficient to induce an electron transfer reaction. As the potential is swept, the current initially rises very slowly. This is due to the background current (residual current and double layer charging). But as the potential is swept to more reducing potentials it reaches values that are capable of inducing the reduction of *A* to *B* at the electrode, and the current starts to rise exponentially with potential (or time). The current increases as the potential is increased due to the increased electron transfer rate. *A* is being consumed and its surface concentration decreases, causing a diffusion gradient to form between the surface of the electrode and the bulk solution. Eventually, as even more negative potentials are reached, the increase becomes less than exponential (due to the surface concentration of *A* approaching zero), and ultimately a maximum

(peak) cathodic current, i_{pc}, is reached at the cathodic peak potential, E_{pc}. The cathodic current then falls as the diffusion gradient extends further into the solution. The rate of mass transport to the working electrode now becomes limiting, and the current now approaches a new equilibrium plateau until the direction of the potential sweep is reversed. A reduction current is observed until the potential at which the peak cathodic current was observed is once more passed. At this point, the current momentarily passes through zero. *B* now begins to re-oxidise, and an oxidative (anodic) current is seen, which again rises until the surface concentration of B approaches zero. This time, a peak anodic current, i_{pa}, is reached at the anodic peak potential, E_{pa}. The current once again decreases as the original potential is once more approached.

The peak separation between the forward and reverse current peaks for a perfectly reversible process can be given by the Nernst equation (Equation 2.21), where $RT/nF = 59/n$ mV, irrespective of the scan rate.

$$E = E^{\ominus} + \frac{RT}{nF} \ln \frac{[A]}{[B]} \qquad (2.21)$$

where E is the equilibrium potential, $E^{\ominus}$ is the potential in volts under standard conditions of temperature and concentration, n is the number of electrons transferred in the reduction or oxidation process in question, R is the molar gas constant (8.31 J K^{-1} mol^{-1}), T is the absolute temperature (in Kelvins) and F is the Faraday constant (9.6 x 10^4 C mol^{-1}). $[A]$ and $[B]$ are the concentrations (activities) of the oxidised and reduced species respectively. Hence, the positions of the peak potentials, E_{pc} and E_{pa}, do not change with scan rate and the ratio of the peak currents, i_{pc} and i_{pa} is equal to 1:

$$\frac{i_{pa}}{i_{pc}} = 1 \qquad (2.22)$$

It has been shown above that in the cyclic voltammetry of *reversible reactions*, i.e. those with fast electrode kinetics relative to the time-scale of the sweep, the product of the initial oxidation or reduction is then reduced or oxidised, respectively, on reversing the scan direction and that the peak potential is constant and independent of sweep rate. However, for completely *irreversible reactions* only the oxidation or reduction corresponding to the initial sweep direction appears, since re-reduction or re-oxidation, respectively, cannot occur. Therefore there is no reverse peak observed and the peak potential shifts to more negative potentials at faster sweep rates. The peak currents are also larger for reversible couples than for an irreversible couple at the same voltage sweep rate. The majority of redox couples fall between the two extremes and exhibit *quasi-reversible* behaviour. This means that the reverse peak appears but is smaller than the forward peak, and unlike the case of reversible reactions, the separation of the two peaks is dependant on the scan rate. Only a very small peak will be seen unless a very fast scan rate is used because the electrode has to be taken to highly anodic potentials so as to 'drive' the *B* to *A* (reverse) reaction. Otherwise, almost all the *B* formed in the forward scan will diffuse into the bulk solution and be unavailable for re-oxidation. By measuring peak potentials for forward and reverse scans it is possible to deduce standard rate constants from values of peak separation for simple electrode processes such as that in Equation 2.19.

However, for any system, reversible or not, the peak currents for both the cathodic and anodic reactions are dependant on the scan rate and directly proportional to the concentration of A, because if the electrode potential is swept more rapidly, relatively less time is available for electrolysis and the depletion of *A* near the electrode is reduced, resulting in a thinner diffusion layer and hence a steeper concentration gradient. The resulting larger flux gives rise to an enhanced peak current, i_p.

2.3.3 Chronoamperometry

Chronoamperometry involves polarising the working electrode at a fixed value, such that a chosen oxidation or reduction reaction occurs at the surface. The resultant current is recorded as a function of time. This is carried out with a static electrode in unstirred solution. The potential is stepped from a potential value where no electroactive species react, E_1, to a potential value where all the species that reach the electrode react, E_2. The corresponding scheme of application and current-time transient (or chronoamperogram) is shown in Figure 2.9:

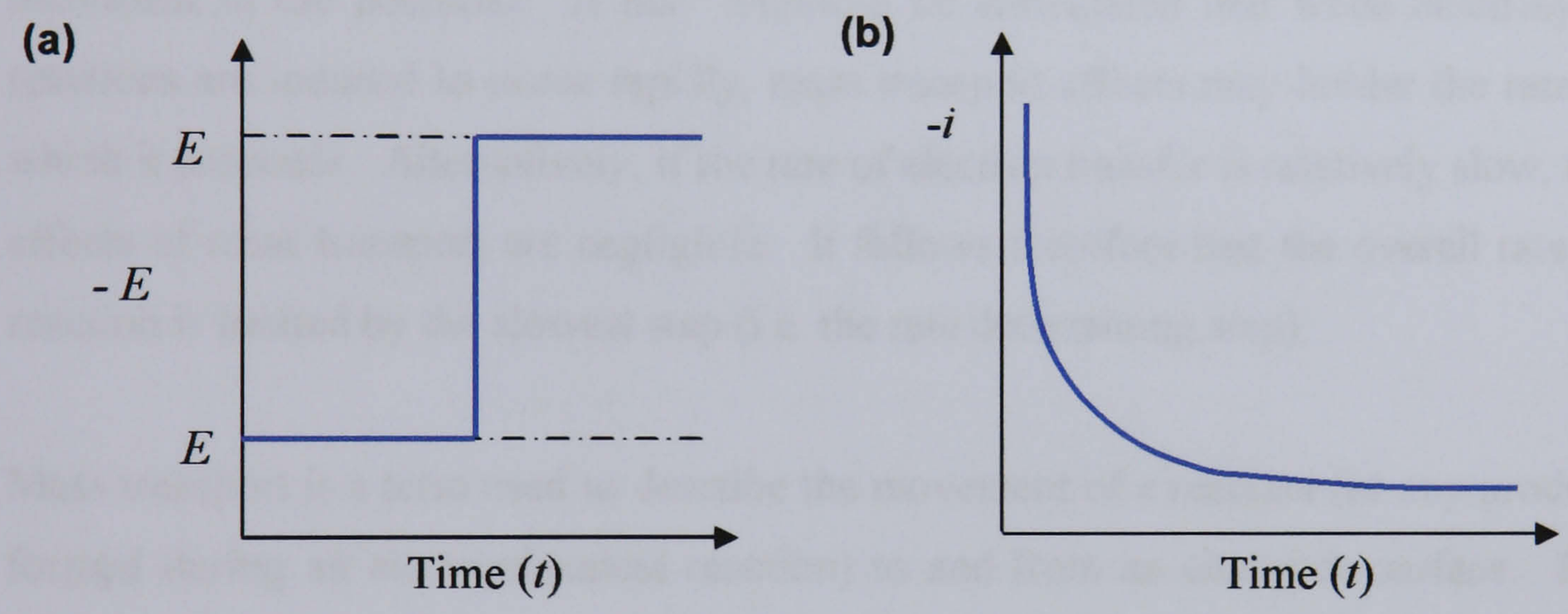

Figure 2.9 (a) Scheme of application for a potential step at an electrode. (b) Current response to potential step as a function of time at a large, static electrode (chronoamperogram).

The concentration gradients shortly after the application of potential, E_2, are extremely large since there has been little time for any depletion of the electroactive material. Consequently, the currents flowing are initially very large. Gradually, as depletion occurs, the diffusion layer thickness increases and the current decreases, ultimately towards zero (albeit never reaching it), as the distance from the electrode into solution increases. Low currents are always observed due to random natural convection in the solution over time. This is further explained in the proceeding section (Section 2.4).

2.4 MASS TRANSPORT

A charged electrode predominately attracts positively and negatively charged species, which may or may not undergo reaction at the surface. However, it should be noted that there is also interaction of the electrode with neutral species through adsorption (Grahame, 1947). Therefore, in the description of any electrode process we have to consider the transport of species to the electrode surface as well as reactions at the surface of the electrode itself. It was shown in Section 2.2, that the electron transfer rate can be experimentally controlled through the electrode potential and that it typically varies by several orders of magnitude for a relatively small increment in the potential. It may therefore be anticipated that when electrolytic reactions are induced to occur rapidly, mass transport effects may hinder the rate at which it proceeds. Alternatively, if the rate of electron transfer is relatively slow, the effects of mass transport are negligible. It follows therefore that the overall rate of reaction is limited by the slowest step (i.e. the rate determining step).

Mass transport is a term used to describe the movement of a reactant (or any product formed during an electrochemical reaction) to and from an electrode surface. For electrolysis to occur, the reactant molecule must be transported from the bulk solution to the electrode interface, and the reactant products, once formed must themselves diffuse away from the electrode (Figure 2.10). This transport can occur by *diffusion, convection or migration* (Brett & Brett, 1986), each of which will be considered in the following sections.

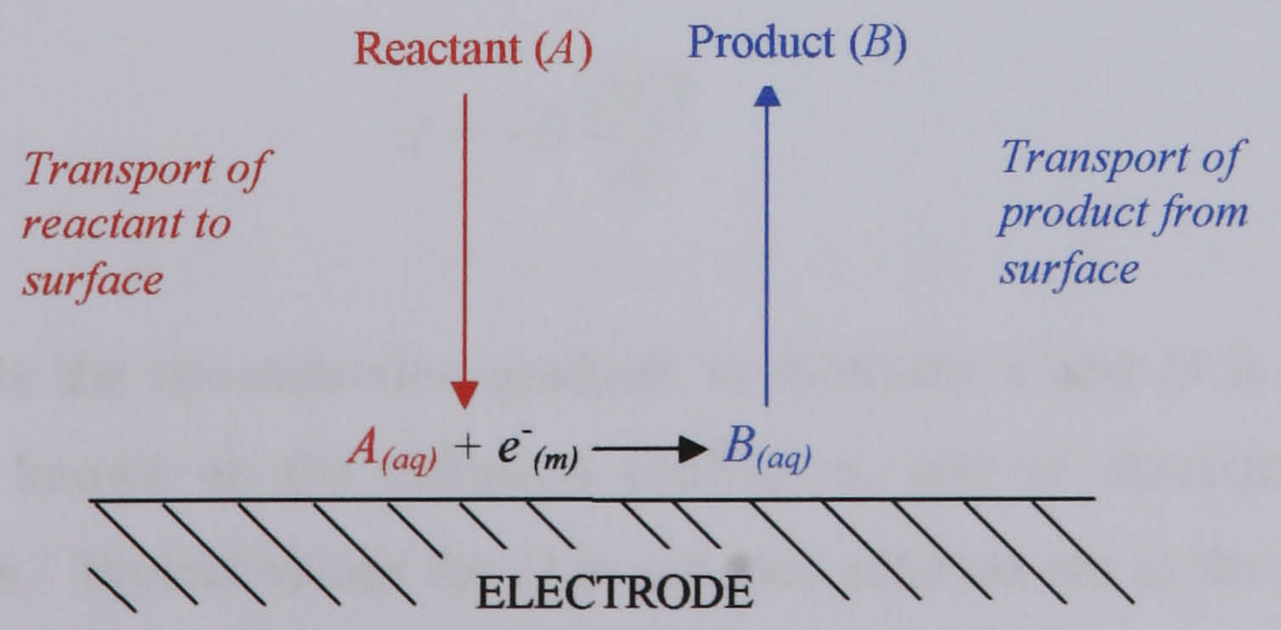

Figure 2.10 Schematic of some of the processes that influence the rate of an electrode reaction in which *A* is reduced to *B*.

2.4.1 Diffusion

Diffusion is the natural movement of species under concentration gradients from a region of high concentration to a region of low concentration. The main driving forces for diffusion are entropy forces, which attempt to equalise these differences in reactant concentrations. Diffusion is shown schematically in Figure 2.11, with the diffusional flux of a species, J (the number of moles of material diffusing through a unit area in one second), into and out of a zone bounded by two planes, x and $x + dx$, which are separated by a distance, dx:

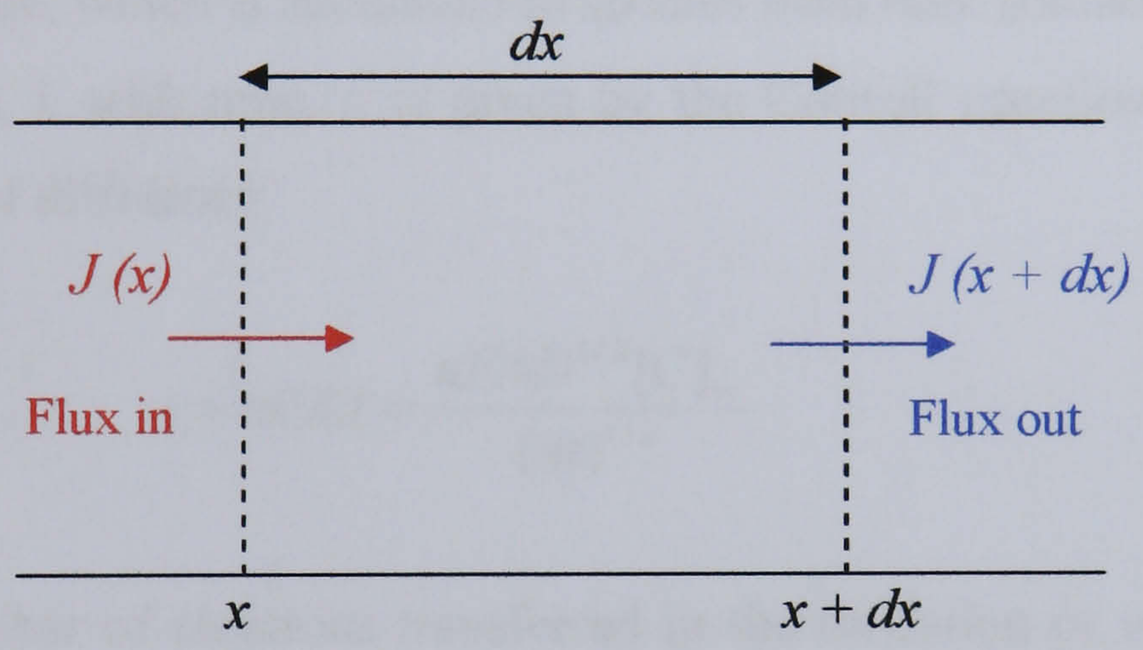

Figure 2.11 Diffusion in one dimension, in the direction opposing the concentration gradient.

Diffusion can be described mathematically by *Fick's first law of diffusion* (Equation 2.23). Fick (1855) first described diffusion by considering the simple case of linear diffusion to a planar surface. He showed experimentally that the 'diffusional flux', J, is:

$$J = -D\frac{\partial[C]}{\partial x} \tag{2.23}$$

where $\partial[C]/\partial x$ is the concentration gradient in direction x and D is the constant proportionality, known as the diffusion coefficient, and is characteristic of the diffusing species. Typical values for D in aqueous solution are in the range 10^{-5} to 10^{-6} cm^2 s^{-1}.

In practice, it is more useful to consider the variation of concentration at a point (such as adjacent to the electrode surface) as a function of time (as opposed to distance). This can be predicted using *Fick's second law of diffusion*:

$$\frac{\partial[C]}{\partial t} = D\left(\frac{\partial^2[C]}{\partial x^2}\right) \tag{2.24}$$

where $\partial[C]/\partial t$ is now the concentration in terms of position and time, and $(\partial^2[C]/\partial x^2)$ is the concentration gradient.

For a planar electrode, which is accessible to species from bulk solution, the resulting variation of current, i, with time, t, is given by the Cottrell equation (derived from Fick's second law of diffusion):

$$i = nFAJ = \frac{nFAD^{1/2}[C]_\infty}{(\pi t)^{1/2}} \tag{2.25}$$

where n is the number of electrons transferred in the oxidation or reduction of the species per mole, F is the Faraday constant (9.6×10^4 C mol^{-1}), A is the electrode area (in cm^2) and $[C]_\infty$ is the bulk concentration of electroactive species.

The effect of *diffusional transport* in electrolysis should also be considered. Consider a large, planar electrode placed in a large container of a reactant, C, which may be oxidised to C^+ according to Equation 2.26:

$$C_{(aq)} \rightarrow C^+_{(aq)} + e^-_{(m)} \tag{2.26}$$

Initially the solution composition is constant and a uniform bulk concentration of C is present throughout the solution. If the electrode is then connected to a potential source, which drives the reaction shown in Equation 2.26 to completion, any C at the electrode interface is converted to C^+. As a result, a concentration gradient is induced between the electrode and the bulk solution. The concentration gradient is

perpendicular to the electrode and acts to force a flux of fresh C from the bulk solution to flow towards the electrode surface (as shown in Figure 2.11). Gradually a diffusion layer is established close to the electrode in which the concentration of C differs from its value in the bulk solution. As electrolysis proceeds, the thickness of this layer becomes progressively larger. The concentration profile at certain times after electrolysis has been initiated can be seen in Figure 2.12, which shows that close to the electrode surface the profile is linear, but beyond this it approaches the bulk concentration asymptotically.

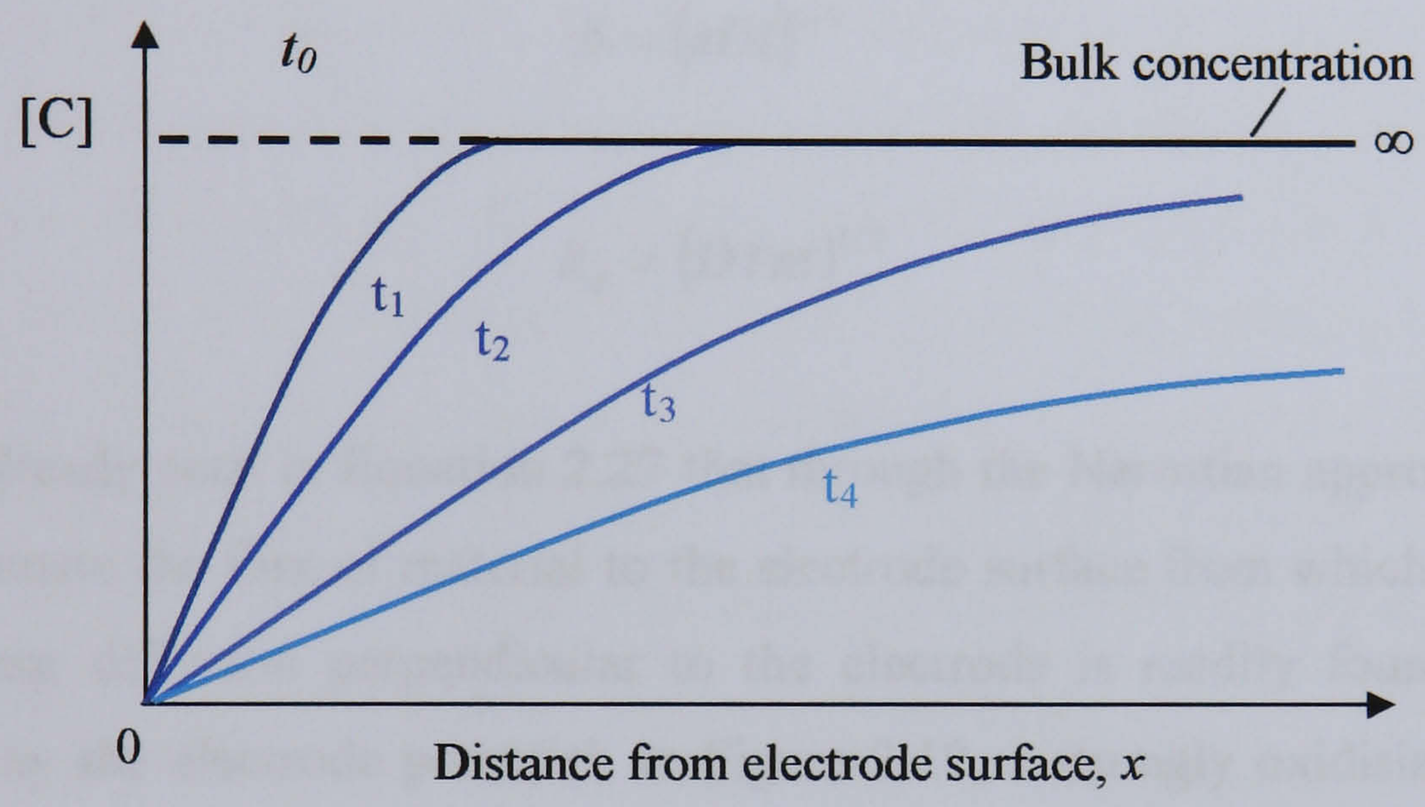

Figure 2.12 Growth of the diffusion layer thickness on a large electrode as a function of time, *t*.

The thickness of the diffusion layer grows steadily as the electrolysis consumes more and more C. In principle, the diffusion layer thickness can grow without limit until it has exhausted all the C within the container (this is the case if the transport effects experienced by C are purely diffusional in nature). For comparison between different types of electrodes and experimental methodology, it is useful to define the diffusion layer thickness, δ, where (according to Nernst):

$$\frac{i}{FA} = D\left(\frac{\partial[C]}{\partial x}\right)_0 = D\frac{([C]_\infty - [C]_0)}{\delta} \qquad (2.27)$$

where $[C]_0$ is the surface concentration of electroactive species.

When $[C]_0 = 0$:

$$\frac{i}{FA} = D\left(\frac{\partial[C]}{\partial x}\right)_0 = D\frac{[C]_\infty}{\delta} = k_d[C]_\infty \tag{2.28}$$

where k_d is the mass transfer coefficient ($=D/\delta$). Thus, the diffusion layer thickness and mass transfer coefficient corresponding to the Cottrell equation (Equation 2.25) are shown in Equations 2.29 and 2.30 respectively:

$$\delta = (\pi Dt)^{1/2} \tag{2.29}$$

$$k_d = (D/\pi t)^{1/2} \tag{2.30}$$

We have already seen in Equation 2.27 that through the Nernstian approach, we are able to estimate the flux of material to the electrode surface from which the current due to linear diffusion perpendicular to the electrode is readily found. This is controlled by the electrode potential; in Figure 2.12, a strongly oxidising electrode potential has been assumed so that the surface concentration of C is indistinguishly close to zero. Since electroactive material must be transported to the electrode surface for electrolysis to occur, it follows that the maximum observable current is limited by the rate at which the reactant reaches the electrode/solution interface. From Equation 2.27, it is clear that if the electrode potential is gradually increased so the surface concentration of the reactant $[C]_0$ eventually becomes zero, a limiting current, i_L, is reached:

$$i_L = \frac{DFA[C]_\infty}{\delta} \tag{2.31}$$

Under these conditions all the electroactive material transported to the electrode is converted to products.

2.4.2 Convection

Convection is the movement of species that occurs when a mechanical force acts on a solution. There are two types of convection; *natural convection*, which can be present in any solution and arises from thermal gradients and/or density differences within the solution, and *forced convection*, which is achieved by external forces such as gas bubbling through solution, pumping, or stirring.

In electrolysis reactions (such as Equation 2.26), the bulk of the solution invariably experiences some mixing due to natural convection and this limits the scale to which the diffusion layer can expand. Obviously, the greater the natural convection in the bulk solution, the thinner the final diffusion layer thickness established. Under these conditions, transport within the diffusion layer is pictured as occurring via diffusion alone, whilst outside the layer, the concentration of C is maintained at its bulk value through natural mixing. In such systems where there is convection in addition to diffusion, extra material is brought to the electrode surface and the currents that flow are larger than those observed when diffusion alone occurs.

Natural convection typically becomes a significant problem with electrodes of conventional size (approximately millimetres or larger) on the time-scale of 10-20 seconds or longer, and is generally undesirable since it is difficult to predict. For this reason, forced convection may be introduced with the aim of swamping any contributions from natural convection (e.g. a hydrodynamic electrode), so ensuring that reproducible experiments can be made beyond the 10-20 second limit. This enables a quantitative description of the flow in solution to be established and the pattern of mass transport to the electrode to be predicted. Concentration changes resulting from the convective movement of solution can be predicted mathematically by Equation 2.32 (where v_x is the velocity of the solution), which is the convective analogue of Fick's second law of diffusion (Equation 2.24):

$$\frac{\partial[c]}{\partial t} = -v_x \frac{\partial[c]}{\partial x} \tag{2.32}$$

2.4.3 Migration

Migration is the movement of charged species under the influence of an applied potential gradient. It represents the mechanism by which charge flows through a solution between two electrodes at which ionic charge is created and destroyed by electron transfer, therefore maintaining the necessary charge balance. However, migration has little importance to the overall rate of mass transport of an electrochemically generated species. This is because a large excess of other ionic species (an inert supporting electrolyte) are present in most cases, providing the passage of the required charge and depressing any potential gradients which may otherwise arise in the solution. Hence, convection and diffusion are typically the only significant mechanisms of mass transport in solutions generally of interest and for most practical purposes the effects of migration can be ignored.

The way in which the supporting (background) electrolyte operates can be understood by examining electrolytic ion addition or removal at the electrode/solution interface. This causes a slight redistribution of the different cations and anions (comprising the background electrolyte) to take place near the interface, so as to maintain near electrical neutrality in the entire interfacial region (except for a very tiny region absolutely adjacent to the electrode). The availability of background ions to maintain electrical neutrality ensures that electrical fields do not build up in the solution as electrolysis proceeds. In this way, transport effects are not subjected to the small charge injection that arises from electrolytic reaction.

Calculations have shown that approximately 100 times the concentration of background electrolyte relative to that of the reactant is required if the measured current is not to be perturbed significantly (<1%) from its value where migration plays no part (Brett & Brett, 1986).

2.5 MICROELECTRODES

We have seen in the previous section that the total rate of mass transport to the electrode surface depends on the bulk concentration of analyte, the area of the electrode, and the diffusion and convection conditions. Although the use of diffusion-limiting membranes can help *limit* the rate of mass transport, in practical situations it may be preferable to *increase* the rate of mass transport. This result can be obtained by using microelectrodes (Edmonds, 1998).

Although the advantageous properties of very small electrodes were recognised by physiologists for many years (Loeb *et al.*, 1995), research in this area did not become very active until the late 1970s when advances in the field of electronics, especially in the measurement of very small currents and the advent of microstructural materials provided the tools necessary to build and use microelectrodes. Fleischmann and co-workers initiated much of this activity with an interest in understanding electrode mechanisms under conditions of high current density (Fleischmann *et al.*, 1987). Around the same time, miniature electrodes were being developed for use within *in vivo* probes (Adams, 1976; Ponchon *et al.*, 1979). By 1981 it was clear that many new areas which were inaccessible to electrodes of larger dimensions could be explored with very small electrodes, and an early review summarises many of these expectations (Wightman, 1981).

Although the question of how small the dimension of an electrode has to be before it is considered to be a true microelectrode has been debated, it is generally accepted that a microelectrode is an electrode which is smaller than the scale of the diffusion layer. Operationally this has been defined as ***an electrode which has at least one dimension (the critical dimension) in the micrometer range, specifically smaller than 25μm*** (Zoski, 2002).

The electrochemical responses at microelectrodes can differ greatly from those seen at conventional (i.e. macro) electrodes. Typically, microelectrodes offer higher

sensitivity, smaller double-layer capacitance, and lower ohmic losses that result in a higher signal-to-noise ratio. The improved diffusion characteristics of microelectrodes allow measurements in both static and stirred solutions (Wightman & Wipf, 1989). This characteristic has opened many new possibilities in electrochemistry and may have a positive effect on the commercial realisation of chemical sensors as it allows a sensor to be used as a 'dip-stick' device. Such sensors may be dipped into the analyte solution without stirring effects (convection) causing unwanted fluctuations in the electrode response. To date, the majority of sensors which have reached commercial success have avoided this problem by inhibiting stirring by some means (e.g. droplets of blood in hand-held glucose sensors are held by surface tension); however, this is not possible for all applications, such as the analysis of non-viscous media or the analysis of analytes present in flowing streams.

A review of the processes that occur at microelectrodes and their resultant properties will be discussed in this chapter. The fabrication of these electrodes will also be discussed.

2.5.1 Diffusion at microelectrodes

Microelectrodes have many different geometries such as a hemisphere, disc, ring, band or cylinder, each of which influences the way in which diffusional mass transport occurs towards the electrode. However, as the type of microelectrodes produced in this work are of a hemispherical diffusional geometry, all further models refer to electrodes of this dimension (and indeed the processes that occur at spherical electrodes during electrolysis exemplify many of the factors which are seen at other geometries of microelectrodes).

Diffusion to and from *macro*-electrode surfaces can be a major problem with electrochemical sensors. This is due to the fact that diffusion occurs at a much slower rate than convection (in the order of a million times slower). If a solution is stirred outside of a macroelectrode based sensor, the measurable signal will fluctuate due to these variable convection rates. This problem can be overcome if the rate of diffusion is made to be larger than the rate of convection. At microelectrodes the predominant mode of mass transport is also diffusion, but now the flux as a result of diffusion is very large. This is because the mass transport of electroactive species is varied from the normal linear diffusion that procures at large, planar electrodes, to a three-dimensional diffusion (hemispherical diffusion profile), and therefore the effects of convection tend to be less apparent than at electrodes of conventional size. This can be explained practically by the fact that a hemispherical electrode is fully and uniformly accessible, as depicted by Figure 2.13b:

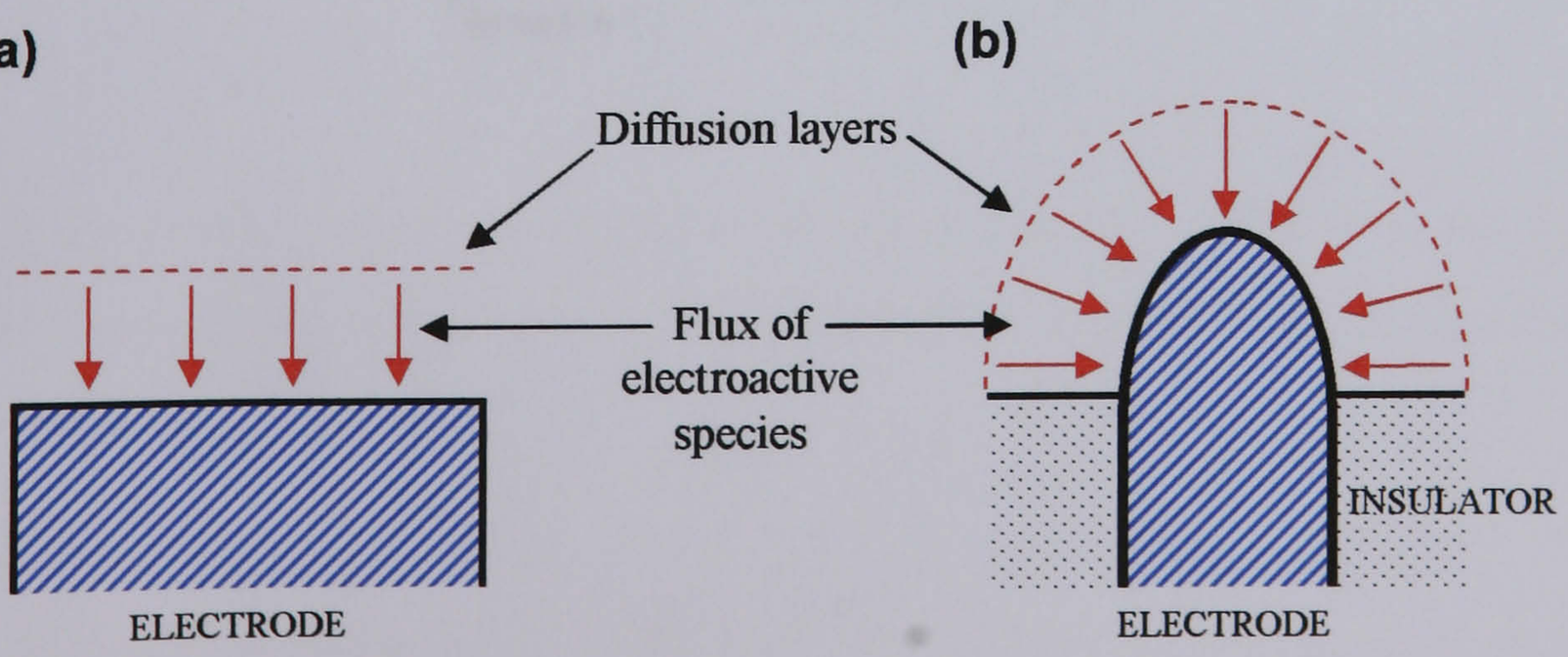

Figure 2.13 Schematic representation of (a) planar diffusion at a macroelectrode and (b) hemispherical diffusion at a microelectrode.

Using the same boundary conditions as for linear diffusion (seen in Section 2.3.3), Cottrell has also calculated the expression for the variation of current with time for a spherical electrode. The result is Equation 2.33:

$$i = nFAD[C]_{\infty}\left[\frac{1}{(\pi Dt)^{1/2}} + \frac{1}{r}\right] \tag{2.33}$$

where r is the radius of the sphere and A is given by $4\pi r^2$ and $2\pi r^2$ for sphere and a hemisphere respectively. At short times the currents at a spherical electrode are identical to those found under conditions of planar diffusion. However, at longer times the current becomes independent of time.

In other words, for a microelectrode the current equation will be the same as above, with the exception of the suppression of the term t, considered negligible due to the very small value of r, since:

$$r = (\pi Dt)^{1/2}/10 \tag{2.34}$$

Hence, the smaller the value of r, the quicker the effect of t decreases and the faster the steady-state is reached. Therefore, Equation 2.33 becomes Equation 2.35 in the case of a microelectrode:

$$i = \frac{nFAD[C]_{\infty}}{r_{hemisphere}} = 2\pi nr_{hemisphere}FD[C]_{\infty} \tag{2.35}$$

Fabrication of microelectodes with the geometry of a disc embedded in an infinite insulating plane is easier to achieve than forming spherical electrodes and is the type fabricated in this work. If the hemisphere dimension is close to the diffusion layer thickness (approximately 10 μm), the result will remain the same if the hemisphere is 'flattened' to a disc shape (Figure 2.14):

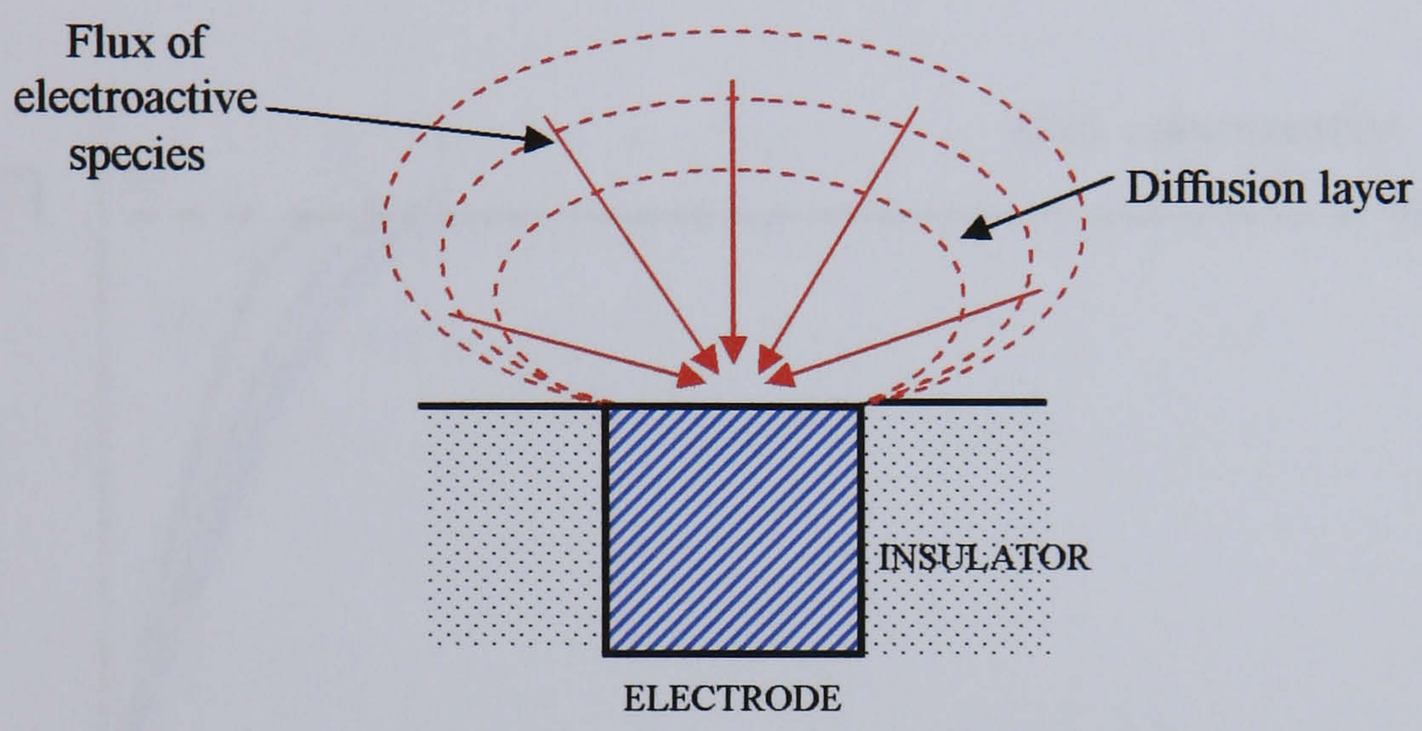

Figure 2.14 Schematic representation of diffusion at a disc microelectrode.

The disc radius becomes a quarter of the sphere perimeter:

$$r_{disc} = \frac{2\pi r_{hemisphere}}{4} \tag{2.36}$$

And so;

$$r_{hemisphere} = \frac{2r_{disc}}{\pi} \tag{2.37}$$

Therefore, by substituting Equation 2.37 into Equation 2.35, the following equation for the steady-state current measured a few seconds after applying a potential step to a disc microelectrode results:

$$i = 4nFr_{disc}D[C]_{\infty} \tag{2.38}$$

In order to explain the effect of diffusion at microelectrodes in more detail, concentration profiles at large and small electrodes must be considered. The Cottrell equation for planar diffusion at a *macroelectrode* (Equation 2.25) predicts that the concentration profile will keep extending into solution as a function of time (Figure 2.12). However, for a *microelectrode*, the concentration profile is quite different, as shown in Figure 2.15:

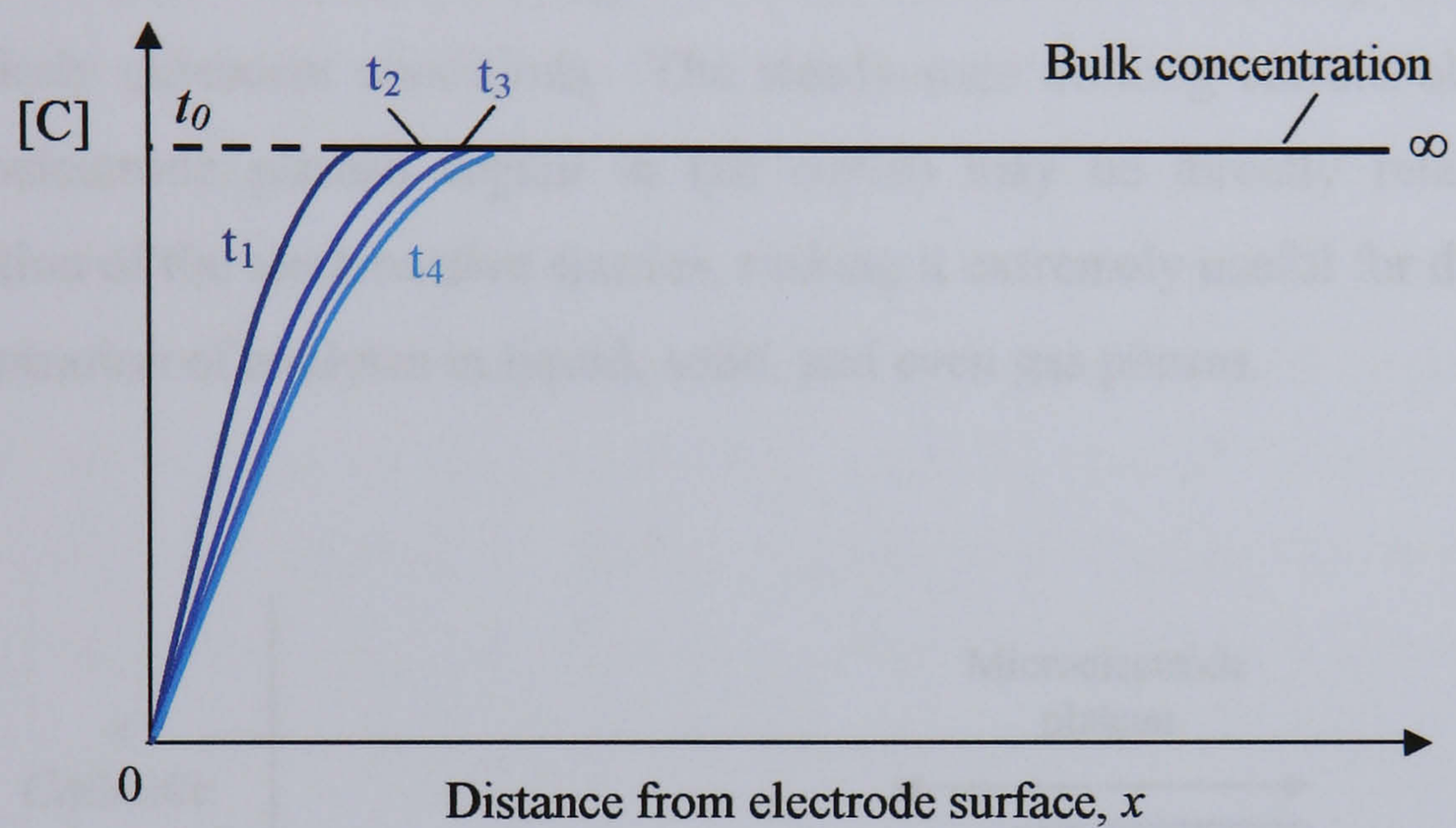

Figure 2.15 Growth of the diffusion layer thickness on a microelectrode with r ~ 10 μm, as a function of time, *t*.

The growth of the diffusion layer is initially similar to that observed at a planar electrode, but at longer times the growth into bulk solution slows considerably. The reason for this behaviour can be described if one considers a different representation of the diffusion layer, as shown in Figure 2.14. As the diffusion layer expands out into the solution, it adopts a hemispherical shape, where its surface area is gradually increasing. Thus, there is an ever-increasing catchment area for reagent, and this compensates for the decreasing concentration/distance profiles at the electrode. In other words, at relatively long experimental timescales, the dimensions of the diffusion layer exceed the radius of the microelectrode, and the originally planar diffusion field transforms into a hemispherical diffusion field. Consequently, the flux of electroactive species to the electrode is substantially higher than for the pure planar diffusion case that is typical of a macroelectrode.

Due to this efficient mass transport, when the applied potential is slowly (at scan rates <50 mVs^{-1}) changed with time (i.e. cyclic voltammetry), the resulting current due to reduction or oxidation of an electroactive species exhibits a sigmoidal-shaped response (i.e. a steady-state response), shown in Figure 2.16, which contrasts with the peak-shaped voltammograms observed at macroelectrodes (Figure 2.8). This sigmoidal shape is characteristic of a microelectrode and is analogous to the polarograms obtained using a dropping-mercury electrode, or a rotating-disk electrode, with the difference being that with microelectrodes, they are observed under entirely quiescent conditions. The steady-state limiting current observed (at the microelectrode plateau region in the curve) may be directly related to the concentration of the electroactive species, making it extremely useful for determining the concentration of analytes in liquid, solid, and even gas phases.

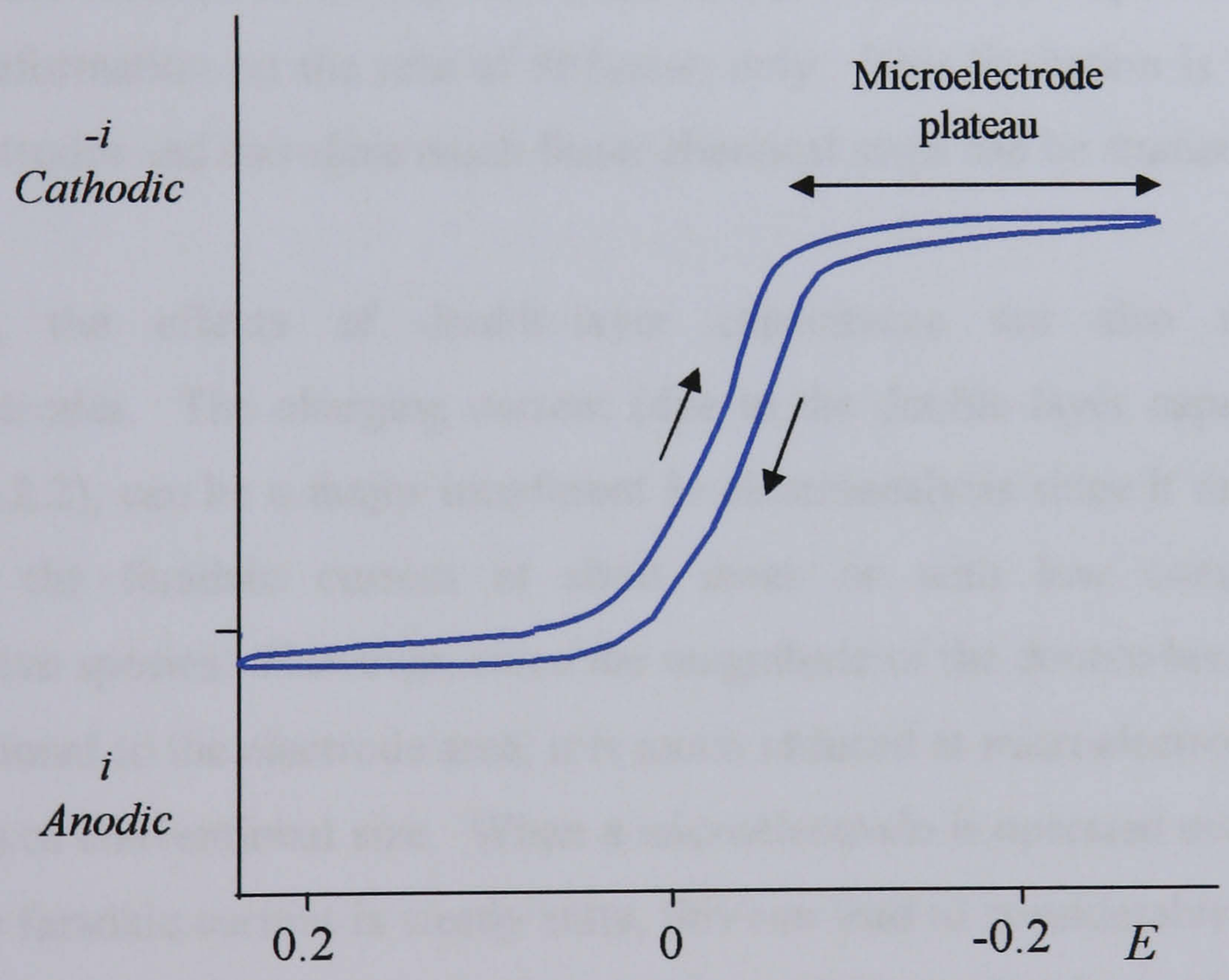

Figure 2.16 Characteristic sigmoidal shaped cyclic voltammogram for a reversible electron transfer reaction at a microelectrode. (Scan rate <50 mVs^{-1}).

2.5.2 Advantages in terms of their use in amperometric sensors

An obvious advantage of microelectrodes is their small size, particularly when voltammetry must be performed in a small volume, such as with *in vivo* measurement systems. However, the advantages of microelectrodes go far beyond the simple restrictions of space.

Firstly, microelectrodes, by virtue of the rate of mass transport being much greater than for macroelectrodes, are very valuable in the study of electrolysis mechanisms when the analysis of very fast processes is required, such as rapid rates of electron transfer between electrode and substrate or a fast chemical reaction forming part of an overall mechanism. Such experiments are limited by the use of macroelectrodes because if the process of interest is faster than the rate of mass transport, the experimental results will simply reflect the rate of the slowest step in the process and provide information on the rate of diffusion only. This limitation is not seen with microelectrodes and therefore much faster chemical steps can be studied.

Secondly, the effects of double-layer capacitance are also minimised at microelectrodes. The charging current (due to the double layer capacitance – see Section 2.2.2), can be a major interferent in electroanalysis since it may exceed the value of the faradaic current at short times or with low concentrations of electroactive species. However, since the magnitude of the double-layer capacitance is proportional to the electrode area, it is much reduced at microelectrodes relative to electrodes of conventional size. When a microelectrode is operated under conditions where the faradaic current is steady state, this can lead to considerable improvement in the faradaic-to-charging current ratio, i_F/i_C (or signal-noise ratio, S/N). For example, at a disk or a spherical electrode, the steady-state current is proportional to the radius, rather than to the area of the electrode, and the i_F/i_C ratio will improve inversely with the value of the radius. The lowered effects of double layer capacitance also allow the rate at which the potential in a cyclic voltammetry experiment can be swept to be made much greater. The capacitative nature of the impedance of any electrochemical cell precludes rapid changes in potential. Thus

electrochemical measurements with conventional electrodes have generally been restricted to millisecond, or longer, time scales. The ability to make fast electrochemical measurements is desirable so that rapid heterogeneous reaction rates can be measured.

Thirdly, the ohmic drop (caused by charging current and given by the product, *iR*) between electrodes may be lowered with the use of microelectrodes. At electrodes of conventional size the problem of ohmic drop is circumvented to a certain degree by the use of a three electrode system and the presence of background electrolyte which acts to lower resistance in the bulk solution (as explained in Section 2.3.1). However, the problem can also be diminished with a decrease in electrode area. This is because the charging current is directly proportional to the area, but resistance is inversely proportional to the smallest electrode dimension. Therefore, it is possible to avoid the addition of background electrolyte with the use of microelectrodes and hence, electrochemical experiments using non-polar solvents such as benzene become possible (non-polar solvents are not capable of dissolving a high concentration of electrolyte). A simplified two-electrode system may also be used instead of the conventional three electrode set-up.

Finally, the current amplitude (total current) is very small at microelectrodes (typically a few nA for a microelectrode with a 10 μm diameter). This means that the quantity of consumed species will remain negligible (1 nA corresponds to 1 nCs^{-1}, i.e. 10^{-4} $Cday^{-1}$). Following Faraday's law, such a current quantity corresponds to 1 nmol (i.e. about 30 ng of oxygen or chlorine consumed on the electrode during one full day). Although the currents at microelectrodes are small, the current density (current per unit area) is high. This leads to good signal resolution and also facilitates low detection limits.

In summary, the major advantages (which are essentially related to each other) of microelectrodes are:

1. The ability to work in highly resistive solutions without adding any supporting electrolyte (reduced effects of solution resistance).

2. A dramatic increase of the signal/noise ratio (reduced effects of double layer capacitance).

3. Access to fast kinetics measurements using high speed (thousands Vs^{-1}) cyclic voltammetry.

4. Negligible consumption of electroactive species during an electroactive redox process at the electrode surface.

5. Establishment of steady-state behaviour, even in static conditions.

6. Low incidence of the solution flow at the electrode surface (i.e. stirring), on the measured current.

2.5.3 Microelectrode arrays

Microelectrodes do suffer from some limitations. The most obvious is the small amperometric signal size (the signal size is proportional to the electrode area) which makes it necessary to protect the electrode from electrical noise, so that the signal does not become buried within a baseline of noise and so rendered undetectable. The instrumentation then becomes of primary importance since the currents registered can be at the picoampere level. Another approach is to use assemblies of microelectrodes all with the same function – a microelectrode array (Figure 2.17). This can increase the total measured current whilst retaining the particular properties of single microelectrodes with respect to high concentration gradients.

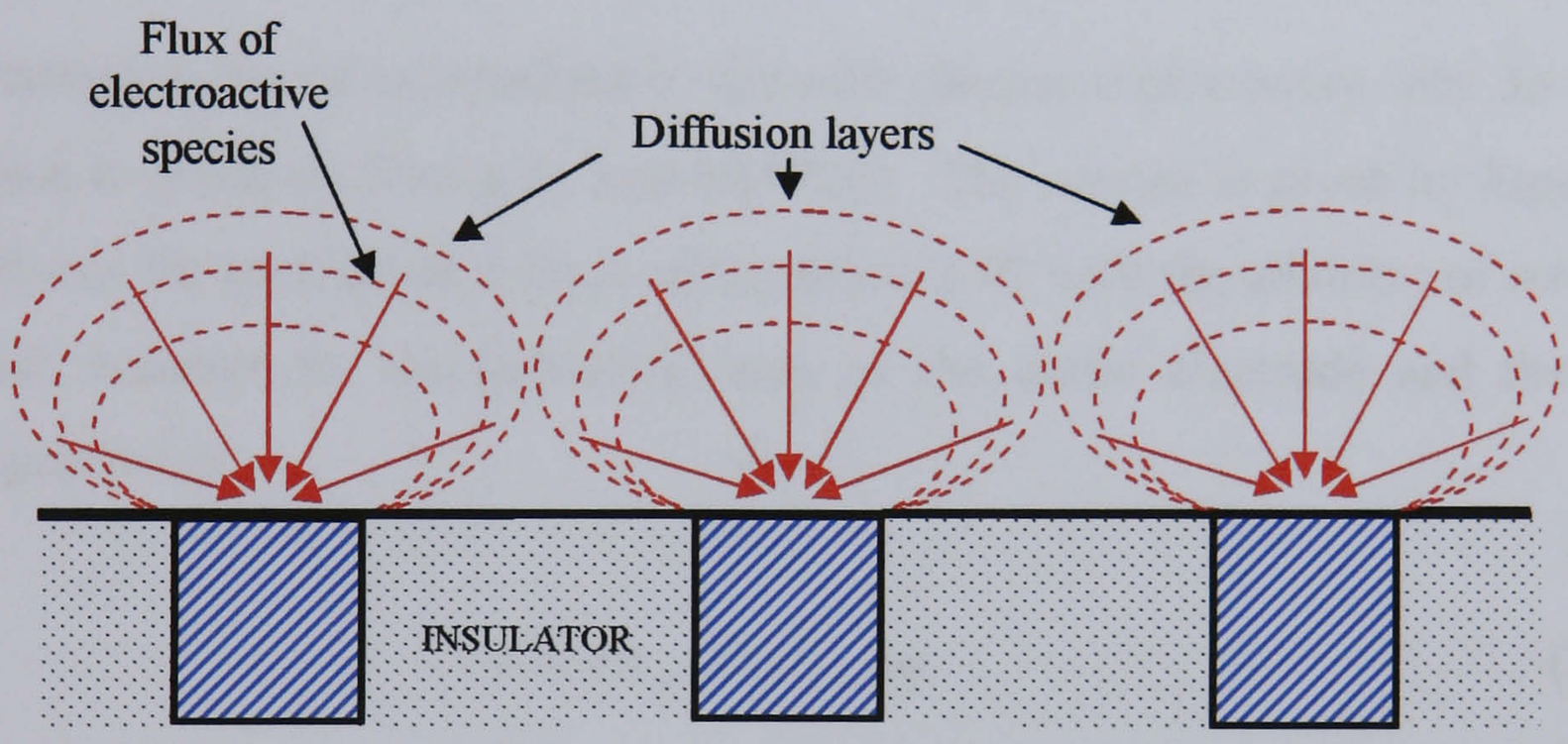

Figure 2.17 Schematic representation of diffusion at a microelectrode array.

It has already been shown that the Nernst diffusion layer has dimensions proportional to the smallest dimension of the electrode. Thus, if two or more microelectrodes are operated at the same potential, the total response of this array of electrodes will depend on the spacing between the individual elements of the array. If the elements are spaced sufficiently far apart, the total response will be the sum of the responses of the individual electrodes (Aoki & Osteryoung, 1981; Caudill *et al.*, 1982). However, if the spacing is sufficiently small such that the diffusion layers overlap as steady-state is approached, the total response will be less than that predicted by the sum for each. This is termed 'shielding' since electrolysis

at adjacent electrodes shields individual elements from the flux they would normally experience.

At very short times, the diffusion layer at each microelectrode acts independently, but as time elapses, the individual diffusion layers grow and start to interact. At sufficiently long times and with sufficiently close spacing between the elements, the array will approach the behaviour of a large electrode whose area is given by the sum of the individual electrode areas and the intervening insulator (Amatore *et al.*, 1983). Hence, to obtain optimum properties, well defined diffusion characteristics have to be established, depending on the electrode radius, their spacing and geometrical arrangement.

The most complete set of expressions to describe chronoamperometry with an array of microdiscs is given by Shoup & Szabo (1984). The current is given by Equation 2.39, which can be considered a form of Equation 2.38 with the addition of terms A and q which account for the geometric area of the entire electrode and the disc density respectively.

$$i = 4nFr_{disc}D[C]_{\infty}Aq \tag{2.39}$$

If the radius of the insulator surrounding each disc is termed r_i, then the condition that must be satisfied in order to prevent the overlapping between the centres of the electrodes is:

$$(r_i - r)^2 \geq 6D\,t \tag{2.40}$$

However, for analytical purposes, a defined array is often unnecessary because a theoretical description of the current is not required since calibration curves will be employed.

2.5.4 Fabrication methods

A recent review of the design and fabrication of single microelectrodes has been given by Zoski (2002). The most popular materials include platinum, carbon fibres, and gold, although mercury, iridium, nickel, silver, and superconducting ceramics have also been used. Microdisc electrodes predominate because of their relative ease of construction, and the ability to polish the sensing surface. They are commonly fabricated by embedding a platinum wire or carbon fibre into tapered glass pipettes that are subsequently sealed with epoxy resin. An active electrode surface is then exposed by mechanical polishing. An alternative procedure involves the electropolymerisation of a passivating polymer film around the carbon fibre electrode. Both of these methods give electrodes with total diameters in the tens-of-micrometres range. However, they are more expensive to fabricate than large electrodes and are therefore often restricted to use within research applications and *in vivo* analysis (such as dopamine monitoring in the mammalian brain).

Multiple microelectrode arrays for electromechanical sensors have been fabricated via photolithographic or laser techniques in a similar manner to the production of printed circuit board and silicon micro-chips or laser ablation, since the late 1970s (Gueshi *et al.*, 1978). Other array fabrication methods include immobilisation of large numbers of metal areas within a non-conducting support and the electrodeposition of mercury and platinum within the pores of a polymer membrane.

With respect to carbon, microelectrodes have been fabricated using conventional techniques such as the suspension of carbon particles or fibres in an insulating matrix, the impregnation of porous carbon within an insulator, or the impregnation of the pores of a host membrane with conducting carbon particles (Wang & Freiha, 1984). Furthermore, glassy carbon electrodes (Horiuchi *et al.*, 1992; Weisshaar & Tallman, 1983; Poon & McCreery, 1986), reticulated vitreous carbon (Sleszynski *et al.*, 1984) and pyrolytic carbon (Niwa & Tabei, 1994; Rojo *et al.*, 1986) arrays have also received considerable attention. Electrodes that are constructed by conventional techniques are subject to great variability in their physical, electrical, and

electrochemical characteristics. Furthermore, these electrodes are difficult to reproducibly fabricate in multi-electrode arrays, and such arrays, when realised, can contain appreciable capacitative coupling between electrodes (Starr *et al.*, 1973).

Different types of carbon array electrodes have also been fabricated using photolithographic techniques (Kittleson *et al.*, 1985; Reller *et al.*, 1984), including microdiscs (Cassidy *et al.*, 1986), microbands (Matsue *et al.*, 1990), and interdigitated array electrodes (Niwa & Tabei, 1994; Aoki *et al.*, 1988; Sanderson & Anderson, 1985). Although such photolithographically produced arrays of microelectrodes exhibit reduced capacitative coupling and can be fabricated reproducibly, they may incur very high costs and are therefore not commercially viable for mass production, especially if disposable tips are required, which is often the case.

Due to this high manufacturing cost, microelectrode arrays have yet to be commercially realised in 'one-shot' sensor applications and consequently, the advantageous properties that they bring with them are also yet to be seen in disposable sensor type applications.

2.6 ELECTRO-POLYMERISED FILMS OF POLY(*o*-PHENYLENEDIAMINE)

Polymer film modified electrodes are used for a variety of applications, such as electrocatalysis (Oyama & Anson, 1980; Bull *et al.*, 1983), analysis (Wierl *et al.*, 1985), and particularly in electrochemical biosensors (Geise *et al.*, 1991). Polymer films were originally constructed using 'bulk technology' such as casting the film on an electrode surface (Sittampalam & Wilson, 1983), using radio frequency plasma or by constructing a discrete, microscopic membrane and subsequently applying it to the electrode (Shichiri *et al.*, 1982). However, all these approaches are difficult to apply to miniaturisation, construction of sensor arrays, or the optimisation of surface microenvironments, as it is nearly impossible to control the reproducibility, uniformity and thickness of the polymer film on an intricately complex surface (such as carbon ink). Therefore, they are essentially limited to two-dimensional electrode surfaces and are not suitable for mass production.

Electropolymerisation may offer a solution to these problems as this method involves 'molecular technology' where deliberate control of the molecular structure of the surface of the electrode can be made to meet specific applications. For example, insulating films show characteristics of molecular self-assembly. They are self regulating films, with uniform thickness, that completely cover the electrode surface regardless of size and shape. The film maintains its uniformity because it only grows thick enough to become an insulator. Polymerisation continues until the conductive surface is completely covered, which is signalled by the current decreasing to a minimum because the monomer cannot penetrate the film. Hence, electrochemistry provides a simple, clean and efficient route to produce a polymer.

Electropolymerised films are generally formed by the oxidation of a monomer, and are insoluble, conducting or insulating polymer films that coat the electrode surface (Emr & Yacynych, 1995). Conducting polymers are capable of transducing energy arising from certain chemical interferents into electrical signals which are easily monitored. The three most common monomers of conducting polymers are pyrrole,

aniline and thiophene. The main disadvantages with these types of films is that they are not very reproducible due to the deposition process, and anions present in the solution or solution pH can influence the conductivity of the film (Curulli *et al.*, 1998). Non-conducting (insulating) polymer films, by contrast, form self-regulating films which have a uniform thickness and cover the surface completely with few defects or pinholes. The most common non-conducting polymers are benzene derivatives such as phenol and phenylenediamines.

The method of polymer deposition exploited in this programme involves the electropolymerisation of an aromatic diamine, *o*PD, onto a conductive surface. This permits essentially defect free, insulating films of PPD to be formed on the electrode of less than 100 nm thickness (Wang *et al.*, 1991). For this reason further discussions will be limited to polymer films of this type.

2.6.1 Electropolymerisation

An introduction and review of electropolymerisation has been given by Deshpande & Amalnerkar (1993), with relevant aspects summarised as follows. Electropolymerisation is carried out in a single- or dual-compartment cell by employing a three electrode configuration (as described in Section 2.3.1) in an electrochemical bath consisting of monomer and supporting electrolyte, both dissolved in an appropriate solvent. Preferential solvents for electropolymerisation have high specific dielectric constants, for example, acetronitrile, propylene carbonate, alcohol, and water. Electrolytes mainly include organic solvent-soluble and ion-dissociating organic or inorganic salts and acids.

Polymerisation is then initiated by applying a suitable driving power supply through the solution in the cell. This can be potentiostatically (constant potential), galvanostatically (constant current) or potentiodynamically (potential scanning) controlled. The initiation of polymerisation may be through oxidation or reduction of an active intermediate from one of the other components in the solution. The

polymer formed will either precipitate onto the electrode surface if it is insoluble or dissolve into the polymerisation medium if soluble (Sun & Sun, 1993). The reaction mechanism can be free radical, anionic, cationic or a combination. Finally, polymer films are deposited at the working electrode.

Electropolymerisation has many advantages compared with other deposition or polymerisation methods. By using different electropolymerising conditions, including monomer concentration, solvent conductivity, pH value, scanning potential range, and applied scanning cycle, different characteristics and functions of the films can be obtained (Imisides *et al.*, 1991). These differences have been found to include thickness, surface topography, pH response, electron transfer kinetics (Chiba *et al.*, 1987b; Martinusz *et al.*, 1994), protection against metal corrosion (Volkov *et al.*, 1980), permselectivity for a dissolved species (Ohnuki *et al.*, 1983), and electrochromic properties (Chiba *et al.*, 1987a).

In summary, electropolymerisation has a number of attractive features:

1. Polymerisation, doping and processing take place simultaneously, which is virtually impossible by other polymerisation methods.

2. A much wider choice of cations and anions as 'dopant' is available.

3. Polymer films can be easily produced on a metallic object of any desired shape, and a uniform doping of film can be accomplished.

4. Both free-standing and supported ultra-thin conducting films applicable in electronics devices can be directly obtained.

5. The thickness of the resulting films can be controlled by varying time at either constant potential or constant current, or varying the number of potential cycles if cyclic voltammetry is used.

6. With suitable control over experimental parameters, it is possible to produce homogenous and dense films.

7. Electrochemical polymerisation reactions (in most cases) can be carried out at room temperature.

2.6.2 Structure, properties and applications

The electrode coating phenomenon of phenylenediamines was first described by Prater in 1973. However, poly(*o*-phenylenediamine) was first prepared as a stable film on an electrode via anodic oxidative polymerisation of *o*-phenylenediamine in acidic solution by Yacynych & Mark in 1976. The electrical conductivity of the PPD film prepared in this way was reported the first time by Yano *et al.* in 1985. Since then a number of papers have appeared on the possible applications of PPD and, as a result, significant progress has been made in recent years in terms of synthetic techniques, characterisation of structure and properties, and the design of functional materials of the polymers.

PPD is an aromatic polyimide resulting from the anodic polymerisation of the aromatic diamine, *o*PD (Figure 2.18).

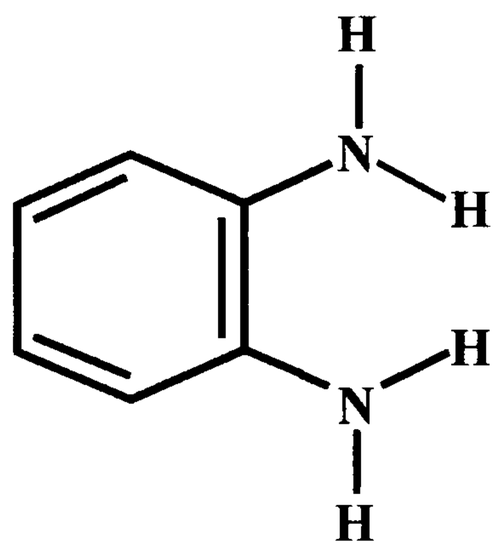

Figure 2.18 Structure of *o*-phenylenediamine.

Aromatic diamine polymers, such as PPD, are more attractive than other aromatic polymers such as polyaniline and polypyrrole, since they exhibit more novel multifunctionality, thought to be partially due to the one free amino group per repeative unit of the polymer. However, despite remarkable research efforts devoted to PPD characterisation (Losito *et al.*, 2001; Li *et al.*, 2002), only limited structural information is available.

Every oxidative polymerisation has its own unique characteristics and therefore produces polymers with specific and peculiar macromolecular and morphological structures. Different analytical techniques have been adopted to draw information on the PPD structure produced at different conditions, which can be summarised as follows. Works based on infrared, Raman and UV-VIS spectroscopies (Losito *et al.*, 2001), quartz crystal microbalance (Martinusz *et al.*, 1994; Dai *et al.*, 1998), radiometry (Martinusz *et al.*, 1995) and electrochemical techniques (Chiba *et al.*, 1987b; Jang *et al.*, 1995), have led to the hypothesis of a ladder polymer possessing a phenazine-like structure for PPD electrosynthesised at very acidic pH values (≤1), although the presence of 1,4-substituted benzenoid-quinoid units along its backbone, involving free NH_2 groups, has also been proposed, either as main repeating units (Yano, 1995), or as defects in the phenazine-like structure (Chiba *et al.*, 1987a). With PPD grown at higher pH (5-7), the extent of conjugation is progressively decreased as suggested by the increasing amount of free NH_2 groups at the surface (Losito *et al.*, 2001). The proposed structure for PPD at higher pH (5-7) is shown in Figure 2.19. This is the structure of PPD applicable to this work.

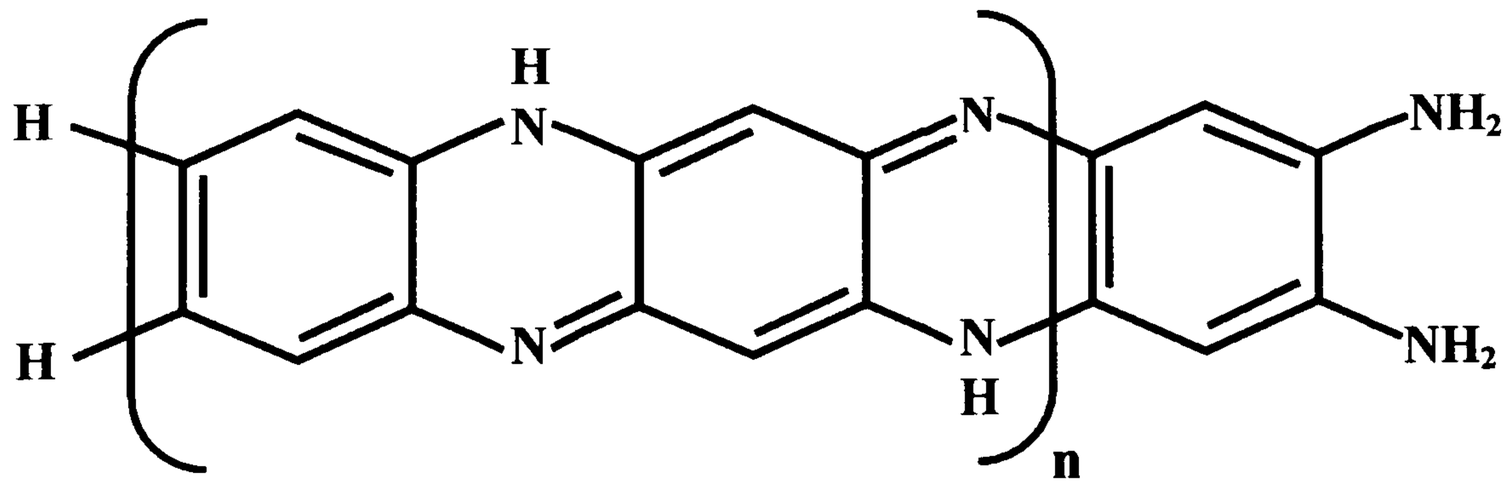

Figure 2.19 Proposed structure of poly(*o*-phenylenediamine) at higher pH (5-7) (Li *et al.*, 2002).

The different macromolecular structures of polymers of the same monomers should be attributed to the peculiar mechanisms of the oxidative polymerisation at different conditions. A general mechanism for *o*PD polymerisation is also still not known definitely, although many mechanisms have been hypothesised. These will be further explored in Chapter 6.

Electropolymerisation of *o*PD offers the advantage of producing a very thin (<100 nm) (Ohnuki *et al.*, 1983) and self-insulating film that can be coated on any conducting, three dimensional surface. Both Yacynych & Mark (1976) and Heineman *et al.* (1980) have shown the oxidation of *o*PD to be irreversible and, with successive cyclic voltammetric scans, forms an insulating polymer film completely covering the electrode surface. The formation of a self-insulating film prevents electropolymerisation on any part of the electrode that has already been coated, thus providing uniform, reproducible coverage of any surface, regardless of its geometry.

Among electrosynthesised polymers, PPD has received a great deal of attention over the past two decades and its possible applications include its use as electron transfer mediators for oxygen reduction (Ohnuki *et al.*, 1983), anticorrosion coatings (Volkov *et al.*, 1980; White *et al.*, 1982), and pH sensitive electrodes (Heineman *et al.*, 1980; Cheek *et al.*, 1983). However, to date, its main role is as an enzyme entrapping membrane (coupled with its peculiar permeability) (Myler *et al.*, 1997). This enables rejection of different species potentially acting as fouling agents or as interferents to a biosensor response. More recently, Malitesta *et al.* (1999) have explored a new possible application for PPD in the field of molecularly imprinted polymers (MIPS), using glucose as a molecular template during the electropolymerisation of *o*PD.

Poly(*o*-phenylenediamine) was investigated within this study for its electropolymerisable capability as an insulating film for use within a sonochemically fabricated microarray and specifically for its insulating properties to chlorine molecules.

2.7 SONOCHEMISTRY

Sound is transmitted through a medium by the induction of vibrational motion of the molecules through which it is travelling and constitutes a series of compression waves separated by rarefaction (stretching) waves in between. The pitch of the sound produced by this series of waves depends upon their frequency, i.e. the number of waves that pass a fixed point in unit time. Sound waves can be represented as a sine wave, as depicted in Figure 2.20, where P_A is the ambient pressure at a fixed point in time, P_W is the wave amplitude and λ is the wavelength.

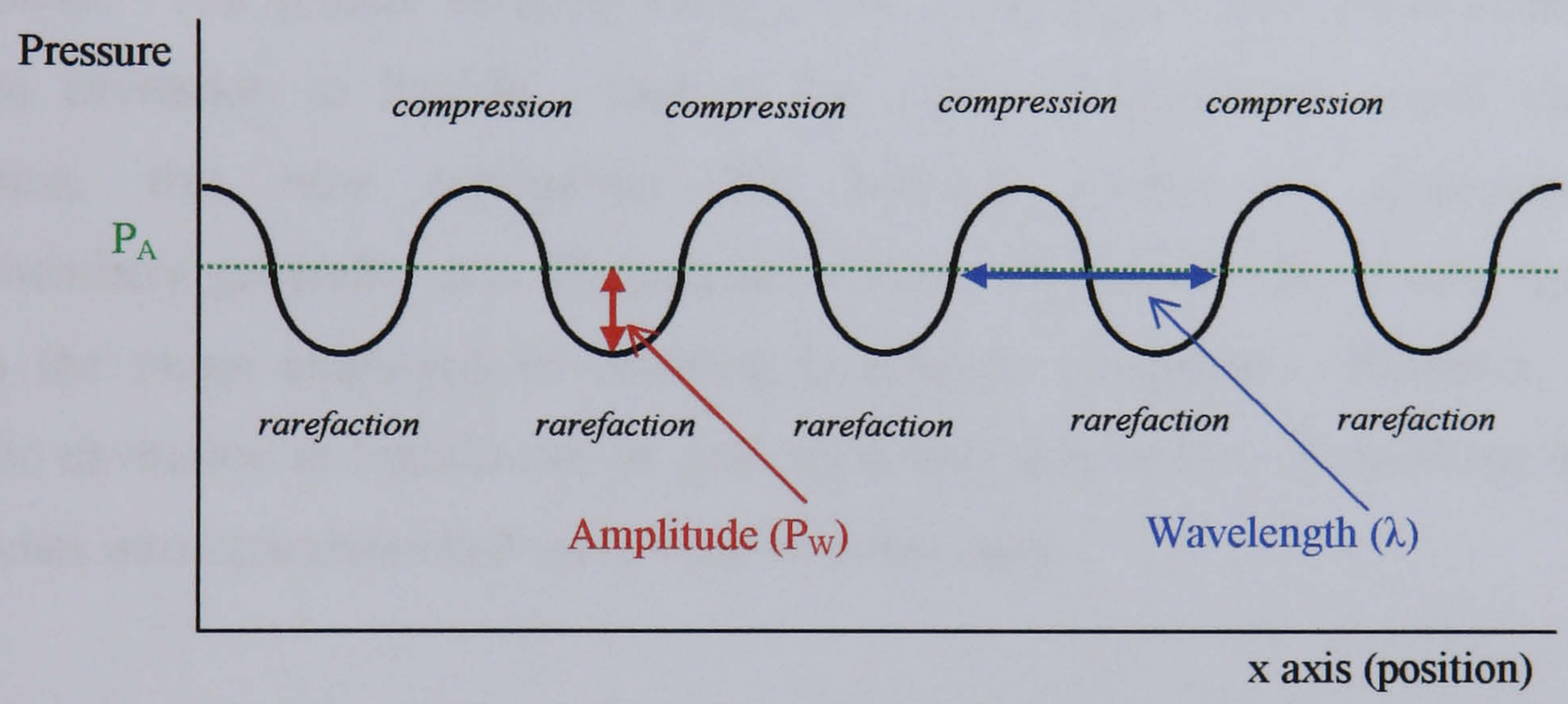

Figure 2.20 Representation of sound motion.

It should be noted here that different materials have different 'impedances' to the passage of sound which are determined by their elastic properties and cross-sectional areas. Efficient energy transfer between two materials is only possible when the impedances are balanced.

The threshold for frequencies of sound that are able to be heard by humans is normally around 18-20 kHz for adults. Sound beyond this limit is inaudible and defined as ultrasound. This broad classification of ultrasound (sound between 20 kHz and 100 MHz) can be subdivided as being used within two distinct applications; power (destructive) and diagnostic imaging.

Diagnostic ultrasound is of high frequency (from around 5 MHz and above) and does not produce cavitation (the formation, growth and implosive collapse of bubbles). Hence, these sound waves have no permanent effect on the physical or chemical character of the material being examined. For this reason, diagnostic ultrasound is used in medical imaging (Williams, 1983), but other applications include echo-ranging, sound velocity measurement and sound attenuation measurement (Povey & Mason, 1998).

However, if a sound wave with a lower frequency (between 20 kHz and approximately 5 MHz) and a higher power is applied to a material, it is possible to induce physical and chemical changes in the material - this is termed *power ultrasound*. The greater acoustic energy that is generated with these conditions induces cavitation in liquids. Due to the chemical effects of sound induced cavitation, this new technology has become known as *sonochemistry*. Sonochemistry generally uses frequencies between 20 and 40 kHz simply because this is the range employed in common laboratory equipment. However, since acoustic cavitation in liquids can be generated well above these frequencies, recent researches into sonochemistry use a much broader range.

Power ultrasound is used in industry for cutting, therapeutic medicine and processing, but two applications in particular, namely welding and cleaning, have provided much of the equipment now commonly commercially available (Frederick, 1965; Abramov, 1998). Sonochemistry itself incorporates many specific uses of ultrasound. These include environmental protection (Yim *et al.*, 2002; Théron *et al.*, 2001); materials science (Xia *et al.*, 2001; Ding *et al.*, 2002) including new catalytic materials, improved extraction, crystallisation, and new methods in polymer technology; electrochemistry (Walton & Phull, 1996; Klima *et al.*, 1994) - providing improvements in plating electrosynthesis and electroanalysis; and biotechnology such as the modification of enzyme and whole-cell activities (Sasaki *et al.*, 2001).

2.7.1 Acoustic cavitation

The chemical effects of ultrasound do not derive from a direct coupling of the acoustic field with chemical species on a molecular level. Instead, the chemical effects of ultrasound derive principally from acoustic cavitation, involving the formation, growth and implosive collapse of bubbles in liquids irradiated with high-intensity ultrasound. A schematic representation of the development and collapse of these bubbles is given in Figure 2.21:

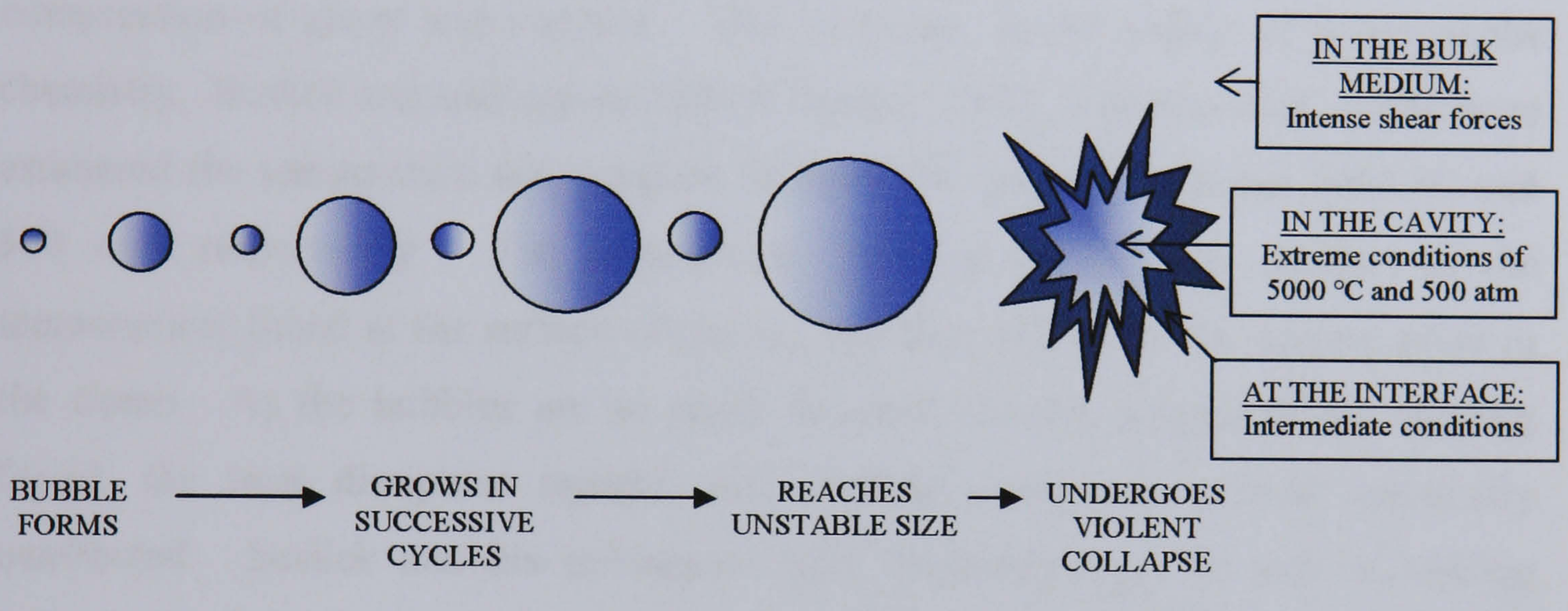

Figure 2.21 Development and collapse of cavitation bubbles.

As we have already seen in Figure 2.20, ultrasound is propagated via a series of compression and rarefaction waves – the molecules of the liquid carrying the ultrasound wave are squashed together and then pulled apart as the wave passes. When the power is sufficiently high, the rarefaction or 'pulling' wave can overcome the attraction forces between the molecules of a liquid, causing cavitation bubbles to form. In other words, nucleation of bubbles occurs at weak points in the liquid (such as at the site of gas filled crevices in suspended particulate matter) or indeed from transient microbubbles from prior cavitation events. At some point, the cavity will reach a resonant size where it can efficiently absorb energy from the sound field (the size depends on the frequency of the ultrasound). Such a cavity, if it is in phase with the sound field, can then grow rapidly in the course of a single expansion cycle.

Once the cavity has overgrown, it can no longer efficiently absorb energy from the sound field and can no longer sustain itself. The surrounding liquid rushes in and the cavity explodes.

The violent collapse of these bubbles generates large shear forces, which can be used for mixing and particle dispersion. In the collapsing bubble itself, high energies and pressures are generated. Many theories exist to explain the energy release involved in cavitation, but the most understandable in a qualitative sense is the 'hot-spot' approach (Suslick *et al.*, 1986) which explains that heat is generated from the rapid compression of gases and vapours. This 'hot-spot' is the source of homogenous chemistry. Suslick and colleagues (Flint & Suslick, 1991; Didenko *et al.*, 1999) have estimated the temperature and pressure of these hot spots to be about 5000 °C and 500 atm respectively. For perspective, these conditions are similar to the temperatures found at the surface of the sun and the pressure at the deepest point in the ocean. As the bubbles are so small compared to the volume of surrounding liquid, the heat dissipates rapidly, and ambient conditions remain essentially unaffected. Suslick and his colleagues have also estimated the rate of cooling following the collapse of a bubble to be of the order of 10^9 Ks^{-1} (Doktycz & Suslick, 1990). This combination of high temperatures, high pressures, and rapid cooling creates conditions unattainable in other fields of chemistry.

The dynamics of cavity growth and collapse vary depending on the local environment. Cavity collapse in a homogenous liquid, as we have previously discussed, is very different from cavitation near a solid-liquid interface. When a bubble collapses near a surface, it implodes asymmetrically because the surface interferes with the in-rushing liquid from the nearest side. As a result, the main in-rush of liquid comes from the side of the bubble opposite the surface. This generates a liquid jet in the direction of the surface, which moves through the bubble at a speed of approximately 100 ms^{-1} (Leighton, 1994). This is shown in Figure 2.22. Such impacts leave behind characteristic microscopic pitting in the surface of the material.

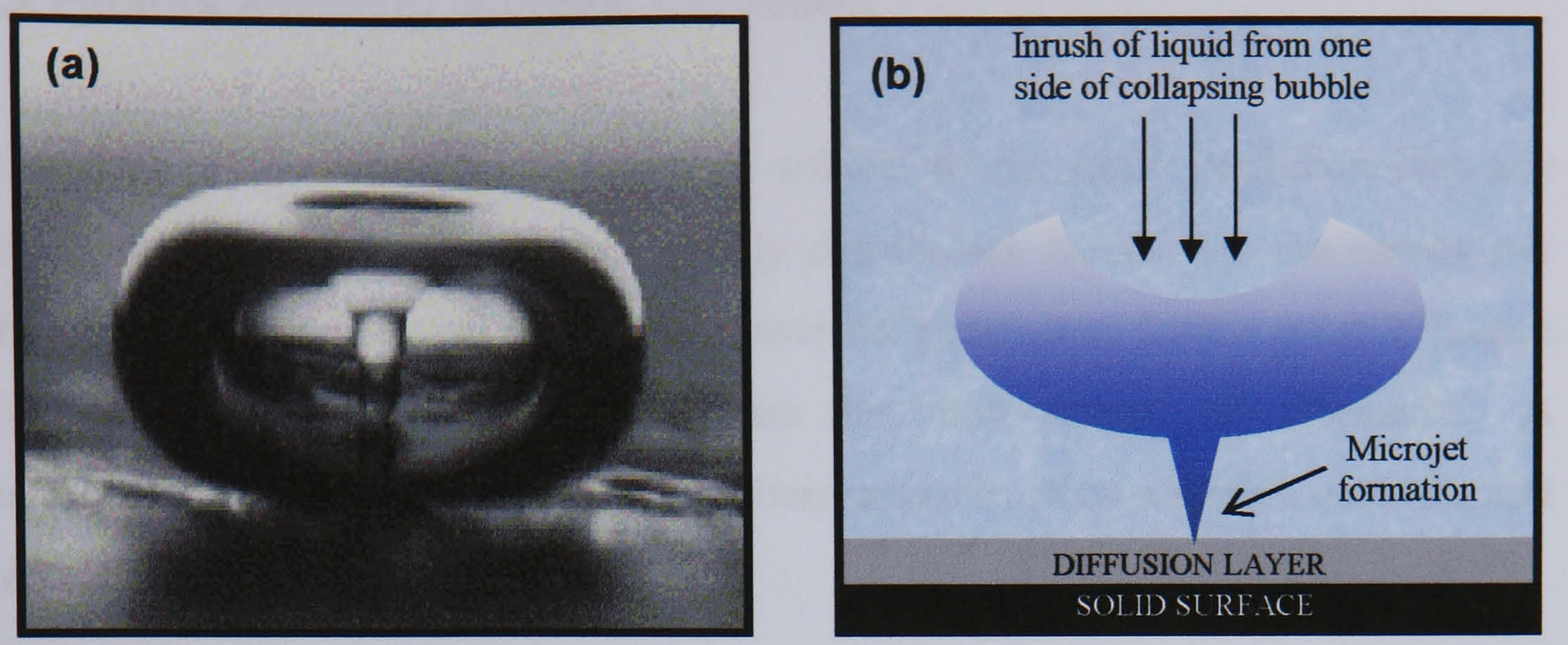

Figure 2.22 (a) A flash microphotograph (Crum, 1982) and (b) a schematic representation, of a microjet of liquid streaming through a bubble upon implosion due to cavitation near a solid surface.

This cavitation is known as *transient (inertial)* since transient cavities generally exist for no more than a few acoustic cycles during which time they expand to at least double their initial radius before collapsing violently within a few microseconds. It is thought that another type of cavitation process exists at surfaces, namely *stable (non-inertial)* (Leighton, 1998). Stable cavities are those are those which oscillate, often non-linearly, about some equilibrium size with a lifetime of tens of cycles. Although it is considered that most of the effects attributed to cavitation are due to the transient type, the oscillation of 'stable' bubbles may make a contribution to the overall sonochemical effect. Shock waves created by cavity collapse in liquid-solid slurries produce high-velocity interparticle collisions, the impact of which can also create surface pitting (Doktycz & Suslick, 1990).

2.7.2 Factors affecting acoustic cavitation

The control of sonochemical reactions is subject to the same limitation that any thermal process has: the Boltzmann energy distribution means that the energy per individual molecule will vary. Therefore, external parameters have a great influence on cavitation and therefore it is important that these factors are discussed. A comprehensive review of these factors has been given by Mason (1999) with relevant aspects summarised below.

Firstly, the *intensity* of sonication must be considered. Intensity, in this context, is directly proportional to the square of the amplitude of vibration of the ultrasonic source and is closely related to the *power* and the *frequency* of the system. In general, an increase in intensity will provide an increase in the sonochemical effects, but there are limits to the ultrasonic energy input to the system. A minimum intensity for sonication is required to reach the cavitation threshold and this minimum depends on the frequency applied.

Essentially, the frequency alters the critical size of the cavitational bubbles. At higher frequencies (into the MHz region), it becomes more and more difficult to produce cavitation in liquids. This is because the rarefaction (and compression) cycle is extremely short and hence occurs faster than the time required for the molecules to be pulled apart (allowing for the bubbles to collapse). In other words, more power is required at a higher frequency if the same cavitational effects are to be maintained. However, transducers which operate at high frequencies are generally not mechanically capable of generating very high ultrasonic power. In addition, when a large amount of ultrasonic power enters a system, a great number of cavitation bubbles are generated in the solution. Many of these will coalesce, forming larger, longer lived bubbles which will act as a barrier to the transfer of acoustic energy through the liquid and consequently dampen the effective ultrasonic energy (Henglein & Gutierre, 1990). This is the main reason why the frequencies generally chosen for sonochemistry are between 20 and 40 kHz with the optimum power then being determined depending on this frequency. Furthermore, the

intensity of sound is attenuated (i.e. it decreases) as it progresses through a medium. The extent of attenuation is inversely related to the frequency. In order to achieve identical intensities in a medium at a given distance from an ultrasonic source using different frequencies, it will be necessary to employ a higher initial power for the source with the higher sound frequency.

Secondly, the *temperature* and *external (applied) pressure* may effect cavitation. Any increase in temperature will raise the vapour pressure of a medium, but decrease the viscosity and surface tension (De Souza-Barboza *et al.*, 1988). This leads to easier but less violent collapse of bubbles and hence a lessened cavitational effect. However, at even higher temperatures (near to the solvent boiling point), large numbers of bubbles will be generated concurrently and again act as a barrier to the transfer of acoustic energy through the medium. Raising the external pressure will give rise to a larger intensity of cavitational collapse and consequently an enhanced sonochemical effect (Cum *et al.*, 1988), although a cavitational threshold (which depends on the system) may be reached where cavitational bubbles are no longer produced .

Thirdly, the *presence and nature of dissolved gases* must be considered. At the beginning of the sonication of a liquid, any gas that is entrapped or dissolved in the liquid will act as nuclei for cavitation and then be removed, making the initiation of further cavitation increasingly difficult. Therefore, the liquid should be ultrasonically degassed before use to produce more uniform cavitational profile.

Finally, the *solvent viscosity, surface tension and vapour pressure* can all influence cavitation. Cavities (microbubbles) are more readily formed using solvents with high vapour pressures, low viscosity and low surface tension. This can be attributed to cavitation producing shear forces in the bulk liquid. Since viscosity is a measure of resistance to shear it is more difficult to produce cavitation in a viscous liquid. The addition of surfactant to a liquid may facilitate cavitation as this would reduce the surface tension of the solvent and thus reduce the threshold for cavitation. It is difficult to induce cavitation in a solvent of low vapour pressure because during the

expansion phase of cavitation bubble generation, vapour from the surrounding liquid will permeate the interface. This produces a small pressure within the bubble, reducing the pressure differential between cavity and bulk. Solvents with high vapour pressures easily generate vapour filled bubbles, but their collapse is cushioned and therefore less energetic.

2.7.3 Ultrasound equipment for sonochemistry applications

The most commonly used equipment for sonochemistry purposes are the ultrasonic bath and the ultrasonic probe. The source of power at both of these systems is generally the piezoelectric transducer, based on ceramics containing piezoelectric materials, such as zirconate titanate. They work on the principle that if charge is applied to one face of a crystal and an equal but opposite charge is applied to the other face, then the whole section of crystal will either expand or contract depending on the polarity of the applied charges, resulting in fluctuations in dimensions (Curie & Curie, 1880). This effect can be harnessed to transmit ultrasonic vibrations from the crystal section through whatever medium it is in contact with.

The most common form of piezoelectric is a disc with a central hole. In a power transducer, it is normal practice to clamp two of these piezoelectric discs between metal blocks in a 'sandwich' (Figure 2.23) which serves to protect the delicate crystalline material and to prevent it from overheating by acting as a heat sink.

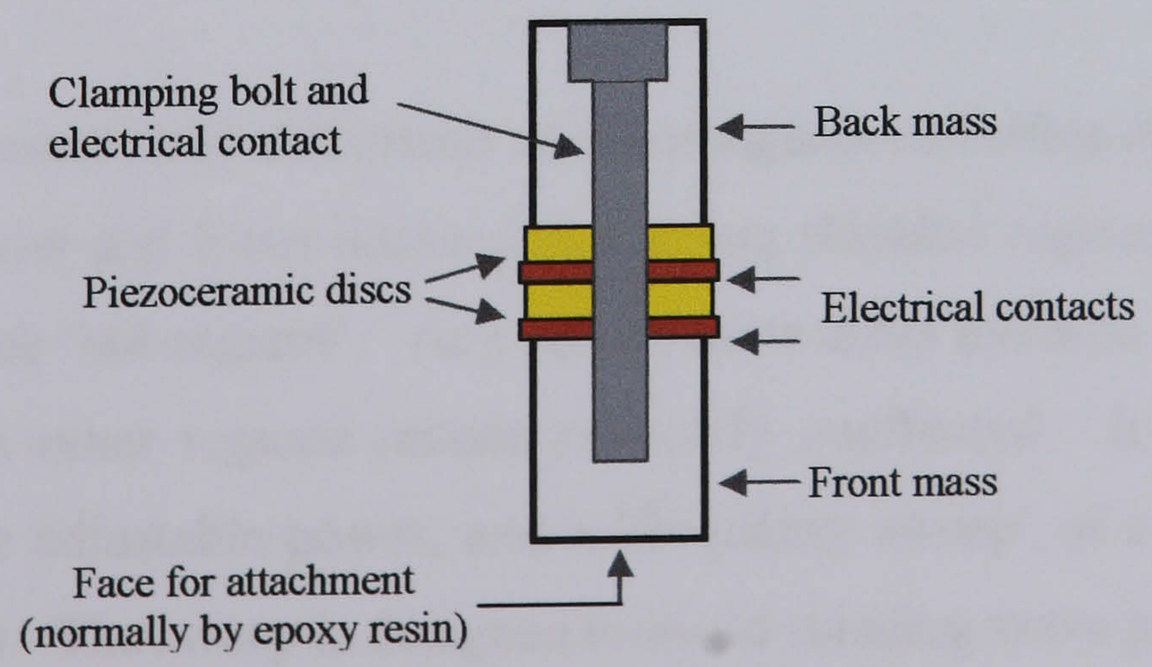

Figure 2.23 Diagram of a piezoelectric sandwich transducer.

The unit is generally one half-wavelength long (although multiples of this can be used) and the peak to peak amplitudes generated by such systems are normally of the order of 10-20 microns. Such transducers are highly efficient (>95%) and, depending on dimensions, can be used over the whole range of ultrasonic frequencies from 20 kHz to many MHz.

The ultrasonic bath is readily accessible, relatively inexpensive and usable on a large scale. For these reasons, an ultrasonic bath is the preferred mode of sonication in this thesis and therefore only ultrasonic baths will be described. An ultrasonic tank is usually made from stainless steel and has either one or several transducers attached underneath the base. The frequency and power depends upon the type and number of transducers used in its construction. Most commercial baths operate at 40 kHz and systems that operate at different frequencies usually require individual commission and purchase. It should be noted here that ultrasonic baths operate at frequencies and powers dependant upon the transducers employed and with geometries that are specific to the particular manufacturer (Reisse *et al.*, 1996). This makes it difficult to make direct comparisons between studies performed in different makes (or models) of ultrasonic baths. The energy input should therefore be assessed for each system because the power per unit volume of the bath will depend on the size of the bath, the reaction vessel type and the thickness of its walls. Reflections take place on the various interfaces between media with different acoustic impedances (Leighton, 1994) and transient cavitation does not occur in all parts of the vessel. Therefore, the sub-domains where sonochemical reactions take place are not necessarily the same (Petrier *et al.*, 1994).

A non-uniform sound field will create an inhomogeneous bubble distribution, which can scatter, channel and focus ultrasound, causing shielded regions and/or localised regions to produce 'hot-regions'. As a result, some areas undergo intense ultrasonic activity, whereas other regions remain relatively unaffected. It may be possible however, to have adjustable power, and a 'frequency sweep' of a few kHz about a central frequency. The sweep is designed to avoid standing wave patterns in the tank and thus disperse bubble aggregations, since the nodes in the waves alternate in

height from the base of the tank. Some tanks, particularly the larger sizes, also have some form of thermostatted temperature control since ultrasonic baths warm up under the influence of transducers and this can, if unchecked, create certain problems in terms of both effectiveness and reproducibility. A schematic representation of a standard ultrasonic bath is shown in Figure 2.24.

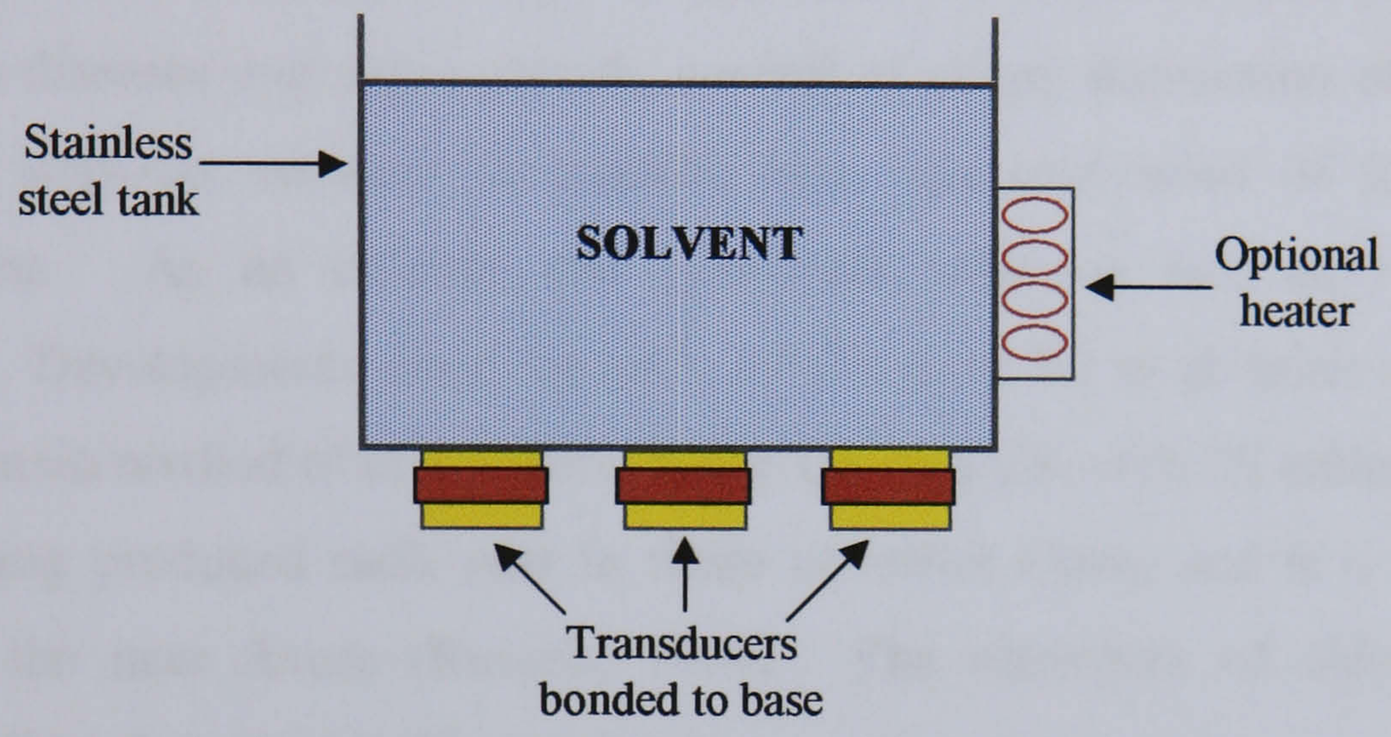

Figure 2.24 Typical ultrasonic bath.

Normal usage of a bath involves the immersion of standard glass reaction vessels into the bath (Mason *et al.*, 1989). However, if non-corrosive and non-volatile reagents are used, the whole bath can be used as a batch reactor. The most intense power will be found directly above the transducers. However, the ultrasound power in the bath liquid will not be uniform with distance from the base. This is because ultrasound passes through water in the form of a wave, and the wave will have positions of maximum amplitude at multiples of the half-wavelength of sound, $\lambda/2$, in the medium. These distances can be calculated using Equation 2.41.

$$v = f\lambda \tag{2.41}$$

where v is the velocity of sound in the medium (1500 ms^{-1} in water) and f is the transducer operating frequency.

2.8 THE DETERMINATION OF AQUEOUS CHLORINE

Chlorine is a powerful oxidising agent that is used widely in the treatment of industrial, recreational, and drinking water. Such processes are heavily dependant on the use of chlorine because of its potency and effectiveness as an oxidant and as a germicide. Other beneficial applications include taste and odour control, prevention of water-borne diseases and algae growth, control of slime, destruction of cyanide and hydrogen sulphide, removal of metallic ions, and prevention of fouling of cooling systems. As an oxidant and germicide, chlorine has no real rival (White, 1978). Developments since the early 1900's have led to chlorine chemistry becoming the main method of disinfection in the UK and US, with 25 million tonnes of chlorine being produced each year in these countries alone, and it is likely to remain so in the near future (Russell, 1994). The chemistry of chlorine and chlorination will be described in Section 2.8.2.

However, in addition to its benefits, chlorination does have some adverse effects. The presence of excessive amounts of chlorine is detrimental to human health and aquatic life. Increasing attention is now being focused on this issue because chlorine has been implicated in the production of potentially carcinogenic chloro-organic compounds such as chloroform (Bellar *et al.*, 1974; Jolley, 1975; Rook, 1976). Taste and odour characteristics of phenols and other organic compounds present in a water supply may be intensified. Furthermore, chlorine is expensive and its overuse increases operational costs.

It follows that to fulfil the primary purpose of chlorination and to minimise any adverse effects, it is essential that proper testing procedures be used with a foreknowledge of the limitations of the analytical determination. Such limitations of contemporary chlorine analysers will be discussed in Section 2.8.4. Due to these limitations and the dissatisfaction of consumers with the analysers in general, new, simplified and reliable procedures are required for the monitoring of chlorine by both users and regulatory agencies in order to assure compliance with regulations. It is

the development of a new sensor for the detection of chlorine in aqueous solutions that is the subject of this work and the theoretical response of such a procedure is discussed in Section 2.8.3.

2.8.1 Applications of chlorine analysers

The scope for chlorine analysis is vast - the Water Research Council estimates that over 20 million chlorine tests are being undertaken across the globe each day (Hall & Hyde, 1992). Chlorine detection is required in a wide variety of industries and its application includes potable and waste water, industrial heating and cooling systems, reverse osmosis filtration systems, environmental testing labs, power plants, food process monitoring, boiler systems, healthcare providers/hospitals, corrosion protection, pharmaceutical processing, desalination, the paper and textile industries, the bottled water industry, environmental and wildlife action groups, merchant and military navies and swimming pools.

The most important use of chlorine, however, is in the disinfection of potable water (White, 1992). The requirements for improved water treatment throughout the world is being driven by demanding drinking water quality standards, based on both health and aesthetic considerations, the foundation for which are the World Health Organisation (WHO) guidelines (1993), that state that for health purposes, chlorine must not exceed 5 mg/l total available chlorine. However, health related problems may be seen with chlorine levels of between 0.6 and 1 mg/l free available chlorine. The monitoring range will therefore normally be covered by a 0-2 mg/l capability. This is accomplished by close scrutiny by Inspectorates (UK Drinking Water Inspectorate, 2000) to ensure that these standards are met. In Europe, the defining moment in the development of prescriptive water quality standards was the adoption of the EC Drinking Water Directive (European Economic Community, 1998). This set the minimum water quality standards to be adopted by all European Union member countries – encompassing a population of over 450 million. Similar

standards have been set in the United States with the introduction of the National Primary Drinking Water Regulations (US Environmental Protection Agency, 2000).

As a result of these regulations, water companies are required to undertake microbiological testing of water to demonstrate effective disinfection. Portable chlorine test systems may therefore be used for 'spot check' measurements of chlorine levels throughout the distribution and/or treatment processes, or for ensuring adequate chlorine residual after completion of work on water mains. Additionally, they may be used for the calibration of online instruments.

Portable chlorine analysers are also used widely in environmental applications, especially since it is very important in these cases to perform analyses 'on-site' (i.e. field analyses). For example, wastewater effluents are often chlorinated to kill pathogens and then dechlorinated before discharge. This common practice has resulted in several comprehensive studies which quantify the toxicity of chlorinated effluents to aquatic life (Brungs, 1973). It has been found that some aquatic species, such as salmon and trout, are very susceptible to poisoning from very low concentrations of chlorine. In the United States, the amount of total residual chlorine in the final effluent is regulated by a 'National Pollutant Discharge Elimination System' (NPDES) permit. Typical limits for total residual chlorine in the final effluent range from 0.002 to 0.05 mg/l. The US Environmental Protection Agency (US Environmental Protection Agency, 1976) also requires such limitations; in this case, the final effluent must be between 0.0075 and 0.013 mg/l. Similar regulations apply in Canada. The Canadian water quality guidelines for aquatic life (Canadian Council of Ministers of the Environment, 1999) state that the maximum concentration of reactive chlorine species (hypochlorous acid and monochloramine) in marine and freshwater should be 0.005 mg/l. Europe has also followed suit with EU law mandating the measurement and limitation in surface water bearing salmon and trout to be 0.005 mg/l (European Economic Community, 1978).

There are several laboratory analytical techniques for the determination of chlorine and chlorinated species. However, the chlorine content of water and in particularly

effluent samples decreases after collection. It is important therefore, that residual chlorine tests should be carried out with a minimum of delay, preferably at the time of sampling. For such on-site testing, portable test kits are useful and there are several of these kits already on the market (see Section 2.8.4). However, most portable analysers cannot accurately measure down to the low levels required by the environment regulators and now that these regulations are increasingly being enforced, the market for new, superior analysers is therefore wide open.

There is also a great dissatisfaction amongst users with the current methods for potable water analysis. One report compiled by the Welsh Environment Agency highlighted this (Boswell, 2001). A quarter of industrial works across Wales were seen to regularly report chlorine dose results which exceeded their consents. Duplicate results obtained by the water treatment operatives were lower than the results reported by the Environment Agency samplers. Similar complaints were received from Severn Trent PLC. The report concluded that analyses may differ from each other due to possible poor use of the test kits or due to potential interferences by competing chemical species. In addition, the test kit detection levels are in the same order of magnitude as the consent i.e. 0.02 mg/l, resulting in erroneous results. All of these factors suggest that there is a great need for a technique that would permit the simplified, rapid, accurate and qualitative analysis of chlorine for both free and total solutions over a wide detection range. It is therefore not surprising that the Environment Agency are sponsoring Microarray Ltd. to develop the chlorine sensor being researched in this work.

2.8.2 Overview of chlorine chemistry

Comprehensive information explaining chlorine chemistry in water treatment is available in several references describing chlorination and chlorination practices (White, 1992; Palin, 1974). An overview emphasising the general chemistry of chlorine disinfection will be presented here.

Chlorination may involve the use of gaseous chlorine (Cl_2), which is dissolved in carrier (motive) water before being added to the water to be treated. When added to water, gaseous chlorine reacts rapidly to form a mixture of hypochlorous acid (HOCl) together with hydrogen and chloride ions (effectively dissolved hydrochloric acid):

$$Cl_2 + H_2O \Leftrightarrow H^+ + Cl^- + HOCl \qquad (2.42)$$

Alternatively, chlorination may involve the use of a solution of hypochlorite, normally sodium hypochlorite (NaOCl). When added to water, sodium hypochlorite also reacts to form hypochlorous acid:

$$NaOCl + H_2O \rightarrow NaOH + HOCl \qquad (2.43)$$

In both cases, the hypochlorous acid partially dissociates to produce the hypochlorite ion (OCl^-) according to Equation 2.44 (since hypochlorous acid is weak, $K = 2.8 \times 10^{-8}$):

$$HOCl \Leftrightarrow H^+ + OCl^- \qquad (2.44)$$

Hence, at equilibrium, molecular chlorine (Cl_2), hypochlorous acid (HOCl) and hypochlorite ions (OCl^-) may exist together. Chlorine in any of these forms is known as ***'free available residual chlorine'***. The equilibrium points in these reactions are pH dependant and are shown in Figure 2.25. Equation 2.42 applies at a pH value of less than approximately 3, with the proportion of gaseous chlorine dropping to zero at a pH of 3. Equation 2.44 covers a pH range of 3-10. Hypochlorous acid dissociates poorly at levels of pH approximately between pH 4-7. Thus,

hypochlorous acid predominates in this region. This is the most germicidal of the free chlorine states due to the ability of the neutral HOCl molecule to diffuse into a cell more rapidly than the OCl^- ion. Hypochlorous acid is fully dissociated to the hypochlorite ion at a pH of around 9.

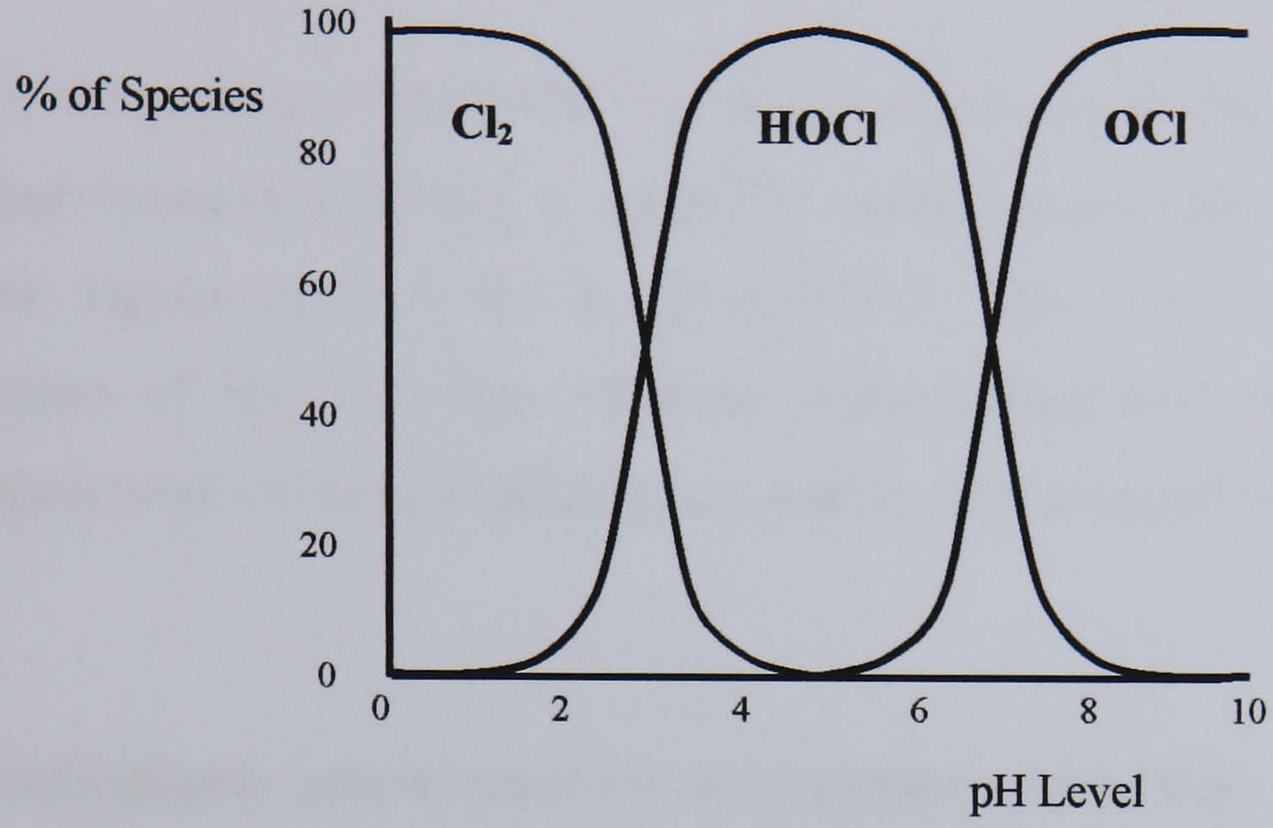

Figure 2.25 The effect of pH on the form of free chlorine in water.

Aqueous free chlorine species are relatively strong oxidising agents and behave as electrophiles, which mean that they readily attack electron rich sites, such as amines. When free chlorine is added to water containing natural or added ammonia, the hypochlorous acid reacts with the ammonium ion to successively replace the hydrogen atoms with chlorine, forming various chloramines depending on several factors including the pH, temperature and the initial Cl_2:NH_3 ratio:

$$NH_3 + HOCl \rightarrow NH_2Cl + H_2O \qquad (2.45)$$

$$NH_2Cl + HOCl \rightarrow NHCl_2 + H_2O \qquad (2.46)$$

$$NHCl_2 + HOCl \rightarrow NCl_3 + H_2O \qquad (2.47)$$

These reactions lead to the successive formation of monochloramine (NH_2Cl), dichloramine ($NHCl_2$) and nitrogen trichloride (NCl_3), as shown in Equations 2.45 to

2.47 respectively. Chlorine is any of these forms is known as ***'combined residual chlorine'***. In general, low pH levels and high Cl_2:NH_3 ratios favour dichloramine formation, dichloramine being the more powerful bactericide, although generally combined chlorine forms are much weaker disinfectants than free chlorine (Binnie *et al.*, 2002).

Historically, the principal analytical problem has been to distinguish between free and combined forms of chlorine, as a positive interference occurs if a portion of the free chlorine measurement is due to chloramines. This would in turn lead to an over-estimation of the true free chlorine concentration and could result in an incorrect assessment of the microbiological quality of the treated water.

2.8.3 Potentiostatic amperometric response to chlorine

We saw in Section 2.8.2 that combined chlorine (i.e. monochloramine, dichloramine and nitrogen trichloride) has some disinfectant capability, but is not as effective as free chlorine (molecular chlorine, hypochlorous acid or hypochlorite ion). Therefore it is usual to distinguish between the two forms (free and combined). This can be done using a potentiostatic amperometric cell.

In a potentiostatic amperometric cell, a fixed potential is applied across the cell (in a three electrode set-up). The current flowing is then proportional to the concentration of chlorine present in the sample (See Section 2.3). Only free available residual chlorine and total residual chlorine may be measured electrochemically. ***'Total available residual chlorine'*** is the sum of the free available residual chlorine and the combined residual chlorine present in the sample. The combined residual chlorine can then be calculated by subtracting the free available residual chlorine from the total available residual chlorine:

$$Total\ chlorine - Free\ chlorine = Combined\ chlorine \qquad (2.48)$$

For free chlorine, the processes that occur at the electrode surfaces are complex, but overall can be represented by the following equations:

At the working electrode: $$HOCl + 2e^- \rightarrow Cl^- + OH^- \quad (2.49)$$

At the counter electrode: $$2H_2O \rightarrow O_2 + 4H^+ + 4e^- \quad (2.50)$$

The small amount of oxygen liberated at the counter electrode is carried away by the sample as dissolved oxygen.

The total available residual chlorine can be measured electrochemically by the addition of acidified potassium iodide (KI). The electrochemical generation of iodine (I_2), is exactly the same as the chemical generation of iodine from the potassium iodide by its stoichiometric reaction with total residual chlorine present in the sample under investigation. Equations 2.51 and 2.52 show the reaction of molecular chlorine (free chlorine) and monochloramine (combined chlorine) respectively, present in the sample solution with iodide.

$$2I^- + Cl_2 \rightarrow I_2 + 2Cl^- \quad (2.51)$$

$$2H^+ + NH_2Cl + 2I^- \rightarrow NH_4^+Cl^- + I_2 \quad (2.52)$$

The generated iodine is then reduced at the working electrode to iodide as shown in Equation 2.53:

At the working electrode: $$I_2 + 2e^- \rightarrow 2I^- \quad (2.53)$$

Hence, both the free and combined chlorine oxidise the iodide ion to liberate free iodine which produces a current through the electrodes in the same way as free available residual chlorine. Therefore, the current produced in the cell is directly proportional to the amount of iodine generated, which in turn corresponds to the

concentration of total residual chlorine. The reaction at the counter electrode is depicted in Equation 2.50.

It is also important to control the pH of the solutions in order to measure chlorine in its correct state in terms of both disinfection and measurement. For example, the form of free chlorine preferred for disinfection is hypochlorous acid as it is a more effective disinfectant than the hypochlorite ion. Therefore, it would be preferable to the consumer if the chlorine measurement instrument were to measure free chlorine in this form, so that a true value of the disinfecting capacity of the sample is attained. From Figure 2.25, one would conclude that the sample should be buffered to a pH of approximately 5 because hypochlorous acid is seen to predominate between about pH 3 and pH 7. This would result in the chlorine being induced into the correct form to allow for electrochemical measurement (i.e. reduction). However, it has also been demonstrated that the response of an amperometric cell to combined chlorine is increased at low pH values (Figure 2.26).

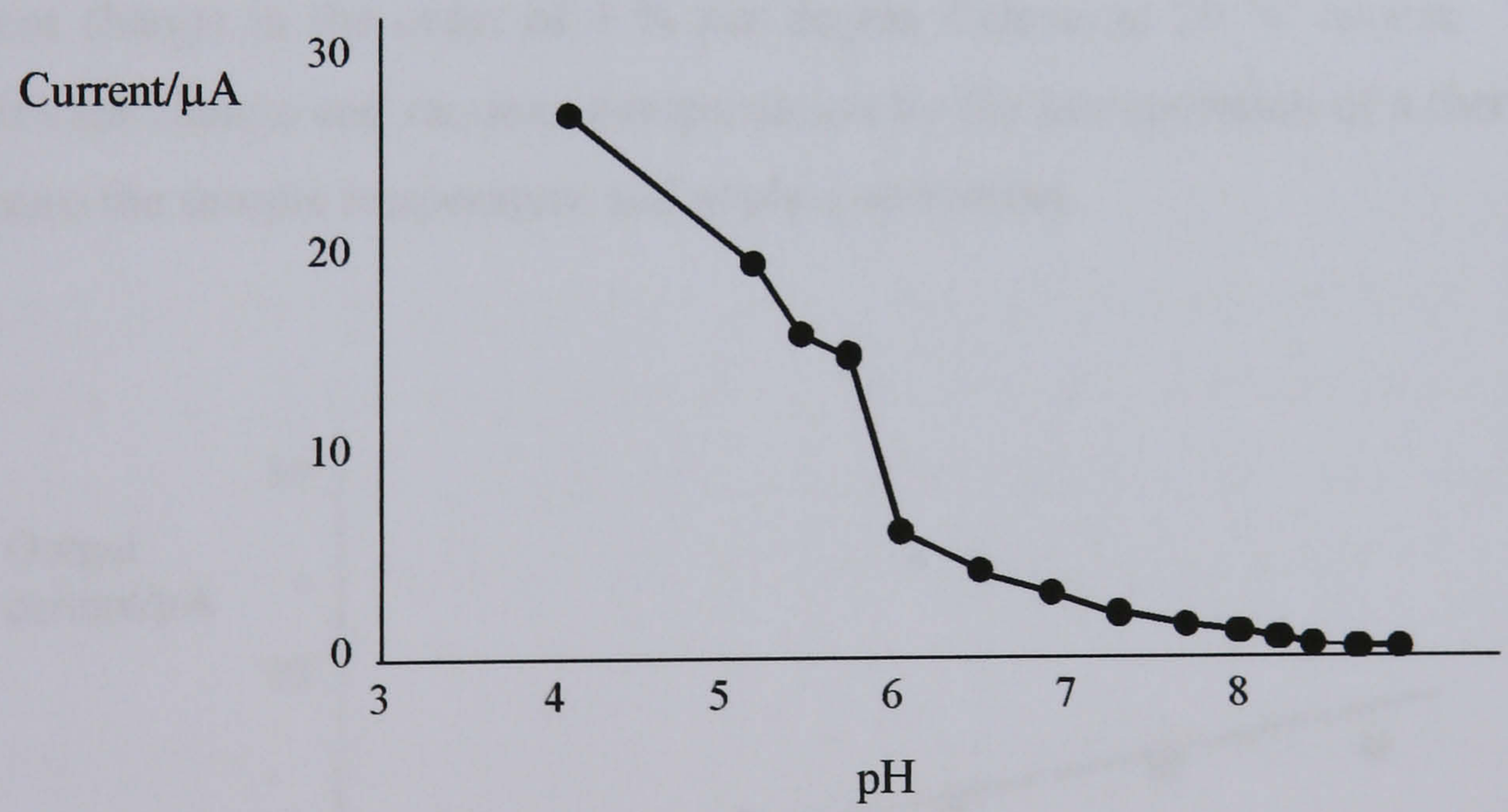

Figure 2.26 Response of a potentiostatic amperometric cell to combined chlorine with varying pH (Moorow & Roop, 1975).

At pH 5 the cell has a high sensitivity to combined chlorine. When substantial combined residuals may be present, the measurement of the free available chlorine component would be unreliable. Therefore, for the measurement of free chlorine, the

solution should be buffered to pH 7, providing a balance between no interference from combined chlorine with the measurement of free chlorine as hypochlorous acid. The measurement of free chlorine in preference to combined chlorine can also be improved by the correct choice of working electrode potential (Moorow & Roop, 1975). Concurrently, as total chlorine measurement should occur at low pH values and direct amperometric measurement has a peak sensitivity to chloramines at pH 4, determinations for total chlorine should be undertaken at this pH (i.e. pH 4). It should also be noted here that good pH stability in amperometric measurements is essential as a pH change of 0.2-0.25 pH units gives approximately a 10% change in reading (Russell, 1994).

It is also important to consider the variation in a potentiostatic amperometric cell with temperature (Russell, 1994). This can be seen in Figure 2.27. Note that the graph responds to a galvanic amperometric cell, which has a similar response characteristic to temperature as a potentiostatic amperometric cell, although the resultant current will be much higher in the galvanic case. It can be seen that a current change in the order of 3 % per degree Celsius at 20 °C occurs. This is a significant change and requires compensation by the incorporation of a thermistor to measure the sample temperature and apply a correction.

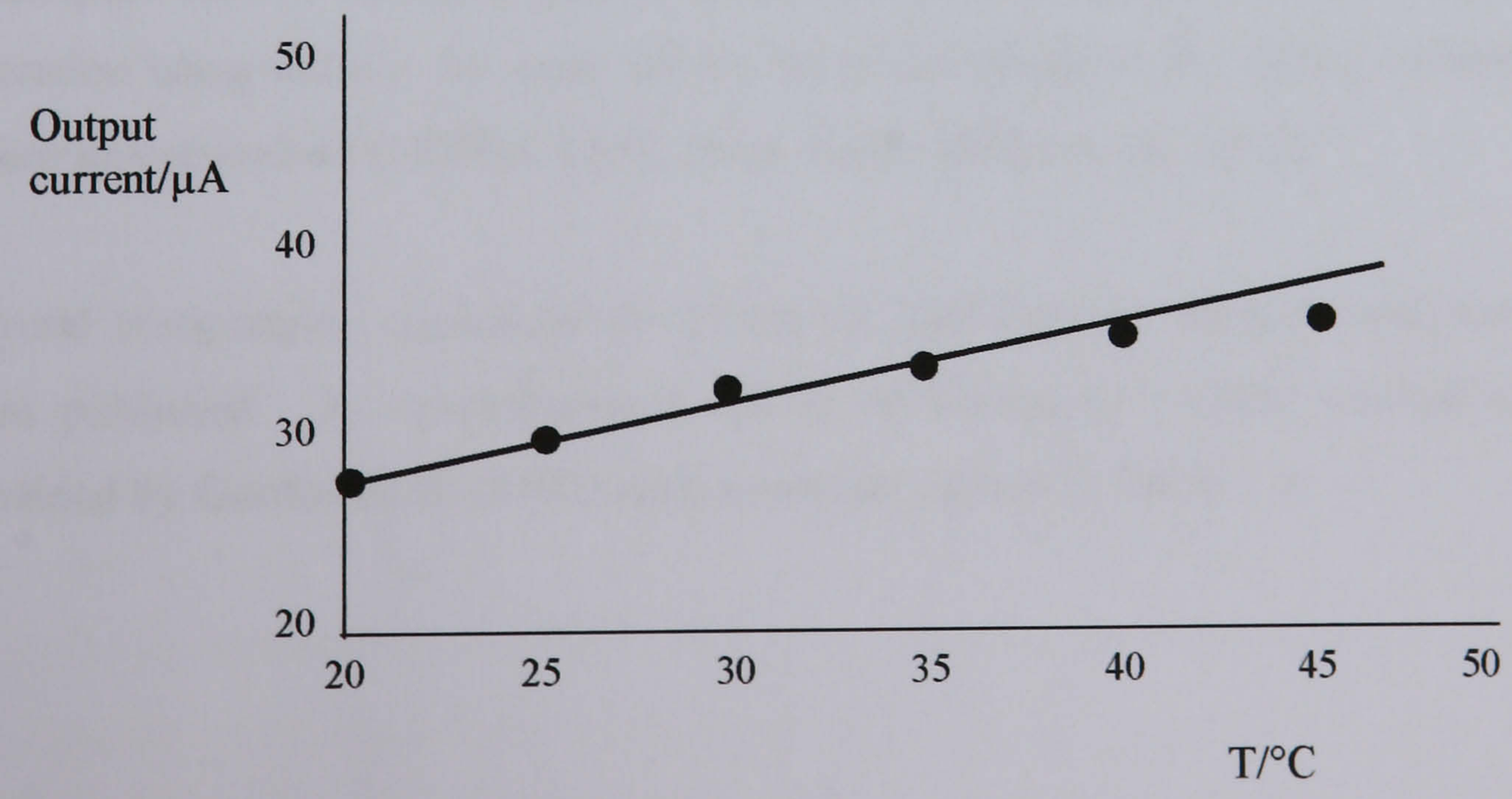

Figure 2.27 Typical temperature variation of a galvanic amperometric cell current with no compensation. (Chlorine concentration 0.32 mg/l, pH 7.6).

It is also important when handling and storing chlorine in water, to remember that aqueous chlorine is unstable due to the decomposition of hypochlorous acid with time to yield hydrochloric acid:

$$2HOCl \rightarrow 2HCl + O_2 \qquad (2.54)$$

The chlorine content of sample solutions, particularly weak solutions, will therefore decrease rapidly. The effect is greater with both rising temperatures and in the presence of organic matter; in addition, it is accelerated by exposure to sunlight or agitation.

2.8.4 Review of contemporary detection methods for the measurement of aqueous chlorine

The use of laboratory chlorine analysers has grown steadily since their introduction in the 1950s. Several analytical techniques for the determination of chlorine and chlorinated species have been described, such as iodometric and amperometric titrations, redox titrations using N,N-diethyl-*p*-phenylenediamine (DPD) as an indicator, and colourimetric methods using either DPD or syringaldazine. All these techniques use the oxidising properties of dissolved chlorine, their exact modes of operation being outside the scope of this introduction and so the reader is referred to references elsewhere (HMSO, 1980; Harp, 1995; APHA *et al.*, 1992).

Several comparative studies of the analytical methods for chlorine analyses have been published. A comprehensive survey of laboratory method comparisons is provided by Gordon *et al.* (1992) with a summary given in Table 2.1.

Table 2.1 Comparison of common analytical methods for free and total chlorine in water.

Method	Analysis Range (mg/L)	Minimum or Estimated Detection Level (mg/L)	Estimated Precision (% RSD)	Application	Skill Level*
DPD colorimetric	0.01-5	0.02	1-2%	Free and Total	1
ULR-DPD colorimetric	0-0.5	0.004	5-6%	Total	2
DPD titration	0.02-5	0.011	2-7%	Free and Total	2
Iodometric titration	1-20	0.15	Not reported	Total	2
Amperometric Titration (Forward)	0.01-2	0.01	1-2%	Free and Total	3
Amperometric Titration (Back)	0.006-0.2	0.006	15%	Total	3
FACTS	0.1-10	0.1	10%	Free	1
Potentiometric Electrode	0-1	0.05	10%	Total	2

*(Harp, 1995) 1=minimal training, 2=moderately skilled with method, 3=experienced

However, for portable field analysis, the most common and accepted methods are the DPD colourimetric and amperometric titration procedures. With both of these methods, free chlorine is measured in the absence of iodide. Combined chlorine is then measured by adding iodide and allowing the combined chlorine to oxidise iodide to iodine.

The DPD colourimetric method, first introduced in 1957 by Palin, is the most widely used method of the two. It is the standard laboratory method in the UK and indeed has been adopted by most members of the European Union as a whole. It is now officially laid down in the USEPA National Primary Drinking Water Regulations (2000) that DPD shall be used for the analysis of residual chlorine in all publicly maintained water supply systems. The method works on the basis that alkylphenylenediamines, such as DPD, are useful colourimetric reduced indicators, the chemistries of which have been reviewed elsewhere (Moore *et al.*, 1984). DPD can be oxidised to a relatively stable semiquinone cationic radical that exhibits a strong adsorption maximum in the red region. Both free and combined chlorine can

be determined. For free chlorine determination, the chlorine sample is added to a previously mixed reagent and buffer solution (pH 6.2), usually supplied as a reagent tablet. The DPD is then oxidised by chlorine to give an intense red colouration, which is measured spectrophotometrically at 515 nm. For combined chlorine determination the same procedure is used, but potassium iodide is added to catalyse the reaction with DPD. This determination gives the total amount of chlorine. The combined fraction is then calculated as the difference between the total and the free chlorine present in the sample.

The amperometric titration technique was first applied to chlorine residual analysis by Marks & Glass (1942). The amperometric titration method measures both free and combined chlorine residuals, but although a low-level method for chlorine below 0.2 mg/l is available, there is no free/combined chlorine discrimination possible in this instance. Amperometric titration uses a potentiostatic amperometric type electrode system to measure the current change as a function of titrant added. In the determination of free chlorine, the sample is titrated with a standard reducing agent of known concentration, usually *N*-phenylarsine oxide (PAO) at pH 7. A small potential is applied across the electrodes before the titration begins. As long as the oxidant (free chlorine) is present in the titrated sample, a current flows through the cell. When all of the oxidant is reacted, the rate of current change is zero, signalling the end point of the titration. After the end point is reached, the solution cannot conduct current even though excess PAO is added. The amount of PAO used at the titration end point is proportional to the chlorine concentration in the sample. If combined chlorine is also required to be measured, potassium iodide solution is added at pH 4. Any combined chlorine present will liberate iodine and the titration is continued until a further null point is reached with the cell current.

A number of commercial instruments exist with most companies producing several variants of their test kit to cater for different sectors of the market. The cost typically varies according to the accuracy and sensitivity of testing required. At the time of writing, on-line chlorine analysers typically range from £1500 to £1700. Portable chlorine measurement systems typically cost around £350. In comparison,

disposable reagent kits for chlorine analysis cost about £65 for a pack of 250 whereas the colour disc for chlorine cost about £23 for a pack of 50 (US Environmental Protection Agency, 2004). The DPD colourimetric instruments range from simple colour disc comparator based devices (a colour comparison wheel is shaded from light to deeper colour in proportion to the concentration of analyte that is being tested) through to portable colourimeters with a digital readout. Amongst the colourimeters there are a number of compact single beam types specific to chlorine such as the Hach® 'pocket' type (Figure 2.28) and the Hanna® Instruments HI-93711™. Portable amperometric titration equipment is also available from these suppliers.

Figure 2.28 The Hach® Company Pocket Colorimeter™.

Although the DPD colourimetric and amperometric titration methods are those currently recommended for chlorine determination, they are less convenient than methods based on a direct reading sensor and indeed, all the current methods have some drawbacks. A summary of their strengths and weaknesses when used for potable water analysis is given by Guter *et al.* (1974) and for their use in wastewaters, by Derrigan *et al.* (1993). For example, in the case of the amperometric titration method, a higher level of operator skill is required to obtain the best reliability and it should also be noted that a loss of chlorine can occur because of rapid stirring. In addition, clean and conditioned electrodes are necessary for sharp end points. Electrode and cell assemblies also require maintenance, which may include, for example, membrane end electrolyte replacement as the cell performance

degrades. With regards to the colourimetric procedure, simple colour and turbidity variations may interfere with end results. The test procedure can also introduce errors such as poor mixing of the reagent tablet. Both methods are based on wet chemistry techniques which necessitate the use of consumables such as reagents and solutions. Calibration standards must also be refreshed on a regular basis. This, coupled with the relatively long time of analysis (a minimum of 3 minutes) renders these methods cumbersome for use by the operator and not at all ideal.

Another disadvantage with all chlorine detection methods is that they are subject to a number of interferences. Some of the most commonly reported interference compounds are shown in Table 2.2, although this list is by no means exhaustive.

Table 2.2 Summary of interferences to a number of common laboratory analytical methods for the detection of aqueous chlorine (shaded blocks represent an interference to the system).

	Method							
Interferences	DPD colourimetric	ULR-DPD colourimetric	DPD titration	Iodometric titration	Amperometric titration (Forward)	Amperometric titration (Back)	FACTS	Potentiometric electrode
Manganese	■	■		■				
Copper	■	■	■	■				
Silver					■	■		■
Dichloramine	■	■			■	■		■
Chlorine dioxide					■	■		
Nitrogen trichloride	■	■			■	■	■	
Monochloramine	■	■	■		■	■		
Bromine	■	■	■				■	■
Iodine	■	■	■				■	■
Chromium	■	■						
Iron	■	■		■				
Iodide	■	■			■	■		
Nitrite	■	■		■				
Ozone	■	■					■	
Manganese oxide	■	■	■	■			■	■

In addition to chemical interferents, it is known that at higher oxidant levels, the formation of the instable colourless imine product is favoured, causing a fading in the solution. This may have serious consequence with regards to measurement. For example, excessive levels of chlorine may be dosed into swimming pools resulting in damaged swimming costumes, eyes, hair and may even result in serious chemical burns. This fading effect, and indeed many interference effects, are not seen with the amperometric reduction of chlorine and is a major advantage with the use of the method.

It is evident then that there presently exists no ideal method for quantifying chlorine in water. Fourteen conceptual qualities of an 'ideal' method for chlorine analyses were presented by Gordon *et al.* (1992):

1. Being method specific to the actual species.
2. Possessing a selectivity of at least 500 times over possible interferences.
3. A detection limit of 1 ppb as Cl_2.
4. Precision of ± 0.1% or better.
5. Accuracy of ± 0.5% or better.
6. A linear working range of four orders of magnitude.
7. Performance with any sample matrix.
8. No requirement for sample dilution to minimise interferences.
9. Working in both batch and automated modes.
10. Maximum sensitivity with traditional laboratory instruments.
11. No specialised skills required to perform the test.
12. Reagent stability in excess of one year.
13. Performance of the test within one minute.
14. Being cost effective.

It is the development of an amperometric chlorine sensor conforming to some, if not all, of the above listed qualities which is the overall aim of this thesis.

CHAPTER 3

MATERIALS AND METHODS

3.1 REAGENTS

Aniline hydrochloride, ferrocenemonocarboxylic acid, gold(I) cyanide, hexaammineruthenium(III) chloride, *o*-phenylenediamine dihydrochloride and potassium ferricyanide(III) (all 'Analytical Reagent' grade) were purchased from Sigma-Aldrich (Gillingham, Dorset, UK).

Maleic acid, potassium chloride, potassium hydroxide, potassium iodide and sodium carbonate (all 'Analytical Reagent' grade) were purchased from Fisher Scientific (Loughborough, Leicestershire, UK).

Acetic acid, chloramine T, orthophosphoric acid and sodium hypochlorite solution (all GPR™ grade), sodium thiosulphate solution 0.1 N (AnalaR Volumetric Solution® grade), Tween®20 ('Organics' grade), disodium hydrogen orthophosphate 12-hydrate, sodium chloride, sodium dihydrogen orthophosphate 1-hydrate and zinc iodide/starch solution (all 'AnalaR®' grade) were purchased from BDH (Lutterworth, Leicestershire, UK).

All chemicals were used without further purification.

3.2 MATERIALS

Menzel 'Superfrost' twin frosted-end microscope slides were purchased from Fisher Scientific (Loughborough, Leicestershire, UK) and were used for the construction of gold-sputter coated working and counter electrodes.

Acheson Electrodag® (1415M) silver conductive paint was purchased from AGAR Scientific Ltd. (Stansted, Essex, UK) and was used for the construction of gold sputter-coated working and counter electrodes, and for the preparation of electron microscopy samples.

Aluminium pin stubs (0.5″ diameter, 6 mm length) and conductive pads were purchased from AGAR Scientific Ltd. (Stansted, Essex, UK) and used for the preparation of electron microscopy samples.

Epoxy resin purchased from RS (Corby, Northamptonshire, UK) and copper multicore wire purchased from Maplins Electronics (Luton, Bedfordshire, UK) were used for the construction of gold sputter-coated working and counter electrodes, and silver/silver chloride reference (Ag/AgCl) electrodes.

Silver wire purchased from J. Blundell & Sons Ltd. (Holborn, London, UK) and soda-lime glass rods purchased from Fisher Scientific (Loughborough, Leicestershire, UK) were used for the construction of silver/silver chloride (Ag/AgCl) reference electrodes.

An E21MOO2 type Ag/AgCl reference electrode was obtained from Radiometer Analytical SAS (Villeurbanne, Cedex, France) and was used for all electrode interrogations involving total chlorine.

Stainless steel gauze ('30' mesh, 0.3 mm wire) was purchased from Fine Mesh Metals (Brierley Hill, West Midlands, UK) and was used as a counter electrode for multi-electrode electropolymerisations.

Perforated stainless steel sheeting (thickness 1 mm, hole diameter 3 mm, pitch 2 mm) was purchased from RM Perforating Ltd. (Warrington, Cheshire, UK) and was used as 'baffling' in the ultrasound tank for sonication investigations.

Electrodes were screen printed at Polyflex Circuits Ltd. (Parlex Corporation, Newport, Isle of Wight, UK) and were specifically designed for the analysis of chlorine in aqueous solutions and therefore possess two carbon working electrodes (working electrode total and working electrode free), in addition to a carbon counter electrode and a silver/silver chloride (Ag/AgCl) reference electrode. However, they may also act as generic disposable templates and may be easily adapted for a range of differing applications.

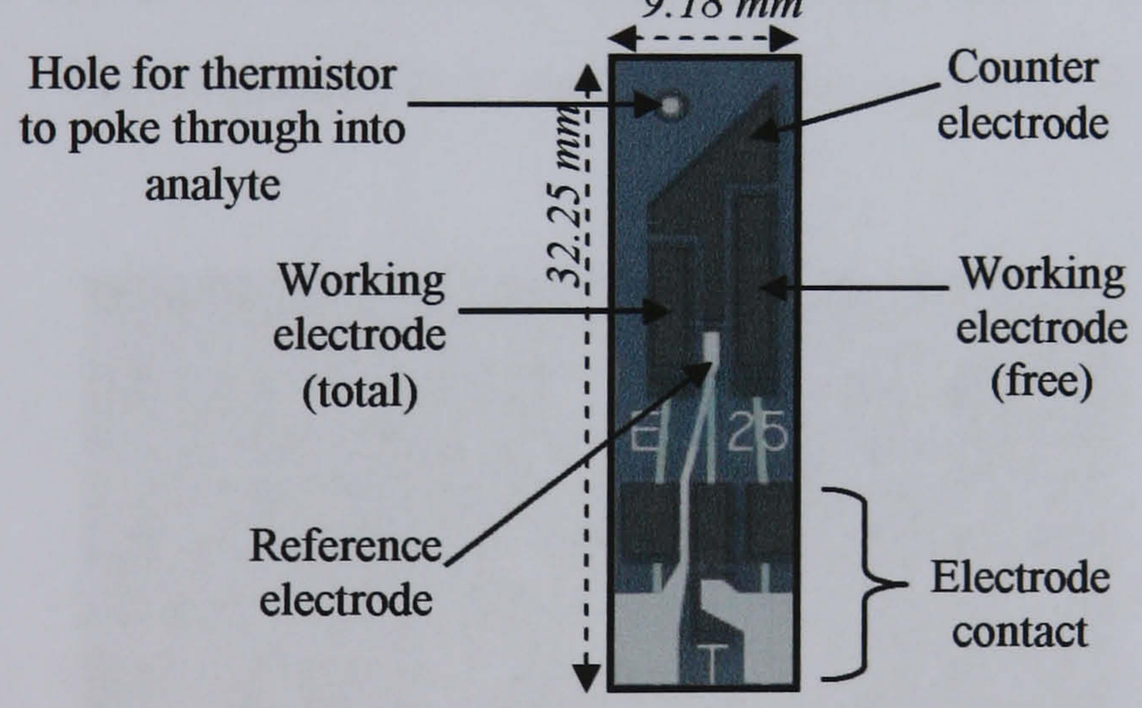

Figure 3.1 Single polycarbonate screen printed electrode.

Two commercial graphite paste-based carbon inks were screen-printed and compared for their use as working electrode materials: product code C2001222R5 from Gwent Electronic Materials Ltd. (Pontypool, Wales, UK) and product code 7102 from DuPont Microcircuit Materials (Bristol, Avon, UK). Silver/silver chloride (product code: 5874), silver (product code: 5028) and dielectric ink (product code: 5018) were all purchased from DuPont Microcircuit Materials (Bristol, Avon, UK) and were

used as the reference electrode, conductive bus bar and for area definition, respectively. The inks were screen printed onto sheets (600 x 450 mm) of 0.375 mm thick Matt Polycarbonate substrate (Cadillac Plastics) purchased from Polyflex Circuits Ltd. (Parlex Corporation, Newport, Isle of Wight, UK), to yield 600 disposable sensors, each of size 32.25 x 9.18 mm (Figure 3.2). Sheets were divided into six individual sheets of 100 sensors for initial investigations. Printing took place in four stages: the silver conductive bus bar was printed first (this enables all 600 sensors to be connected together for electropolymerisation), followed by the carbon working and counter electrodes. This was followed by the dielectric which defined the working electrode geometries to be 8.82 mm^2 and 12.96 mm^2 for working electrode total (for total chlorine measurement) and working electrode free (for free chlorine measurement) respectively, resulting in an apparent total geometric area of 21.78 mm^2. The counter electrode has geometry of 26.92 mm^2. Finally the silver/silver chloride (Ag/AgCl) reference was printed. Post-printing of each ink, electrodes underwent a heat curing and drying process with a conveyor-belt system under heated air. The temperature was ramped from 25 °C to 120 °C over 30 seconds, held at 120°C for 45 seconds and then cooled back to room temperature over 20 seconds. The dielectric layer was also cured under a UV light source for 5 seconds.

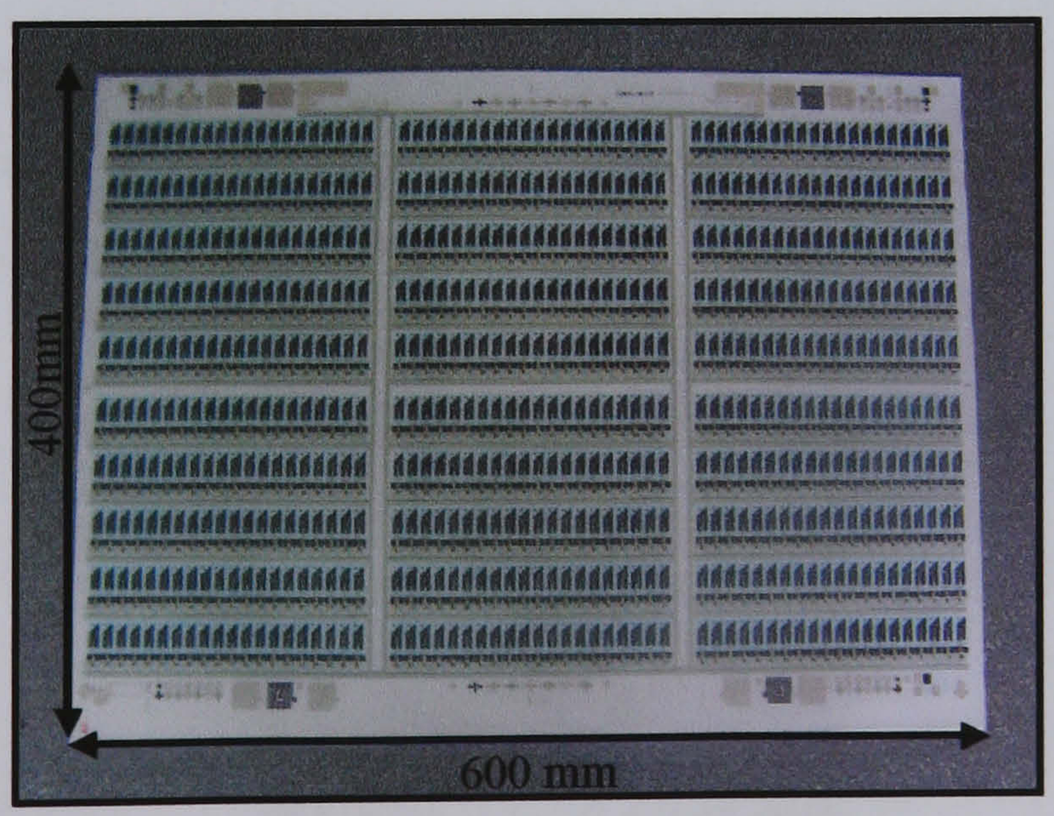

Figure 3.2 Photograph of a sheet of 600 sensors.

All inks and electrodes were used as supplied. Each screen-printed electrode was used in a single experiment, without any pre-treatment, unless otherwise stated.

3.3 EQUIPMENT AND APPARATUS

3.3.1 Potentiostats

A Sycopel Analytical Electrochemical Workstation Model AEW2 potentiostat (Sycopel Scientific Ltd, Washington, Tyne & Wear, UK) controlled by a PC equipped with an ECProg3 software program was used for all lab-scale electrochemical studies.

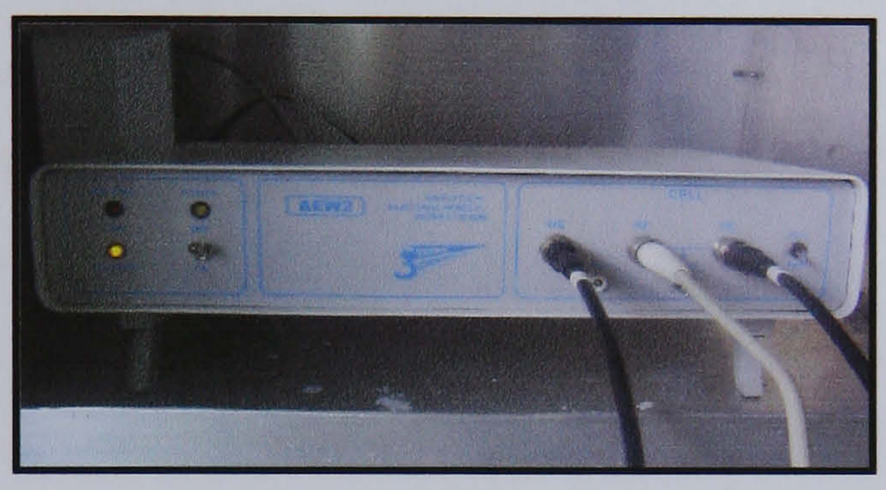

Figure 3.3 Sycopel AEW2 potentiostat.

A 40 channel potentiostat system (± 200 mA compliance per I/E channel, 4 decade current resolution, single auxiliary and reference) with an integrated PC control system was custom built (Sycopel Scientific Ltd, Washington, Tyne & Wear, UK) and used for the electropolymerisation of all electrodes unless otherwise stated.

Figure 3.4 Custom built Sycopel 40-channel potentiostat.

3.3.2 Ultrasonic tanks

A Transsonic, 25 kHz, laboratory-scale ultrasound tank was used for the sonochemical fabrication of microelectrode arrays upon individual electrodes. Large-scale sonication experiments were performed using a custom built (Ultrawave Ltd., Cardiff, UK) 2 kW, 25 kHz ultrasound tank (Figure 3.5a) with internal dimensions of 750 x 750 x 660 mm (working volume 3.57 x 10^8 mm^2), employing 10 transducers geometrically arranged and bonded to the base of the stainless steel housing. The tank incorporates a frequency sweep of ± 1 kHz in 100 Hz steps three times per second, and a temperature control system allowing for the temperature to be varied between 10 to 50 °C. Software incorporated within the power generation system allows for the power to be varied between 50 and 100%, and the sonication time to be varied between 1 and 99 seconds. A sonic pulse system is also programmed in the software to allow for de-oxygenation of the water prior to sonication.

A baffle, designed such that a 50 mm gap was present around all sides, was constructed from perforated stainless steel and supported at the base of the tank via rubber stoppers, again to allow a 50 mm gap between the base of the baffle and the base of the tank (Figure 3.5b). This was constructed with the aim of reducing standing waves and wave reflections occurring from the tank walls, leading to a more uniform sonication profile across the tank.

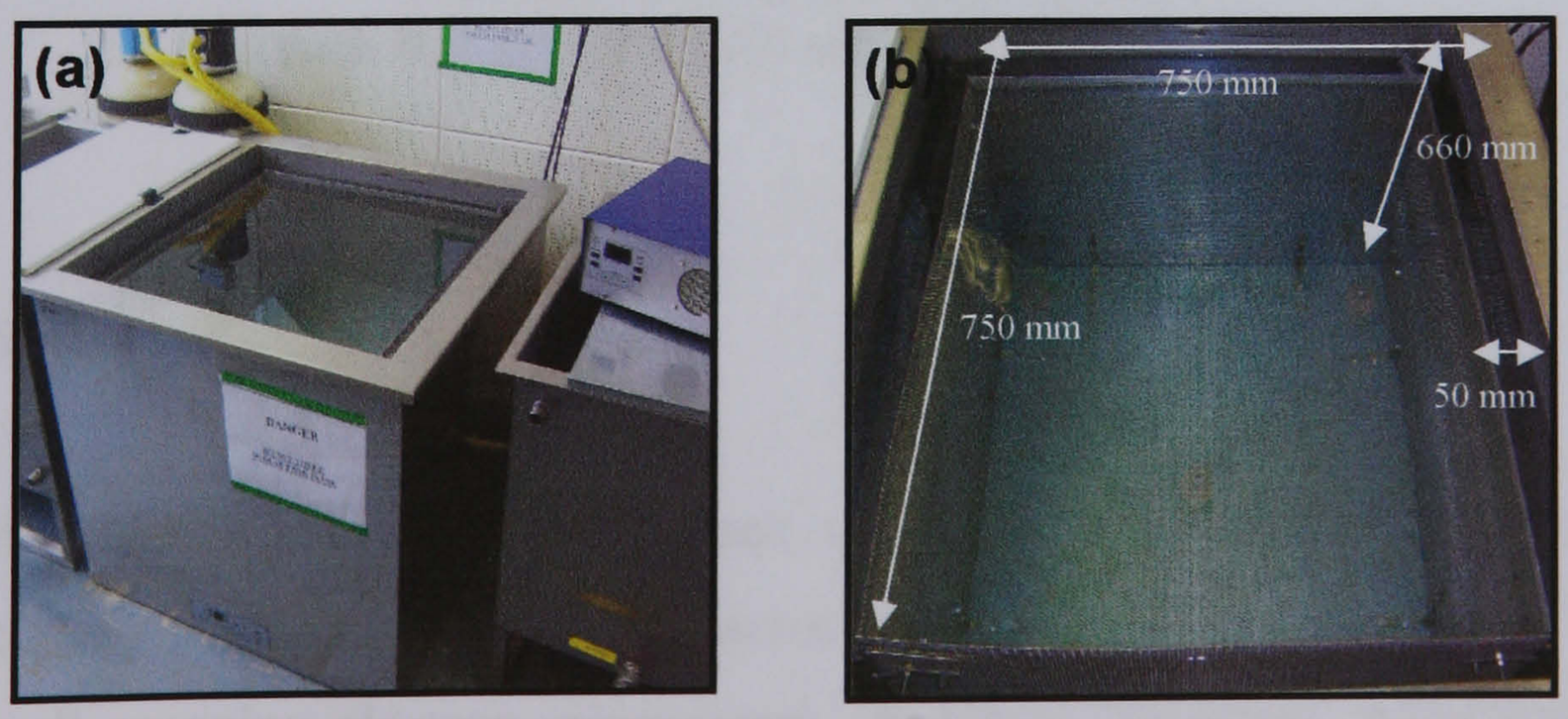

Figure 3.5 (a) Custom built Ultrawave ultrasound tank (b) Ultrasound tank showing incorporated baffling.

Ultrasound tank specifications of frequency and power are set and calibrated by the manufacturer and were verified using a crystal microphone connected to a Tektonix TDS 1002 digital storage oscilloscope (RS, Corby, Northamptonshire, UK), and a USPM200/2 Ultrasonic Power Meter (Ultrawave Ltd., Cardiff, UK), respectively.

A Transsonic T460, 35 kHz, 30W ultrasound tank (Fisher Scientific, Loughborough, Leicestershire, UK) was used for the removal of electrode surface bubbles prior to the electropolymerisation of carbon electrodes, to ensure a homogenous polymer layer.

3.3.3 Sputter coating

An AGAR B7341 Automatic Sputter Coater (AGAR Scientific Ltd., Essex, UK), in conjunction with a Pfeiffer Rotary Vane Vacuum Pump (Pfeiffer Vacuum Ltd., Newport Pagnell, UK), was used for the preparation of gold working and counter electrodes and samples for investigation under SEM.

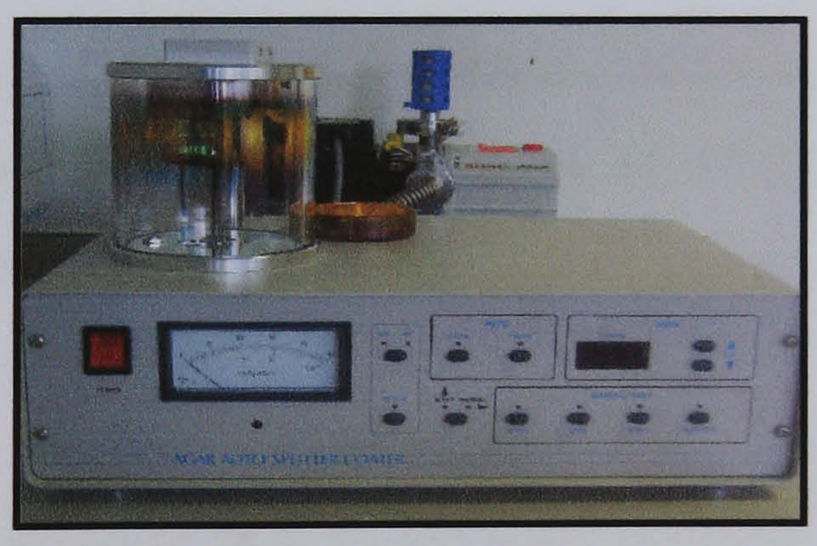

Figure 3.6 AGAR B7341 automatic sputter coater.

3.3.4 Microscopy

A Hitachi Denshi Limited, KPM1 black and white CCD camera (x2 lens, x25 magnification) was used for all light microscopy. A Philips XL30 FEG-SEM was used for all scanning electron microscopy. A Veeco 'Explorer' AFM (triangular cantilever of spring constant 0.032 Nm^{-1}) was used for all atomic force microscopy.

3.3.5 Chemical modifying layer deposition

A BioDot Inc. AD3200™ dispense platform in combination with a BioJet Plus™ 3000 dispensing system (Europe BioDot Ltd., Huntingdon, Cambridgeshire, UK), controlled by PC driven AxSys™ software, was used for the deposition of chemical modifying layers.

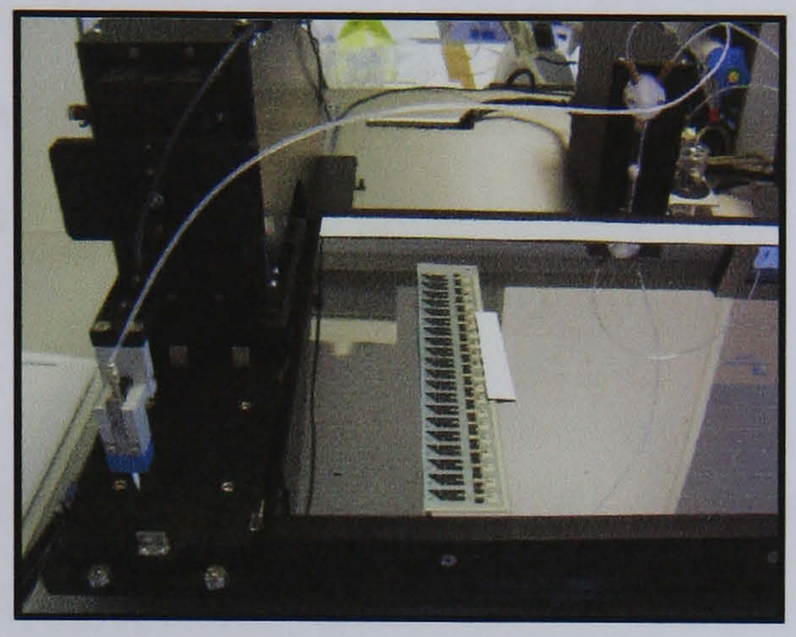

Figure 3.7 Biodot AD3200™ platform with BioJet Plus™ 3000 dispensing system.

3.3.6 Validation

A Hach® Company Pocket Colorimeter™ Chlorine Analysis System (Camlab, Over, Cambridgeshire, UK) was used for the validation all of chlorine solutions and as a comparator for sensor interrogation studies.

Figure 3.8 Hach® Pocket Colorimeter™.

A LaMotte 1200 Colorimeter™ was also used as a comparator for sensor interrogation studies.

3.4 BUFFERS AND SOLUTIONS

3.4.1 Solutions for the pre-treatment of carbon electrodes

A saturated solution of sodium carbonate and separately, a pH 7.0 buffer comprising 2.01×10^{-2} M sodium dihydrogen orthophosphate 1-hydrate, 2.98×10^{-2} M disodium hydrogen orthophosphate 12-hydrate and 0.1 M sodium chloride, were used for investigations into the activation of bare carbon electrodes.

3.4.2 Solutions for the electrodeposition of polymer films

A 5.0×10^{-3} M *o*-phenylenediamine dihydrochloride solution was prepared in a pH 7.4 buffer comprising 5.28×10^{-2} M disodium hydrogen orthophosphate 12-hydrate, 1.30×10^{-2} M sodium dihydrogen orthophosphate 1-hydrate and 5.10×10^{-3} M sodium chloride.

A 0.2 M aniline hydrochloride solution used for electrode modification studies was prepared in a pH 2.0 buffer comprising 4.6×10^{-3} M malaic acid, 5.3×10^{-3} M potassium hydroxide and 8.6×10^{-3} M potassium chloride.

3.4.3 Redox couple solutions for electrode characterisation

A 1.0×10^{-3} M ferrocenemonocarboxylic acid solution, a 1.0×10^{-3} M hexxaaminеruthenium(III) chloride solution and a 5.0×10^{-3} M potassium ferricyanide(III) solution were all prepared in pH 7.8 buffer comprising 3.18×10^{-2} M disodium hydrogen orthophosphate 12-hydrate, 4.35×10^{-3} M sodium dihydrogen orthophosphate 1-hydrate and 0.1 M potassium chloride.

3.4.4 Chlorine solutions for electrode performance analysis

All chlorine solutions were prepared according to Merck analytical standard procedures (Merck, 1998) as follows:

A 1000 ppm (1000 mg/l) stock solution of total chlorine was prepared by dissolving 1.42×10^{-2} M chloramine T in 1 litre of deionised water.

A pH 4.0 buffer comprising 9.0×10^{-3} M orthophosphoric acid, 9.0×10^{-2} M sodium dihydrogen orthophosphate 1-hydrate and 0.5 M potassium chloride was used for the preparation of any further dilutions.

A stock solution of free chlorine was prepared by diluting 10 ml of sodium hypochlorite solution into 100 ml of distilled deionised water in a conformity checked 100 ml borosilicate glass volumetric flask. A precise assay of the stock concentration was found by titration using iodide/thiosulphate as follows: 5 ml of the stock solution, 5 ml of acetic acid, 2 g of potassium iodide and 30 ml distilled deionised water was sealed together in a 250 ml conical flask and shook for 10 seconds. This mixture was then left for 5 minutes to eliminate the iodine. The resulting iodide was then titrated against 0.1 mol/l sodium thiosulphate solution until a pale yellow colour developed. 2 ml of zinc iodide/starch solution was then added and the titration was completed until the solution turned from deep blue to colourless. The procedure was repeated until concurrent results were obtained for each titrations (0.0 ml accuracy). The exact assay of the stock solution was then calculated according to Equation 3.1:

$$\textit{ml sodium thiosulphate (0.1 mol/L)} \times 710 = \textit{x mg/L free chlorine} \qquad (3.1)$$

A pH 7.0 buffer comprising 4.30×10^{-3} M sodium dihydrogen orthophosphate 1-hydrate, 5.60×10^{-3} M disodium hydrogen orthophosphate 12-hydrate and 0.1 M sodium chloride was used for the preparation of any further dilutions.

3.4.5 Chemical modifying layer solution

A solution (pH 4.0) comprising 9.0 x 10^{-3} M orthophosphoric acid, 9.0 x 10^{-2} M sodium dihydrogen orthophosphate 1-hydrate, 0.5 M potassium chloride and 0.7 M potassium iodide was used for the preparation of a modifying layer for a total chlorine sensing electrode. The solution was prepared in a borosilicate glass volumetric flask and used immediately after preparation in order to minimise the oxidation of iodide to iodine.

3.4.6 Water purification

All solutions were prepared using deionised water (18 MΩcm^{-1} resistivity at 25 °C) sourced from an Elga Purelab UHQ-II Water System (Elga, Hugh Wycombe, Buckinghamshire, UK) unless otherwise stated. Water used for the preparation of free chlorine solutions requires purification to the highest standard and therefore deionised water was subsequently double distilled using a simple laboratory still (Figure 3.9) to aid removal of any residual organics that may combine with the free chlorine present in the sample.

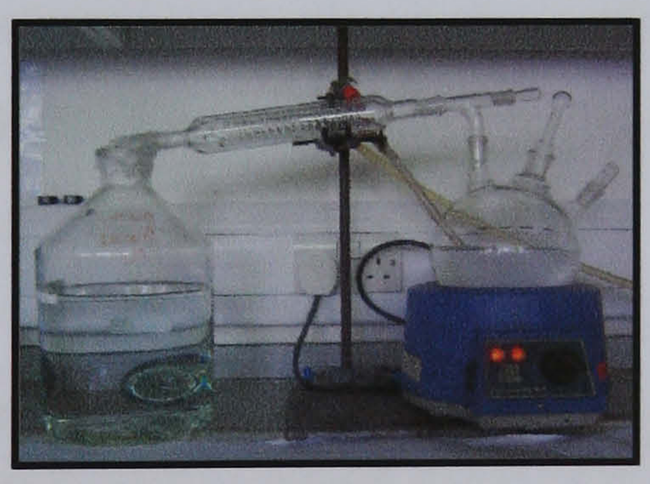

Figure 3.9 Laboratory still for water purification.

The purity of water used in the sonication process is critical to the efficiency of the cavitation process and should be no less than 18 MΩcm^{-1} resistivity at 25 °C. Water used to fill the ultrasound tank is therefore continuously pumped through a particulate filter (mesh size of 100 µm) and two separate purifying cylinders, types DC9 and CC9 (Purite Ltd., Thame, Oxfordshire, UK), to remove organics and inorganics respectively, for at least three hours prior to sonication. An integrated conductivity meter is incorporated and the conductivity is checked prior to each use.

3.5 EXPERIMENTAL PROCEDURES

3.5.1 Preparation of electrodes

A silver/silver chloride (Ag/AgCl) reference electrode was constructed by heat sealing silver wire (1.5 mm diameter) within a hollow soda glass tube, leaving 10 mm of silver wire exposed at one end of the glass tube. The opposing end of the silver wire was joined to copper multi-core wire. The silver electrode was pre-anodised for 10 minutes in a saturated solution of potassium chloride at +1.0 V (vs. SCE) to allow the silver chloride layer to be electrodeposited onto the surface of the silver rod.

The ground glass edge of twin frosted microscope slides (cut to size ~ 25 x 15 mm) were sputter coated with gold for 2 minutes in order to render one face electrically conductive. Mulitcore wires were attached to this face using silver conductive paint. Glass slide/wire junctions were coated with epoxy resin in order to insulate the joint and provide additional mechanical strength to the electrode assembly (Figure 3.10). The conductive faced glass slide/wire assemblies were then used as both counter electrodes and working electrode templates for the electrochemical fabrication of microarrays.

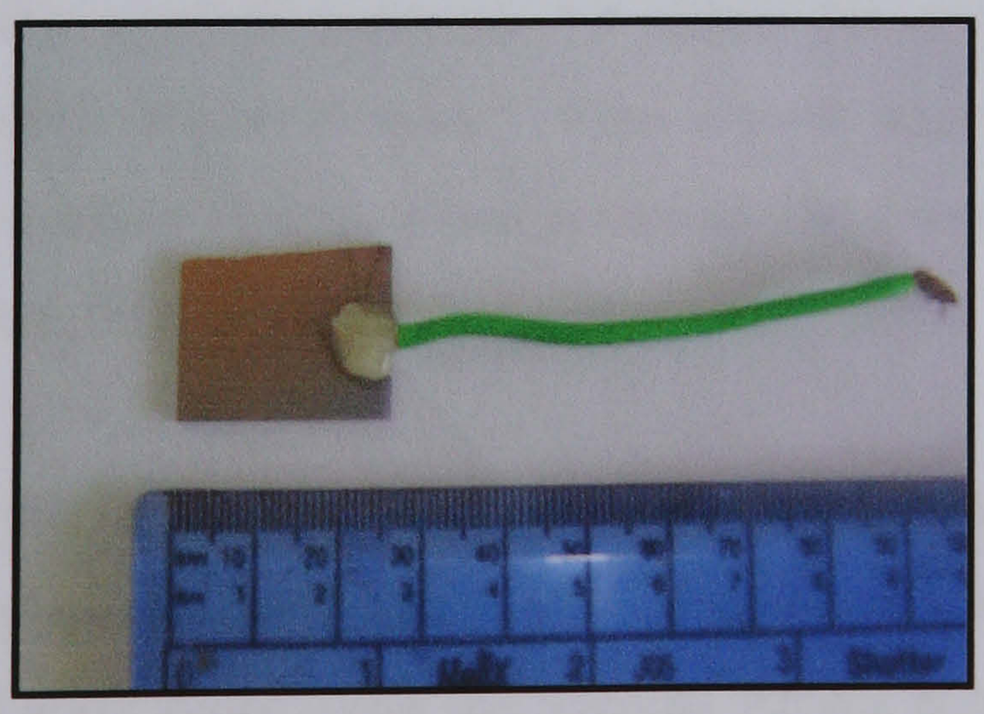

Figure 3.10 Gold sputter coated glass slide electrode.

3.5.2 Pre-treatment of electrodes

The electrochemical pre-treatment of carbon electrodes was carried out by applying anodic potentials of +1.2 and +1.0 V (vs. Ag/AgCl) in electrolyte solutions of 0.05 M phosphate buffer (pH 7.0) and saturated (>3 M) sodium carbonate respectively, for a period of 120 seconds and 300 seconds respectively. Electrodes were immediately rinsed with deionised water in each case.

The sonochemical pre-treatment of carbon electrodes was carried out by sonication of electrodes for 5, 30 and 300 seconds at 100% power and a water temperature of 25 °C.

3.5.3 Electropolymerisation of electrodes

For initial studies on the modification of bare (planar) carbon electrodes with polyaniline films, aniline hydrochloride was electropolymerised on to single screen printed carbon electrodes using the Sycopel AEW2 potentiostat as follows: an aniline hydrochloride/buffer solution was de-oxygenated by purging with nitrogen for 20 minutes in a sealed cell. The cell was prepared with a working electrode to be coated, a gold sputter coated ground glass slide counter electrode and a silver/silver chloride (Ag/AgCl) reference electrode. Polymerisation was carried out by potentially cycling the applied potential 15 times between -0.2 to +0.8 V (vs. Ag/AgCl) at a sweep rate of 50 mVs^{-1}. Film growth was terminated at -0.2 V (vs. Ag/AgCl). The working electrode was removed, the excess monomer washed off with deionised water, then left to air dry.

For initial studies of the insulating layer component of the sonochemically formed microarrays, *o*-phenylenediamine was first electropolymerised on to gold sputter-coated ground glass slides using the Sycopel AEW2 potentiostat as follows: an *o*-phenylenediamine dihydrochloride/buffer solution was de-oxygenated by purging with nitrogen for 20 minutes in a sealed cell. The cell was prepared with a

working electrode to be coated, a gold sputter coated ground glass slide counter electrode and a silver/silver chloride (Ag/AgCl) reference electrode. Polymerisation was carried out by cycling the applied potential in the range from 0 to +0.8 V (vs. Ag/AgCl) at a sweep rate of 50 mVs^{-1} for 20 cycles. The working electrode was removed, the excess monomer washed off with deionised water, then left to air dry (unless subsequently sonicated, in which case, the electrode must be sonicated before the polymer layer is left to dry).

Studies towards the optimisation of electrodeposited *o*-phenylenediamine films upon single screen-printed carbon electrodes were performed using the Sycopel AEW2 potentiostat by adjusting the potential scan range, the potential sweep rate and the number of potential sweeps (i.e. coatings) independently as detailed in Chapter 6, as follows: an *o*-phenylenediamine dihydrochloride/buffer solution was de-oxygenated by purging with nitrogen for 20 minutes in a sealed cell. The cell was prepared with a working electrode to be coated, a gold sputter coated ground glass slide counter electrode and a pseudo silver/silver chloride (Ag/AgCl) reference electrode. The working electrode was removed, the excess monomer washed off with deionised water, then left to air dry (unless subsequently sonicated, in which case, the electrode must be sonicated before the polymer layer is left to dry).

Multiple screen-printed carbon electrodes (sheets of 100 sensors) were electropolymerised in a solution of de-oxygenated (via nitrogen purging for ~20 minutes) and de-gassed (via pulsed sonication for ~30 minutes) *o*-phenylenediamine dihydrochloride/buffer, housed in a glass cell of volume 2.2 litres (Figure 3.11).

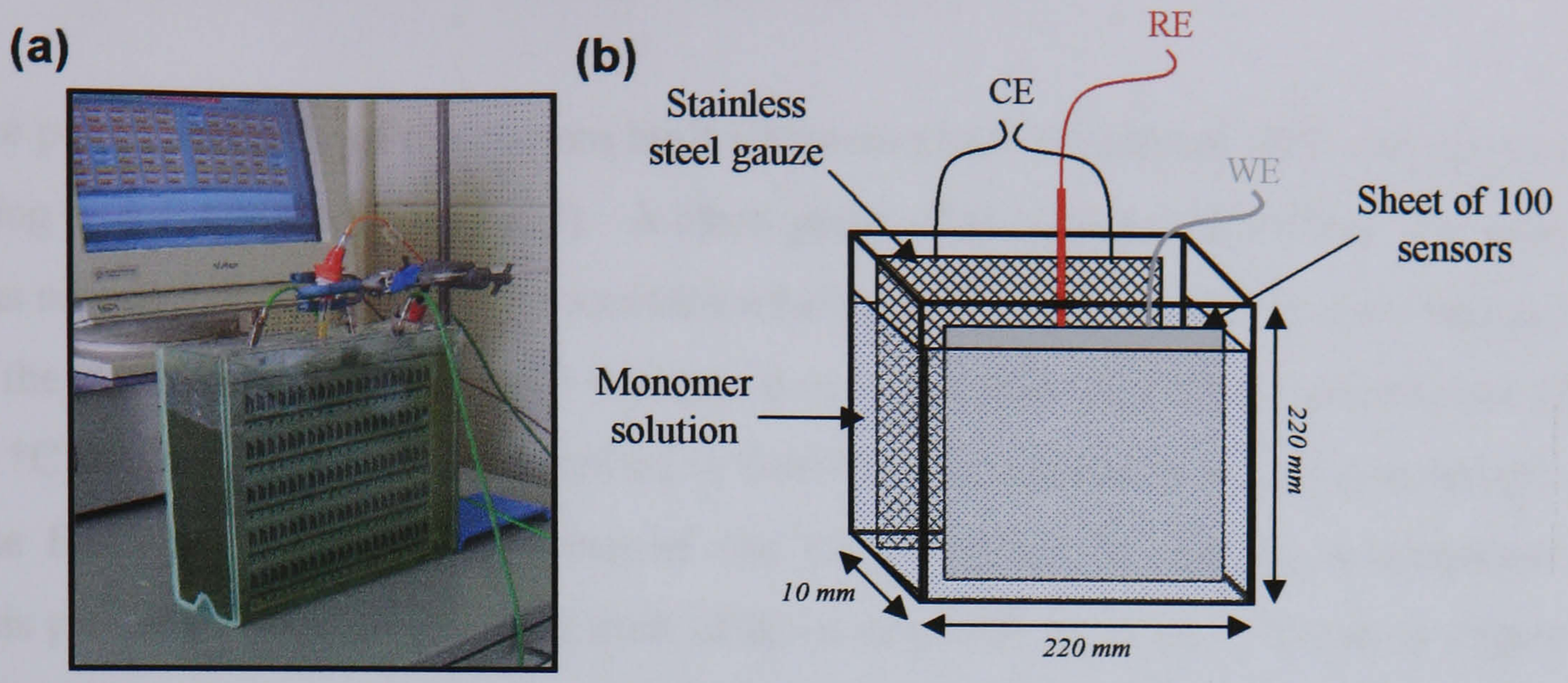

Figure 3.11 (a) Photograph and, (b) Schematic, of electropolymerisation cell.

The cell contained two shallow wells which served to hold the counter electrode and screen printed working electrode sheet at a fixed distance from one another. The counter electrode was made from stainless steel gauze to allow a large total surface area. The cell was made airtight via sealing with laboratory film, while reference electrodes were clamped overhead and able to enter the cell through sealed holes in the lid. Immediately prior to polymerisation, the cell was placed inside a Transsonic T460 sonication tank and pulse-sonicated until all bubbles were visibly removed from the surface of the carbon working electrodes.

Polymerisation was carried out by cycling the applied potential in the range from 0 to +1.0 V (vs. Ag/AgCl) at a sweep rate of 50 mVs^{-1} for 50 cycles. The sheet was removed, the excess monomer washed off with deionised water, then left to air dry (unless subsequently sonicated, in which case, the electrode must be sonicated before the polymer layer is left to dry).

3.5.4 Ultrasound tank intensity mapping

The power intensity of the custom built Ultrawave Ltd. ultrasound tank was mapped using a 'foil test' (Mason, 1999). A clean piece of aluminium foil (450 x 400 mm) was suspended vertically in the sonication bath (shown in Figure 3.12) and sonicated in the stationary position for 10 minutes at 100% power (at a water temperature of 25 °C), *without* the baffling described in Section 3.3.2 present in the ultrasound tank. The foil was then carefully removed and photographed for further investigation. This procedure was repeated for each of the tank positions, A to F, shown in Figure 3.13. The ultrasound tank was then mapped in a similar manner *with* the baffling present. In this case the foil was sonicated for 20 minutes at 100% (at 25 °C) as little damage to the foil was observed after a 10 minute sonication period.

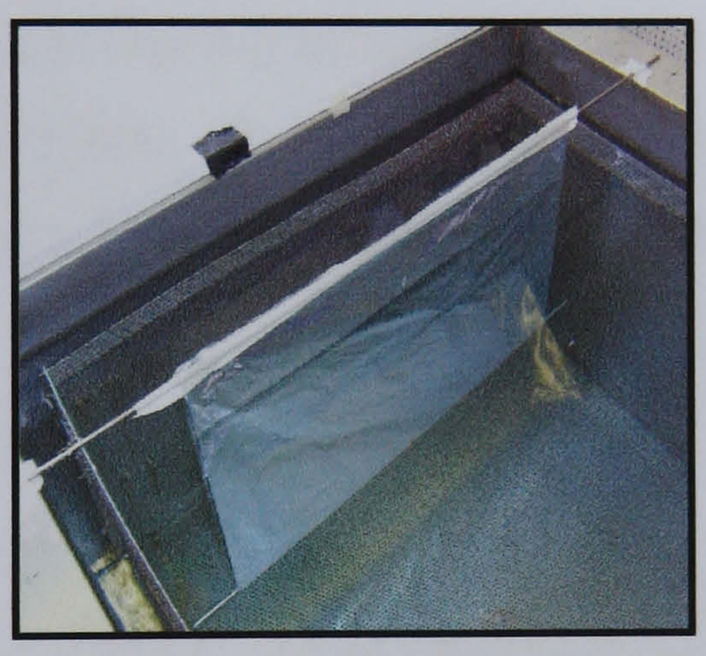

Figure 3.12 Method of suspending foil sheets.

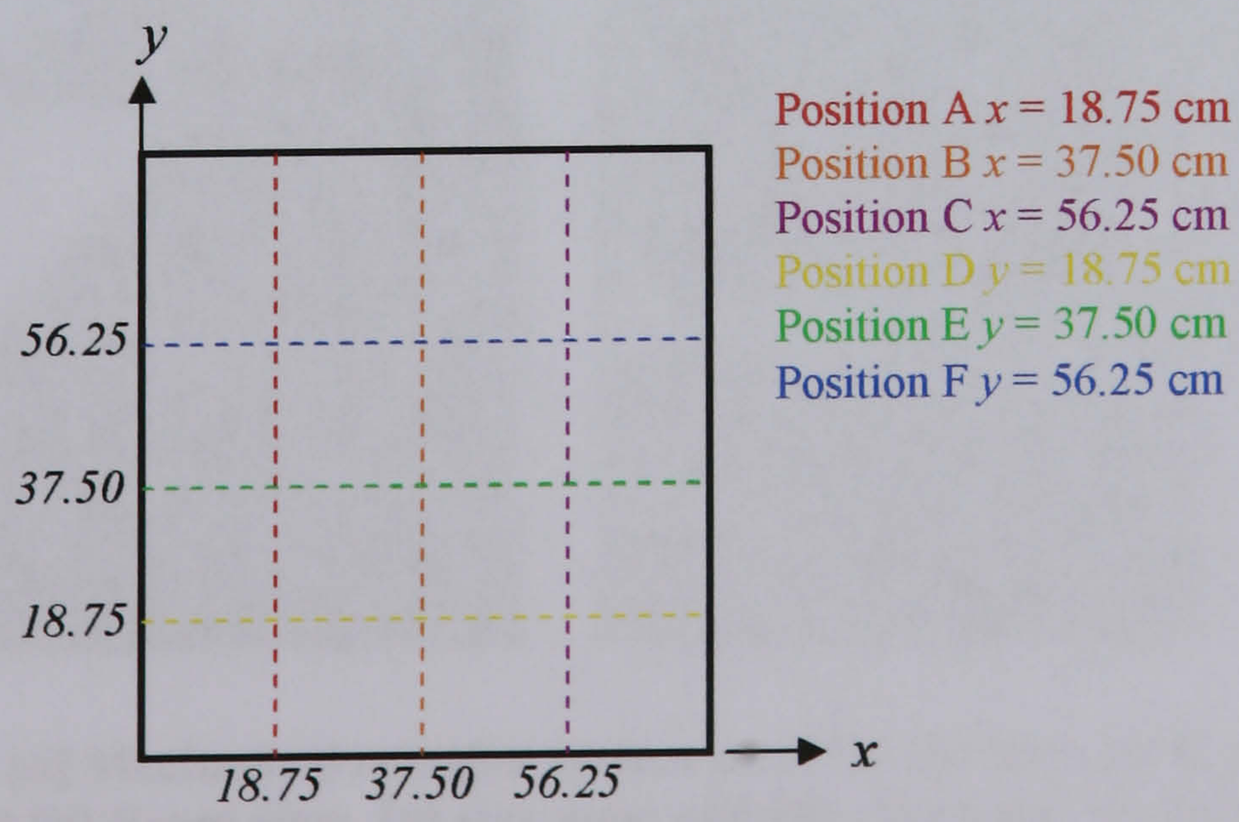

Figure 3.13 Schematic of grid for foil sheet positioning.

3.5.5 Sonochemical ablation of polymer films

Gold sputter-coated glass slides and single screen printed carbon electrodes for initial studies were immersed in a glass beaker containing deionised water. The beaker was subsequently suspended at the centre point of the ultrasound tank so that the water level within the beaker is in line with the water level in the tank and sonicated for 20 seconds at 100 % power and a water temperature of 25 °C.

Sonochemical ablation optimisation studies were performed by adjusting the sonication time, tank power and electrode positioning independently. The solvent used for the sonication step was always water, degassed for ~30 minutes prior to sonication (via the internal tank pulse de-gassing system).

Further sonication experiments were performed by rotating the electrode sheets in the tank whilst sonication took place. A mechanical rotation system was built from Meccano® '40' motion system kit and controlled by a KIKA Labortechnik RW 28 basic motor system.

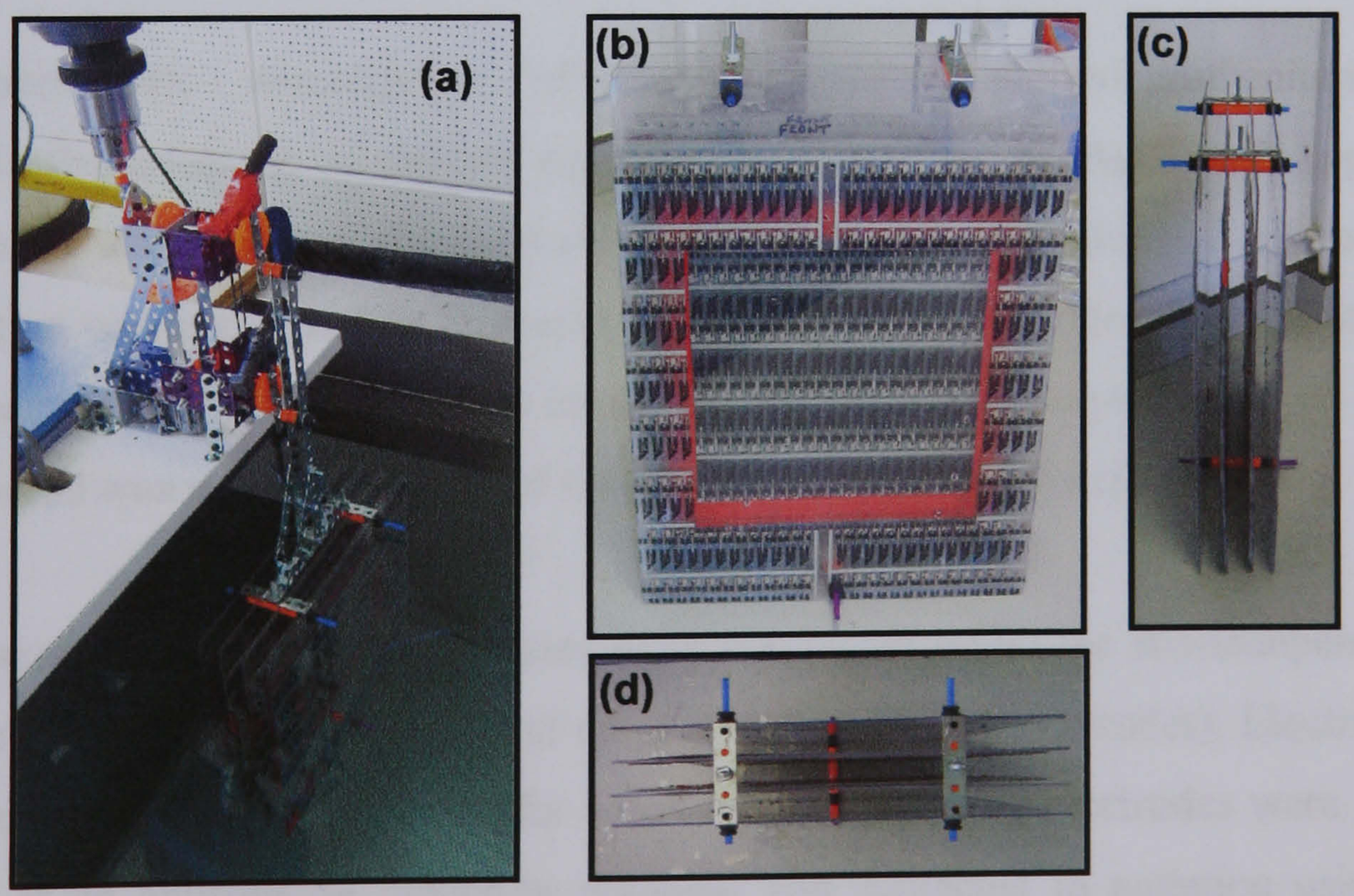

Figure 3.14 (a) Mechanical rotation system used for the sonication of multiple sensor sheets and (b) Front view, (c) side view and (d) plan view, of sensor placement structure.

3.5.6 Electrochemical characterisation in redox solutions.

Electrochemical characterisation of both macroelectrode (planar) and microelectrode array assemblies was performed via connection to a potentiostat. An open three-electrode cell was used for all electrochemical studies unless stated otherwise.

Cyclic voltammetric techniques were used to characterise the response of electrodes to reversible solution bound redox couples. Electrodes characterised in potassium ferricyanide(III)/buffer solutions were recorded between -0.2 and +0.7 V (vs. Ag/AgCl), electrodes characterised in ferrocenemonocarboxylic acid/buffer solutions were recorded between -0.3 and +0.55 V (vs. Ag/AgCl) and electrodes characterised in hexaammineruthenium(III) chloride/buffer solutions were recorded between -0.4 and +0.1 V (vs. Ag/AgCl). All characterisations were performed at a scan rate of 20 mVs^{-1} unless stated otherwise.

Linear voltammetric techniques were performed in buffer solutions to elucidate the background current levels of planar electrodes by scanning between -1.0 and +1.0 V (vs. Ag/AgCl) at a scan rate of 20 mVs^{-1}.

For amperometric interrogation of electrodes in hexaammineruthenium(III) chloride/buffer solutions, a constant potential of -0.35 V (vs. Ag/AgCl) was applied for 1 minute and the resultant current-time transient was recorded. Coulometric interrogation was performed in hexaammineruthenium(III) chloride/buffer solutions in the same manner as amperometric interrogations, with the exception that the total charge passed was recorded instead of the total current after each experiment.

Amperometric voltammetric techniques were used to examine the stir-independent behaviour of the microelectrodes (and compared with planar electrodes). Electrodes were submerged within a redox/buffer solution. The working electrodes were then polarised at an appropriate reduction potential and subjected to agitation using a Jenway 1100 magnetic stirrer and flea (Jenway Ltd., Dunmow, Essex, UK). The response was then recorded in both unstirred (quiescent) and stirred solutions.

3.5.7 Analysis of chlorine solutions

All electrodes were connected to a potentiostat for interrogation and were interrogated by both amperometric and coulometric techniques.

For amperometric interrogation of total chlorine/buffer solutions, a three-electrode cell comprising the working electrode, a counter electrode and an external silver/silver chloride (Ag/AgCl) reference electrode (with integrated frit) was used in order to avoid the iodisation of the reference electrode from iodide present in the chlorine sample. A constant potential of -0.08 V (vs. Ag/AgCl) was applied for 60 seconds in all cases unless stated otherwise, and the resultant current-time transient recorded.

For amperometric interrogation of electrodes in free chlorine/buffer solutions, a constant potential of -0.1 V (vs. Ag/AgCl) was applied for 60 seconds in all cases unless otherwise stated, and the resultant current was recorded.

3.5.8 Surface topography studies

For light microscopy studies of microelectrode arrays, a gold cyanide/sodium carbonate solution was deposited into the microelectrode array 'pores' using a constant potential method. The exact solution formulary and deposition procedure is currently company confidential.

The following procedure was followed for the examination of electrode surfaces using scanning electron microscopy techniques: Samples were mounted on aluminium stages by adhesion with conductive tape. The samples were then sputter-coated with gold for 30 seconds. Conductive silver paint was then applied to the sample perimeter to ensure good electrical conductivity between the stage and the specimen and to decrease the risk of sample charging. During microscope modelling, great attention was paid in selecting a typical picture of the surface, fully characterising each material.

3.5.9 Deposition of the chemical modifying layer

Three techniques to apply a chemical modifying layer to sonochemically fabricated sensors were investigated;

(i) the deposition of the modifying chemicals in the form of an emulsion by screen printing,

(ii) the immersion of the electrodes in an aqueous reagent solution (dip-coating) and,

(iii) the deposition of the modifying chemicals in the form of an aqueous solution via an ink-jet printing type procedure.

An emulsion suitable for screen printing was developed in conjunction with Gwent Electronic Materials Ltd. (Pontypool, Wales, UK) and screen printed upon sonochemically fabricated microelectrode arrays at Polyflex Circuits Ltd. (Parlex Corporation, Newport, Isle of Wight, UK). Electrodes were stored under desiccation until testing.

An aqueous total chlorine modifying layer solution (as described in Section 3.4.5) was used to dip-coat electrodes. Prior to immersion, the reference electrodes of the sensor strips were protected using insulating tape, so that the iodide in the reagent solution could not cause iodisation of the silver/silver chloride reference electrode. Electrodes were immersed perpendicularly in the solution for ~3 seconds and removed. Following immersion, the electrodes were dried flat in an oven for 10 minutes at 40°C and stored under desiccation until testing.

For investigations towards the suitability of an 'ink-jet' type printing system as a method for the deposition of aqueous modifying layer solutions, a BioDot AD3200™ dispense platform in conjunction with a BioJet Plus™ aspirate/dispense system was used (a schematic of which is given in Figure 3.14). Process settings specific to the sensor and solution types were pre-programmed by BioDot Ltd. prior to machine

delivery (the dispense positions are programmed as co-ordinates with the drops programmed in terms of drop volume and open time).

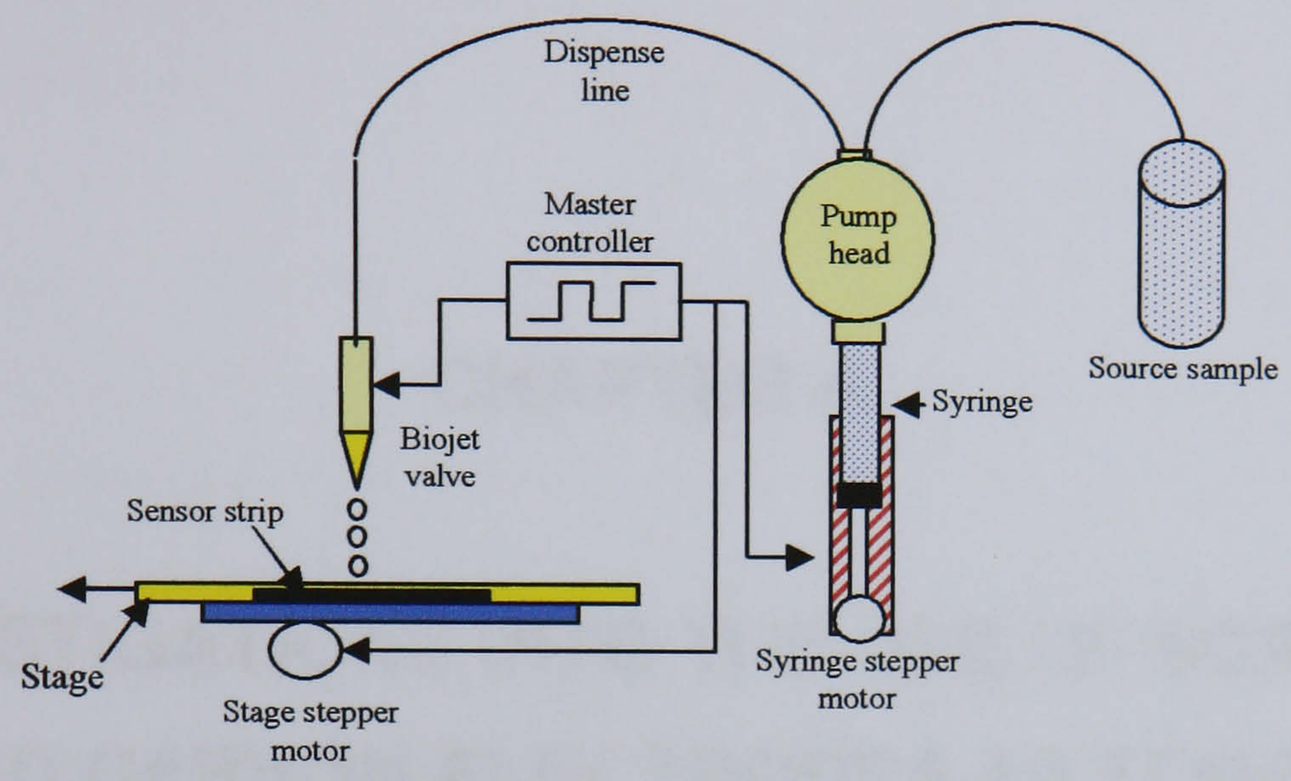

Figure 3.15 Schematic of the BioJet Plus™ aspirate/dispense technology.

A strip of 20 electrodes was cut from a sheet of sonochemically fabricated microelectrode arrays and placed in a fixed position on the dispense platform (see Figure 3.7). The total chlorine modifying layer solution (as described in Section 3.4.5) was placed in the sample source cylinder and 'primed' through the system in order to initialise the syringes and fill the feed lines, syringes and dispensers before dispensing. A sensor strip consisting of 20 sensors was then placed in a fixed position on the dispense platform. The solution was then deposited on each of the working electrodes via the 'line' dispense function according to the following settings: 28 drops of 0.3 mm drop pitch (the distance between each dispense) and 80 nL drop volume (amount of each drop dispensed). There was no need to protect the reference electrodes from the dispense solution since the accuracy of deposition is great enough to avoid any 'spill over' to this area. The sensor strip was then removed and dried in a still oven at 40 °C for 10 minutes and stored under desiccation until testing.

CHAPTER 4

INVESTIGATIONS INTO THE USE OF SCREEN PRINTED CARBON ELECTRODES AS TEMPLATES FOR SONOCHEMICALLY FABRICATED MICROELECTRODE ARRAYS – Part 1: Electrochemical Characterisation

4.1 INTRODUCTION

As discussed in Chapter 1, the primary aim of this research programme is to develop a disposable sensor for the determination of chlorine in aqueous solutions that exploits the sonochemical fabrication approach for microelectrode array production. Microarray Limited believes that this production format may provide a solution to the lack of commercial viability of chemical microelectrode-based sensors, due to the simplicity and inexpensiveness of the approach. It follows therefore, that to fully exploit the economic benefits of this new technology, an equally cost-effective base electrode material needs to be sought. One approach is to utilise miniaturised electrodes, screen printed using carbon inks. Therefore, the early intentions of this work are to examine the suitability of commercially available carbon inks as hosts for the fabrication and subsequent mass production of sonochemically produced microelectrode arrays.

The microfabrication of electrodes by way of thick-film (screen-printing) techniques presents the most promising route for the mass production of inexpensive and yet highly reproducible chemical sensing devices (Alvarez-Icaza & Bilitewski, 1993). Screen-printing methods and materials are already highly developed for the manufacture of capacitors, resistors and conductors used in hybrid electronic circuits, and resultantly, multilayer patterns deposited are repeatable in thickness and geometry. Miniaturisation is feasible, along with a high degree of electrochemical activity of the devices deriving from their specific area and microporous structure (Prudenziati, 1994). In addition, screen printing is a simple process and, because screen-printable inks have been highly developed, problems with mutual compatibility, sealing at the interface and adhesion to substrates may already have been solved.

It is not surprising then, that during recent years, the screen printing technology applied to sensor and biosensor construction has been considerably improved, and a large number of papers and reviews have appeared in the literature

(Hart & Wring, 1997; Albareda-Silvert *et al.*, 2000). Indeed, screen printed sensors are expected to be widely used in numerous real-life applications of controlled-potential techniques, and are already the devices of choice for the commercialisation of 'one-shot' glucose (Green & Hilditch, 1991) or metal (Wang, 1994) sensors.

In general, the screen-printing process involves a conductive or dielectric film being applied to a substrate by forcing through a patterned screen. The film is then baked (either by heating or photocuring) to drive off solvents from, and thus to cure, the patterned ink. This procedure may be repeated as often as screens are required to realise the final design of the sensor.

A wide range of inks and substrate materials may be used to mass produce low cost sensor strips. Silver-based inks are usually employed for obtaining reference electrodes and dielectric plus metallic oxides or some other binding material, are used for dielectric inks. Carbon or metal (such as platinum, gold or silver) ink formulations are commonly used for printing working electrodes. Such inks may also be utilised as bonding pads for electrical connections to the sensor instrumentation and/or as counter electrodes. In particular, carbon inks are attractive for sensing applications because they are relatively inexpensive and exhibit lower background currents over a wider potential window than metal electrodes, particularly in the cathodic region (Niwa & Tabei, 1994). Moreover, they exist in a variety of forms such as glassy carbon, carbon fibres or carbon (graphite) inks (Gilmartin & Hart, 1995). These attractive properties of carbon facilitate its use in various applications. Although glassy carbon is mostly used for research purposes, it is very difficult to machine due to its hard and brittle nature, thus confining itself to dimensions and shapes supplied by the manufacturer. Compared with glassy carbon, carbon (graphite) ink has the advantage of a lower residual current leading to higher signal/noise responses and correspondingly lower detection limits (Keller *et al.*, 1976; Caliguri & Mefford, 1984). Graphite based carbon ink electrodes also have the advantage of being robust, so they can be used as amperometric sensors in stirred solutions (Wring *et al.*, 1990). They can also be produced in large numbers at low

cost and since they are designed to be used once and then discarded, they are more convenient to use than solid electrodes, which need to be renewed or repolished.

In general, carbon inks are composed of graphite particles, a polymer binder and other additives (for the dispersion, printing and adhesion tasks). The exact ink formulation is regarded by the manufacturer as proprietary information. Such differences in this heterogeneous surface and composition of inks (e.g. type, size or loading of graphite particles), and in the printing and curing conditions, may strongly affect the electron transfer reactivity and overall analytical performance of the resulting carbon sensors. It is important therefore, to study in detail the analytical performance of the base (planar) carbon ink electrodes before any further research is undertaken. For that reason, this chapter will focus towards investigations into the performance of planar screen printed carbon electrodes with the intention of demonstrating the sensing utility of such electrodes for generic applications, and in order to facilitate the selection of the appropriate carbon for the specific application described in this study.

Previous studies by Wang *et al.* (1998) have shown (from data on the background currents, potential windows and the electrochemical activity of carbon inks to redox systems), that different compositions and preparations of carbon electrodes have a profound effect upon their electrochemical behaviour and electroanalytical utility. Section 4.2 therefore evaluates and compares the performance of two different commercially available carbon inks via interrogation with benchmark redox couples in terms of reversibility, operational potential range, background currents and steady-state response characteristics. In order to describe the electrochemical behaviour of carbon ink electrodes as reliably as possible, carbon inks were also subjected to investigations onto their surface structure using scanning electron microscopy techniques. Microscopic studies on the surface of the screen printed carbon ink electrodes provides further understanding of the electrochemical behaviour of the carbon inks by correlation to the carbon microstructures and morphology. This section also serves to identify a suitable redox couple for the characterisation of microelectrode arrays in further chapters.

As with any electrode material, the choice of working electrode should depend upon the specific electroanalytical application and technique used. For example, studies by Wang *et al.* (1998) have shown that a particular carbon ink may possess, for example, low dependency on background contributions, making it ideal for amperometric interrogation, but may also be accompanied with high residual currents that render it less desirable for voltammetric adsorptive or stripping determinations. It is important then to characterise the base electrodes to their response to chlorine probes via amperometry. The sensing utility of both carbon inks is therefore demonstrated for free and total chlorine probes in Section 4.3. Experiments were also performed to establish the true reduction potentials for free and total chlorine and the optimum amount of potassium iodide required for the measurement of total chlorine at carbon screen printed ink electrodes.

Conclusions made in this chapter will determine the carbon ink composition for the base sensor used in all further chapters and will help in the development of screen printed carbon electrodes for other sensing applications with easily available carbon inks.

4.2 ELECTROCHEMICAL BEHAVIOUR OF STANDARD REDOX COUPLES AT BARE (PLANAR) CARBON ELECTRODES

As different carbon inks can differ strongly in their electrochemical properties, the aim of this section is to compare the electrochemical behaviour and analytical performance of screen-printed sensors fabricated from two different carbon inks. Planar (macroscopic) electrodes fabricated from carbon inks supplied by both Gwent Electronic Materials (GEM) and DuPont Microcircuit Materials are examined in each case (detailed descriptions of the electrodes are given in Section 3.2). The electrochemical characterisation was initially performed by cyclic voltammetry in pH 7.8 phosphate buffer at a scan rate of 20 mVs^{-1} in three different redox couples, chosen as their investigation should find broad utility for electroanalytical and future sensing applications. Figures 4.1a, 4.1b and 4.1c display cyclic voltammograms for 5 mM potassium ferricyanide(III), 1 mM hexaammineruthenium(III) chloride and 1 mM ferrocenemonocarboxylic acid, respectively. The resulting cyclic voltammetric peak separations (ΔE_p), anodic peak potentials (E_{pa}) and anodic peak currents (i_{pa}) of each ink are compared and summarised in Table 4.1.

Table 4.1 Summary of voltammetric peak separations, anodic peak potentials and anodic peak currents for three redox systems at two different carbon electrodes.
(All potentials quoted vs. Ag/AgCl).

		GEM	DuPont
Potassium Ferricyanide(III)	ΔE_p (mV)	–	–
	E_{pa} (mV)	421	420
	i_{pa} (μA)	8.7	4.3
Hexaammineruthenium(III) chloride	ΔE_p (mV)	101	80
	E_{pa} (mV)	289	293
	i_{pa} (μA)	10.3	9.2
Ferrocenemonocarboxylic acid	ΔE_p (mV)	115	100
	$E_{,a}$ (mV)	220	220
	i_{pa} (μA)	15.7	14.7

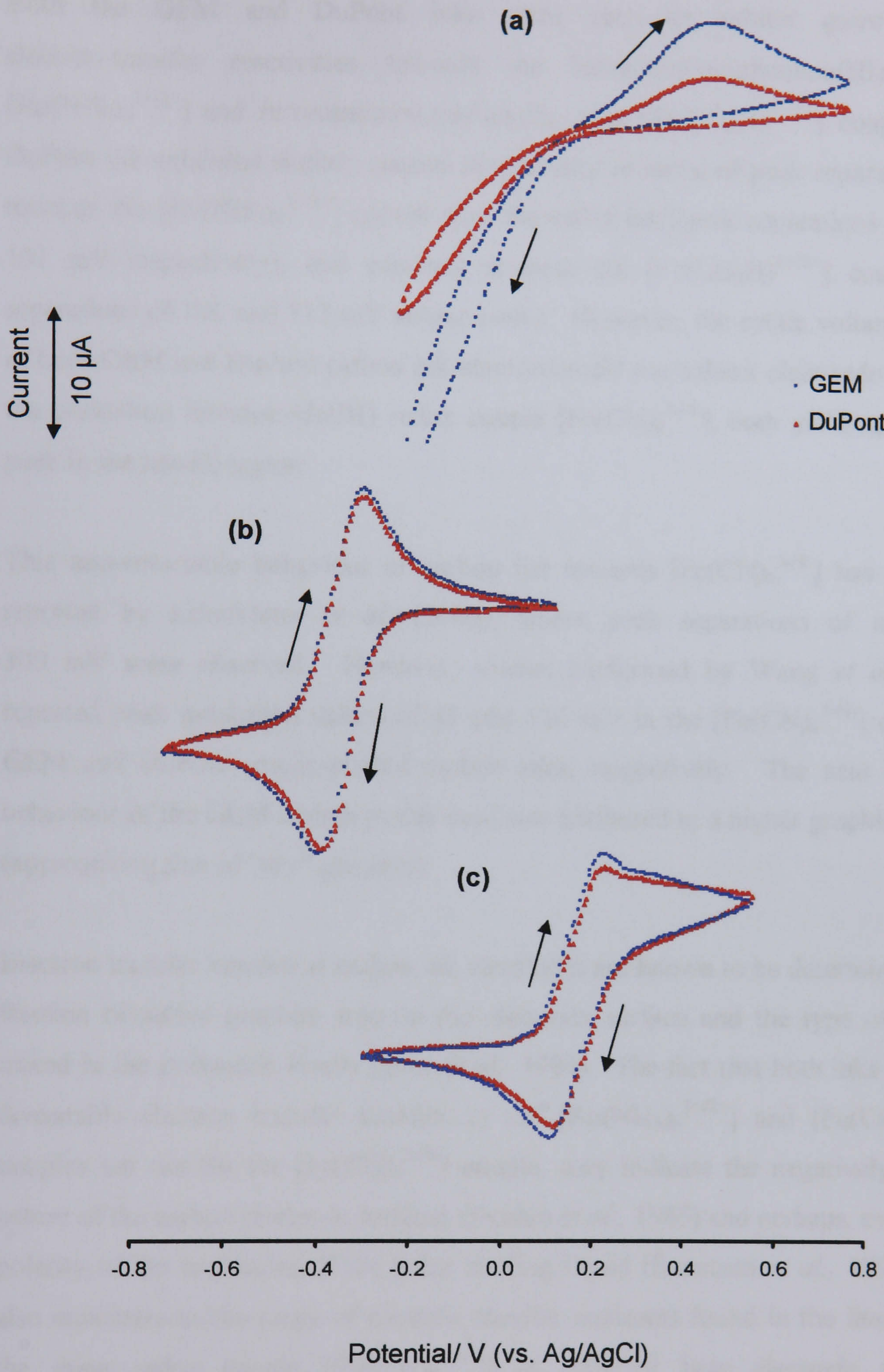

Figure 4.1 **Cyclic voltammograms for three different redox couples; (a) 5 mM potassium ferricyanide(III) (b) 1mM hexaammineruthenium(III) chloride and (c) 1mM ferrocenemonocarboxylic acid, at screen printed electrodes prepared with two different commercial carbon inks; GEM and DuPont.**
[Supporting electrolyte: phosphate buffer (pH 7.8, 0.1 M). Scan rate: 20 mVs^{-1}].

Both the GEM and DuPont inks were seen to exhibit *quasi*-reversible electron-transfer reactivities towards the hexaammineruthenium(III) chloride [$Ru(NH_3)_6^{3+/2+}$] and ferrocenemonocarboxylic acid [$Fc(CO_2H)^{3+/2+}$] couples. The DuPont ink exhibited slightly greater reversibility in terms of peak separation (ΔE_p) towards the [$Ru(NH_3)_6^{3+/2+}$] system than the GEM ink (peak separations of 80 and 101 mV respectively), and similarly towards the [$Fc(CO_2H)^{3+/2+}$] couple (peak separations of 100 and 115 mV respectively). However, the cyclic voltammograms of both GEM and DuPont carbon ink electrodes did not exhibit clear redox peaks to the potassium ferricyanide(III) redox couple [$Fe(CN)_6^{3-/4-}$], both yielding only one peak in the anodic region.

This non-reversible behaviour of carbon ink towards [$Fe(CN)_6^{3-/4-}$] has also been reported by Erlenkötter *et al.* (2000), where peak separations of more than 300 mV were observed. However, studies performed by Wang *et al.* (1998), reported peak separation values of 63 and 126 mV in the [$Fe(CN)_6^{3-/4-}$] couple for GEM and DuPont screen-printed carbon inks, respectively. The near Nernstian behaviour of the GEM carbon in this case was attributed to a higher graphite loading (approaching that of "dry" graphite).

Electron transfer kinetics at carbon ink electrodes are known to be determined by the fraction of active graphite area on the electrode surface and the type of graphite mixed in the polymeric binder (Rice *et al.*, 1983). The fact that both inks exhibited favourable electron transfer kinetics to the [$Ru(NH_3)_6^{3+/2+}$] and [$Fc(CO_2H)^{3+/2+}$] couples but not for the [$Fe(CN)_6^{3-/4-}$] couple, may indicate the negatively charged nature of the carbon electrode surfaces (Deakin *et al.*, 1985) and perhaps, even by the polarity of the molecules of the polar binding liquid (Švancara *et al.*, 1996). This also correlates to the range of electron transfer constants found in the literature for the same redox couple ([$Fe(CN)_6^{3-/4-}$]) at different base electrode materials: 2.2×10^{-3} cm s^{-1} at a screen printed carbon ink electrode from GEM, 8.2×10^{-3} cm s^{-1} for the same carbon ink after pre-treatment and 1.2×10^{-2} cm s^{-1} for glassy carbon (Grennan *et al.*, 2001).

In all cases (i.e. for each redox couple at both carbon inks), the peak separation values are considerably greater than the ~59 mV expected for a Nernstian diffusion controlled one-electron transfer reaction. The non-homogenous nature of screen printed electrodes has been postulated as the reason for the often observed (Patel *et al.*, 2001; Wang *et al.*, 1998), non-reversible or *quasi*-reversible behaviour of some redox couples at carbon electrodes. It has been suggested (Rice *et al.*, 1993), that the ΔE_p values are an indicator for the charge transfer inhibition within the materials, consistent with the presence of a pasting or binding liquid. Due to the non-homogenous surface composition of screen-printed electrodes, the active area of those electrodes may be much smaller than the geometrical electrode area. These factors are typical of the constraints of the screen printing process, resulting in the redox activity and overall analytical performance of the electrodes to be compromised to some extent.

The peak current values (i_{pa}) suggest a greater electroactivity of the GEM ink than the DuPont ink. This is especially apparent in the $[Fe(CN)_6^{3-/4-}]$ couple, where the peak current for the GEM ink is nearly double that of the DuPont (8.7 and 4.3 μA respectively). Again, this large difference in electron transfer kinetics for the $[Fe(CN)_6^{3-/4-}]$ couple among the inks may be attributable primarily to the type or ratio of propriety polymer binders and/or graphite used in the two pastes. The difference in peak current values between the inks when tested in the $[Ru(NH_3)_6^{3+/2+}]$ and $[Fc(CO_2H)^{3+/2+}]$ couples is ~1 μA, with the GEM ink again providing the highest i_{pa} value in both cases. These results suggest that the GEM ink would be favourable in cases where a negatively charged complex is to be analysed.

Figure 4.2 compares linear background voltammograms for pH 4.0 and pH 7.0 phosphate buffers at both GEM and DuPont electrodes. The buffers were chosen as they are the electrolytes required for the analysis of chlorine solutions in further investigations within this work, in addition to being typical of the buffers that may be required for use when developing future intended sensing applications.

The GEM and DuPont ink electrodes exhibit comparable background responses, although the GEM ink exhibits the narrower potential window in both electrolyte solutions, particularly with respect to the cathodic potential limit (i.e. the potential at which oxygen is reduced). The difference in background response (in terms of signal size) of the GEM and DuPont inks can be attributed to the marginally stronger electrochemical reactivity of the GEM ink seen previously in Table 4.1. The differences in background currents exhibited by the two inks may only have a profound effect upon their analytical utility if the intended electroanalytical application allows it. For example, it is generally considered that amperometric sensing is less dependant on background currents (as they are usually performed after the decay of transient currents to steady-state values) than other modes of electroanalysis, such as voltammetric or stripping work.

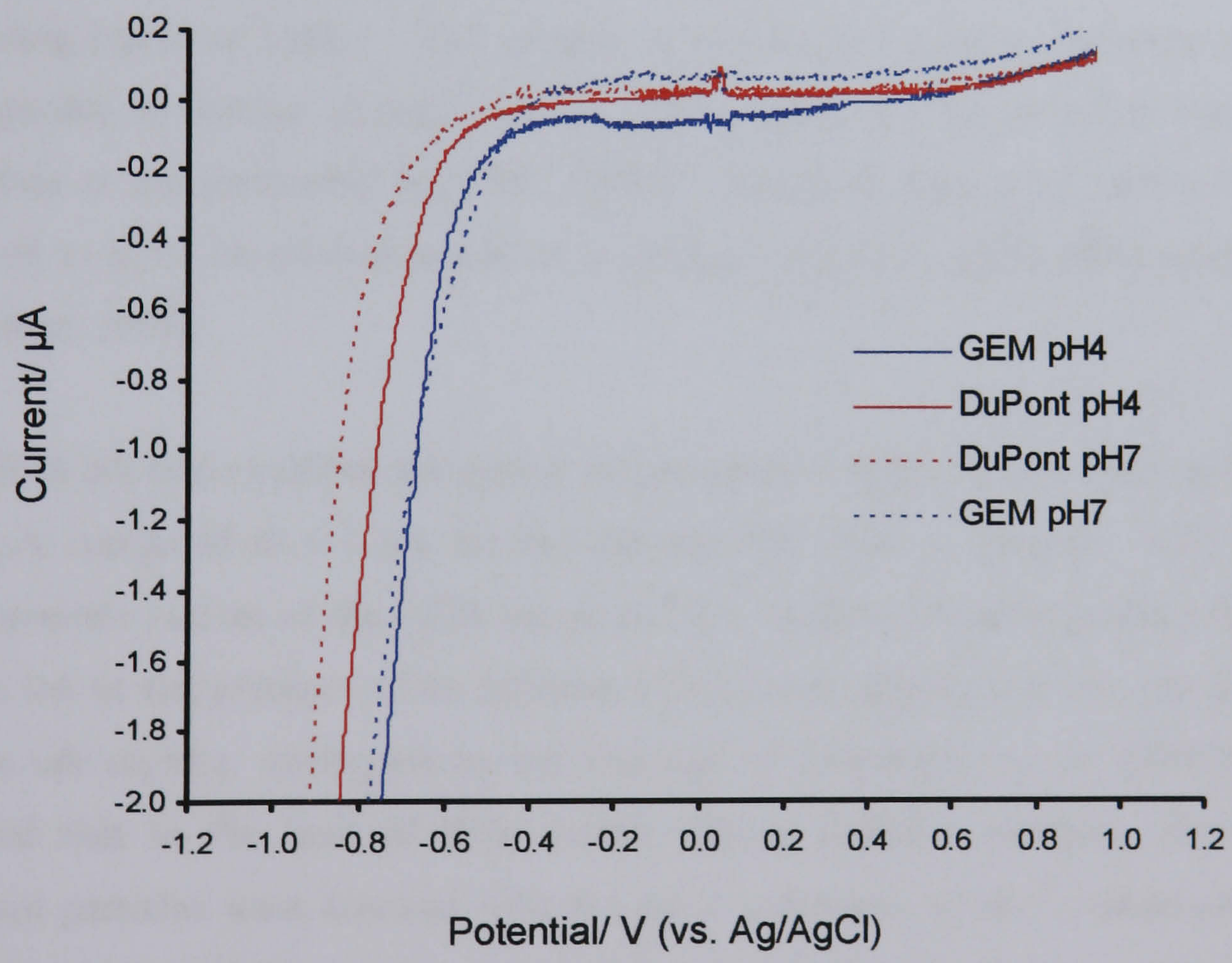

Figure 4.2 Linear scan background voltammograms for two different electrolyte solutions: (a) phosphate buffer (pH 7.0, 0.1 M) and (b) phosphate buffer (pH 4.0, 0.5 M), at screen printed electrodes prepared with two different commercial carbon inks from GEM and DuPont.

[Scan rate: 20 mVs^{-1}. Solutions purged with nitrogen for 20 minutes].

It is useful however, to compare the amperometric response of both electrodes in terms of reproducibility, time to steady-state response and signal magnitude, in order to demonstrate the practical utility, in these terms, of each carbon ink. Ten electrodes (both GEM and DuPont inks) were polarised at -0.35 V (vs. Ag/AgCl) in 1 mM hexaammineruthenium(III) chloride (chosen because of its favourable reversibility out of the three redox couples previously examined), for 1 minute. Figure 4.3 compares the resulting current-time transients obtained at GEM (Figure 4.3a) and DuPont (Figure 4.3b), carbon ink electrodes. Both inks exhibit a slow 'wet-up' (i.e. time to reach a steady-state response), as compared to gold electrodes (not shown). A slow decay in current is characteristically measured during chronoamperometric experiments on carbon inks and is consistent with the presence of surface functional groups which undergo slow electrolysis reactions during area measurement experiments (Zhang & Coury, 1993). This suggests that the active surfaces of some graphite particles are covered partly or completely by a microfilm of pasting liquid or binder. The surface of carbon electrodes is therefore largely hydrophobic in nature (Kalcher *et al.*, 1995), affecting the character electrode processes at the electrodes (Kalcher, 1990). The slow wet-up of carbon inks is reported to often be misinterpreted as a surface roughness (area) effect (Coury & Heineman, 1988).

The GEM ink again exhibits the greater electroactivity, with a steady-state current of 10.8 μA compared to 9.3 μA for the DuPont ink (after 1 minute). This larger amperometric current of the GEM ink could be a result of a higher graphite loading of this ink or the presence of an adherent (inhibitory) organic layer on the DuPont carbon ink surface, analogous to the findings of Erlenkötter *et al.* (2000), who reported that in the case of their screen printed platinum working electrodes, platinum particles were covered with the ink's polymeric binder component, thus rendering these particles inaccessible to electrochemical reactions. Interestingly, the DuPont ink, although providing a smaller steady-state current, is seen to be more reproducible than the GEM ink, possessing a relative standard deviation (RSD) of response of 0.78 % compared to 1.7 % for the GEM ink. This may be due to the

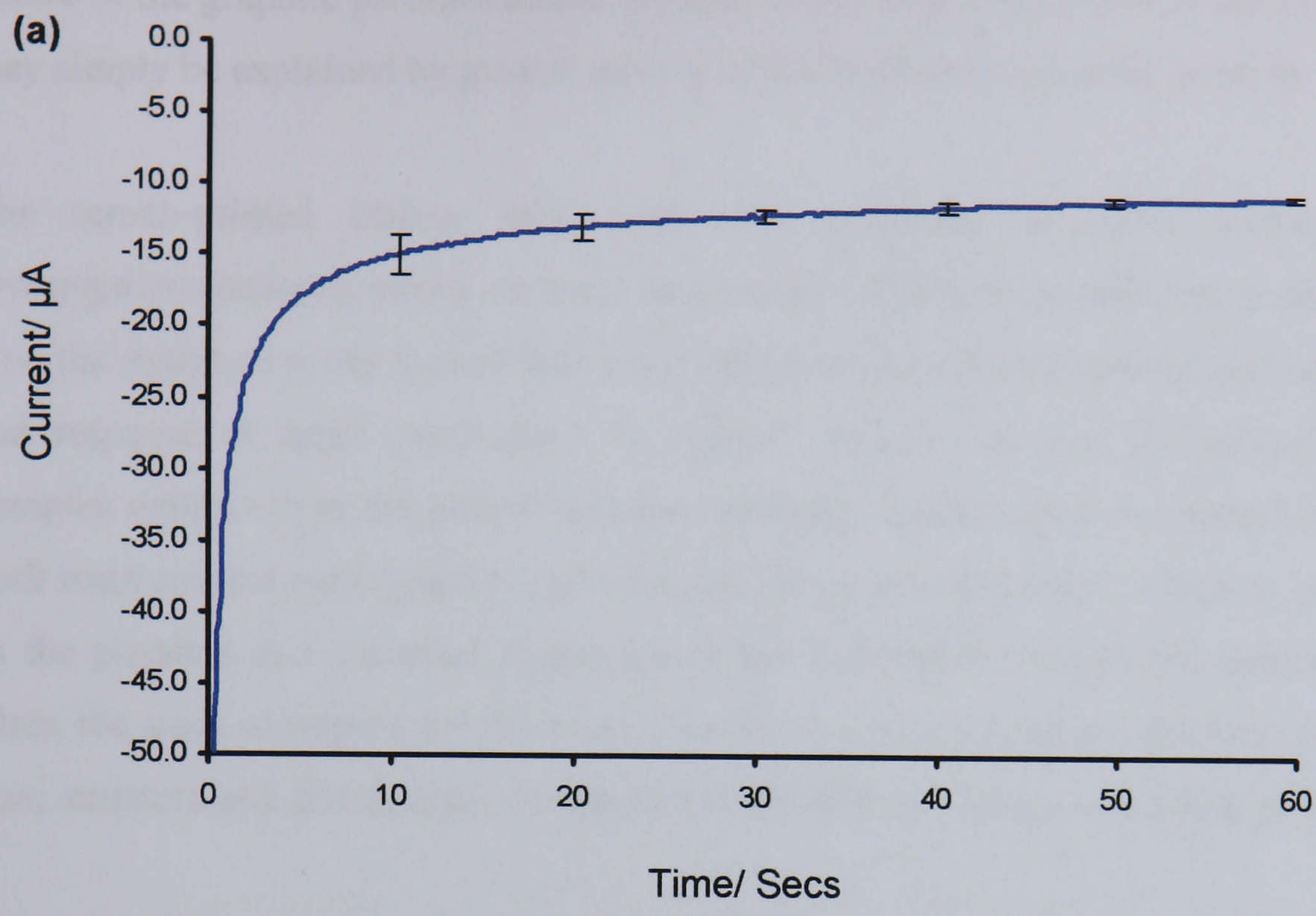

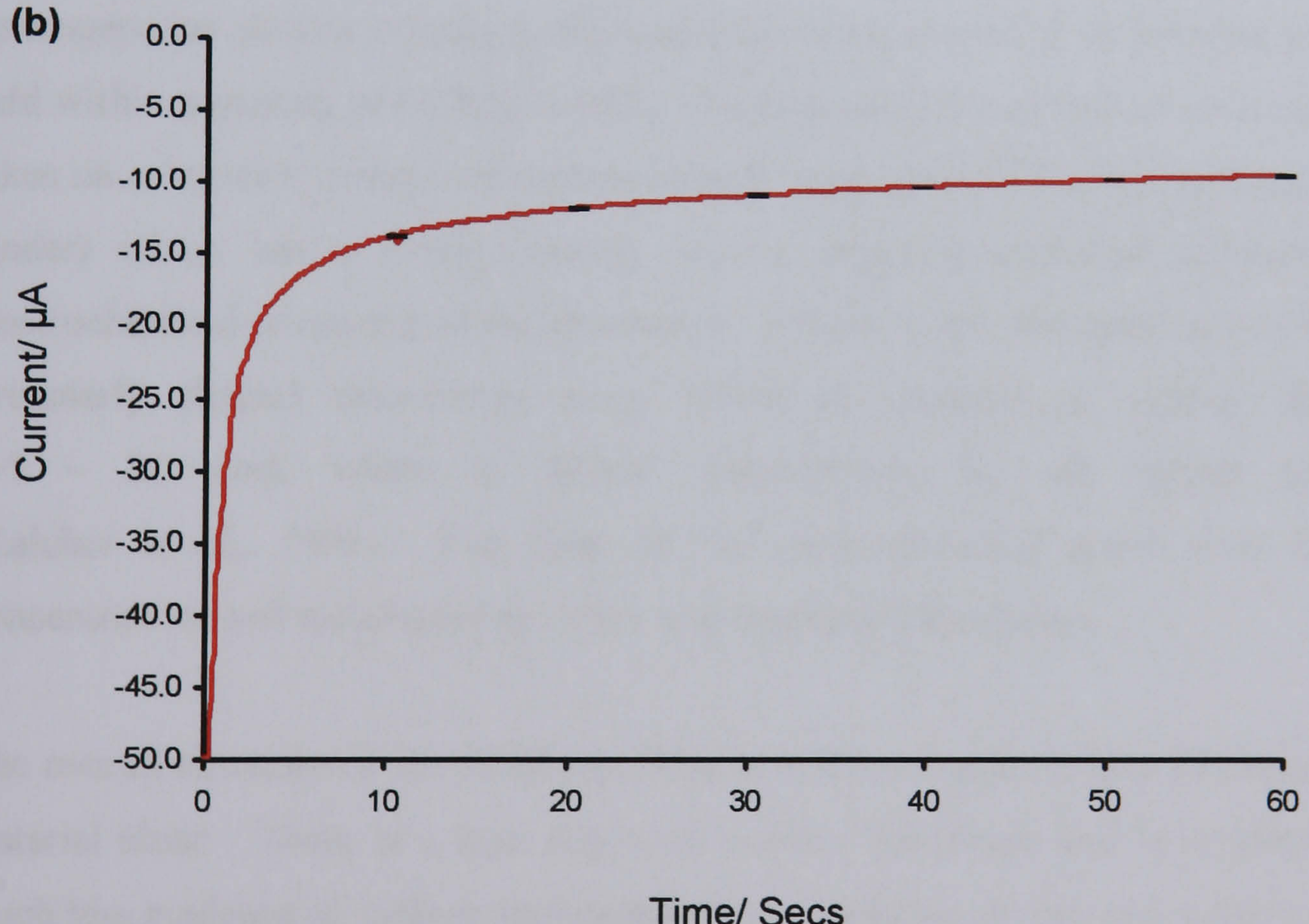

Figure 4.3 Current-time transients of 1mM hexaammineruthenium (III) chloride at screen printed (a) GEM and (b) DuPont, carbon electrodes.
[Supporting electrolyte: phosphate buffer (pH 7.8, 0.1 M) purged with nitrogen for 20 minutes. Polarising potential: -0.35 V (vs. Ag/AgCl)].

nature of the graphite particles and/or oxygen-containing surface functionalities, or it may simply be explained by greater mixing of the DuPont ink prior to printing.

The screen-printed carbon inks were also subjected to direct microscopic investigations using scanning electron microscopy (SEM), in an effort to understand how the structure of the carbon inks may influence the electrochemical conductivity and response at these electrodes. In general, carbon ink (and its surface) is a complex matrix where the overall structure strongly depends upon the mutual ratio of both main components (graphite particles and the polymeric binder or liquid), as well as the physical and chemical properties of the individual components themselves. Thus, the areas of interest are the overall surface topography and the graphite particle size, structure and distribution in relation to the surface coverage of binding polymer.

Figure 4.4 shows the typical morphological features of a GEM (Figure 4.4a) and DuPont (Figure 4.4b) carbon ink electrode before use. Both micrographs display a heterogeneous surface structure, characterised as an ensemble of graphite particles held within a pasting or binding liquid. Consequently, the surface of such materials takes on a 'mosaic' pattern of microstructures (aggregates of carbon and regions of binder) which has a strong bearing on the resulting electrical resistance and electrochemical properties of the electrodes. In both cases, the surface is formed by irregularly shaped micrometer sized flakes of graphite of various diameter (~5 – 20 μm), which is almost characteristic for all carbon powders (Kalcher *et al.*, 1995). The form of the electrochemical active sites (surface concentrations and distributions) varies with each ink formulation.

The overall structure of the GEM ink (Figure 4.4a) is similar to that of the graphite material alone. There is a high degree of surface roughness and void spaces with much less evidence of surface binding polymer, producing a film with a microporous structure. The DuPont ink (Figure 4.4b) shows a more uniform surface topography formed by either the close assembling of the graphite particles or an increased amount of polymeric binder. The more uniform and lighter shading of grey would

(a)

(b)

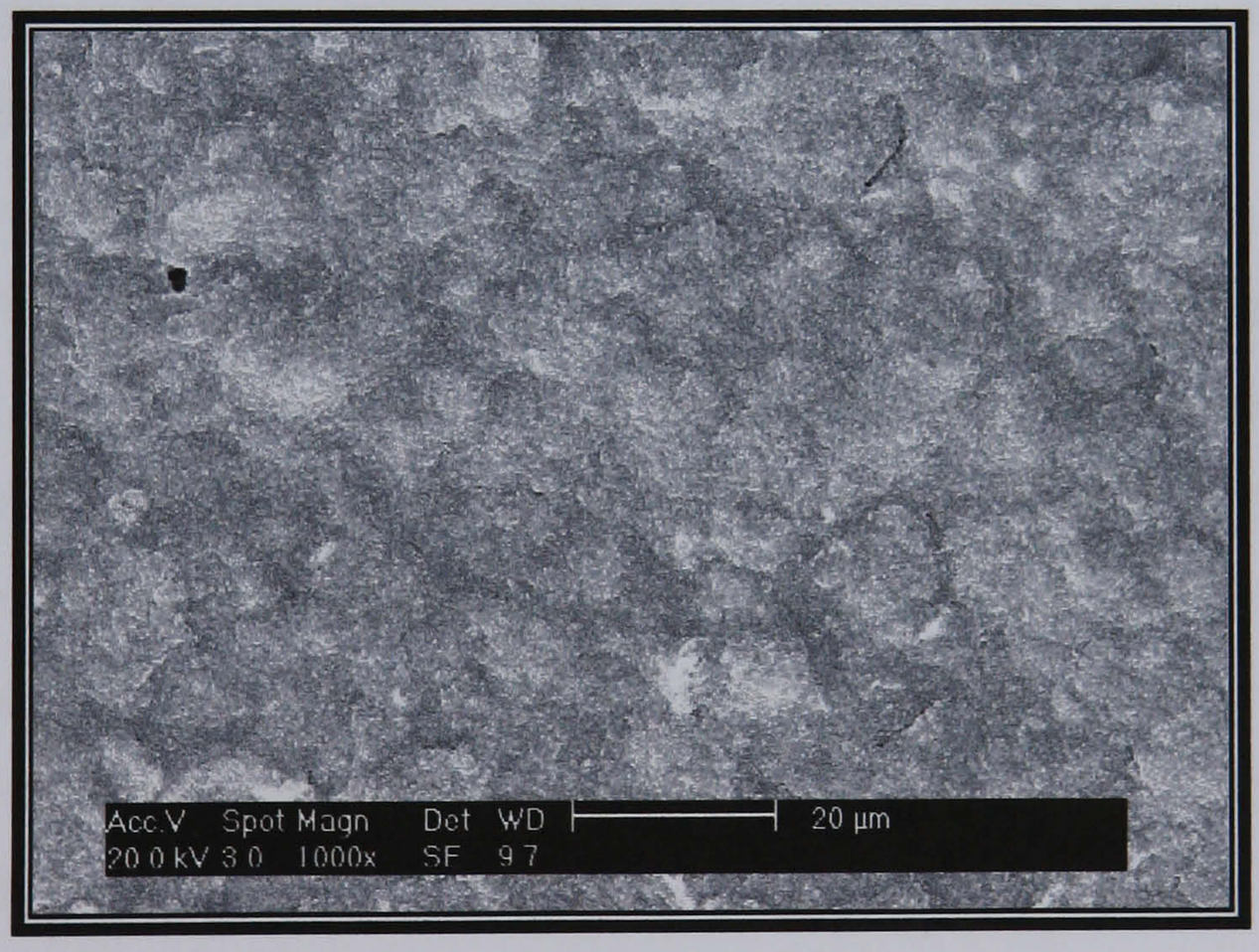

Figure 4.4 Scanning electron micrographs of the carbon reactive surface of screen printed electrodes fabricated from (a) GEM, and (b) DuPont, carbon inks.
(x 1000 magnification).

possibly lead one further towards the conclusion that the graphite flakes are embedded more evenly inside a polymeric binder and that the graphite particles are covered by a thin film of binder liquid.

The micrographs serve to confirm the conclusions made from the electrochemical analyses described earlier in the chapter. Valentini *et al.* (2003) have shown, albeit in the case of carbon nanotube electrodes, that those with a composition similar to dry carbon powder (i.e. *less binder*) exhibit an enhanced electroanalytical response in terms of higher currents and lower peak separations. Results here have shown that the best performance, in terms of anodic peak current in cyclic voltammetric experiments and steady-state current with amperometric interrogation, was obtained for the GEM ink. The micrographs confirm that this is indeed due to the apparent high ratio of graphite/binder.

Previous work by Rice *et al.* (1983) reported that the electroactivity of carbon inks with *higher binder* composition resulted in a wider peak separation for the $[Fe(CN)_6^{3-/4-}]$ redox couple. Rice *et al.* concluded that this was due to the amount of graphite particles decreasing with increasing binder, producing a higher resistance at the ink surface. We have already demonstrated a lower electroactivity of the DuPont ink in this work, showing a lower anodic peak current with cyclic voltammetry (in the case of $[Fe(CN)_6^{3-/4-}]$) and a lower steady-state current in amperometric experiments (in the case of $[Ru(NH_3)_6^{3+/2+}]$) as compared to the GEM ink. Again, the micrograph of the DuPont electrode surface suggests this is due to the high amount of binder, hampering the electrical communications between graphite particles and thus resulting in a higher resistance and thus a lower current.

The difference in surface topography features of the inks may explain why the DuPont ink electrode shows better reproducibility of amperometric signal in $[Ru(NH_3)_6^{3+/2+}]$ than the GEM ink electrode. Coury & Heineman (1988) have suggested that during electrochemical experiments, local pH gradients may arise in the pores of highly uneven surface carbon inks, as redox reactions of the surface carbon oxides invariably involve coupled proton transfers. Furthermore, it is

envisaged that the smoother and more homogenous surface of the base DuPont carbon ink electrode would be more favourable for the further processes involved in the sonochemical fabrication of the microelectrode arrays since large void areas and pores may act as irregular nucleation sites for sonochemical ablation.

Film resistance measurements were performed using a digital voltmeter with a centimetre separation between points. Film resistance is affected by several factors, including the dielectric nature of the polymer and the conductivity of the carbon components, as well as the proportions of these materials within the formulation and their distribution in the dried film. Resistance values for the carbon inks were determined across the film and are expressed here in terms of ohms per cm of the coating. The GEM and DuPont inks have a film resistance of 560 Ω cm^{-1} and 1.3 kΩ cm^{-1}, respectively. The lesser quantity of insulating binder in the GEM ink increases the tendency for the graphite particles to form tracks of conducting aggregates throughout the film, resulting in a lower electrical resistance as compared to the DuPont ink. The consequence of this decreased surface conductivity exhibited by the DuPont ink is reflected in lower currents obtained at this electrode with the electrochemical characterisations previously made. The fact that there was little difference in the peak separations between the two carbon inks, despite their differing resistivities, can be explained by looking at the work of Seddon *et al.* (1997). Seddon *et al.* calculated that reasonable changes in bulk resistances (based on the sensitivity of resistance with respect to carbon content as being 81 Ω per percentage change in carbon in the film) would contribute to shifts in ΔE_p values of only a few millivolts. By using the method of Seddon *et al.*, we can estimate the difference in carbon content between the GEM and DuPont inks as being approximately 9.13 %.

To obtain more detailed information about the influence of the physical and chemical properties of carbon, microscopic observations using SEM could be further adapted for sub-micrometer scale or combined with other techniques such as scanning tunnelling microscopy.

4.3 ELECTROCHEMICAL BEHAVIOUR OF CHLORINE PROBES AT BARE (PLANAR) CARBON ELECTRODES

Previous studies on the performance of screen-printed carbon electrodes have concluded that the choice of carbon ink should depend upon the analyte under investigation and specific electrochemical technique used (Wang *et al.*, 1998). It is important therefore to investigate the behaviour of the chosen carbon ink to chlorine species via amperometric interrogation.

As discussed in Chapter 2 (Section 2.8.3), only free available residual chlorine and total available residual chlorine can be measured electrochemically (combined chlorine can be quantified by subtracting the amount of free chlorine from the total). For free chlorine, the process that occurs at the working electrode can be represented by Equation 4.1:

$$HOCl + 2e^- \rightarrow Cl^- + OH^- \qquad (4.1)$$

Total available chlorine is measured electrochemically by the addition of potassium iodide, which reacts with the chlorine present in the sample to liberate iodine. Iodine is then reduced at the working electrode to according to Equation 4.2:

$$I_2 + 2e^- \rightarrow 2I^- \qquad (4.2)$$

Thus, screen printed carbon electrodes were characterised in this section with respect to the possibility of them amperometrically and reproducibly measuring the two couples, [$HOCl/Cl^-$] and [$I_2/2I^-$].

4.3.1 Selection of applied potential for amperometric determination of free and total chlorine solutions

The choice of the applied potential at the working electrode is fundamental to achieve the lowest detection limit, whilst avoiding possible electrochemical interfering species. Therefore, before measuring the sensitivity of the planar carbon screen printed electrodes to chlorine solutions, the optimal polarisation potentials for both iodine (total chlorine determination) and hypochlorous acid (free chlorine determination) were firstly determined using DuPont screen-printed carbon electrodes. Comparable results were obtained at GEM electrodes and therefore, for clarity, plots are not repeated here.

Figure 4.5 shows a cyclic voltammogram of a carbon electrode in 10 mg/l (10 ppm) total chlorine (with added iodide). From this cyclic voltammogram, it can be seen that the reduction peak relating to the reduction of iodine (I_2) to iodide ($2I^-$) occurs at approximately -0.08 V (vs. Ag/AgCl). To verify this, the electrode current as a function of polarisation potential was measured in a background phosphate buffer (pH 4.0) with (upper curve) and without (lower curve) 10 mg/l total chlorine, at seven different values of potential near to 0.0 V (vs. Ag/AgCl) (Figure 4.6).

Both iodide and oxygen can give rise to a reductive signal. The lower curve shows that at the most cathodic potential of -0.3 V (vs. Ag/AgCl), the reduction of oxygen begins and an offset current due to this reduction is reflected in the upper curve. At potentials greater than approximately -0.15 V (vs. Ag/AgCl), this offset current is largely suppressed. From the upper curve a current plateau can be observed between +0.05 and -0.15 V (vs. Ag/AgCl). Here exists a "potential window" where iodine reduction is relatively potential independent and there is no interference from the reduction of dissolved oxygen. Therefore, -0.08 V (vs. Ag/AgCl) was taken as the optimal working potential to prevent any interference from dissolved oxygen whilst providing a sufficiently high reduction current to be measured without difficulty.

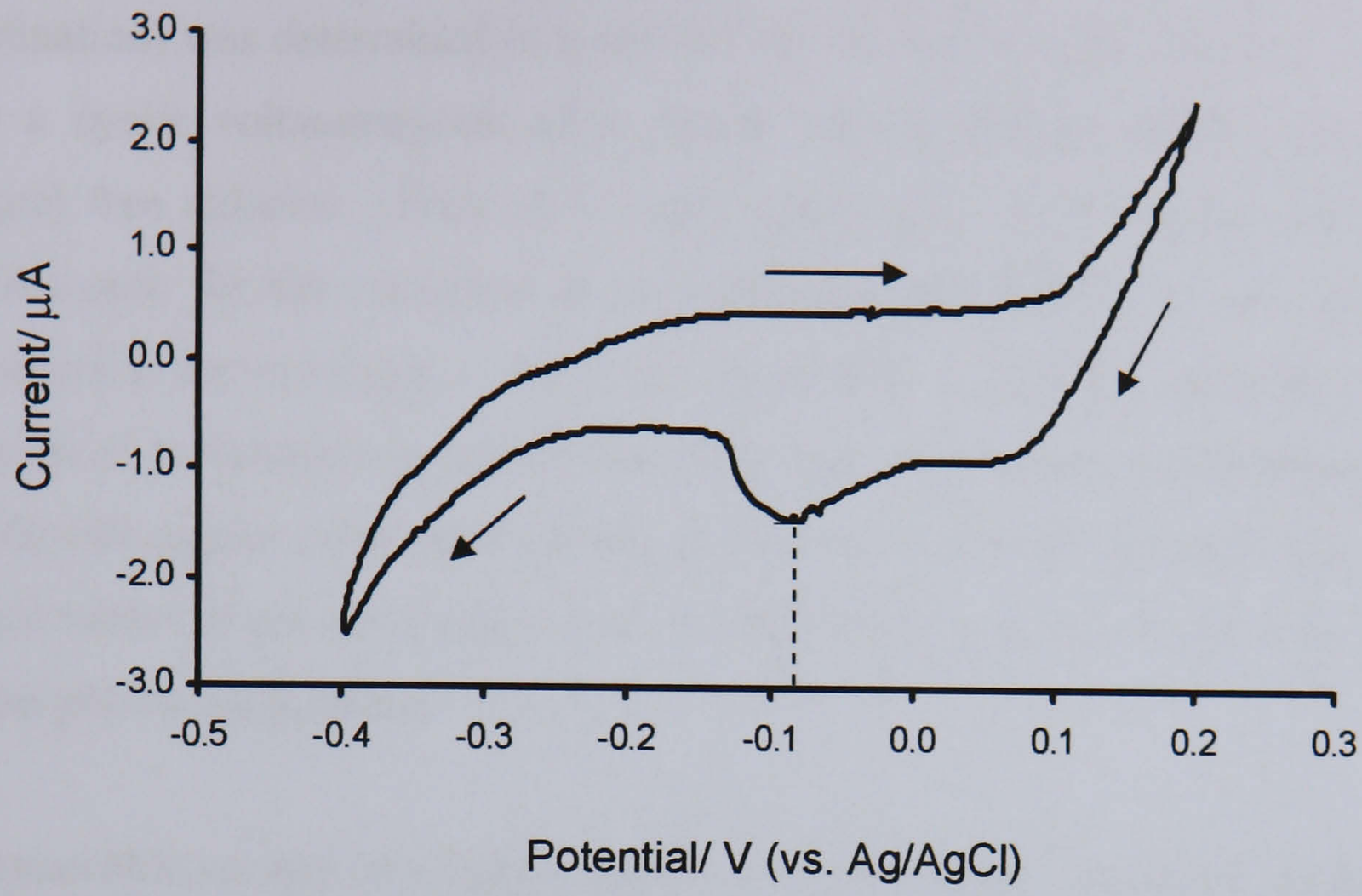

Figure 4.5 Cyclic voltammogram of 10 mg/l total chlorine.
[Supporting electrolyte: phosphate buffer (pH 4.0, 0.5 M). Scan rate: 20 mVs^{-1}].

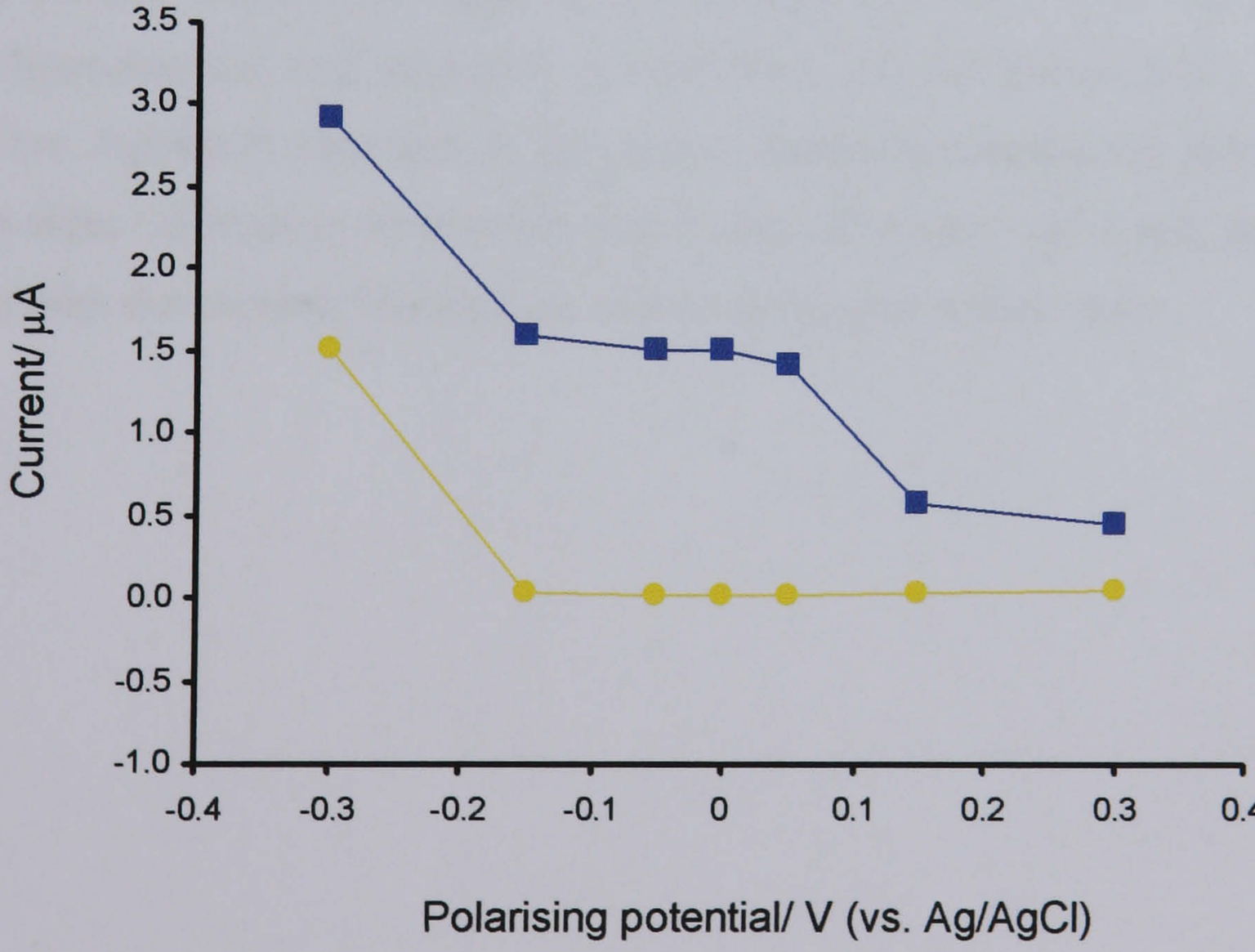

Figure 4.6 Current as a function of polarisation potential with (upper curve) and without (lower curve) 10 mg/l total chlorine.
[Supporting electrolyte: phosphate buffer (pH 4.0, 0.5 M)].

The optimal polarisation potential for hypochlorous acid (free chlorine determination) was determined in a similar way to that of total chlorine. Figure 4.7 shows a cyclic voltammogram of a screen printed carbon electrode in 10 mg/l (10 ppm) free chlorine. From this cyclic voltammogram, it can be seen that the reduction peak for the reduction of hypochlorous acid (HOCl) to the chloride ion (Cl^-) occurs at approximately -0.06 V (vs. Ag/AgCl). Again, the electrode current as a function of polarisation potential was measured in a background phosphate buffer (pH 7.0) with (upper curve) and without (lower curve) 10 mg/l free chlorine, at seven different values of potential near 0.0 V (vs. Ag/AgCl) (Figure 4.8), in order to verify the ideal polarising potential.

Both hypochlorous acid and oxygen gave a reductive signal. However, it can be seen from the lower curve that it is at potentials more cathodic than -0.15 V (vs. Ag/AgCl), that the reduction of oxygen begins and the offset current due to the oxygen reduction is again observed in the upper curve. At potentials more *anodic* than -0.15 V (vs. Ag/AgCl), this offset current is largely suppressed. In this case, no current plateau exists in the upper curve and therefore there is no region, as such, where hypochlorous acid reduction is relatively potential independent. Therefore, -0.1 V (vs. Ag/AgCl) was taken as the optimal reduction potential for free chlorine as this provides the highest interference/signal ratio allowable whilst still being able to be confident that no interference from dissolved oxygen would occur.

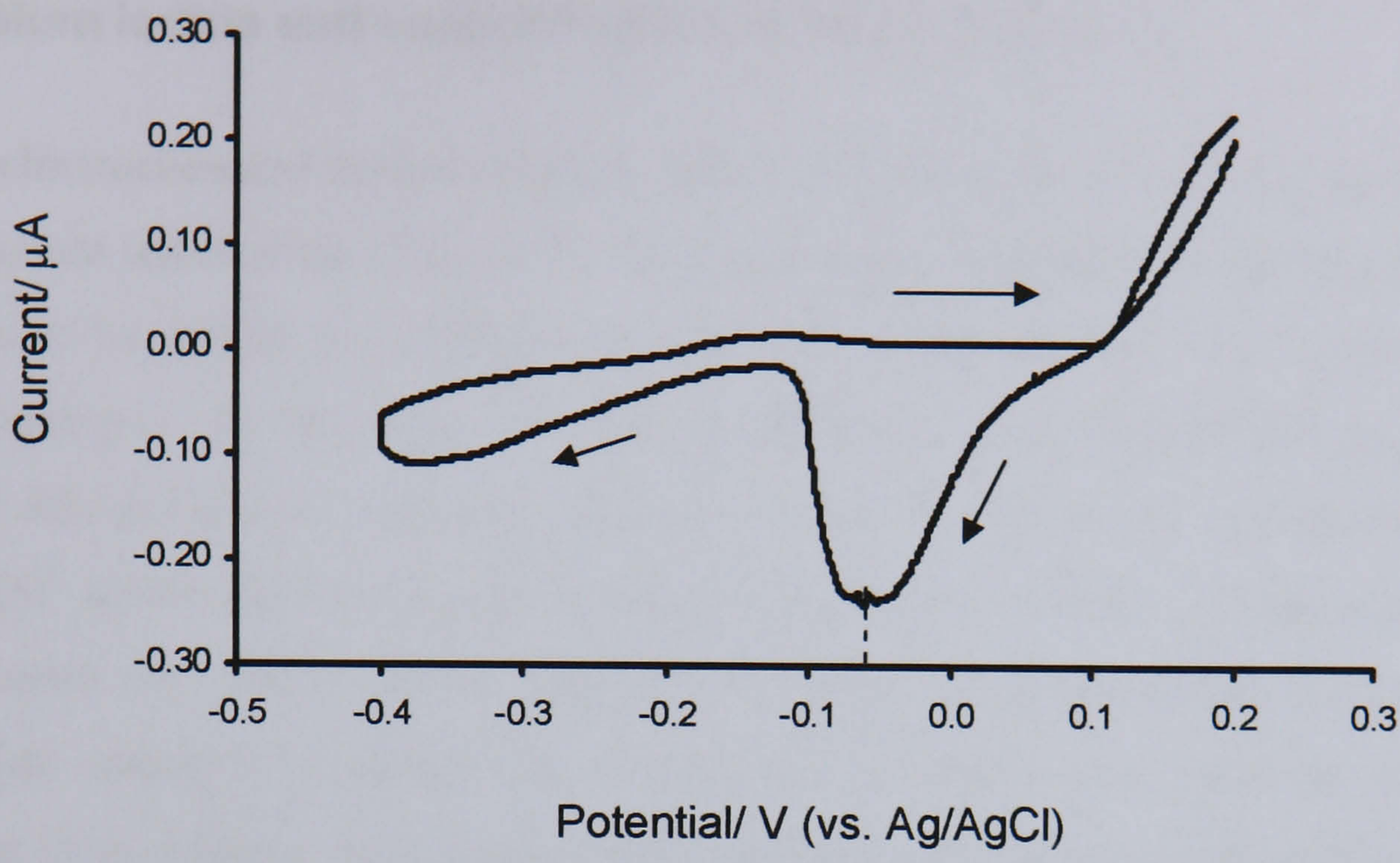

Figure 4.7 Cyclic voltammogram of 10 mg/l free chlorine.
[Supporting electrolyte: phosphate buffer (pH 7.0, 0.1 M). Scan rate: 20 mVs^{-1}].

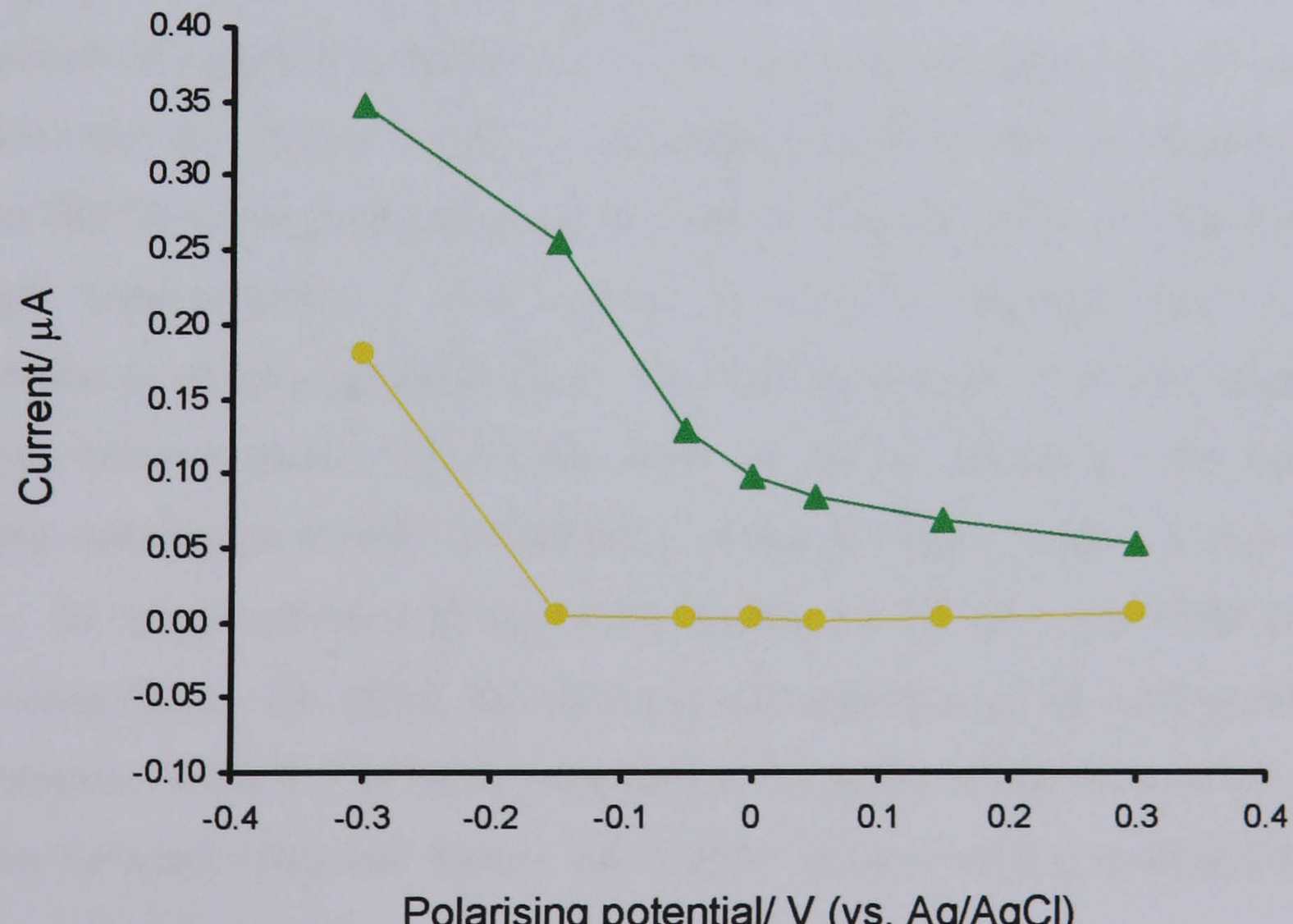

Figure 4.8 Current as a function of polarisation potential with (upper curve) and without (lower curve) 10 mg/l free chlorine.
[Supporting electrolyte: phosphate buffer (pH 7.0, 0.1 M)].

4.3.2 Dependency of total chlorine measurement to the amount of potassium iodide and supporting electrolyte in solution

As the electrochemical measurement of total available chlorine requires the addition of potassium iodide (See Chapter 2), it is important to establish the optimal quantity that needs be added to solutions in order to obtain accurate and reproducible determinations. In this work, experiments involving total chlorine are performed using a fritted external Ag/AgCl reference electrode, due to the iodisation of the 'on-board' screen-printed pseudo-Ag/AgCl reference electrode. Therefore, initial experiments were performed to establish the optimum concentration of supporting electrolyte required to obtain reproducible measurement (i.e. minimal variation resulting from changes in *iR* drop). These results will also serve to ensure the validity of the experiments performed to determine the optimal iodide concentration.

Fixed-potential experiments were performed at DuPont carbon ink electrodes in solutions of 10 mg/l total chlorine (this concentration is considered to be 'mid-range'), in pH 4.0 phosphate buffer at -0.08 V (vs. Ag/AgCl). The concentration of supporting electrolyte was varied between values of 0.05 and 1.0 M potassium chloride. Figure 4.9 shows the relationship between the relative standard deviation (RSD) of measurements (a), and signal size (b), with varying supporting electrolyte concentrations. The current is seen to increase with increasing concentration of supporting electrolyte. The RSD is seen to be initially high at low electrolyte concentrations (40 % for 0.05 M KCl), lowering with increasing electrolyte concentration until 0.5 M KCl, where the RSD reaches a minimum of 2.08 %. At concentrations of electrolyte above 0.5 M KCl, the RSD begins to increase once more. Therefore, the optimum concentration of supporting electrolyte was determined to be 0.5 M KCl, since this is the point where there is the greatest separation between plots and hence, the highest current with a corresponding low relative standard deviation.

Similarly, fixed-potential experiments were performed at DuPont carbon ink electrodes to establish the optimal quantity of potassium iodide required to obtain

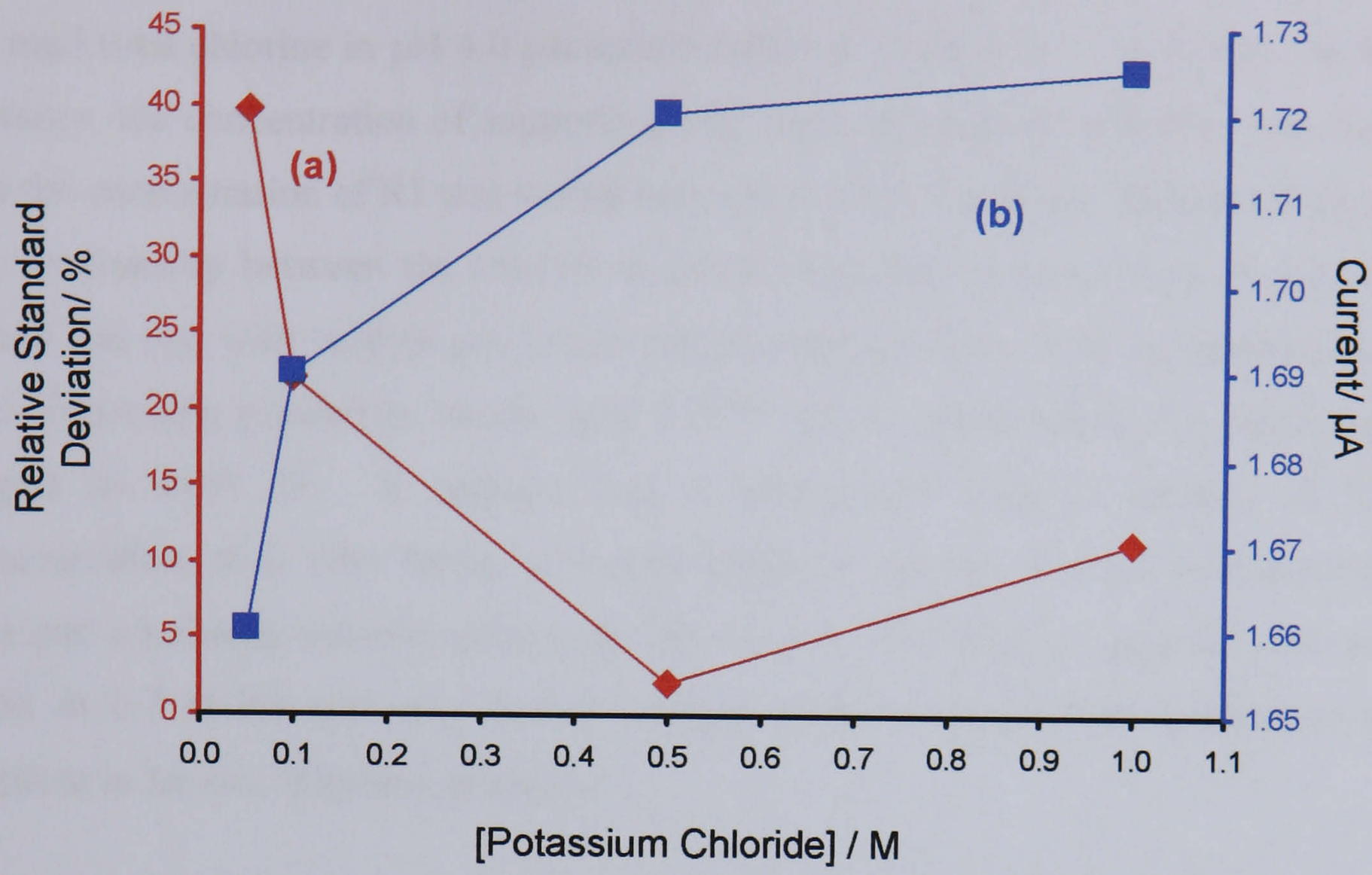

Figure 4.9 Relationship between relative standard deviation (a), and signal size (b), with varying supporting electrolyte concentration for a 10 mg/l total chlorine solution.
[Supporting electrolyte: phosphate buffer (pH 4.0, potassium chloride concentration varied as shown in the graph). Polarising potential: -0.08 V (vs. Ag/AgCl)].

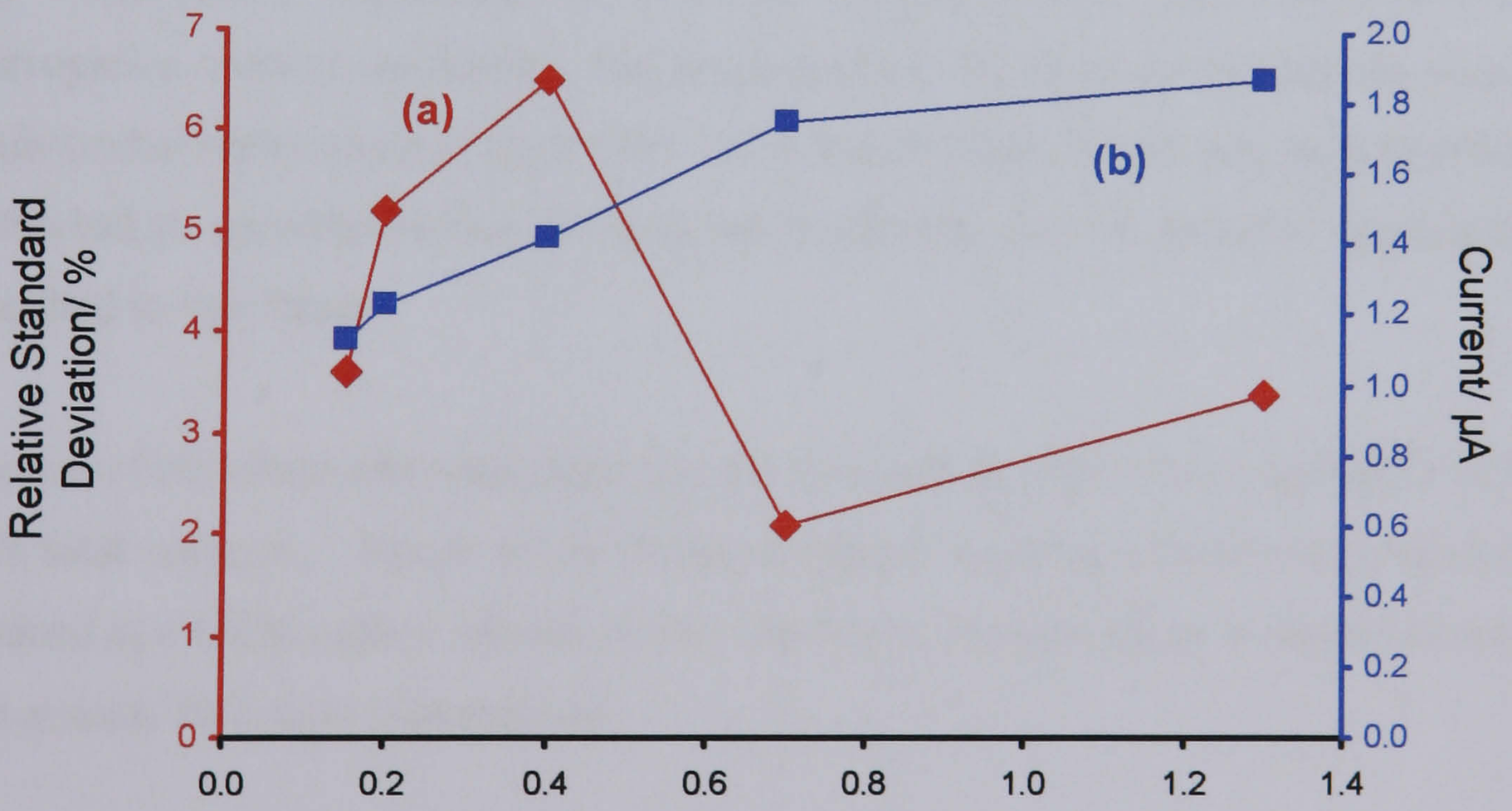

Figure 4.10 Relationship between relative standard deviation (a), and signal size (b), with varying potassium iodide concentration for a 10 mg/l total chlorine solution.
[Supporting electrolyte: phosphate buffer (pH 4.0, 0.5 M).
Polarising potential: -0.08 V (vs. Ag/AgCl)].

accurate and reproducible results. Again, electrodes were tested in solutions of 10 mg/l total chlorine in pH 4.0 phosphate buffer at -0.08 V (vs. Ag/AgCl). In this instance, the concentration of supporting electrolyte (potassium chloride) was fixed and the concentration of KI was varied between 0.1 and 1.3 M KI. Figure 4.9 shows the relationship between the relative standard deviation of measurements (a), and signal size (b), with varying potassium iodide concentrations. The current increases with increasing potassium iodide until 0.7 M KI, at which point, the signal size begins to level off. It appears that a 'saturation' point is reached at this concentration, with there being sufficient iodide in solution to react with both the free and combined chlorine present in the sample. The RSD is also at its lowest point at 0.7 M KI with any further increase in KI concentration resulting in an increase in relative standard deviation.

4.3.3 Amperometric response to chlorine probes

We have seen from Section 4.2, that the electrochemical response of carbon inks may vary considerably depending on both the chosen analyte and electrochemical interrogation method employed. The amperometric interrogation of chlorine probes at electrodes screen printed from both GEM and DuPont carbon inks was therefore performed to ascertain which ink may be favourable for the intended application described in this thesis.

A series of ten electrodes were polarised for 1 minute at -0.08 V (vs. Ag/AgCl) in 10 mg/l total chlorine. Figure 4.11a shows a typical resulting current-time transient obtained at a GEM carbon ink electrode. The error from the mean is shown as error bars at each 10 second time interval.

The current is seen to reach a quasi-steady state at approximately 50 seconds after the initial polarisation. This relatively slow wet-up is probably due to the hydrophobicity of the carbon surface (consistent with the presence of surface

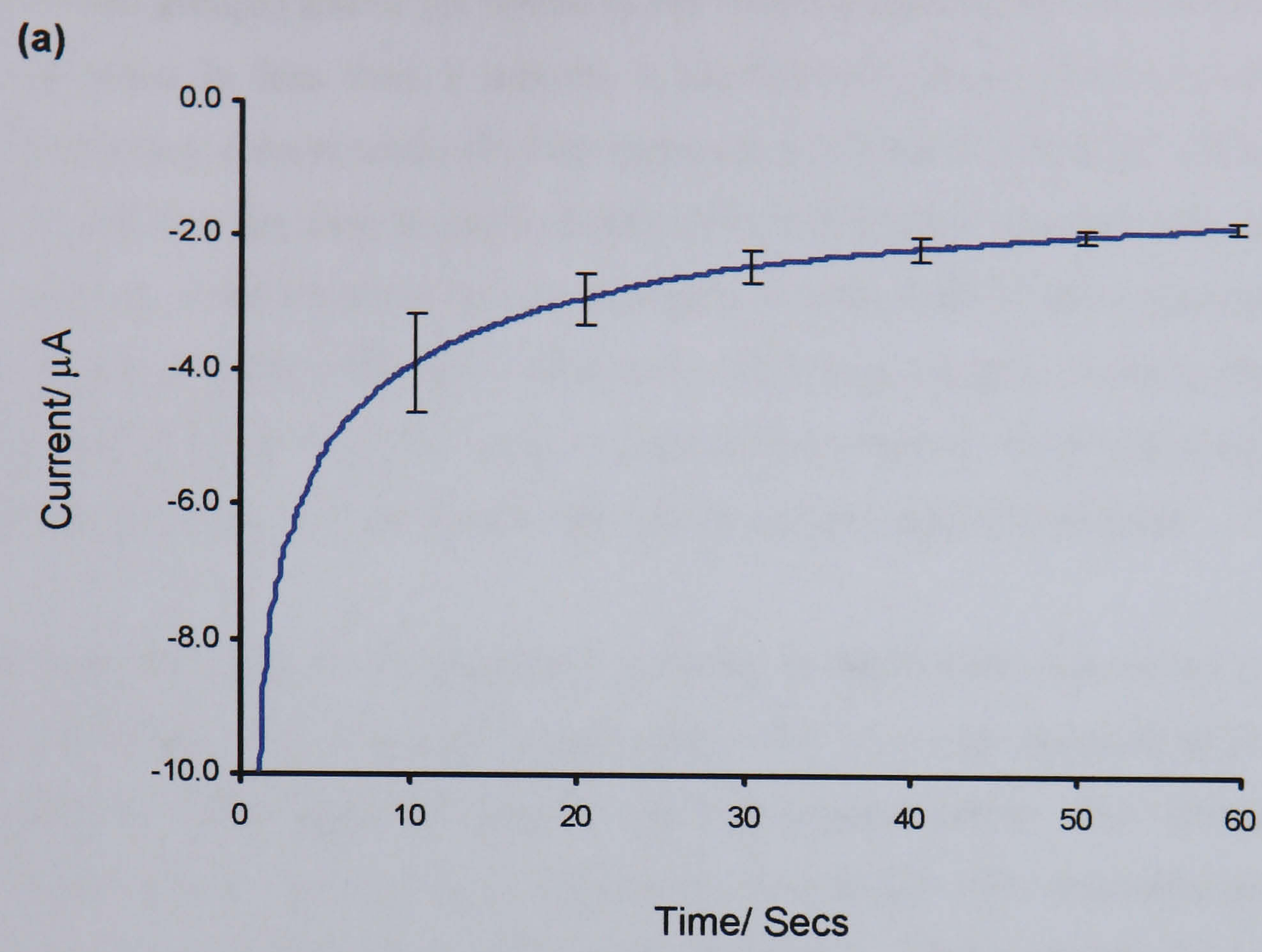

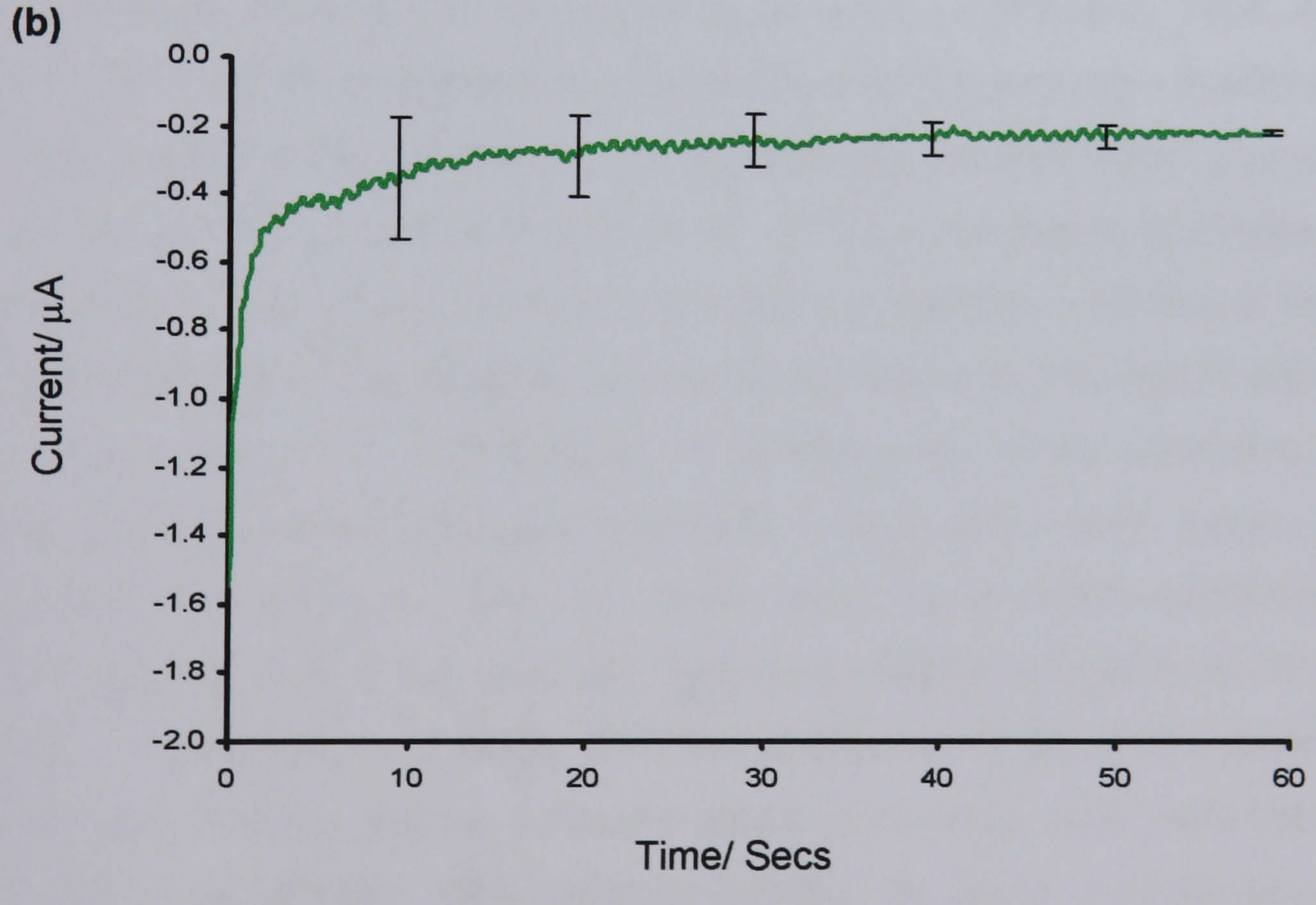

Figure 4.11 **Current-time transients at GEM screen printed carbon electrodes of (a) 10 mg/l total chlorine: [Supporting electrolyte: phosphate buffer (pH 4.0, 0.5 M). Polarising potential: -0.08 V (vs. Ag/AgCl)], and, (b) 10 mg/l free chlorine [Supporting electrolyte: phosphate buffer (pH 7.0, 0.1 M). Polarising potential -0.1 V (vs. Ag/AgCl)].**

functional groups) and/or the nature of the iodine molecule, and still allows readings to be taken in less than 1 minute, a significantly shorter time period than the contemporary colourimetric chlorine measurement kits (~3 minutes). Of course, it is envisaged that the time to reach steady-state will further decrease after subsequent processing of the electrodes (i.e. sonochemical fabrication of microelectrode arrays), as microelectrodes offer advantages over their macroscopic counterparts, namely, enhanced rates of mass transport of electroactive species to the electrodes surface and reduced double layer capacitance (surface area greatly diminished).

Another advantage with using screen printing methods with commercial inks is that the print should be repeatable in thickness. The electrode repeatability for a set of ten different electrodes was checked via chronoamperometry. The relative standard deviation of the current values obtained at 60 seconds after the initial polarisation was less than 6.0 % (6.8 % after 50 seconds). These results are particularly significant as some work involving non-modified carbons have reported evidence of the extraction of iodine into the carbon pastes (Davis & Everhart, 1964; Farsang, 1965). Methods for the determination of iodide at carbon electrodes usually involve chemical modification, utilising ion-pairing of the analyte with tetraalkylammonium (Lu *et al.*, 1995), cinchonine (Kwak *et al.*, 1996) or rhodamine B (Vydra *et al.*, 1976). Davis & Everhart (1964) first admitted a potentional solubility of iodine in carbon pastes when classifying this process as a spontaneous diffusion of iodine onto the paste interior with entrapping of its molecules by strong adsorptive forces. Farsang (1965) studied the redox behaviour of the $[I_2/2I^-]$ system using a carbon paste electrode made with silicon oil. In his report, a poor signal reproducibility of both iodine and iodide was attributed again to a solubility of iodine in the pasting liquid. Analogically to Farsang, the redox behaviour of the $[I_2/2I^-]$ system was investigated with the silicone oil based carbon paste using cyclic voltammetry by Švancara *et al.* (1998). After repetitive cycling, the peaks corresponding to the reaction shown in Equation 4.2, gradually increased. This phenomenon was already interpreted by Farsang (1965) as a consequence of markedly better solubility of iodine in silicone oil compared to that in aqueous phase. It was ascertained more recently (Konvalina, 1997) that in the presence of lipophilic cations, ion-pairing with

iodide is performable with any unmodified carbon paste electrode (independent of the type of binder). The good reproducibility of response observed here (in a given batch as well as for electrodes of different batches) shows that iodine diffusion into the carbon ink, if at all, does not present any practical hindrance to the electrodes due to either the ink composition or the short and 'one-shot' use of the electrodes.

GEM carbon inks electrodes were also examined in 10 mg/l *free* chlorine. Electrodes were polarised for 1 minute at -0.1 V (vs. Ag/AgCl). Figure 4.11b shows a typical resulting current-time transient obtained. Again, the error from the mean is shown as error bars at each 10 second time interval. The current is seen to reach a *quasi*-steady state at a shorter time than for the total chlorine measurement, at approximately 40 seconds after the initial polarisation. This may be a result of the smaller current obtained for free chlorine than total chlorine at the same concentrations (0.21 and 1.86 μA respectively), but may also suggest that there is indeed some solubility of iodine into the carbon ink with total chlorine measurement, resulting in slower diffusion compared to that of free chlorine. There is no data available to compare the results obtained here with previous studies. This is largely because previous methods for the electrochemical reduction of hypochlorous acid have always involved the use of metal-based electrodes. Electrodes fabricated by screen printing of commercial carbon inks have not, to the author's knowledge, been investigated before this work. Again, the time to reach a steady-state value will further decrease after fabrication to a microelectrode array, allowing for the 'on-the-spot' results currently required by the consumer.

The electrode repeatability for a set of ten different electrodes in 10 mg/l free chlorine was also checked via chronoamperometry. The relative standard deviation of the current values obtained at 40 seconds after the initial polarisation was 20.9 % and after 60 seconds, approximately 4.0 %. Hence, values would have to be taken at 60 seconds in order to obtain reproducible sensors with electrodes fabricated from this ink.

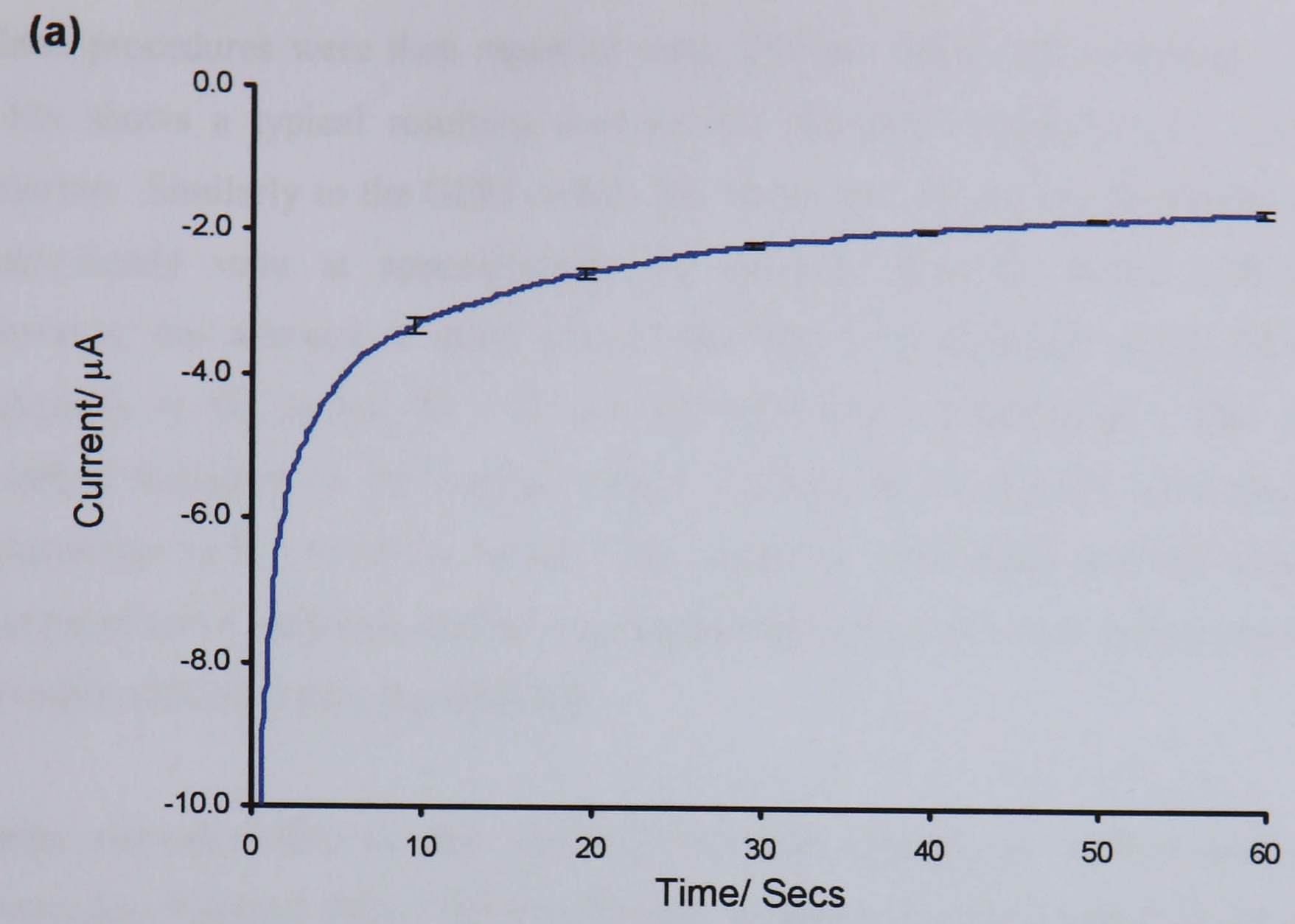

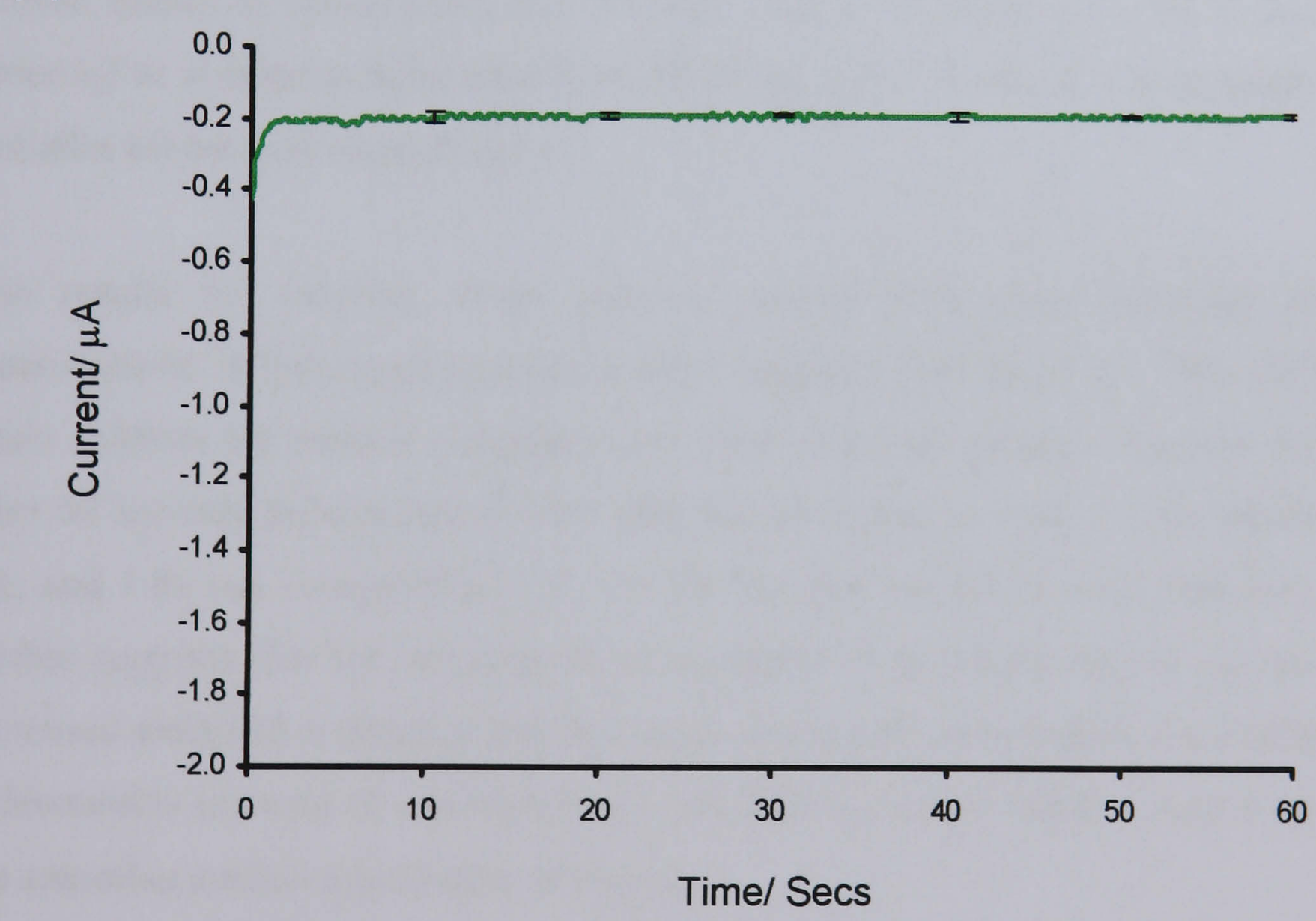

Figure 4.12 **Current-time transients at DuPont screen printed carbon electrodes of (a) 10 mg/l total chlorine: [Supporting electrolyte: phosphate buffer (pH 4.0, 0.5 M). Polarising potential: -0.08 V (vs. Ag/AgCl)], and, (b) 10 mg/l free chlorine [Supporting electrolyte: phosphate buffer (pH 7.0, 0.1 M). Polarising potential -0.1 V (vs. Ag/AgCl)].**

These procedures were then repeated using DuPont carbon ink electrodes. Figure 4.12a shows a typical resulting current-time transient obtained in 10 mg/l total chlorine. Similarly to the GEM carbon ink electrodes, the current is seen to reach a *quasi*-steady state at approximately 50 seconds after the initial polarisation. However, the response is more reproducible here in comparison to the GEM ink, especially in the period 10 - 40 seconds after initial polarisation. The relative standard deviation of the current values obtained at 60 seconds after the initial polarisation is 2.5 % (0.54 % after 50 seconds). This enhanced reproducibility compared to the GEM electrodes may suggest that the DuPont ink is less susceptible to iodine solubility than the GEM ink.

Better reproducibility is also observed for free chlorine at DuPont carbon ink electrodes (Figure 4.12b). There is far less variation in current values in the period 10 - 40 seconds after initial polarisation and the relative standard deviation of the current values at steady-state (2.4 %) and after 60 seconds (2.1 %) is less than observed at electrodes fabricated from GEM ink (20.9 % and 4.0 % at steady-state and after 60 seconds respectively).

The results for chlorine probe analysis concur with those obtained for the measurement of hexaammineruthenium(III) chloride (Section 4.2). The GEM ink again exhibits the greater electroactivity, with observed current values of 0.21 μA after 60 seconds polarisation in free chlorine compared to 0.18 μA for the DuPont ink, and 1.86 μA compared to 1.72 μA for the DuPont ink in total chlorine. This further suggests that the presence of an increased of polymeric binder results in an increased electrical resistance and thus, a lower current. Once again, the DuPont ink is favourable in terms of reproducibility, confirming further that this is as a result of the smoother surface topography of this ink.

The DuPont ink composition was then used to investigate the response of carbon electrodes for 15 different concentrations of total chlorine (Figure 4.13). The DuPont ink was chosen due to a combination of its better reproducibility for chlorine measurements, and its smoother and more homogenous surface.

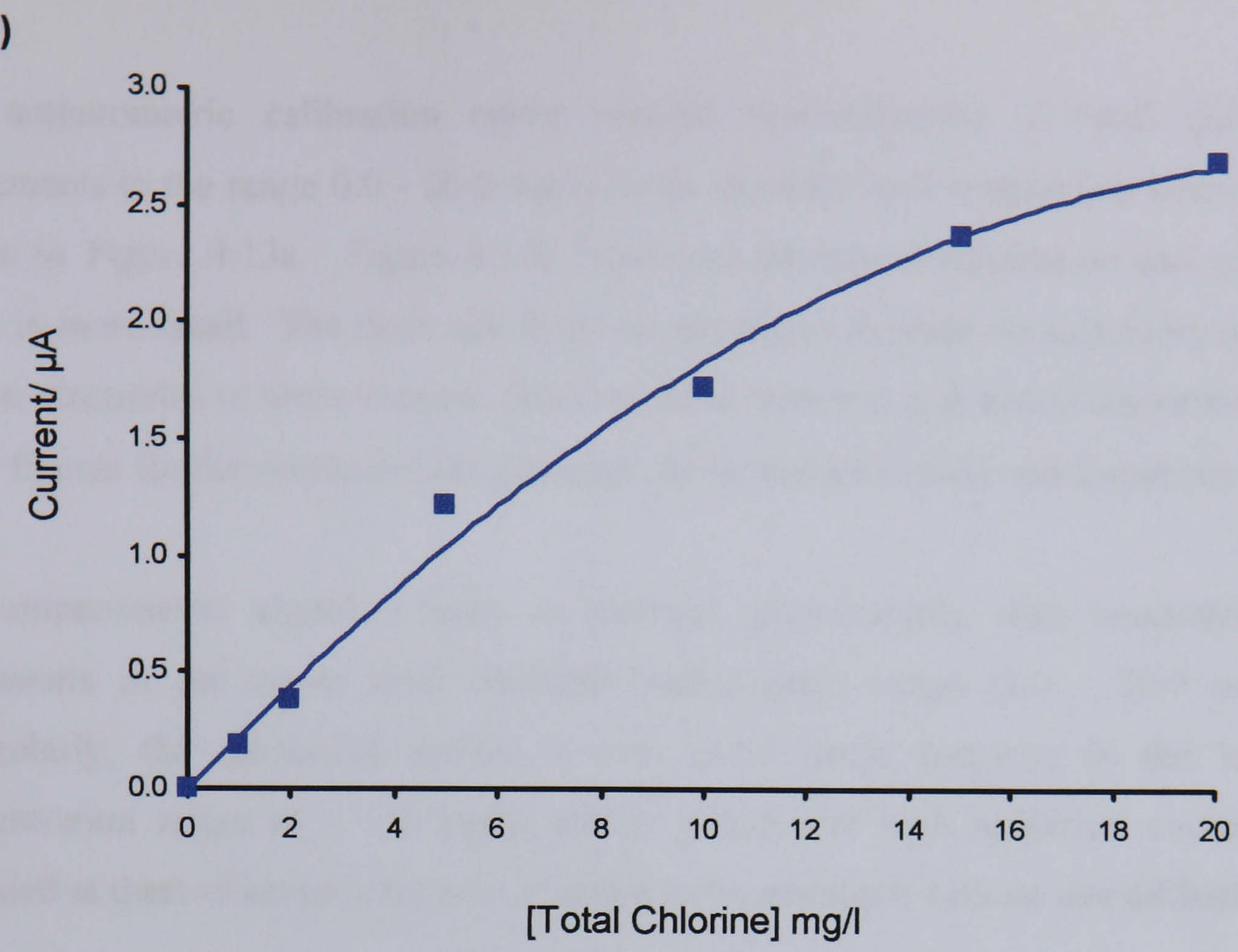

Figure 4.13 **Amperometric calibration curves at DuPont screen printed carbon electrodes for (a) high-range total chlorine measurement and (b) low-range total chlorine measurement.**
[Supporting electrolyte: phosphate buffer (pH 4.0, 0.5 M).
Polarising potential: -0.08 V (vs. Ag/AgCl)].

The amperometric calibration curve relating concentrations of total chlorine (increments in the range 0.0 - 20.0 mg/l) to the resultant iodine reduction current, is shown in Figure 4.13a. Figure 4.13b illustrates the low concentration part of the curve in more detail. The main aim here was simply to indicate the suitability of the carbon electrodes to amperometric chlorine measurements, and not to determine the exact figures for the response time, detection limit, linearity range and sensitivity.

The amperometric signal is seen to increase *quasi*-linearly with concentration increments in the upper total chlorine measurement range (1.0 - 20.0 mg/l). Particularly, the electrodes exhibit a very good linear response in the lower concentration range (0 - 1.0 mg/l), and a sufficiently high reduction current is provided at these electrodes for total chlorine to be measured without any difficulty.

The calibration plot resulting from amperometric measurements of 15 concentrations of free chlorine is shown in Figure 4.14. The electrodes are seen to respond to these additions, the magnitude of which is near linearly dependant on the concentration of electroactive species. However, the desired measurement range for the determination of free chlorine in drinking water for example, is in the range 0-1 mg/l, with a desired detection limit of 0.01 mg/l. Unfortunately, the sensor current becomes very low in this region (Figure 4.14b). A new electrode design with a larger surface area could be studied as a first solution, but it is important to remember here that a greater sensitivity in electrochemical measurements is observed at microelectrodes compared to their macroelectrode equivalents (due to increased rates of mass transport), and that, combined with modern circuitry to desired sensitivities being constructed fairly routinely, should conclude that full scale measurements of both free and total chlorine over a wide concentration range is achievable at carbon electrodes.

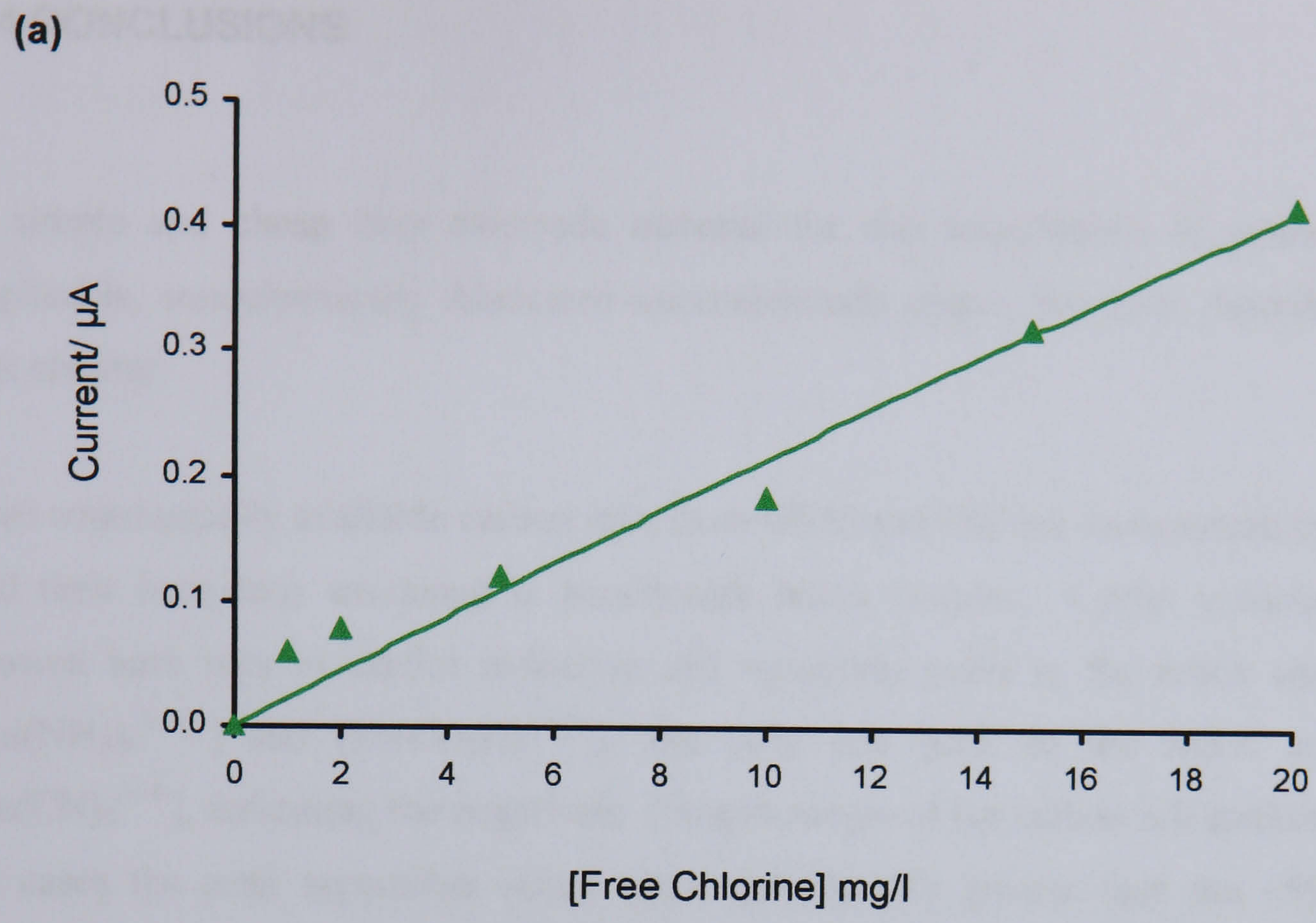

Figure 4.14 Amperometric calibration curves at DuPont screen printed carbon electrodes for (a) high-range free chlorine measurement and (b) low-range free chlorine measurement.
[Supporting electrolyte: phosphate buffer (pH 7.0, 0.1 M).
Polarising potential: -0.1 V (vs. Ag/AgCl)].

4.4 CONCLUSIONS

A simple and cheap base electrode material for the manufacture of generically applicable, sonochemically fabricated microelectrode arrays, has been described in this chapter.

Two commercially available carbon inks from GEM and DuPont were screen printed and their behaviour examined in benchmark redox couples. Cyclic voltammetry showed both inks to exhibit oxidation and reduction peaks to the redox couples, $[Ru(NH_3)_6^{3+/2+}]$ and $[Fc(CO_2H)^{3+/2+}]$, but only one peak to the redox couple, $[Fe(CN)_6^{3-/4-}]$, indicating the negatively charged nature of the carbon ink surfaces. In all cases the peak separation values were considerably greater than the ~59 mV expected for a Nernstian diffusion controlled one-electron transfer reaction, consistent with the non-homogenous composition of carbon inks.

Electrodes fabricated from GEM ink exhibited a narrower potential window and greater charging current compared to those fabricated from DuPont ink, when subjected to linear scan background voltammetric experiments in both neutral and acidic buffers.

Chronoamperometric experiments in $[Ru(NH_3)_6^{3+/2+}]$ at both types of carbon ink electrode showed a slower decay in current compared to that seen at gold electrodes, consistent with the presence of surface functional groups at the electrode surface and the hydrophobic nature of the inks. However, at both inks, the steady-state response times were found to be <1 minute. Electrodes fabricated from the GEM carbon ink resulted in a larger amperometric current than those fabricated from the DuPont ink, suggesting a higher graphite loading of the GEM ink, or the increased presence of an insulating binder in the DuPont ink. However, the DuPont ink was seen to be favourable in terms of reproducibility.

Scanning electron microscopy investigations showed both inks as having a heterogeneous surface structure, characterised as an ensemble of graphite particles (5 – 20 μm diameter) held within a binding liquid. The GEM ink was seen to have a rough and microporous topography compared to the smooth surface of the DuPont ink. The DuPont ink contained a higher amount of polymeric binder than the GEM ink which was seen to be similar to graphite alone. The electrochemical properties were seen to correlate with the carbon structure established from SEM images.

Film resistance measurements revealed the DuPont ink to have a more resistive surface than the GEM ink, again confirming the increased presence of polymeric binder in this ink.

At properly defined reduction potentials (-0.08 and -0.1 V (vs.Ag/AgCl) for total and free chlorine respectively), electrodes showed sensitivity to aqueous chlorine, whilst excluding any interference from dissolved oxygen. The optimal amount of potassium iodide (0.7 M KI) and supporting electrolyte (0.5 M KCl) required for accurate and reproducible total chlorine measurements was established.

Chronoamperometric experiments in both free and total chlorine solutions were performed with electrodes screen printed from both GEM and DuPont carbon inks. In all cases, GEM electrodes produced a higher current whilst DuPont electrodes exhibited a superior reproducibility. Relative standard deviations of less than 3% were observed at DuPont electrodes for both free and total chlorine solutions. For both inks the electrode steady-state response times were found to be <1 minute.

Amperometric calibration curves demonstrated a near linear response of electrodes to both total and free chlorine solutions in the concentration ranges of interest. A sufficiently high reduction current for total chlorine to be measured without difficulty was obtained at all concentrations tested. Whilst low currents were observed for the reduction of free chlorine, increased mass transport at microelectrode arrays (combined with advanced instrument circuitry), should allow for its measurement at the very low concentrations required.

Screen printed carbon electrodes were demonstrated to be effective for the measurement of both common redox complexes and aqueous chlorine solutions, and therefore their use in the development and production of generic sensors for widespread applications looks promising. Electrodes fabricated from both inks showed good electrochemical behaviour, with the DuPont carbon ink being most favourable due to its enhanced reproducibility and smooth surface topography. Future research will focus on methods to increase the current for free chlorine (Chapter 5).

CHAPTER 5

INVESTIGATIONS INTO THE USE OF SCREEN PRINTED CARBON ELECTRODES AS TEMPLATES FOR SONOCHEMICALLY FABRICATED MICROELECTRODE ARRAYS – Part 2: Effects of pre-treatments and modifiers

5.1 INTRODUCTION

Chapter 4 described the use of two commercially available screen printed carbon electrodes for use in the manufacture of generically applicable, sonochemically fabricated, microelectrode arrays. Such electrodes were demonstrated to be effective for the measurement of both common redox complexes and aqueous chlorine solutions, although due to the constraints imposed by the screen printing process (i.e. the low carbon content allowable for a smooth print), the redox activity and overall analytical performance were observed to be compromised when compared to metal electrodes, particularly when considering the measurement of free chlorine. However, SEM investigations indicated that the observed electrochemical properties varied according to ink composition. This effect has been the subject of numerous investigations (McCreery, 1991), the majority of which have concluded that such electrodes may lend themselves to improvement in terms of electrochemical performance by modification and pre-treatment.

Engstrom (1982; 1984) has shown that pre-treatment can be made specific to certain analyte species. It may be possible then, in this way, to enhance the performance of carbon electrodes further, enabling specific pre-treatments to be applied for specific sensor applications or for the measurement of particular analytes (such as free chlorine). Various activation procedures have thus been shown to influence the electrochemical reactivity of these electrodes. This approach is more practical than formulating new and specific inks, partly due to the proprietary nature of carbon inks and the specialist knowledge required to develop ink compositions, but also because modification of the ink composition (for enhancing redox activity) may compromise the binding and adhesion properties of the ink.

The main focus of this chapter is therefore to develop and explore simple activation and modification procedures, with a view to maximising the electrode response, particularly to free chlorine, and with the overall intention of easily and inexpensively incorporating such procedures into the fabrication and/or working of the sensors.

Many modifying and activation chemistries for carbon electrodes have been considered, all of which have attempted to improve the reproducibility, selectivity or sensitivity of the sensor. Polishing (Bodalbhai & Brajter-Toth, 1988), vacuum-heat (Fagan *et al.*, 1985), radio-frequency plasma (Chi-Sing Tse & Kuwana, 1978) and laser (Poon & McCreery, 1986) pre-treatments have all been successfully used, but these methods may not be compatible with the single- use and field operation of the sensors described in this thesis.

Therefore, three methods that may be applied *in situ* to either the sensor/instrument operation, or the fabrication procedure, are investigated in this chapter. These comprise of electrochemical, chemical and physical treatments, and their application is described in Section 5.2. The effect of each treatment on the physical properties of the screen printed carbon electrodes is also investigated in this section, using scanning electron microscopy techniques.

The modified and pre-treated electrodes are also examined using electrochemical techniques in Section 5.3. The electrodes are firstly examined with respect to their cyclic voltammetric behaviour in the redox couples $[Fc(CO_2H)^{3+/2+}]$ and $[Fe(CN)_6^{3-/4-}]$. Secondly, the electrodes are subjected to amperometric investigations in free chlorine solutions. Comparisons are made to the responses seen for unmodified electrodes in Chapter 4.

Information resulting from SEM studies (Section 5.2) is compared and correlated with the conclusions of the voltammetric and amperometric investigations performed in Section 5.3, thus providing a way of further characterising their overall chemical performance and to establish how differences in the carbon surface translate into changes in the performance characteristics of the electrodes.

The results drawn from all these investigations will be concluded in Section 5.4 and will aid the development of sonochemically fabricated microelectrode array sensors based upon substrates screen printed with easily available commercial carbon inks.

5.2 PRE-TREATMENT AND MODIFYING PROCEDURES

The advantages of using modified and pre-treated electrodes have been compounded in recent years. It is now recognised that improvements in sensitivity and selectivity, as well as the ability to detect electro-inactive species, can be realized using appropriately modified surfaces (McCreery, 1991). In order to keep the activation or modification of electrodes simple and compatible with the production or measurement instrumentation, methods that will be consistent with the field-based application of these disposable devices have been attempted. From an analytical standpoint, pre-treatment procedures were sought that would provide a reproducibly active surface, in addition to enhancing the rate of electron transfer via the introduction of chemical functionality to the surface of the electrode.

The aim of this section is therefore to discuss the most suitable pre-treatment procedures and examine their effect on the surface structure of the screen printed carbon electrodes.

5.2.1 Electrochemical pre-treatment methods

It has long been reported that *electrochemical* pre-treatments of carbon electrodes can improve their electrochemical behaviour (Valentini, 2003). Electrochemical activations have been seen to improve the performance of glassy carbon (Engstrom & Strasser, 1984), carbon fibre (Wang *et al.*, 1987) and graphite epoxy (Falat & Cheng, 1982) electrodes. The exact alterations of the electrodes and the mechanisms of the activation techniques are not known, but are thought to primarily involve the presence of surface functional groups, especially of the carbon–oxygen type (i.e. carbonyl, hydroxyl, quinine, lactone, phenol etc.) during the electro-activation (Bowers & Yenser, 1991; Nagaoki & Yoshino, 1986).

Blaedel and Mabbot (1978) were the first to systematically study the effects of electrochemical pre-treatment of a carbon film electrode, using square wave treatments at various potentials and frequencies. The majority of further studies involved the application of relatively large, positive or negative potentials at the working electrode. However, in 1986, Rojo *et al.* showed that cathodic treatments, although having no affect on the faradaic response, seemingly degrade the residual current, and consequently are not useful for electrodes intended for analytical use. Works since have therefore concentrated on electrodes preconditioned by applying anodic potentials in acidic or basic electrolyte solutions.

The exact amplitude and duration of the applied potentials varies considerably within the literature. To find an appropriate electrochemical pre-treatment condition for the electrodes available to us, we must first refer back to their cyclic voltammetric behaviour which was examined in Section 4.2. The electrodes were seen to exhibit clear redox peaks to the positively charged redox bound couples, $[Ru(NH_3)_6^{3+/2+}]$ and $[Fc(CO_2H)^{3+/2+}]$, but not to the negatively charged $[Fe(CN)_6^{3-/4-}]$ couple, yielding only one peak in the anodic region. It was postulated that this may be due to the negatively charged nature of the carbon surfaces.

Wang *et al.* (1996) have shown that short pre-anodisation (<2 minutes) in phosphate buffer solutions via the application of high oxidation potentials (+1.5 to +2.0 V vs. SCE), improved the electron transfer kinetics at carbon electrode surfaces. The application of such high positive potentials seemed to lower the static barrier, increase the surface functionality and roughness, and/or remove surface contaminants in a manner analogous to activation of other carbon electrodes, resulting in enhanced electrochemical activity for a variety of irreversible and *quasi*-reversible redox systems. Similarly, Cui *et al.* (2001a) showed that activation of characteristically irreversible screen printed carbon electrodes in saturated sodium carbonate solution resulted in enhanced electrochemical characteristics for a number of negatively charged redox compounds. Furthermore, the methods of Wang *et al.* (1996) and Cui *et al.* (2001a), due to the relatively short electrochemical activation period employed, would be compatible with the decentralised operation of the

sensors required here. Both treatments can be considered as '*in situ*' and resultantly, may be easily incorporated (programmed) into the operation of the sensing instrumentation or performed during the electrode fabrication process.

Thus, electrodes were activated in; (i) a 0.05 M phosphate buffer (pH 7.0) solution by applying an anodic potential of +1.2 V (vs. Ag/AgCl) for 2 minutes, according to the method of Wang *et al.* (1996), and (ii) a saturated solution (>3 M) of sodium carbonate by applying an anodic potential of +1.0 V (vs. Ag/AgCl) for 5 minutes according to the method of Cui *et al.* (2001a).

Scanning electron microscopy was employed to characterise the surfaces before and after activation in phosphate buffer and saturated sodium carbonate solutions (Figures 5.1b and 5.1c, respectively). Results indicate that the surface topography changes significantly between the untreated (Figure 5.1a) and treated electrodes. Prior to pre-treatment, the electrode exhibits a smooth morphology formed by either the close assembling of the graphite particles or a considerable amount of polymeric binder. The inclusion of a pre-treatment step in the procedure results in the microparticulate nature and surface roughness of the graphite particles to increase. The organic binder is largely removed and graphite particles, whose size are in the 10-20 μm range, are clearly exposed at the surface. However, there is little observable difference between the images shown in Figures 5.1b and 5.1c, apart from perhaps an indication of a more even pre-treatment effect with the phosphate buffer method (Figure 5.1b), as there is an area in Figure 5.1c (the lower left quadrant), where the surface is comparable to that of the untreated electrode (Figure 5.1a).

Many previous studies have also reported that the electrode surface structure became very porous by electrochemical treatment (Nagaoki *et al.*, 1988; Kepley & Bard, 1988), and the effective electrode surface area increased (Eswaramoorthy *et al.*, 1999; Murata *et al.*, 2000). Since a greater level of exposure of graphite edges is evident, improvements in electrochemical responses might be expected to result from such pre-treated electrodes.

(a)

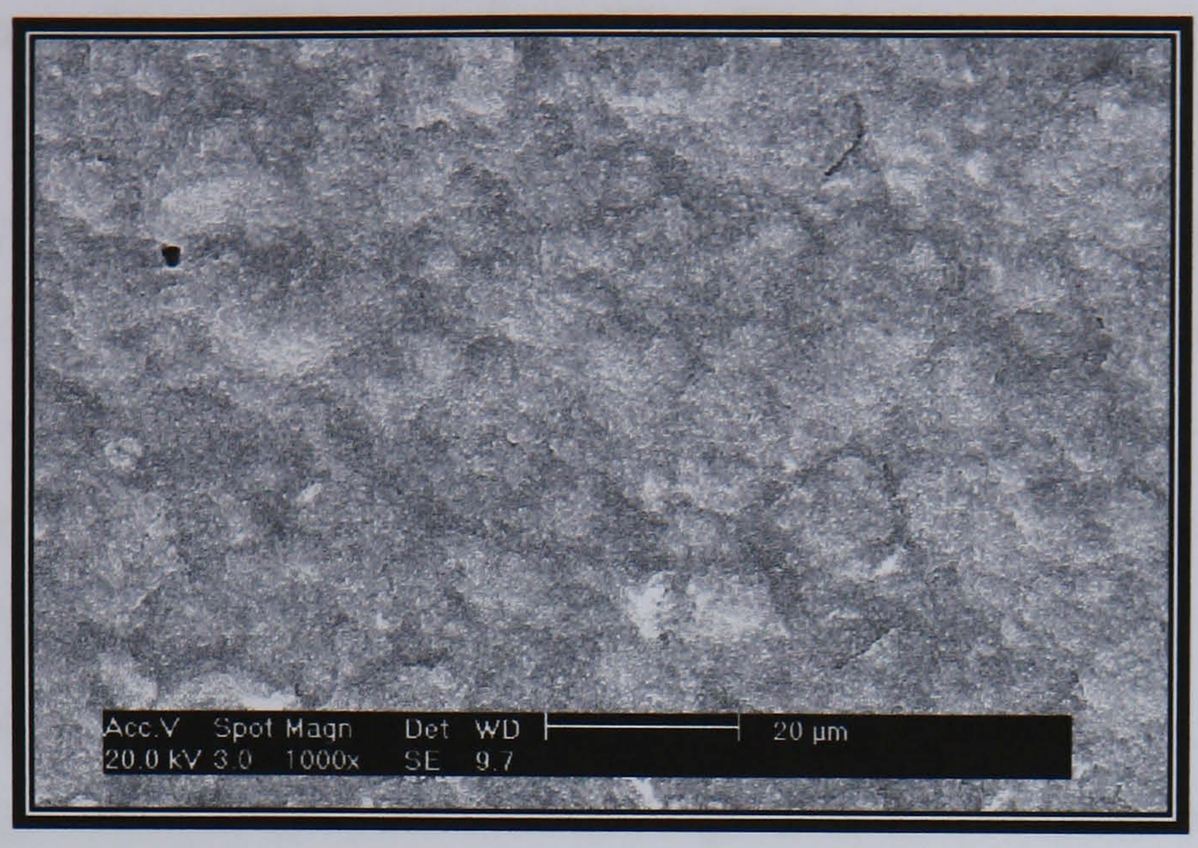

(b)

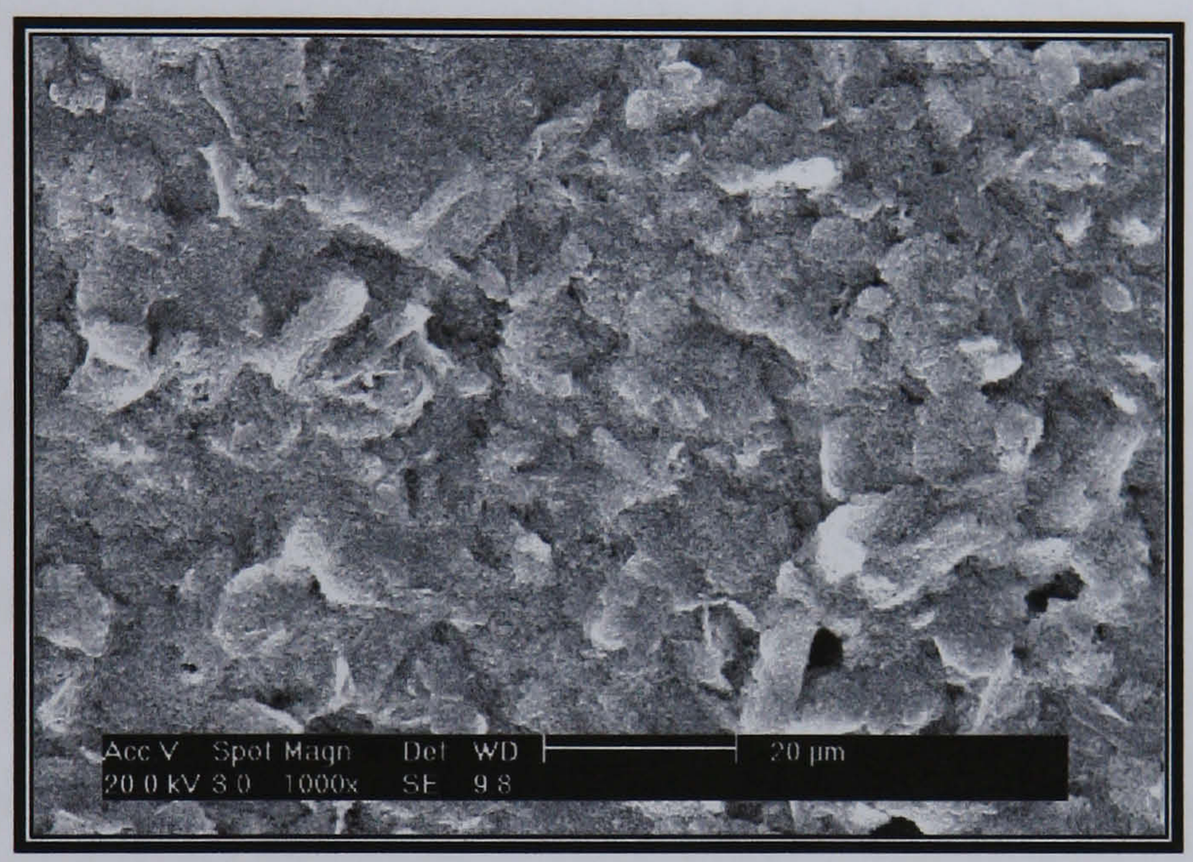

(c)

Figure 5.1 **Scanning electron micrographs of the carbon reactive surface of screen printed electrodes, (a) untreated, and then subsequently pre-treated by anodisation in (b) phosphate buffer and (c) sodium carbonate.**
(x 1000 magnification).

5.2.2 Deposition of modifying polyaniline films

It has previously been demonstrated that the use of polymer coatings to produce modified surfaces provides advantages during analysis (Imisides *et al.*, 1991 and references therein). Perhaps the most significant of these is that a multilayered, dynamic polymer coating provides a three dimensional reaction zone at the surface. This may give rise to an increase in the flux of reactions that occur there, which in turn may increase sensitivity. Polymer materials have been attached to substrates by covalent bonding, adsorption, physical mixing, or electrodeposition. Due to its simplicity and many advantages (as previously described in Chapter 2.6.1), it is the latter of these mechanisms of attachment that is utilised for this investigation.

One group of monomers that can be electropolymerised and that display marked analytical utility are those based upon substituted aromatics, such as aniline. Aniline undergoes oxidation at positive potentials to form polyaniline. The mechanism of growth and attachment of polyaniline is known to vary with substrate (Rodriguez *et al.*, 1987). A reaction scheme for the anodic polymerisation of aniline at carbon electrodes was first proposed by Yasui (1935). The process involves the incorporation of counterions into the polymer matrix during synthesis and resultantly, polyaniline may exist in four different redox states (Friend, 1993). Within low acidic environments (<pH 4), polyaniline exists as the conductive emeraldine salt form, (for the most conductive form, y = 0.5), depicted by Equation 5.1:

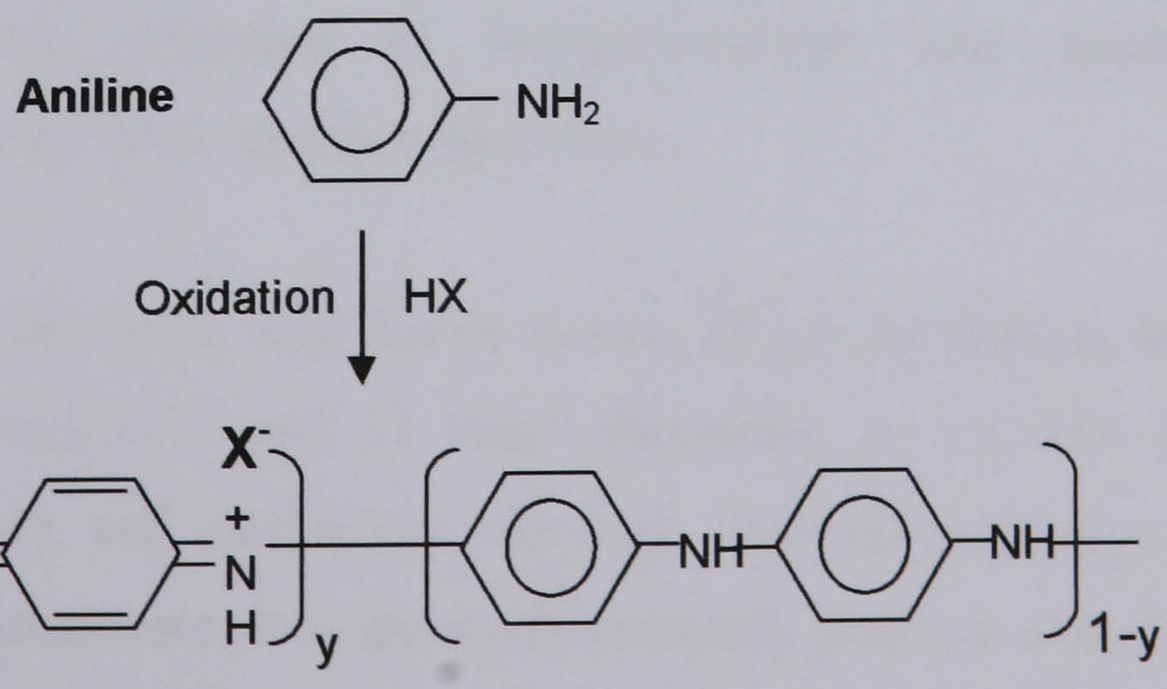

As the pH is increased, the polymer undergoes deprotonation (Equation 5.2), and at pH values greater than approximately pH 5, the polymer essentially becomes non-conductive (Doblhofer & Zhong, 1991).

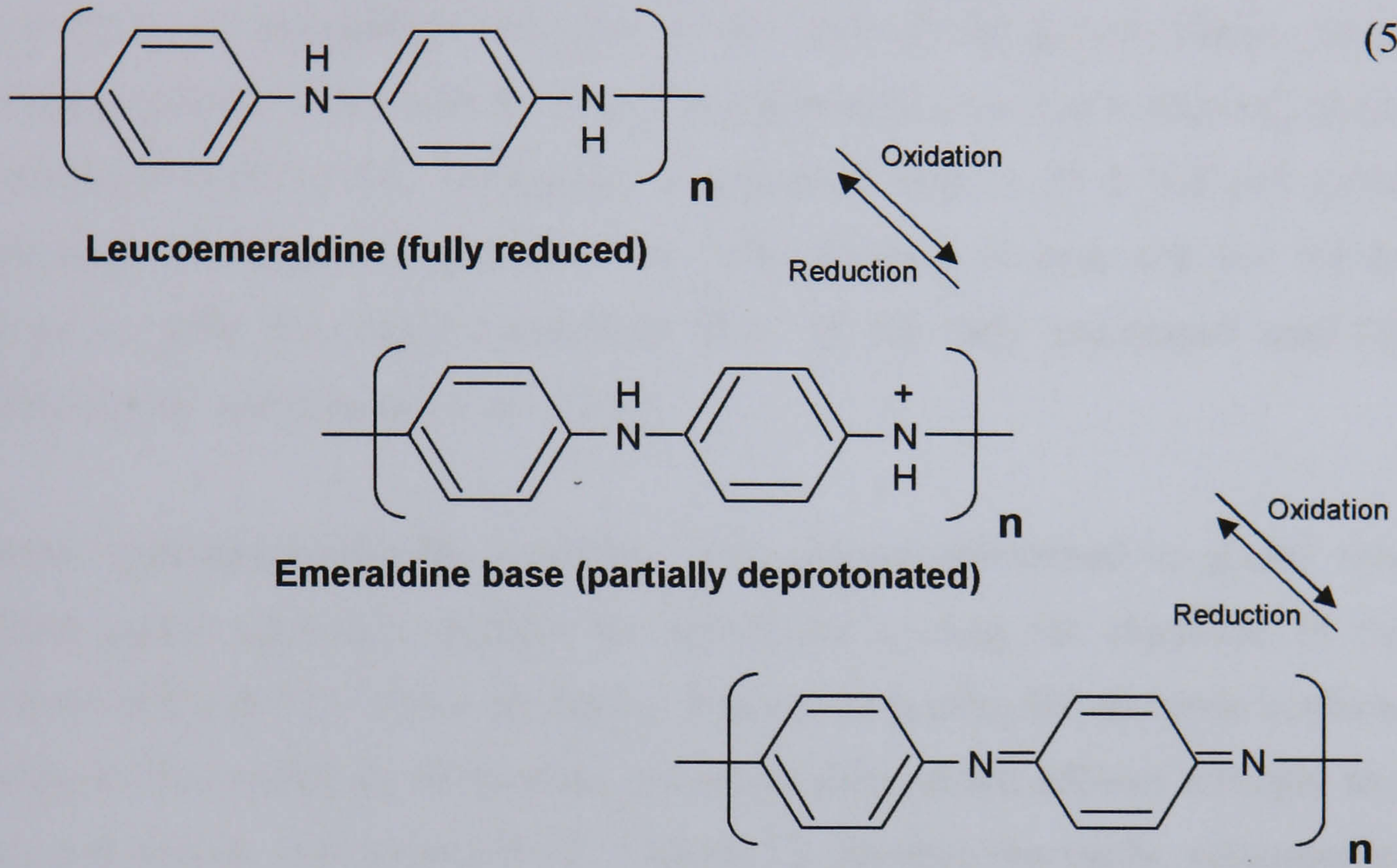

(5.2)

Leucoemeraldine (fully reduced)

Emeraldine base (partially deprotonated)

Pernigraniline (fully depronated)

The polymerisation is initiated in acidic medium by the formation of an aniline radical cation, whose charge is localised mainly on the nitrogen atom. The monomer units are then connected by C-N bonds in *para* positions (head to tail couplings), to form leucoemeraldine, which is essentially non-conducting in both the base and protonised form. Strong oxidation of leucoemeraldine base leads to a non-conductive semi-quinone form, pernigraniline base.

Polyaniline is the polymer of choice here due to its ease of polymerisation, low cost, high conductivity of between 0.01 and 13 Scm^{-1} depending on the film forming conditions (Li *et al.*, 2002), and particularly, its high chemical durability against oxygen and moisture. Furthermore, it is thermodynamically possible that dissolved redox species may be oxidised or reduced by the oxidised or reduced form of the

polyaniline film. This means that the film may behave as an electron-transfer mediating catalyst (Yano *et al.*, 1992a).

In order to maximise the current response of any polyaniline modified electrode, efforts must be made to maintain the conductive state of the film. As the conductivity of polyaniline decreases as the pH of the polymerisation solution increases (and the electroactivity cannot be regenerated in a non-conducting polymer produced at higher pHs), polyaniline is deposited from a pH 2 buffered solution containing 0.2 M aniline *hydrochloride*. The presence of hydrochloride has been shown to yield the highly conductive form of the fully protonated emeraldine hydrochloride salt (Ohsaka *et al.*, 1984).

Aniline hydrochloride/buffer solutions were electropolymerised at planar screen printed carbon electrode surfaces by potentially cycling the electrode 15 times between -0.2 and +0.8 V (vs. Ag/AgCl). Potentially cycling the electrode in this way results in the deposition of an even polymeric film which adheres strongly to the electrode surface (McGurk, 2002). Figure 5.2 presents the cyclic voltammogram recorded for the electropolymerisation.

The first scan exhibits a discernable and irreversible anodic peak due to monomer oxidation at +0.79 V (vs. Ag/AgCl). As cycling continues, this peak shifts to slightly less positive potentials and decreases in intensity. No cathodic peak corresponding to the irreversible anodic peak is observed. In the second scan, one redox system at +0.32 (anodic)/+0.28 (cathodic) V (vs. Ag/AgCl) appears. The currents on the anodic and cathodic waves increase steadily with potential sweep time, reflecting the growth of the conductive polyaniline film. The irreversible anodic peak corresponds to the oxidation of aniline to the corresponding polyemeraldine cation radical and then of this cation radical oxidising to the corresponding polyemeraldine dication. The absence of a cathodic peak (corresponding to the irreversible anodic peak), indicates a fast consumption of the electrogenerated monocation radicals and dications by following chemical reactions to form the electroactive polyaniline film

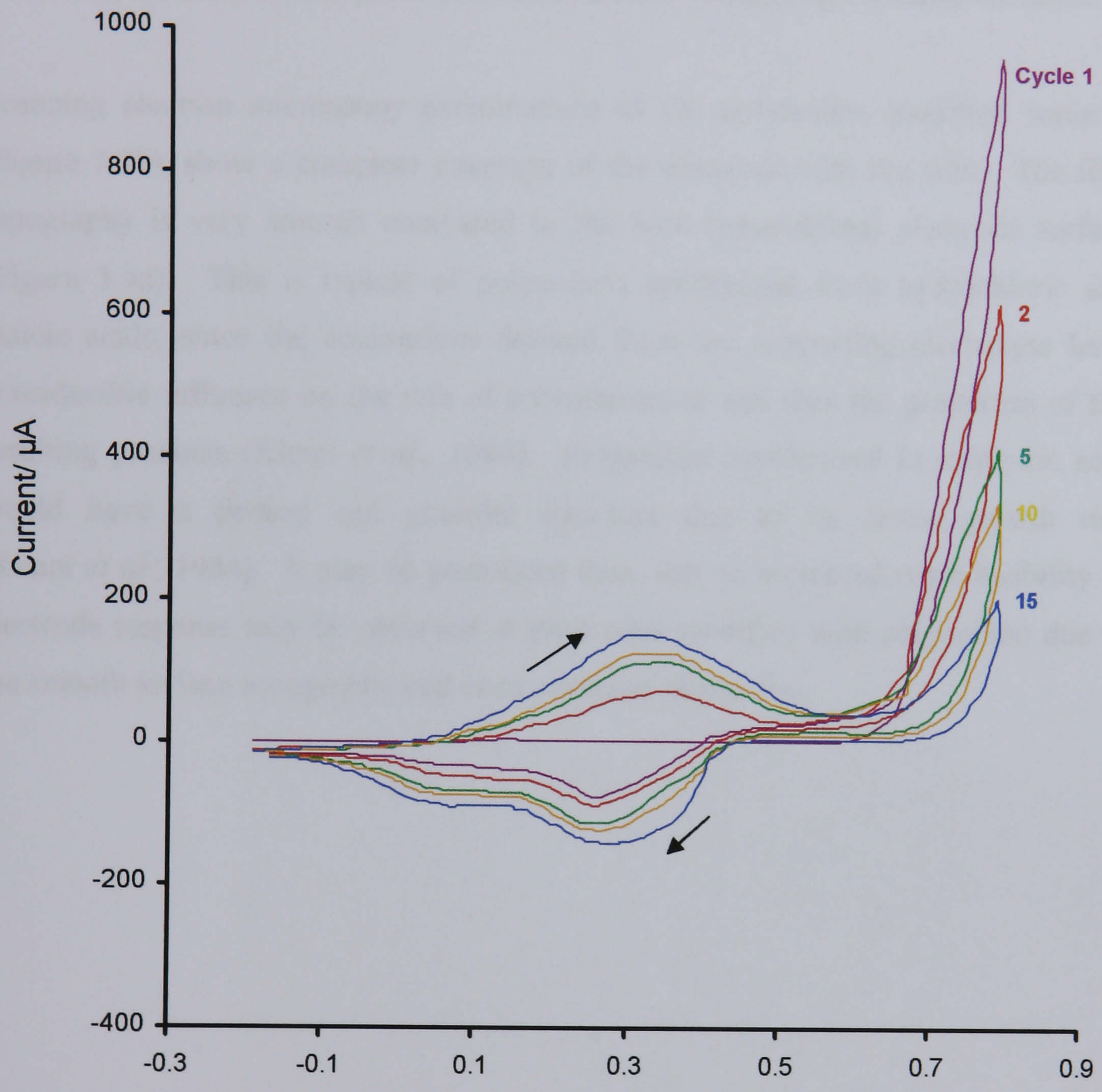

Figure 5.2 **Cyclic voltammogram of the electrodeposition of polyaniline at the surface of a planar screen printed carbon electrode.**
[Supporting electrolyte: maleate buffer (pH 2.0, 8.6×10^{-3} M).
Scan rate: 50 mVs^{-1}]

on the electrode. This is confirmed by the appearance of new redox peaks in the second scans in the potential regions more negative than those at which the irreversible oxidation peak of the monomer appeared. The cyclic voltammogram observed here is similar to those obtained by Oyama *et al.* (1989) and Meneguzzi *et al.* (1999), for the electrodeposition of other electro-conducting aromatic diamines.

Scanning electron microscopy examinations of the polyaniline modified surfaces (Figure 5.3b), show a complete coverage of the electrode with the film. The film topography is very smooth compared to the bare (unmodified) electrode surface (Figure 5.3a). This is typical of polyaniline synthesised from hydrochloric and maleic acids, since the counterions derived from the supporting electrolyte have considerable influence on the rate of polymerisation and thus the properties of the resulting products (Kitani *et al.*, 1984). Polyaniline synthesised in sulphuric acid would have a porous and granular structure due to its faster growth rate (Kitani *et al.*, 1984). It may be postulated then, that an increased reproducibility in electrode response may be observed at electrodes modified with polyaniline due to the smooth surface topography and even coverage of the film.

(a)

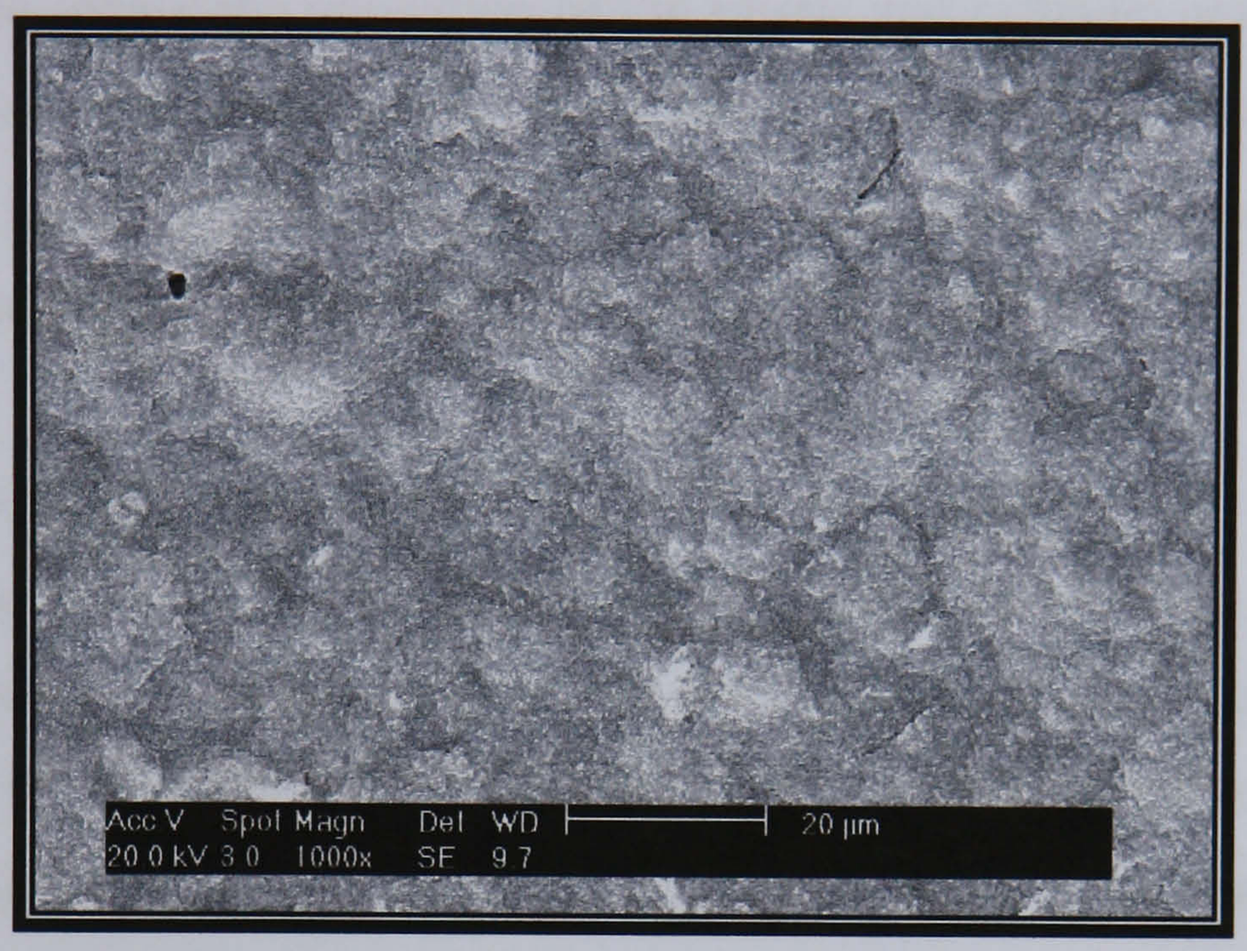

(b)

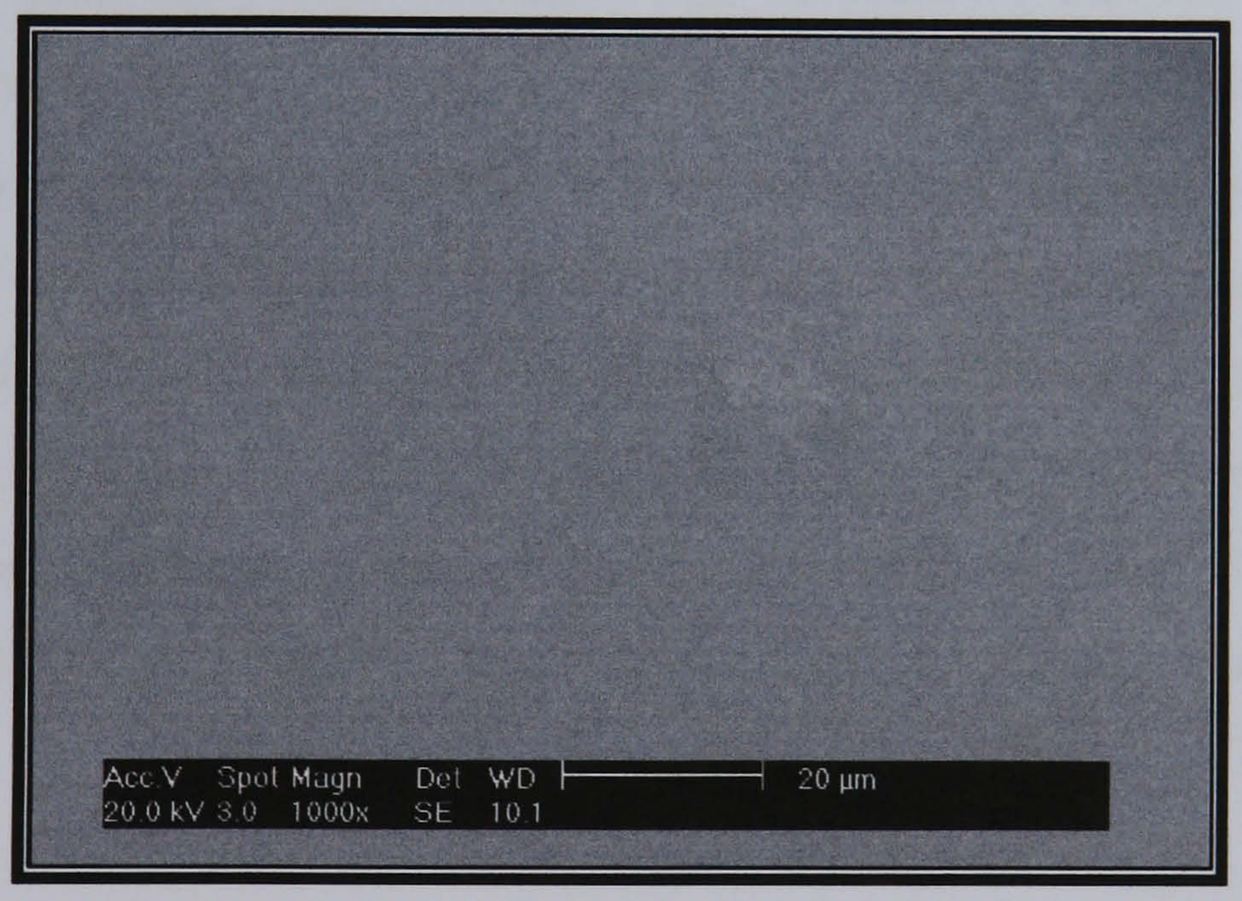

Figure 5.3 **Scanning electron micrographs of carbon screen printed electrodes: (a) before any modification and (b) modified with a film of electrodeposited polyaniline.**
(x 1000 magnification).

5.2.3 Sonochemical activation methods

A number of early investigations into the activation of glassy carbon electrodes reported the cleaning of electrodes prior to use through mechanical polishing. This method was seen to reduce the separation of the anodic and cathodic peak potentials for various redox couples when placed in aqueous solution (Wightman *et al.*, 1984; Hu *et al.*, 1985). However, the nature of screen printed carbon electrodes prevents the use of such mechanical polishing methods for activation purposes.

Later studies showed that glassy carbon electrodes which have been sonicated with 20 kHz ultrasound in relatively non-volatile organic solvents (e.g. dioxane), also exhibit enhanced heterogeneous electron-transfer rates for a variety of aqueous redox probes (Zhang & Coury, 1993) and consequently, tremendous increases in current levels are observed (Dewald & Peterson, 1990). In principle, these results may be attributed to any combination of increased rate of electron transfer, changes in electrode area or changes in the physical and chemical properties of the electrode surface. The advantages of this ultrasonic activation approach include the simplicity of the method and the low cost of the equipment used. In addition, ultrasonic activation of electrodes may be easily incorporated into the overall production of sensors, particularly in relation to the work of this thesis, due to the sonochemical fabrication of microelectrode arrays in this work being produced at a similar frequency (25 kHz) to that used by Zhang & Coury (1993) in previous activation studies (20 kHz).

Water was selected as the solvent in this work since it has commonly been successfully used for other studies in the field of sonochemistry (Suslick, 1990; Doktycz & Suslick, 1990), and furthermore, water is also the solvent of choice to produce sonochemically fabricated microelectrode arrays. It would therefore be far more practical and economical to utilise a common solvent for both the activation and electrode subsequent array production processes.

To determine the effect of extended sonication times on the activation as well as to determine whether a correlation between enhanced electron-transfer rates exists, screen printed carbon electrodes were sonicated in water for 5, 30 and 300 seconds, according to the procedure described in Chapter 3.

Ultrasonic irradiation at frequencies in the 20-30 kHz range has varying effects on electrode surfaces. Non-metals such as glassy carbon have been observed to become severely pitted after only a few minutes of sonication in aqueous media (Zhang & Coury, 1993). Since the current monitored in a voltammetric experiment increases with increasing electrode area, it is important to ascertain the extent of surface damage sustained by the screen printed carbon electrodes during sonication in an effort to explain and understand any correlation there may be between the surface damage and the electrochemical results obtained in Section 5.3. Scanning electron micrograph images (Figure 5.4), were obtained for untreated electrodes, and electrodes sonicated for each time period, at the same magnification. Prior to pre-treatment, the surface of the electrode is relatively smooth, with few discernable cracks or grooves (Figure 5.4a), and can be characterised as an ensemble of graphite particles held within a pasting liquid. As the sonication time is increased, the microparticulate nature of the carbon ink is observed to increase accordingly (Figures 5.4b, 5.4c and 5.4d, respectively), suggesting a 'sonochemical surface roughening effect' due to cavitational 'hotspots' generated during bubble implosion and the subsequent generation of interfacial fluid microjets (See Chapter 2, Section 2.7). The appearance of cracks and grooves is consistent with the decomposition of the polymeric binder resulting in greater definition of the graphite particle surface area. This observation is consistent with the work of Suslick (1990), who found that particles of brittle, layered, inorganic materials underwent fragmentation during sonication. It would be expected that these observed increases in the effective graphite surface areas using topographical studies would result in concomitant increases in current response.

(a)

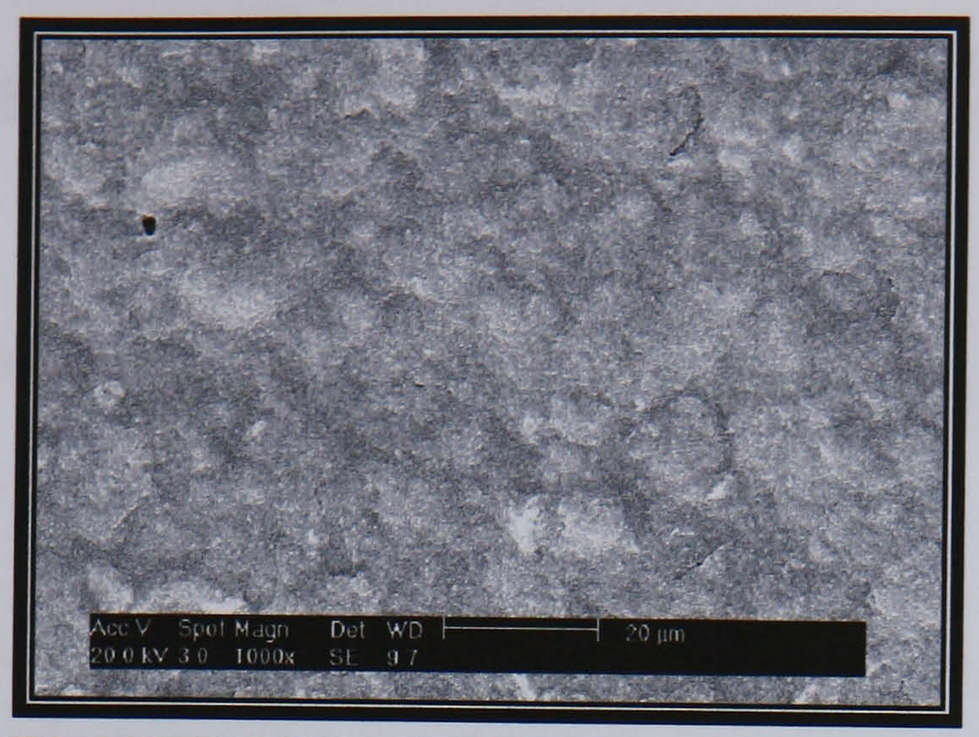

(b)

(c)

(d)

Figure 5.4 **Scanning electron micrographs of: (a) the carbon reactive surface of bare screen printed electrodes and electrodes subsequently pre-treated by, (b) sonication in water for 5 seconds, (c) sonication in water for 30 seconds and, (d) sonication in water for 300 seconds.**
(x 1000 magnification).

5.3 CHARACTERISATION OF MODIFIED ELECTRODES

5.3.1 Cyclic voltammetric behaviour of redox couples at modified electrodes

In order to explore the nature of the modification (if any) of the carbon electrodes by the various treatment procedures, cyclic voltammetry was first performed to investigate the electrochemical behaviour of $[Fe(CN)_6^{3-/4-}]$ and $[Fc(CO_2H)^{3+/2+}]$ at all modified/pre-treated screen printed carbon electrodes. The voltammetric conditions are described in Chapter 3, Section 3.5.6. $[Fe(CN)_6^{3-/4-}]$ and $[Fc(CO_2H)^{3+/2+}]$ were chosen as the redox couples for this analysis since they exhibited the least reversibility when investigations at untreated carbon electrodes were performed in Chapter 4. In addition, their investigation should find broad utility in electroanalysis and may provide an indication of any effects upon the surface barrier of the treatments due to their differing charge.

The anodic peak potentials (E_{pa}), peak separations (ΔE_p), and the anodic peak currents (i_{pa}) of the cyclic voltammograms observed for the reduction of two redox couples before and after each pre-treatment are summarised in Table 5.1.

Table 5.1 Summary of voltammetric peak separations, anodic peak potentials and anodic peak currents for two redox systems at carbon electrodes before and after various pre-treatments (all potentials quoted vs. Ag/AgCl).

	Potassium Ferricyanide			Ferrocenecarboxylic acid		
	ΔE_p (mV)	E_{pa} (mV)	i_{pa} (μA)	ΔE_p (mV)	E_{pa} (mV)	i_{pa} (μA)
Bare (untreated)	–	448	4.3	100	220	14.7
Phosphate buffer	–	540	3.4	150	230	12.0
Sat. Na_2CO_3	–	380	36.1	140	250	12.0
PANI modified	–	–	–	365	350	8.5
5 secs sonication	–	–	0.61	262	326	9.2
30 secs sonication	–	–	0.75	188	270	11.1
5 mins sonication	–	–	1.74	166	254	11.2

Figure 5.5 compares cyclic voltammograms for 5 mM potassium ferricyanide (Figure 5.5a) and 1 mM ferrocene carboxylic acid (Figure 5.5b), at untreated screen printed carbon electrodes, and carbon electrodes activated in 0.05 M phosphate buffer according to the method described in Section 5.2.1. Neither the untreated or treated electrodes exhibit clear redox peaks to the $[Fe(CN)_6^{3-/4-}]$ couple, displaying only one broad peak in the anodic region. The untreated and treated electrodes also exhibit comparable behaviour to the $[Fc(CO_2H)^{3+/2+}]$ couple, both displaying *quasi*-reversible electron transfer reactivities towards this analyte.

It can be seen in Figure 5.5 that no improvement in the electron transfer kinetics is observed for both compounds and in fact, the electron transfer kinetics actually seem to have slowed in both cases. For example, there is an increase in the separation of the cathodic and anodic peak potentials for the $[Fc(CO_2H)^{3+/2+}]$ couple (values of +100 mV and +150 mV are observed for the untreated and treated electrodes, respectively), and the anodic peak obtained for the $[Fe(CN)_6^{3-/4-}]$ couple is shifted further in the anodic region from +448 mV at the untreated electrode, to +540 mV at the electrode pre-anodised in phosphate buffer. Note also the decrease in peak current response as a result of pre-treatment in both cases: a 0.9 μA decrease for the $[Fe(CN)_6^{3-/4-}]$ couple and a 2.7 μA decrease for the $[Fc(CO_2H)^{3+/2+}]$ couple.

These results are surprising since previous studies on pre-treated carbon electrodes by Wang *et al.* (1996), using similar pre-treatment procedures, have shown an improvement in reaction kinetics for several benchmark redox couples. We know however, from the comparisons of two different commercial carbon inks made in Chapter 4, that the degree of electrochemical reversibility depends on the electrode material and varies between carbon inks. The type of carbon ink (supplied from Ercon, USA) used by Wang *et al.* may have been far enough removed in composition from the formulation of carbon ink used in this work, that marked differences in the effects of pre-treatment are observed.

The rate of electron transfer at carbon electrodes in aqueous solution is affected by several factors, many of which are poorly understood. Changes in observed reaction

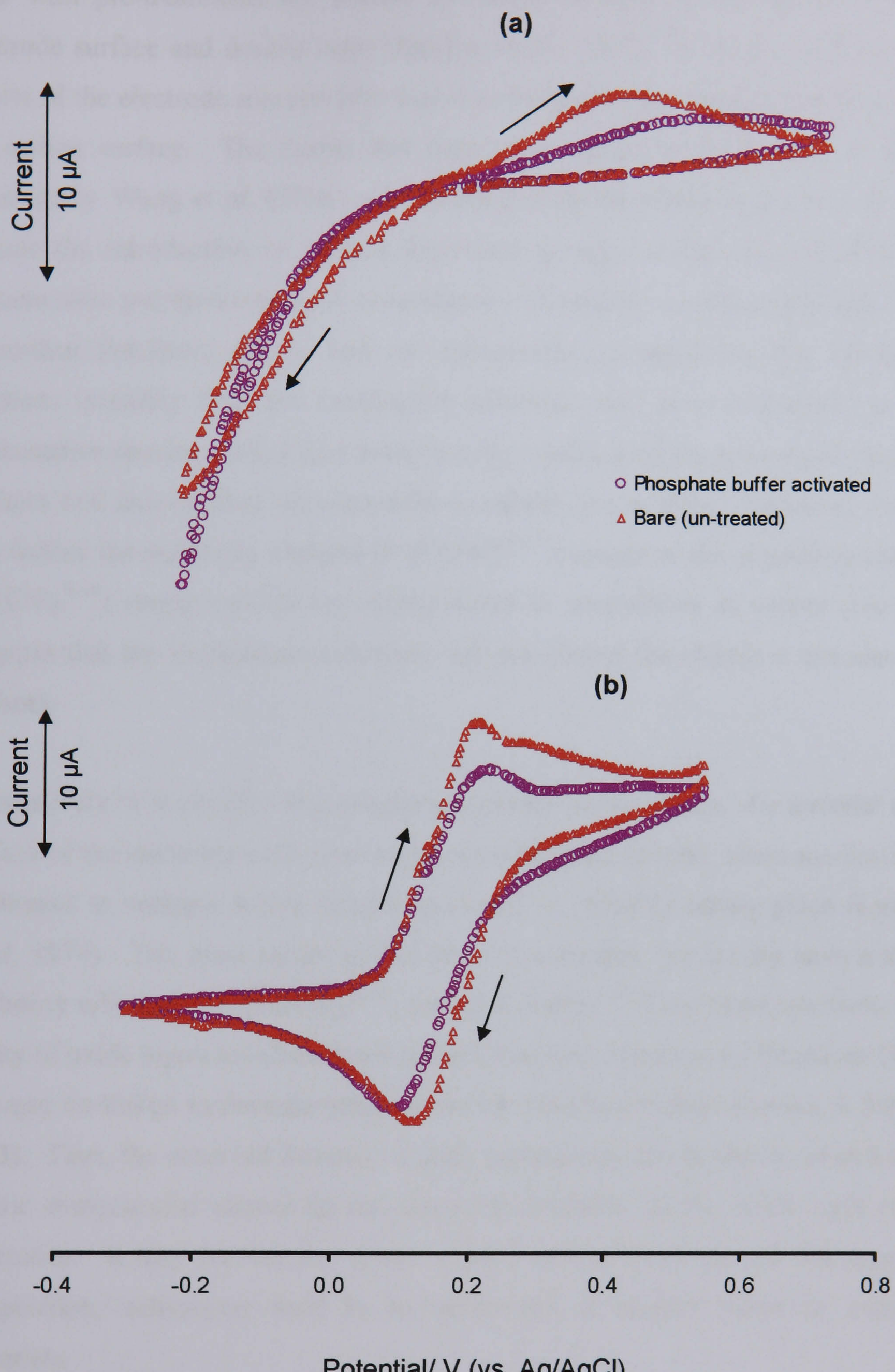

Figure 5.5 **Cyclic voltammograms at bare (un-treated) electrodes and electrodes pre-treated by anodisation in phosphate buffer, for two different redox compounds: (a) 5 mM potassium ferricyanide, and (b) 1 mM ferrocenecarboxylic acid.**
[Supporting electrolyte: phosphate buffer (pH 7.8, 0.1M). Scan rate: 20 mVs^{-1}].

rates with pre-treatments are known to reflect changes in the character of the electrode surface and double layer (Deakin *et al.*, 1985). A likely origin of these effects of the electrode solution interface is a change in the chemical functionality of the carbon surface. The events that may have caused the favourable activation observed by Wang *et al.* (1996) were postulated by his research group to possibly include the introduction of surface functional groups, or the removal of surface contaminants and detrimental ink constituents. Therefore, we can assume that *a lack of* surface functional groups and *an introduction* of impurities that hinder the reactions (possibly from the anodisation solution), may have contributed to both electroactive species studied here being poorly catalysed on the pre-treated electrode surfaces and thus causing the electrodes to exhibit low activity. However, the fact that neither the positively charged $[Fc(CO_2H)^{3+/2+}]$ couple or the negatively charged $[Fe(CN)_6^{3-/4-}]$ couple exhibit any improvement in reversibility at treated electrodes suggests that the anodisation procedure has not altered the charge at the electrode surfaces.

Alternatively, it is possible that anodisation causes the formation of a material at the surface of the electrode such as an oxide layer of some species, since anodisation is performed at voltages where oxygen evolution is probably taking place (Laser & Ariel, 1974). The exact nature of this layer is uncertain, but it may have a strong inhibitory effect on the $[Fe(CN)_6^{3-/4-}]$ and $[Fc(CO_2H)^{3+/2+}]$ electrode reactions. The ability of oxide layers to inhibit reactions has also been observed by Engstrom (1982) and may be linked to the adsorption of the electroactive species (Anson & Schultz, 1963). Thus, the observed increase in peak separations may be due to some kind of kinetic overpotential caused by the increased thickness of the oxide layer on the electrodes. It may be that for screen printed carbon electrodes of this type and composition, activations need to be performed at shorter times or increased potentials.

Cyclic voltammetry was then performed in both 5 mM potassium ferricyanide and 1 mM ferrocene carboxylic acid, at electrodes treated by anodisation in a saturated sodium carbonate solution, according to the procedure described in Section 5.2.1.

The influence of the pre-treatment upon the voltammograms obtained compared to untreated electrodes, is represented in Figure 5.6. The $[Fe(CN)_6^{3-/4-}]$ couple (Figure 5.6a) displays irreversibility at the untreated carbon ink electrode, as reported in the previous chapter. However, *quasi*-reversible behaviour is observed at the treated electrode. Both the untreated and treated electrodes exhibit a broad anodic peak response, with a lowering of the anodic peak potential at the treated electrode from +448 mV (for the untreated electrode) to +380 mV. Most significantly, at -0.22 V (vs. Ag/AgCl), a small cathodic peak that is not present in the voltammogram obtained at the untreated electrodes, is present at the pre-anodised electrode. In addition, it can be seen that there is a dramatic increase in peak current response for this redox compound as a result of pre-anodisation in saturated sodium carbonate solution, increasing by 31.8 μA.

The improvement in electron transfer kinetics for the $[Fe(CN)_6^{3-/4-}]$ couple observed at the pre-treated electrodes would also be expected for the $[Fc(CO_2H)^{3+/2+}]$ redox couple. On the contrary, the electroactivity of the treated electrode seemed to decrease at $[Fc(CO_2H)^{3+/2+}]$ and a higher peak separation value (+140 mV) than the untreated electrode (+100 mV) was obtained. In contrast to the method of anodisation in phosphate buffer, pre-treatment by anodisation in saturated sodium carbonate solution does appear to alter the charge at the electrode surface, as a deactivation is seen with the positively charged $[Fc(CO_2H)^{3+/2+}]$ couple, as compared to the improvement in electrochemistry observed for the $[Fe(CN)_6^{3-/4-}]$ compound. This may be due to the removal of the thin polymeric binding layer present on the graphite particles (confirmed with the SEM images shown in Figure 5.1c), rendering the electrodes more hydrophilic and therefore more accessible to solution species (Rice *et al.*, 1983). This is unlikely to have resulted in the activation of electrodes to the $[Fe(CN)_6^{3-/4-}]$ couple, however, as SEM images (Figure 5.1b) also show a very similar removal of binder at electrodes anodised in phosphate buffer solution, although an accompanying improvement in electroactivity for $[Fe(CN)_6^{3-/4-}]$ was not observed at those electrodes.

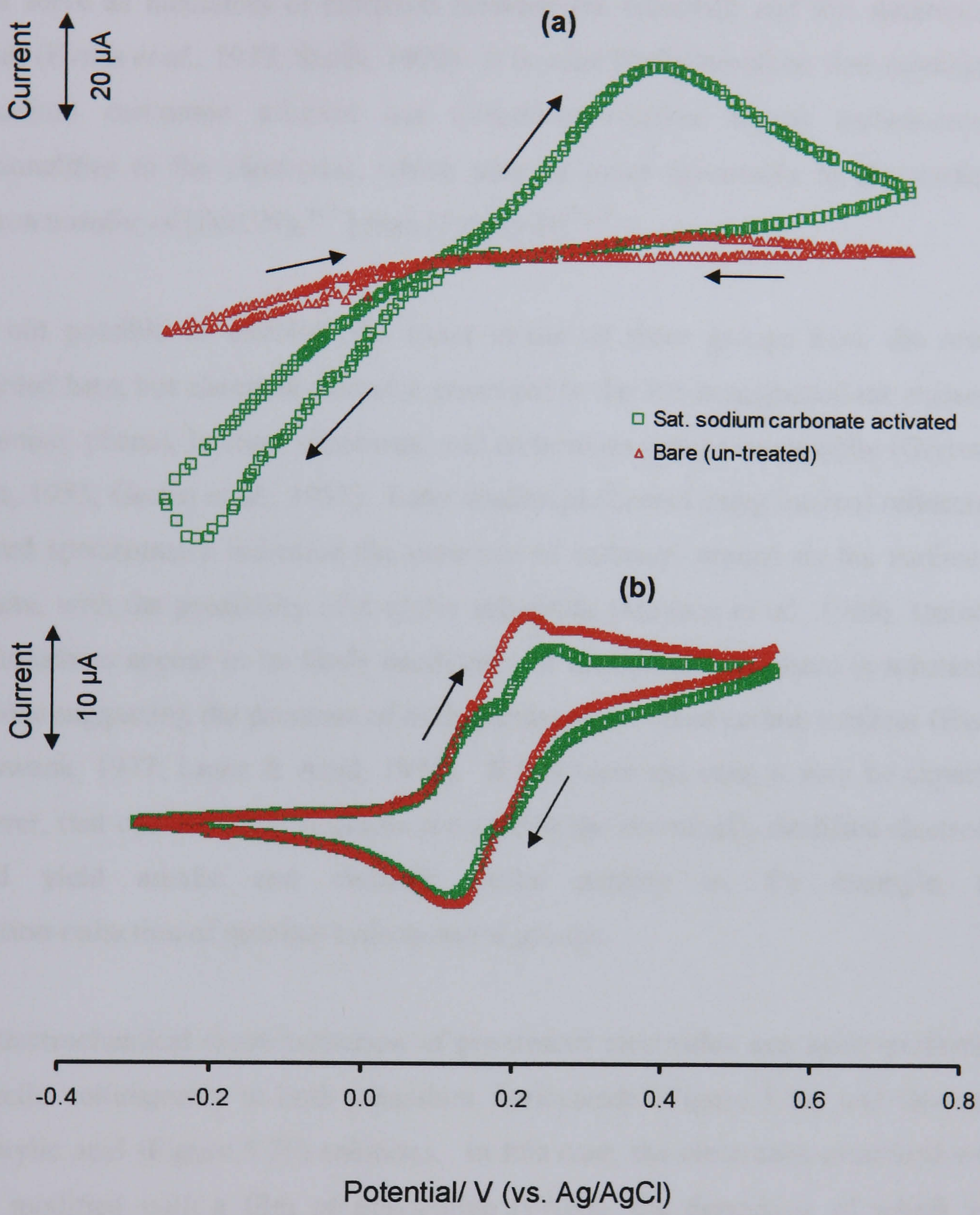

Figure 5.6 **Cyclic voltammograms at bare (un-treated) electrodes and electrodes pre-treated by anodisation in saturated sodium carbonate solution, for two different redox compounds: (a) 5 mM potassium ferricyanide, and (b) 1 mM ferrocenecarboxylic acid.**
[Supporting electrolyte: phosphate buffer (pH 7.8, 0.1M). Scan rate: 20 mVs^{-1}].

It has also been suggested that pre-treatment introduces, or alters, the nature of functional groups on the electrode surface (Hu *et al.*, 1985) and that such groups might serve as mediators of electrons between the electrode and the electroactive species (Evans *et al.*, 1977; Štulík, 1992). It is more likely therefore, that anodisation in sodium carbonate solution has introduced surface bound carbon-oxygen functionalities to the electrodes, which may be more favourable to the mediated electron transfer of $[Fe(CN)_6^{3-/4-}]$ than $[Fc(CO_2H)^{3+/2+}]$.

It is not possible to establish the exact nature of these groups from the results presented here, but chemical evidence presented in the 1950s suggested the existence of quinine, phenol, lactone, chromene, and carbonium groups on graphite (Garten & Weiss, 1955; Garten *et al.*, 1957). Later studies performed using internal reflectance infrared spectrometry indicated the presence of carbonyl groups on the surface of graphite, with the possibility of a cyclic anhydride (Mattson *et al.*, 1969). Quinone functionalities appear to be likely candidates as mediators since there is substantial evidence suggesting the presence of such groups on oxidised carbon surfaces (Evans & Kuwana, 1977; Laser & Ariel, 1974). If this were the case, it may be expected however, that cyclic voltammograms recorded at the chemically modified electrodes would yield anodic and cathodic peaks relating to, for example, the oxidation-reduction of quinine-hydroquinone groups.

The electrochemical characterisation of pre-treated electrodes was again performed by cyclic voltammetry in both potassium ferricyanide (Figure 5.7a) and ferrocene carboxylic acid (Figure 5.7b) solutions. In this case, the electrodes examined were those modified with a film of polyaniline (PANI), the deposition of which was described in Section 5.2.2. The voltammograms obtained at these new modified electrodes were compared with those obtained at conventional screen printed carbon electrodes, having no pre-treatment or modification.

Although many studies on the properties of polyaniline have been driven by the wide variety of possible applications, little attention has been paid to the electrochemical

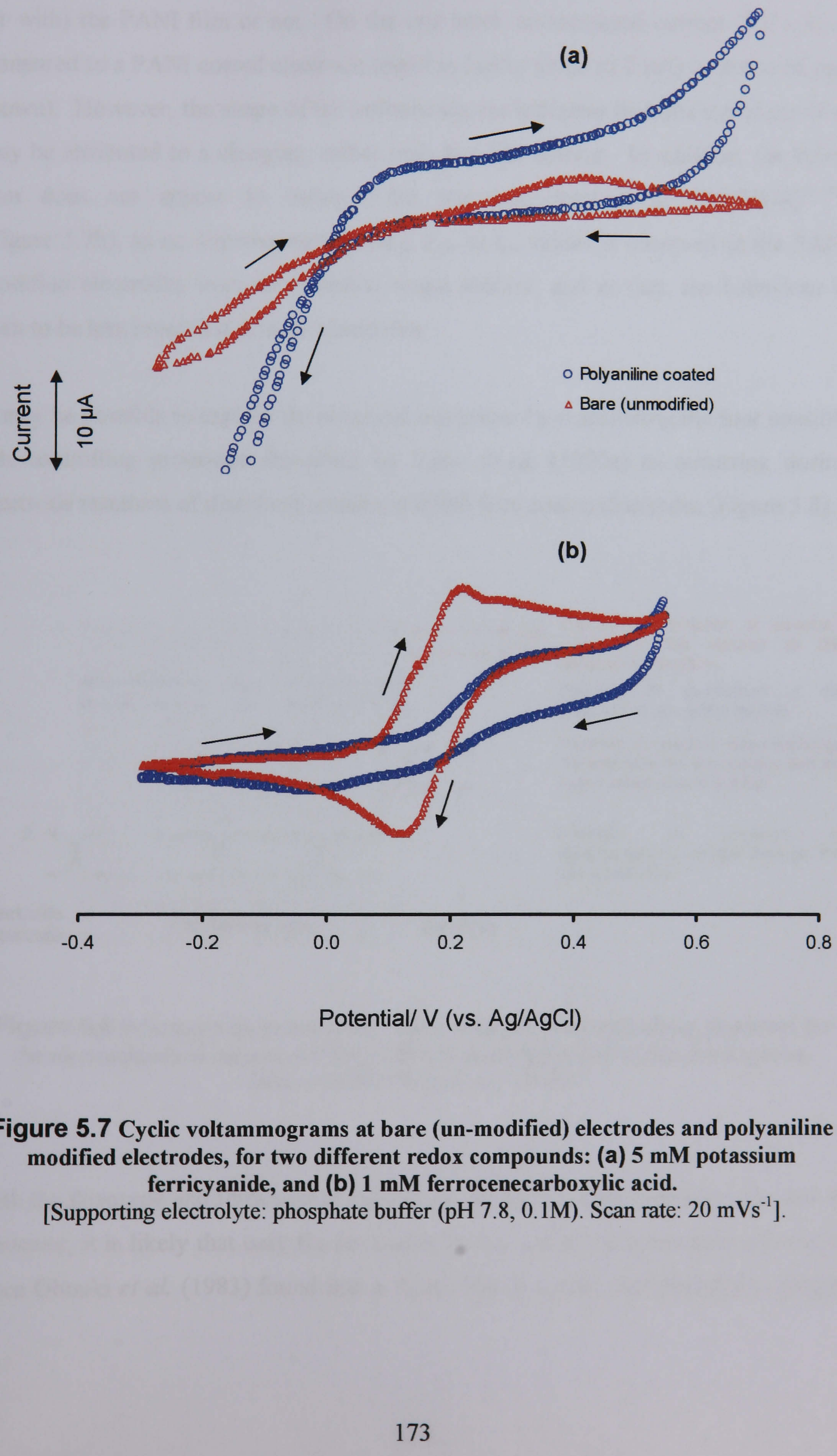

Figure 5.7 **Cyclic voltammograms at bare (un-modified) electrodes and polyaniline modified electrodes, for two different redox compounds: (a) 5 mM potassium ferricyanide, and (b) 1 mM ferrocenecarboxylic acid.**
[Supporting electrolyte: phosphate buffer (pH 7.8, 0.1M). Scan rate: 20 mVs^{-1}].

response of PANI films to dissolved species. It is hard therefore to conclusively determine from Figure 5.7a whether a reaction of $[Fe(CN)_6^{3-/4-}]$ is occurring at (or with) the PANI film or not. On the one hand, an increased current (6.0 μA) as compared to a PANI coated electrode tested in buffer alone (0.2 μA) is observed (not shown). However, the shape of the voltammogram indicates that this signal increase may be attributed to a charging, rather than faradaic current. In addition, the PANI film does not appear to catalyse the electrode reaction of $[Fc(CO_2H)^{3+/2+}]$ (Figure 5.7b), as no improvement in ΔE_p, E_{pa} or i_{pa} values is observed at the PANI modified electrodes over the potential range studied, and in fact, the behaviour is seen to be less reversible at such electrodes.

It may be possible to explain the observed behaviour by considering the four possible rate-controlling processes described by Yano *et al.* (1992a) as occurring during electrode reactions of dissolved species at PANI film coated electrodes (Figure 5.8):

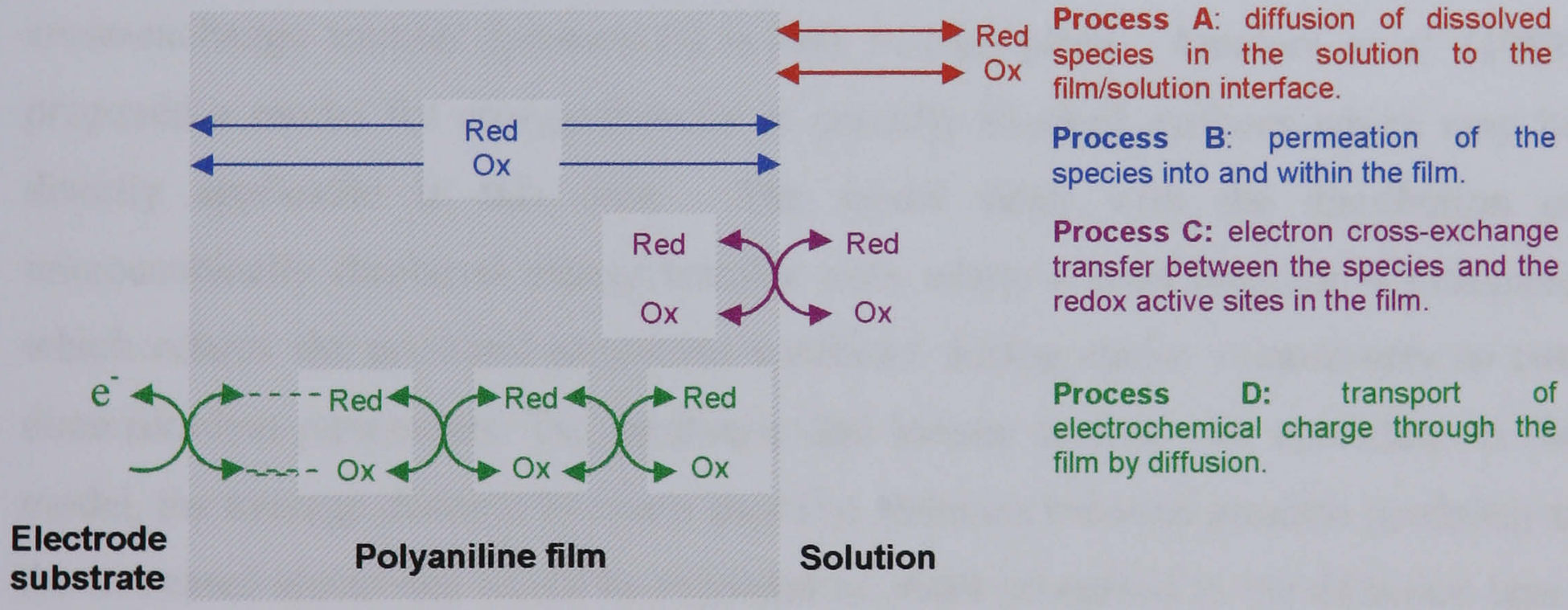

Figure 5.8 Schematic representation of four possible rate-controlling processes for the electrochemical response of PANI film coated electrodes to dissolved species. (Adapted from Yano *et al.*, 1992a).

Both the ferrocene and ferricyanide species would be expected to undergo process A. However, it is likely that only the ferrocene species would progress onto process B, since Ohnuki *et al.* (1983) found that a PANI film is nearly impermeable to species

having a Stokes radii (γ_s) of more than 2 Å. Ferrocene, having a γ_s of 1.7 Å (Salmon & Jutzi, 2001), can permeate the film and therefore some activity is observed at the PANI coated electrodes (Figure 5.7b). Ferricyanide however, whose γ_s is 2.7 Å (Yano *et al.*, 1992b), is unable to fully permeate the film and thus does not display activity (except as a result of increased charging) at the PANI coated electrodes.

The low activity exhibited by the PANI film coated electrodes, when compared to unmodified electrodes, may simply be attributed to the films possessing only a few redox active sites near the film/solution interface, thus inhibiting their ability to act as electron-transfer-mediating catalysts. However, the changes observed in the cyclic voltammograms at polyaniline modified electrodes to $[Fc(CO_2H)^{3+/2+}]$ may also be a consequence of a gradual progression from macroscopic electrode characteristics to microscopic electrode characteristics. If the redox electroactive sites within the film are sufficient in number and spacing, the PANI film coated electrode may behave similarly to a randomly spaced microelectrode array, with each individual active site acting as a microscopic electrode where electron cross-exchange transfer (process C) is able to take place. Amatore *et al.* (1983) proposed a model for charge transfer at partially blocked surfaces which may be directly applicable in this case. The model deals with the distribution of microscopically displaced charge transfer sites where a zone diagram is presented which relates the principal properties exhibited during cyclic voltammetry to two dimensionless parameters: the geometric and kinetic factors. So according to the model, the average distance between sites (i.e. distance between graphite particles) at the untreated electrodes would be regarded as small compared to the diffusion layer thickness and therefore the diffusion layers will overlap. The peak shaped voltammogram obtained here relates to the overlapping of the active sites, resulting in the electrode to behave as a macroelectrode. However, at the PANI coated electrode, the average distance between sites (i.e. the redox active points in the film) is greater and thus the diffusion layers no longer overlap and physically the electrode may begin to exist as a random array of microelectrodes. Electrochemically, the increase in distance between sites manifests itself as an increase in the peak to peak separations (ΔE_p) for a particular redox reaction, leading one to believe the effect is

due to a decrease in the apparent heterogeneous rate constant of electron transfer.

Figure 5.9 shows cyclic voltammograms at screen printed carbon electrodes pre-treated by sonication in water for 5, 30 and 300 seconds, in 5 mM potassium ferricyanide (Figure 5.9a), and 1 mM ferrocenecarboxylic acid (Figure 5.9b). Broader peaks, with accompanying higher values of ΔE_p (data shown in Table 5.1) are observed at all sonicated electrodes and indeed, for both the $[Fe(CN)_6^{3-/4-}]$ and $[Fc(CO_2H)^{3+/2+}]$ redox couples, the highest reversibility was observed at the untreated electrodes.

The extent of deactivation ranges from moderate to severe with sonication time. This result is both surprising and interesting since cavitation is generally more facile in water than some organic liquids, and thus cavitation (and activation) effects at *least* as great as those in organic systems would be expected. The occurrence of concomitant deactivation reactions of the carbon surface involving aqueous sonolysis products is a possible explanation. Such reactions would be expected to result in a higher density of surface oxides on the carbon. This agrees with the findings of Zhang & Coury (1993), who, by square wave voltammetry, observed surface oxides to be present at glassy carbon electrodes sonicated in water.

The fact that the reversibility and electroactivity of the electrodes appears to decrease with increasing sonication time is also perhaps surprising, since significantly greater surface roughening (and therefore an increase in the apparent area available for electron transfer) with increased sonication time was observed from SEM imaging of the sonicated electrodes (Figure 5.4). It appears from the cyclic voltammograms obtained here therefore, that significant increases in electrode area are accompanied by decreases in heterogeneous electron transfer rates. Zhang & Coury (1993) have also observed that electrodes sonicated in water (albeit glassy carbon) do not result in any significant enhancement in heterogeneous electron transfer rates, even though enhancements for the same redox couples were observed when electrodes were sonicated in dioxane. Furthermore, a similar *degradation* of the rate of electron

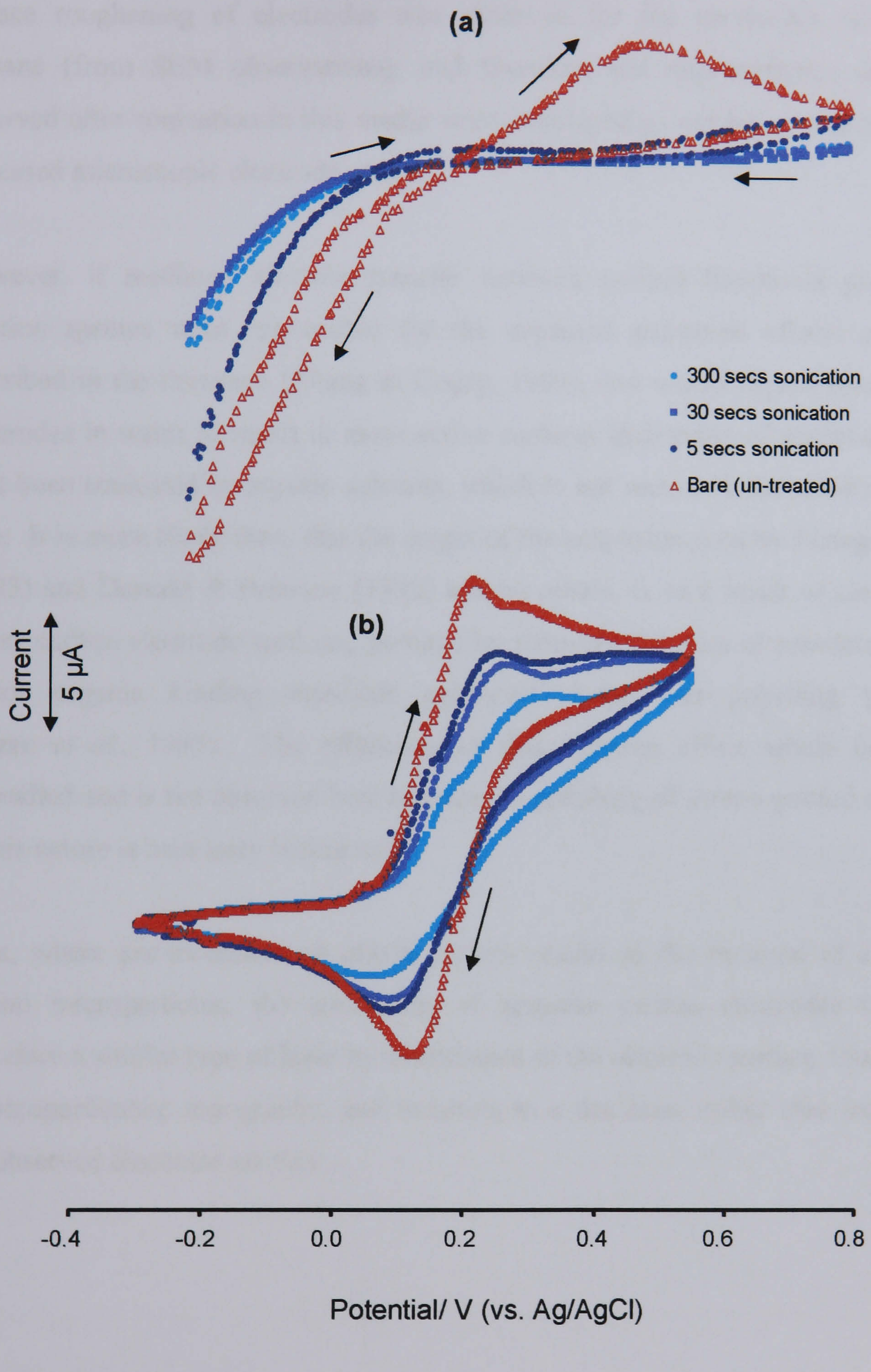

Figure 5.9 **Cyclic voltammograms at bare (un-treated) electrodes, electrodes pre-treated by sonication for 5 seconds, electrodes pre-treated by sonication for 30 seconds, and electrodes pre-treated by sonication for 300 seconds, for two different redox compounds: (a) 5 mM potassium ferricyanide, and (b) 1 mM ferrocenecarboxylic acid.**
[Supporting electrolyte: phosphate buffer (pH 7.8, 0.1M). Scan rate: 20 mVs^{-1}].

transfer, with increases in the peak separation, was routinely observed. However, no surface roughening of electrodes was observed for the electrodes sonicated in dioxane (from SEM observations), and therefore the improvements in kinetics observed after sonication in this media were concluded as not being associated with increased microscopic electrode area.

However, if mediated electron transfer between surface functional groups and solution species were responsible for the expected activation effects previously described in the literature (Zhang & Coury, 1993), one would expect sonication of electrodes in water to result in more active surfaces than those of electrodes which have been sonicated in organic solvents, which is not seen with the results obtained here. It is more likely then, that the origin of the activation seen by Zhang & Coury (1993) and Dewald & Peterson (1990) among others, is as a result of cleaning the glassy carbon electrode surfaces, perhaps by removal of layers of powdered carbon and/or organic binding materials produced during the polishing procedure (Kazee *et al.*, 1985). The efficiency of this cleaning effect would be solvent dependant and is not observed here because no polishing of screen printed electrodes of this nature is necessary before use.

Thus, where pre-treatment on glassy carbon results in the removal of a layer of carbon microparticles, the sonication of graphite carbon electrodes here may *introduce* a similar type of layer by disturbance of the electrode surface, thus creating a microparticulate topography, and resulting in a decrease, rather than increase, of the observed electrode activity.

5.3.2 Amperometric response of modified electrodes to free chlorine

Amperometry was used to evaluate each of the pre-treated/modified electrodes as sensors for aqueous chlorine, in terms of their ability to enhance the signal size resulting from the reduction of free chlorine. All electrodes were polarised at -0.1 V (vs. Ag/AgCl) for 1 minute in a 10 mg/l free chlorine/buffer solution. Figure 5.10 compares the mean steady-state current obtained at each pre-treated/modified electrode both in free chlorine and in buffer alone. Current values for the untreated electrodes are also provided for comparison.

Figure 5.10 indicates an improvement in the electrochemical reactivity of the pre-treated electrodes towards the reduction free chlorine (as compared to untreated electrodes), with the exception of those pre-treated by sonication methods. The sonicated electrodes exhibit a 10-20 nA decrease in current as compared to the bare electrodes, which correlates with the 'deactivation' observed at such electrodes in the previous section. However, such small changes in signal may simply be a result of experimental error. The most significant changes in free chlorine response were observed with electrodes treated by the two electrochemical pre-anodisation methods, with increases in current of 0.78 and 0.35 μA for pre-anodisation in saturated sodium carbonate and 0.05 M phosphate buffer, respectively. The PANI modified electrodes also exhibited an enhanced response, with a 0.25 μA increase in the current recorded after 60 seconds polarisation.

Comparable background currents were registered with most of the untreated and treated electrodes, with the most significant increase being at those modified with polyaniline. The fact that the electrodes pre-treated by all other methods, despite possessing an increased surface area from SEM investigations made in Section 5.2, do not exhibit large changes in background current, is further prove that the increase in observed current is not a direct result of increasing electrode surface area available for electron transfer. These results are favourable compared to those reported previously in the literature. For example, Bjelica *et al.* (1980) reported that the

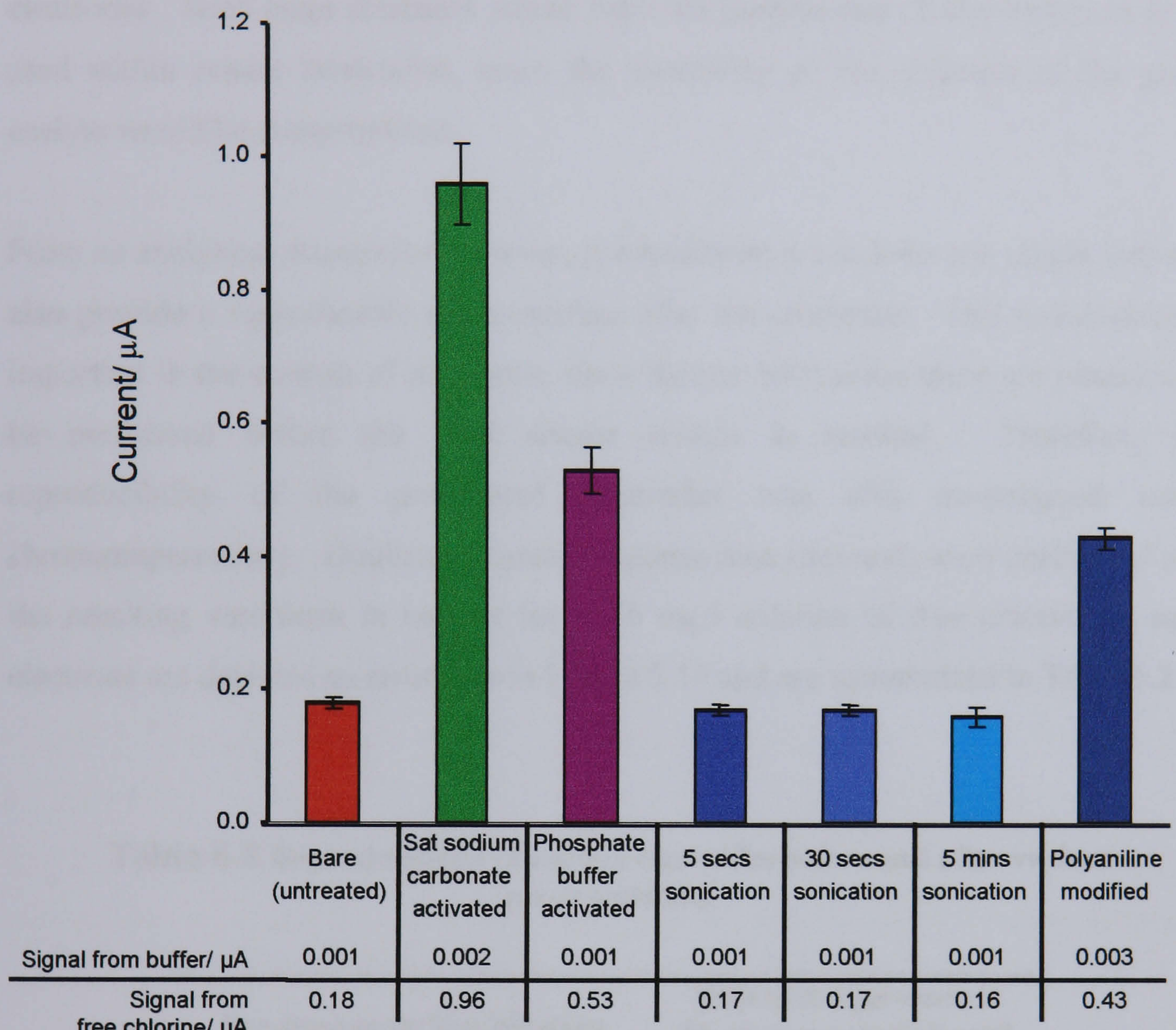

Figure 5.10 Amperometric responses of screen printed carbon electrodes after various pre-treatment to 10 mg/l free chlorine.
[Supporting electrolyte: phosphate buffer (pH 7.0, 0.1M).
Polarising potential: -0.1 V (vs. Ag/AgCl)].

differential capacity of glassy carbon increased by more than an order of magnitude upon anodic pre-oxidation, resulting in increased background currents. Similar increases in the background current have been reported for anodised glassy carbon (Engstrom & Strasser, 1984; Bjelica *et al.*, 1980) and carbon paste (Rice *et al.*, 1983) electrodes. Such large increases would limit the possibilities of the treatment to be used within sensor fabrication, since the sensitivity of the electrode to the given analyte would be compromised.

From an analytical standpoint however, pre-treatment procedures are sought that can also provide a *reproducibly* active surface after the treatment. This is particularly important in the context of this work, since further fabrication steps are intended to be performed before the final sensor outline is reached. Therefore, the reproducibility of the pre-treated electrodes was also investigated using chronoamperometry. Duplicate current response measurements were performed and the resulting variations in current for a 10 mg/l solution of free chlorine at each electrode are depicted as error bars in Figure 5.10 and are summarised in Table 5.2:

Table 5.2 Reproducibility of carbon electrodes before and after various pre-treatments.

Pre-treatment/Modification	RSD of Amperometric Measurement of 10 mg/l Free Chlorine
No pre-treatment (bare)	2.1 %
Pre-anodisation in sat. Na_2CO_3	6.4 %
Pre-anodisation in 0.05 M phosphate buffer	6.4 %
Sonication in water for 5 secs	2.2 %
Sonication in water for 30 secs	2.2 %
Sonication in water for 300 secs	4.3 %
PANI modified	3.6 %

There is little change in the reproducibility of the electrodes sonicated for 5 and 30 seconds, as would be expected since no change in signal size for free chlorine measurement was observed at these electrodes. Contrastingly, the RSD approximately doubles from 2.1 % at the bare electrodes to 4.3 % at those sonicated for 300 seconds. This is not surprising since a greater degree of surface disruption is observed at electrode sonicated for such a long period (Figure 5.4). Both pre-anodisation procedures result in a 4.3 % increase in RSD as compared that obtained at a bare (un-treated) electrode, which is probably too high for their use in practical terms. The only procedure that combines an increase in current with a sustainable reproducibility for the amperometric measurement of free chlorine is the modification of electrodes with a film of conducting polyaniline, yielding electrodes whose reproducibility performance of responses is under 4 % RSD. Good reproducibility is likely to occur at PANI modified electrodes since SEM analysis (Figure 5.3) has shown the deposited PANI film to possess a very smooth surface topography.

Figure 5.11 displays typical current-time transients obtained for 10 mg/l free chlorine at electrodes pre-anodised in saturated sodium carbonate solution, electrodes pre-anodised in 0.05 M phosphate buffer and electrodes modified with a film of polyaniline, in order to demonstrate the practical sensing utility of such activated carbon strip electrodes in terms of their 'wet-up' characteristics (i.e. response time to steady-state). The error from the mean is shown for each electrode as error bars at each 10 second time interval and the current-time transient at an untreated electrode is again provided for comparison. Plots for the measurement of free chlorine at pre-sonicated electrodes are not shown for clarity, since it has already been seen that no improvement in signal size for free chlorine reduction is obtained at such electrodes.

At the untreated electrodes, the current is seen to reach a steady state at approximately 40 seconds after the initial polarisation. The phosphate buffer activation, despite yielding a higher current, also reaches a steady state at approximately 40 seconds, although the reproducibility at this point is compromised

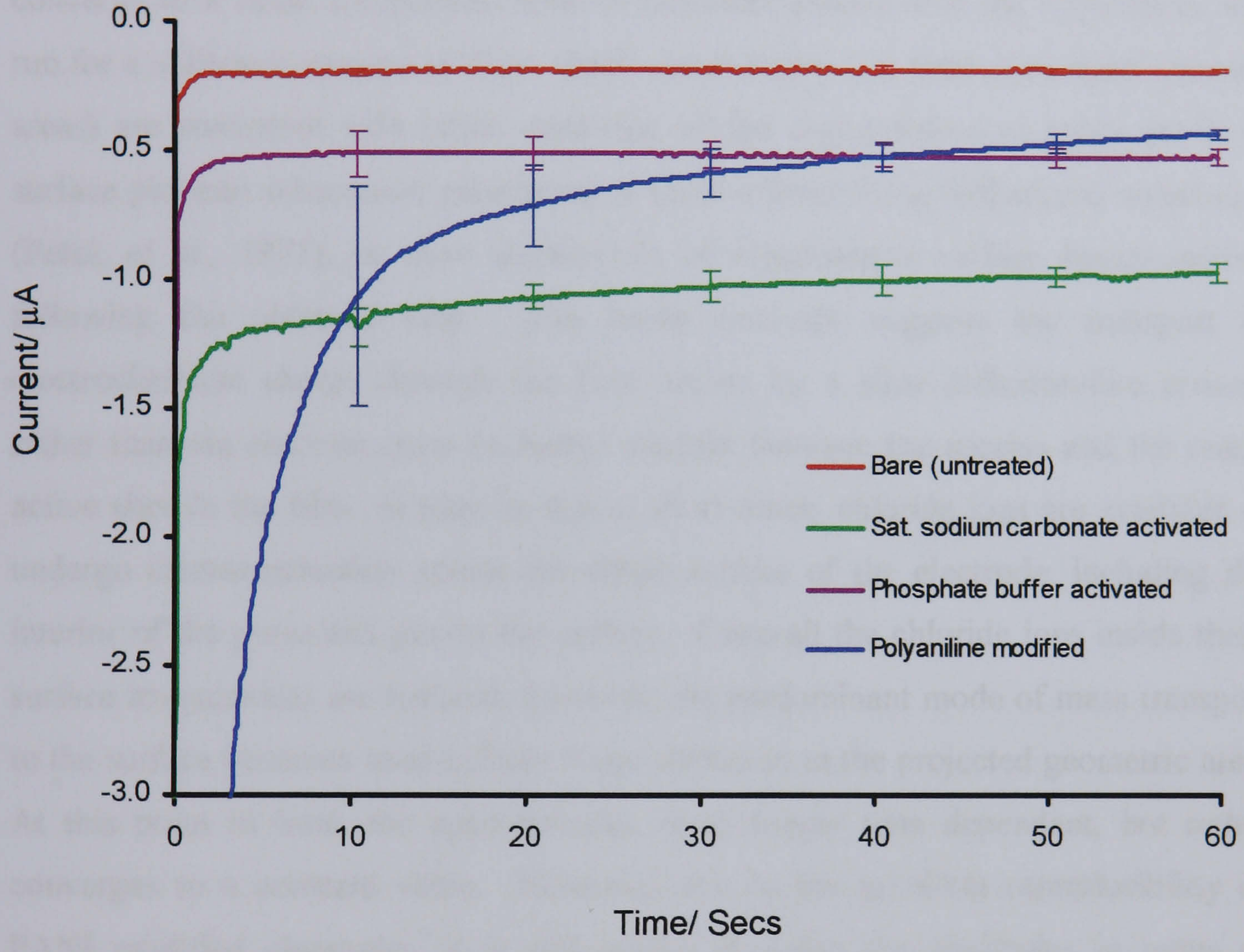

Figure 5.11 Current-time transients of 10 mg/l free chlorine at screen printed carbon electrodes after various pre-treatments.
[Supporting electrolyte: phosphate buffer (pH 7.0, 0.1M).
Polarising potential: -0.1 V (vs. Ag/AgCl)].

somewhat. Similarly, the saturated sodium carbonate activation method produces electrodes that reach a *quasi*-steady state in less than 1 minute, but again, the reproducibility is not sufficient enough to enable their use in real terms. Significant increases in the charging current at electrodes modified with polyaniline are observed and the electrodes never reach a true steady-state within the time interval performed. The nature of the transient curve could lead one to believe that the current may converge to a value comparable with an untreated electrode if the experiment was run for a sufficient amount of time. Such observations (i.e. time dependant apparent areas) are consistent with either depletion of the concentration of redox probe in surface pits and subsequent generation of semi-infinite linear diffusional conditions (Petek *et al.*, 1971), or slow electrolysis of electroactive surface functionalities following the potential step. The result certainly suggests the transport of electrochemical charge through the film occurs by a slow diffusion-like process rather than via electron cross exchange transfer between the species and the redox active sites in the film. It may be that at short times, chloride ions are available to undergo electro-reduction across the entire surface of the electrode, including the interior of the pores and pits in the surface. Once all the chloride ions inside these surface irregularities are reduced, however, the predominant mode of mass transport to the surface becomes semi-infinite linear diffusion to the projected geometric area. At this point in time, the apparent area is no longer time dependant, but rather converges to a constant value. However, due to the excellent reproducibility of PANI modified electrodes, it is still viable to utilise the electrodes in terms of providing an enhanced signal size for free chlorine measurement, since values can be reliably recorded in less than one minute, at a point in the transient where the reduction signal is still comparatively more than that measured at untreated electrodes after the same response time has passed.

There are a number of possible explanations as to why increases in free chlorine signal are observed at both the pre-anodised and PANI modified electrodes despite no improvement in the cyclic voltammetric behaviour of such electrodes being seen to $[Fe(CN)_6^{3-/4-}]$ and $[Fc(CO_2H)^{3+/2+}]$ (with the exception of $[Fe(CN)_6^{3-/4-}]$ at carbonate activated electrodes). The most obvious of these is that different

electrochemical species are being measured, since the effectiveness of electrochemical pre-anodisation has already been found by Engstrom (1982) to be dependant upon the electrochemical species undergoing electrolysis. Engstrom showed that the process which activated the electrode with respect to hydroquinone actually deactivated the electrode with respect to ferricyanide and thus analogically, the process which activated the electrodes tested here to free chlorine may also have resulted in deactivation with respect to $[Fe(CN)_6^{3-/4-}]$ and $[Fc(CO_2H)^{3+/2+}]$.

As discussed previously, another explanation may be that anodisation causes the formation of an oxide layer at the surface of the electrodes which may have a strong inhibitory effect on the reactions of $[Fe(CN)_6^{3-/4-}]$ and $[Fc(CO_2H)^{3+/2+}]$, but not to the reduction of free chlorine. The activation in relation to free chlorine must involve either the oxidation of the surface to produce functionalities capable of catalysing the electrochemical reaction or the oxidative removal of impurities from the surface, and may occur directly by electrochemical oxidation or indirectly by oxygen production during anodisation. It is more likely that the effect is direct since previous studies involving the measurement of oxygen output at electrodes upon the application of pre-anodisation potential have indicated that the presence of oxygen alone is not sufficient to activate the electrode (Engstrom & Strasser, 1984). If the presence of such an oxide layer is the cause of the differences in activity observed between species at pre-anodised electrodes, it may be possible to overcome the inhibitory nature of the oxide layer to the reduction of $[Fe(CN)_6^{3-/4-}]$ and $[Fc(CO_2H)^{3+/2+}]$ via the incorporation of a further pre-cathodisation step. Engstrom & Strasser (1984) reported that in cases where the anodisation step of the pre-treatment produced a layer on the electrode that inhibited the reduction of ferricyanide, a further cathodisation step reduced this layer, leaving a surface with increased activity. A similar phenomena for the measurement of hydrazine was observed by Wang *et al.* (1996) - a short pre-cathodisation period (20 seconds at -0.5 V vs. SCE) was required for activation and was attributed to the cathodic removal of inhibitory layer. This procedure may result in a surface that would be active towards all of the species investigated and is certainly an area for further work.

Alternatively, the increases in peak separations observed at pre-anodised electrodes when tested in $[Fe(CN)_6^{3-/4-}]$ and $[Fc(CO_2H)^{3+/2+}]$ may not be as a result of a decrease in electroactivity at these electrodes, but instead may be a consequence of a gradual progression from macroscopic to microscopic electrode characteristics. As discussed in Chapter 4, Rice *et al.* (1993) suggested that ΔE_p values are an indicator for the charge transfer inhibition within a material and hence, the increase in ΔE_p values observed here would suggest a decrease in the charge transfer at the treated electrodes. This may be due to the breakdown of the polymeric binder in the ink (which is supported by the SEM images shown in Figure 5.1) resulting in an introduction of void spaces and an increase in spacing between the graphite particles, in addition to disturbing the conductive stratum that exists throughout the printed film. This loss of conductivity in itself may be the cause of the lesser electroactive surface, but furthermore, it is possible that the topography of carbon ink is disturbed by the treatment such that individual graphite particles now act as microelectrodes whose diffusion layers no longer overlap. A true microelectrode array would yield a sigmoidal shaped voltammogram however, the hysteresis observed at the cyclic voltammograms obtained here may have resulted from the random nature of the pre-treatment resulting in some overlapping of diffusion layers and some increase in linear diffusion. Microelectrode behaviour at treated carbon electrodes was also observed by Cui *et al.* (2001b) - sigmoidal shaped curves were obtained at very slow scan rates (1 mVs^{-1}) implying that pre-treated electrodes behave as random microelectrode arrays, as was also suggested by Brainina & Bond (1995). This would also contribute towards the increased sensitivity of the electrodes to free chlorine amperometric experiments.

The increase in current observed at the PANI film coated electrodes is somewhat surprising since it is thought that PANI films only respond to dissolved species over the potential region where PANI itself is redox active (Oyama *et al.*, 1983). For PANI films deposited in acidic media (as was undertaken here), PANI is electro-active (i.e. present as the emeraldine salt form) in the potential region between -0.05 and +0.6 V (vs. Ag/AgCl) (McGurk, 2002). For the measurement of free chlorine, the electrodes are polarised at -0.1 V (vs. Ag/AgCl), which is just

outside the electro-active active region of the PANI film and therefore, one would not expect to see an increase in free chlorine signal at PANI coated electrodes polarised at this potential. However, Yano *et al.* (1992b) have also opposed this theory, reporting responses of several organic and inorganic species at PANI coated electrodes in spite of such an electro-inactive potential region of PANI.

The increase in current at the PANI coated electrodes outside the electroactive region is probably caused by interactions between the PANI film and the chlorine species. PANI releases dopant anions over the electro-inactive potential region because of the deprotonation of the PANI nitrogens that accompanies oxidation to the imine form (Chiang & MacDiarmid, 1986). The limited dopant anions that exist near the film/solution interface are expected to be released from the films due to their small diffusion co-efficient of approximately 10-13 cm^2s^{-1} (Yano *et al.*, 1992b), and the redox active sites still remain inside the film. The chloride species, having a Stokes radii of 1.2 Å (Sata, 2000), is able to permeate through the PANI film to reach the oxidised sites. The redox active sites are oxidised to give the films their oxidised quinone products. The quinones are incorporated into areas within the film containing the deprotonated nitrogens and play the role of dopant anions, promoting electron hopping between the redox active sites within the films, since they are π-electron-rich species. Similarly, we can predict that enhanced current responses would be observed for the measurement of total chlorine at PANI modified electrodes, since I^- has a size roughly equal to that of Cl^- (Yano *et al.*, 1992b).

5.5 CONCLUSIONS

This chapter has described a number of methods (and their subsequent analysis) for the pre-treatment and modification of screen printed carbon electrodes and their exploitation within electrochemical sensor production methodology has been discussed.

Sonochemical pre-treatment, despite causing considerable electrode surface roughening, did not increase the observed current resulting from the amperometric reduction of free chlorine and in addition, appeared to deactivate electrodes to ferricyanide and ferrocenecarboxylic acid solutions.

Electrochemical polymerisation of aniline at screen printed carbon electrodes yielded smooth films of polyaniline at the electrode surfaces under SEM analysis. Electrodes modified by such films did not respond to ferricyanide and showed only a small response to ferrocenecarboxylic acid. However, the current resulting from the reduction of free chlorine was seen to more than double at PANI modified electrodes. In addition, a relative standard deviation in measurements of less than 4% allows for electrode responses to be recorded in less than 60 seconds.

Electrochemical anodisation pre-treatment methods were proposed to remove some of the polymeric binder present in the carbon ink and thus, increase the microparticulate nature and roughness of the carbon electrode surfaces. Despite this, no improvement in the electron transfer kinetics of ferricyanide or ferrocenecarboxylic acid was observed at electrodes pre-anodised in phosphate buffer solution, although some improvement was seen with electrodes having pre-anodisation in saturated sodium carbonate solution. However, significant increases in the response to free chlorine were seen at electrodes pre-anodised in both solutions, although an accompanying increase in the relative standard deviation of results was also observed in both cases.

However, deductions on the relationship between the electrochemical behaviour of the treated electrodes and the physio-chemical properties have not been confirmed by these studies. One would assume that such an important parameter as the surface treatments giving rise to structural alteration would be directly responsible for changes in the observed electrochemical behaviour. However, it seems more likely from the results shown here that incidental structural alterations are caused by other factors that are not observable at the microscopic scale chosen.

Whether or not electrochemical pre-treatment is indicated as useful was seen to depend upon the nature of the system under study. A number of possible reasons for this behaviour were hypothesised including: (i) the formation of a selectively inhibitory oxide layer at pre-anodised electrodes, (ii) a decrease in charge transfer between graphite particles at treated electrodes resulting in such electrodes to act as randomly spaced microelectrode arrays, and (iii), in the case of PANI modified electrodes, the transport of electrochemical charge through the film by a diffusion dominated process and subsequent electron cross exchange transfer between the analyte species and the redox active sites in the film.

The increased electrochemical reactivity and selectivity of the pre-treated carbon ink electrodes presented in this chapter offer many possibilities in the field of electrochemical sensing. Their application in chlorine sensing devices is particularly promising and indeed, the results presented here may have a profound effect upon the ability of screen printed carbon ink substrates to be used for the electrochemical measurement of free chlorine, in particular for the programme of work undertaken within this study.

CHAPTER 6

EVALUATION AND OPTIMISATION OF POLY(*o*-PHENYLENEDIAMINE) FILMS FOR USE AS INSULATING LAYERS WITHIN SONOCHEMICALLY FABRICATED MICROELECTRODE ARRAYS

6.1 INTRODUCTION

Electropolymerisation of heteroaromatic compounds on electrode surfaces has become one of the many effective methods used to modify electrodes. Among electrodeposited polymers, the material obtained by electropolymerisation of *o*-phenylenediamine (*o*PD), commonly known as poly(*o*-phenylenediamine) (PPD) or polydiaminobenzene, has received a great deal of attention over the last 20 years. Since the first report on the polymerisation of *o*-phenylenediamine on conducting substrates via electrochemical oxidation (Yacynych & Mark, 1976), a number of papers have appeared on possible applications of the resultant polymer films. Electrochemical diodes (Ohnuki *et al.*, 1983), anticorrosion coatings (White *et al.*, 1982), pH measurements (Cheek *et al.*, 1983) and in particular, enzyme entrapping permselective membranes in biosensor design (Heineman *et al.*, 1980), represent the main fields of application. More recently, we have explored a new possible application for PPD in the field of sonochemically fabricated microelectrode arrays (Myler, 2000). A film of PPD may be electrochemically deposited at an underlying conductive substrate in order to insulate the electrode and then, due to its extremely thin depth (in the order of nanometres), may be subsequently sonicated in order to expose microscopic pores in the film (discussed further in Chapter 7), thus forming a microelectrode array.

As has previously been discussed in Chapter 2.6, PPD films in particular lend themselves to this application since they are strongly adherent, highly reproducible membranes (Malitesta *et al.*, 1990), which completely cover the electrode surface regardless of dimension. The use of such films not only provides an economic advantage, but the electropolymerisation of *o*PD from phosphate buffers may yield non-conducting and electro-inactive PPD films. Such synthesis also offers possibilities of producing self regulating, ultra-thin and essentially defect free films with uniform thickness, since they only grow thick enough to become insulators (Liu *et al.*, 1992).

However, in order to exploit these properties successfully for the intended application, a number of challenges regarding both the preparation and characterisation of the films have to be overcome. This chapter will therefore describe the optimisation of the electro-polymerisation process so that the most ideal films (i.e. the most insulating/reproducible) are produced.

The formation of ultra-thin insulating layers of PPD via the electrochemically initiated polymerisation of *o*PD was initially performed upon the surface of gold supporting electrodes and is described in Section 6.2.1. Cyclic voltammetry was used to both polymerise *o*PD and to study the electroactivity of the resulting PPD coated electrodes. The mechanism of the film formation process is discussed in Section 6.3.

Section 6.4 describes the electrodeposition of PPD upon *carbon* supporting electrodes, with comparisons being made to the deposition upon gold electrodes made in Section 6.2. The effects of various experimental parameters on the chemical and physical properties of the film will also be described, thus allowing for optimisation of the layer upon carbon supporting electrodes (Section 6.4.2). The optimal polymerisation conditions concluded from Section 6.4.2 are the electropolymerisation parameters used to simultaneously deposit PPD films upon sheets of 100 electrodes (Section 6.4.3), and again cyclic voltammetry is used to study the electroactivity of the resulting electrodes, in order to ascertain the success of simultaneous polymerisation upon multiple electrodes.

Microscopic examinations of the films deposited upon gold and carbon electrodes are performed in Sections 6.2.2 and 6.4.4 respectively, and finally the insulating properties of the layer in respect to its use in an amperometric sensor are determined using hexaammineruthenium(III) chloride and total chlorine as electrochemical probes.

6.2 ELECTRODEPOSITION OF POLY(*o*-PHENYLENEDIAMINE) UPON GOLD HOST ELECTRODES

6.2.1 Electrodeposition of the polymer film

Poly(*o*-phenylenediamine) (PPD) films were initially grown on the working electrode surfaces of gold sputter-coated ground glass slides as previously reported by Myler *et al.* (1997). PPD can be formed electrochemically using a constant potential or cyclic voltammetric method, however, previous work has shown that the use of cyclic voltammetry results in a more useful film for use within sensors in terms of enhanced resistance to interferents (Curulli *et al.*, 1998). Therefore, electrodes were scanned between 0 and +0.8 V (vs. Ag/AgCl) at a scan rate of 50 mVs^{-1} in pH 7.4 buffered solutions of 5 mM *o*PD, as described in Chapter 3. The polymerisation was stopped after 20 potential cycles. The cyclic voltammogram corresponding to the electrodeposition of the film is shown in Figure 6.1a (the cycles are sequentially numbered). Figure 6.1b shows the total charge involved in the polymer deposition as a function of the number of potential cycles.

The voltammogram is depicted by a large anodic irreversible oxidation peak on the first scan, which is characteristic of almost all aromatic diamines and its position is believed to be specific to each differing monomer (Li *et al.*, 2002). The shape of the deposition is very similar to that seen by Malitesta *et al.* (1990), in that the anodic current starts to rise at approximately +0.1 V with two peaks being observed at +0.3 V and +0.5 V (vs. Ag/AgCl), respectively. Early hypotheses of the mechanism of film formation (Lui *et al.*, 1992; Martin *et al.*, 1991) suggest a classical 'gel-point' mechanism. The gel-point mechanism shows two temporal windows; (i) an induction period during which soluble polymer particles are produced, but no polymer is obtained followed by (ii) an instantaneous production of solid polymer gel. This explosive growth occurs because the concentration of polymer particles has been increased to the point where these particles can interact. This produces a

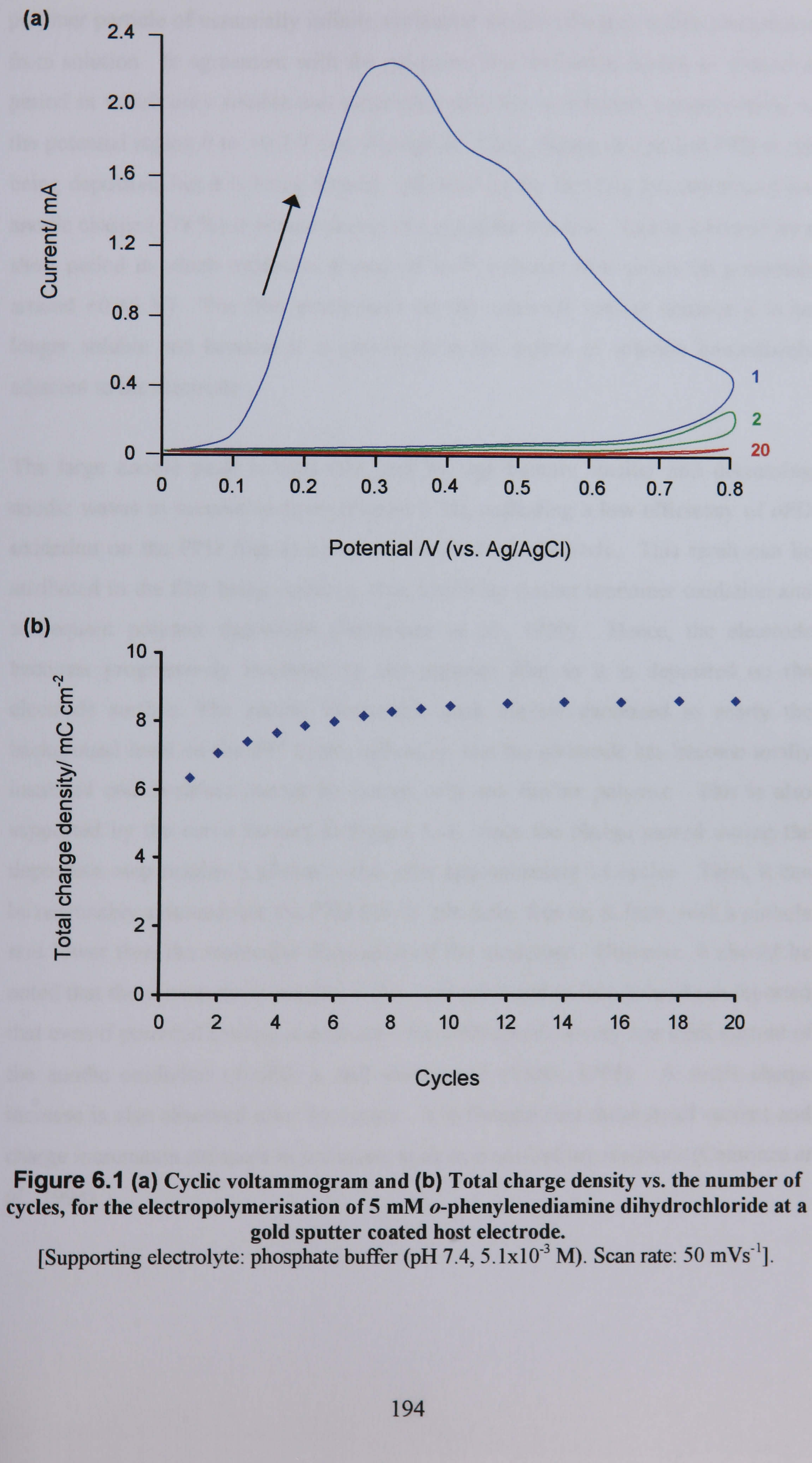

Figure 6.1 (a) Cyclic voltammogram and (b) Total charge density vs. the number of cycles, for the electropolymerisation of 5 mM *o*-phenylenediamine dihydrochloride at a gold sputter coated host electrode.
[Supporting electrolyte: phosphate buffer (pH 7.4, 5.1×10^{-3} M). Scan rate: 50 mVs^{-1}].

polymer particle of essentially infinite molecular weight (the gel) which precipitates from solution. In agreement with the gel-point film formation model, an induction period in which only soluble and suspended polymer is obtained, corresponding to the potential region 0 to +0.3 V (vs. Ag/AgCl). Thus, during this period PPD is not being deposited, but it is being formed, indicated by the fact that the majority of the anodic charge (~73 %) is passed during this potential window. This is followed by a short period in which explosive growth of solid polymer film occurs (at potentials around +0.35 V). The film precipitates on the electrode surface because it is no longer soluble and because it is generated in the region of solution immediately adjacent to the electrode.

The large anodic peak is then followed by significantly smaller and decreasing anodic waves in successive scans (Figure 6.1a), indicating a low efficiency of *o*PD oxidation on the PPD film as compared to the bare electrode. This result can be attributed to the film being resistive, thus hindering further monomer oxidation and subsequent polymer deposition (Heineman *et al.*, 1980). Hence, the electrode becomes progressively insulated by the polymer film as it is deposited on the electrode surface. The anodic irreversible peak current decreased to nearly the background level on the 20^{th} cycle, indicating that the electrode has become totally insulated and therefore cannot be coated with any further polymer. This is also supported by the curve formed in Figure 6.1b, since the charge passed during the deposition step reaches a plateau value after approximately 14 cycles. Thus, it can be reasonably assumed that the PPD film is 'pin-hole' free or, at least, with a pinhole size lower than the molecular dimension of the monomer. However, it should be noted that the current never reaches a true zero point and in fact, it has been reported that even if potential cycling is continued for 1000 cycles, a very low peak current of the anodic oxidation of *o*PD is still maintained (Yano, 1995). A small charge increase is also observed after 20 cycles. It is thought that these small current and charge increments are spent in processes such as cross-linking reactions (Centonze *et al.*, 1994).

6.2.2 Microscopic examination of the film surface topography

The surfaces of both bare gold sputter-coated assemblies and PPD coated glass slides were examined using scanning electron microscopy and the images obtained are shown in Figure 6.2. There is no obvious difference in surface topography between the bare (Figure 6.2a) and PPD coated (Figure 6.2b) electrodes, as would be expected with such a thin film since it is known that most thin film deposition techniques result in the imperfections of one layer being transferred from a (solid) substrate through a thin film to the surface (Tolan *et al.*, 1996). This leads to 'so-called' conformal or correlated roughness (i.e. the polymer does not 'fill in' the cavities on the substrate). However, the difference in shading between the two images does suggest a difference in conductivity between the electrodes, since the consistent bright contrast of the PPD coated electrode is probably a film interference effect. This has also been observed with SEM analysis of similar insulating films by Liu *et al.* (1992).

The section of electrode surface imaged here was consistent with the electrode as a whole. Thus, the consistency of the contrast and topography, indicates that the films obtained have uniform thickness and are contiguous across the entire electrode surface. This is an especially important feature because for a diffusion-controlled process, the current at the outer edge of the electrode will always be somewhat higher than the current at the centre (Liu *et al.*, 1992). As a result, the region of solution near the outer edge reaches the gel-point concentration before the region of solution adjacent to the centre. Once the outer edge is covered, however, current only flows at the centre. Thus, the region of solution adjacent to the centre ultimately reaches the gel-point, and the centre of the electrode is subsequently covered. This slight non-uniformity of current distribution is proven by SEM analysis to not produce a significant non-uniformity in film thickness.

Thus, scanning electron microscopy of a PPD coated gold electrode confirms that its surface is largely featureless and that the electrode is coated by an essentially defect free film of PPD.

(a)

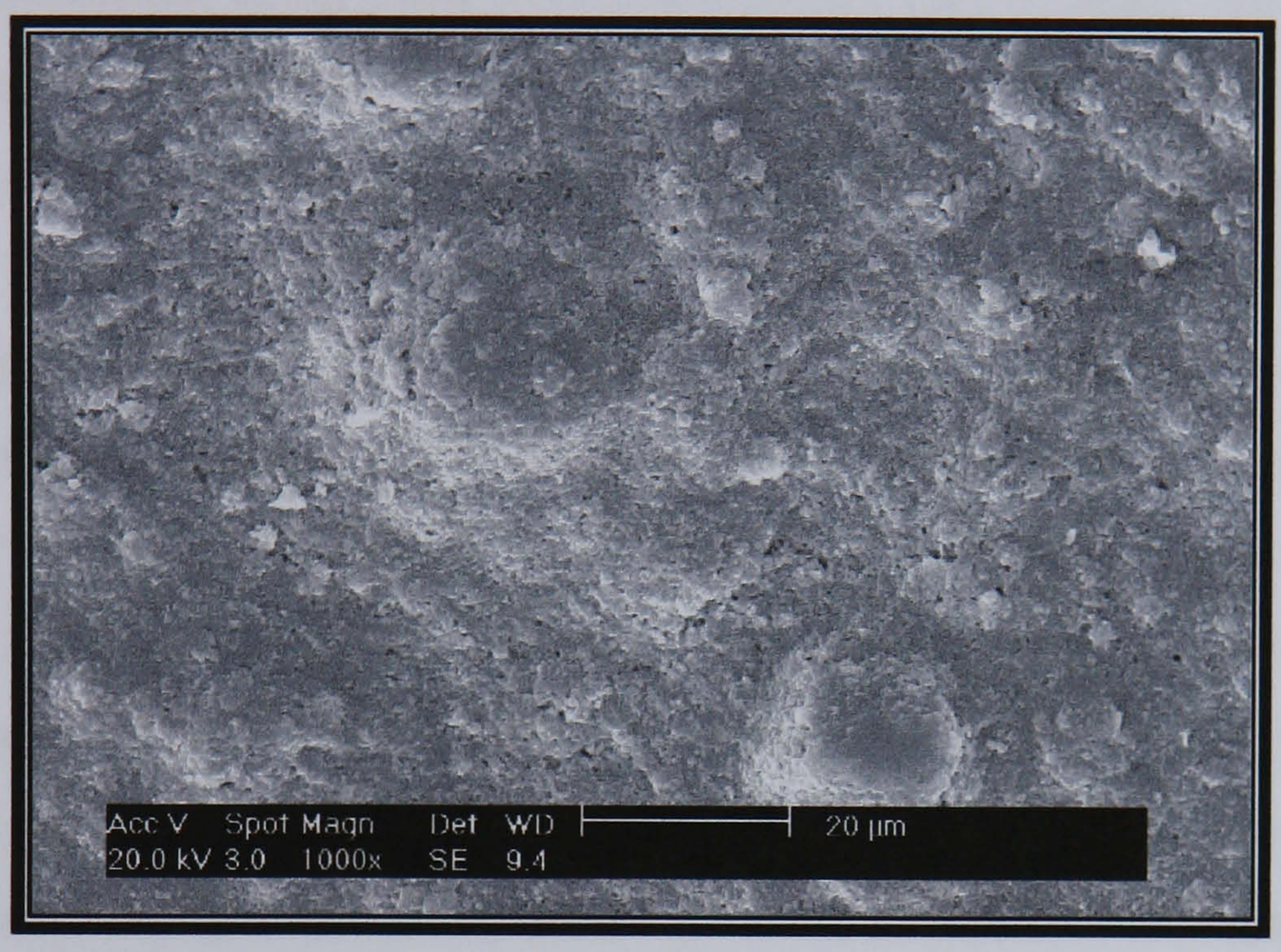

(b)

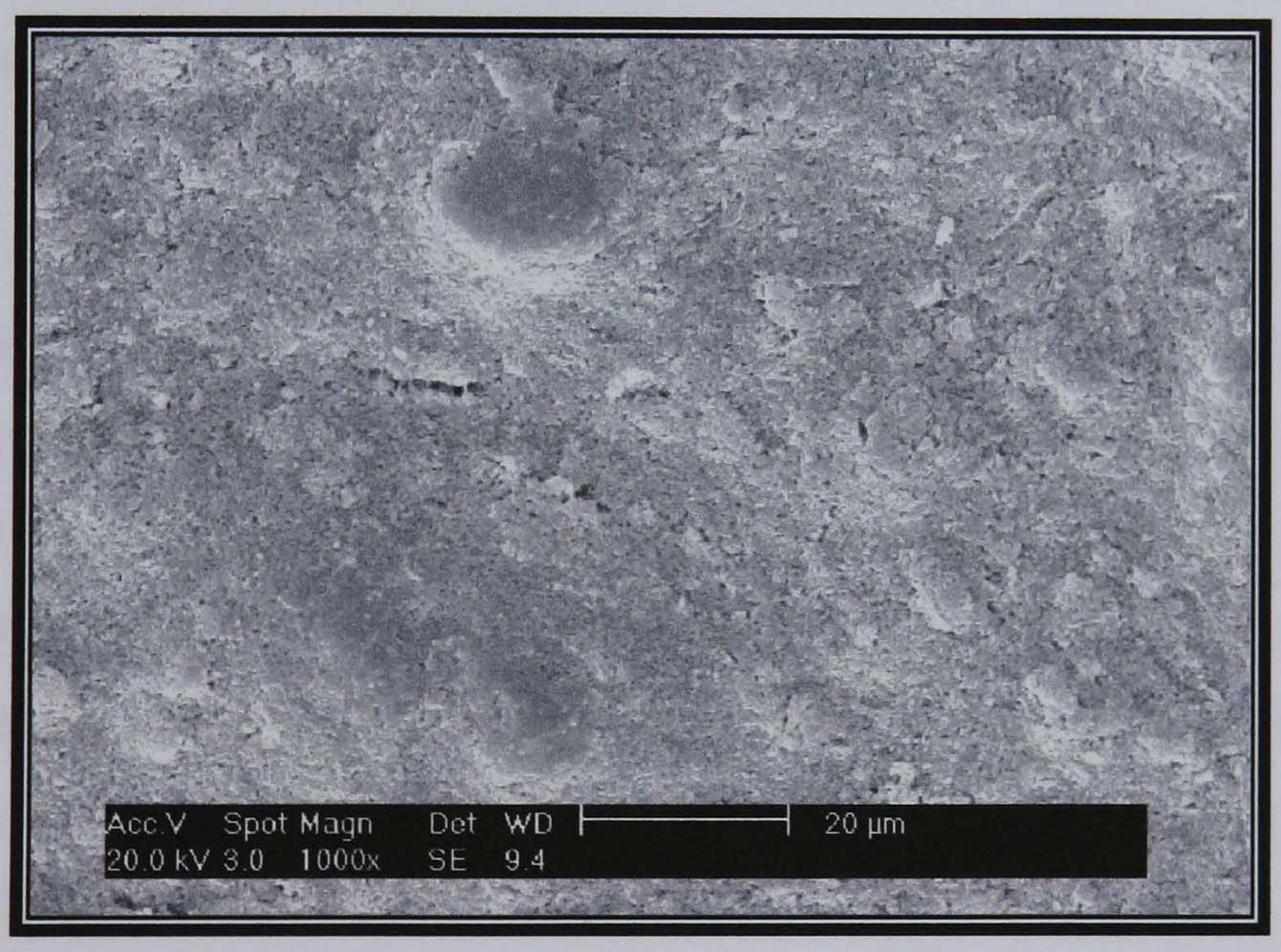

Figure 6.2 Scanning electron micrograph of (a) a bare sputter coated glass slide electrode and (b) a similar electrode coated by an electrodeposited film of poly(*o*-phenylenediamine).
(x1000 magnification).

6.2.3 Estimation of the film thickness using charge integration techniques

Thickness calculations using SEM were found to be experimentally difficult to verify at glass slide/gold electrodes since it was hard to obtain a non-distorted and clean cross sectional cut of the glass backed electrode assemblies. However, since the thickness of films is known to affect the mass transport (Nell & Bohn, 1993) and charge transport (Kondratiev *et al.*, 1999) through the films, in addition to surface roughness and morphology (Chi *et al.*, 2001), it is important to try and estimate the thickness of the films deposited here. A number of instruments and techniques to examine the magnitude of film thickness have been developed recently, for example infra-red spectrophotometry (Kawata & Takeuchi, 1991), alpha-step profiling (Spangler *et al.*, 1990), laser-ultrasound (Dewhurst *et al.*, 1990) and ellipsometry (Villette *et al.*, 1997). However, most of these measurement methods must be performed in vacuum and be accompanied by a series of complicated samples or pre-treatments.

One way in which the film thickness can be calculated is by measuring the total charge passed during the deposition process (Holdcroft & Funt, 1988), which has already been performed experimentally, as shown in Figure 6.1b. This, combined with the fact that electropolymerisation of *o*PD occurs via a two-electron process, along with each monomer unit having an area of ~1.5 x 10^{-19} m^2 and each polymer monolayer having a depth of ~1.4 x 10^{-10} m^2 i.e. the diameter of the largest molecule – carbon (Myler *et al.*, 1997), the thickness of the film, *d*, can therefore be calculated according to Equation 6.1:

$$d = M_n \times M_d \tag{6.1}$$

where M_d is the depth of a single *o*PD monolayer (in metres) and M_n is the total number of *o*PD *monolayers* deposited during the polymerisation (according to Equation 6.2).

$$M_n = U_{tot} / U_{mono} \tag{6.2}$$

where U_{tot} is the total number of *o*PD *units* deposited during the polymerisation and U_{mono} is the number of monomer units per monolayer. U_{tot} and U_{mono} can be calculated from Equations 6.3 and 6.4 respectively:

$$U_{tot} = \frac{Q_{tot}}{n \times Q_{ox}} \tag{6.3}$$

where Q_{tot} is the total charge passed during the polymerisation (in Coulombs), Q_{ox} is the charge passed by one electron (1.6×10^{-19} C) and n is the number of electrons associated with polymer formation.

$$U_{mono} = \frac{A_{electrode}}{A_{mono}} \tag{6.4}$$

where $A_{electrode}$ is the area of the working electrode and A_{mono} is the area of a monomer unit (both in square metres).

Therefore, the thickness of the film formed here on gold sputter-coated glass slides is estimated to be 56 nm, which is slightly thicker than that previously obtained by cross-sectional SEM imaging by Myler *et al.* (1997) on a gold sputter coated polycarbonate membrane electrode (~35 nm).

6.2.4 Electrochemical characterisation of the polymer film

The electroactivity and permeability of the electrochemically deposited PPD films grown on gold substrates was tested by cyclic voltammetry in solutions of 1mM potassium ferricyanide dissolved in pH 7.8 buffer. Figure 6.3 shows cyclic voltammograms recorded at a bare gold electrode (Figure 6.4a) and a similar electrode coated with a film of PPD (Figure 6.3b). The voltammogram corresponding to the bare gold electrode reveals an approximate 59 mV peak separation as would be expected for a one electron diffusional controlled reversible reduction/oxidation process. Contrastingly, very little voltammetric response is observed at the PPD coated electrode, confirming that it has been insulated by the film. The absence of $[Fe(CN)_6^{3-/4-}]$ peaks on the voltammogram corresponding to the PPD covered electrode (Figure 6.3b) agrees with the little data already reported at similar pH values for PPD grown onto gold (Levi & Pisarevskaya, 1992) and platinum (Ohnuki *et al.*, 1983), and serves to exclude the permeation and direct electrochemistry of $[Fe(CN)_6^{3-/4-}]$ (adsorbed onto the film or diffusing from the solution) at PPD modified electrodes. Indeed, it would be expected that $[Fe(CN)_6^{3-/4-}]$ electrochemistry would only be observed on electrodes coated with PPD synthesised at lower pH, where it arises from the direct oxidation of $[Fe(CN)_6^{3-/4-}]$ adsorbed on the polymer surface. This process is hindered on PPD films synthesised at pH 7.4, thus confirming the low electroactivity of these materials, compared to the ones obtained at lower pH.

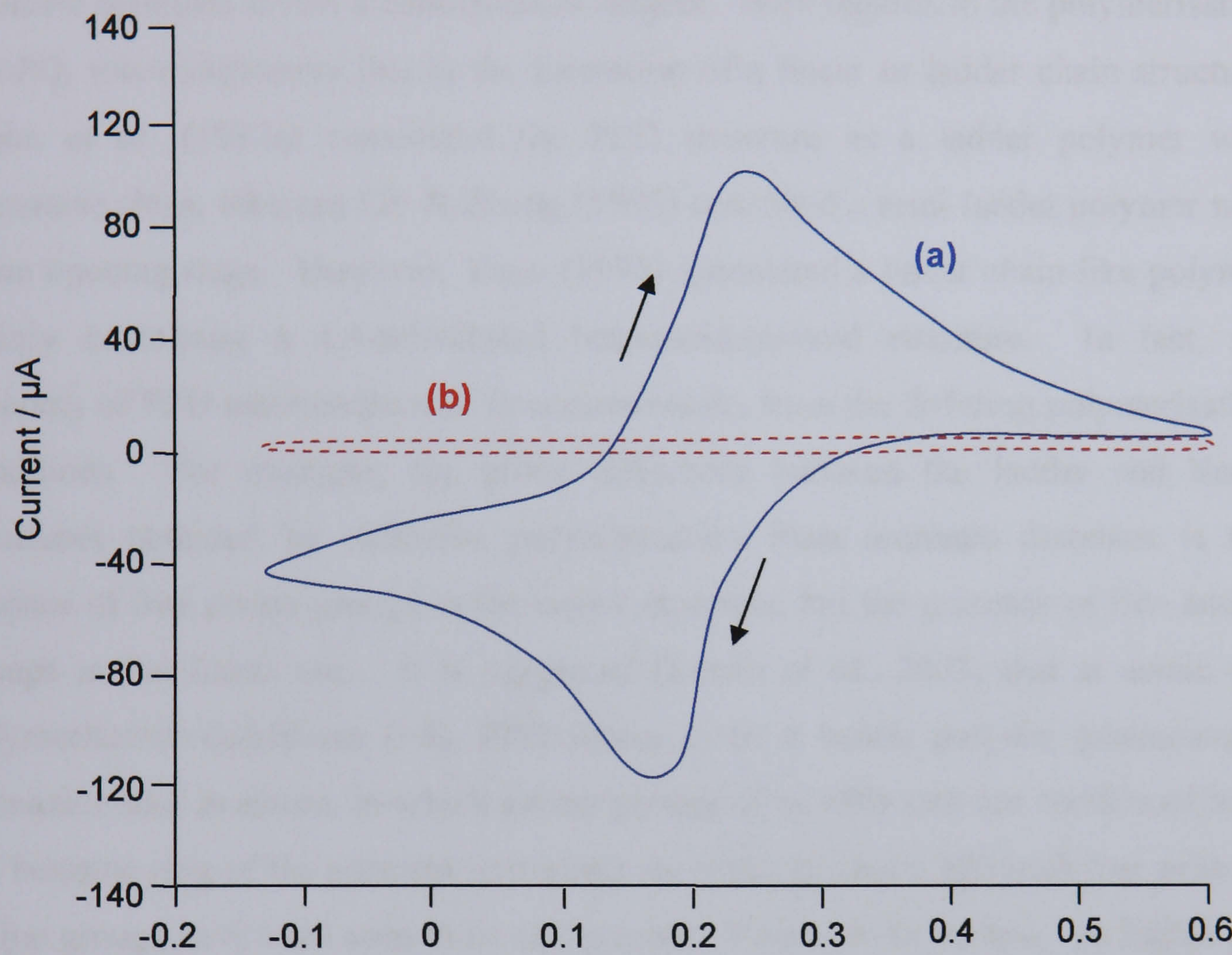

Figure 6.3 **Cyclic voltammetry of 5 mM potassium ferricyanide at (a) a bare sputter coated glass slide electrode and (b) a similar electrode coated by an electrodeposited film of poly(*o*-phenylenediamine).**
[Supporting electrolyte: phosphate buffer (pH 7.8, 0.1M). Scan rate: 20 mVs^{-1}].

6.3 FILM STRUCTURE AND POLYMERISATION MECHANISM

The macromolecular structure of most polymers resulting from the polymerisation of aromatic diamines is still a controversial subject. With regards to the polymerisation of *o*PD, this controversy lies in the formation of a linear or ladder chain structure. Chiba *et al.* (1987a) considered the PPD structure as a ladder polymer with phenazine rings, whereas Lin & Zhang (1996) described a semi-ladder polymer with some opening rings. However, Yano (1995) speculated a linear chain-like polymer mainly containing a 1,4-substituted benzenoid-quinoid structure. In fact, the diversity of PPD macromolecular structures results from the differing polymerisation conditions. For example, the prime difference between the ladder and linear structures obtained by oxidative polymerisation from aromatic diamines is the absence of free amino groups in the ladder structure, but the presence of free amino groups in the linear one. It is suggested (Losito *et al.*, 2003) that at acidic pH polymerisation conditions (<5), PPD seems to be a ladder polymer possessing a phenazine-like structure, in which amino groups of an *o*PD unit are condensed with the benzene ring of the adjacent unit along the polymer chain, although free primary amino groups have been seen to be still present, at least at the surface. At higher pH (>5) conditions, the extent of conjugation is progressively decreased, since there is an increasing amount of free amino groups at the surface. These structures also show some agreement with the properties of PPD synthesised at the particular pH values, for example, the better electroactivity exhibited by the polymer obtained at low pH and the ability of PPD grown at high pH to interact with enzymes (probably due to the presence of neutral or protonated amino groups that interact with enzymes or small molecules). The different macromolecular structures of PPD can thus be attributed to the peculiar mechanisms of the oxidative polymerisation at different conditions.

An understanding of the mechanism of electropolymerisation of *o*PD is important for correlations between oxidation conditions, performance and functionality of the PPD films to be made. The mechanism of oxidative polymerisation of aromatic diamines

is a complicated and diverse process depending on the monomer type, oxidant feature, and polymerisation method and conditions, and as a result, there is no *one* complete mechanism of oxidative polymerisation that is universally accepted for the whole family of aromatic diamines as yet. Due to this uncertainty, a number of different analytical techniques have been adopted to draw information on the PPD structure and to make hypotheses on the polymerisation mechanism. Yano (1995) used FTIR spectroscopy to suggest that one of the amino groups of *o*PD in acidic aqueous solution must be protonated. The positively charged ammonium group without a lone electron pair probably hinders the formation of the phenazine ring during electropolymerisation and then has the *meta* orientation effect. Therefore the head-to-tail coupling is most favourable for the *o*PD polymerisation. Dai *et al.* (1998) proposed a slightly different electropolymerisation mechanism of *o*PD based upon electrochemical quartz crystal microbalance (EQCM) techniques. They reported that the monomers are initially oxidised anodically to give a monocationic radical and then undergo chemical coupling to form a dimer, which can be further oxidised to produce a bi-cation. The bi-cation will undergo polymerisation to form a linear chain polymer or become cyclised to yield a cyclic ladder polymer. Very similarly, Jang *et al.* (1995) used a combination of FT-NMR spectroscopy, cyclic voltammetry and hydrodynamic experiments (RDE and RRDE) to suggest that during electropolymerisation of *o*PD at least two different polymeric components which are responsible for electron mediation are formed: an active component containing phenazine (a cyclic dimer of *o*PD) mainly in the early stage of polymerisation, and an inactive component containing a non-cyclically coupled species.

However, a general mechanism for the polymerisation of *o*PD that could explain the observed changes in cyclic voltammetric behaviour as well as in polymer structure observed with pH variations, was still lacking until the pioneering work of Losito *et al.* (2003). They used a combination of data previously reported for polyaniline (Deng & Van Berkel, 1999) and X-ray photoelectron spectroscopy (XPS) (Centonze *et al.*, 1994), combined with integration of cyclic voltammetry, and electrospray ionisation-ion trap mass spectroscopy (ESI-ITMS). This resulted in

Losito *et al.* (2003) proposing that chain propagation appears to compete with two different intramolecular oxidation processes, leading to the formation of phenazine or 1,4-benzoquinonediimine units, whose relative importance is in turn, dictated by polymerisation conditions (pH and potential).

The mechanism proposed by Losito *et al.* (2003) is represented schematically by Figure 6.4. From Figure 6.4 is can be seen that in any pH condition the first stage of polymerisation is monomer oxidation to the corresponding radical cation, followed by radical coupling (head-to-head, head-to-tail, tail-to-tail) to give three possible different dimers (A1, A2 and A3) that can be further oxidised, by a two electron, two proton process to B1. The fully reduced dimer A1 may be involved in three different and competitive processes: (i) further radical coupling (i.e. chain propagation) to form a trimer, E, (ii) oxidation to the B1 dimer or (iii) internal coupling (intramolecular oxidation followed by cyclisation) leading to the intermediate species B2, which rapidly evolves into its fully oxidised form, 2,3-diaminophenazine (2,3-DAP) (D). The last possibility is strongly supported by cyclic voltammetric experiments performed on a 2,3-DAP standard by Losito *et al.* (2003), which revealed that the dimer B2 (i.e. the reduced form of 2,3-DAP) is more easily reduced than the *o*PD monomer. The fully reduced trimer, E, then plays a role similar to that of the A dimer, leading to either partially (H) or fully (F) oxidised trimers or to the fully reduced tetramer (I).

The key point in the polymerisation mechanism seems to be the competition between oxidative coupling, leading to chain propagation, and intramolecular oxidation processes leading to the formation of (i) phenazine, (ii) 1,4-benzoquinonediimine units or (iii) both. For instance, D and F (the main forms of F1 and F2) arise from phenazine-forming processes, whereas B and H arise from 1,4-benzoquinonediimine forming processes. All these processes (including initial monomer oxidation) are favoured by an increase of polymerisation pH, yet oligomer intramolecular oxidations, especially phenazine-forming ones, seem to occur at potentials lower than those of chain propagation processes, since high amounts of phenazine-like dimers are found in the electrolytic solutions at low pH or potential conditions. On

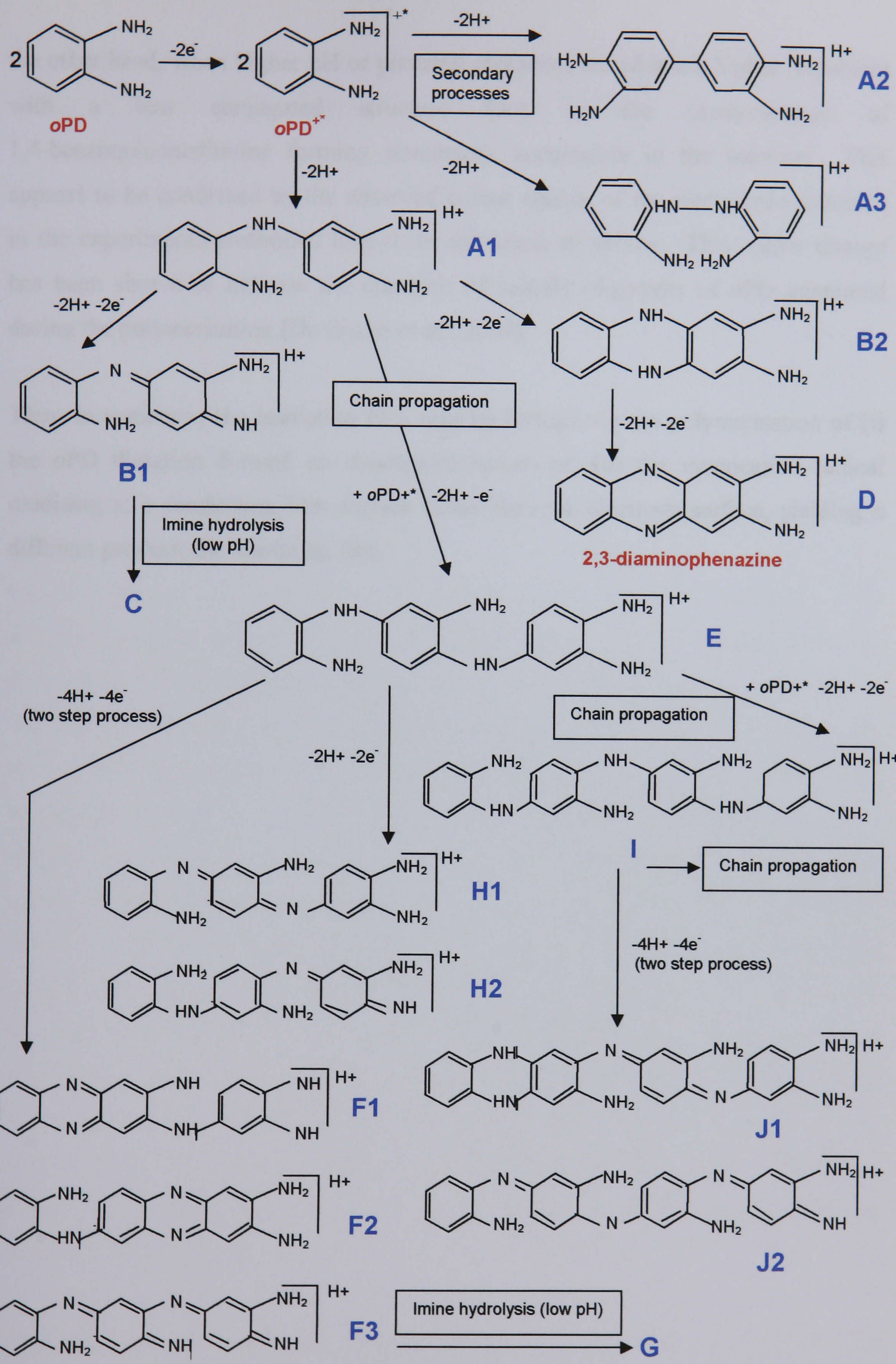

Figure 6.4 Schematic representation of the *o*PD polymerisation mechanism proposed by Losito *et al.* (2003).

the other hand, when higher pH or potential processes are adopted, higher oligomers with a less conjugated structure (due to the predominance of 1,4-benzoquinonediimine forming processes), accumulate in the solution. This appears to be confirmed by the observed colour change of the electrolytic solutions in the experiments preformed here from colourless to yellow. This colour change has been shown to indicate the presence of soluble oligomers of *o*PD generated during the polymerisation (De Giglio *et al.*, 2003).

Thus, in summary, the insulating film may be formed via the polymerisation of (i) the *o*PD di-cation formed on disproportionation or, (ii) the monocation radical oxidising at a conducting film surface rather than the electrode surface, yielding a different product, the insulating film.

6.4 ELECTRODEPOSITION OF POLY(*o*-PHENYLENEDIAMINE) UPON SCREEN PRINTED CARBON HOST ELECTRODES

6.4.1 Electrodeposition of the polymer film onto single electrodes

*o*PD was subsequently electropolymerised onto screen printed *carbon* electrodes, using the same electrochemical conditions as used for the electropolymerisation of *o*PD onto gold electrodes. The voltammogram resulting from the electrodeposition is shown in Figure 6.5a, with the total charge passed after each potential cycle given in Figure 6.5b.

The first anodic scan demonstrates the same features as those observed for *o*PD oxidation on gold electrodes seen in the previous section, i.e. a complex oxidation peak, where the current intensity of the peak decreases upon cycling, suggesting the deposition of an insulating film on the electrode surface. However, in this case, only one maximum is seen in the anodic direction with its peak occurring at approximately +0.6 V (vs. Ag/AgCl), which is more anodic than both the peaks observed at the gold electrode. Furthermore, the potential at which the anodic current starts to rise is also shifted to a more positive potential (+0.2 V compared to +0.1 V (vs. Ag/AgCl) for deposition at a gold electrode). This shift explains why the anodic scans appear to be 'cut-off' at +0.8 V (vs. Ag/AgCl). The differences observed between the voltammograms of PPD deposited upon gold and carbon substrates is likely to be due to the difference in electroactivity of the two working electrode materials. The shape difference between the voltammograms may also be related to the difference in substrate material since it has been postulated that polymerisation upon gold may occur in two separate stages giving the two current maxima peaks (Warrington, 2001).

Figure 6.5b indicates that less charge per unit area is deposited during polymerisation upon carbon electrodes (~1.1 mC) than that expelled during polymerisation upon gold electrodes (~8.6 mC), under the same electropolymerisation conditions. This

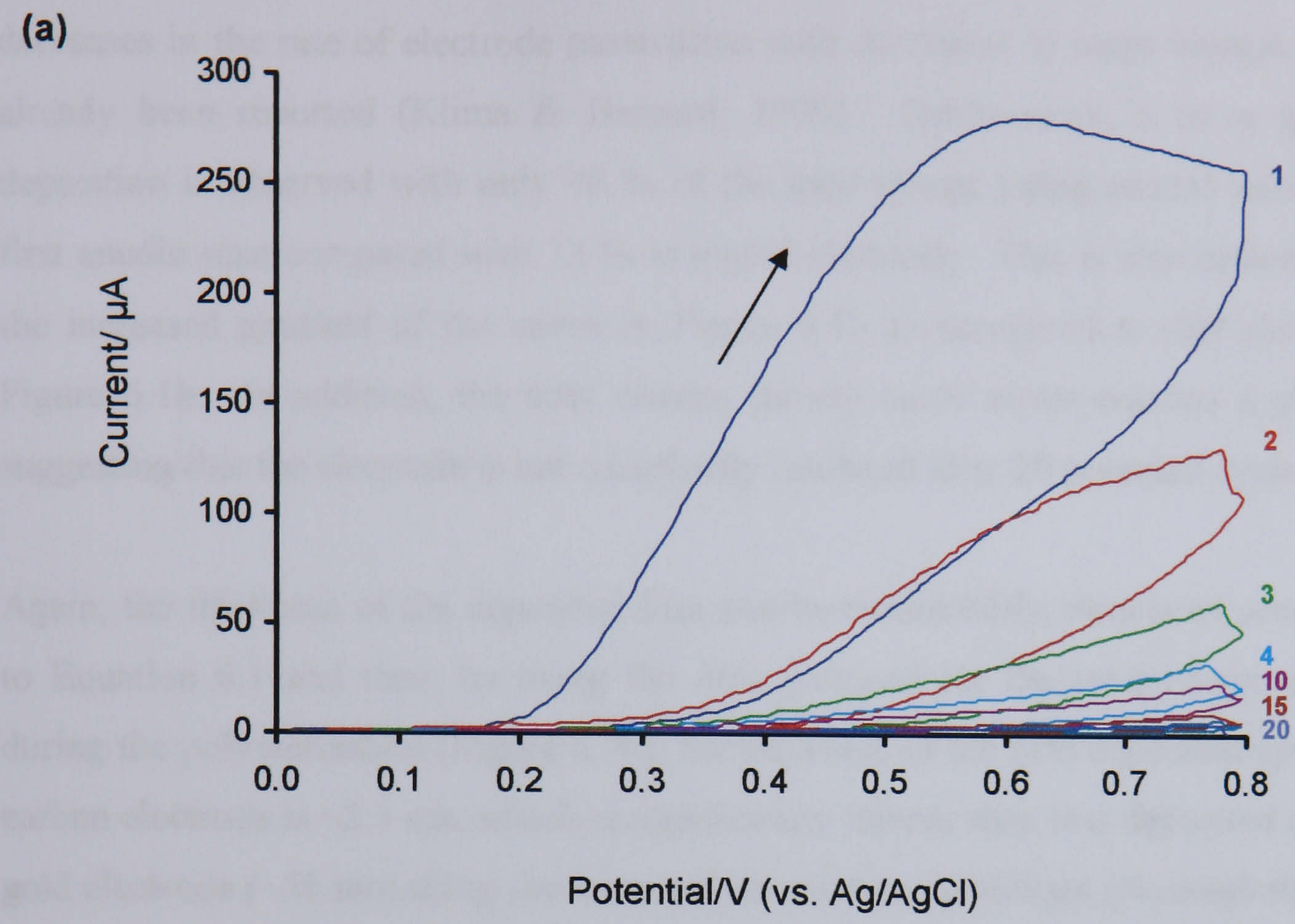

Figure 6.5 (a) Cyclic voltammogram and (b) Total charge density vs. the number of cycles, for the electropolymerisation of 5 mM *o*-phenylenediamine dihydrochloride at a screen printed carbon electrode.
[Supporting electrolyte: phosphate buffer (pH 7.4, 5.1×10^{-3} M). Scan rate: 50 mVs^{-1}].

would be expected since graphite carbon is much less conductive than gold and decreases in the rate of electrode passivation with decreases in mass transport have already been reported (Klima & Bernard, 1999). Furthermore, a more gradual deposition is observed with only 48 % of the total charge being passed during the first anodic scan compared with 73 % at a gold electrode. This is also indicated by the increased gradient of the curve in Figure 6.5b as compared to that shown in Figure 6.1b. In addition, the total charge density curve never reaches a plateau, suggesting that the electrode is not completely insulated after 20 potential cycles.

Again, the thickness of the deposited film can be theoretically calculated according to Equation 6.1 and thus, by using the data obtained for the total charge passed during the polymerisation (Figure 6.5b), the thickness of the film deposited upon the carbon electrode is ~2.3 nm, which is significantly thinner than that deposited upon a gold electrode (~56 nm) using the same polymerisation conditions (although the film may actually be slightly thicker than this since the apparent area of a graphite electrode may not be equal to the electroactive area). This is not surprising since it has been found that electropolymerised films can have significantly different characteristics when formed on different electrode materials (Emr & Yacynych, 1995). Therefore, in order to obtain a similar thickness of PPD film (and therefore a similar insulating property to that seen in Figure 6.3) on a carbon electrode as that deposited upon a gold electrode, the electropolymerisation conditions must be optimised.

6.4.2 Optimisation of the insulating properties of the polymer film

From the discussions made in Section 6.3, it was concluded that the electrochemical induced formation of polymer films on electrode surfaces involves diffusional transport of the monomer to the electrode surface, its oxidation at an appropriate electrode potential to a radical cation, radical-radical coupling, electrochemical oxidation of the oligomers formed, chain propagation due to further coupling reactions, and finally precipitation of the polycationic polymer on the anode surface.

Based on these considerations, optimal conditions for the polymer formation process can be presumed. For example, the concentration of radical cations (i.e. that of monomeric species) in the diffusion zone in front of the electrode surface has to be high, a solvent has to be used in which the solubility of the formed oligomers and polymer chains is low, and the electrode potential has to be sufficiently high to allow fast electron transfer (Bilger & Heinze, 1993). In addition, the potential sweep rate and the number of potential cycles must be sufficient to allow time for the deposition of a film of desired thickness.

The electropolymerisation conditions have already been somewhat optimised; the electrolyte solution is de-oxygenated prior to deposition since the exclusion of oxygen and the absence of nucleophilic species in the polymerisation solution are indispensable for the reproducible deposition of the film due to the intermediate radical cations possibly undergoing reactions with nucleophilic species, thus decreasing the probability of chain propagation. In addition, the carbon electrodes are subjected to five short bursts of sonication (at a frequency of 25 kHz and each lasting ~0.5 secs), upon initial immersion within the polymerisation solution in order to remove surface bubbles and reduce the hydrophobicity of the electrode surfaces. This is important because the surface bubbles may hinder diffusional mass transport towards the electrode surface and thus the formation of a sufficiently high concentration of radical cations within the reaction zone may be prevented.

However, the investigations performed in the previous section have indicated a number of additional ways in which the electrodeposition of the PPD films may be optimised. The fact that the deposition upon carbon was observed to be a slower process (less charge was expelled during the initial scan and a more gradual decrease in peak currents with time was seen), suggests that the polymerisation needs to be performed over a longer period of time. Furthermore, as the charge density vs. cycles curve did not reach a plateau (Figure 6.5b) after 20 cycles, indicating that more potential cycles (i.e. coatings) need to be deposited in order to obtain a similar thickness film to that obtained upon gold electrodes. Liu *et al.* (1992) have investigated the effects of sweep rate, monomer concentration and electrolyte

concentration on the thickness of a poly(DVB/EVB) film. At any monomer concentration and at any electrolyte concentration the thickness of the film obtained was seen to decrease with increasing scan rate. Therefore, it would appear far more beneficial initially to vary the scan rate since this will have more of an effect on the film thickness than varying the monomer or electrolyte concentration (which may also affect the conductivity of the film).

Therefore, it was decided to investigate the effects of varying the scan rate and of varying the number of potential cycles in terms of the efficiency of the differently electropolymerised films to the blockage of the chosen analyte. This was determined by evaluation of the decrease in steady-state response (current) for the amperometric reduction of 1mM hexaammineruthenium(III) chloride. In addition, all electrodes were polymerised by sequentially cycling the electrodes between 0 and +1.0 V (vs. Ag/AgCl), instead of 0 and +0.8 V (vs. Ag/AgCl) as was previously used, since both the anodic peak potential and the potential at which the current starts to rise on the first scan is shifted by approximately 0.1 V in the anodic direction.

Figure 6.6a shows the relationship between current and the number of potential cycles for electrodes polymerised for 1, 2, 5, 20, 50 and 100 potential cycles at a scan rate of 50 mVs^{-1}. By comparison of the data obtained at different numbers of cycles, a decrease in the current for the $[Ru(NH_3)_6^{3+/2+}]$ reaction is observed with increase of cycles. The electrodes are clearly not completely insulated after 1, 2, 5 or 20 cycles. However, a significant reduction in the signal is observed after 50 potential cycles. The best coverage appeared to be obtained after 100 cycles although it is likely that if more data points were obtained, the curve would be seen to reach a *quasi*-plateau at some value between 50 and 100 potential cycles. Yano (1995) attempted to control the thickness of PPD films deposited upon indium-tin oxide coated glass electrodes by altering the number of potential cycles, but a film thicker than 0.85 μm was not obtainable (Yano, 1995). The film thickness was seen to increase linearly from 50 to 800 nm with increasing the number of potential cycles from 60 to 360 and remained at a nearly constant thickness of between 800-850 nm above 360 voltammetric cycles.

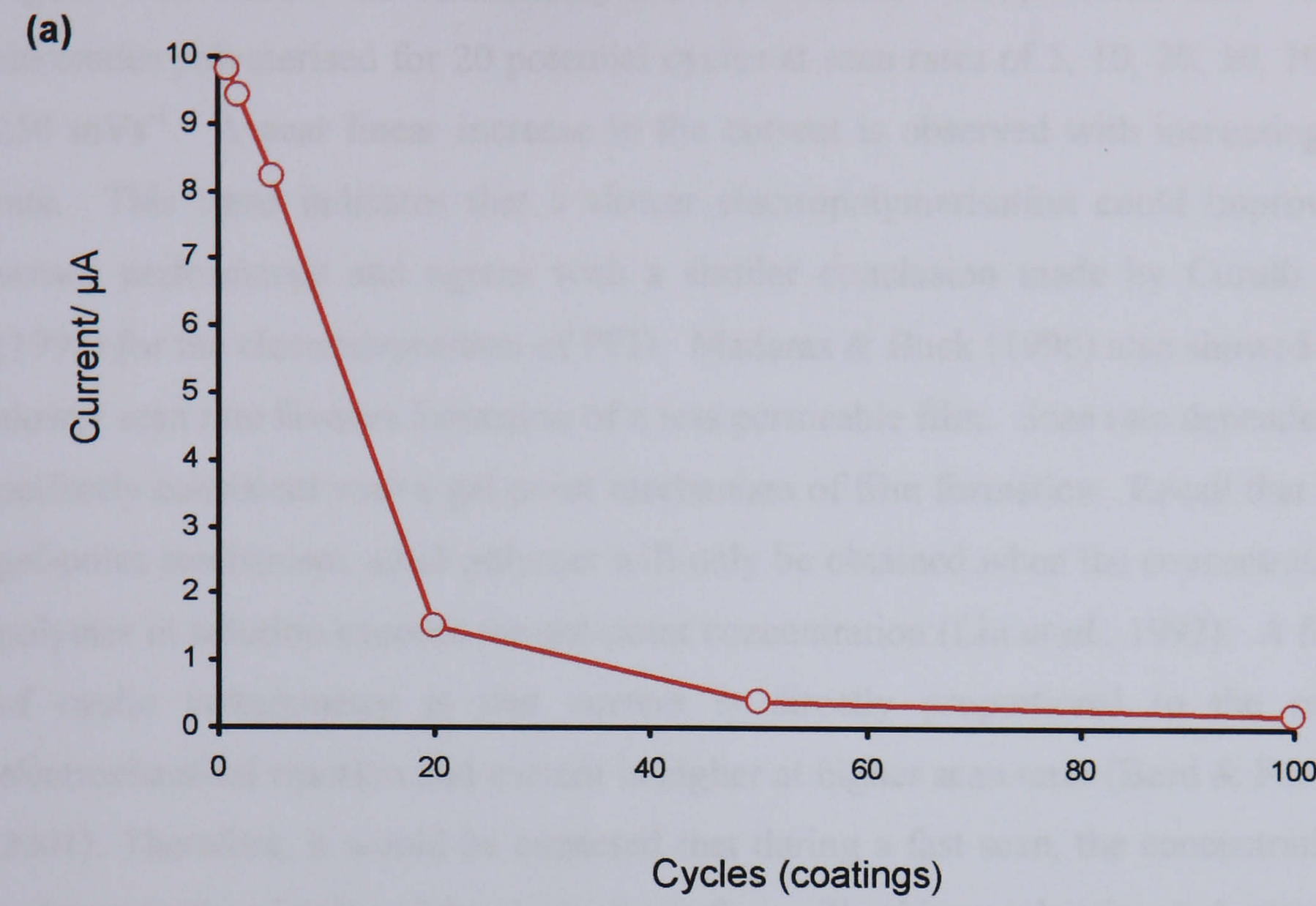

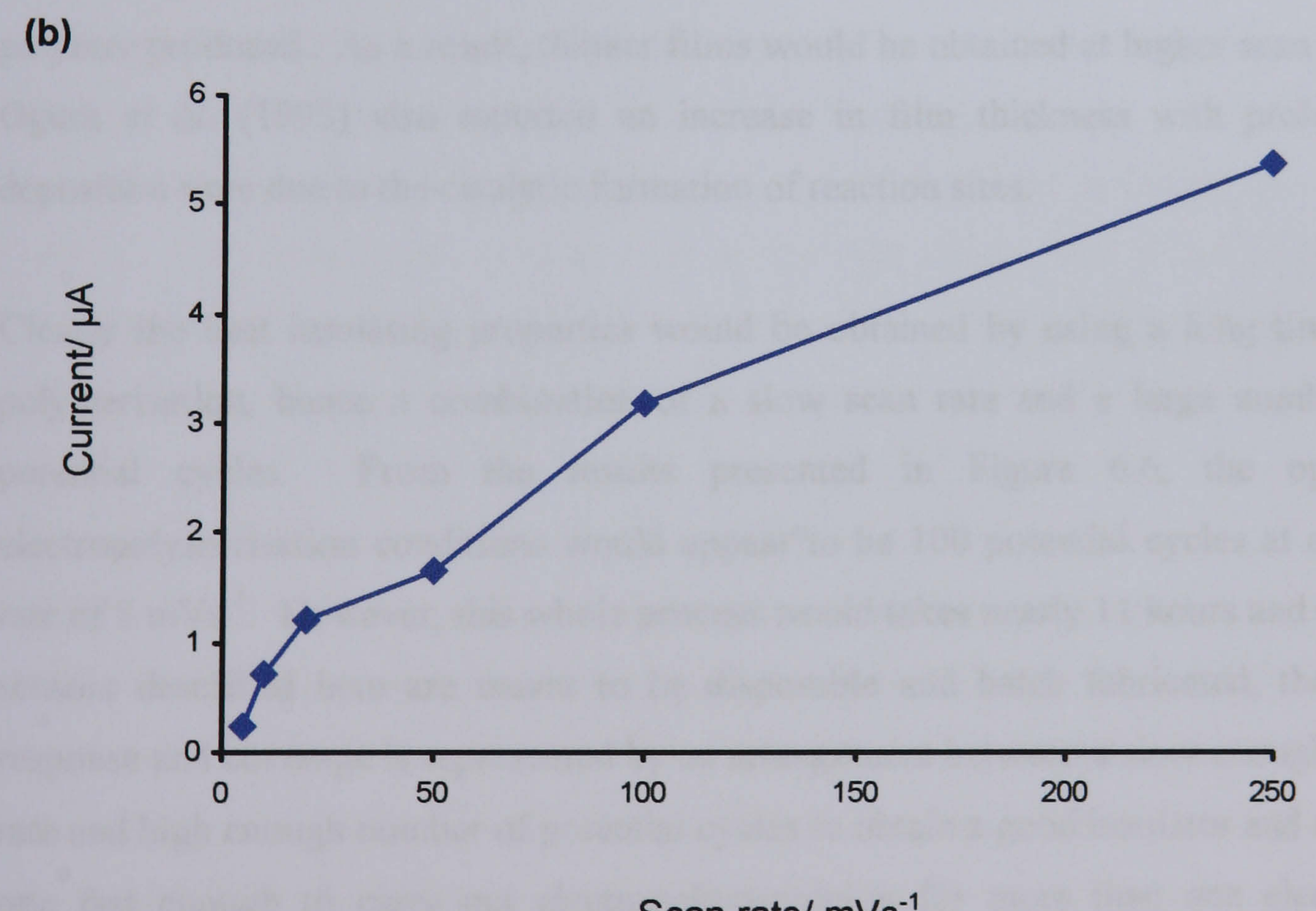

Figure 6.6 **Plot of amperometric reduction current [Polarisation potential: -0.35 V (vs. Ag/AgCl)] for 1 mM hexaammineruthenium(III) chloride at PPD coated electrodes vs. (a) number of cycles and (b) scan rate during the electrodeposition of the film.**

Figure 6.6b shows the relationship between current and potential scan rate for electrodes polymerised for 20 potential cycles at scan rates of 5, 10, 20, 50, 100 and 250 mVs^{-1}. A near linear increase in the current is observed with increasing scan rate. This trend indicates that a slower electropolymerisation could improve the sensor performance and agrees with a similar conclusion made by Curulli *et al.* (1998) for the electrodeposition of PPD. Madaras & Buck (1996) also showed that a slower scan rate favours formation of a less permeable film. Scan rate dependence is perfectly consistent with a gel-point mechanism of film formation. Recall that in the gel-point mechanism, solid polymer will only be obtained when the concentration of polymer in solution exceeds the gel-point concentration (Liu *et al.*, 1992). A feature of cyclic voltammetry is that current is directly proportional to the rate of electrochemical reaction and current is higher at higher scan rates (Bard & Faulkner, 2001). Therefore, it would be expected that during a fast scan, the concentration of polymer in the vicinity of the electrode surface will achieve gel-point at shorter times and this gel-point concentration will be achieved for a smaller total amount of polymer produced. As a result, thinner films would be obtained at higher scan rates. Ogura *et al.* (1995) also reported an increase in film thickness with prolonged deposition time due to the catalytic formation of reaction sites.

Clearly the best insulating properties would be obtained by using a long time for polymerisation, hence a combination of a slow scan rate and a large number of potential cycles. From the results presented in Figure 6.6, the optimal electropolymerisation conditions would appear to be 100 potential cycles at a scan rate of 5 mVs^{-1}. However, this whole process would takes nearly 11 hours and as the sensors described here are meant to be disposable and batch fabricated, the best response and coverage is represented by an arrangement between a slow enough scan rate and high enough number of potential cycles to obtain a good insulator and a scan rate fast enough to carry out electropolymerisation for more than one electrode simultaneously. A condition of 50 potential cycles deposited at a scan rate of 50 mVs^{-1} (total polymerisation time of approximately 33 minutes), would initially appear to satisfy these requirements and is interrogated for the electrodeposition of PPD at multiple carbon electrodes simultaneously in Section 6.4.3.

6.4.3 Electrodeposition of the polymer film upon multiple carbon electrodes

Using the optimal conditions of scan rate and the number of potential cycles postulated in the previous section, *o*PD was simultaneously electropolymerised onto 100 screen printed *carbon* electrodes. A custom built potentiostat and specially designed and printed electrode sheets (silver busbars connect the electrodes allowing the passage of current from a single source) were used (see Chapter 3). Thus, electrodes were scanned between 0 and +1.0 V (vs. Ag/AgCl) at a scan rate of 50 mVs^{-1} in pH 7.4 buffered solutions of 5 mM *o*PD for 50 potential cycles.

The voltammogram resulting from the electrodeposition is shown in Figure 6.7a, with the total charge passed after each potential cycle given in Figure 6.7b. The first anodic scan demonstrates the same features as those observed for *o*PD oxidation on individual electrodes i.e. one oxidation peak, where the current intensity of the peak decreases upon cycling, suggesting the deposition of an insulating film on the electrode surface. Once again, the potential at which the peak occurs has shifted to a more anodic potential (~ +0.75 V), possibly due to the presence of the connecting busbars. The anodic peak current seen on the first anodic scan is approximately 28.5 mA, which is slightly more than 100 times the peak current observed upon polymerisation of a single sensor (280 μA), possibly due to the resistivity of the busbars.

Figure 6.7b shows that more charge per unit area is spent during polymerisation upon sheets of carbon electrodes (~6.1 mC) than that expelled during polymerisation upon single carbon electrodes (~1.1 mC), although this is most probably a direct result of the difference in electropolymerisation conditions (i.e. more potential cycles over a wider potential range) rather than a factor of the simultaneous polymerisation of electrodes. The deposition is slightly more gradual yet again (indicated by the increased gradient of the curve in Figure 6.7b as compared to that shown in Figures 6.1b and 6.5b) which would be expected due to the resistance offered by the busbars.

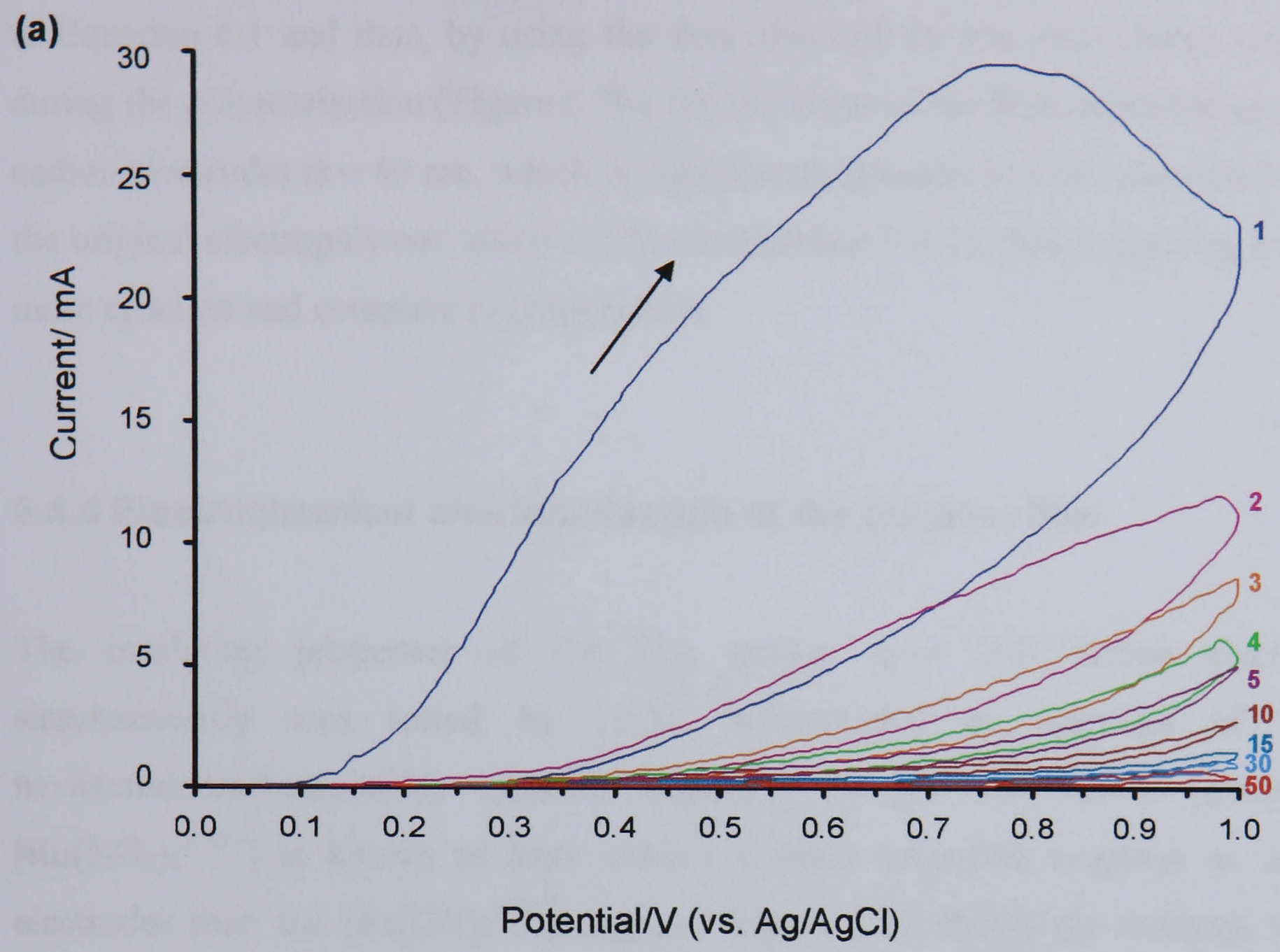

Figure 6.7 (a) Cyclic voltammogram and (b) Total charge density vs. the number of cycles, for the electropolymerisation of 5 mM *o*-phenylenediamine dihydrochloride at a sheet of 100 screen printed carbon electrodes.
[Supporting electrolyte: phosphate buffer (pH 7.4, 5.1×10^{-3} M). Scan rate: 50 mVs^{-1}].

Again, the thickness of the deposited film can be theoretically calculated according to Equation 6.1 and thus, by using the data obtained for the total charge expelled during the polymerisation (Figure 6.7b), the thickness of the film deposited upon the carbon electrodes is ~ 40 nm, which is significantly greater than that deposited using the original electropolymerisation conditions (Section 6.4.1), thus suggesting a much more efficient and complete polymerisation.

6.4.4 Electrochemical characterisation of the polymer film

The insulating properties of the film grown upon 100 carbon electrodes simultaneously was tested by cyclic voltammetry in solutions of 1mM hexaammineruthenium(III) chloride dissolved in pH 7.8 buffer (since the $[Ru(NH_3)_6^{3+/2+}]$ is known to have exhibit a more reversible response at carbon electrodes than the $[Fe(CN)_6^{3-/4-}]$ couple). Figure 6.10 shows the resultant cyclic voltammograms recorded at a bare carbon electrode (Figure 6.10a) and a similar electrode coated with a film of PPD (Figure 6.10b). While the redox behaviour of $[Ru(NH_3)_6^{3+/2+}]$ at the bare electrode is clearly present, there is little faradaic current flowing at the PPD coated electrode, since no peaks are observable on the voltammogram, suggesting that $[Ru(NH_3)_6^{3+/2+}]$ cannot permeate through the film to the carbon electrode surface.

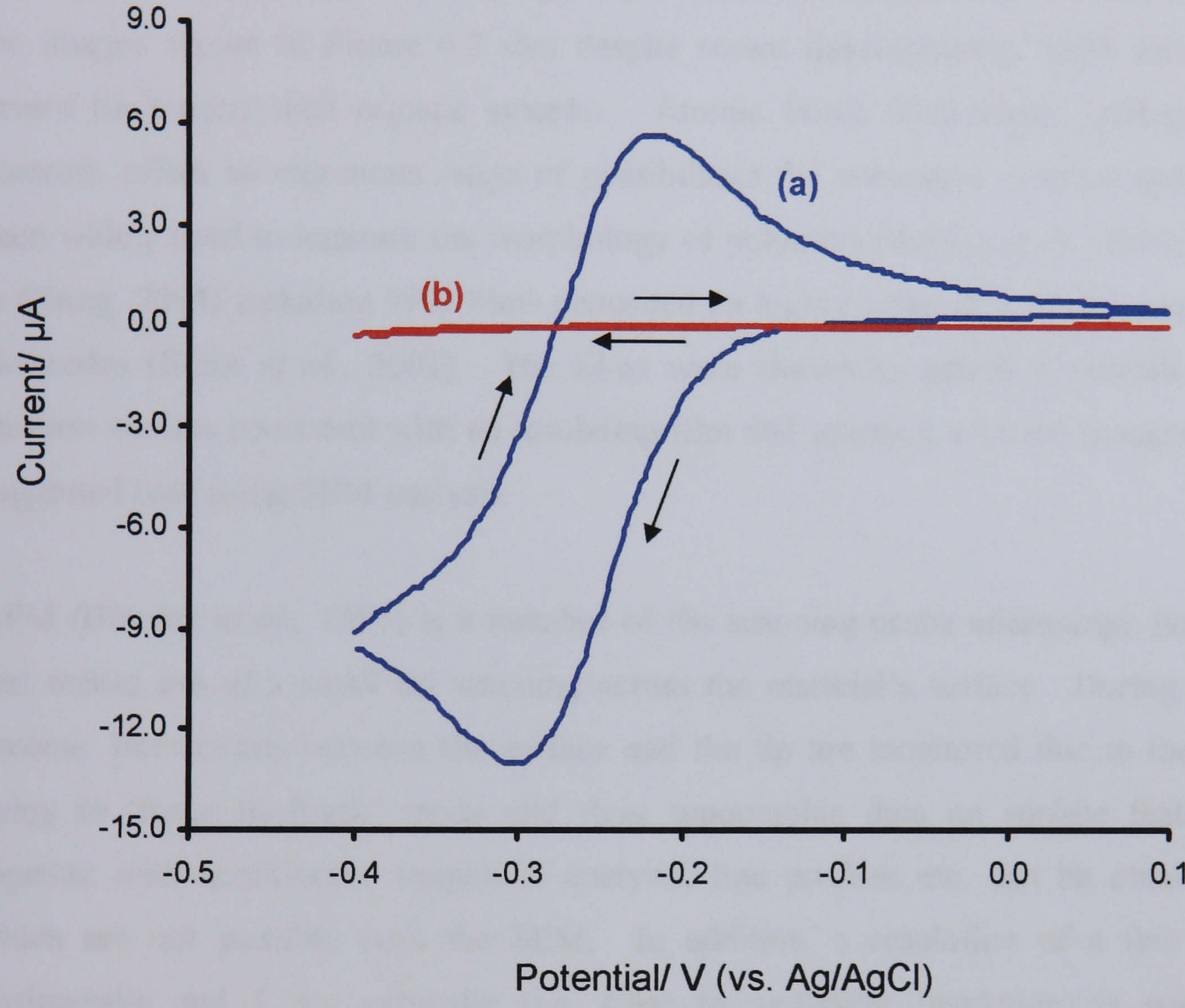

Figure 6.8 Cyclic voltammetry of 1 mM hexaammineruthenium(III) chloride at (a) a bare screen printed carbon electrode and (b) a similar electrode coated by an electrodeposited film of poly(*o*-phenylenediamine).
[Supporting electrolyte: phosphate buffer (pH 7.8, 0.1M). Scan rate: 20 mVs^{-1}].

6.4.5 Microscopic investigations of the film surface topography

There may be some difference in the surface topography of PPD films electropolymerised upon carbon electrodes (and/or electrodes simultaneously polymerised) than the films deposited upon gold electrodes. SEM is the imaging method traditionally used for studying sample surfaces, however, we have seen from the images shown in Figure 6.2 that despite recent developments, SEM still has severe limitations with organic systems. Atomic Force Microscopy (AFM), by contrast, offers an enormous range of possibilities for polymeric systems and has been widely used to measure the morphology of polymers (Barisci *et al.*, 2000; Wu & Chang, 2004) including PPD films deposited on highly ordered pyrolytic graphite electrodes (Elliot *et al.*, 2001). The films were shown to exhibit a smooth and uniform surface consistent with an insulating film and agreeing with the topography suggested here using SEM analysis.

AFM (Binning *et al.*, 1986) is a member of the scanning probe microscope family that makes use of a small tip scanning across the material's surface. During this process, interactions between the surface and the tip are monitored due to the tip being in 'force feedback' mode and thus, topographic data on surface features together with quantitative roughness analysis, line profiles etc. can be obtained, which are not possible with the SEM. In addition, a resolution of a few nm horizontally and 1 nm vertically (i.e. close to molecular resolution) is readily achieved on smooth surfaces. The samples in this study are potentially suitable for AFM analysis techniques since they consist of an electrically conductive substrate coupled with a non-conductive polymer film and thus the potential to distinguish and analyse different regions of electrode.

AFM in the simplest contact mode was therefore used to examine the surfaces of the carbon electrodes. The rough topography caused some instabilities in feedback and therefore the scan size is restricted to 20 μm to prevent the vertical movement going out of range (absolute limit of 12 μm). Figure 6.9 shows topographic images of the screen printed carbon electrodes with (Figure 6.9a) and without (Figure 6.9b)

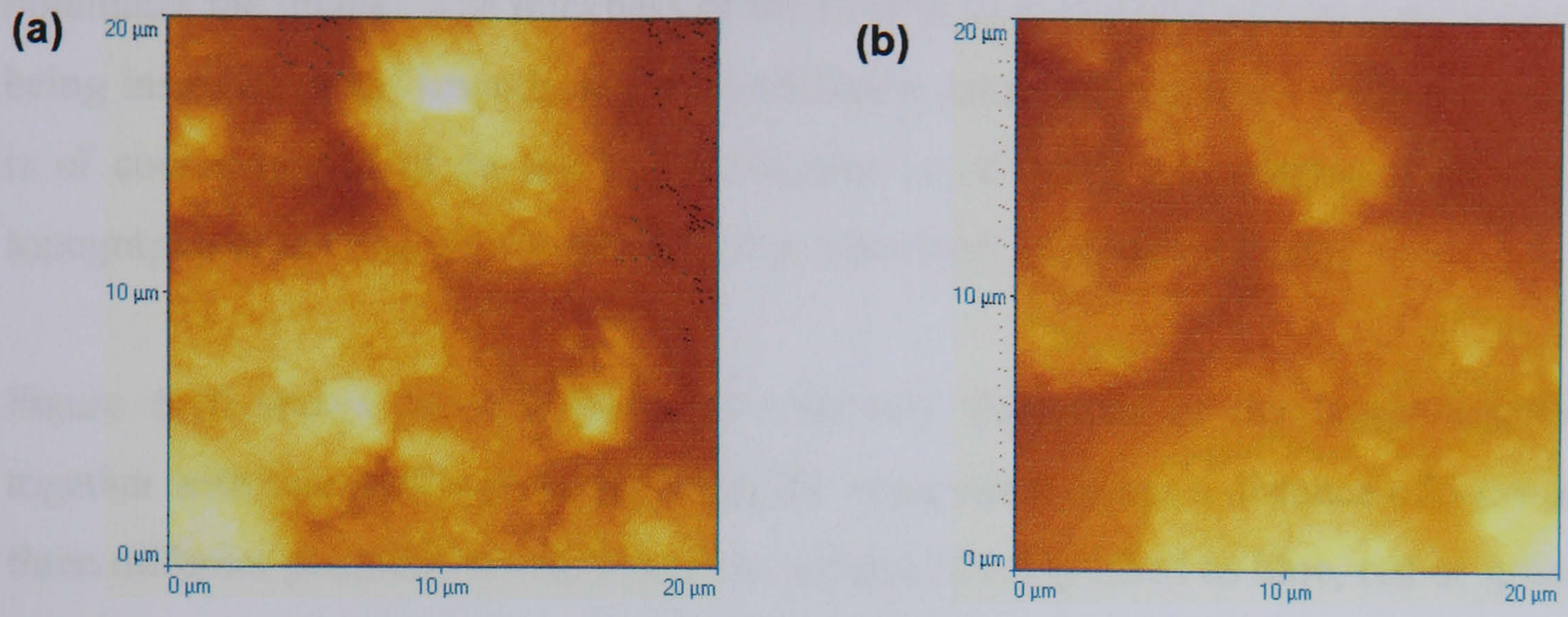

Figure 6.9 **Atomic force micrograph of (a) a bare screen printed carbon electrode and (b) a similar electrode coated by an electrodeposited film of poly(*o*-phenylenediamine).**
[Contact mode, Scan size: 20µm].

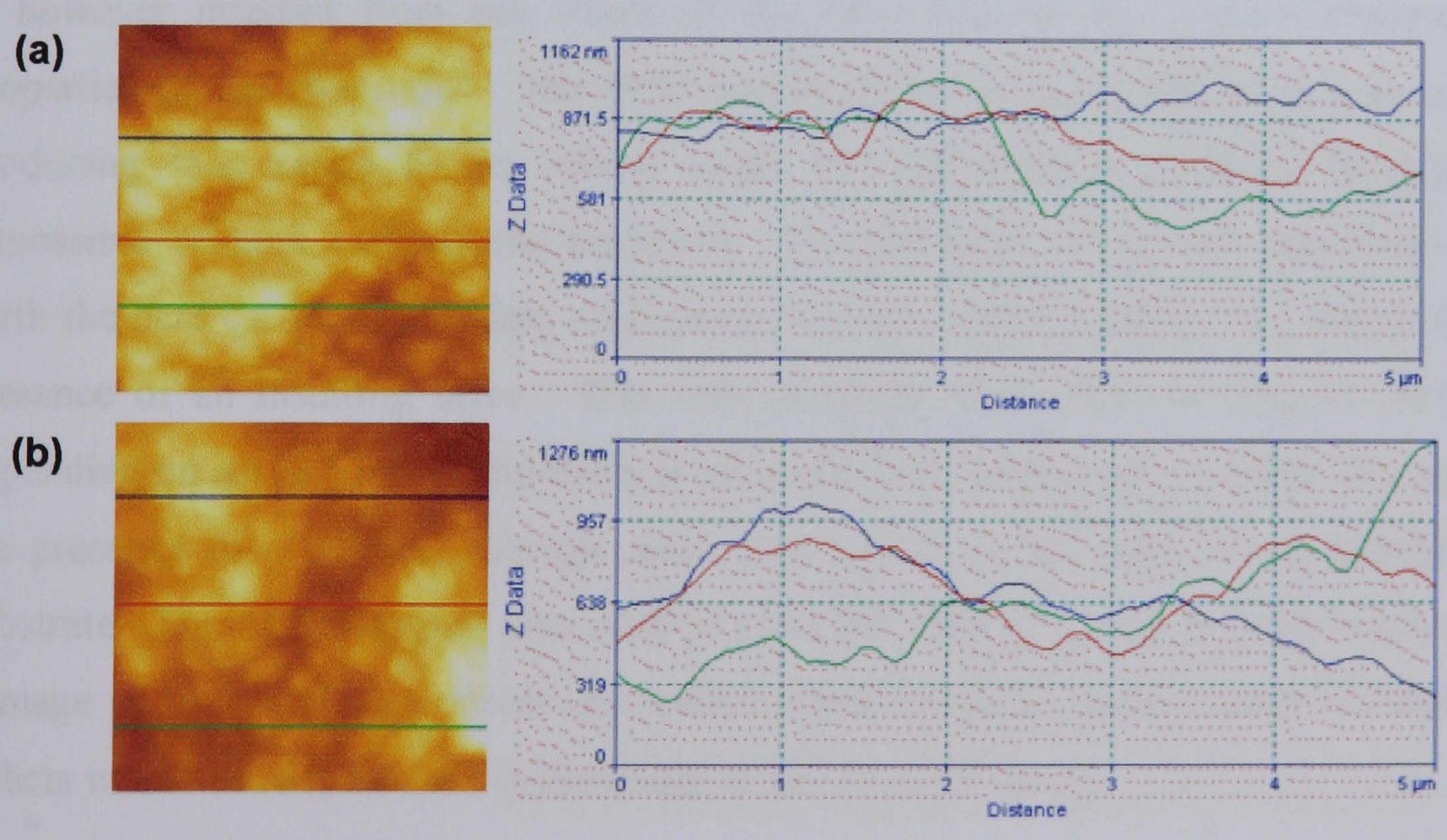

Figure 6.10 **AFM line profiles of (a) a bare screen printed carbon electrode and (b) a similar electrode coated by an electrodeposited film of poly(*o*-phenylenediamine).**
[Contact mode, Scan size: 5 µm].

electrodeposited PPD. In both cases, the rough topography of the carbon electrodes dominates the image. The thickness of the PPD layer would initially be construed as being insufficient to 'smooth out' the underlying granular structure. However, this is of course typical of an insulating polymer i.e. the film topography mirrors the topography of the underlying substrate (the correlated roughness effect).

Figure 6.10 shows zoomed views of relatively flat areas of the larger images, together with line profile plots depicting the topography across a distance of 5 μm at three different positions on the electrode surface (distinguished as blue, red or green lines), to see if the thickness of the polymer film can be seen. Figure 6.10a is the planar carbon and Figure 6.10b is the same carbon subsequently coated with PPD. Due to the topography of the carbon ink, it is impossible to distinguish any height difference from being due to the topography of the graphite particles or due to the polymer layer itself. The lack of any distinction between the images is disappointing, but not surprising since the carbon substrate is very rough and the polymer film very thin. The presence of an insulating layer, even though not visible, is however inferred from the effect of the PPD film on the surface electrical properties of the electrodes. The PPD coated electrodes appeared to be charged, producing long range forces, which made the achievement of force feedback impossible without earthing the electrode. Contrastingly, it was not necessary to earth the bare carbon electrodes, confirming that this charging effect was due to the presence of an insulting layer. This also illustrates that other variants of AFM, depending on surface forces and thermal properties etc. might easily be able to image the presence of a polymer, though again this would be facilitated by a smoother substrate. The AFM imaging also confirms that the PPD film is very robust since no damage is observed as a result of contact mode imaging (conspicuous streaking effects would usually be seen in the image if this were the case).

6.5 EVALUATION OF THE POLYMER FILM COATING AS AN INSULATING LAYER FOR USE IN AN AMPEROMETRIC ELECTRODE

We have briefly looked at the electroactivity of the electrodeposited films using cyclic voltammetry (Figure 6.8), however, since the intended use of the electrodes is within an amperometric microarray sensor, it is useful to interrogate the films using amperometric techniques. The permeation rate through *polyionic* films has been found to be dependant on the permeant charge and molecular size (Finklea & Vithanage, 1984; Leddy *et al.*, 1985). However, although different permeability to neutral versus charged electroactive solutes can also be exhibited by *non-ionic* films (Finklea & Vithanage, 1984), Centonze *et al.* (1994) have concluded that the access of several redox couples to the carbon-polymer interface, where the electrode process occurs, is governed by properties more selective than molecular size and charge. Thus, in principal, for a non-ionic, pristine film such as PPD, the electrochemistry of redox solutes would be influenced by several factors, such as the solubility of redox species and their mass transport characteristics inside the polymer bulk, film porosity and kinetics of charge transfer reaction at the carbon-polymer interface. It is thought (Centonze *et al.*, 1994) that these processes would be controlled by specific chemical interactions between probe and film, for example involving hydrophobic interactions or hydrogen bonding.

Experiments were initially polarised in a pH 7.8 buffered solution of 1mM hexaammineruthenium(III) chloride. The $[Ru(NH_3)_6^{3+/2+}]$ redox couple is a positively charged and commonly used electrochemical redox probe known to exhibit a good response at carbon electrodes. Both bare and PPD coated carbon electrodes were polarised at a potential of -0.35 V (vs. Ag/AgCl) for 3 minutes. Further interrogation was performed via the introduction of convection (forced stirring) to the test solution 1 minute after the initial polarisation, which was further increased in magnitude after 2 minutes. The resulting current-time transients are shown in Figure 6.11a. The electrochemistry of $[Ru(NH_3)_6^{3+/2+}]$ appears to completely suppressed at the PPD

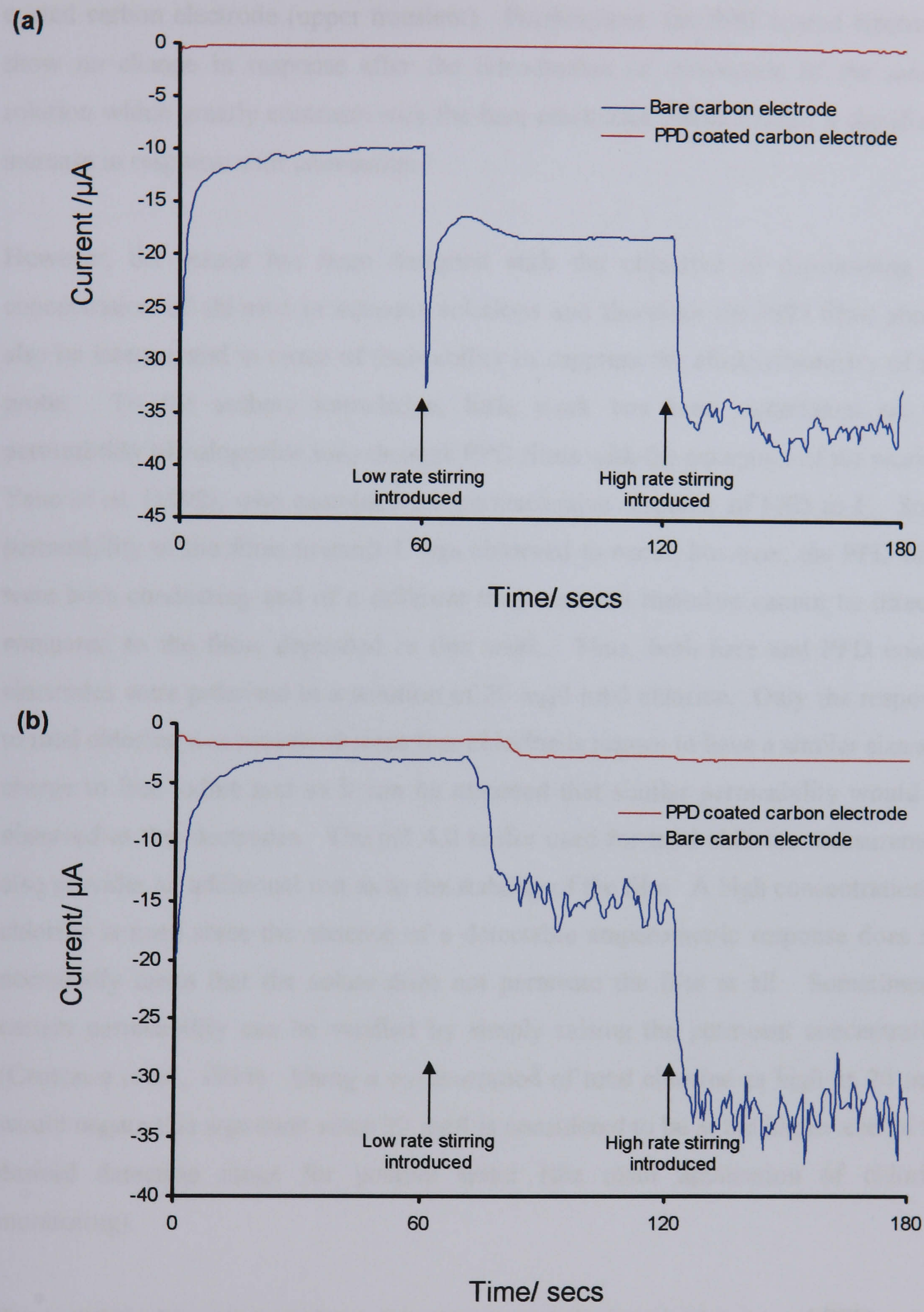

Figure 6.11 **Current-time transients at bare and PPD coated carbon electrodes stirred in: (a) 1mM hexaammineruthenium(III) chloride [Supporting electrolyte: phosphate buffer (pH 7.8, 0.1 M). Polarising potential: -0.35 V (vs. Ag/AgCl)] and (b) 20 ppm total chlorine [Supporting electrolyte: phosphate buffer (pH 4.0, 0.5 M). Polarising potential: -0.08 V (vs. Ag/AgCl)].**

coated carbon electrode (upper transient). Furthermore, the PPD coated electrodes show no change in response after the introduction of convection to the sample solution which greatly contrasts with the bare electrodes which exhibit a significant increase in response with convection.

However, the sensor has been designed with the objective of determining the concentration of chlorine in aqueous solutions and therefore the PPD films should also be interrogated in terms of their ability to suppress the electrochemistry of this probe. To the authors knowledge, little work has been undertaken on the permeability of halogenide ions through PPD films with the exception of the work of Yano *et al.* (1992), who examined the permselective response of PPD to I^-. Some permeability of the films towards I^- was observed to occur, however, the PPD films were both conducting and of a different thickness and therefore cannot be directly compared to the films deposited in this work. Thus, both bare and PPD coated electrodes were polarised in a solution of 20 mg/l total chlorine. Only the response to total chlorine was measured since free chlorine is known to have a similar size and charge to free iodine and so it can be assumed that similar permeability would be observed at the electrodes. The pH 4.0 buffer used for total chlorine measurement also provides an additional test as to the stability of the film. A high concentration of chlorine is used since the absence of a detectable amperometric response does not necessarily mean that the solute does not permeate the film at all. Sometimes a certain permeability can be verified by simply raising the permeant concentration (Centonze *et al.*, 1994). Using a concentration of total chlorine as high as 20 mg/l would negate this argument since 20 mg/l is considered to be at the higher end of the desired detection range for potable water (the main application of chlorine monitoring).

Figure 6.11b shows the resultant current-time transients at both bare and PPD coated electrodes polarised for 3 minutes at -0.08 V (vs. Ag/AgCl) in 20 mg/l total chlorine. Again, convection was introduced to the test solutions at 1 minute after the initial polarisation and subsequently increased in magnitude at 2 minutes. The electrochemistry of chlorine is somewhat, although not completely, suppressed at the

PPD coated electrodes (upper transient), probably due to the very high concentration employed. However, very little variation in response was seen upon the introduction of convection as compared to that observed at the bare electrodes. This is very promising, especially considering that in reality the concentrations of chlorine present in the test samples are more likely to be in the 0-2 mg/l range.

Thus, the electrodeposited films appear to be quite impermeable and, considering their thickness, exhibit noticeable transport barrier characteristics in both redox probes. Furthermore, the low permeability of redox species through the film indicates that it is not well swollen by water. Madaras & Buck (1996) have also shown that electropolymerised PPD films have excellent lifetimes and indeed, the lifetime of most biosensors incorporating such films has depended to a great extent on the operational stability of the enzyme layer and not the PPD itself. This problem is of course negated in a chlorine sensor since no enzymes are required for its operation. It appears therefore, that PPD films deposited upon carbon substrates according to the optimal electropolymerisation conditions determined in this chapter are both stable and impermeable and yet thin enough to theoretically be punctured by sonochemical means.

6.6 CONCLUSIONS

This chapter has described the development and optimisation of poly(*o*-phenylenediamine) films and their exploitation within amperometric sonochemically fabricated microelectrode arrays has been discussed.

PPD films were initially deposited at a gold electrode by potentially cycling the electrode assembly until it became fully insulated by the polymer (after 20 potential cycles). Cyclic voltammograms relating to the electrodeposition of the film revealed the electropolymerisation as being a self-regulating and thus highly reproducible process, since diminishing peak currents were observed as the electrode became progressively insulated by the film.

Scanning electron micrographs of both a bare gold electrode and an electrode coated with a film of PPD confirmed that its surface is largely featureless and essentially defect free. The thickness of the film deposited upon the gold electrode was estimated via charge integration to be approximately 56 nm and in addition, was found to be electrochemically inactive when interrogated by cyclic voltammetry in solutions of ferricyanide.

Mechanisms relating to both the growth of the PPD films across the electrode surfaces, and the polymerisation of *o*PD itself, were hypothesised. Growth of the film was thought to occur via the classical 'gel-point' mechanism. The polymer itself was postulated as being formed via either the polymerisation of the *o*PD di-cation formed on disproportionation, or the monocation radical oxidising at a conducting film surface rather than the electrode surface, yielding a different product, the insulating film.

PPD was also deposited at a carbon electrode in a manner analogous to that at the gold electrode. Again, diminishing peak currents were seen in the cyclic voltammogram relating to the electrodeposition, however, it was seen the electrode

was not completely insulated after 20 potential cycles since the total charge expelled during the polymerisation did not reach a plateau value. This was thought to be due to the difference in conductivity between the gold and carbon electrodes and was confirmed by the film being calculated as having a thickness of only 2.3 nm under these polymerisation conditions.

The electropolymerisation conditions were optimised in order to obtain fully insulated films of PPD at carbon electrodes. An arrangement between a slow enough scan rate and a high enough number of potential cycles in order to obtain a good insulator over a reasonable time scale was determined, by amperometry in ruthenium complexes, to be 50 cycles at a scan rate of 50 mVs^{-1}.

The optimal polymerisation conditions were employed to deposit PPD films upon 100 carbon electrodes simultaneously. Cyclic voltammograms relating to the simultaneous electropolymerisation of carbon electrodes correlated well with those observed for the electropolymerisation at individual electrodes. The deposited films were calculated as having a thickness of approximately 40 nm and were seen to be essentially electrochemically inactive when tested in solutions of hexaammineruthenium using cyclic voltammetry. The surface topography of the films was also investigated using AFM. Although it was impossible to distinguish between the bare and PPD coated electrodes, the presence of an insulating film was confirmed by the need to earth the PPD coated carbon samples.

Finally, the electrodeposited films were interrogated amperometrically using both ruthenium and chlorine probes. The amperometric response relating to the reduction of the probe species was seen to dramatically reduce to negligible levels at the electrodes insulated with PPD and furthermore, no variation in this response was observed upon the introduction of convection to the test solutions.

CHAPTER 7

FABRICATION AND CHARACTERISATION OF SONOCHEMICALLY FORMED MICROELECTRODE ARRAYS

7.1 INTRODUCTION

As has been discussed in Chapter 2.5, microelectrodes offer many advantages over conventional macroelectrodes since they experience hemispherical solute diffusional profiles. It is this phenomenon that can impart stir-independence to the responses of sensors, whilst also offering lowered limits of detection. However, although microelectrodes yield extremely large current densities, they generate very small total current responses. One approach to overcoming this problem, without substantial loss of the benefits gained from the individual microelectrodes, is by the use of *microelectrode arrays*.

Microelectrode arrays may be fabricated by a number of approaches, although the most commonly used techniques of photolithography and laser ablation have to date proved cost prohibitive for the mass production of disposable sensor strips. However, a novel approach for the fabrication of microelectrode arrays that lends itself to mass production is that of sonochemical fabrication. The method takes advantage of acoustic cavitation; the nucleated formation, growth and subsequent collapse of vapour filled bubbles due to the passage of an ultrasonic ($2 \times 10^4 \sim 10^9$ Hz) wave through the medium. Sonochemical theory and experimentation has suggested that when such a bubble collapses near a solid surface, it implodes asymmetrically, and the in-rush of liquid from the side of the bubble away from the solid surface can move at a speed of approximately 100 ms^{-1} (Leighton, 1994). This phenomenon is commonly termed 'ultrasonic microjetting'.

It has previously been shown that *o*-phenylenediamine may be electropolymerised at conductive electrode surfaces via a two-electron process to form essentially defect free insulating polymer films of less than 100 nm thickness (Chapter 6). The rationale underpinning of this work is that sonochemical ablation of such thin films at electrode surfaces may expose areas of the underlying conductive electrode on the basis of ultrasonic microjetting i.e. the microjets of solution cause microscopic

pitting of the insulating film, and each exposed area can act as a localised microelectrode and thus collectively as a microelectrode array.

Madigan *et al.* first reported that the sonication of insulating polymer films may possibly result in the formation of a microelectrode array in 1994. However, their use of an ultrasonic probe system meant that sonication times were required to be long due to the streaming and coalescence of bubbles that occurs with such probe systems. The true potential of the method for the fabrication of electrochemical sensors was not recognised until Higson patented the procedure for such an application in 1996. This led to the pioneering work of Myler (2000), who used an ultrasonic bath as opposed to a probe system to induce cavitation, allowing for the cavitation bubbles to be formed as separate entities throughout the sonicated liquid medium, resulting in much reduced sonication times and thus, the potential for mass fabrication of such electrodes.

This chapter is therefore focussed towards the fabrication and characterisation of sonochemically formed microelectrode arrays using screen printed carbon working electrode templates, a material which lends itself to mass fabrication due to its low cost, excellent reproducibility and ease of fabrication (See Chapter 4). Microelectrode arrays are initially prepared upon gold working electrode templates in order to characterise the process (Section 7.2). Arrays are then prepared upon carbon working electrode templates, as described in Section 7.3, and subsequently interrogated using both cyclic voltammetric and hydrodynamic amperometric techniques to assess if the behaviour of the produced arrays is in agreement with known microelectrode theory. In both cases, the prepared arrays are imaged using scanning electron microscopy. Gold cyanide labelling is also used to enable the density and distribution of the resultant microelectrodes to be estimated so that theories upon the diffusion at such arrays may be discussed.

The results of this chapter will aid investigations towards the mass production of the thus formed sensors, presented in Chapter 8.

7.2 FABRICATION OF MICROELECTRODE ARRAYS UPON GOLD ELECTRODES

o-phenylenediamine was first polymerised on gold sputter coated glass slide electrode assemblies as described in Chapter 6. The film is known to be insulating since cyclic voltammetry for the electrodeposition of the film revealed diminishing peak currents as the electrode became progressively insulated by the polymer film (Figure 6.1). Sonochemically fabricated microelectrodes were prepared via ablation of the poly(*o*-phenylenediamine) films using 20 seconds exposure to ultrasound at a frequency of 25 kHz according to the method of Myler (2000), thus exposing micro-sized areas of the underlying conductive gold substrate. This process is shown schematically in Figure 7.1:

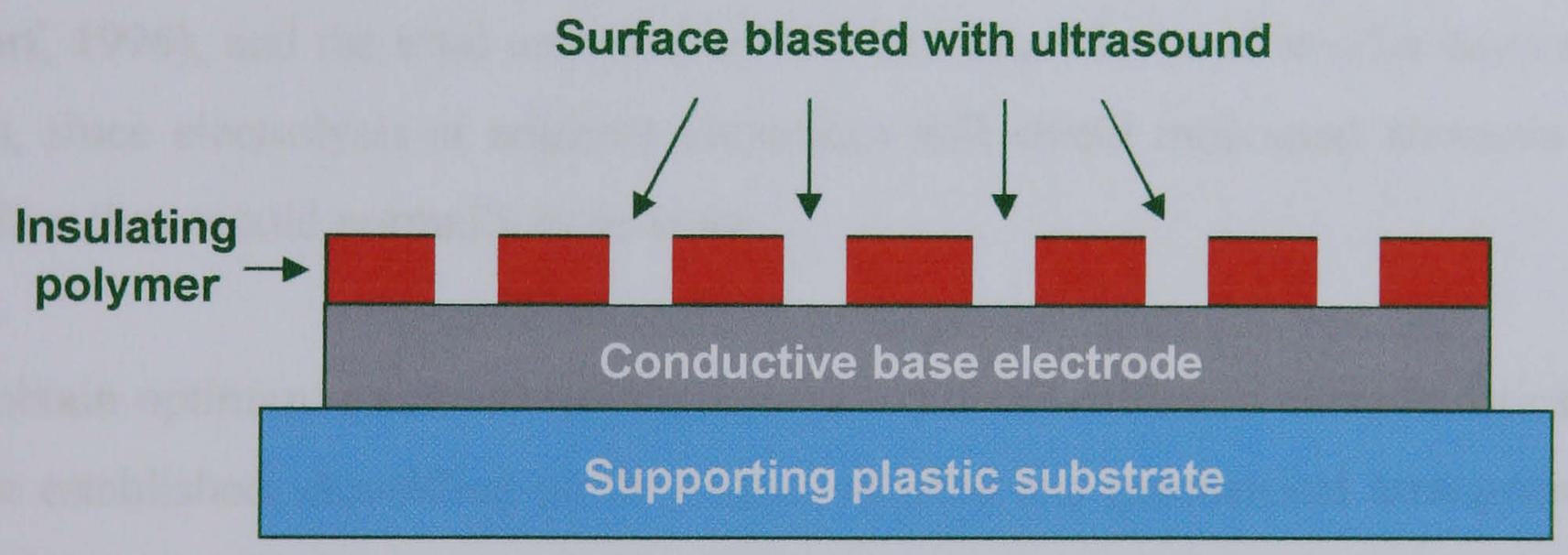

Figure 7.1 Schematic of the sonochemical formation of microelectrode arrays.

When an electrochemical sensor is designed that incorporates a microelectrode array, the optimum geometry of the array will depend on the proposed application and operation of the sensor. For voltammetric microsensors, radial diffusion is highly advantageous, as it permits the acquisition of steady-state measurements and the use of very fast scan rates. Furthermore, if a flow independent sensor is desirable, radial diffusion will minimise the convection dependence of the sensor. Morf & de Rooij (1997) presented theoretical calculations of the current output of arrays of different

packing densities using steady-state and chronoamperometric responses and found that such an ideal response behaviour of microelectrode arrays can be only be achieved if a nearly radial diffusion geometry is maintained at the individual microelectrodes, thus implying that the centre-centre spacing, d_c, between individual microelectrodes must be sufficiently large. If this is the case, the microelectrode array will behave as multiple single electrodes in parallel and produce a limiting current $i_L q$, where q is the number of individual electrodes in the array (Morf & de Rooij, 1997). In contrast, when very short distances of d_c are employed, the advantages of using microelectrodes will be greatly reduced, as the individual diffusion fields will merge to form a linear diffusion layer analogous to macroelectrodes of the same total surface area (Wittstock *et al.*, 1998). Microelectrode arrays with intermediate spacing will exhibit a mixed diffusional profile, where diffusion is assumed to be radial in the regions bordering a microelectrode - but planar in areas further away from the active surfaces in the outer region of the diffusion layer. This is because there is some diffusional 'overlap' (Morf, 1996), and the total response will be less than that predicted by the sum for each, since electrolysis at adjacent electrodes will shield individual elements from the flux they would normally experience.

To obtain optimum microelectrode properties, defined diffusion characteristics have to be established, depending on the radius, spacing and geometrical arrangement of the electrodes in the array. It is useful therefore, to attempt to characterise the sonochemically fabricated microelectrode arrays in terms of their pore size and distribution, so that a better understanding of the diffusion process occurring at such electrodes and predictions of the expected current amplitudes may be made. Thus, scanning electron microscopy was used to image the sonicated electrodes.

The scanning electron micrograph corresponding to a PPD coated electrode sonicated for 60 seconds is shown in Figure 7.2b. This time was chosen since it provided the clearest images of the cavitation induced micropores present in the polymer - it is very difficult to image pores within the polymer film at lower sonication times since the topography of the polymer mimics that of the

(a)

(b)

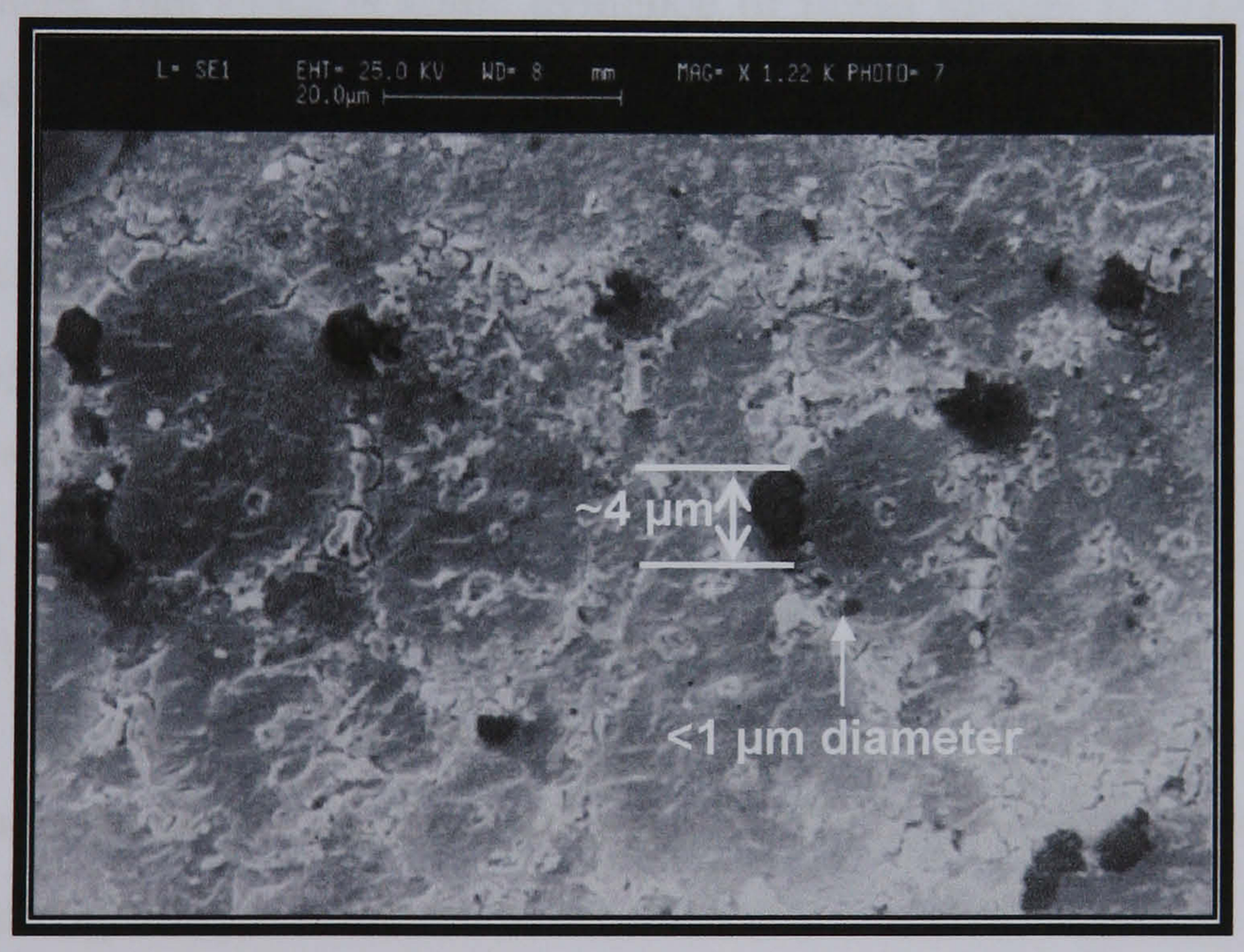

Figure 7.2 Scanning electron micrographs of (a) a gold electrode coated with PPD and (b) a similar electrode subsequently sonicated in water at 25 kHz for 60s. (x 1000 magnification).

underlying sputter-coated gold electrode. By comparison with an untouched PPD coated gold electrode (Figure 7.2a), micro-sized 'pores' may clearly be seen within the surface of the polymer film. The distribution of pores is random since ultra-sonic cavitation is a chaotic process. It also appears that most of the cavities are bimodal in size, possessing either ~4 μm (±1 μm) or sub-micron diameters. There is little evidence of cavities with diameters falling in between this range. It is likely that the smallest of the cavities observed are formed by the initial impact of the micro-jets of fluid which are expelled following the collapse of vapour bubbles within the water (Suslick, 1990). These initial cavities are known to act as nucleation sites for the formation of further bubbles (Suslick, 1990). The cavity would then grow as new bubbles implode within the confines of the original cavity, giving rise to a quantum enlargement in the diameter of the cavity. Since pores no larger than ~4 μm are seen, it is believed that pores of this size are too large to act as nucleation sites. In addition, it can be seen from the pores formed in the bottom right corner of Figure 7.2b for example, that there is some evidence of pores joining to form 'dumb-bell' shaped cavities when two pores are formed within close proximity to one another.

Cyclic voltammetry is a simple diagnostic tool that can be used to establish if an electrode array is sufficiently distributed so that it exhibits microelectrode behaviour, since microelectrodes are known to exhibit sigmoidal shaped cyclic voltammograms for reversible solution bound redox species, a characteristic feature that results from the development of radial diffusion at each microelectrode surface. This is in contrast with the characteristic peak shaped voltammograms expected at a planar, *macro*-electrode surface, (or indeed an array in which the microelectrodes are too closely packed together).

Figure 7.3 shows a series of cyclic voltammograms recorded in 1mM potassium ferricyanide at a planar gold electrode (Figure 7.3a), a PPD coated electrode as a control (Figure 7.3b), and a similar electrode subsequently sonicated in water at 25 kHz for 20 seconds (Figure 7.3c). The voltammogram corresponding to the planar gold electrodes exhibits well-defined reversible electrochemical responses, which are attributed to the reduction/oxidation of $[Fe(CN)^{3-/4-}]$. The separation

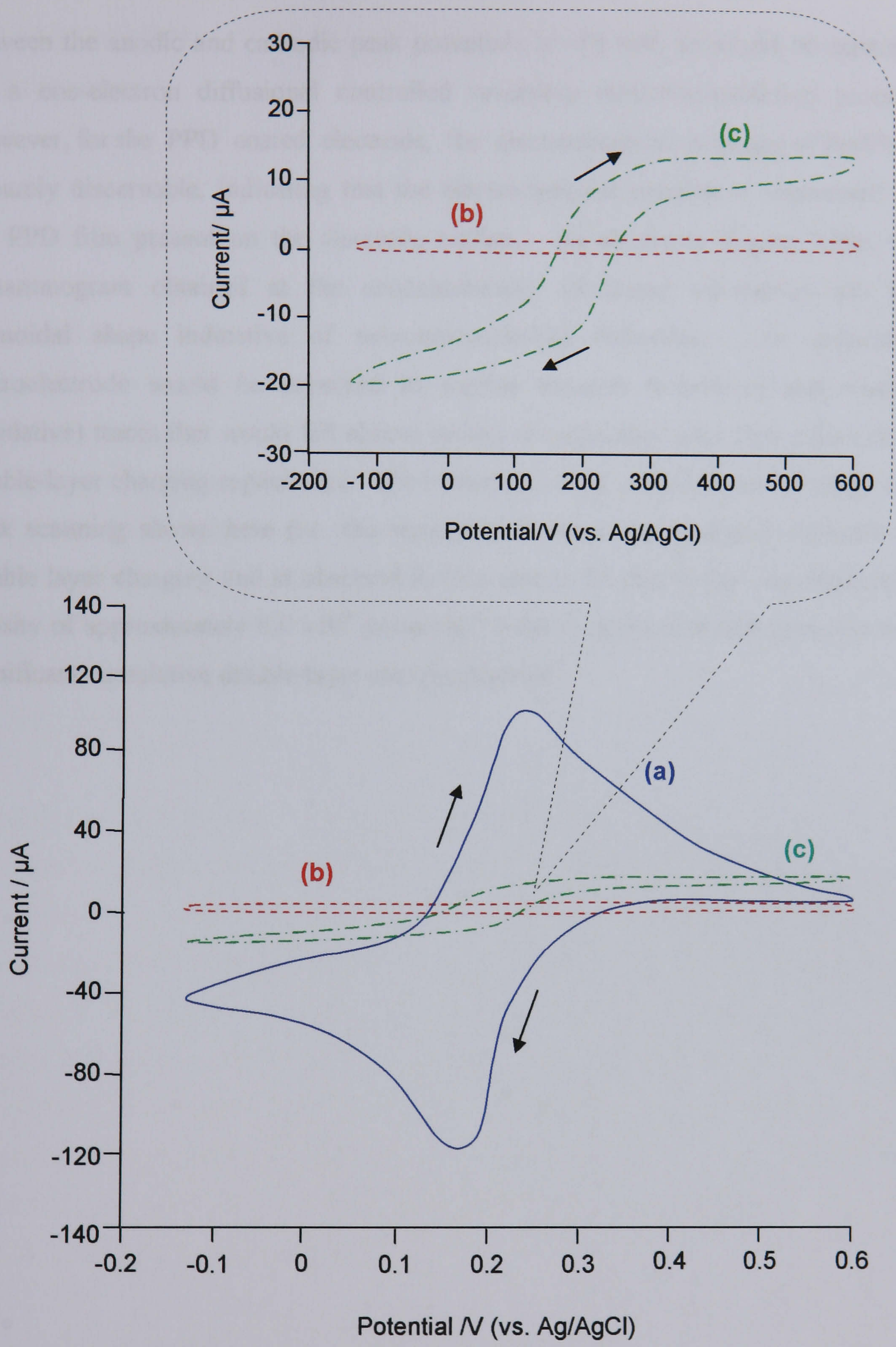

Figure 7.3 **Cyclic voltammetry of 1 mM potassium ferricyanide at (a) a bare gold electrode (b) a PPD coated gold electrode and (c) a PPD coated electrode subsequently sonicated for 20 seconds. (b) and (c) are also shown enlarged in the bubble caption for clarity.** [Supporting electrolyte: phosphate buffer (0.1 M, pH 7.8). Scan rate: 50 mVs^{-1}].

between the anodic and cathodic peak potentials is ~59 mV, as would be expected for a one-electron diffusional controlled reversible reduction/oxidation process. However, for the PPD coated electrode, the electrochemical response of $Fe(CN)^{3-}$ is barely discernable, indicating that the electrochemical reaction is suppressed by the PPD film present on the electrode surface. As shown in Figure 7.23c, the voltammogram obtained at the sonochemically fabricated microarray has the sigmoidal shape indicative of microelectrode-like behaviour. An individual microelectrode would be expected to exhibit forward (reductive) and reverse (oxidative) traces that would fall almost on top of each other with little evidence of double-layer charging capacitance. The hysteresis of the curve between forward and back scanning shown here (i.e. the separation between the peaks) is evidence of double layer charging and is observed in this case to be due to the very large pore density of approximately 8.0 $x10^4$ pores cm^{-2} (Myler, 2000), that will give rise to a significant cumulative double-layer charging current.

7.3 FABRICATION OF MICROELECTRODE ARRAYS UPON CARBON ELECTRODES

Previous investigations relating to the sonochemical fabrication of microelectrode arrays have involved either the use of gold sputter-coated glass slide assemblies (Myler, 2000) or screen printed gold (Myler *et al.*, 2004) as electrode templates. Although such electrode substrates have proved useful for characterising the fabrication procedure and producing individual microelectrode arrays required for specialist applications, they do not lend themselves as templates for the mass fabrication of *disposable* sensor arrays due to their high cost. Contrastingly, screen printed carbon electrodes have proved themselves to be attractive for sensing applications because they are relatively inexpensive and exhibit lower background currents over a wider potential window than their metal electrode counterparts (Niwa & Tabei, 1994).

Microelectrodes were thus fabricated upon PPD coated, screen printed carbon electrode templates in the same manner as described in the previous section. Again, it was very hard to obtain quantitative images of the microscopic pores produced with 20 seconds sonication using scanning electron microscopy, since it is very difficult to distinguish the differences in shading resulting from the ablated areas, with the shading differences produced as a result of the surface topography of the electrodes (since the polymer film mimics the surface topography of the underlying carbon electrode). However, the fact that the polymer films are being ablated via exposure to sonication is confirmed since the individual ablated areas of the film can clearly be seen at higher magnifications (Figure 7.4a).

In attempt to image the distributions of the pores more easily, gold cyanide was electrochemically deposited at the sonicated electrodes. The gold will only deposit in the areas where the underlying conductive carbon substrate has been exposed (Figure 7.4b). In addition, due to its high conductivity and light reflectance, when

(a)

(b)

Figure 7.4 **Scanning electron micrographs of PPD coated carbon electrodes showing (a) a micropore (x 2700 magnification) and (b) a micropore filled with deposited gold (x 4000 magnification).**

placed at an angle to a light source, the areas of deposited gold can easily be observed under a high magnification light microscope. Figure 7.5 (overleaf) shows a typically representative area of an electrode sonicated for 20 seconds with gold subsequently deposited electrochemically within the ablated pores of the insulating polymer. A similar distribution of micro-pores to that observed with SEM imaging of sonicated gold electrodes (Figure 7.2) is observed. Again, their appears to be a bi-modal distribution of pores, although it hard to establish their exact size, since there is an unavoidable but slight increase in the area following electroplating, i.e. the growth of gold will 'overlap' the actual perimeter of the pores to some extent (this can be seen in Figure 7.4b). The pore density was estimated from the gold cyanide imaging to be ~7.3 x 10^4 pores cm^{-2} for 20 seconds sonication. This is in good agreement to the population density of ~8 x 10^4 pores cm^{-2} calculated by Myler (2000) for a PPD coated gold electrode sonicated for the same time period.

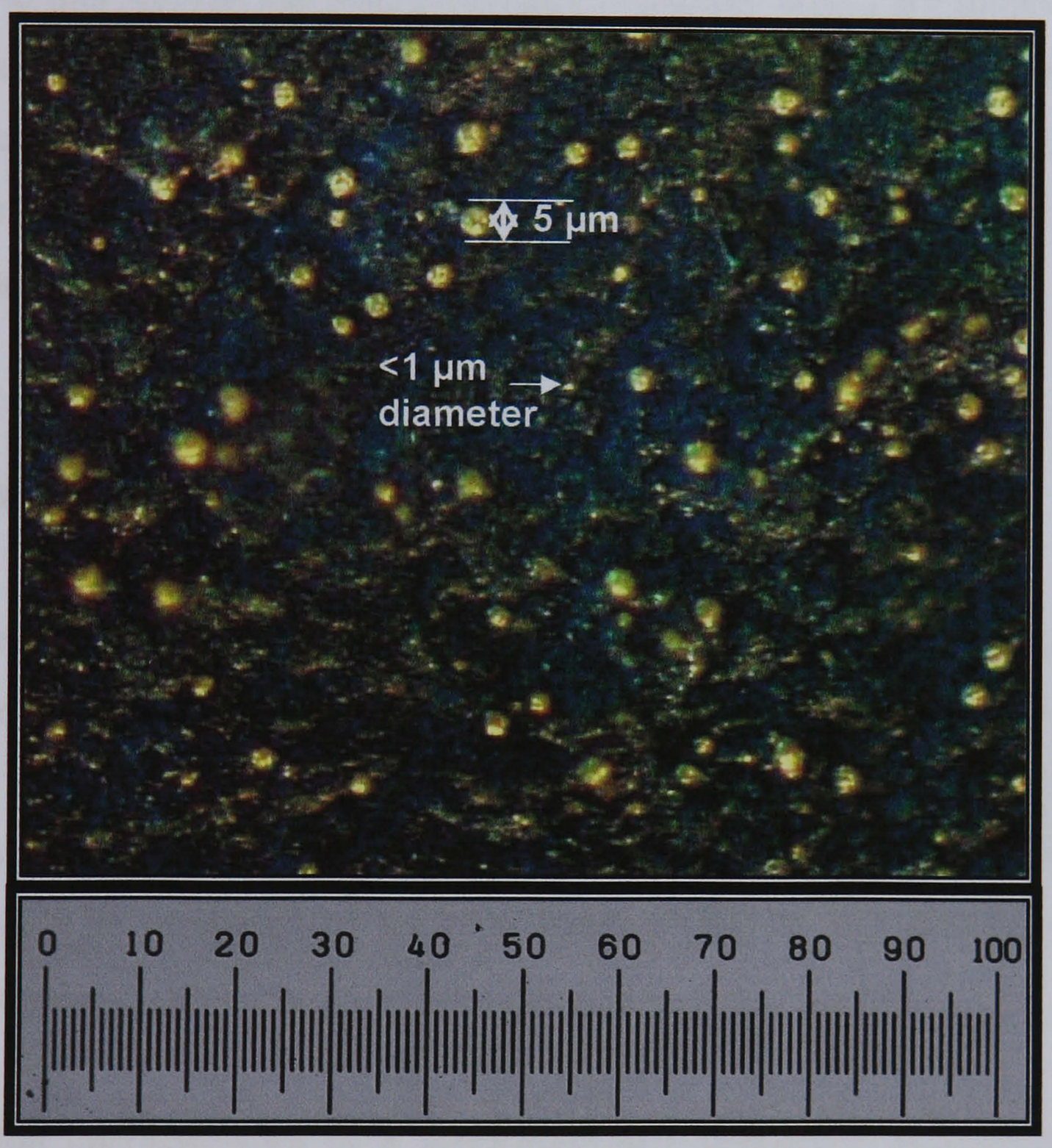

Figure 7.5 High magnification light microscope image of a sonochemically fabricated microelectrode array depicting the labelling of cavitational induced micro-pores with gold cyanide.
(Graticule shows micrometres).

7.4 ELECTROCHEMICAL CHARACTERISATION OF CARBON MICROELECTRODE ARRAYS

Microelectrodes may be easily characterised using electrochemical techniques due to the unique properties that hemispherical diffusion profiles impart on such sensors. Therefore, in this section, the sonochemically fabricated arrays are subjected to both cyclic voltammetric and chronoamperometric interrogation in order to assess whether the arrays exhibit these properties, namely sigmoidal-shaped cyclic voltammograms, stir-independence, scan rate independence and enhanced sensitivity. Comparisons to known microelectrode theory are also made.

7.4.1 Sigmoidal voltammograms

It has already been mentioned in Section 7.2 that cyclic voltammetry under steady-state conditions produced by non-linear diffusion results in S-shaped waves rather than the usual peak-shaped responses, since the hemispherical diffusion profile of microelectrodes allows for a substantially increased flux of electroactive species to the electrode - as compared to the pure linear diffusion case that is typical of a macroelectrode.

The diffusion characteristics of a sonochemically fabricated microelectrode array were therefore examined using slow applied potential cyclic voltammetry in 1 mM solutions of the reversible redox systems, hexaammineruthenium (III) chloride (Figure 7.6a) and ferrocenemonocarboxylic acid (Figure 7.6b). Voltammograms (i) and (ii) are those recorded at bare and PPD coated carbon electrodes respectively, in both cases. The voltammograms corresponding to the planar carbon electrodes exhibit well-defined reduction/oxidation peaks, typical of linear diffusion profiles. The separation between the anodic and cathodic peaks is greater than ~59 mV (as is usual for a one-electron diffusional controlled reversible reduction/oxidation process) for both redox systems, which would be expected since

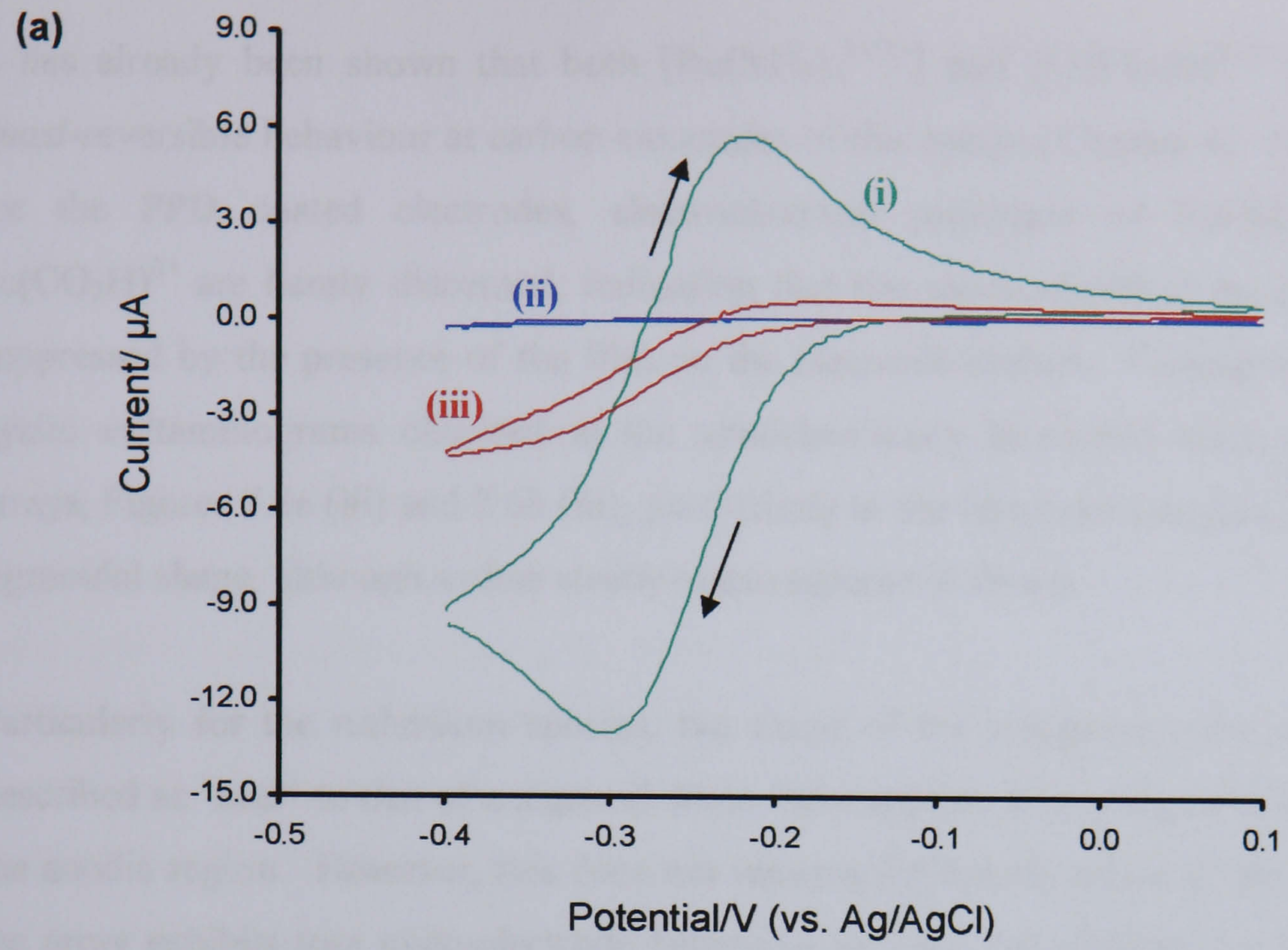

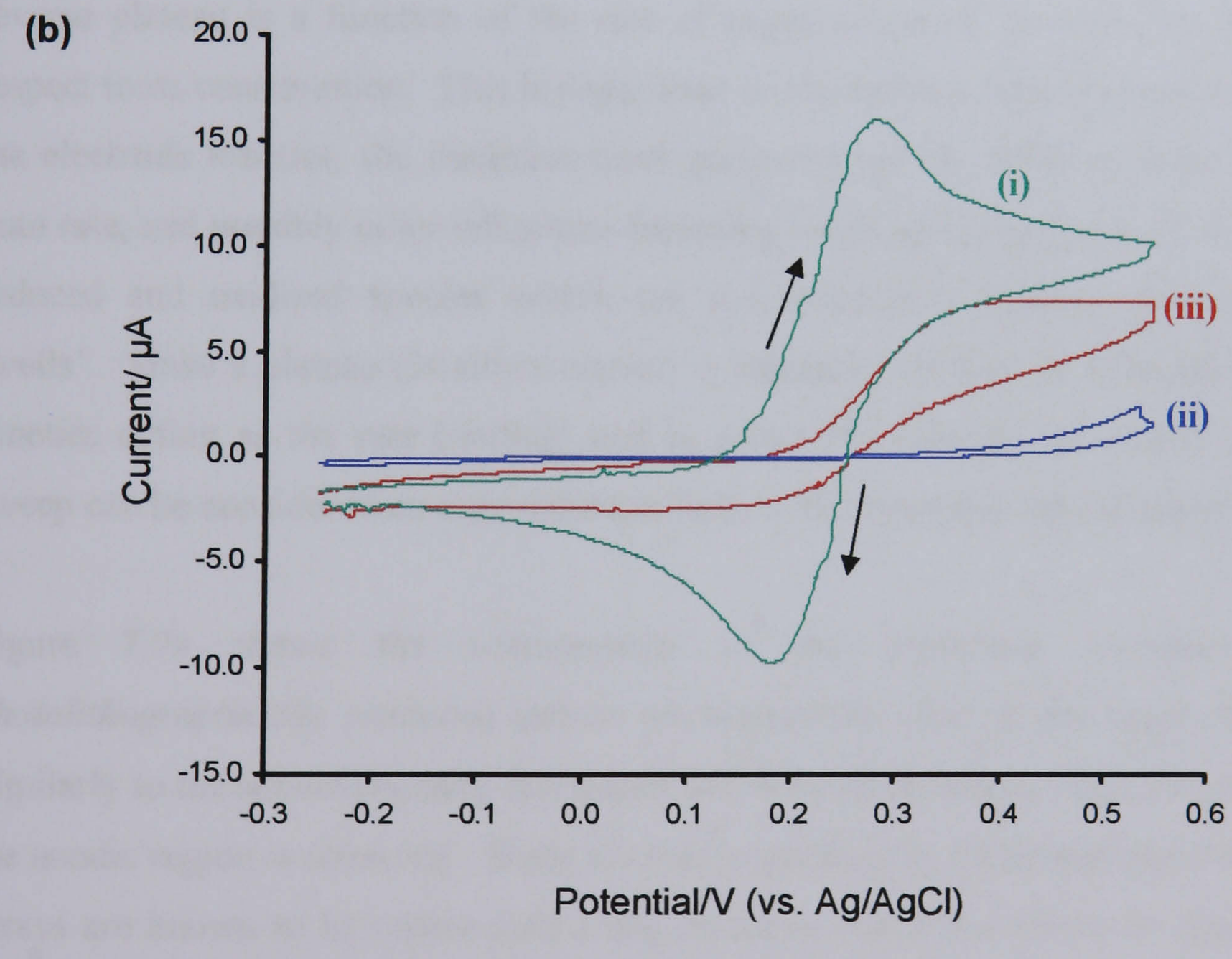

Figure 7.6 Cyclic voltammetry of **(a)** 1 mM hexaammineruthenium(III) chloride and **(b)** 1 mM ferrocenemonocarboxylic acid, at (i) a bare carbon electrode, (ii) a PPD coated carbon electrode and (iii) a similar electrode subsequently sonicated for 20 seconds. [Supporting electrolyte: phosphate buffer (0.1 M, pH 7.8). Scan rate: 20 mVs^{-1}].

it has already been shown that both $[Ru(NH_3)_6^{3+/2+}]$ and $[Fc(CO_2H)^{3+/2+}]$ exhibit *quasi*-reversible behaviour at carbon electrodes of this nature (Chapter 4). However, for the PPD coated electrodes, electrochemical responses of $Ru(NH_3)_6^{3+}$ or $Fc(CO_2H)^{3+}$ are barely discerned, indicating that the electrochemical reactions are suppressed by the presence of the film on the electrode surface. Contrastingly, the cyclic voltammograms obtained at the sonochemically fabricated microelectrode arrays, Figures 7.6a (iii) and 7.6b (iii), particularly in the ferrocene complex, hint at a sigmoidal shape, although a clear steady-state response is absent.

Particularly for the ruthenium species, the shape of the voltammograms could be described as 'near' to that of a sigmoid since there appears to be only one plateau in the anodic region. However, this does not necessarily directly relate to the whether the array exhibits true microelectrode behaviour or not. The presence or lack of a reverse plateau is a function of the rate of regeneration of the redox couple with respect to its consumption. This is dependant on the balance between factors such as the electrode kinetics, the thickness (and geometry) of the diffusion layer and the scan rate, and possibly other influences including localised concentrations of both the reduced and oxidised species within the sonochemically formed microelectrode 'wells'. Since a plateau (in either region) is indicative of lack of diffusion control, kinetics acting as the rate limiting step in *either* the cathodic or anodic transient sweep can be considered an appropriate indicator for microelectrode behaviour.

Figure 7.7a shows the voltammetry of the ruthenium complex at a *photolithographically* produced carbon microelectrode array at the same scan rate. Similarly to the sonochemically fabricated microelectrode arrays, only one plateau in the anodic region is observed. Since photolithographically fabricated microelectrode arrays are known to be constructed using carefully calculated electrode spacings, it can be concluded that the lack of a reverse plateau in both cases is due to the electron transfer kinetics of this complex at the carbon underlying electrodes, not a factor of the electrode spacing and distribution in the sonochemically fabricated microarrays. Furthermore, Swan (1979) and Amatore *et al.* (1983) have suggested that microelectrode arrays will be more sensitive to electron transfer rates than larger

electrodes, explaining why the arrays exhibit greater irreversibility than the planar electrodes under the same conditions.

The separation between the forward and reverse traces in Figures 7.6a and 7.6b (iii), which are larger than one would expect, are also likely to be a function of the reaction kinetics at the carbon underlying electrode. Similar voltammograms run at photolithographically produced amorphous carbon and gold microelectrode arrays (Figures 7.7a and 7.7b, respectively) with the same electrode centre-centre spacing/electrode radius ratios (manufacture quoted), seem to confirm this since much tighter traces are observed at the gold array than the amorphous carbon one, despite their identical d_c/r_{disc} ratio. The separation is further pronounced at the sonochemically fabricated arrays due to comparatively very large pore density (~7.3×10^4 pores cm^{-2}) at these electrodes.

As previously discussed in Chapter 2.5.3, the Cottrell equation is derived by solving Fick's second law of diffusion by assuming semi-infinite, linear diffusion to a horizontal plane and therefore cannot be used to describe microelectrode behaviour. Instead, a time-independent correction term must be incorporated to express the current profile of a microelectrode after the application of a potential step. The resulting equation for a single, inlaid, microdisc electrode yields a limiting current, i_L, that is time independant and varies with radius, r_{disc}, rather than area. Hence, microelectrode current density varies inversely with r_{disc} and thus the smaller the microelectrode, the greater the current density. For a defect–free microelectrode *array* and pure radial diffusion without overlap of the diffusion layers at individual electrodes, the current response from the array should be a simple sum of the current from each electrode according to the well-known equation:

$$i = 4nFr_{disc}D[C]_{\infty}Aq \qquad (7.1)$$

where n is the number of electrons involved in the reaction, F is the Faraday constant, D is the diffusion coefficient of the electroactive species ($cm^2\ s^{-1}$), $[C]_{\infty}$ is its concentration (mM), r_{disc} is the radius of each individual microelectrode (cm) and

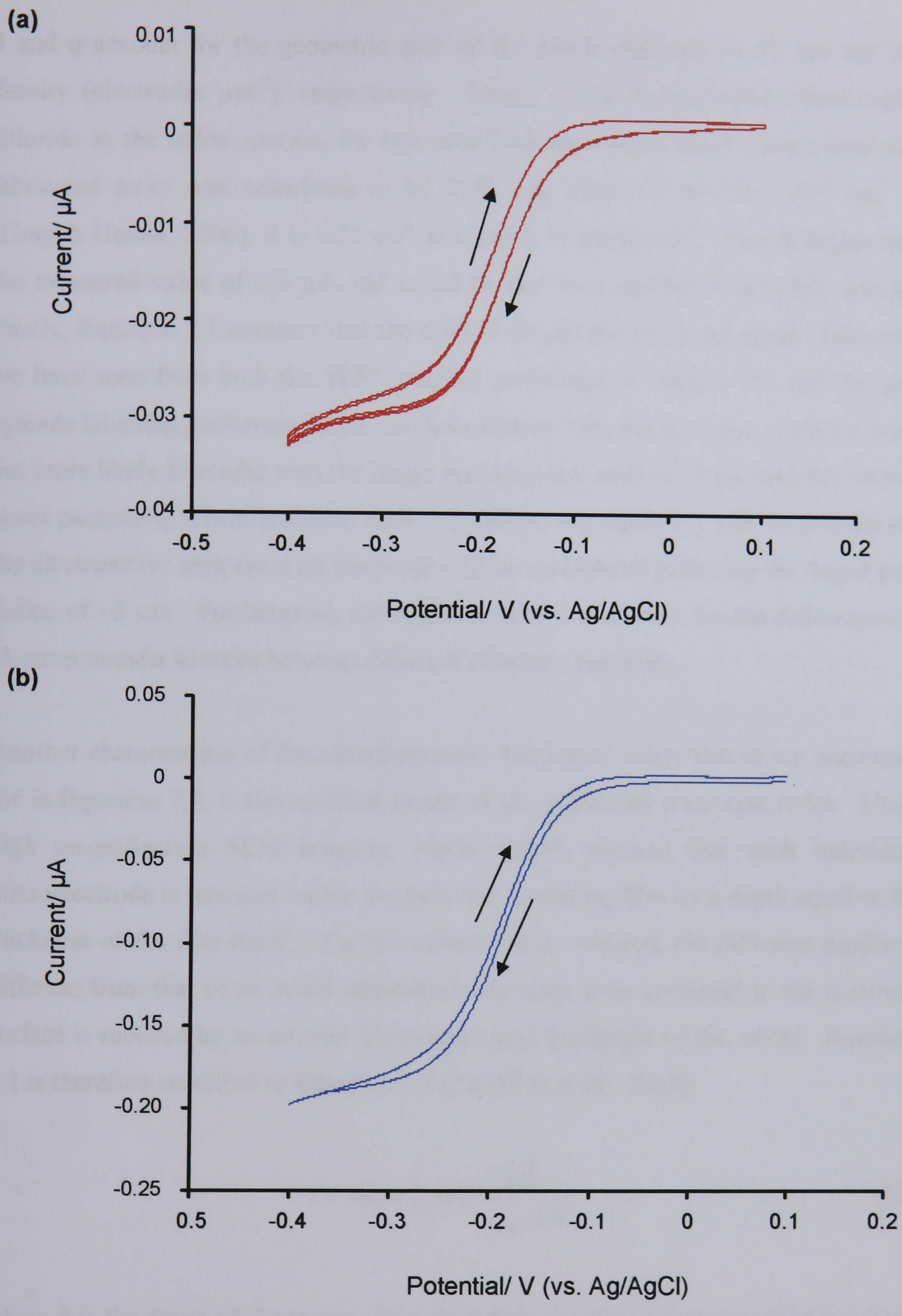

Figure 7.7 **Cyclic voltammetry of 1 mM hexaammineruthenium(III) chloride at photolithographically fabricated;**
(a) amorphous carbon and (b) gold, microelectrode arrays.
[Supporting electrolyte: phosphate buffer (0.1 M, pH 7.8). Scan rate: 20 mVs^{-1}].

A and *q* account for the geometric area of the entire electrode (cm^2) and the disc density (electrodes μm^{-2}), respectively. Using 1 mM hexaammineruthenium(III) chloride as the redox species, the expected limiting current for the sonochemically fabricated array was calculated to be 0.98 μA, where *D* is 8.6×10^{-6} cm^2 s^{-1} (Gray & Unwin, 2000), *A* is 0.21 cm^2 and *q* is 0.73 pores μm^{-2}. This is higher than the measured value of 0.6 μA and could be due to a number of possible reasons. Firstly, Equation 7.1 assumes that the radii of the all the pores are equal. However, we have seen from both the SEM imaging performed in Section 7.2 and the gold cyanide labelling performed in the previous section, that the pore size is not constant, but more likely bi-modal with the larger pores having radii of ~2 μm and the smaller pores possessing sub-micrometer radii. Therefore, the value of *q* will 'over-estimate' the electroactive area since all the pores will be considered as having the larger pore radius of ~2 μm. Furthermore, the equation does not account for the differences in electron transfer kinetics between different electrode materials.

Another characteristic of the sonochemically fabricated arrays that is not accounted for in Equation 7.1, is the recessed nature of the individual microelectrodes. Using high magnification SEM imaging, Myler (2000) showed that each individual microelectrode is recessed within the polymer insulating film by a depth equal to the thickness of the film itself. If a microelectrode is recessed, the diffusion profile is different from that of an inlaid microelectrode since mass transport to the electrode surface is reduced by an amount dependant upon the height of the recess. Equation 7.1 is therefore modified to Equation 7.2 (Sandison *et al.*, 2002):

$$i = Aq\pi r_{disc}^2 nFD\frac{[c]_\infty}{r_{disc}+h} \qquad (7.2)$$

where *h* is the depth of the recess. The thickness of poly(*o*-phenylenediamine) films electrochemically deposited upon carbon electrodes was calculated in Chapter 6 to be approximately 40 nm. Thus, accounting for the recessed nature of the individual microelectrodes using Equation 7.2, the expected limiting current at the sonochemically fabricated microelectrode array is now 0.76 μA, which is closer to

the experimentally determine value than that given by Equation 7.1. It should be noted however, that although recessed electrodes may exhibit a reduced diffusion compared to inlaid microelectrodes of the same dimensions, the recess part may also block convection of the electroactive species near the electrode, thus improving the stir-independence of such electrodes (Aoki, 1993). Furthermore, it has also been shown that the overlap between the diffusion fields of the individual electrodes will occur to a lesser degree for recessed electrodes (Zhu *et al.*, 1998), suggesting that a greater electrode density can be employed.

The difference between the theoretically and experimentally determined limiting currents that still occurs even with the use of Equation 7.2 is not surprising, since the equation still assumes a uniformly (hexagonal or square lattice) distributed arrangement of the individual microelectrodes in the array. The sonochemically fabricated arrays are randomly spaced and therefore 'missing' electrodes may cause a further reduction in the actual electrode area and thus current, since the lower symmetry of such an arrangement means that a lower electrode density must be employed to allow no overlap between the diffusion layers to occur. In fact, although several papers (Morf, 1997; Beriet *et al.*, 2000; Lee *et al.*, 2001) concerning the theory and simulation of microelectrode array behaviour have been published in recent years, together with some experimental investigations, to the author's knowledge, only one attempt (Scharifker, 1988) has been made to describe the current corresponding to random arrays of microelectrodes, probably because it is far easier to calculate the diffusion overlap at electrodes with known and uniform separations. However, the model of Scharifker also makes a number of assumptions that do not directly apply to sonochemically fabricated microelectrodes, such as that the number density and radius of the microelectrodes within the array is constant.

7.4.2 Scan rate independence

Another typical feature of microelectrodes is that cyclic voltammograms exhibit the same shape and nearly the same current regardless of scan rate, indicating a typical response for a radial diffusion profile.

Cyclic voltammograms of the sonochemically fabricated microelectrode arrays at various scan rates are compared with cyclic voltammograms performed at planar electrodes using the same scan rates, in Figure 7.8. As can be seen, the microelectrode arrays (Figure 7.8b) produce a near steady-state current which varies little with increasing scan rate, contrasting with the planar electrodes (Figure 7.8a), whose peak shaped response varies greatly with scan rate due to the linear limiting diffusion occurring at these electrodes.

Figure 7.9 compares plots of the peak (or limiting) current vs. log scan rate for a planar carbon electrode (Figure 7.9a) and a sonochemically fabricated microelectrode array (Figure 7.9b). The slope of a log i vs. log v_s line relating to a planar electrode governed by linear diffusion should be 0.5 for a reversible redox couple (Bard & Faulkner, 2001). The slope of the line shown in Figure 7.9a is 0.43, which is less than the expected value of 0.5, yet not surprising since we already know that hexaammineruthenium(III) chloride exhibits only *quasi*-reversible behaviour at carbon electrodes of this type. The slope of the line relating to the microelectrode array is clearly less (0.13), signalling an approach to a radial diffusion governed case. However, in this instance there appears to be no region where pure radial diffusion and thus complete scan rate independence is achieved (i.e. the slope of the line relating to the microelectrode array never reaches zero), indicating some mixed mass transport modes, although since the planar electrode slope was not equal to 0.5, it could also be argued that the microelectrode slope does not reach zero due to the electron transfer kinetics and reversibility of the redox couple at the underlying carbon electrode templates, and not because of the microelectrode geometry.

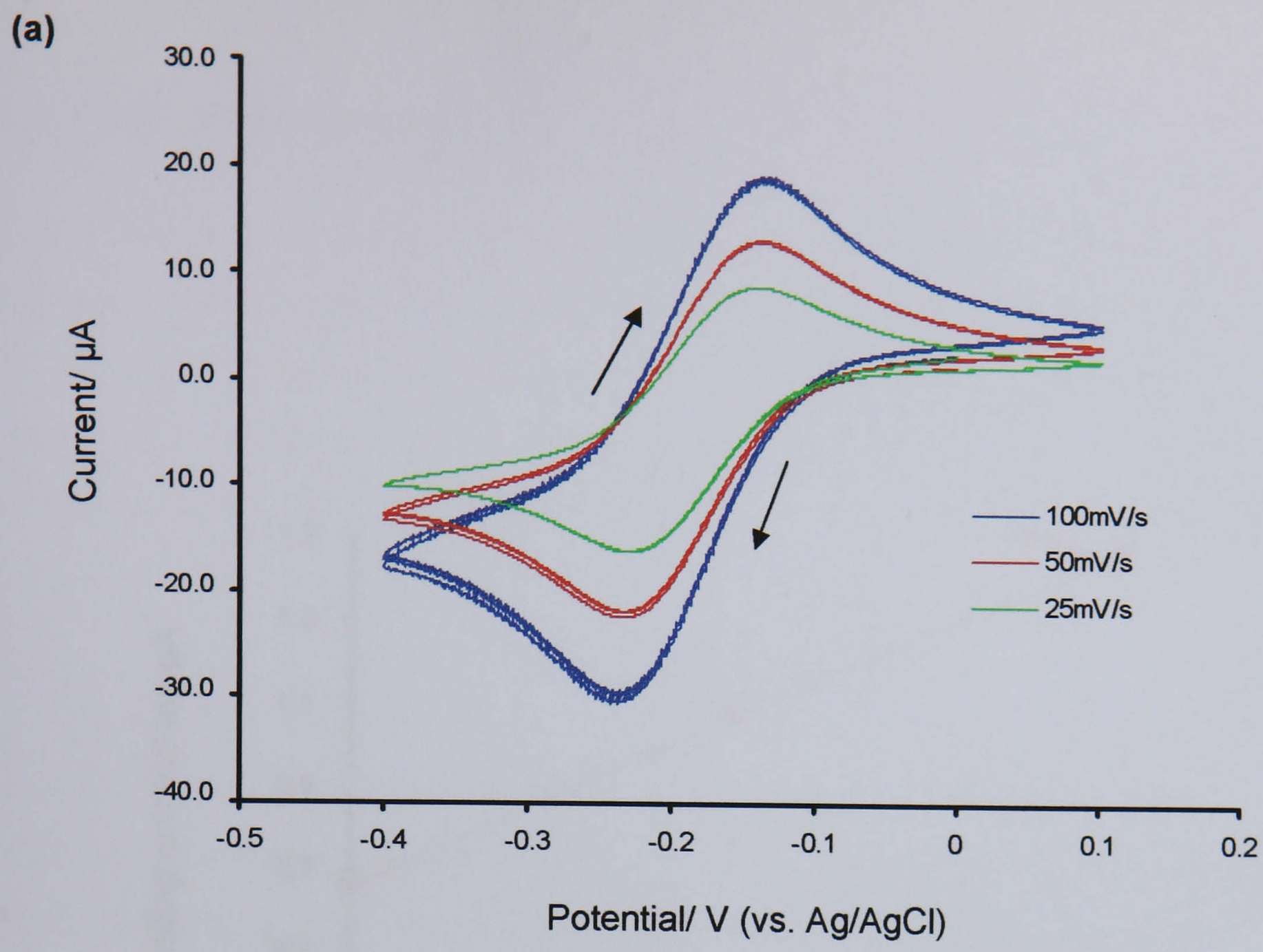

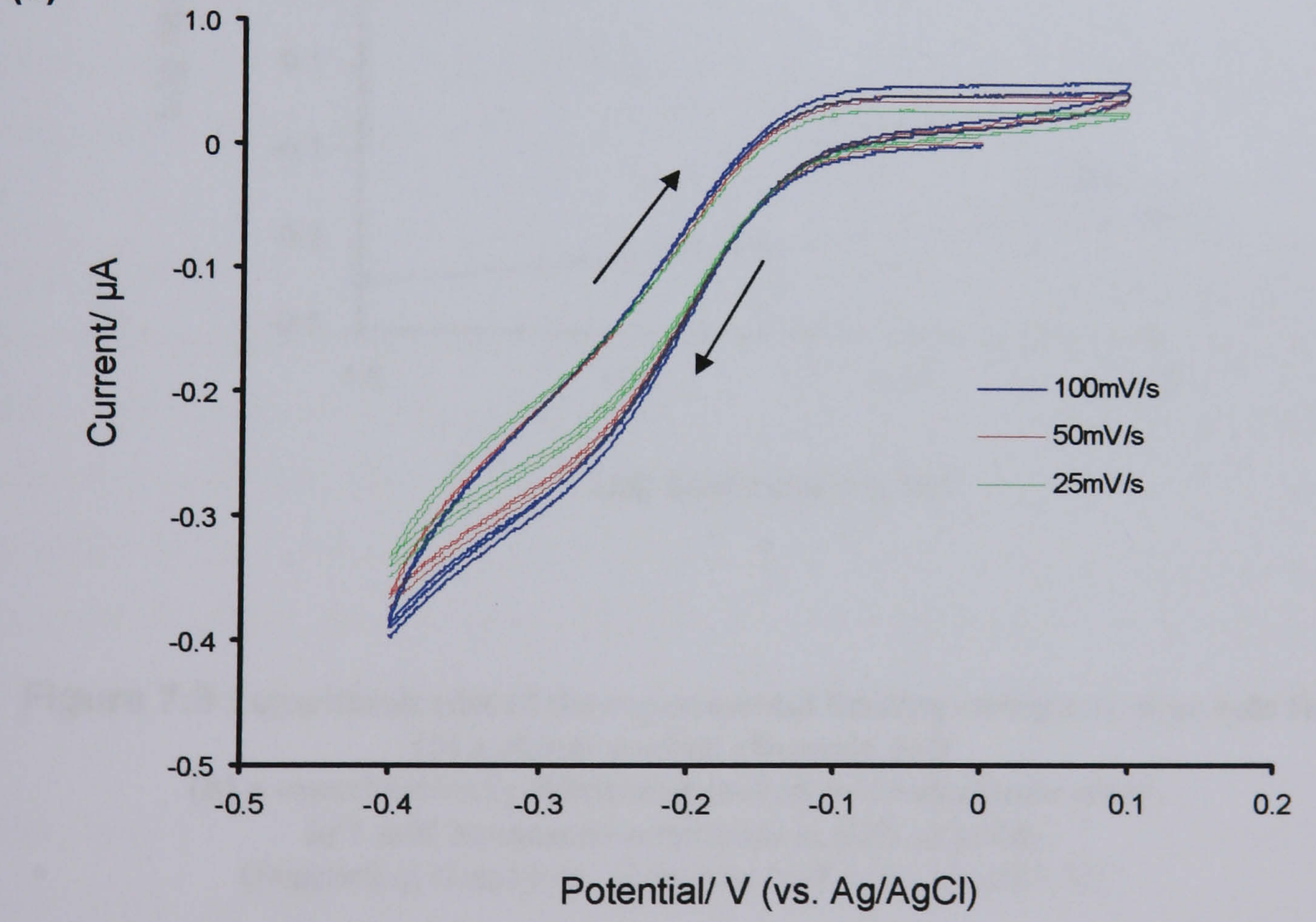

Figure 7.8 Dependence on scan rate of cyclic voltammograms in 1 mM hexaammineruthenium(III) chloride at:
(a) bare electrodes and (b) sonochemically fabricated microelectrode arrays.
[Supporting electrolyte: phosphate buffer (0.1M, pH 7.8)].

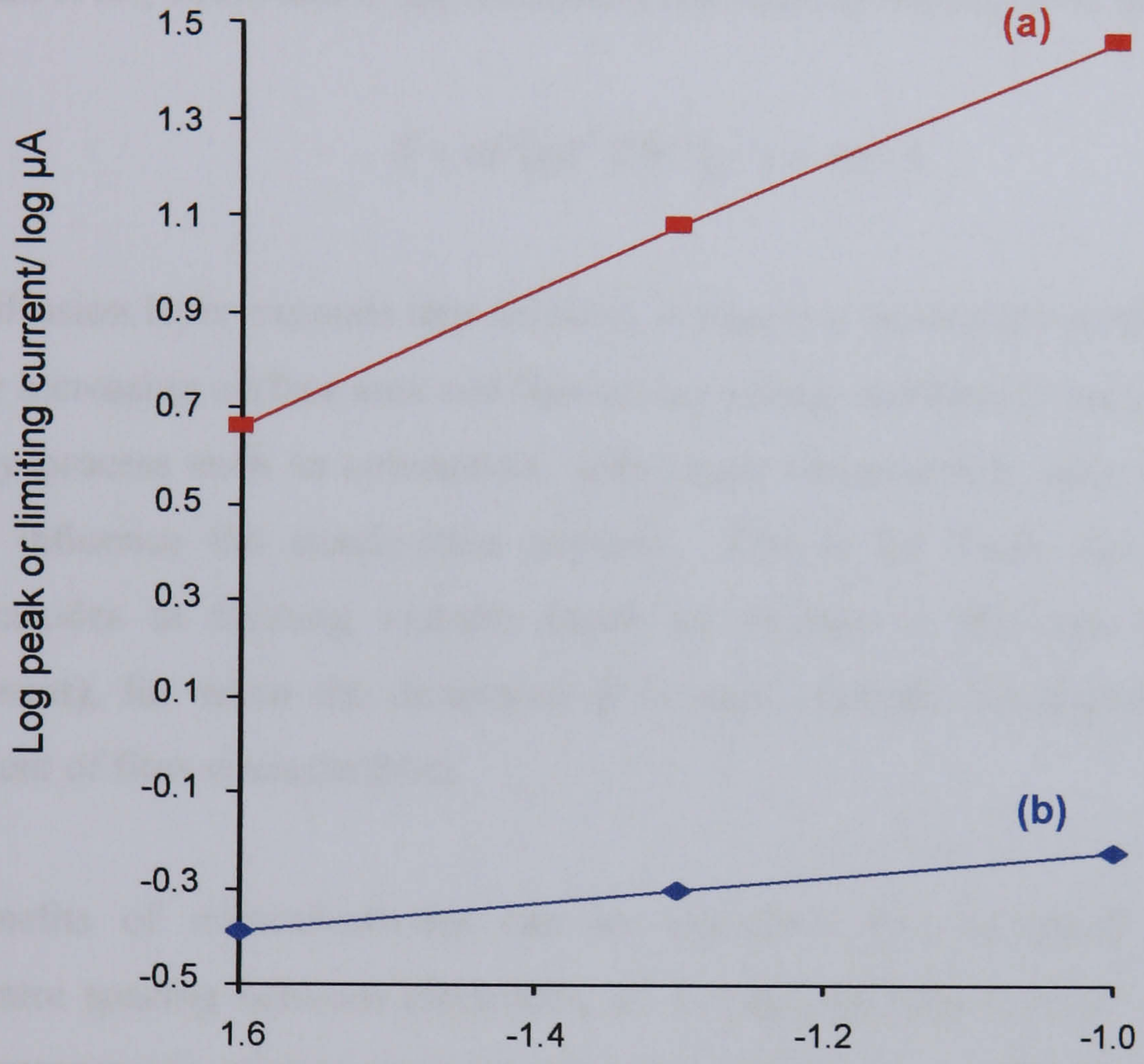

Figure 7.9 **Logarithmic plot of the experimental limiting current vs. scan rate for (a) a planar carbon electrode and (b) a sonochemically fabricated carbon microelectrode array, in 1 mM hexaammineruthenium (III) chloride. [Supporting electrolyte: phosphate buffer (0.1M, pH 7.8)].**

7.4.3 Stir-independence

One of the most significant advantages of microelectrodes is that the steady-state current, which is reached extremely quickly after the application of the potential step, is essentially convection independent. For a single microelectrode, the steady-state diffusion layer thickness, δ, is given by Equation 7.3 (Wightman *et al.*, 1982) and is approximately the same as the electrode dimension, β.

$$\delta = nF\left(\pi\beta^2\right)D[C]_\infty / i = \pi\beta / 4 \qquad (7.3)$$

As the diffusion layer expands into solution, it adopts a hemispherical shape, with a gradually increasing surface area and thus an increasing 'catchment' area for reagent. Thus, any process such as convection, with larger characteristic layer thicknesses, will not influence the steady-state current. This is the basis for the use of microelectrodes in flowing systems (such as streams in the case of chlorine measurement), for when the dimension β is small enough, the signal should be independent of flow characteristics.

Such benefits of microelectrodes can be exploited only in arrays where the centre-centre spacing between electrodes, d_c, is kept sufficiently large. Therefore, chronoamperometric stirring experiments were performed to indicate whether the sonochemically fabricated arrays meet this requirement since stirring the solution should have little influence on the measured current and a near-steady-state current response should be noted after a short time (and correspondingly, the non-faradaic current should be seen to be small).

Sonochemically fabricated carbon microarrays (Figure 7.10c) were polarised at -0.35 V (vs. Ag/AgCl) in 1 mM hexaammineruthenium(III) chloride/buffer solutions for 180 seconds. Both planar (Figure 7.10a) and PPD coated (Figure 7.10b) carbon electrodes were also examined as controls. Convection was applied to the solution 80 seconds after the initial polarization using a magnetic stir plate (a magnetic flea

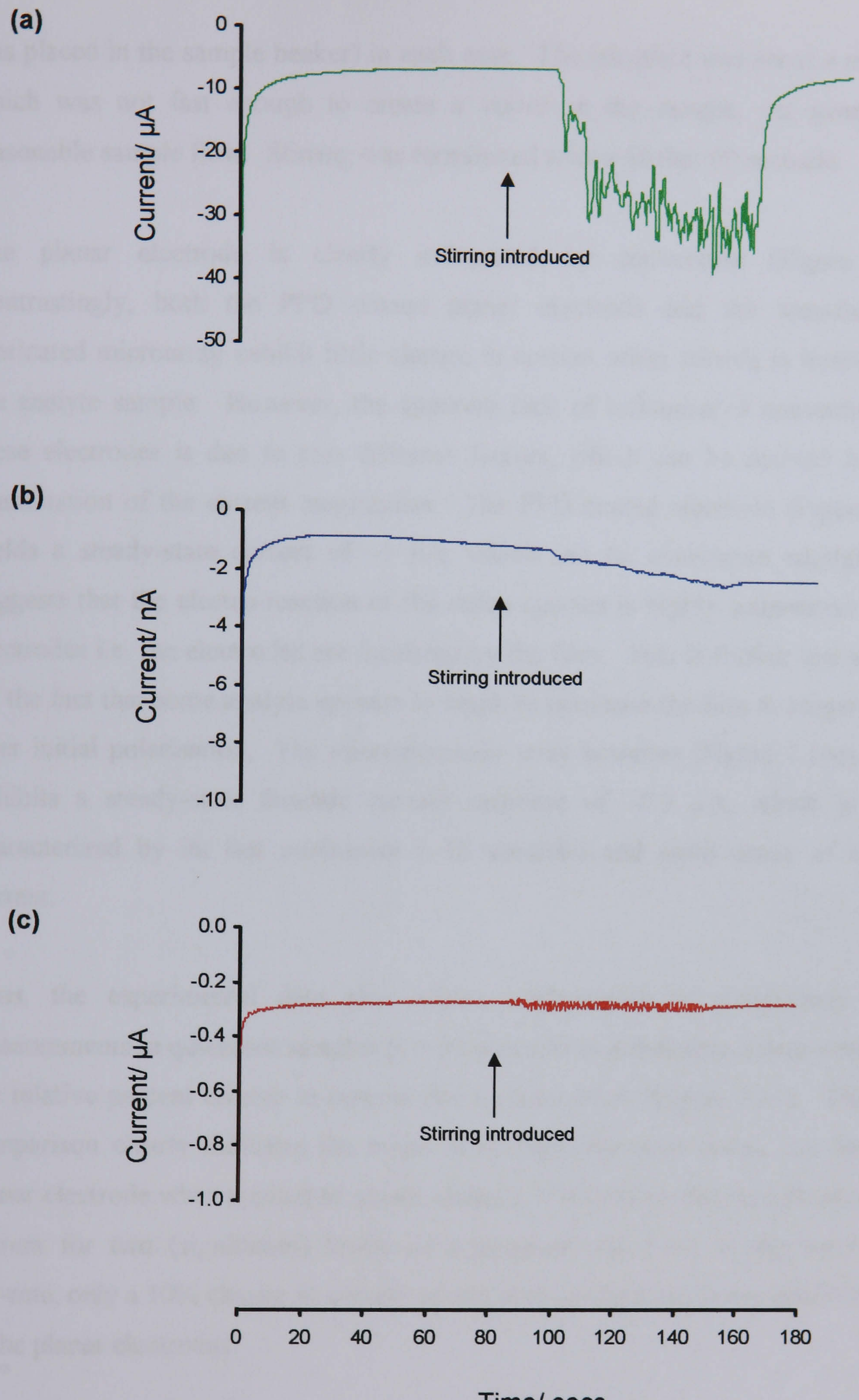

Figure 7.10 Current transients in 1 mM hexaammineruthenium(III) chloride showing variation in steady-state response with stirring at (a) a bare carbon electrode, (b) a PPD coated electrode and (c) a sonochemically fabricated microelectrode array.
[Supporting electrolyte: phosphate buffer (0.1 M, pH 7.8).
Polarising potential: -0.35V (vs. Ag/AgCl)].

was placed in the sample beaker) in each case. The stir-plate was set at a mid-value which was not fast enough to create a vortex in the sample, yet generating a reasonable sample flow. Stirring was terminated after a further 60 seconds.

The planar electrode is clearly influenced by convection (Figure 7.10a). Contrastingly, both the PPD coated planar electrode and the sonochemically fabricated microarray exhibit little change in current when stirring is introduced to the analyte sample. However, the apparent lack of influence of convection upon these electrodes is due to two different factors, which can be defined by closer examination of the current magnitudes. The PPD coated electrode (Figure 7.10b) yields a steady-state current of ~1 nA, which can be considered negligible and suggests that the electro-reaction of the redox species is highly suppressed at these electrodes i.e. the electrodes are insulated by the film. This is further characterized by the fact that some analyte appears to begin to permeate the film at longer periods after initial polarisation. The microelectrode array however (Figure 7.10c), clearly exhibits a steady-state faradaic current response of ~0.3 μA, which is further characterized by its fast attainment (~15 seconds) and rapid decay of charging current.

Thus, the experimental data also allows comparisons of steady-state current measurements in quiescent samples (t = 60 seconds) and therefore a determination of the relative percent change in current due to convection (Figure 7.11). This direct comparison clearly indicates the major advantage that such arrays can have over planar electrode when applied to sensor systems. Convection has no influence on the current for two (significant) levels of convection and even at the very highest stir-rate, only a 10% change in current occurs at the microarrays compared with 65 % at the planar electrodes.

It may be noted that the chronoamperometric steady-state current obtained at the arrays is much lower than that yielded by the planar electrodes. It is known that the chronoamperometric response of microelectrode arrays with intermediate packing densities is influenced by several parameters including the electrode radius, the

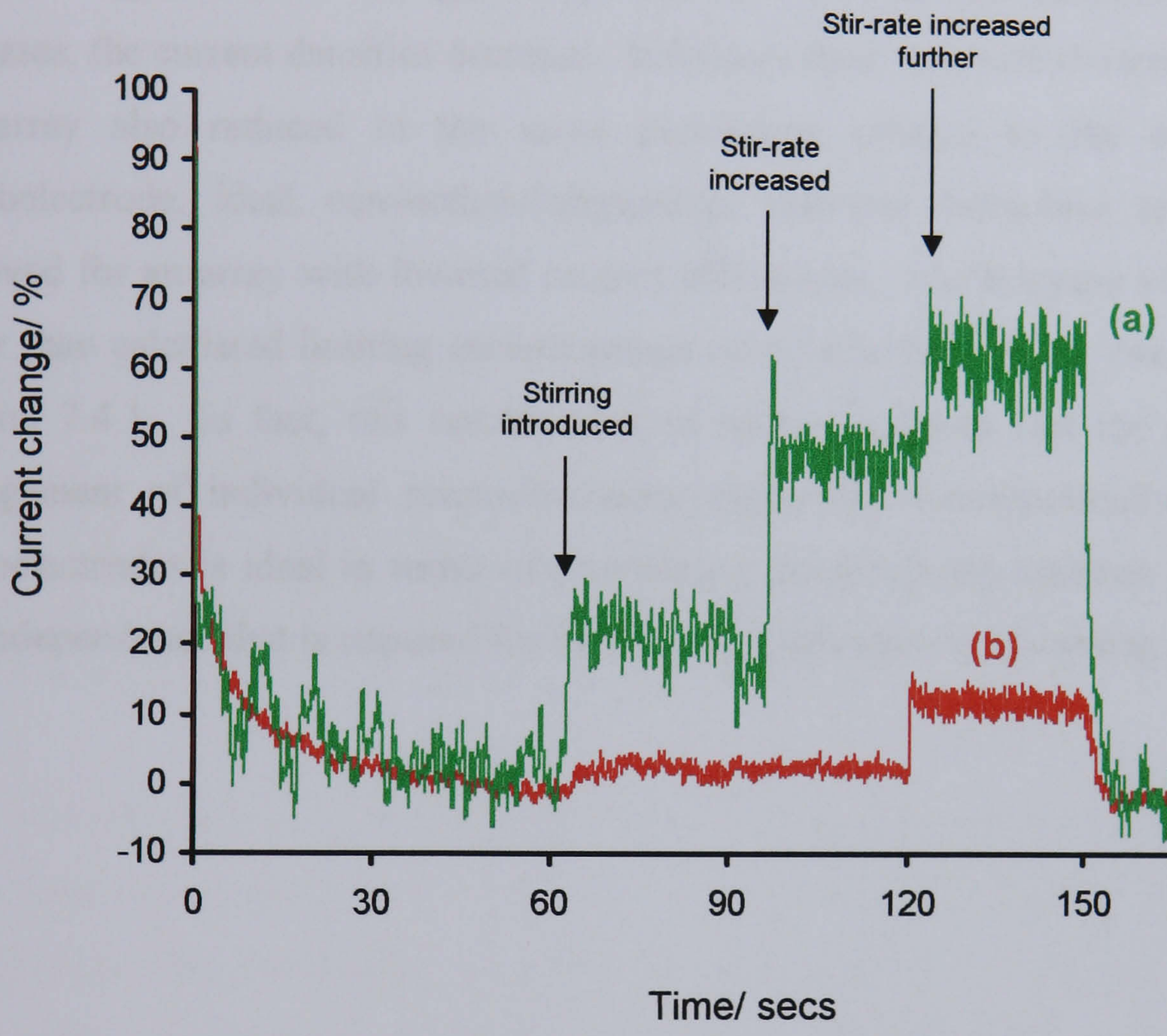

Figure 7.11 **Stir-rate dependence in terms of percentage current change for; (a) a bare carbon electrode and (b) a sonochemically fabricated microelectrode array, in 1 mM hexaammineruthenium(III) chloride.**
[Supporting electrolyte: phosphate buffer (0.1 M, pH 7.8).
Polarising potential: -0.35 V (vs. Ag/AgCl)].

diffusion layer thickness and the transition, which has been found to roughly corresponds to half of the inter electrode distance (Morf, 1996). Considering these parameters, Morf (1997) calculated that for a reduction of the convection independent contribution to be <10 % of the signal, the general requirement $d_c^2 > 4\beta\delta$, must be fulfilled. Morf (1996) concluded that the average inter-electrode distance between electrodes is the most critical parameter to optimise the array output response regardless of the geometry but, as the distance between electrodes increases, the current densities decrease. It follows then, that with the total current of the array also reduced to the same percentage relative to the output of a macroelectrode, ideal convection-independent response behaviour can only be achieved for an array with lowered current efficiencies, which agrees well with the lower than calculated limiting current values calculated from cyclic voltammetry in Section 7.4.1. In fact, this combination of results suggests that the geometrical arrangement of individual microelectrodes within the sonochemically fabricated microelectrodes is ideal in terms of providing a good balance between current and stir-independence that is required for their use as electrochemical sensing devices.

7.4.4 Enhanced sensitivity

Lower detection limits are obtained at microelectrodes since the capacitative current at planar electrodes is greater than at microelectrodes. This can be explained by comparing Equations 7.4 and 7.5 which give the capacitative current for a planar ($i_{c,p}$) and a microelectrode ($i_{c,m}$), respectively:

$$i_{c,p} = v_s C_d A \tag{7.4}$$

$$i_{c,m} = v_s C_d A_a \tag{7.5}$$

where v_s is the scan rate, C_d is the is the double layer capacitance, A is the geometric area of the electrode and A_a is the electroactive area of the electrode. A_a will always be less than the A and thus, $i_{c,m}$ will always be less than $i_{c,p}$. Since the faradaic current is proportional to electrode area, the ratio of faradaic to background (capacitative) current should increase with decreasing electrode radius.

Thus, electroanalytical detection limits at microelectrode arrays can, in principle, be lower than detection limits at analogous macrosized electrodes and indeed, West (1993) found that for densely packed arrays of small microelectrodes, significant improvements in the signal to noise ratio are observed, although ohmic interactions were also found to increase with the number of neighbouring electrodes and remain significant if the separation distance is less than ten times the radii.

The sensitivity of the sonochemically fabricated microelectrode arrays is assessed here using free chlorine, since not only does EU law require very low levels of free chlorine to be measured in aqueous solutions, but as we have seen from Chapter 4, this offers a considerable challenge due to the low currents obtained for free chlorine at planar carbon electrodes. Chronoamperometry was performed in phosphate buffer at a sonochemically fabricated microelectrode (Figure 7.12) by polarising the electrode at -0.1 V (vs. Ag/AgCl). Very low concentrations of free chlorine were added to the sample at regular time intervals as indicated on the current-time

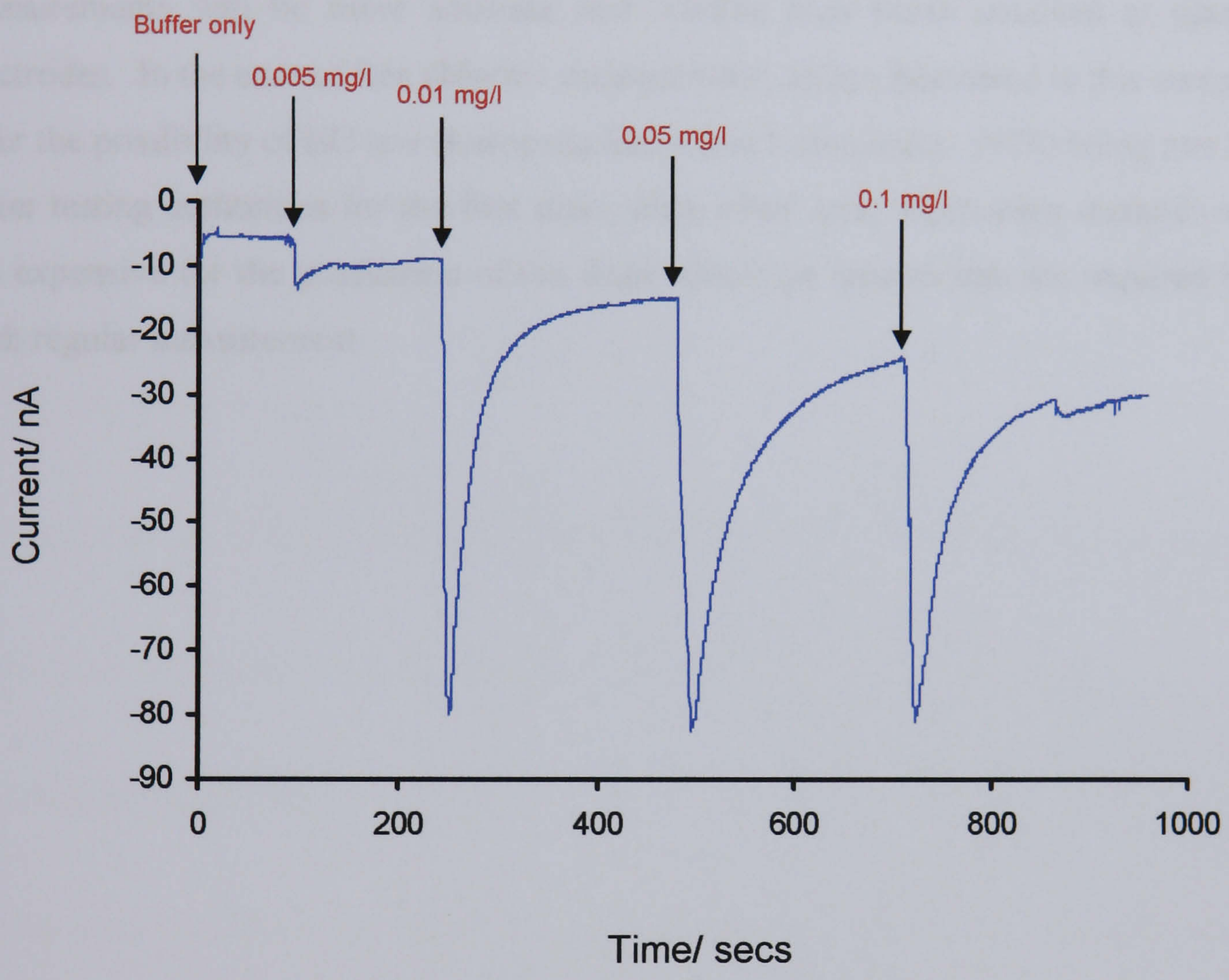

Figure 7.12 Current-time transient showing the response of sonochemically fabricated microelectrode arrays to successive additions of free chlorine at very low concentrations.
[Supporting electrolyte: phosphate buffer: (0.1 M, pH 7.0).
Polarising potential: -0.1 V (vs. Ag/AgCl)].

transient shown in Figure 7.12. Defined responses to each of the chlorine additions are observed, suggesting a greater sensitivity of the sonochemically fabricated microelectrodes as compared to their planar counterparts. If we define the detection limit as being that concentration that gives a faradaic signal which is equal to the background current, the arrays can be seen to have a detection limit for free chlorine of <0.005 mg/l. Furthermore, since the thus fabricated microelectrode arrays have also been seen in the previous section to impart stir-independent responses, the measurements will be more accurate and reliable than those obtained at planar electrodes. In the case of free chlorine measurement, arrays fabricated in this manner offer the possibility of EU law (European Economic Community, 1978) being met by water testing authorities for the first time, since other array fabrication methods are too expensive for the production of the disposable-type sensors that are required for such regular measurement.

7.5 CONCLUSIONS

This chapter described the sonochemical fabrication of microelectrode arrays upon both gold and screen printed carbon electrodes. Imaging of the sonochemically fabricated arrays suggested a random distribution of pores with bi-modal diameters. This distribution provided an optimal centre-to-centre spacing between pores to allow radial diffusion at the individual microelectrodes, yielding arrays that exhibited a good balance between the following typical microelectrode characteristics:

1. Sigmoidal shaped cyclic voltammograms.

2. Low stir-dependence of less than 10 % change in base current even at the very highest flow rates.

3. Rapid (<20 seconds) steady-state responses in chronoamperometric experiments.

4. Scan rate independent cyclic voltammetry.

5. Enhanced sensitivity.

Furthermore, a defined geometric arrangement is not required since calibration curves may be employed and this, combined with the simplicity and inexpensiveness of the approach, suggests that sonochemically fabricated microelectrode arrays offer widespread applicability in the field of electrochemical sensors.

CHAPTER 8

OPTIMISATION OF ULTRASOUND CONDITIONS TO FACILITATE THE MASS FABRICATION OF MICROELECTRODE ARRAYS

8.1 INTRODUCTION

We have seen from the results presented in Chapter 7 that carbon microelectrode arrays may be fabricated via the sonochemical ablation of insulating polymer films, and that such electrodes exhibit typical microelectrode behaviour, including for example, stir-independence, sigmoidal shaped voltammograms and enhanced sensitivity. Furthermore, these electrodes may lend themselves to mass fabrication due to the simplicity and inexpensiveness of the sonochemical approach. Since we have already shown in Chapter 6 that *o*-phenylenediamine may be reproducibly deposited upon 100 electrodes simultaneously, the question of scale-up lies with the ultrasound process and thus, the purpose of this chapter is to prove that sonochemical fabrication of microelectrode arrays can be undertaken on a scale larger than that used in the research laboratory, by investigating the homogeneity of the ultrasound process itself.

Over the last few years a number of groups have become interested in solving the problems of scale-up (Martin & Law, 1983; Mason & Berlan, 1992). It appears in this context that the problem is largely based on whether it is possible to achieve a uniform sonication profile throughout the whole tank or whether it is easier to localise the ultrasound into a particular region of the reacting system. However, such studies have focussed upon scale-up for the purpose of ultrasonic cleaning – scale-up in terms of microelectrode array production has no precedent, to date.

This chapter investigates the possibility of 'scale-up' of the sonochemical approach of microelectrode array fabrication both in terms of producing multiple electrodes simultaneously *and* in terms of the use of industrial size ultrasound tanks for such purposes. Section 8.2 describes a method of 'mapping' the cavitation properties of sonication tanks and relates the observed cavitation patterns with ultrasound propagation theory. The effect of the incorporation of a 'baffling' system (i.e. a system to distort standing wave formation) to the ultrasonic tank is also investigated in this section. The tank cavitation patterns determined in Section 8.2 are correlated

with the electrochemical performance of electrodes sonicated in the tank as described in Section 8.3.

Section 8.4 examines possible improvements to the sonication protocol with the aim of increasing the reproducibility of electrodes fabricated in this way. Optimal sonication conditions for this improvement are determined using both cyclic voltammetric and chronoamperometric interrogation techniques. Calibration curves for sensors produced according to the parameters found by the experiments described in Section 8.4 are presented in Section 8.5. An alternative interrogation method resulting in enhanced reproducibility of results is also presented.

8.2 ULTRASONIC CAVITATION 'MAPPING' STUDIES

The production of reproducible microelectrode arrays upon multiple electrodes simultaneously is not a case of simply immersing the sensor sheets in the water and applying an ultrasonic pulse. The construction of the tank and the distribution of the ultrasonic intensity within this vessel must be firstly considered in order for the correct positioning of the sheets within the tank to be determined. Thus, correlations between the electrochemical behaviour of the individual electrodes at different positions in the sheet can be made. For a single sensor in a small ultrasound bath with a single transducer, this is a simple task, since the electrode should be located vertically above the transducer. However, for a large bath with multiple transducers, the electrode sheets must be placed in the most homogeneous regions of intensity, which are unique to each individual sonication bath, since power is known to vary with tank size and manufacturer (Mason, 1999). Once optimal positions have been identified, these can be used as templates for mass production.

A number of methods can be employed to locate these regions. Pugin (1987), for example, used thermistor probes to measure localised temperature differences at various places within sonication tanks. Maxima and minima were found depending on the tank shape, the liquid height and input power. Another approach involves exploiting sonochemically enhanced luminescence. For example, luminol is known to degrade in the presence of hydroxyl radicals and hydrogen peroxide, resulting in the emission of light (Mason, 1999). This light emission is intensified if the radical and peroxide generation is concentrated into a small region. Such conditions occur at the interface between carbon tetrachloride and water during sonication. A series of bright sparks of light are subsequently emitted from the carbon tetrachloride/water interface upon agitation by the sonic waves. However, the simplest and most effective way of characterising the areas of intensity within a given tank is probably via the well-known 'foil test' (Pugin, 1987; Mason, 1999). The test works on the basis that when a cavitation bubble collapses close to a surface, it causes considerable surface damage due to microstreaming of the high velocity jets of

solvent. Using a series of foil sheets, the location of the areas with and without transient cavitation can be discriminated and consequently, the nodal regions of the bath can be identified since perforations in the foil will occur at the areas of maximum ultrasonic intensity. Thus, clean pieces of aluminium foil (450 x 400 mm) were suspended vertically within the sonication tank at various positions as described in Chapter 3.5.4 (page 110). The sheets were subsequently sonicated at 100% power for 10 minutes. A number of perforations within the foil sheets were observed to begin to appear after approximately 3 minutes sonication. On removal, the foil sheets were photographed and the resultant images are shown in Figure 8.1 overleaf (x and y are the distances from the side and base of the tank, respectively). The intensity of the perforations can be seen to vary according to the positions of the foils within the tank, and were found to be particularly intense at positions B and E. From the images corresponding to these two locations (and indeed the other images to a certain extent), it appears that the maximum cavitation occurs in horizontal lines or planes parallel to the surface of the liquid. This pattern suggests the presence of standing waves in the tank – that give rise to concentrated regions of sonic energy in the positions of maximum amplitude. Schram (1991) used a suspension of copper bronze particles to confirm that for large baths, the standing wave pattern corresponds to the half-wavelength of ultrasound in a particular solution. Upon the application of ultrasound, the originally uniform suspension of copper particles changed to a set of horizontal bright 'metallic' lines separated by distances of the half-wavelength of the ultrasound, correlating to the copper bronze particles being collected at the nodes and anti-nodes of the sound waves in the solution.

As was discussed in Section 2.7, the wavelength of ultrasound within a particular system can be calculated according to Equation 8.1:

$$v = f\lambda \qquad (8.1)$$

The velocity (v) of sound through water is approximately 1500 ms^{-1} and thus for a transducer operating frequency (f) of 25 kHz, the wavelength (λ) of the ultrasound in

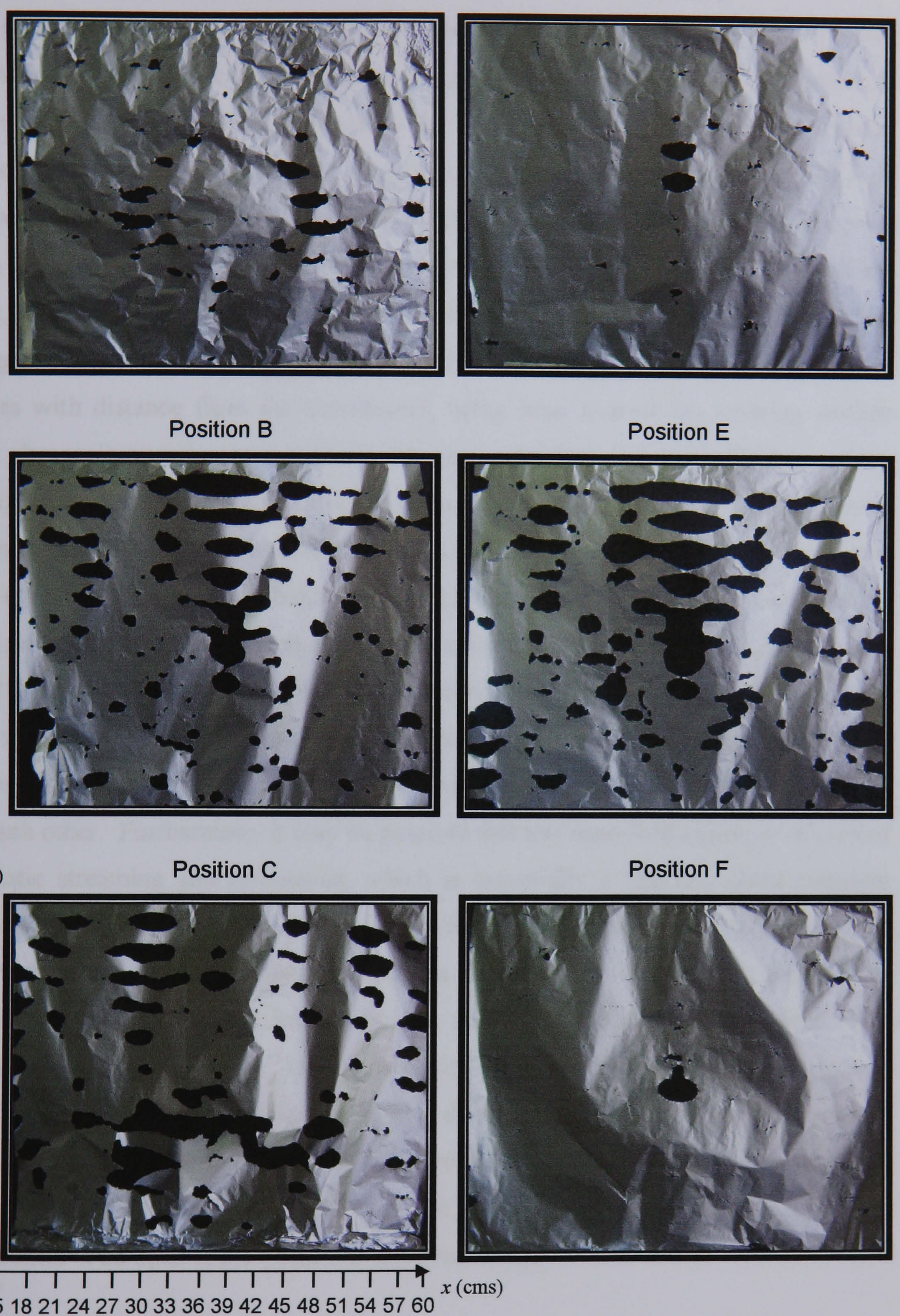

Figure 8.1 **Photographic representation of the 'foil test' showing the ultrasonic cavitation induced damage on sheets of aluminium foil placed at various positions within the ultrasonic tank.**

the system is ~6 cm. Hence, for the system used in this work, the maximum cavitation effect can be expected to occur at vertical intervals of ~3 cm (half the wavelength), which indeed appears to be the case since horizontal perforations corresponding to this distance can clearly be located on most of the sonicated foils shown in Figure 8.1. In positions B and E, the foil was most rapidly destroyed in the area nearest to the solvent surface, at approximately 48 cm from the bottom of the tank, which suggests intense cavitation in this area. In fact, it appears from these images that the intensity of the ultrasound corresponding to the standing waves varies with distance from the transducers, being least nearest the emitting surface (the ultrasonic transducers are attached to the underside of the metallic base of the bath). This is surprising since acoustic intensity is thought to decrease with distance away from the source (Klima & Bernard, 1999), and therefore it would imply that less evidence of ablation should be observed at the top of the foil sheet. One possible explanation for the results seen here is that towards the base of the bath, close to the emitting surface, there is destructive interference in the standing wave pattern, with the standing waves being disrupted and therefore appearing less intense. This is quite feasible in a system comprising of a number of transducers in close proximity to each other. Furthermore, it may be possible that this near-field region is an area of acoustic streaming and turbulence, which is essentially a region *without* transient cavitation (Klima & Bernard, 1999). If this were true, the results presented in Figure 8.1 would also serve as further proof that a surface is not disturbed by the flow of solution associated to acoustic streaming and/or turbulence, but is indeed only punctured as a result of transient cavitation on the basis of microjetting. Alternatively, the increase in ablation with distance away from the emitting surface may be a factor related to internal reflectances within the metallic tank, since the majority of calculations for the decrease of intensity have been based upon sonication in an open space (Klima & Bernard, 1999).

In order to elucidate the effect of the locations of the transducers (see Figure 8.2a) on the shape and intensity of the foil perforations shown in Figure 8.1, their positions in relation to the positioning of the foil sheets is plotted in Figure 8.2b. Each of the transducers is denoted numerically for ease of explanation. It is thought that the

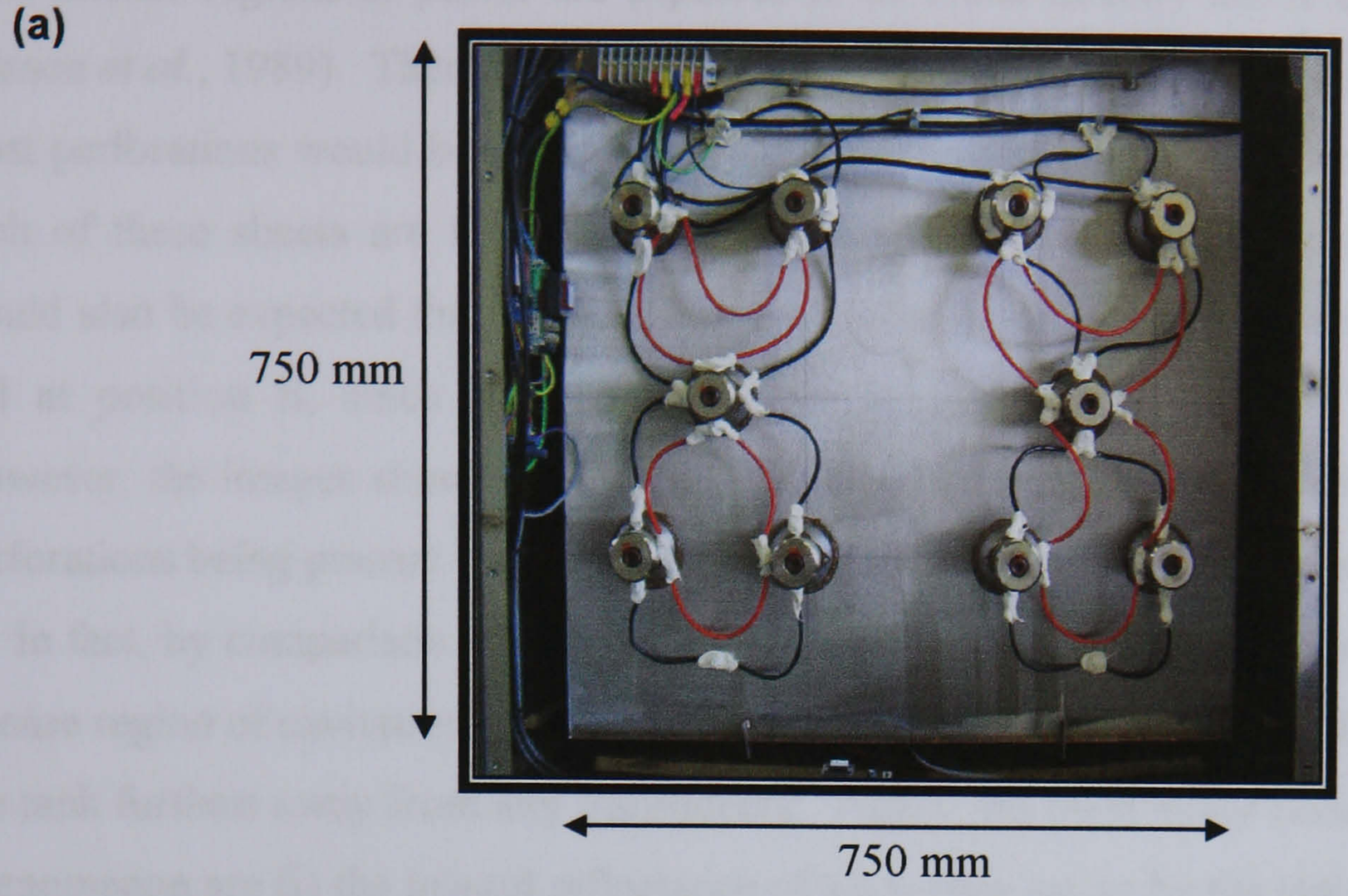

Figure 8.2 (a) Photograph of the underside of the ultrasonic tank showing the positions of the transducers, and (b) diagram to show the positions of the transducers in relation to the positioning of the aluminium foil.

most intense regions of power are expected to be found directly above a transducer (Mason *et al.*, 1989). Therefore, from studying Figure 8.2, one would expect that the most perforations would be observed on the foils located in positions D and F, since each of these sheets are located directly above four transducers. Accordingly, it would also be expected that the least evidence of ablation would be observed on the foil at position B, since no transducers are located directly beneath this sheet. However, the images shown in Figure 8.1 exhibit the opposite effect, with the *most* perforations being present on the foil from position B and the *least* at positions D and F. In fact, by comparison of all the images shown in Figure 8.1, it appears the most intense region of cavitation is at the centre of the tank, which is actually the region in the tank furthest away from any transducers. Again, the most likely reasons for this phenomenon are (i) the inward reflectance of ultrasonic waves by the tank walls, and (ii) disruption of the ultrasonic waves as a result of the transducers being relatively close together. To try and establish more confidently which of these two factors is the most prominent, the *vertical* areas of most perforation observed on the foil sheets have been marked with a cross on the transducer/foil diagram of Figure 8.3.

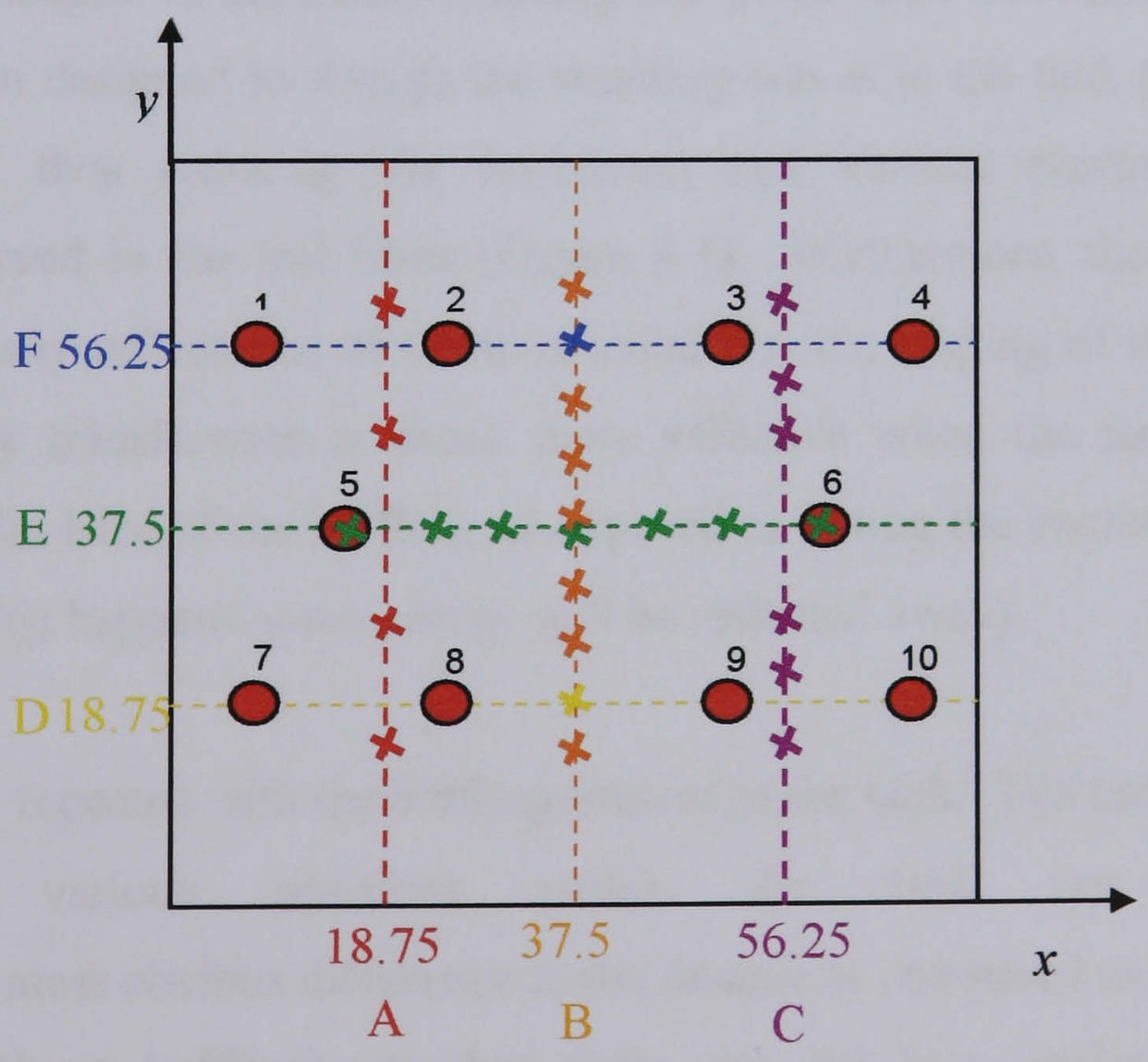

Figure 8.3 Diagram to show the locations of maximum perforation (vertical) in relation to the positioning of the transducers.

Most noticeable is the evidence of symmetry between the areas of maximum intensity (with the exception of some anomalies in the foil at position C). However, although some intense ablation occurs at the centre of the tank, away from the transducers, there is also evidence of intense ablation directly above transducers 5 and 6 (foil E) and in close proximity to transducers 2 and 8 (foil A) along with transducers 3 and 9 (foil C). Thus it would appear that the pattern of ablation is primarily due to internal reflectance in the tank rather than the disruption of ultrasound between transducers. Interestingly, the tank is manufactured with the inside base angled downwards towards the centre to aid drainage. As the ultrasonic energy is radiating vertically as sound waves from the transducers, this arrangement may further add to inwards reflectance of the ultrasound observed.

Consequently, the inner base and sides of the tank were then lined with a perforated stainless steel 'baffling' sheet comprising a hexagonal arrangement of 3mm diameter perforations (see Chapter 3.3.2). Ultrawave Ltd. (the tank manufacturers) have determined perforations of this size to be optimal for the disruption of ultrasound in the KHz frequency range. In addition, such baffling is often used for the construction of 'stages' in ultrasonic cleaning and small-scale laboratory tanks. This baffling has been designed to disrupt the standing waves in the tank (i.e. the nodes and antinodes), thus reducing the horizontal and vertical perforation pattern previously observed in the foil films (Figure 8.1). Furthermore, the baffling may compensate for any reflectance of the ultrasound due the angling of the base panel, since the energy transference is much more effective when the sound impinges directly on the flat base of the baffling as opposed to hitting the angled underside of the tank (when this happens some energy will be reflected away).

The foil test was repeated with the baffling present in the tank. The foils having been sonicated at various positions within the tank are shown in Figure 8.4. The most obvious difference in the images as compared to those given in Figure 8.1 (without baffling), is that there are far less perforations in the foils at all positions. Furthermore, the foils were sonicated for twice the time period

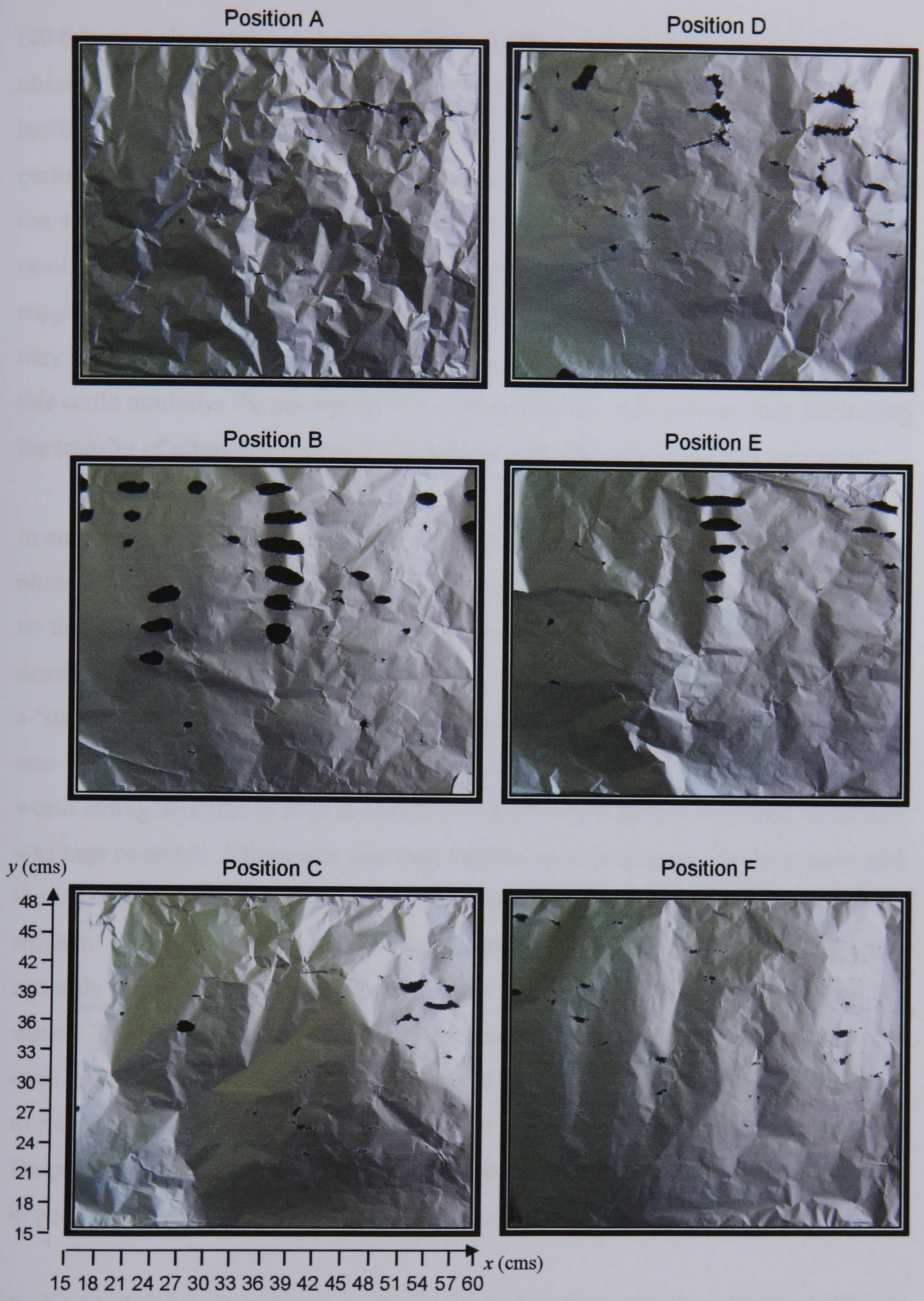

Figure 8.4 **Photographic representation of the 'foil test' showing the ultrasonic cavitation induced damage on sheets of aluminium foil placed at various positions within the ultrasonic tank having a baffling incorporated within.**

(20 minutes) since those in the tank without baffling, since no sign of perforation was observed after 10 minutes sonication. Thus, it appears on first analysis that the baffling has suppressed the intensity of the cavitation to some degree, since less perforation is observed. However, it may also be possible that cavitation occurs to the same degree in the bulk solvent overall, but is simply more evenly dispersed, resulting in the appearance of less intensely perforated regions. Furthermore, suppression of the transient cavitation via the incorporation of a baffling structure may improve the coupling between the horns and the water within the baffling, since this could minimise the adsorption of ultrasound by the bulk solvent, thus facilitating the transfer of ultrasonic energy to the solvent bulk (the area of desired cavitation).

In an attempt to further visualise the effect of the baffling on the homogeneity of the ultrasound, a small amount of blue ink was carefully pipetted into a beaker of water so that it formed a separated layer at the bottom of the beaker (due to its higher density). Two experiments were undertaken; firstly the beaker was placed on top of a 'stage' comprising a 3 mm hole diameter perforated sheet and secondly, the beaker was suspended by means of a retort stand within the sonication tank itself. It is worth noting here that in both instances the height of the beaker above the transducer was kept constant. Ultrasound was then applied to both systems. In the system with the baffling, the ink was observed to gradually and evenly disperse throughout the solvent. However, without the baffling in place, the ink was seen to rapidly surge upwards from directly above the transducer and unevenly disperse throughout the water. This suggests that the baffling improves the energy field continuity between each transducer (i.e. the transducers appeared to act as one energy source as opposed to many separate point sources), resulting in a more evenly dispersed energy field. Despite this, Figure 8.4 still shows some evidence of the presence of standing waves in positions B and E, indicating that complete homogeneity has not been achieved.

It should also be remembered in this context that the level of cavitation (which is partly dependant on the tank power and sonication time) required to ablate the aluminium foil, is far greater than that required to ablate the ~40 nm thick polymer that insulates the carbon electrodes. The foil test simply provides an indication as to

the location of the ultrasonic 'hot-spots' within the tank, but of course there may exist 'warm-spots' that are not intense enough to manifest themselves as perforations in the foil, but will be sufficiently energetic to perforate the thin polymer film. It is important therefore, to assess the effect (if present) of such 'warm-spots' or indeed the ultrasonic 'hot-spots' on the performance and reproducibility of the resultant electrode arrays.

8.3 EFFECTS OF ULTRASONIC INTENSITY PROFILE UPON ELECTRODE PERFORMANCES

Following on from the successful and simultaneous polymerisation of multiple sensors (see Chapter 6), a sheet of 100 insulated sensors was sonicated for 20 seconds at 100% power in the top left hand corner of the sonication tank (in position A), since the foil tests showed that there was less evidence of standing waves at this position and the location allowed for easy positioning of the sheets due to the length of the holding clamp used. The electrode sheets consist of five rows (labelled A-E) of 20 sensors (see Figure 8.5).

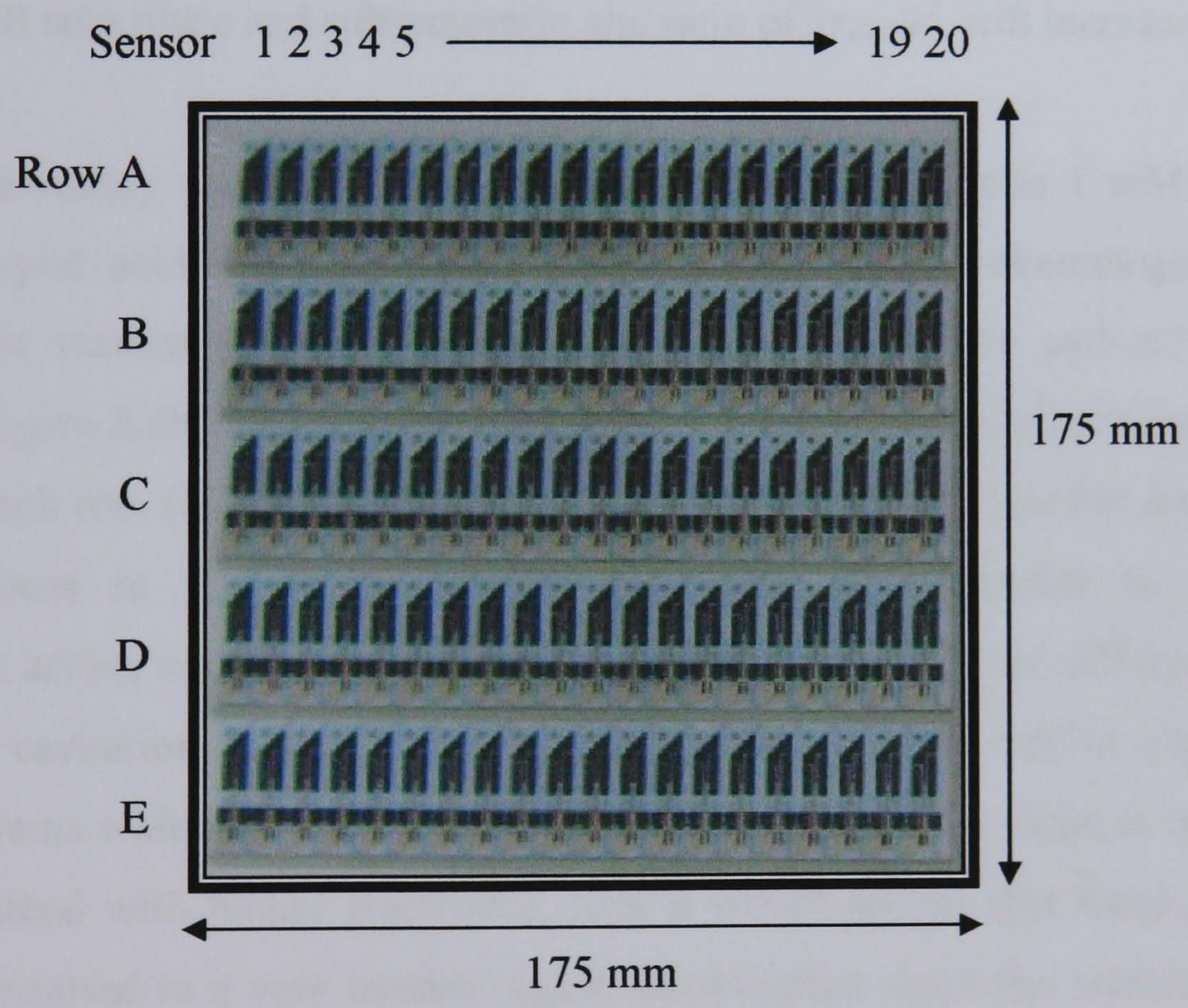

Figure 8.5 A sheet of 100 sensors.

A number of electrodes from each strip were interrogated using cyclic voltammetry in order to establish the consistency of the formation of electrodes exhibiting microelectrode behaviour (i.e. sigmoidal shaped voltammograms). Cyclic voltammetry allows for this analysis since, as was discussed in the previous chapter,

the diffusion profile of an electroactive species towards an array of microelectrodes may follow: a hemispherical profile, when the individual microelectrodes operate independently of each other; a linear profile, when diffusion fields of the individual microelectrodes merge completely; or be mixed in nature, when the individual diffusion layers partially merge. Furthermore, according to microelectrode array theory (Wightman & Wipf, 1989), the size (diameter, $2r_{disc}$) and the distance (d_c) between the centres of adjacent microelectrodes determines the diffusion behaviour of the microelectrode array. The larger the ratio of $2r_{disc}/d_c$, the more diffusion cross-talk between the electrodes occurs, and the more planar electrode characteristics will be shown. Thus, the shape of the voltammograms obtained here may be correlated with the intensity of cavitation at the location of the particular sensor, since the greater the intensity, the more cavitation (and consequently ablation) will take place and subsequently, the ratio of $2r_{disc}/d_c$ will increase.

Cyclic voltammetry was preformed at the sonicated electrodes in 1 mM ferrocene monocarboxylic acid/buffer solutions. Figure 8.6a shows voltammograms from electrodes at various positions *horizontally across* the middle row of the sheet (row C). Figure 8.6b depicts voltammograms corresponding to electrodes from the middle of each row (electrodes 10), i.e. at positions *vertically down* the sheet. There are differences in the electrochemical behaviour of electrodes as one goes horizontally across and down a sheet. Figure 8.6a suggests three different vertical regions of cavitation intensity. Electrodes 1 and 5 both exhibit peak-shaped voltammograms which are nearly identical to each other. This shape is comparable to that obtained with planar electrodes, thus it would appear that these electrodes have been exposed to a very intense region of cavitation since the presence of both anodic and cathodic peaks suggests destruction of the insulating film to a form approaching a planar electrode like surface. The voltammograms corresponding to electrodes 15 and 20 are also very similar to each other, but their shape is more sigmoidal than that of electrodes 1 and 5, with evidence of a near plateau in the cathodic region. It would therefore follow that these electrodes were exposed to a region of less intense cavitation, being sufficient to result in the ablation of some microscopic areas of the film that are sufficient in size and distribution to result

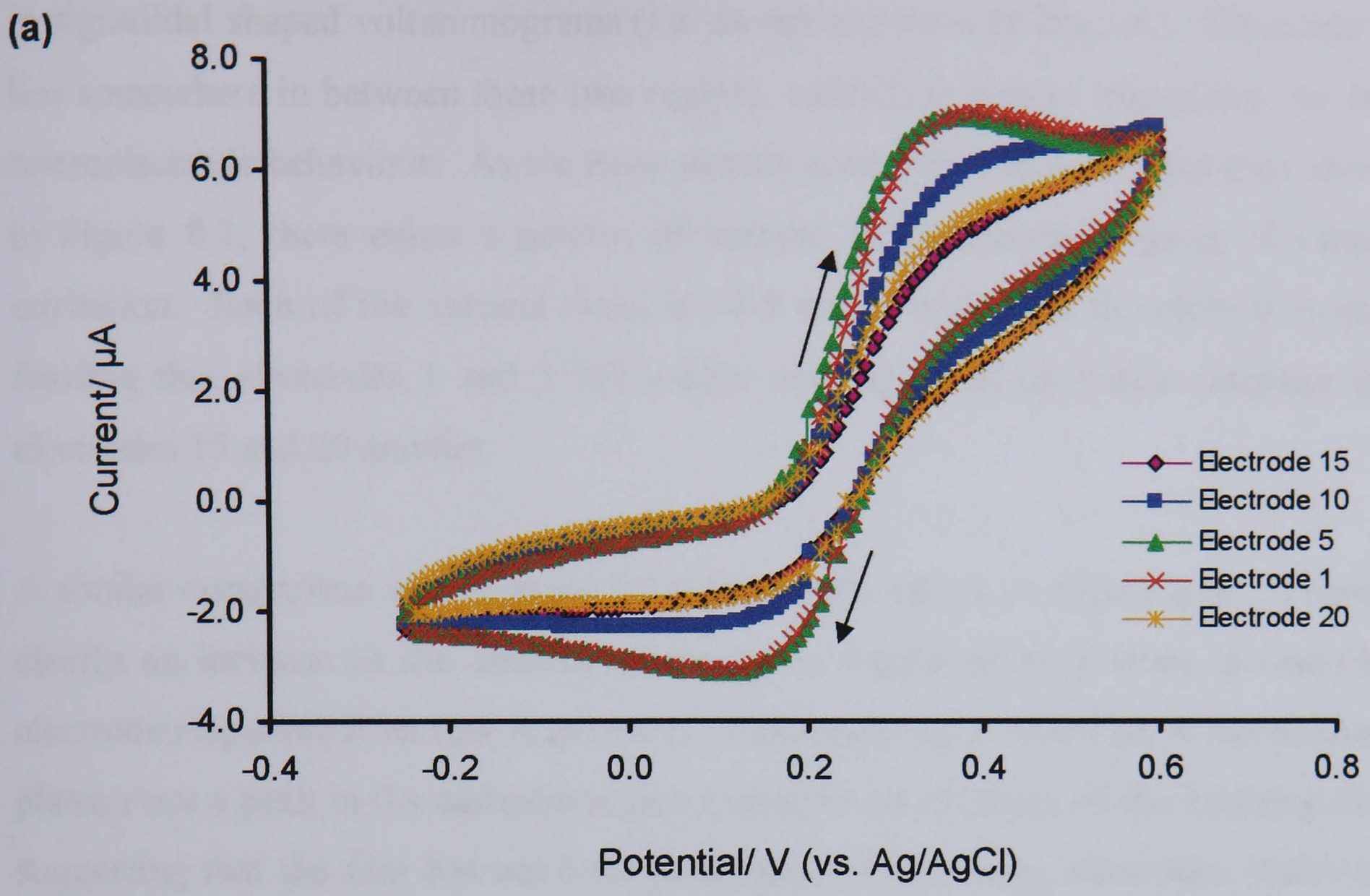

Figure 8.6 Cyclic voltammograms in 1 mM ferrocenemonocarboxylic acid at **(a) electrodes selected from different positions in the same row (row C) and (b) electrodes selected at the same position (electrode 10) from different rows.** [Supporting electrolyte: phosphate buffer (0.1M, pH 7.8). Scan rate: 20 mVs^{-1}].

in sigmoidal shaped voltammograms (i.e. an optimal ratio of $2r_{disc}/d_c$). Electrode 10 lies somewhere in between these two regions, exhibiting neither true planar nor true microelectrode behaviour. As we have already seen from the perforated foils shown in Figure 8.1, there exists a pattern of vertical and horizontal regions of intense cavitation. Each of the vertical areas is ~3-5 cm in width and therefore it is quite feasible that electrodes 1 and 5 fall within one region of cavitation intensity and electrodes 15 and 20 another.

A similar comparison can be made from the results shown in Figure 8.6b. There is clearly an increase in the amount of cavitation (observed as a more 'planar-like' electrode response) from row A to row E. The sensor taken from row A has neither a plateau nor a peak in the cathodic region owing to the presence of the insulting film, suggesting that the film has not been penetrated. Conversely, electrodes positioned on the second row (row B) restored a signal of ferrocene with a quasi-sigmoidal shape. The current is observed to increase further towards the bottom of the sheet, with the shape of the corresponding voltammograms changing step-wise to those of the type exhibiting both anodic and cathodic peaks, owing to the destruction of the film (or at least enough destruction to result in an unfavourable $2r_{disc}/d_c$ ratio). Since the electrode sheets were perpendicularly suspended within the tank with row E of sensors (see Figure 8.5) nearest the surface, it can be said that the cyclic voltammograms shown in Figure 8.6b correlate with the conclusions made from the foil tests from the previous section, in that there appears to be an increase in cavitational events away from the base of the tank.

8.4 IMPROVEMENTS TO THE SONICATION PROTOCOL

The previous sections have shown that the cavitation within the ultrasonic tank is not entirely homogenous and that in fact, there exist standing waves that manifest themselves as variations between the electrochemical responses of the resultant microelectrode arrays. There are two possible solutions to this problem: the first approach could involve methods for increasing the homogeneity of the ultrasound within the tank, or secondly, modifying the sonication protocol to account for the various regions of different cavitation intensity. Since improving the homogeneity of ultrasound within the tank would likely involve expensive tank modifications, the latter approach is described here.

One obvious possibility is to incorporate movement into the sonication protocol. If the sensor sheet is rotated during sonication, each sensor within the sheet should theoretically be exposed to the same intensity of cavitation. Since we have already mapped the cavitation areas within the tank and determined the separation distance between the nodes and anti-nodes, the degree of movement can be calculated so that each sensor moves through the nodes and anti-nodes both vertically and horizontally (this will be explained in more detail later). Furthermore, such a method can be easily incorporated into any tank system that has previously been mapped. However, since the intended movement method of sonication should involve the sensors being exposed to both the intense *and* moderate cavitation regions within the tank, it is likely that the ultrasonic exposure time will have to be decreased to a certain degree. This is further supported by the fact that most of the cyclic voltammograms shown in Figure 8.6 suggest 'over sonication' since they exhibit peaks analogous to those resulting from planar electrodes (due to the destruction of the insulating film).

Thus, the first step to improvement of the sonication protocol is to establish the optimum sonication time and power required to produce arrays exhibiting microelectrode behaviour. Electrodes were consequently sonicated *in a position of high intensity* using combinations of 50, 75 or 100% power with 5 or 10 seconds

duration. The resultant cyclic voltammograms are compared with those obtained at a planar electrode in Figure 8.7a. The voltammograms corresponding to electrodes sonicated for 10 seconds at both 75 and 100% power exhibit quasi-reversible behaviour, suggesting that sonication to this extent is too great for the production of microelectrode arrays.

From the information ascertained from the cyclic voltammograms, there was seen to be very little difference in the voltammetric profiles for sensors sonicated for 5 seconds (at 75% and 100% power) and 10 seconds at 50% power. Therefore, the stir-independence behaviour of the microelectrode arrays previously produced were analysed to further interrogate their microelectrode-like behaviour (Figure 8.7b). Electrodes were polarised at -0.35 V (vs. Ag/AgCl) in a solution of 1 mM hexaammineruthenium(III) chloride, and were subsequently subjected to forced convection after 100 seconds, which was increased further in intensity after 200 seconds. Stirring was terminated after 300 seconds polarisation. Again, arrays prepared via 10 seconds sonication indicate a microelectrode population density reaching a value where the hemispherical diffusion profiles of the individual microelectrodes begin to overlap, consequently leading to a progressive loss of stir-independent response behaviour. However, arrays prepared via 5 seconds sonication do exhibit microelectrode-like behaviour, with electrodes having been sonicated at 75% power reaching complete stir-independence of the sensor response. It can therefore be concluded that 5 seconds sonication at 75% power are optimal conditions for the production of microelectrode arrays in the context of the system described here.

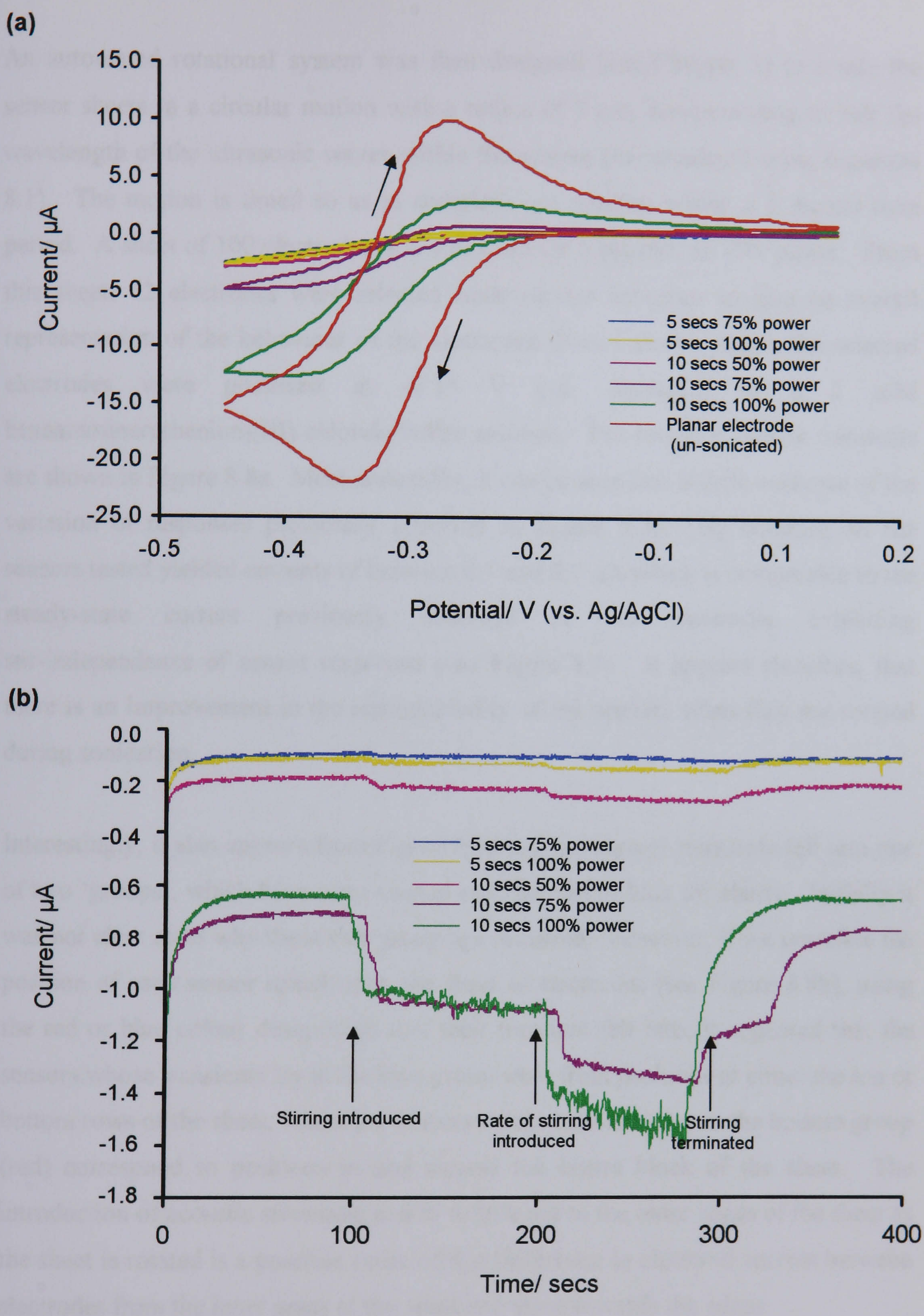

Figure 8.7 (a) Cyclic voltammetry (Scan rate: 50 mVs^{-1}) and (b), current transients, showing the variation in steady-state response with stirring (Polarising potential: -0.35 V (vs. Ag/AgCl), at electrodes sonicated for various time periods and tank power in 1 mM hexaammineruthenium(III) chloride.
[Supporting electrolyte: phosphate buffer (0.1M, pH 7.8)].

An automated rotational system was then designed (see Chapter 3) to rotate the sensor sheets in a circular motion with a radius of 3 cm, corresponding to half the wavelength of the ultrasonic waves within the system (as calculated using Equation 8.1). The motion is timed so as to complete one rotation within a 5 second time period. A sheet of 100 electrodes was sonicated for 5 seconds at 75% power. From this sheet, 12 electrodes were selected from various locations to give an overall representation of the behaviour of the electrodes from a sheet. Again, the selected electrodes were polarised at -0.35 V (vs. Ag/AgCl) in a 1 mM hexaammineruthenium(III) chloride/buffer solution. The resultant current transients are shown in Figure 8.8a. Most noticeably, it can be seen that is little evidence of the variation of responses previously observed in Figure 8.7b. By contrast, all the sensors tested yielded currents of between 0.1 and 0.2 μA which is comparable to the steady-state current previously observed at the electrodes exhibiting stir-independence of sensor responses (see Figure 8.7). It appears therefore, that there is an improvement in the reproducibility of the sensors when they are rotated during sonication.

Interestingly, it also appears from Figure 8.8a that the current transients fall into one of two 'groups', which have been shaded as either red or blue for clarity. Initially it was not clear as to why these two groupings occurred. However, if we correlate the position of each sensor tested upon the sheet of electrodes (see Figure 8.8b), using the red or blue colour designation that their transient fell into, it appeared that the sensors whose transients lay in the blue group were from positions at either the top or bottom rows of the sheet, whilst the sensors whose transients lay in the bottom group (red) correspond to positions in and around the centre block of the sheet. The introduction of acoustic streaming and/or turbulence to the outer edges of the sheet as the sheet is rotated is a possible cause of this difference in observed current between electrodes from the inner areas of the sheet and those towards the edges.

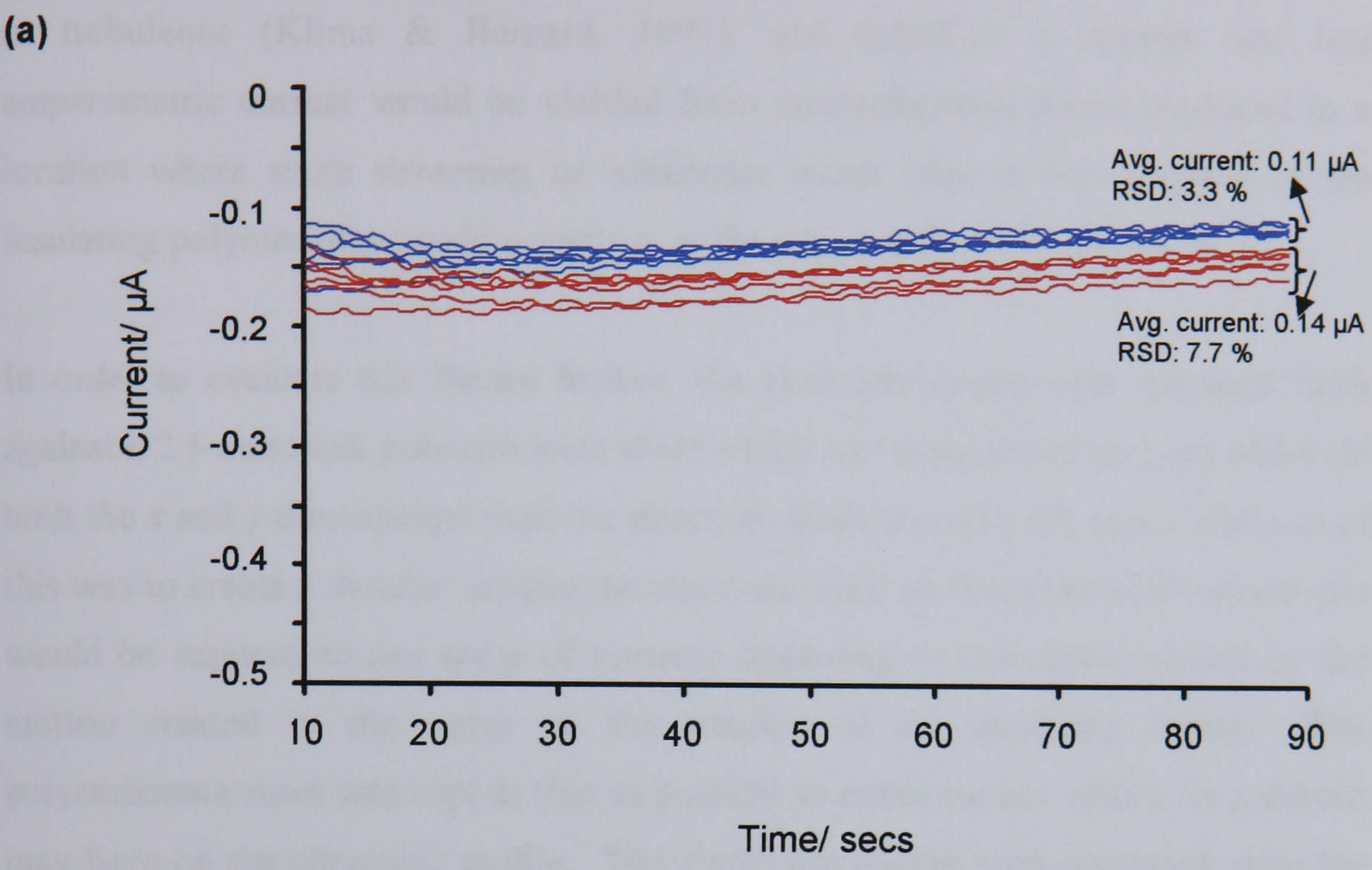

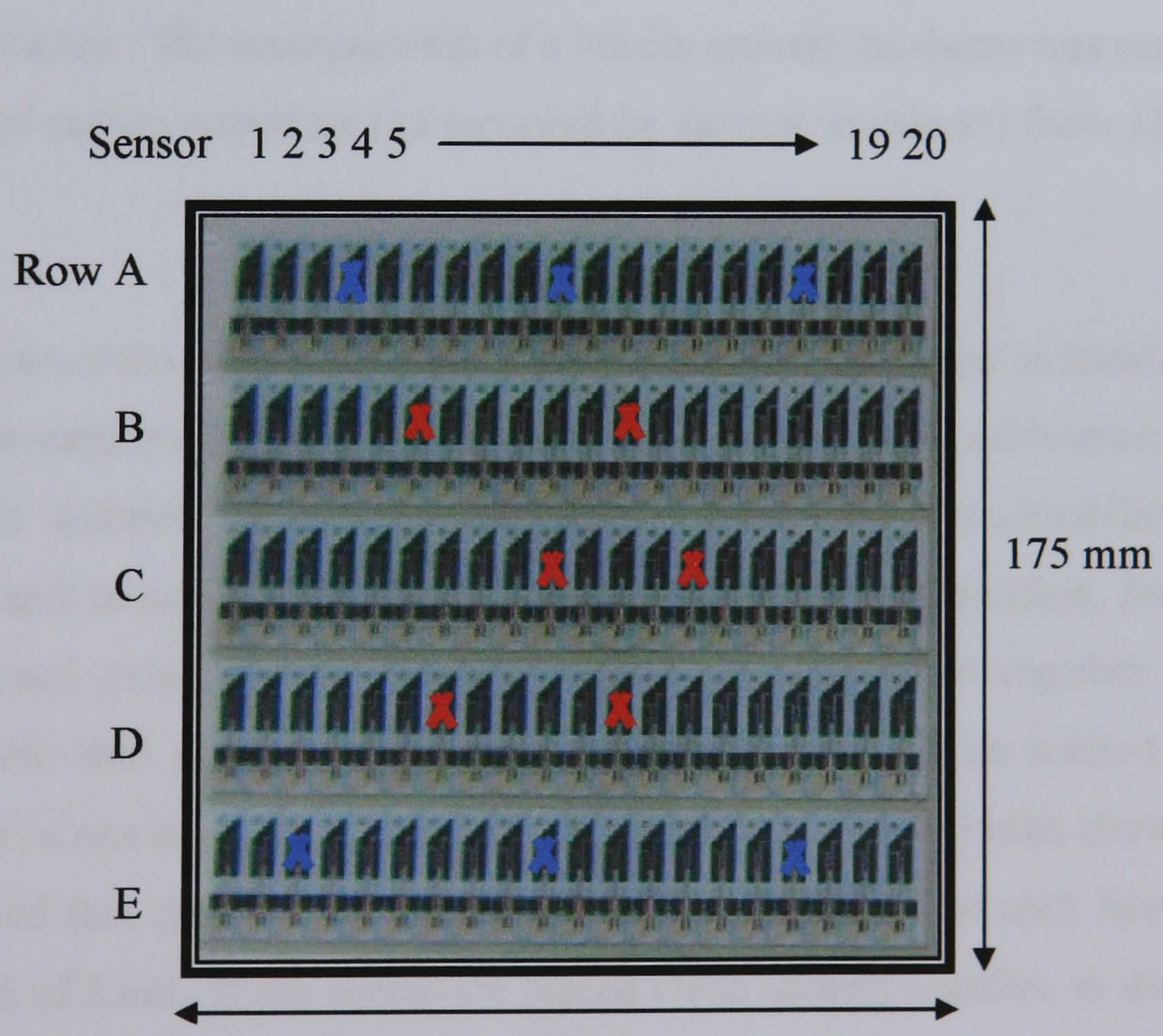

Figure 8.8 (a) Current transients at electrodes sonicated for 5 secs at 75% power using the automated rotation system. (b) Diagram to indicate the position of the electrodes tested in (a) within a sheet, in 1mM hexaammineruthenium(III) chloride.
[Polarising potential: -0.35 V (vs. Ag/AgCl).
Supporting electrolyte: phosphate buffer (0.1M, pH 7.8)].

It is known that transient cavitation does not occur in regions of acoustic streaming or turbulence (Klima & Bernard, 1999), and therefore it confers that less amperometric current would be yielded from microelectrode arrays produced in a location where some streaming or turbulence exists (due to less ablation of the insulating polymer film would occur) i.e. at the edges of the 100 sensor sheets.

In order to evaluate this theory further, the electrode sheets were mounted flush against a 2.5 mm thick polycarbonate sheet which was designed to be 3 cm wider (in both the *x* and *y* dimensions) than the electrode sheet around each edge. The aim of this was to create a 'border' around the electrode sheet so that none of the electrodes would be exposed to any areas of acoustic streaming or turbulence caused by the motion created in the water by the rotation of the electrode sheets. The polycarbonate sheet was kept as thin as possible to minimise any effects its presence may have on the ultrasonic profile. The electrodes having been sonicated using the polycarbonate backing sheet were interrogated amperometrically in the same manner as described previously. The incorporation of a border around the sheets was seen to reduce the RSD of sensor responses (as recorded by current transients) from 13.2% to 4.86%.

The crucial question arriving from this work is whether this behaviour is translated across different concentration ranges and so whether or not a reliable calibration plot is obtainable. In addition, it is important to investigate the reproducibility of electrodes from batch to batch. Therefore, further to the border modification, four of the above mentioned polycarbonate backing sheets were connected together in a design that allowed 400 sensors (4 x sheets of 100 sensors) to be rotated and sonicated together in one batch (see Chapter 3, Figure 3.14). The foil tests shown in Section 8.2 showed that the vertical regions of cavitation within the tank have an approximate width of 5 cm. If the sheets are placed close enough together so that all four of them lie within 5 cm of each other, each sheet should be exposed to similar cavitation intensity since they all lie within the same region. The reproducibility of microelectrode arrays (taken from different batches) produced in this manner is investigated within the next section.

8.5 CHARACTERISATION AND REPRODUCIBILITY OF ELECTRODES

A number of batches of electrodes were produced via sonication for 5 seconds at a power intensity setting of 75% using the system described in the preceding section (each batch comprising four sheets of 100 electrodes). 12 electrodes from each sheet were selected from locations within the sheets that would serve to yield on overall representation of the behaviour of the electrodes. Calibration curves for hexaammineruthenium(III) chloride produced are plotted using both final current value and total charge integration approaches in Figures 8.9a and 8.9b, respectively; error bars are also shown with these plots. A minimal Y axis intercept (i.e. response) at zero concentration coupled with a near linear relationship between both the current or charge and the concentration of the analyte is observed in both cases. It is noticeable that the error bars (and therefore the standard deviation) are lower throughout when the charge integral approach is used. For example, for a concentration of 10 mM hexaammineruthenium(III) chloride (the concentration at which maximum error occurs), the relative standard deviation of results using the final current value approach is 6.8%. However, whilst this shows that good reproducibility can be obtained between batches of multiple sensors, the relative standard deviation of responses for the same concentration using the charge integration produce is only 0.68 %.

It can therefore be concluded that the charge integral method clearly offers a more reliable approach for interrogating the sensors even though it might be expected that double layer charging current might cause spreading of the data at shorter time durations. In addition, the charge integral approach decreases the RSD (over the final current approach) over all the concentration ranges with the exception of zero concentration (i.e. 0 mM), further proving how well this approach works, since this is where the faradaic component has been completely removed. In fact, some more recent designs of measurement instruments for use with blood glucose sensors are using both charge integration and initial current transient slope approaches (Heller *et al.*, 2003).

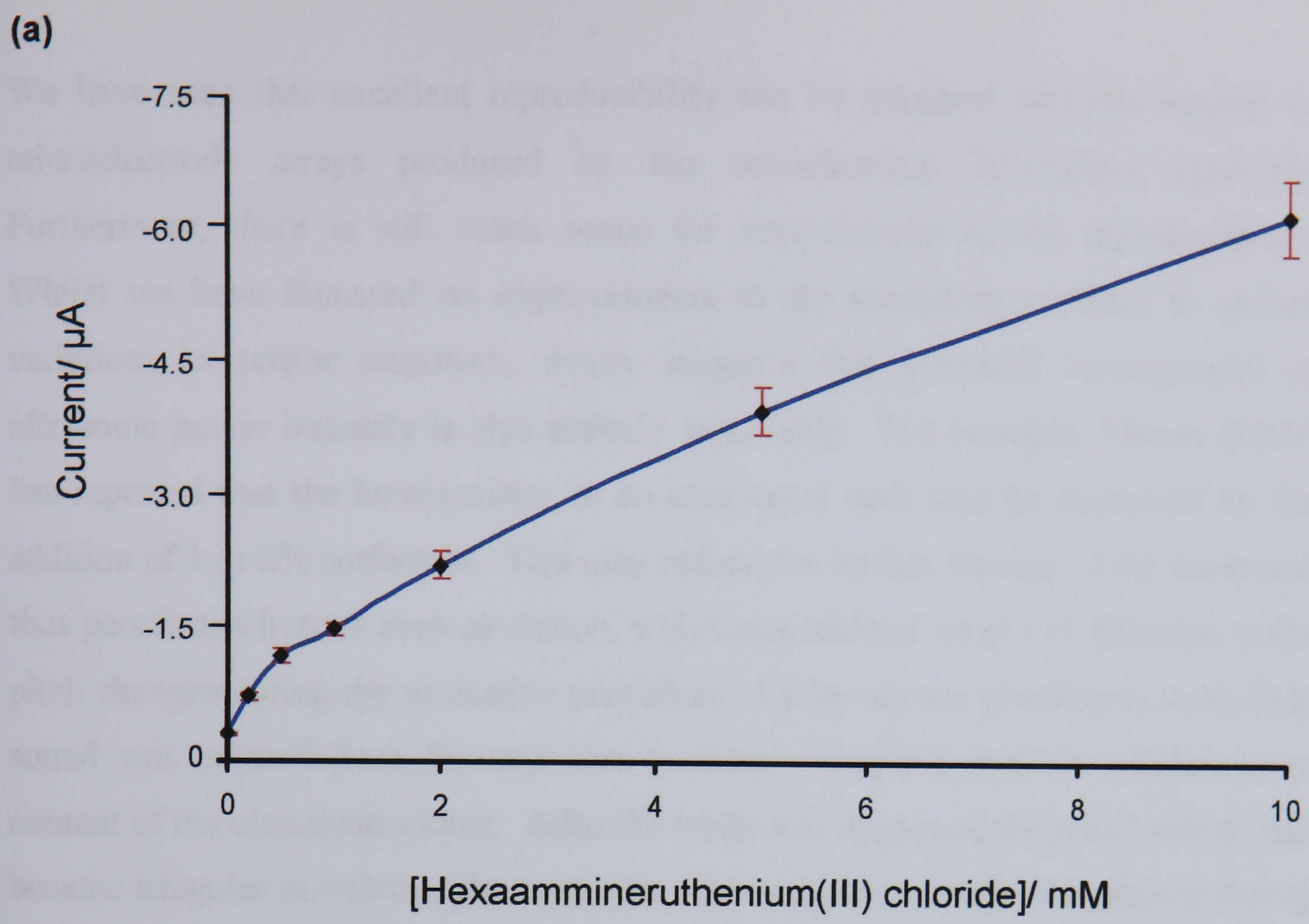

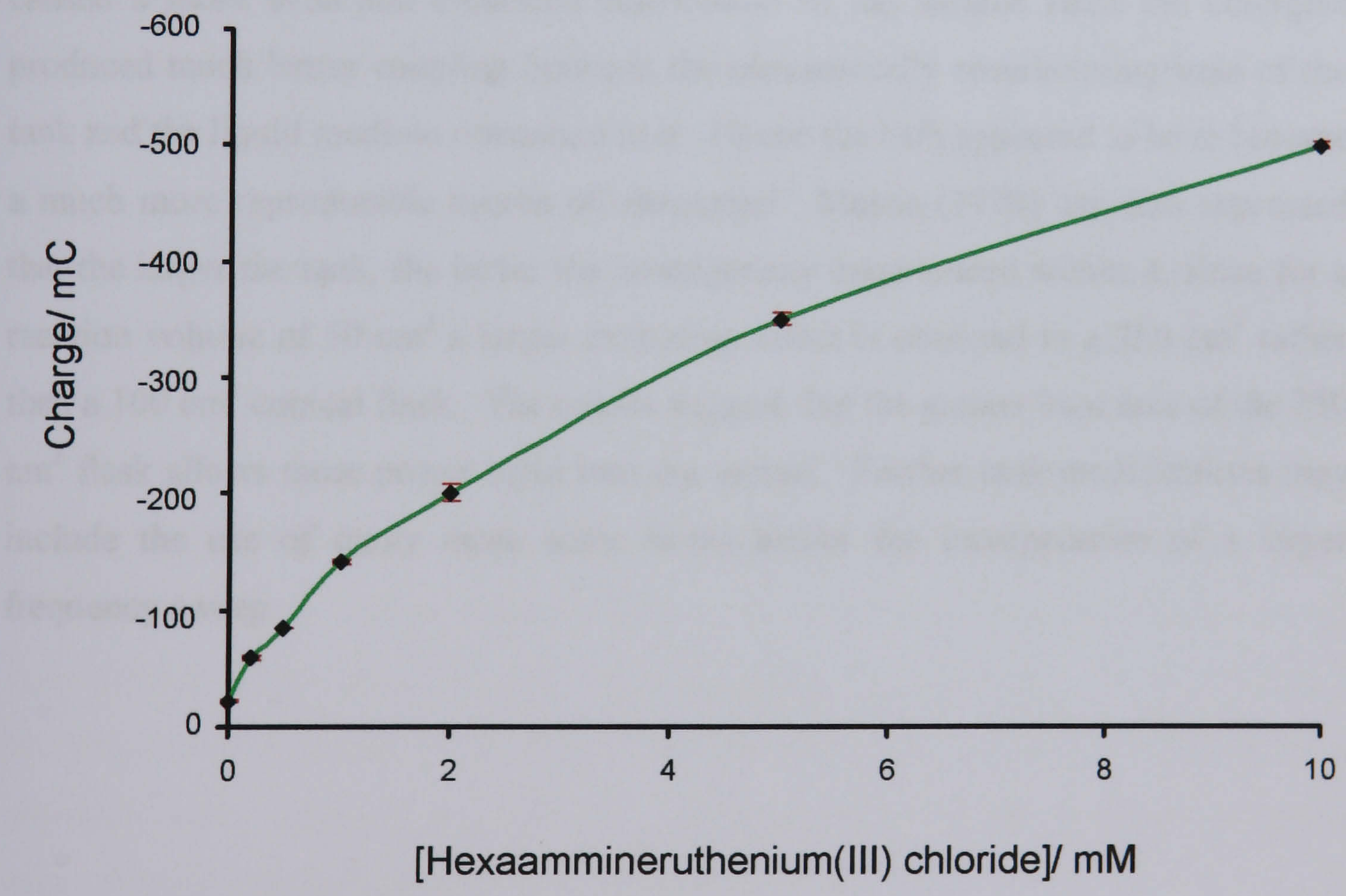

Figure 8.9 **Calibration curves of: (a) current and (b) charge, resulting from the amperometric reduction of hexaammineruthenium(III) chloride at sonochemically fabricated microelectrode arrays.**
[Supporting electrolyte: phosphate buffer (pH 7.8, 0.1M).
Polarising potential: -0.35 V (vs. Ag/AgCl)].

We have seen that excellent reproducibility can be obtained between batches of microelectrode arrays produced by the sonochemical fabrication approach. Furthermore, there is still much scope for improvement of the reproducibility. Whilst we have focussed on improvements to the sonication protocol to reduce variations in sensor responses, theory suggests that increased homogeneity of ultrasonic power intensity is also entirely achievable. For example, Mason (1999) has reported that the homogeneity in an ultrasound tank may be improved by the addition of 1 or 2% surfactant. This may reduce the surface tension of the water and thus permit much more even cavitation, which was realised simply by listening to the pitch changes during the sonication procedure. Under normal conditions, an audible sound was emitted from the tank due to metal vibrations and the sub-harmonic content of the ultrasonic source. After the water was degassed, the sound settled and became irregular in volume (the surface is often subject to erratic disturbance during this period). After the addition of surfactant, the note of the sound changed and caused a more even and enhanced distribution of the surface since the detergent produced much better coupling between the ultrasonically reverberating base of the tank and the liquid medium contained in it. Hence the bath appeared to have become a much more reproducible source of ultrasound. Mason (1999) has also expressed that the larger the tank, the better the homogeneity experienced within it, since for a reaction volume of 50 cm^3 a larger cavitation effect is obtained in a 250 cm^3 rather than a 100 cm^3 conical flask. The results suggest that the greater base area of the 250 cm^3 flask allows more power input into the system. Further tank modifications may include the use of many more sonic horns and/or the incorporation of a larger frequency sweep.

8.6 CONCLUSIONS

This chapter has described investigations made into the ultrasound process in order to optimise sonochemical ablation procedure to facilitate the mass production of carbon microelectrode array based sensors.

Results presented in this chapter have allowed an enhanced understanding of the ultrasound process when applied to large-scale tanks. Initial investigations, using a series of foil-film tests, showed the presence of standing waves in the tank. Findings from various profiling approaches gave evidence of localised regions of enhanced ultrasonic intensity. These regions were calculated to occur at separations equal to the half-wavelength of the ultrasound applied and were observed to increase in intensity away from the emitting surface. By corresponding the locations of the ultrasonic transducers with those of the intense cavitation regions, this behaviour was concluded to be due to tank dimensions and internal reflections.

The incorporation of a stainless steel perforated 'baffling' system to the tank interior appeared to lower the ultrasound intensity within the tank, and imparted a more evenly dispersed energy field, due to an improved energy field continuity between each transducer (i.e. the transducers appeared to act as one energy source as opposed to many separate point sources). A representative series of electrodes selected from a sheet of 100 sonicated simultaneously within the tank were interrogated using cyclic voltammetry. The resultant voltammograms were found to be dependant upon their position within the tank upon sonication and correlated well with the cavitation mapping performed previously. This confirmed that improvements to the sonication protocol were required in order to produce reproducible sensors exhibiting microelectrode array behaviour on a large scale.

The sonication parameters were optimised in terms of power and duration in order to obtain microelectrode arrays that possess sigmoidal voltammetric behaviour and stir-independence of final sensor performance. These parameters were determined

via a combination of cyclic voltammetry and chronoamperometry to be 5 seconds sonication at 75% power.

The sonication protocol was further enhanced via the use of a custom made mechanical system which rotated the electrode sheets during sonication by a distance sufficient to expose each individual electrode to approximately the same intensity of cavitation. A further enhancement was achieved by introducing a border around outer edges of the electrode sheets to avoid variation in electrode responses as a result of exposure to regions of acoustic turbulence and streaming as the sheet is rotated during sonication.

Finally, the reproducibility between batches, and across a range of ruthenium probe concentrations, of electrodes produced according to the enhanced sonication regime was characterised using chronoamperometry using both final current value and charge integral techniques. The charge integral method was seen to offer a more reliable approach for interrogating sensors, decreasing the relative standard deviation over the final current approach across the entire concentration range.

Although there is still much scope for improvement of the homogeneity of ultrasound within large-scale tanks, a relative standard deviation of response of 0.68% was obtained between batches of microelectrode arrays produced using the improvements made to the sonication protocol as a result of the findings of this chapter.

CHAPTER 9

INITIAL EXPLORATION OF TECHNIQUES FOR MODIFICATION LAYER DEPOSITION AND SUBSEQUENT COMPARISON OF MODIFIED SENSORS WITH CONTEMPORARY CHLORINE MEASUREMENT DEVICES

9.1 INTRODUCTION

This chapter examines methods for the deposition of a chemical modifying layer, to allow the immobilisation of the reagents at the sensor surface. The immobilisation of the modifying components of a sensor is critical for its use and would enable the sensors to specifically measure analytes at remote locations so minimising the risk of sample degradation during transport to the laboratory, without the necessity for wet chemical techniques.

Throughout this thesis, the realisation of reproducible and mass fabricated microelectrode arrays using sonochemical ablation techniques has been described. The parallel development of a chemical modifying layer, coupled with deposition technology, is of prime importance to maintain the advantages that microelectrode arrays offer to an end user. This is an area which is often overlooked when considering the commercialisation of such devices and indeed, if a suitable deposition method is not sought, the advantages of this fabrication method and the microelectrode arrays that result may be compromised.

In consequence, surface modification technologies that lend themselves to mass sensor production, such as screen printing (Kulys & D'Costa, 1991) and ink-jet type printing approaches (Kimura *et al.*, 1988) are investigated as methods for reagent deposition. Surface modified sonochemically fabricated microelectrode array based sensors are used as model systems in order to demonstrate the relative advantages and disadvantages of each of these deposition approaches. Important parameters in this context include control of the reagent layer thickness, adhesion of the reagents and the reproducibility of the final sensor. A novel method for packaging the final sensor strips is also described.

Finally, the performance of sonochemically fabricated microelectrode arrays having being modified with a reagent layer are compared with contemporary methods for the measurement of chlorine in Section 9.3. Calibration curves for the sensors in

concentrations of total chlorine are obtained. Responses in both standard chlorine solutions and 'real' samples are compared in terms of precision, accuracy and ease of measurement.

9.2 COMPARISON OF TECHNIQUES FOR THE DEPOSITION OF CHEMICAL MODIFYING LAYERS

Three techniques to apply the reagents are investigated and described in this section;

(i) the deposition of the modifying chemicals in the form of an emulsion by screen-printing,
(ii) the immersion of the electrodes in an aqueous reagent solution (dip-coating) and,
(iii) the deposition of the modifying chemicals in the form of an aqueous solution via an ink-jet printing type procedure.

9.2.1 Screen-printing of low-viscosity emulsions

Screen-printing techniques present a promising route for the deposition of reagents upon mass produced electrochemical sensors, since the process is both highly reproducible and yet relatively inexpensive. As was previously discussed in Chapter 4, screen-printing methods and materials are already highly developed for the manufacture of sensing devices. In addition, screen printing is a simple and rapid process which can be fully automated.

Thus, an emulsion suitable for screen printing was developed in conjunction with Gwent Electronic Materials Ltd. and was screen printed upon sonochemically fabricated microelectrode arrays at Polyflex Circuits Ltd. as described in Chapter 3. The exact formulation of the emulsion is GEM proprietary information, but the formulation basically comprised a solvent coupled with binding and setting agents and of course, the reagents required to measure total chlorine.

Upon visual inspection, the emulsions appeared to be accurately and reproducibly deposited upon the sensing surfaces. However, the fact that the modifying layers were so visible upon the surface was detrimental since this suggested that the ink

layers were too thick. This was confirmed when the electrodes were tested amperometrically in standard solutions of total chlorine in concentrations ranging from 0 to 1 mg/l total chlorine since this represented the lower range of measurement. It was not possible to obtain reliable results with the screen printed electrodes, since responses with significant signal fluctuations were obtained. This made it very difficult to distinguish between differing concentrations of total chlorine under investigation. The 'wet-up' (i.e. the time to reach a steady-state signal) of the electrodes was also observed to be slow and irreproducible, suggesting that the modifying layer is not thin enough to allow for rapid solute diffusion and thus for rapid response times. Therefore, the thickness of the layer was observed to negate the advantageous properties of the microelectrode arrays by making diffusion the rate-limiting step in the analysis. Subsequent modifications to the viscosity of the emulsion proved that it is very difficult to formulate reagent solutions sufficiently thin for reproducible measurements to be made, whilst still retaining the properties of adhesion required for printing. There is also the risk that the screen-printing process may damage the insulating polymer layer, and thus the microelectrode array, if contact is made between the screen-printing squeegee and the surface of the sensor. Resultantly, it was concluded that screen-printing is not a suitable method for the deposition of the non-viscous substances required for use with our sonochemically fabricated microelectrode arrays.

9.2.2 Dip-coating of aqueous buffer solutions

Preliminary experiments for the 'dip-coating' of sensors using aqueous reagent solutions were performed. A pH 4.0 phosphate buffer solution comprising 0.7 M KI and 0.5 M KCl (as calculated to be the optimum amounts required for total chlorine measurement in Chapter 4), was formulated without the addition of any surfactant or binding agent, since we have seen from investigations towards the screen-printing deposition method (Section 9.2.1) that they may compromise the response of the sensors. Prior to immersion, the reference electrodes of the sensor strips were protected using insulating tape, so that the iodide in the reagent solution could not

cause iodisation of the silver/silver chloride reference electrode. The sonochemically fabricated microelectrode arrays were then immersed perpendicularly in the modifying layer solution for ~3 seconds and removed. Following immersion, the electrodes were dried flat in an oven for 10 minutes at 40°C and stored under desiccation until testing.

Visual inspection of the electrodes showed that the reagent solution was not evenly dispersed and resulted in reagent deposits which were not uniform in shape. Altering other parameters such as the time of exposure to solution and the angle that the electrodes were dipped, did not appear to have any significant effect on the appearance of the deposits. Another drawback with this method was that it was not simple to quantify the amount of material being deposited.

For a disposable single-use sensor, reproducibility is vital. The reproducibility of responses for a batch of ten dip-coated electrodes is shown in Table 9.1 (interrogated amperometrically in standard solutions of total chlorine).

Table 9.1 **Reproducibility of ten dip-coated, sonochemically fabricated, microelectrode array based chlorine sensors.**

[Total Chlorine] (mg/l)	Mean Current (nA)	Standard Deviation (nA)
0	2.4	1.0
0.1	5.8	9.6
0.2	11.0	13.9
0.3	20.9	2.6
0.4	29.5	0.7
0.5	42.6	5.2
1.0	76.5	8.4

Electrodes fabricated using dip-coating as a method of reagent application exhibited poor reproducibility over the range of total chlorine concentrations tested, although there was less signal noise than those produced using screen printing. This is not surprising since there was little control over the amount of reagent being deposited upon each electrode. It was, therefore, concluded that the 'dip-coating' deposition was not a suitable method for laying down the chemical modifying layer. However, the 'dip-coating' technique investigations did show that the deposition of aqueous reagents is possible without the addition of any surfactant or adhesives. The more hydrophilic surface of the poly(*o*-phenylenediamine) of the microelectrode arrays, in comparison to the screen-printed carbon substrate, lends itself more readily to surface modification by the deposition of aqueous soluble reagents.

9.2.3 Ink-jet printing of aqueous buffer solutions

An 'ink-jet' type printing system was also evaluated as a method for depositing the aqueous reagent solution used for the 'dip-coating' technique with the aim of obtaining a more reproducible layer. The ink-jet process is most familiar in the form of the office based ink-jet printer. Such machines operate by circulating a solution through a small hole (typically 35-75 μm diameter) in a nozzle under a pressure of about 3 bar (42 psi). Shock waves are sent through the fluid via the drive rod, which is activated by a piezoelectric crystal, and this breaks the jet into individual droplets, under the control of a microprocessor, using the charging electrode. The charged drops are then deflected on passing through two parallel high voltage deflector plates. A pattern is hence built up in a dot-matrix form.

The method offers an interesting route towards the deposition of reagents upon electrochemical sensors, and indeed, an ink-jet type printing deposition process has previously been used by Newman *et al.* (1992:1995) for printing antibodies onto membranes in diagnostic kits. Non-viscous fluids may be easily deposited by the process and, due to the microprocessor control of ink-jet machines, it is extremely simple to change print patterns and volumes of reagent dispensed. It is also a

non-contact process, thus being ideal for deposition of material on non-planar and delicate surfaces. Furthermore, the fluid is deposited as small droplets (typically about 1 nl) which can be placed accurately and at high speed.

Newman *et al.* (1992:1995) used a commercially available ink-jet machine, the Microdoser™, specifically designed by Biodot Ltd. (Huntingdon, Cambridgeshire) for the deposition of labile and valuable materials. A more recent system that is commonly used for the deposition of reagents upon sensing surfaces is the BioDot Inc. AD3200™, which combines a dispense platform with one or more BioJet Plus™ dispensers (Figure 3.15). This machine is a more advanced model of the original ink-jet print type systems, comprising a proprietary dispense technology that combines the high-resolution displacement capabilities of a syringe pump with a high-speed micro solenoid valve. The dispensing system has the syringe pump connected to the backside of the valve, as shown in Chapter 3, Figure 3.15. The dispensing system is hydraulically driven and requires a fluid medium to be present from the syringe to the microsolenoid valve. The dispensing process involves the following steps:

1. the syringe is displaced by a given amount,
2. the valve is opened for a short period of time (milliseconds),
3. fluid is released from the valve and travels to the tip,
4. the fluid increases its linear velocity as it passes through the tip orifice and ejects as a drop (or a stream if the volume of fluid is large). One valve actuation results in one drop.

The key to the BioJet Plus™ system dispensing the proper volume is the steady-state pressure (SSP) in the dispensing system, which is achieved by displacement of fluid by the syringe pump. Thus, the SSP is displacement (drop size) dependant, increasing with increasing drop size. Once the SSP is established, the amount of fluid displaced by the syringe pump will equal the amount dispensed.

For simplicity, the dispensing system can also be modelled as an electrical circuit with the pressure acting as the voltage, the flow rate as the current, the system compliance as capacitative elements, the valve, tip, and feed lines as resistive elements, and the valve as a switch. This model shows the syringe pump as a current source, which provides an advantage over a pressure source (e.g. gas pressure) in that any changes in resistance will not affect the flow rate. In contrast a pressure source will be affected by changes in resistance in the system.

A strip of 20 electrodes was cut from a sheet of sonochemically fabricated microelectrode arrays and placed in a fixed position on the dispense platform as shown in Chapter 3, Figure 3.7. It should be noted here that deposition can be performed upon full-size sensor sheets if required, since larger stage sizes are readily available commercially. Process settings specific to the sensor and solution types were pre-programmed by BioDot Ltd. prior to machine delivery (the dispense positions are programmed as co-ordinates with the drops programmed in terms of drop volume and open time), with care taken so that the dispensing tip and the substrate do not touch, thus avoiding any damage to the surface of the underlying microelectrode arrays. The total chlorine modifying layer solution (as described in Section 3.4.5) was placed in the sample source cylinder and 'primed' through the system in order to initialise the syringes and fill the feed lines, syringes and dispensers before dispensing. The solution was then deposited on each of the working electrodes via the 'line' dispense function according to the following settings: 28 drops of 0.3 mm drop pitch (the distance between each dispense) and 80 nL drop volume (amount of each drop dispensed). There was no need to protect the reference electrode from the dispense solution since the accuracy of deposition is great enough to avoid any 'spill over' to this area. The source solution and all feed supply lines were protected from light to avoid significant iodisation of the present within the modifying layer solution. After deposition, the sensor strip was dried in a still oven at 40 °C for 10 minutes and stored under desiccation until testing (higher drying temperatures visually caused increased coalescence of reagent moieties, as did no forced drying at all). The depositions dried quickly and maintained their shape very well.

Upon drying, the depositions appeared to be very evenly dispersed across the entire electrode surface, contrasting to those resulting from the 'dip-coating' method of deposition. The reproducibility of a batch of ten electrodes produced with the BioDot ink-jet printing technique is shown in Table 9.2:

Table 9.2 Reproducibility of ten BioDot deposited, sonochemically fabricated, microelectrode array based chlorine sensors.

[Total Chlorine] (mg/l)	Mean Current (nA)	Standard Deviation (nA)
0	24	0.7
0.1	27.5	1.2
0.2	33.8	1.3
0.3	41.3	2.7
0.4	63.4	2.2
0.5	77.8	4.9
1.0	134.7	3.8

The results achieved with this method of deposition are seen to be very encouraging. Despite the additional deposition of the modifying layer to the sonochemically fabricated microelectrode arrays, the inter-electrode reproducibility of sensor responses (average RSD = 4.3 %) was comparable to that obtained for the electrodes after fabrication (see Chapter 8).

Whereas all of the electrodes fabricated using dip-coating as the method of reagent application produced small currents and exhibited poor reproducibility (Table 9.1), the BioDot coated electrodes produced significantly higher currents (approximately double), whilst still retaining their microelectrode like behaviour. This is most likely because the amount of reagent upon each electrode is controlled and dispersed evenly across the entire electrode surface, so that all of the analyte upon contact is converted into the correct chemical state required for measurement, before reaching

the electrode surface. Furthermore, the electrodes were found to be more stable than those produced by 'dip-coating', again suggesting a very uniform distribution of reagents. In addition, the results compare very favourably with other techniques that have previously been used for the deposition of reagents upon disposable electrochemical sensors (Hu & Turner, 1991) in terms of response time (in the order of 1 minute).

There are many other advantages to the ink-jet printing process which are particularly significant when considering its use for the mass fabrication of electrodes, such as the economy of the process. Since the reagent solutions are only placed where they are required, there is very little wastage. This may not be the most important consideration in the design of a chlorine sensor (where the reagents are relatively inexpensive), but for many other sensing purposes where the components may be extremely valuable, this could be of prime importance. Furthermore, producing chlorine sensing electrodes via this approach eliminates the need for a separate step to provide protection of the reference electrode during manufacture. This deposition technology has the additional advantage of being able to be adapted to many applications, since it is possible to use a row of multiple ink-jet nozzles, in order to deposit several different reagents in a desired sequence so that multi-analyte or multilayer sensors can be fabricated.

One of the most significant advantages with the use of the BioDot Inc. AD3200™ for the deposition of the reagents required for a total chlorine sensor, is that the whole process may be performed within a glove box operated environmental chamber for humidity control and dust reduction. In addition, a degasser module may also be used. This is important in this context since iodide in the modifying layer solution is readily oxidised and thus should be protected from exposure to air and light until packaged.

During consideration of methods for the protection of the final sensors from environmental exposure, a novel method for the packaging of electrochemical sensors (and indeed many other analytical devices), by means of a heat-sealed

protective film was realised and subsequently patented (Higson, 2004). Traditionally, electrochemical sensors are stored in a foil or plastic package, with sealing of the package being by means of an adhesive seal and/or a lacquer film. However, known disadvantages associated with these methods are both the cost (which may be a significant proportion of the total cost of sensors as a whole, up to 40% of the total cost of some commercially available sensors), and the slow speed at which the manufacturing can proceed. Furthermore, the use of adhesive in the presence of sensors is particularly undesirable for medical purposes since, in general, the sensors require clean and uncontaminated conditions. However, the use of a protective film which is heat-sealed to the substrate so as to be partially or wholly removable by peeling, results in sensors being easy to produce and highly amenable to mass fabrication techniques. In addition, such packaging is of high quality and provides excellent protection for the sensor. As the protective film may be hermetically sealed to the substrate, the integrity of the analyte sensing material can be maintained - for example, the film may protect the sensor from the ingress of moisture from the environment, alternatively moisture may be entrapped by the film so as to maintain the sensor at a defined humidity. The film may also be opaque to protect the analyte detection means from exposure to light.

9.3 COMPARISONS WITH CONTEMPORARY METHODS FOR THE MEASUREMENT OF CHLORINE

In order to compare the responses of electrodes fabricated within this work with those of contemporary methods for the measurement of chlorine in aqueous solutions, a series of sonochemically fabricated microelectrode array sensors, prepared with reagent solution ink-jet printed onto their sensing surface were tested for their response to a range of total chlorine concentrations from 0 through to 10 mg/l. Ten electrodes were polarised for 60 seconds at -0.08 V (vs. Ag/AgCl) at each concentration of total chlorine. Representative calibration graphs are shown in Figure 9.1.

Good response characteristics are obtained with changes in the concentration of total chlorine solution and generally, the sensors are seen to exhibit *quasi*-linearity over concentrations relevant to the target analyte (i.e. both the high and low range chlorine concentrations). The current responses do not decline significantly at higher concentrations of total chlorine (i.e. the curve does not plateau), indicating that both the quantity of reagent deposited and the thickness of the modifying layer does not limit the response of the sensor to chlorine.

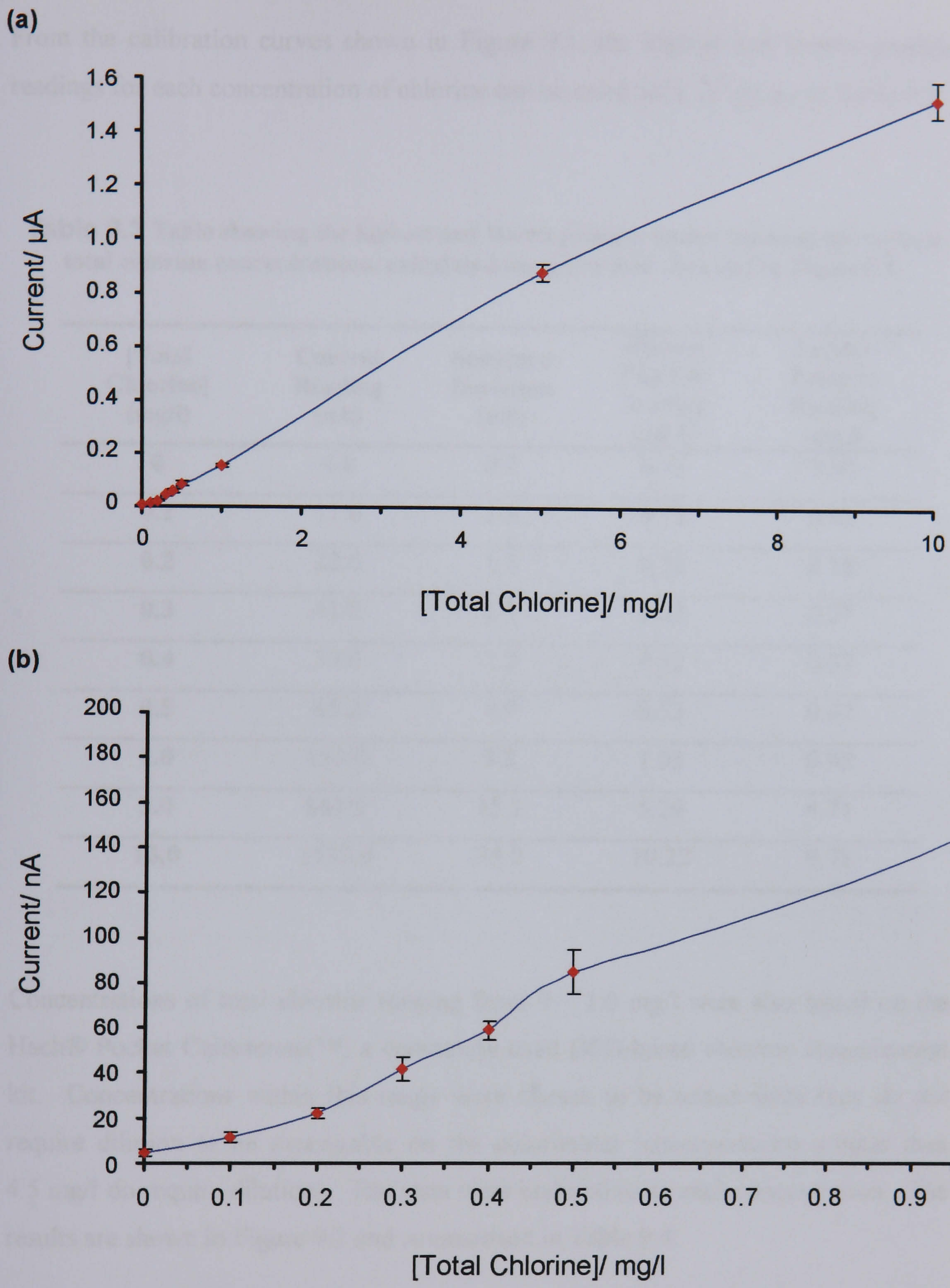

Figure 9.1 Amperometric calibration curves at BioDot coated sonochemically fabricated microelectrode arrays for (a) high-range total chlorine measurement and (b) low-range total chlorine measurement.
[Polarising potential: -0.08 V (vs. Ag/AgCl)].

From the calibration curves shown in Figure 9.1, the highest and lowest possible readings for each concentration of chlorine can be calculated, as shown in Table 9.3:

Table 9.3 Table showing the highest and lowest possible sensor readings for various total chlorine concentrations, calculated using the data obtained in Figure 9.1.

[Total Chlorine] (mg/l)	Current Reading (nA)	Standard Deviation (nA)	Highest Possible Reading (mg/l)	Lowest Possible Reading (mg/l)
0	4.8	0.7	0.01	0.00
0.1	11.6	1.2	0.12	0.08
0.2	22.0	1.3	0.22	0.18
0.3	41.8	2.7	0.33	0.27
0.4	59.0	2.2	0.43	0.37
0.5	85.2	4.9	0.53	0.47
1.0	153.0	3.8	1.05	0.95
5.0	881.2	15.1	5.29	4.71
10.0	1532.0	35.0	10.22	9.78

Concentrations of total chlorine ranging from 0 – 1.0 mg/l were also tested on the Hach® Pocket Colorimeter™, a commonly used DPD-based chlorine measurement kit. Concentrations within this range were chosen to be tested since they do not require dilution to be measurable on the colorimeter (concentrations greater than 4.5 mg/l do require dilution). Ten tests were undertaken at each concentration. The results are shown in Figure 9.2 and summarised in Table 9.4.

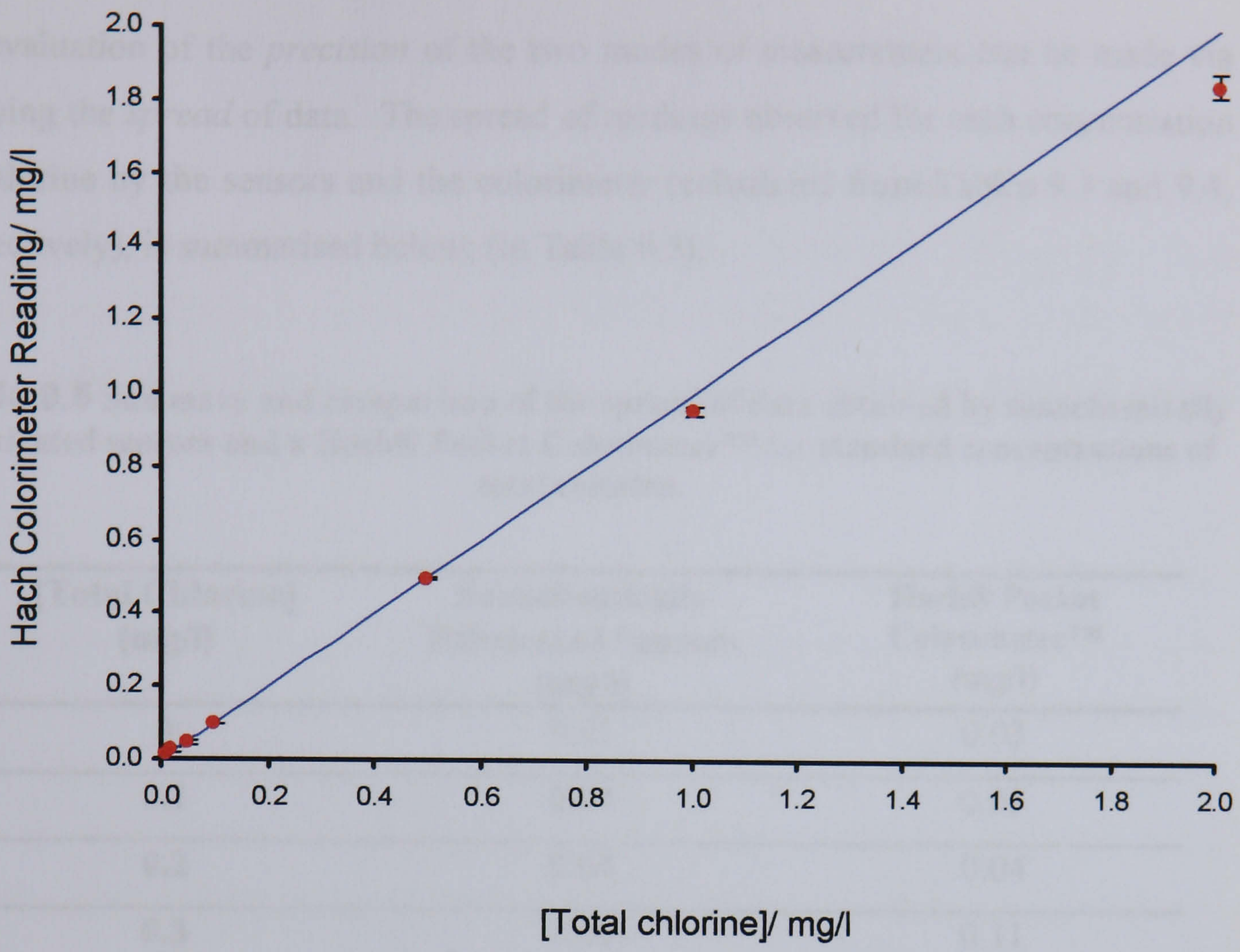

Figure 9.2 Hach® Pocket Colorimeter™ instrument readings of standard chlorine concentrations.

Table 9.4 Table showing the highest and lowest predicted and actual readings for various concentrations of total chlorine using the Hach® Pocket Colorimeter™.

[Total Chlorine] (mg/l)	Mean Reading (mg/l)	Standard Deviation (mg/l)	Highest Predicted Reading* (mg/l)	Lowest Predicted Reading* (mg/l)	Highest Actual Reading (mg/l)	Lowest Actual Reading (mg/l)
0.0	0.02	0.012	0.02	0.00	0.03	0.00
0.1	0.09	0.016	0.12	0.08	0.12	0.07
0.2	0.19	0.016	0.22	0.18	0.21	0.17
0.3	0.35	0.037	0.32	0.28	0.40	0.29
0.4	0.40	0.031	0.42	0.38	0.52	0.42
0.5	0.47	0.037	0.52	0.48	0.52	0.42
1.0	0.97	0.035	1.02	0.98	1.02	0.93

*The highest and lowest predicted reading are predicted by the ±0.02 error stated by Hach.

An evaluation of the *precision* of the two modes of measurement can be made via studying the *spread* of data. The spread of readings observed for each concentration of chlorine by the sensors and the colorimeter (calculated from Tables 9.3 and 9.4, respectively), is summarised below; (in Table 9.5).

Table 9.5 Summary and comparison of the spread of data obtained by sonochemically fabricated sensors and a Hach® Pocket Colorimeter™ for standard concentrations of total chlorine.

[Total Chlorine] (mg/l)	Sonochemically Fabricated Sensors (mg/l)	Hach® Pocket Colorimeter™ (mg/l)
0	0.01	0.03
0.1	0.04	0.05
0.2	0.04	0.04
0.3	0.06	0.11
0.4	0.06	0.10
0.5	0.06	0.10
1.0	0.10	0.09

The sensors are clearly more precise than the colorimeter over this concentration range, exhibiting a smaller spread of data for all concentrations of total chlorine, with the exception of 1.0 mg/l. These results are particularly encouraging since, not only do they suggest that the ink-jet method of depositing reagents is successful, it should also be remembered that the sensors have been fabricated in the laboratory and are thus essentially only prototypes. It should also be noted here that although the accompanying literature to the Hach® Pocket Colorimeter™ quotes a precision of ±0.02 mg/l, from the results shown in Table 9.4, it is can clearly be seen that this is not, in practice, correct. In many cases, the colorimeter gives readings which are either significantly higher or lower.

As a further control, i.e. to prove that the results are not just comparable to contemporary methods due to a factor of the contemporary method being erroneous, an additional DPD-based colorimetric measurement kit, the LaMotte 1200 Colorimeter™, was also interrogated. As both the colorimeters only measure total chlorine concentrations up to 4.5 mg/l (without dilution), a standard solution of 1 mg/l total chlorine was prepared. Ten tests were performed by each method of measurement, the results being presented in Figure 9.3.

As we already know from the results shown in Table 9.5, the Hach® Pocket Colorimeter™ is slightly more precise at this concentration (although it is seen to be *less* precise over all the other concentrations tested), exhibiting a standard deviation of ±0.045 mg/l total chlorine compared with ±0.05 mg/l for the sensors. However, the sensors are more precise than the LaMotte 1200 Colorimeter™ which has a standard deviation of ±0.06 mg/l for 1 mg/l total chlorine. Furthermore, since *known* chlorine standards are used, the *accuracy* of both the sensors and the colourimeters can also be compared (of course, the accuracy can never be determined exactly since we cannot assume that the true value is known with absolute certainty). The sensors can be seen to be more accurate than both the Hach and LaMotte colorimeters, exhibiting a relative error of 1% compared to 2% and 3% for the LaMotte 1200 Colorimeter™ and the Hach® Pocket Colorimeter™, respectively.

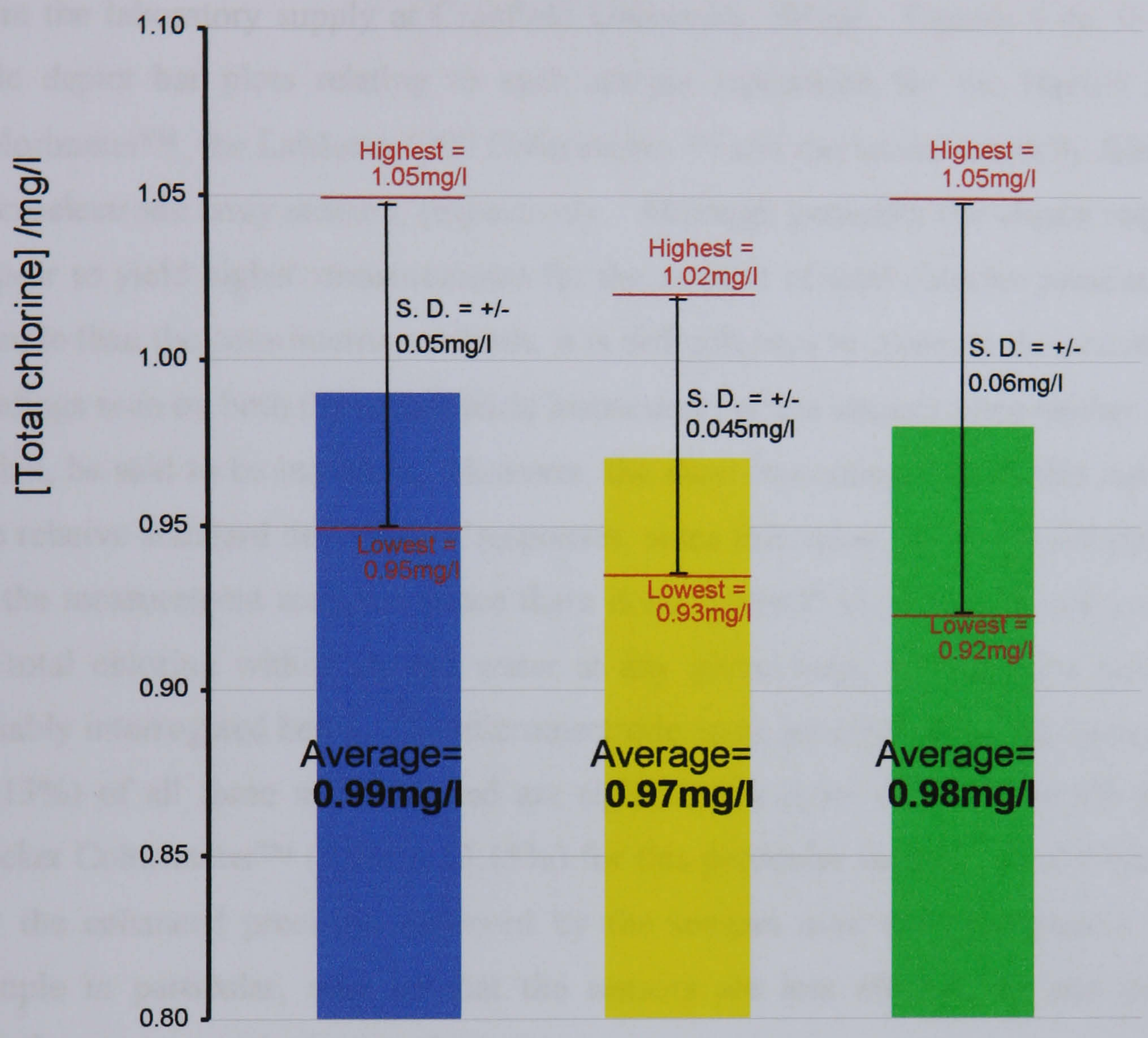

Figure 9.3 **Comparison of the responses of two contemporary methods for the measurement of total chlorine with that of sonochemically fabricated microelectrode array sensors, in a standard solution of 1 mg/l total chlorine.**

The sensors were then evaluated for the determination of total chlorine in a 'real' sample of tap water and compared with the two DPD colorimetric measurement methods. Results were recorded concurrently using the same water sample drawn form the laboratory supply at Cranfield University, Silsoe. Figures 9.4a, 9.4b and 9.4c depict bar plots relating to each sample replication for the Hach® Pocket Colorimeter™, the LaMotte 1200 Colorimeter ™ and the sonochemically fabricated microelectrode array sensors, respectively. Although generally the sensor responses appear to yield higher measurements for the amount of total chlorine present in the sample than the colorimetric methods, it is difficult here to compare the *actual* mean readings seen by both the colorimetric instruments or the sensors since neither can, in effect, be said to be incorrect. However, the most interesting data in this context is the relative standard deviation of responses, since this value represents the precision of the measurement methods (since there is no 'correct' value for the concentration of total chlorine within the tap water at any given time, the accuracy cannot be reliably interrogated here). The microelectrode array sensors exhibit the lowest RSD (3.13%) of all three methods, and are significantly more precise than the Hach® Pocket Colorimeter™ (RSD = 13.15%) for this particular sample. One explanation for the enhanced precision observed by the sensors over the colorimeters in this sample in particular, may be that the sensors are less affected by any possible interferents present in the sample matrix.

In addition to the precision and accuracy, there a many other advantages to using the sensors developed here as opposed to contemporary optical wet chemistry kits. Firstly the time taken to perform a measurement is much less, being in the order of 1 minute as compared to 5 minutes for the Hach® Pocket Colorimeter™, for example. Secondly, it is much simpler to place a sensor into an instrument, add the sample and press 'read' as opposed to the need for accurate measurements of the sample volume, the addition of reagents, mixing of the sample and reagents, and also calibration of the instrument. In addition, the sensor can measure at least 0 to 10 mg/l total chlorine on one electrode, whereas the Hach instrument only permits measurements within the range 0 to 4.5 mg/l total chlorine (higher concentrations require dilution which is both time consuming and prone to error).

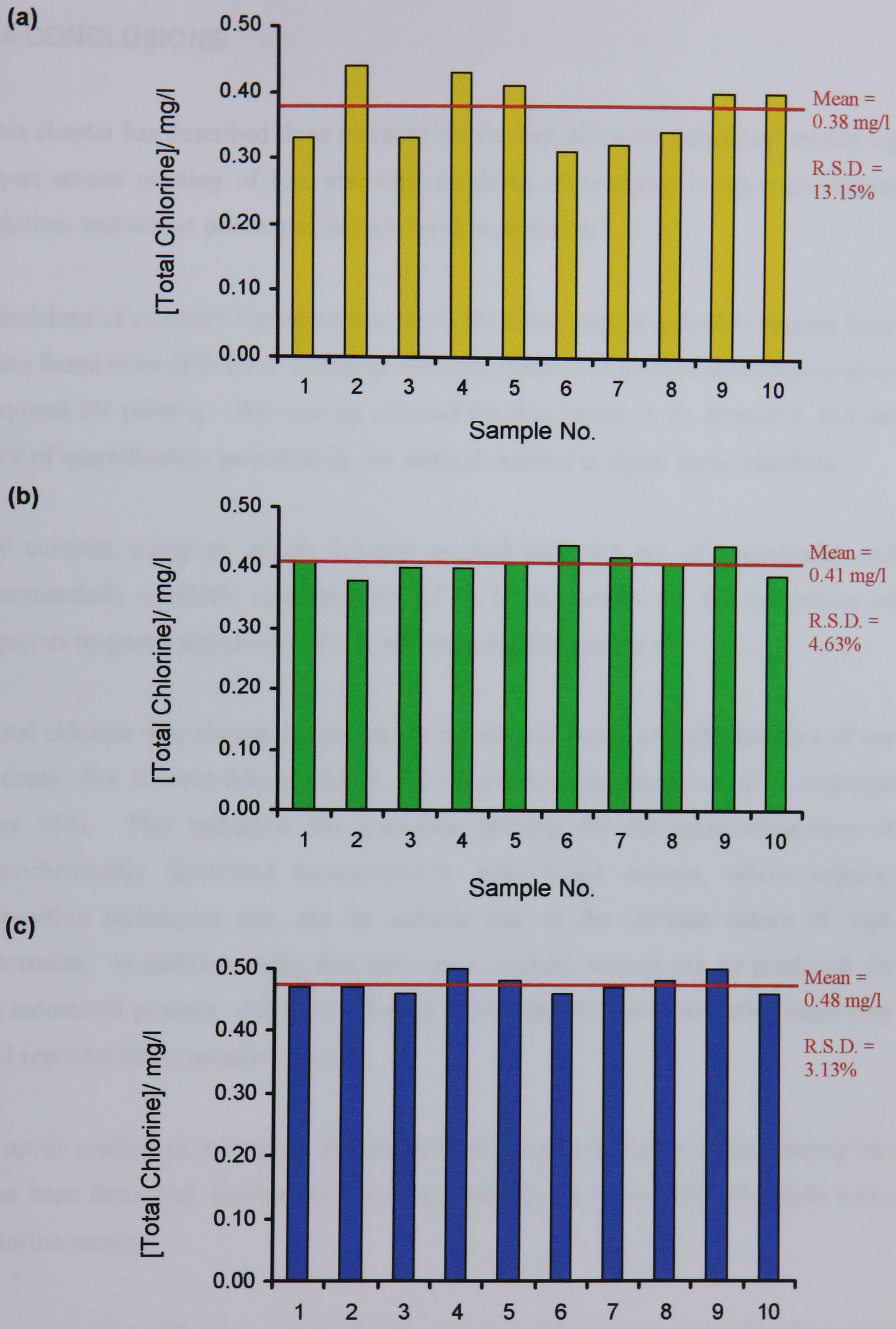

Figure 9.4 **Comparison of the concentration of total chlorine within a sample of tap water determined by (a) Hach® Pocket Colorimeter™, (b) Lamotte 1200 Colorimeter ™ and (c) sonochemically fabricated microelectrode array sensors.**

9.4 CONCLUSIONS

This chapter has described three methods for the deposition of a chemical modifying layer; screen printing of low viscosity emulsion, dip-coating in aqueous reagent solution, and ink-jet printing of aqueous reagent solution.

Emulsions of viscosity low enough to allow for a thin and reproducible reagent layer were found to be difficult to formulate without compromising the adhesion properties required for printing. Dip-coating allowed for thin layers to be deposited, but the lack of quantification permitted by the method resulted in signal irreproducibility.

By contrast, using an ink-jet printing method with the aid of a specialist and commercially available machine, proved to be successful for the deposition of aqueous reagent solutions of defined and reproducible geometry.

Total chlorine was chosen as the analyte for demonstrating the effectiveness of the process. For 10 electrodes produced, the relative standard deviation of the response was <5%. This technique has particular benefits for the mass fabrication of sonochemically fabricated microelectrode array based sensors, where existing deposition techniques may not be suitable due to the intricate nature of such electrodes. In addition, using this fabrication method, sensors can be produced via an automated process, with their inherent advantages of mass production capability and reproducibility remaining intact.

A novel method of packaging electrochemical sensing devices via heat-sealing has also been described, having particular applicability to coated microelectrode array chlorine sensors.

Amperometric calibration curves for the ink-jet printed, sonochemically fabricated microelectrode arrays were produced. The sensors exhibited *quasi*-linearity over the range 0 – 10 mg/l total chlorine and responses showed no significant decrease with increasing concentration, thus indicating that the quantity of the reagents and the

thickness of the reagent layer was sufficient not to restrict the flux of chlorine to the sensing surface.

The spread of data was estimated from the calibration curves and compared with that experimentally obtained by DPD-based colorimetric measurement kits. The sensors were seen to exhibit less spread (and thus greater precision) over the majority of chlorine concentrations tested. Further comparative analyses in known solution standards showed the sensors to exhibit greater accuracy than two contemporary methods for the measurement of total chlorine.

Sensors were also interrogated in terms of their response to tap water samples. The sensors exhibited the lowest RSD (3.13%) of response in this sample matrix when compared with two contemporary methods for the measurement of total chlorine. Furthermore, the sensors demonstrated many other advantages over the colorimetric methods in terms of ease of measurement and time of analysis.

CHAPTER 10

GENERAL CONCLUSIONS

This thesis has described investigations towards the fabrication of microelectrode arrays, utilising novel sonochemical techniques, for application within electrochemical sensors. The applicability of this technique for the mass production of simple-to-use, disposable sensors for the rapid determination of chlorine in aqueous media, has also been demonstrated.

The intermediary aims of the research programme were to optimise each of the fabrication stages involved in the sonochemical fabrication process, namely, screen-printing of carbon electrodes onto a base substrate, electrodeposition of an insulating polymer, sonication of the insulating polymer to expose underlying areas of conductive electrode and finally, the deposition of a chemical modifying layer.

Chapters 4 and 5 focussed upon the use of screen printed carbon electrodes as templates for sonochemically fabricated microelectrode arrays. The behaviour of two commercially available carbon inks (GEM and DuPont) was examined in benchmark redox couples. Both inks exhibited oxidation and reduction peaks to the redox couples, $[Ru(NH_3)_6^{3+/2+}]$ and $[Fc(CO_2)^{3+/2+}]$, but only one peak to $[Fe(CN)_6^{3-/4-}]$. The non-homogenous and therefore non-ideal composition of carbon ink as an electrode surface was confirmed since peak separation values were considerably greater than those expected for a Nernstian diffusion controlled one-electrode transfer reaction.

Chronoamperometric experiments at electrodes screen-printed using both types of carbon inks showed a slower decay in current response (i.e. time to reach steady-state) compared to that seen at gold electrodes, consistent with the presence of surface functional groups at the electrode surfaces and the hydrophobic nature of the inks. Despite this, the steady-state response times were observed to be <1 minute. Electrodes fabricated from the GEM carbon ink exhibited a narrower usable potential window and greater charging current coupled with a larger amperometric current, than those fabricated from DuPont ink. However, the DuPont ink was found to impart a greater reproducibility to sensor responses. These results suggested a higher graphite loading of the GEM ink, as compared to the DuPont ink. This was

confirmed by scanning electron micrographs. The micrographs also revealed that the electrodes printed using GEM ink had a rough and microporous topography compared to the smoother surface of the DuPont ink electrodes, and it was postulated that this contributed to the greater reproducibility observed at the DuPont ink electrodes when interrogated electrochemically. Further confirmation of the presence of an increased amount of binder in the DuPont electrodes was provided by film resistance measurements.

Reduction potentials for total and free chlorine sensing carbon ink electrodes were defined. At these potentials, electrodes showed sensitivity to aqueous chlorine solutions without interference from dissolved oxygen. The optimal concentration of potassium iodide and supporting electrolyte required for accurate and reproducible total chlorine measurements was also established. Amperometric calibration curves demonstrated a near linear response of electrodes to both total and free chlorine solutions in the concentration ranges of interest, with a relative standard deviation for responses of <3 %. Although low currents were observed for the reduction of free chlorine, a sufficiently high reduction current for the determination of total chlorine was obtained at all the concentrations tested.

Carbon ink electrode pre-treatment and modification methods were investigated in an effort to increase the observed current resulting for the amperometric reduction of free chlorine. Sonochemical pre-treatment appeared to deactivate electrodes to two redox solutions tested and did not increase the response to free chlorine. Electrochemical pre-treatment methods also did not result in significant improvement in the electron transfer kinetics of redox bound solutions, despite resulting in an increase in the microparticulate nature and roughness of the carbon electrode surfaces. However, considerable increases in the response to free chlorine were seen with electrodes having pre-anodisation in both saturated sodium carbonate and phosphate buffer solutions, although an accompanying increase in the relative standard deviation of responses was also observed. The most successful means of modification was shown to be the electrodeposition of films of polyaniline upon the electrode surfaces. With these electrodes, current responses to free chlorine were

seen to double in comparison to those observed at bare electrodes, whilst still retaining a response time of <60 seconds and a relative standard deviation of responses of <4 %. It was postulated that this enhanced response was caused by interactions between the PANI film and the chlorine species. The chlorine species was able to permeate through the PANI film to reach the redox active sites within the film, thus allowing electron cross exchange transfer between the analyte species and the redox active sites. Electrodes modified by polyaniline in this way offer many possibilities in the field of electrochemical sensing and may have a profound effect upon the ability of screen printed carbon ink substrates to be used for the electrochemical measurement of free chlorine.

Since Chapters 4 and 5 proved that screen printed electrodes are effective for the measurement of both common redox couples and aqueous chlorine solutions, (and therefore being useful in the development and production of generic sensors for widespread applications), Chapter 6 described the development and optimisation of poly(*o*-phenylenediamine) films upon such electrodes, and their exploitation within sonochemically fabricated microelectrode arrays. Poly(*o*-phenylenediamine) films were deposited on both gold and carbon electrodes. Cyclic voltammograms relating to the electrodeposition of the films revealed the electropolymerisation as being a self-regulating and thus highly reproducible process, since diminishing peak currents were observed as the electrode became progressively insulated by the film. However, although the gold electrodes were completely insulated after 20 potential cycles, carbon electrodes were not insulated until 50 potential cycles had passed, due to the difference in conductivity of these electrodes. Scanning electron micrographs of both a bare gold electrode and an electrode coated with a film of PPD confirmed that its surface is largely featureless and essentially defect free.

Mechanisms relating to both the growth of the PPD films across the electrode surfaces, and the polymerisation of *o*PD itself, have been discussed. Growth of the film was thought to occur via the classical 'gel-point' mechanism. The polymer itself was postulated as being formed via either the polymerisation of the *o*PD di-cation formed on disproportionation, or the monocation radical oxidising at a

conducting film surface rather than the electrode surface, yielding a different product, the insulating film.

PPD films were also deposited upon sheets of 100 carbon electrodes. Cyclic voltammograms relating to the simultaneous electropolymerisation of carbon electrodes correlated well with those observed for the electropolymerisation on individual electrodes. The deposited films were calculated as having a thickness of approximately 40 nm. The surface topography of the film was also investigated using AFM. Although it was impossible to distinguish between the bare and PPD coated electrodes, the presence of an insulating film was confirmed by the need to earth the PPD coated carbon samples. Amperometric interrogation of the films using both ruthenium and chlorine probes showed negligible responses which did not vary upon the introduction of convection to the test solutions.

Chapters 7 and 8 described the formation of microelectrode arrays via the sonochemical ablation of the insulating PPD films as previously described in Chapter 6. Imaging of the sonochemically fabricated microelectrode arrays suggested a random distribution of pores with a bi-modal size distribution. This distribution provided an optimal centre-to-centre spacing between pores to allow radial diffusion at the individual microelectrodes, yielding arrays that exhibited a good balance between typical microelectrode characteristics such as sigmoidal shape and scan rate independent cyclic voltammograms, rapid steady-state responses in chronoamperometric experiments, low stir-dependence of less than 10 % change in base current even at the very highest flow rates, and enhanced sensitivity.

The ultrasound process was investigated further in order to optimise the sonochemical ablation procedure to facilitate the mass production of carbon microelectrode array based sensors. Initial investigations using a series of foil tests showed the presence of standing waves in the ultrasonic tank. The standing waves were calculated to occur at separations equal to the half-wavelength of the ultrasound applied and were observed to increase in intensity away from the emitting surface. It

was concluded that this behaviour was due to tank dimensions and internal reflection effects.

A stainless steel 'baffling' system incorporated into the tank interior appeared to lower the ultrasound intensity within the tank, and imparted a more evenly dispersed energy field, due to an improved energy field continuity between each transducer (i.e. the transducers appeared to act as one energy source as opposed to many separate point sources).

The responses of sensors having been sonochemically fabricated within the tank were found to be dependant upon their position within the tank and corresponded with the cavitation mapping established by the foil tests. This confirmed that improvements to the sonication protocol were required in order to produce reproducible sensors exhibiting microelectrode array behaviour on a large scale. Therefore, the sonication parameters were optimised. The optimal power and duration required to obtain sigmoidal shaped voltammograms and stir-independence of responses was determined to be 5 seconds at 75 % power (for the system studied). The use of a mechanical system which rotated the electrode sheets during sonication by a distance sufficient to expose each individual electrode to approximately the same intensity of cavitation, in addition to the introduction of a border around the outer edges of the sheets, resulted in a decrease in the variation of responses of electrodes. Consequently, even though, as discussed, there is still much scope for improvement of the homogeneity of ultrasound within large-scale tanks, a relative standard deviation of coulometric responses of 0.68 % was obtained between batches of microelectrode arrays produced.

Chapter 9 described the final stage involved in the sonochemical production of disposable microelectrode array based sensors, namely the deposition of a chemical modifying layer. It was found that emulsions of sufficiently low viscosity to allow for the printing of thin and reproducible reagent layers were difficult to formulate without comprising the adhesion properties required for printing. Dip-coating allowed for thin layers to be deposited, but the lack control of quantification

permitted by the method resulted in irreproducibility on the final sensor responses. However, an ink-jet type printing technique proved very successful for the deposition of aqueous reagent solutions, resulting in depositions of defined and reproducible geometry, having a relative standard deviation of responses of <5 %. This technique has particular benefits for the mass fabrication of microelectrode arrays, since existing deposition techniques may not be suitable due to the intricate nature of such electrodes. Furthermore, using an 'ink-jet' type printing method, sensors can be produced via an automated process, with their adherent advantages of mass production capability and reproducibility remaining intact.

The completed sensors exhibited *quasi*-linearity over a total chlorine concentration range of 0 – 10 mg/l, with no suggestion of the curve plateauing with increasing concentration, thus suggesting that the quantity of the reagents and the thickness of the reagent layer was sufficient not to restrict the flux of chlorine to the sensing surface. Data obtained from the calibration curves was compared with that obtained experimentally from DPD-based colourimetric measurement kits. The sonochemically fabricated sensors exhibited a greater precision over the majority of chlorine concentrations tested. The sensors also exhibited a greater accuracy than two contemporary methods for the measurement of total chlorine. A greater precision was also demonstrated by the sensors as compared to the contemporary measurement methods when interrogated in tap water samples. Furthermore, the sensors demonstrated many other advantages over the colourimetric methods in terms of ease of measurement and time of analysis. A novel method for packaging of the complete sensors via heat-sealing was also described in the context of this work.

The results presented within this thesis, combined with the simplicity and inexpensiveness of the sonochemical approach to microelectrode array fabrication suggests that such sensors offer widespread applicability in the field of electrochemical sensors.

CHAPTER 11

SUGGESTIONS FOR FURTHER WORK

This thesis has described the development of generically applicable and disposable electrochemical sensors via exploitation of a sonochemical approach to microelectrode array fabrication. Although this work has gone far towards answering questions regarding whether this method may be rendered suitable for mass fabrication, as with many projects, by answering these questions, many more have arisen which must be fulfilled to fully demonstrate the potential of the process. This chapter therefore provides a number of suggestions for future research.

Whilst this thesis has demonstrated that is it possible to sonochemically fabricate 400 sensors within one production batch to within <4% RSD using a laboratory constructed rotation system, it is recognised that further modifications towards the homogeneity of the ultrasound process (for example, the addition of surfactant to the solvent or the incorporation of a frequency sweep), and the use of an industrially constructed automation device, may be explored as further avenues towards the minimisation of this value. Furthermore, a larger tank design should be explored to facilitate studies of the sonication of full 600 electrode sheets.

Both screen and ink-jet printing were investigated as methods to deposit buffering salts upon the working electrode surfaces. Approaches to negate the need for this fabrication step could be explored. For example, we have demonstrated within this study that conducting polyaniline films may enhance amperometric current responses when electrochemically deposited at planar carbon electrodes. Since previous work performed within this research group has also shown that is it possible to electrochemically grow enzyme containing protrusions at each microelectrode within an array (Myler, 2000), it may be viable to grow iodide containing protrusions at the sonochemically fabricated arrays. The protrusions may serve not only to modify the electrodes to the desired pH for measurement, but also to enhance the current responses at the electrodes to certain analytes.

During the undertaking of this thesis, a novel and patented (Higson, 2004) method for the packaging and protection of disposable sensors was realised. Further studies could be undertaken to establish the commercial potential of this technology. For

example, electrode longevity studies may determine the success of such packaging in terms their protection of the electrode to ultra-violet light, humidity and temperature changes, along with prevention of physical damage.

With a view to commercialisation of such sensors, a collaboration was established with an instrument manufacturing company. A prototype sensor instrument was constructed and is shown in Figure 11.1.

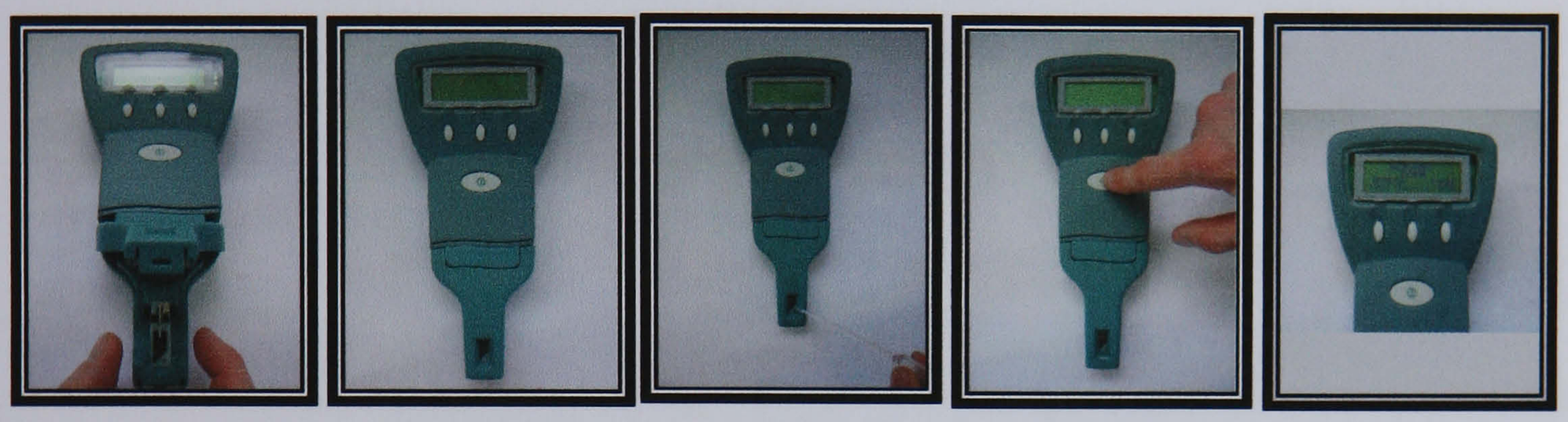

Figure 11.1 Prototype of the chlorine sensing instrument.

The instrument requires to be fully calibrated and interrogated both analytically and via customer beta testing.

We have within this study demonstrated the use of sonochemically fabricated microelectrodes as sensors for the measurement of chlorine in aqueous solutions. The fabrication method could be further employed to produce, for example, sensors for other analytes of environmental importance.

REFERENCES

Abramov, O. V. (1998). *High Intensity Ultrasound: Theory and Industrial Applications*, London: Gordon & Breach.

Adams, R. N. (1976). Probing brain chemistry with electroanalytical techniques. *Anal Chem* **48**, A1126-A1138.

Albareda-Silvert, M., Merkoci, A. & Alegret, S. (2000). Configurations used in the design of screen printed enzymatic biosensors. A review. *Sens Actuat* **69,** 153-163.

Alvarez-Icaza, M. & Bilitewski, U. (1993). Mass production of biosensors. *Anal Chem* **65**, A525-A533.

Amatore, C., Savéant, J. M. & Tessier, D. (1983). Charge transfer at partially blocked surfaces: A model for the case of microscopic active and inactive sites. *J Electroanal Chem* **147**, 39-51.

Anson, F. C. & Schultz, T. A. (1963). Effect of adsorption and electrode oxidation on the oxidation of oxalic acid at platinum electrodes. *Anal Chem* **35**, 1114-1116.

Aoki, K. (1993). Theory of ultramicroelectrodes. *Electroanalysis* **5**, 627-639.

Aoki, K., Morita, M., Niwa, O. & Tabei, H. (1988). Quantitative-analysis of reversible diffusion-controlled currents of redox soluble species at interdigitated array electrodes under steady-state conditions. *J Electroanal Chem* **256**, 269-282.

Aoki, K. & Osteryoung, J. (1981). Diffusion-controlled current at the stationary finite disk electrode. *J Electroanal Chem* **122**, 19-35.

APHA, AWWA & WEF (1992). *Standard Methods for the Examination of Water and Wastewater*, 18th edn. Washington DC: American Public Health Association.

Bard, A. J., Abruna, H. D., Chidsey, C. E., Faulkner, L. R., Feldburg, S., Itaya, K., Majda, M., Melroy, O., Murray, R. W., Porter, M. D., Sorlaya, M. P. & White, H. S. (1993). The electrode-electrolyte interface – A status report. *J Phys Chem* **97**, 7147-7173.

Bard, A. J. & Faulkner, L. R. (2001). *Electrochemical Methods: Fundamentals and Applications*, 2nd edn. New York: John Wiley & Sons.

Barisci, J. N., Stella, R., Spinks, G. M. & Wallace, G. G. (2000). Characterisation of the topography and surface potential of electrodeposited conducting polymer films using atomic force and electric force microscopies. *Electrochim Acta* **46**, 519-531.

Bellar, T. A., Lichenburg, J. J. & Kromer, R. C. (1974). The occurrence of organohalides in chlorinated drinking water. *J Am Water Works Assoc* **66**, 703-706.

Beriet, C., Ferrigno, R., Girault, H. H. (2000). Simulation of the chronoamperometric response of a regular array of micro-disc electrodes. *J Electroanal Chem* **486**, 56-64.

Bilger, R. & Heinze, J. (1993). Role of the formation potential on the redox processes of polypyrrole studied by an electrochemical quartz microbalance. *Synth Met* **55**, 1424-1429.

Bilitewski, U. & Turner, A. P. F. (2000). *Biosensors for Environmental Monitoring,* Amsterdam: Harwood Academic Publishers.

Binnie, C., Kimber, M. & Smethurst, G. (2002). *Basic Water Treatment*, 3rd edn. London: Thomas Telford Ltd.

Binning, G., Quate, C. F. & Gerber, C. H. (1986). Atomic force microscopy. *Phys Rev Lett* **56**, 930-933.

Bjelica, L., Parsons, R. & Reeves, R. M. (1980). Electrochemical studies on different glassy carbon electrodes II. Corrosion and double layer characteristics. *Croat Chem Acta* **53,** 211-231.

Blaedel, W. J. & Mabbot, G. A. (1978). A pyrolytic carbon film electrode. *Anal Chem* **50,** 933-936.

Bodalbhai, L. & Brajter-Toth, A. (1988). Different methods of graphite electrode treatment and their effect on the electrochemical behaviour of a small adsorbing biological molecule, 2,6-Diamino-8-purinol. *Anal Chem* **60**, 2557-2561.

Boswell, J. (2001). *Investigations into Discrepancies between Environment Agency Wales and DCWW in Measuring Free Chlorine in the Field.* (Unpublished).

Bowers, M. L. & Yenser, B. A. (1991). Electrochemical behaviour of glassy carbon electrodes modified by electrochemical oxidation. *Anal Chim Acta* **243,** 43-53.

Brainina, K. Z. & Bond, A. M. (1995). Characterization of thick-layer graphite disposable voltammetric electrodes. *Anal Chem* **67,** 2586-2591.

Brett, C. M. A. & Brett, A. M. C. F. O. (1986). Hydrodynamic Electrodes. In *Comprehensive Chemical Kinetics,* pp355-441, Amsterdam: Elsevier.

Brett, C. M. A. & Brett, A. M. O. (1998). *Electroanalysis*, Oxford: Oxford University Press.

Brungs, W. A. (1973). Effects of residual chlorine on aquatic life. *J Water Poll Control Fed* **45**, 2180-2193.

Bull, R. A., Fan, F. R. & Bard, A. J. (1983). Polymer films on electrodes: Incorporation of catalysts into electronically conductive polymers: Iron phthalocyanine in polypyrrole. *J Electrochem Soc* **130**, 1636-1638.

Butler, J. A. V. (1924). Studies in heterogenous equilibria part iii: a kinetic theory of reversible oxidation potentials at inert electrodes. *Trans Faraday Soc* **19**, 734-739.

Caliguri, E. J. & Mefford, I. N. (1984). Femtogram detection limits for biogenic amines using microbore HPLC with electrochemical detection. *Brain Res* **296**, 156-159.

Canadian Council of Ministers of the Environment (1999). Canadian Water Quality Guidelines for the Protection of Aquatic Life. In *Canadian Environmental Quality Guidelines, No. 1299*, Winnipeg.

Cass, A. E. G., Davis, G., Francis, D. G., Hill, H. A. O., Aston, W. J., Higgins, I. J., Plotkin, E. V., Scott, L. D. L. & Turner, A. P. F. (1984). Ferrocene-mediated enzyme electrode for amperometric determination of glucose. *Anal Chem* **56**, 667-671.

Cassidy, J., Ghoroghchain, J., Safarazi, F., Smith, J. J. & Pons, S. (1986). Simulation of edge effects in electroanalytical experiments by orthogonal collocation – VI Cyclic voltammetry at ultramicroelectrode ensembles. *Electrochimica Acta* **31**, 629-636.

Cattrall, R. W. (1997). *Chemical Sensors*, Oxford: Oxford University Press.

Caudill, W. L., Howell, J. O. & Wightman, R. M. (1982). Flow rate independent amperometric cell. *Anal Chem* **54**, 2532-2535.

Centonze, D., Malitesta, C., Palmisano, F. & Zambonin, P. G. (1994). Permeation of solutes through an electropolymerised ultrathin poly-*o*-phenylenediamine film used as an enzyme-entrapping membrane. *Electroanalysis* **6**, 423-429.

Chapman, D. L. (1913). A contribution to the theory of electrocapillarity. *Phil Mag* **25**, 475-481.

Cheek, G., Wales, C. P. & Nowak, R. J. (1983). pH response of platinum and vitreous carbon electrodes modified by electropolymerised films. *Anal Chem* **55**, 380-381.

Chi-Sing Tse, D. & Kuwana, T. (1978). Electrocatalysis of dihydronicotinamide adenosine diphosphate with quinines and modified quinine electrodes. *Anal Chem* **50**, 1315-1318.

Chiang, J. C. & MacDiarmid, A. G. (1986). Polyaniline- Protonic acid doping of the emeraldine form to the metallic regime. *Synth Met* **13**, 193-205.

Chiba, K., Ohsaka, T., Ohnuki, Y. & Oyama, N. (1987a). Electrochemical preparation of a ladder polymer containing phenzine rings. *J Electroanal Chem* **219**, 117-124.

Chiba, K., Ohsaka, T. & Oyama, N. (1987b). Electrode kinetics of electroactive electropolymerised polymers deposited on graphite electrode surfaces. *J Electroanal Chem* **217**, 239-251.

Clark, L. C. (1970). Membrane polarographic electrode system and method with electrochemical compensation. US Pat. No. 3539455.

Clark, L. C. (1956). Monitor and control of blood and tissue oxygen tensions. *Trans Am Soc Artif Intern Organs* **2**, 41-51.

Clark, L. C. & Lyons, C. (1962). Electrode systems for continuous monitoring in cardiovascular surgery. *Ann NY Acad Sci* **102**, 29-45.

Coury, L. A. & Heineman, W. R. (1988). Electrochemical examination of unusual properties of spectroscopic graphite-electrodes. *J Electroanal Chem* **256**, 327-341.

Cox, B. G. (1994). *Modern Liquid Phase Kinetics*, Oxford: Oxford University Press.

Crum, L. A. (1982). Acoustic cavitation. *Ultrason Symp* **1**, 1-11.

Cui, G., Yoo, J. H., Lee, J. S., Yoo, J., Uhm, J. H., Cha, G. S. & Nam, H. (2001a). Effect of pre-treatment on the surface and electrochemical properties of screen-printed carbon paste electrodes. *Analyst* **126**, 1399-1403.

Cui, X., Hetke, J. F., Wiler, J. A., Anderson, D. J. & Martin, D. C. (2001b). Electrochemical deposition and characterization of conducting polymer polypyrrole/PSS on multichannel neural probes. *Sens Actuators A-Phys* **93**, 8-18.

Cum, G., Gallo, R., Spadaro, A. & Galli, G. (1988). Effect of static pressure on the ultrasonic activation of chemical reactions - selective oxidation at benzylic carbon in the liquid phase. *J Chem Soc Perk Trans 2* **11**, 375-383.

Curie, J. & Curie, P. (1880). Cristallophysique- développement, par pression, de l'électricité polaire dans les cristaux hémièdres à faces inclinées. *Compt Rend* **91**, 294-295.

Curulli, A., Kelly, S., O'Sullivan, C., Guilbault, G. G. & Palleschi, G. (1998). A new interference-free lysine biosensor using a non-conducting polymer film. *Biosensors & Bioelectronics* **13,** 1245-1250.

Dai, H. P., Wu, Q. H., Sun, S. G. & Shiu, K. K. (1998). Electrochemical quartz crystal microbalance studies on the electropolymerisation processes of ortho-phenylenediamine in sulphuric acid solutions. *J Electroanal Chem* **456**, 47-59.

Davis, D. G. & Everhart, M. E. (1964). Chronopotentiometry of the bromide-bromine couple at platinum and carbon paste electrodes. *Anal Chem* **36**, 38-40.

De Giglio, E., Losito, I., Torsi, L., Sabbatini, L. & Zambonin, P. G. (2003). Electroanalytical and spectroscopic characterisation of poly(*o*-phenylenediamine) grown on highly orientated pyrolytic graphite. *Ann Chim* **93**, 209-221.

De Souza-Barboza, J. C., Petrier, C. & Luche, J. L. (1988). Ultrasound in organic synthesis: 13. Some fundamental aspects of the sonochemical Barbier reaction. *J Org Chem* **53**, 1212-1218.

Deakin, M. R., Stutts, K. J. & Wightman, R. M. (1985). The effect of pH on some outer-sphere electrode reactions at carbon electrodes. *J Electroanal Chem* **182,** 113-122.

Deng, H. & Van Berkel, G. J. (1999). Electrochemical polymerisation of aniline investigated using on-line electrochemistry/electrospray mass spectrometry. *Anal Chem* **71**, 4284-4293.

Derrigan, J., Lin, L. & Jensen, J. (1993). Comparison of free and total chlorine measurement methods in municipal wastewaters. *Water Environ Res* **65**, 205-212.

Deshpande, M. V. & Amalnerkar, D. P. (1993). Biosensors prepared from electrochemically synthesized conducting polymers. *Prog Polym Sci* **18**, 623-649.

Dewald, H. D. & Peterson, B. A. (1990). Ultrasonic hydrodynamic modulation voltammetry. *Anal Chem* **62,** 779-782.

Dewhurst, R. J., Noui, L. & Shan, Q. (1990). Polymer film thickness measurement using laser-ultrasound techniques. *Rev Sci Instrum* **61**, 1736-1742.

Diamond, D. (1998). *Principles of Chemical and Biological Sensors*, Canada: John Wiley & Sons.

Didenko, Y. T., McNamara III, W. B. & Suslick, K. S. (1999). Hot spot conditions during cavitation. *J Am Chem Soc* **121**, 5817-5818.

Dietrich, A. M., Jensen, J. N. & Da Costa, W. F. (1996). Chemical species. *Water Environ Res* **68**, 391-406.

Ding, T., Wang, H., Xu, S. & Zhu, J. J. (2002). Sonochemical synthesis and characterizations of monodispersed PbSe nanocrystals in polymer solvent. *J Cryst Growth* **235**, 517-522.

Doblhofer, K. & Zhong, C. J. (1991). The mechanism of electrochemical charge-transfer reactions on conducting polymer films. *Synth Met* **43,** 2865-2870.

Doktycz, S. J. & Suslick, K. S. (1990). Interparticle collisions driven by ultrasound. *Science* **247,** 1067-1069.

Edmonds, T. E. (1998). *Chemical Sensors*, p193. Glasgow: Blackie & Son Ltd.

Elliott, J. M., Cabuche, L. M. & Bartlett, P. N. (2001). Electrochemical characterization of a templated insulating polymer-modified electrode. *Anal Chem* **73**, 2855-2861.

Emr, S. A. & Yacynych, A. M. (1995). Use of polymer-films in amperometric biosensors. *Electroanalysis* **7,** 913-923.

Engstrom, R. C. (1982). Electrochemical pre-treatment of glassy carbon electrodes. *Anal Chem* **56,** 2310-2314.

Engstrom, R. C. & Strasser, V. A. (1984). Characterization of electrochemically pre-treated glassy carbon electrodes. *Anal Chem* **56,** 136-141.

Erlenkötter, A., Kottbus, M. & Chemnitius, G. C. (2000). Flexible amperometric transducers for biosensors based on a screen printed three electrode system. *J Electroanal Chem* **481,** 82-94.

European Economic Community (1998). Drinking water directive: Council directive 80/778/EEC of 3 November 1998 on the quality of water intended for human consumption. *Official Journal of the European Community* **L330,** 32-54.

European Economic Community (1978). Freshwater and fisheries directive: Council directive 78/659/EEC of 18 July 1978 on the quality of fresh waters needing protection or improvement in order to support fish life. *Official Journal of the European Community* **L222**, 1-10.

Eswaramoorthy, M., Sen, R. & Rao, C. N. R. (1999). A study of micropores in single-walled carbon nanotubes by adsorption of gases and vapors. *Chem Phys Lett* **304,** 207-210.

Evans, J. F. & Kuwana, T. (1977). Radiofrequency oxygen plasma treatment of pyrolytic graphite electrode surfaces. *Anal Chem* **49**, 1632-1635.

Evans, J. F., Kuwana, T., Henne, M. T. & Royer, G. P. (1977). Electrolysis of solution species using modified electrodes. *J Electroanal Chem* **80**, 409-416.

Fagan, D. T., Hu, I. F. & Kuwana, T. (1985). Vacuum heat-treatment for activation of glassy carbon electrodes. *Anal Chem* **57**, 2759-2763.

Falat, L. & Cheng, H. Y. (1982). Voltammetric differentiation of ascorbic acid and dopamine at an electrochemically treated graphite/epoxy electrode. *Anal Chem* **54**, 2108-2111.

Farsang, G. (1965). Voltammetric properties and analytical uses of carbon paste electrodes prepared with silicone oil. *Acta Chim Hung Tomus* **45**, 163-175.

Fiaccabrino, G. C. & Koudelka-Hep, M. (1998). Thin-film microfabrication of electrochemical transducers. *Electroanalysis* **10**, 217-222.

Fick. A. (1855). On liquid diffusion. *Phil Mag* **10,** 30-39.

Finklea, H. O. & Vithanage, R. S. (1984). Non-electroactive electrode coatings formed by electrochemical polymerisation. *J Electroanal Chem* **161**, 283-294.

Fleischmann, M., Pons, S., Rolison, D. R. & Schmidt, P. P. (1987). Ultramicroelectrodes, Morganton NC: Datatech. Systems.

Flint, E. B. & Suslick, K. S. (1991). The temperature of cavitation. *Science* **253,** 1397-1399.

Frederick, J. R. (1965). *Ultrasonic Engineering*, London: John Wiley & Sons.

Friend, R. H. (1993). Report 62: Conductive polymers II – From science to applications. *RAPRA Review Reports* **6**, 3-28.

Galan-Vidal, C. A., Munoz, J., Dominguez, C. & Alegret, S. (1995). Chemical sensors, biosensors and thick-film technology. *Trac-Trends In Anal Chem* **14,** 225-231.

Garten, V. A. & Weiss, D. E. (1955). The quinine-hydroquinone character of activated carbon and carbon black. *Aust J Chem* **8**, 68-95.

Garten, V. A., Weiss, D. E. & Willis, J. B. (1957). A new interpretation of the acidic and basic structures in carbons 1. Lactone groups of the ordinary and fluorescent types in carbons. *Aust J Chem* **10**, 295-309.

Geise, R. J., Adams, J. M., Barone, N. J. & Yacynych, A. M. (1991). Eletropolymerised films to prevent interferences and electrode fouling in biosensors. *Biosensor & Bioelectronics* **6**, 151-160.

Gilmartin, M. A. T. & Hart, J. P. (1995). Sensing with chemically and biologically modified carbon electrodes. A review. *Analyst* **120,** 1029-1045.

Gordon, G., Cooper, W., Rice, R. & Pacey, G. (1992). *Disinfectant Residual Measurement Methods,* 2nd edn. AWWA Research Foundation and American Water Works Association.

Gouy, M. (1910). Électricité –sur la constitution de la charge électrique à la surface d'un electrolyte. *Compt Rend* **149,** 654-657.

Grahame, D. C. (1947). The electrical double layer and the theory of electrocapillarity. *Chem Rev* **41**, 441-501.

Gray, N. J. & Unwin, P. R. (2000). Simple procedure for the fabrication of silver/silver chloride potentiometric electrodes with micrometre and smaller dimensions: Application to scanning electrochemical microscopy. *Analyst* **125**, 889-893.

Green, M. & Hilditch, P. (1991). Disposable single-use sensors. *Anal Proc* **28,** 374-376.

Grennan, K., Killard, A. J. & Malcolm, R. S. (2001). Physical characterisations of a screen-printed electrode for use in an amperometric biosensor system. *Electroanalysis* **13,** 745-750.

Gueshi, T., Tokuda, K. & Matsuda, H. (1978). Voltammetry at partially covered electrodes. Part 1: Chronopotentiometry and chronoamperometry at model electrodes. *J Electroanal Chem* **89**, 247-260.

Guilbault, G. G. (1983). Determination of formaldehyde with an enzyme-coated piezoelectric crystal detector. *Anal Chem* **55**, 1682-1684.

Guter, K. J., Cooper, W. J. & Sorber, C. A. (1974). Evaluation of existing field test kits for determining free chlorine residuals in aqueous solutions. Water Technology/Quality in *J Am Water Works Assoc* **66**, 38-43.

Hall, T. & Hyde, R. A. (1992). *Water Treatment Processes and Practices*, Marlow, Buckingham: WRc PLC.

Harp, D. L. (1995). *Current Technology of Chlorine Analysis for Water and Wastewater*, USA: Hach Company.

Hart, J. P. & Wring, S. A. (1997). Recent developments in the design and application of screen-printed electrochemical sensors for biomedical, environmental and industrial analyses. *TRAC* **16,** 89-103.

Heineman, W. R., Wleck, H. J. & Yacynych, A. M. (1980). Polymer film chemically modified electrode as a potentiometric sensor. *Anal Chem* **52**, 345-346.

Heller, A., Say, J., Vreeke, M. & Feldman, B. J. (2003). *Small volume in vitro analyte sensor*. United States Patent Number US2003201194.

Helmholtz, von H. (1853). Ueber einige gesetze der vertheilung elektrischer ströme in körperlichen leitern mit anwendung auf die thierisch-elektrischen versuche. *Ann Physik* **89,** 211-233.

Henglein, A. & Gutierre, M. J. (1990). Chemical effects of continuous and pulsed ultrasound: A comparative study of polymer degradation and iodide oxidation. *J Phys Chem* **94,** 5169-5172.

Higson, S. P. J. (2004). *Heat-sealed protective film for electrochemical sensors.* International Patent Number WO2004029609.

Higson, S. P. J. (2003). *Analytical Chemistry*, Oxford: Oxford University Press.

Higson, S. P. J. (1996). *Sensor.* European Patent Number EP0823050.

HMSO (1980). Chemical Disinfecting Agents in Water and Effluents, and Chlorine Demand. In *Methods for the Examination of Waters and Associated Materials.*

Holdcroft, S. & Funt, B. L. (1988). Preparation and electrocatalytic properties of conducting films of polypyrrole containing platinum microparticulates. *J Electroanal Chem* **240**, 89-103.

Horiuchi, T., Niwa, O., Morita, M. & Tabei, H. (1992). Stripping voltammetry of reversible redox species by self-induced redox cycling. *Anal Chem* **64**, 3206-3208.

Hu, J. & Turner, A. P. F. (1991). An enzyme electrode for glucose consisting of glucose-oxidase immobilised at a benzoquinone-modified carbon electrode. *Anal Lett* **24**, 15-24.

Hu, I. F., Karweik, D. H. & Kuwana, T. (1985). Activation and deactivation of glassy-carbon electrodes. *J Electroanal Chem* **188**, 59-72.

Imisides, M. D., John, R., Riley, P. J. & Wallace, G. G. (1991). The use of electropolymerization to produce new sensing surfaces: A review emphasizing electrodeposition of heteroaromatic compounds. *Electroanalysis* **3**, 879-889.

Janata, J. (2001). Centennial retrospective on chemical sensors. *Anal Chem* **73**, A150-A153.

Janata, J., Josowicz, M., Vanysek, P. & DeVaney, D. M. (1998). Chemical sensors. *Anal Chem* **70**, 179R-208R.

Jang, D. H., Yoo, Y. S. & Oh, S. M. (1995). Electropolymerization mechanism for poly(*o*-phenylenediamine) (PPD) and its electrocatalytic behaviour for O_2 reduction. *Bull Korean Chem Soc* **16**, 392-397.

Jensen, J. N. & Johnson, J. D. (1990). Interferences by monochloramine and organic chloramines in free available chlorine methods: 1. Amperometric titration. *Environ Sci Technol* **24**, 981-985.

Jolley, R. L. (1975). Chlorine-containing organic constituents in chlorinated effluents. *J Water Poll Control Fed* **47**, 601-618.

Kalcher, K. (1990). Chemically modified carbon paste electrodes in voltammetric analysis. *Electroanalysis* **2,** 419-433.

Kalcher, K., Wang, J., Kauffmann, J.-M., Švancara, I., Vytřas, K., Neuhold, C. & Yang, Z. (1995). Sensors based on carbon paste in electrochemical analysis - A review with particular emphasis on the period 1990-1993. *Electroanalysis* **7,** 5-22.

Kawata, S. & Takeuchi, K. (1991). Infrared thin-film analysis with 2 transmission spectra measured at different incident angles. *J Opt Soc Am A* **8**, 1055-1061.

Kazee, B., Weisshaar, D. E. & Kuwana, T. (1985). Evidence for the presence of a thin carbon-particle layer on polished glassy carbon electrodes. *Anal Chem* **57**, 2736-2739.

Keller, R., Oke, A., Mefford, I. & Adams, R. N. (1976). Liquid chromatographic analysis of catecholamines routine assay for regional brain mapping. *Life Sci* **19**, 995-1003.

Kepley, L. J. & Bard, A. J. (1988). Ellipsometric, electrochemical, and elemental characterization of the surface phase produced on glassy carbon electrodes by electrochemical activation. *Anal Chem* **60,** 1459-1467.

Kimura, J., Kawana, Y. & Kuriyama, T. (1988). An immobilised enzyme membrane fabrication method using an ink-jet nozzle. *Biosensors* **4**, 41-52.

Kitani, A., Izumi, J., Yano, J., Hiromoto, Y. & Sasaki, K. (1984). Basic behaviours and properties of electrodeposited polyaniline. *Bull Chem Soc Jpn* **57**, 2254-2257.

Kittleson, G. P., White, H. S. & Wrighton, M. S. (1985). A microelectrochemical diode with submicron contact spacing based on the connection of two microelectrodes using dissimilar redox polymers. *J Am Chem Soc* **107**, 7373-7380.

Klima, J. & Bernard, C. (1999). Sonoassisted electrooxidative polymerisation of salicyclic acid: role of acoustic streaming and microjetting. *J Electroanal Chem* **462**, 181-186.

Klima, J., Bernard, C. & Degrand, C. (1994). Sonoelectrochemistry: effects of ultrasound on voltammetric measurements at a solid electrode. *J Electroanal Chem* **367**, 297-300.

Kondratiev, V. V., Tikhomirova, A. V. & Malev, V. V. (1999). Study of charge transport processes in Prussian-blue modified electrodes. *Electrochim Acta* **45**, 751-759.

Konvalina, J. (1997). MSc Thesis, University of Pardubice, Pardubice. Cited In: Koochaki, Z., Cumming, R. H., Rowell, F. J. & Stewert, I. W. (1995). Monitoring of hazardous biochemicals in the workplace atmosphere. *Process Biochem* 30, 589-597.

Koochaki, Z., Cumming, R. H., Rowell, F. J. & Stewert, I. W. (1995). Monitoring of hazardous biochemicals in the workplace atmosphere. *Process Biochem* **30**, 589-597.

Koopal, C. G. J., Bos, A. A. C. M. & Nolte, R. J. M. (1994). Third-generation glucose biosensor incorporated in a conducting ink. *Sens Actuators B* **18**, 166-170.

Kulys, J. & D'Costa, E. J. (1991). Printed amperometric sensor based on TCNQ and cholinesterase. *Biosens Bioelectron* **6**, 109-115.

Kwak, M. K., Park, D. S., Woon, M. S. & Shim, Y. B. (1996). Anodic differential pulse voltammetric analysis of iodide with a cinchonine-modified carbon paste electrode. *Electroanalysis* **8**, 680-684.

Laser, D. & Ariel, M. (1974). The anodic behaviour of glassy carbon in acid solution – A spectroelectrochemical study. *J Electroanal Chem* **52**, 291-303.

Leddy, J., Bard, A. J., Maloy, J. T. & Saveant, J. M. (1985). Kinetics of film-coated electrodes – Effect of a finite mass transfer rate of substrate across the film-solution interface at steady state. *J Electroanal Chem* **187**, 205-227.

Lee, H. J., Beriet, C., Ferrigno, R. & Girault, H. H. (2001). Cyclic voltammetry at a regular microdisc electrode array. *J Electroanal Chem* **502**, 138-145.

Leighton, T. G. (1994). *The Acoustic Bubble*, London: Academic.

Leighton, T. G. (1998). The principles of cavitation. In *Ultrasound in Food Processing*, pp. 151-182. Edited by M. J. W. Povey & T. J. Mason. London: Thomson Science.

Levi, M. D. & Pisarevskaya, E. Y. (1992). Cyclic and steady-state voltammetric studies of the mechanism and kinetics of some solute inorganic redox-species reactions at a gold electrode covered with poly-ortho-phenylenediamine. *Electrochimica Acta* **37**, 635-641.

Li, X. G., Huang, M. R., Duan, W. & Yang, Y. L. (2002). Novel multifunctional polymers from aromatic diamines by oxidative polymerizations. *Chem Rev* **102**, 2925-3030.

Lin, X. Q. & Zhang, H. Q. (1996). In situ external reflection FTIR spectroelectrochemical investigation of poly(*o*-phenylenediamine) film coated on a platinum electrode. *Electrochim Acta* **41**, 2019-2024.

Liu, C., Chen, W. J. & Martin, C. (1992) Electrochemical synthesis of ultrathin film composite membranes. *J Memb Sci* **65**, 113-128.

Loeb, G. E., Peck, R. A. & Martyniuk, J. (1995). Toward the ultimate metal microelectrode. *J Neurosci Methods* **63**, 175-183.

Losito, I., Palmisano, F. & Zambonin, P. G. (2003). *o*-phenylenediamine electropolymerisation by cyclic voltammetry combined with electrospray ionisation-ion trap mass spectroscopy. *Anal Chem* **75**, 4988-4995.

Losito, I., De Giglio, E., Cioffi, N. & Malitesta, C. (2001). Spectroscopic investigation on polymer films obtained by oxidation of *o*-phenylenediamine on platinum electrodes at different pHs. *J Mater Chem* **11**, 1812-1817.

Lu, G. H., Yang, M., Zheng, Q. F., Wang, A. L. & Jin, Z. X. (1995). Anodic-stripping voltammetry for the determination of trace iodide. *Electroanalysis* **6,** 591-593.

Madaras, M. B. & Buck, R. P. (1996). Miniaturised biosensors employing electropolymerised permselective films and their use for creatine assays in human serum. *Anal Chem* **68**, 3832-3839.

Madigan, N. A., Hagan, C. R. S. & Coury, L. S. (1994). Preparation of microarray electrodes by sonochemical ablation of polymer films. *J Electrochem Soc* **141,** L23-L24.

Malitesta, C., Losito, I. & Zambonin, P. G. (1999). Molecularly imprinted electrosynthesized polymers: New materials for biomimetric sensors. *Anal Chem* **71**, 1366-1370.

Malitesta, C., Palmisano, F., Torsi, L. & Zambonin, P. G. (1990). Glucose fast-response amperometric sensor based on glucose-oxidase immobilised in an electropolymerised poly(ortho-phenylenediamine) film. *Anal Chem* **62**, 2735-2740.

Marcus, R. A. (1963). On the theory of oxidation-reduction reactions involving electron transfer – comparison and properties of electrochemical and chemical rate constants. *J Phys Chem* **67**, 853-857.

Marks, H. C. & Glass, J. R. (1942). A new method of determining residual chlorine. *J Am Water Works Assoc* **34**, 1227-1240.

Martin, M. K., Ward, T. C. & McGrath, J. E. (1981). Anionic Polymerisation: Kinetics, Mechanisms and Synthesis. In: *ACS Symposium Series No. 166, Am Chem Soc,* Edited by J. E. McGrath. Washington D.C. pp. 557-580.

Martin, C. J. & Law, A. N. R. (1983). Design of thermistor probes for measurement of ultrasound intensity distributions. *Ultrasonics* **21**, 85-90.

Martinusz, K., Czirok, E. & Inzelt, G. (1994). Studies of the formation and redox transformation of poly(*o*-phenylenediamine) films using a quartz crystal microbalance. *J Electroanal Chem* **379**, 437-444.

Martinusz, K., Inzelt, G. & Horanyi, G. (1995). Coupled electrochemical and radiometric study of anion migration in poly(*o*-phenylenediamine) films. *J Electroanal Chem* **395**, 293-297.

Mason, T. J. (1999). *Sonochemistry*, Oxford: Oxford University Press.

Mason, T. J. & Berlan, J. (1992). Ultrasonics in Industrial Processes: The Problems of Scale-up. *Current Trends in Sonochemistry*, Edited by G. Price, Royal Society of Chemistry. pp. 148-157.

Mason, T. J., Lorimer, J. P. & Moorhouse, J. P. (1989). Sonochemistry – using ultrasonic baths. *Education in chemistry* **26,** 13-15.

Matsue, T., Aoki, A., Ando, E. & Uchida, I. (1990). Multichannel electrochemical detection system for flow analysis. *Anal Chem* **62**, 407-409.

Mattson, J. S., Mark, H. B. & Weber, W. J. (1969). Identification of surface functional groups on active carbon by infrared internal-reflection spectroscopy. *Anal Chem* **41,** 355-358.

McCreery, R. L. (1991). Carbon electrodes: Structural Effects on Electron-Transfer Kinetics. In *Electroanalytical Chemistry*. Edited by A. J. Bard. New York: Dekker.

McGurk, A. (2002). *Studies towards the development of novel electrochemical biosensors utilising NAD(P) dependant enzymes.* PhD Thesis, UMIST.

Meneguzzi, A., Pham, M. C., Ferreira, C. A., Lacroix, J. C., Aeiyach, S. & Lacaze, P. C. (1999). Electroactive poly(aromatic-amine) films deposited on mild steel. *Synth Met* **102**, 1390-1391.

Merck (1998). Standard or Free and Total Chlorine, Analytical Quality Assurance Procedures 1.14826.0001 and 1.100430001. www.merck.de/servlet/PB/menu.htm (accessed October 1998).

Moore, H. E., Garmendia, M. J. & Cooper, W J. (1984). Kinetics of monochloramine oxidation of N,N-diethyl-para-phenylenediamine. *Envir Sci & Technol* **18**, 348-353.

Moorow, J. J. & Roop, R. N. (1975). Advances in chlorine-residual analysis. *J Am Water Works Assoc* **67**, 184-186.

Morf, W. E. (1997). Theoretical treatment of the current vs. time response of microelectrode arrays to changes of potential, concentration, or flow. *Anal Chim Acta* **341**, 121-127.

Morf, W. E. (1996). Theoretical treatment of the amperometric current response of multiple microelectrode arrays. *Anal Chim Acta* **330**, 139-149.

Morf, W. E. & de Rooij, N. F. (1997). Performance of amperometric sensors based on multiple microelectrode arrays. *Sens Actuators B* **44,** 538-541.

Mosbach, K. & Danielsson, B. (1981). Thermal bioanalyzers in flow steams – enzyme thermistor devices. *Anal Chem* **53**, A83-A94.

Murata, K., Kaneko, K., Kokai, F., Takahashi, K., Yudasaka, M. & Iijima, S. (2000). Pore structure of single-wall carbon nanohorn aggregates. *Chem Phys Lett* **331**, 14-20.

Myler, S. (2000). *The exploitation of thin-polymer-films and microelectrode arrays for the development of electrochemical biosensors.* PhD Thesis, UMIST.

Myler, S., Davis, F., Collyer, S. D. & Higson, S. P. J. (2004). Sonochemically fabricated microelectrode arrays for biosensors-part II: Modification with a polysiloxane coating. *Biosensors & Bioelectronics* **20**, 408-412.

Myler, S., Eaton, S. & Higson, S. P. J. (1997). Poly(*o*-phenylenediamine) ultrathin polymer-film composite membranes for enzyme electrodes. *Anal Chim Acta* **357**, 55-61.

Nagaoki, T., Fukunaga, T., Yoshino, T., Watanabe, I., Nakayama, T. Okazaki, S. (1988). Uptake of ions by electrochemically treated glassy carbon. *Anal Chem* **60,** 2766-2769.

Nagaoki, T. & Yoshino, T. (1986). Oxygen reduction at electrochemically treated glassy carbon electrodes. *Anal Chem* **58,** 1953-1955.

Newman, J. D., White, S. F., Tothill, I. E. & Turner, A. P. F. (1995). Catalytic materials, membranes, and fabrication technologies suitable for the construction of amperometric biosensors. *Anal Chem* **67**, 4594-4599.

Newman, J. D., Turner, A. P. F. & Marrazza, G. (1992). Ink-jet printing for the fabrication of amperometric glucose biosensors. *Anal Chim Acta* **262**, 13-17.

Niwa, O. & Tabei, H. (1994). Voltammetric measurements of reversible and quasi-reversible redox species using carbon film based interdigitated array microelectrodes. *Anal Chem* **66**, 285-289.

Ogura, K., Kokura, M., Yano, J. & Shiigi, H. (1995). Spectroscopic and scanning tunnelling microscopic characterisation of virgin and recast films of electrochemically prepared poly(*o*-phenylenediamine). *Electrochim Acta* **40,** 2707-2714.

Ohnuki, Y., Matsuda, H., Ohsaka, T. & Oyama, N. (1983). Permselectivity of films prepared by electrochemical oxidation of phenol and amino-aromatic compounds. *J Electroanal Chem* **158**, 55-67.

Ohsaka, T., Ohnuki, Y., Oyama, N., Katagiri, G. & Kumisako, K. (1984). IR Adsorption spectroscopic identification of electroactive and electroinactive polyaniline films prepared by the electrochemical polymerisation of aniline. *J Electroanal Chem* **161**, 399-405.

Oyama, N. & Anson, F. C. (1980). Catalysis of electrode processes by multiply-charged metal complexes electrostatically bound to polyelectrolyte coatings on graphite electrodes, and the use of polymer-coated rotating disk electrodes in diagnosing kinetic and conduction mechanisms. *Anal Chem* **52**, 1192-1198.

Oyama, N., Ohnuki, Y., Chiba, K. & Ohsaka, T. (1983). Selectivity of poly(aniline) film coated electrode for redox reactions of species in solution. *Chem Lett* **11**, 1759-1762.

Oyama, N., Sato, M. & Ohsaka, T. (1989). Preparation of thin polymeric films on electrode surfaces by electropolymerization of aromatic compounds with amino groups. *Synth Met* **29**, E501-E506.

Palin, A. T. (1974). *Chemistry of Modern Water Chlorination*, Water Services.

Palin, A. T. (1957). The determination of free and combined chlorine in water by the use of diethyl-*p*-phenylene diamine. *J Am Water Works Assoc* **49**, 873-880.

Patel, N. G., Meier, S., Cammann, K. & Chemnitius, G. C. (2001). Screen-printed biosensors using different alcohol oxidases. *Sens Act B* **75,** 101-110.

Penner, R. M., Heben, M. J., Longin, T. L. & Lewis, N. S. (1990). Fabrication and use of nanometre-sized electrodes in electrochemistry. *Science* **250**, 1118-1121.

Petek, M., Neal, T. E. & Murray, R. W. (1971). Spectroelectrochemistry. Application of optically transparent minigrid electrodes under semiinfinite diffusion conditions. *Anal Chem* **43**, 1069-1074.

Peterson, J. I., Goldstein, S. R., Fitzgerald, R. V. & Buckhold, D. K. (1980). Fiber optic pH probe for physiological use. *Anal Chem* **52**, 864-869.

Petrier, C., Lamy, M. F., Francony, A., Benahcene, A., David, B., Renaudin, V. & Gondrexon, N. (1994). Sonochemical degradation of phenol in dilute aqueous solutions: Comparison of the reaction rates at 20 and 487 kHz. *J Phys Chem* **98**, 10514-10520.

Ponchon, J. L., Cespuglio, R., Gonon, F., Jouvert, M. & Pujol, J. F. (1979). Normal pulse polarography with carbon fiber electrodes for in vivo determinations of catecholamines. *Anal Chem* **51**, 1483-1486.

Poon, M. & McCreery, R. L. (1986). In situ laser activation of glassy carbon electrodes. *Anal Chem* **58**, 2745-2750.

Povey, M. J. W. & Mason, T. J. (1998). *Ultrasound in Food Processing*, London: Thomson Science.

Prater, K. B. (1973). Electrode filming in ring substituted anilines. *J Electrochem Soc* **120**, 365-366.

Prudenziati, M. (1994). *Thick Film Sensors*, Amsterdam: Elsevier.

Pugin, B. (1987). Qualitative characterisation of ultrasound reactors for heterogeneous sonochemistry. *Ultrasonics* **25**, 49-55.

Reisse, J., Caulier, T. D. C., Fabre, O., Vandercammen, J., Delplancke, J. L. & Winard, R. (1996). Quantitative sonochemistry. *Ultrasonics Sonochemistry* **3,** S147-S151.

Reitnauer, P. G. (1972). Verfahren und einrichtung zur enzymatisch-polarometrischen bestimmung von glucose. GDR Pat. No. 101.

Reller, H., Kirowaeisner, E. & Gileadi, E. (1984). Ensembles of microelectrodes - Digital-simulation by the two-dimensional expanding grid method - Cyclic voltammetry, IR effects and applications. *J Electroanal Chem* **161**, 247-268.

Rice, M. E., Galus, Z. & Adams, R. N. (1983). Graphite paste electrodes – Effects of paste composition and surface states on electron transfer rates. *J Electroanal Chem* **143,** 89-102.

Rodriguez, I., Marcos, M. & Gonzalez-Velasco, J. (1987). Mechanism of electrochemical growth of polypyrrole on a glass electrode doped with SnO_2 (ITO) from aqueous solutions. *Electrochim Acta* **32**, 1181-1185.

Rojo, A., Rosenstratten, A. & Anjo, D. (1986). Characterization of a conductive carbon-film electrode for voltammetry. *Anal Chem* **58**, 2988-2991.

Rook, J. J. (1976). Haloforms in drinking water. *J Am Water Works Assoc* **68**, 168-172.

Russell, S. (1994). *Residual Chlorine: A Guide to Measurement in Water Applications*, Marlow, Buckingham: WRc PLC.

Salmon, A. & Jutzi, P. (2001). Water soluble ferrocenyl and polyferrocenyl compounds: synthesis and electrochemistry. *J Organometallic Chem* **637-639**, 595-608.

Sanderson, D. G. & Anderson, L. B. (1985). Filar electrodes: Steady-state currents and spectroelectrochemistry at twin interdigitated electrodes. *Anal Chem* **57**, 2388-2393.

Sandison, M. E., Anicet, N., Glidle, A. & Cooper, J. M. (2002). Optimization of the geometry and porosity of microelectrode arrays for sensor design. *Anal Chem* **74**, 5717-5725.

Sasaki, K., Yumita, N., Nishigaki, R., Sakata, I., Nakajima, S. & Umemura, S. (2001). Pharmocokinetic study of a gallium-porphyrin photo- and sono-sensitizer, ATX-70, in tumor-bearing mice. *Jpn J Cancer Res* **92**, 989-995.

Sata, T. (2000). Studies on anion exchange membranes having permselectivity for specific anions in electrodialysis- effect of hydrophobicity of anion exchange membranes on permselectivity of anions. *J Memb Sci* **167,** 1-31.

Scharifker, B. R. (1988). Diffusion to ensembles of microelectrodes. *J Electroanal Chem* **240**, 61-76.

Schram, C. J. (1991). The manipulation of particles in an ultrasonic field. In *Advances In Sonochemistry* **2,** 293-322. Edited by T. J. Mason, London: JAI Press.

Seddon, B. J., Osborne, M. D., Lagger, G., Dryfe, R. A. W., Loyall, U., Schäfer, H. & Girault, H. H. (1997). Micro-glassy carbon inks for thick-film electrodes. *Electrochim Acta* **42,** 1883-1894.

Seiyama, T., Nakahara, T. & Takeuchi, T. (1994). Environmental oriented electrochemistry. *Stud Environ Sci* **59**, 233-272.

Shichiri, M., Kawamori, R., Yamasaki, Y., Hakui, N. & Abe, H. (1982). Wearable artificial endocrine pancreas with needle-type glucose sensor. *Lancet* **250,** 1129-1131.

Shoup, D. & Szabo, A. (1984). Chronoamperometry at an ensemble of microdisk electrodes. *J Electroanal Chem* **160**, 19-26.

Sittampalam, G. & Wilson, G. S. (1983). Surface-modified electrochemical detector for liquid chromatography. *Anal Chem* **55**, 1608-1610.

Sleszynski, N., Osteryoung, J. & Carter, M. (1984). Arrays of very small voltammetric electrodes based on reticulated vitreous carbon. *Anal Chem* **56**, 130-135.

Spangler, L. L., Torkelson, J. M. & Royal, J. S. (1990). Influence of solvent and molecular-weight on thickness and surface topography of spin-coated polymer-films. *Polym Eng Sci* **30**, 644-653.

Starr, A., Wise, K. D. & Csongradi, J. (1973). An evaluation of photoengraved microelectrodes for extracellular single-unit recording. *IEEE Transactions on Biomedical Engineering* **20**, 291-293.

Stern, H. O. (1924). Zur theorie der elektrolytischen doppelschicht. *Zeitschrift Elektrochemie* **30**, 508-516.

Štulík, K. (1992). Activation of solid electrodes. *Electroanalysis* **4,** 829-834.

Sun, H. C. & Sun, B. T. (1993). Some dynamic regression simulated equations for electrochemical doping processes of polypyrrole. *J Appl Electrochem* **23**, 741-744.

Suslick, K. S. (1990). Sonochemistry. *Science* **247**, 1439-1445.

Suslick, K. S., Hammerton, D. A. & Cline, R. E. (1986). The sonochemical hot spot. *J Am Chem Soc* **108**, 5641-5642.

Švancara, I., Hvízdalová, M., Vytřas, K., Kalcher, K. & Novotný, R. (1996). A microscopic study on carbon paste electrodes. *Electroanalysis* **8,** 61-65.

Švancara, I., Konvalina, J., Schachl, K, Kalcher, K. & Vytřas, K. (1998). Stripping voltammetric determination of iodide with synergistic accumulation at a carbon paste electrode. *Electroanalysis* **10**, 435-441.

Swan, D. (1979). PhD Thesis, University of Southampton. Cited In: Sleszynski, N., Osteryoung, J. & Carter, M. (1984). Arrays of very small voltammetric electrodes based on reticulated vitreous carbon. *Anal Chem* **56**, 130-135.

Tafel, J. (1905). Über die Polarisation bei kathodischer Wasserstoffentwicklung. *Z Physik Chem* **50A**, 641-712.

Théron, P., Pichat, P., Petrier, C. & Guillard, C. (2001). Water treatment by TiO_2 photocatalysis and/or ultrasound: degradations of phenyltrifluoromethylketone, a trifluoroactic-acid-forming pollutant, and octan-1-ol, a very hydrophobic pollutant. *Water Sci Technol* **44**, 263-270.

Tolan, M., Vacca, G., Wang, J., Sinha, S. K., Li, Z., Rafailovich, M. H., Sokolov, J., Gibaud, A., Lorenz, H. & Kotthaus, J. P. (1996). Thin polymer films on rough surfaces. *Physica B* **221**, 53-59.

Turner, A. P. F. (1989). *Biosensors: Fundamentals and Applications*, Suffolk, UK: St Edmundsbury Press.

UK Drinking Water Inspectorate (2000). List of Approved Products and Processes. www.dwi.detr.gov.uk/soslist. (accessed November 2001).

Updike, S. J. & Hicks, G. P. (1967). The enzyme electrode. *Nature* **214**, 986-988.

US Environmental Protection Agency (2004). Chemical Sensor: Water and Wastewater Security Product Guide - Chlorine Measurement System www.epa.gov/safewater/security/guide/chlorinemeasurementsensor.html (accessed April 2004).

US Environmental Protection Agency (2000). National Primary and Secondary Drinking Water Regulations. www.epa.gov/safewater/mcl.htm (accessed October 2001).

US Environmental Protection Agency (1976). Water Quality Criteria: Effects of Chlorine on Fish and Aquatic Organisms. www.hach.com/h2ou/h2wtrqual.htm (accessed December 2001).

Valentini, F., Amine, A., Orlanducci, S., Terranova, M. L. & Palleschi, G. (2003). Carbon nanotube purification: preparation and characterisation of carbon nanotube paste electrodes. *Anal Chem* **75,** 5413-5421.

Villette, S., Valignat, M. P., Cazabat, A. M., Schabert, F. A. & Kalachev, A. (1997). Ultrathin liquid films. Ellipsometric study and AFM preliminary investigations. *Physica A* **236,** 123-129.

Volkov, A., Tourillon, G., Lacaze, P. C. & Dubois, J. E. (1980). Electrochemical polymerization of aromatic amines: IR, XPS and PMT study of thin film formation on a Pt electrode. *J Electroanal Chem* **116**, 279-291.

Volmer, M. & Erdey-Gruz, T. (1930). Zur Theorie der Wasserstoffiiberspannung. *Z Physik Chem* **150A**, 203-213.

Vydra, F., Štulik, K. & Juláková, E. (1976). *Electrochemical Stripping Analysis,* Chichester: Ellis Horwood.

Walton, D. J. & Phull, S. S. (1996). Sonoelectrochemistry. In *Advances In Sonochemistry*, pp. 205-285. Edited by T. J. Mason. London: JAI Press.

Wang, J. (1994). Decentralized electrochemical monitoring of trace-metals from disposable strips to remote electrodes – plenary lecture. *Analyst* **119,** 763-766.

Wang, J. & Freiha, B. A. (1984). Vitreous carbon-based composite electrode as an electrochemical detector for liquid chromatography. *J Chromatogr* **298**, 79-87.

Wang, J., Leech, D., Ozsos, M., Martinez, S. & Smyth, M. R. (1991). One-step fabrication of glucose sensors based on entrapment of glucose oxidase within poly(ester-sulfonic acid) coatings. *Anal Chim Acta* **245**, 139-143.

Wang, J., Pedrero, M., Sakslund, H., Hammerich, O. & Pingarron, J. (1996). Electrochemical activation of screen-printed carbon strips. *Analyst* **121,** 345-350.

Wang, J., Tian, B., Nascimento, V. B. & Agnes, L. (1998). Performance of screen-printed carbon electrodes fabricated from different carbon inks. *Electrochim Acta* **43,** 3459-3465.

Wang, J., Tuzhi, P. & Villa, V. (1987). Activation of carbon fibre microelectrodes by alternating-current electrochemical treatment. *J Electroanal Chem* **234,** 119-131.

Warrington, R. J. (2001). *Studies towards developing a suitable electrode for the reduction/oxidation of NAD^+/NADH.* PhD Thesis, UMIST.

Weisshaar, D. E. & Tallman, D. E. (1983). Chronoamperometric response at carbon-based composite electrodes. *Anal Chem* **53,** 1146-1151.

West, A. (1993). Ohmic interactions within electrode ensembles. *J Electrochem Soc* **140**, 134-139.

White, H. S., Abruna, H. D. & Bard, A. J. (1982). Semiconductor electrodes XII Improvement of performance of n-WSe_2 electrodes by electrochemical polymerization of *o*-phenylenediamine at surface imperfections. *J Electrochem Soc* **129**, 265-271.

White, G. C. (1992). *Handbook of Chlorination and Alternative Disinfectants*, 3rd edn. New York: Van Nostrand Reinhold.

White, G. C. (1978). *Water Chlorination: Environmental Impact and Health Effects*, Michigan: Ann Arbor Science Publishers Inc.

Wierl, L. M., Guadalupe, A. R. & Abruna, H. D. (1985). Multiple-use polymer-modified electrodes for electroanalysis of metal ions in solution. *Anal Chem* **57**, 2009-2011.

Wightman, R. M. (1981). Microvoltammetric electrodes. *Anal Chem* **53**, A1125-A1135.

Wightman, R. M., Caudill, W. L. & Howell, J. O. (1982). Flow rate independent amperometric cell. *Anal Chem* **54,** 2532-2535.

Wightman, R. M., Deakin, M. R., Kovach, P. M., Kuhr, W. G. & Stutts, K. J. (1984). Methods to improve electrochemical reversibility at carbon electrodes. *J Electrochem Soc* **131**, 1578-1583.

Wightman, R. M. & Wipf, D. O. (1989). Voltammetry at Ultramicroelectrodes. In *Electroanalytical Chemistry*, Edited by A. J. Bard. New York: Marcel Dekker.

Williams, A. R. (1983). *Ultrasound: Biological Effects and Potential Hazards*, New York: Academic Press.

Wittstock, G., Grundig, B., Strehlitz, B. & Zimmer, K. (1998). Evaluation of microelectrode arrays for amperometric detection by scanning electrochemical microscopy. *Electroanalysis* **10**, 526-531.

World Health Organisation (1993). *Guidelines for Drinking Water Quality, Volume 1 – Recommendations*, 2nd edn. Geneva: WHO.

Wring, S. A., Hart, J. P., Bracey, L. & Birch, B. J. (1990). Development of screen-printed carbon electrodes, chemically modified with cobalt phthalocyanine, for electrochemical sensor applications. *Anal Chim Acta* **231**, 203-212.

Xia, H., Zhang, C. & Wang, Q. (2001). Study on ultrasonic-induced encapsulating emulsion polymerization in the presence of nanoparticles. *J Appl Polym Sci* **80**, 1130-1139.

Yacynych, A. M. & Mark, H. B. (1976). The spectroelectrochemical study of the oxidation of 1,2-diaminobenzene: Alone and in the presence of Ni(II). *J Electrochem Soc* **123**, 1346-1351.

Yano, J. (1995). Electrochemical and structural studies on soluble and conducting polymer from *o*-phenylenediamine. *J Polym Sci Pol Chem* **33**, 2435-2441.

Yano, J., Kitani, A., Vasquez, R. E. & Sasaki, K. (1985). Polymer film coated electrodes prepared by electroxidation of aniline derivatives. *Nippon Kagaku Kaishi* **6,** 1124-1130.

Yano, J., Ogura, K., Kitani, A. & Sasaki, K. (1992a). The kinetic difference between hydroquinone and Fe^{2+} in the electrochemical reponse of a polyaniline-film-coated electrode. *Synthetic Metals* **52**, 21-31.

Yano, J., Ogura, K., Kitani, A. & Sasaki, K. (1992b). Unique electrochemical response of a polyaniline-film coated electrode to several dissolved organic species. *Canadian J Chem* **70,** 1009-1010.

Yano, J., Shimoyama, A. & Ogura, K. (1992c). Poly(*o*-phenylenediamine)-film-coated electrode having a permselective response to halogenide ions. *J Electrochem Soc* **139**, L52-L53.

Yasui, T. (1935). Electrolytic oxidation of aniline oil. *Bull Chem Soc Jpn* **10**, 305-311.

Yim, B., Nagata, Y. & Maeda, Y. (2002). Sonolytic degradation of phthalic acid esters in aqueous solutions. Acceleration of hydrolysis by sonochemical ablation. *J Phys Chem* **106**, 104-107.

Zoski, C. G. (2002). Ultramicroelectrodes: design, fabrication and characterisation. *Electroanalysis* **14**, 1041-1051.

Zhang, H. H. & Coury, L. A. (1993). Effects of high-intensity ultrasound on glassy-carbon electrodes. *Anal Chem* **65,** 1552-1558.

Zhu, H. X., Lo, T. C., Lenigk, R. & Renneberg, R. (1998). Fabrication of a novel oxygen sensor with CMOS compatible processes. *Sens Actuators* **B 46**, 155-159.

APPENDIX

Available online at www.sciencedirect.com
SCIENCE DIRECT®
Biosensors and Bioelectronics 20 (2004) 328–337
BIOSENSORS & BIOELECTRONICS
www.elsevier.com/locate/bios

Sonochemically fabricated microelectrode arrays for biosensors offering widespread applicability: Part I

Andrew C. Barton[a], Stuart D. Collyer[a], Frank Davis[a], Davinia D. Gornall[a], Karen A. Law[a], Emma C.D. Lawrence[a], Daniel W. Mills[a], Suzy Myler[b], Jeanette A. Pritchard[b], Mark Thompson[c], Seamus P.J. Higson[a,*]

[a] *Institute of Bioscience and Technology, Cranfield University at Silsoe, Cranfield Centre for Analytical Science Silsoe, Cranfield, Bedfordshire MK45 4DT, UK*
[b] *Manchester Materials Science Centre, University of Manchester and UMIST Grosvenor Street, Manchester M1 7HS, UK*
[c] *Microarray Ltd., The Fairbairn Building, 72 Sackville Street, P.O. Box 88, Manchester M60 1QD, UK*

Received 27 November 2003; received in revised form 4 February 2004; accepted 4 February 2004

Available online 11 March 2004

Abstract

A novel and patented procedure is described for the sonochemical fabrication of a new class of microelectrode array based sensor with electrode element populations of up to 2×10^5 cm^{-2}. For some years it has been accepted that microelectrode arrays offer an attractive route for lowering minimum limits of detection and imparting stir (convectional mass transport) independence to sensor responses; despite this no commercial biosensors, to date, have employed microelectrode arrays, largely due to the cost of conventional fabrication routes that have not proved commercially viable for disposable devices. Biosensors formed by our sonochemical approach offer unrivalled sensitivity and impart stir independence to sensor responses. This format lends itself for mass fabrication due to the simplicity and inexpensiveness of the approach; in the first instance impedimetric and amperometric sensors are reported for glucose as model systems. Sensors already developed for ethanol, oxalate and a number of pesticide determinations will be reported in subsequent publications.

Keywords: Sonochemistry; Electropolymerisation; Biosensor; Microelectrodes; Glucose

1. Introduction

Biosensor technology has developed into an ever expanding and multidisciplinary field since the Clark enzyme electrode was first reported (Clark and Lyons, 1962). Biosensors generically offer simplified reagentless analyses for a range of biomedical and industrial applications and for this reason this area has continued to develop into an ever expanding and multidisciplinary field during the last couple of decades. Since more than half of the sensors reported in the literature are based on electrochemical transducers (Meadows, 1996) and at the time of writing approximately 85% of the world commercial market for biosensors is for blood glucose monitoring (Newman et al., 2002), we will as the first model system of this sonochemically fabricated microelectrode array biosensor, report a glucose oxidase based impedimetric sensor. We have already within our laboratory demonstrated the fabrication of enzymatic and affinity based sensors that lend themselves to interrogation by either (i) amperometric or (ii) impedimetric approaches. Enzymatic sensors have been developed for analytes including ethanol, oxalate and a series of pesticides. Affinity sensors have been developed using antibody/antigen and DNA hybridisation based approaches. These will all be reported in a series of further publications.

Microelectrodes offer advantages over conventional larger working electrodes within biosensors since they experience hemispherical solute diffusional profiles, and it is this phenomenon that can impart stir-independence to sensor responses, whilst also offering lowered limits of detection.

Individual microelectrodes offer very small responses and one approach for overcoming this problem is to use many microelectrodes together in the form of an array to allow a cumulative and so larger response to be measured.

* Corresponding author. Tel.: +44-1525-863-453; fax: +44-1525-863-503.
E-mail address: s.p.j.higson@cranfield.ac.uk (S.P.J. Higson).

0956-5663/$ – see front matter © 2004 Elsevier B.V. All rights reserved.
doi:10.1016/j.bios.2004.02.002

Microelectrode arrays may be fabricated by a number of approaches although techniques such as photolithography or laser ablation have to date proved cost prohibitive for the mass production of disposable sensor strips. We will within this paper describe a novel sonochemical fabrication approach (Higson, 1996) for the production of microelectrodes, that lends itself to the mass production of sensor arrays.

2. Experimental

Glucose oxidase from *Asperigillus niger* (80% protein, 132,000 units/g solid), was purchased from the Sigma Chemical Company (Poole, Dorset, UK), D-glucose, aniline, potassium hydrogen phthalate, disodium hydrogen orthophosphate 1-hydrate, sodium dihydrogen orthophosphate 12-hydrate, sodium chloride, and diaminobenzene dihydrochloride (all 'AnalaR' grade), were purchased from BDH (Poole, Dorset, UK). All chemicals were used without further purification.

Glucose oxidase was prepared using 250 units/ml, in distilled water for deposition at microelectrode arrays.

Anhydrous α-D-glucose solutions were prepared to a range of concentrations, from 1 to 40 mM, in pH 7.4 phosphate buffer.

A small volume, 2.7 ml, PTFE cell was milled for the co-deposition of aniline/enzyme. The cell held the glass slide working and counter electrodes at a fixed distance from each other, whilst the reference electrode was clamped overhead.

A Sycopel PCI- 100 MK3 Potentiostat computer interface was used in conjunction with a 'Ministat Potentiostat', H.B. Thompson and Associates, (Newcastle-upon-Tyne) for all electrochemical studies: current/charge transients were recorded using a PC with dedicated software. AC impedance measurements were performed using a ACM Auto AC DSP frequency response analyser and potentiostat again linked to a PC.

A Philips XL30 FEG SEM was used for all scanning electron microscopy.

2.1. Electrode preparation

Polymer modified insulated electrodes were prepared on gold-coated glass slides as reported earlier (Myler et al., 1997).

2.2. Sonochemical ablation of polydiaminobenzene ultra-thin films

The polymer modified electrodes were then immersed in a beaker containing distilled water, and then sonicated for 1, 5, 10, 20, 30, 40, 50, 60 and 90 s using a Camlab Transsonic T460, 25 kHz sonic bath. This is set and calibrated by the manufacturer and we have verified this using a crystal microphone and recording the sound waves on a digital storage oscilloscope. The sonic bath employed 12 transducers geometrically arranged and bonded to the base of the stainless steel tank housing.

2.3. Polymerisation of microelectrode arrays

For the polymerisation of glucose oxidase enzyme microelectrode arrays, a pH 4.5 phthalate buffer was first prepared using 0.2 M potassium hydrogen phthalate and 0.2 M NaCl. A 0.2 M aniline solution was then prepared in the phthalate buffer. Glucose oxidase, (500 units ml^{-1}) was prepared in distilled water, to avoid denaturing the enzyme. 2.7 ml of the buffer and enzyme preparation (1.35 ml each) were mixed in a small volume PTFE cell, immediately prior to the electrochemical coating procedure being performed.

Aniline/GOD was polymerised by potentially sequentially cycling for 5 min between −200 and +800 mV versus Ag/AgCl at 50 mV s^{-1}, film growths were terminated at −0.2 V. Immediately following polymerisation, the working electrode was submerged in pH 7.4 phosphate buffer to prevent enzyme denaturisation.

2.4. Voltammetric techniques

Hydrodynamic voltammetric techniques were used to examine the stir-independent behaviour of the microelectrodes. Polydiaminobenzene coated electrodes, sonicated for 1, 10, 20, 30, 40, 50, 60, and 90 s, were placed in the glass stage within the cell along with a gold sputtered counter electrode and Ag/AgCl reference electrode. The electrodes were submerged within a 5 mM ferricyanide/phosphate buffer solution previously purged for 20 min with N_2; the working electrode was then polarised at −300 mV versus Ag/AgCl. A magnetic stirrer was used to agitate the solution. Current responses were recorded using a PC with dedicated software. We have determined the reproducibility of sensor responses to be <5% variability in a series of trials.

2.5. AC impedance analysis

A sealed glass cell assembly contained a gold sputtered auxiliary, a Ag/AgCl reference and an enzyme/polyaniline microelectrode array in pH 7.4 phosphate buffer solution previously purged with nitrogen for 20 min for the removal of oxygen prior to any electrochemical investigation. Serial additions of glucose were introduced to the cell giving 1, 5, 10, 20, 30 and 40 mM concentrations. Ac impedance measurements were performed using an ACM Auto AC DSP frequency response analyser between the frequencies of 0.1 Hz and 10 kHz.

3. Results and discussion

We have within our laboratory previously shown that 1,2-diaminobenzene dihydrochloride may be electropolymerised

at conductive surfaces via a $2e^-$ process to form essentially defect free insulating polymer films of less than 100 nm thickness (Myler et al., 1997).

The rationale underpinning this work is that sonochemical ablation of thin insulating polymer films at electrode surfaces may expose localised areas, each of which can act as localised microelectrodes and collectively as a microelectrode array.

Many other workers have studied the immobilisation of enzymes (e.g. the oxidases and dehydrogenases) within conducting polymers such as polyaniline or polypyrrole for use within sensors (Foulds and Lowe, 1986, Shaolin et al., 1992). We will, in this paper, describe a technique that allows the co-deposition of glucose oxidase within the conducting polymer, polyaniline, at conducting microelectrode cavities to form "mushroom" shaped microelectrode protrusions.

The interrogation of enzymatic microelectrode sensors of this type is described by both amperometric or ac impedance approaches to demonstrate their versatility. Scanning electron micrographs of electrode surfaces are included at each stage of the electrode fabrication process.

1,2-Diaminobenzene was first electropolymerised on gold sputter coated ground glass slides as previously reported (Myler et al., 1997) and this is shown schematically in Fig. 1(a). Cyclic voltammetry for the electrodeposition of insulating polydiaminobenzene film, Fig. 1(b), shows that diminishing peak currents are seen as the electrode becomes progressively insulated by the polymer film as it is deposited at the electrode surface (Myler et al., 1997).

Scanning electron microscopy of a polydiaminobenzene coated gold substrate, Fig. 1(c), confirms that its surface is largely featureless and that the electrode is coated and so insulated by an essentially defect free polymer film of polydiaminobenzene. Charge integration calculations for the current passed during the electropolymerisation would suggest that the polymer film is ~30–40 nm in thickness, in close agreement with previously calculated and experimentally determined thicknesses (Myler et al., 1997).

Ultrasound (in the kHz range) passing through a solvent such as water causes thermal agitation and localised hotspots of up to several hundred to a few thousand K, which in turn gives rise to the formation of superheated vapour bubbles (Suslick, 1990; Taleyarkan et al., 2002). These bubbles are, however, cooled by the solvent at ambient temperature (in our studies 25 °C) and asymmetrically implode with the ejection of micro-jets of solvent at speeds of up to several hundred ms^{-1}. These micro-jets may cause the shattering of hard brittle solids and this is exploited, for example, within medicine for the shattering of kidney stones. Soft solid surfaces such as polymers may, however, be ablated by such jets (Suslick, 1990).

Sonochemically fabricated microelectrodes were prepared via the ablation of polydiaminobenzene films using an ultra-sonic frequency of 25 kHz as shown schematically within Fig. 1(d), for a range of differing time durations from 1 through to 90 s.

Scanning electron micrographs for a 60 s sonicated electrode assembly are shown in Fig. 1(e). These were chosen since these provided the clearest images of the cavitation at the polymer surface. There are several features of interest within these micrographs. Firstly the distribution of the pores is random since ultra-sonic cavitation is a chaotic process. It is also evident that almost all of the cavities are bimodal in size, possessing either ~3 μm (±1 μm) or sub-micron diameters. We believe that the smallest of the cavities observed are formed by the initial impact of the micro–jets of fluid (Suslick, 1990). These cavities are known to act as nucleation sites for further bubble formation (Suslick, 1990) and it is thought that the cavity grows as new bubbles implode within the confines of the original cavity. This process gives rise to a quantum enlargement in the diameter of a cavity. Since no larger pores are seen it is believed that the 3 μm diameter pores no longer act as nucleation sites. In some instances there is evidence of a few pores joining to form dumbbell shaped cavities when two pores form in close proximity to each other, Fig. 1(e). Fig. 1(f) shows a close-up of the pores, showing how the polymer coating has been peeled back from the substrate.

3.1. Electrochemical characterisation

Electrochemical evaluation of microelectrode assemblies was performed for possible use within sensors or biosensors. Microelectrodes characteristically exhibit sigmoidal shaped cyclic voltammograms (Southampton Electrochemistry Group, 1985) for reversible solution bound redox couples such as $Fe(CN)_6^{3-}/Fe(CN)_6^{4-}$, in contrast to the characteristic diffusion limited reversible voltammograms expected at a planar electrode surface.

Fig. 2 shows a series of cyclic voltammograms recorded at a scan rate of 50 mV s^{-1} for a 1 mM solution of $Fe(CN)_6^{3-}$ at (i) planar gold electrodes, the (ii) sonochemically fabricated microelectrode arrays and (iii) polydiaminobenzene coated gold electrodes as a control. The voltammogram corresponding to the plain gold slides reveals an approximate 59 mV peak separation as would be expected for a $1e^-$ diffusional controlled reversible reduction/oxidation process. Cyclic voltammograms for the polymer insulated electrode and the microelectrode array are also shown in the enlarged bubble caption of Fig. 2 for clarity. Very little voltammetric response is observed at the polydiaminobenzene coated electrode, confirming that its has been insulated. The microelectrode array electrodes yield sigmoidal shaped voltammetric profiles suggesting that all of the microelectrode arrays formed in this way were indeed exhibiting true microelectrode-like behaviour. Individual microelectrodes would be expected to see forward (reductive) and reverse (oxidative) current transients that would fall almost on top of each other with little evidence of double-layer charging

capacitance, however separate forward and reverse peaks displaying evidence of double-layer charging are observed in this case due to the very large pore density (115,000 microelectrodes cm^{-2}) that will give rise to a significant cumulative double-layer charging current.

3.2. Microelectrode population density and reproducibility of sensor arrays

It is important to understand in this context both how microelectrode population densities grow with increasing

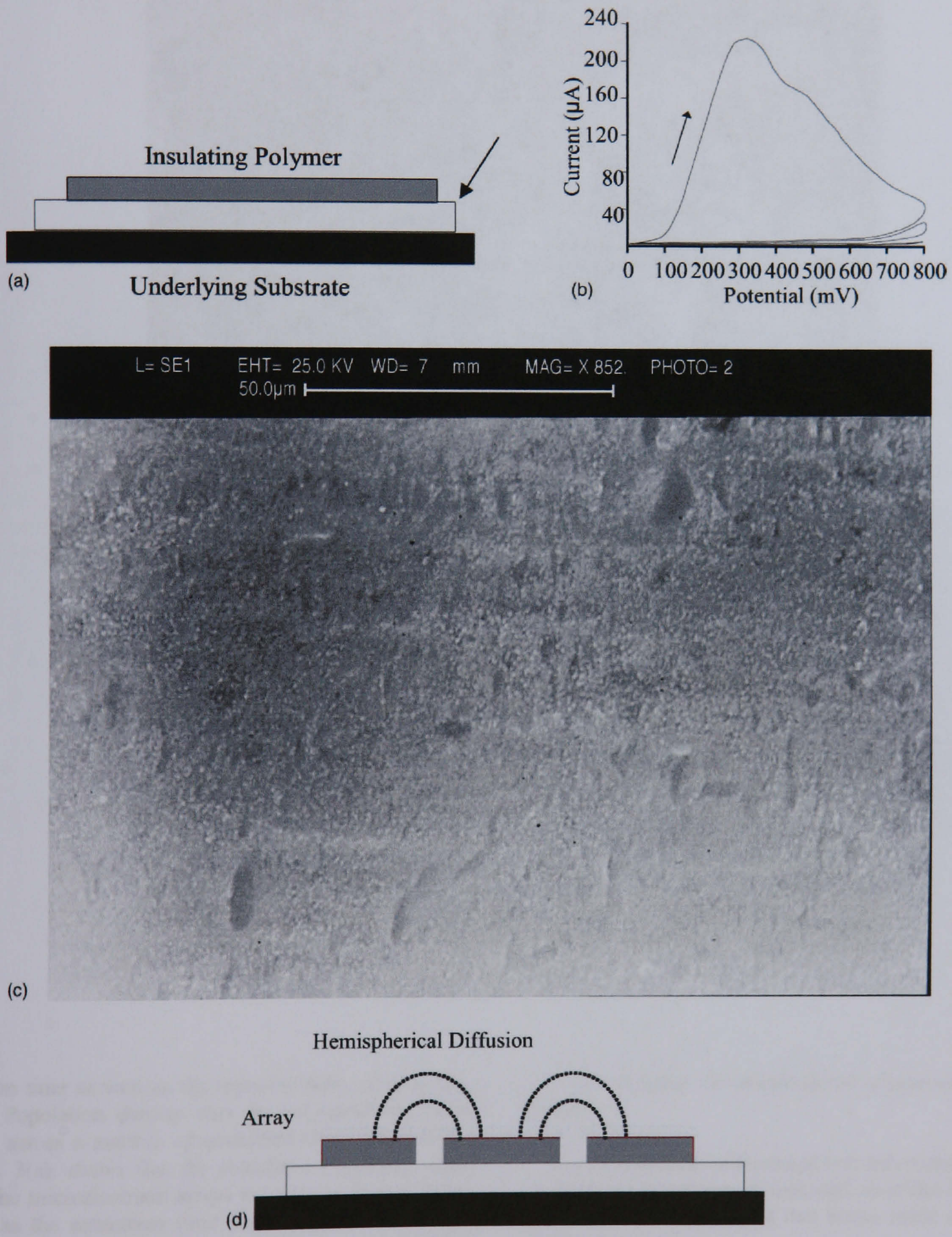

Fig. 1. Deposition of polydiaminobenzene to form an insulating film. (a) Schematic of polymer insulated electrode. (b) Cyclic voltammogram for polymerisation of 5 mM *o*-phenylenediamine dihydrochloride at a potential scan rate of $50\,mV\,s^{-1}$. (c) Electron micrograph of polydiaminobenzene insulated gold electrode surface. (d) Schematic of microelectrode array (e) Electron micrograph of sonochemically fabricated microelectrode array. (f) Close-up of sonochemically fabricated microelectrode array showing pore structure.

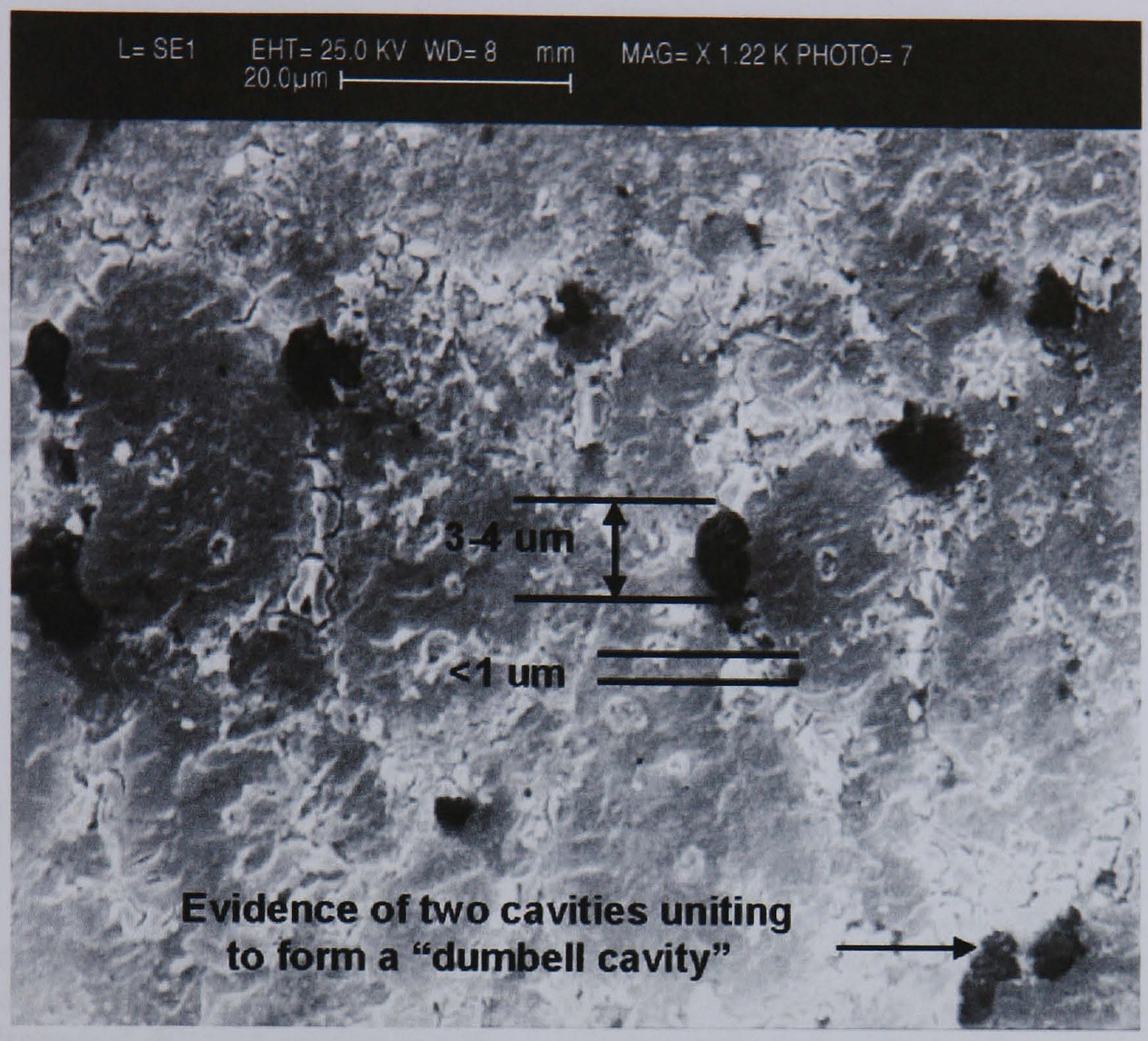

(e)

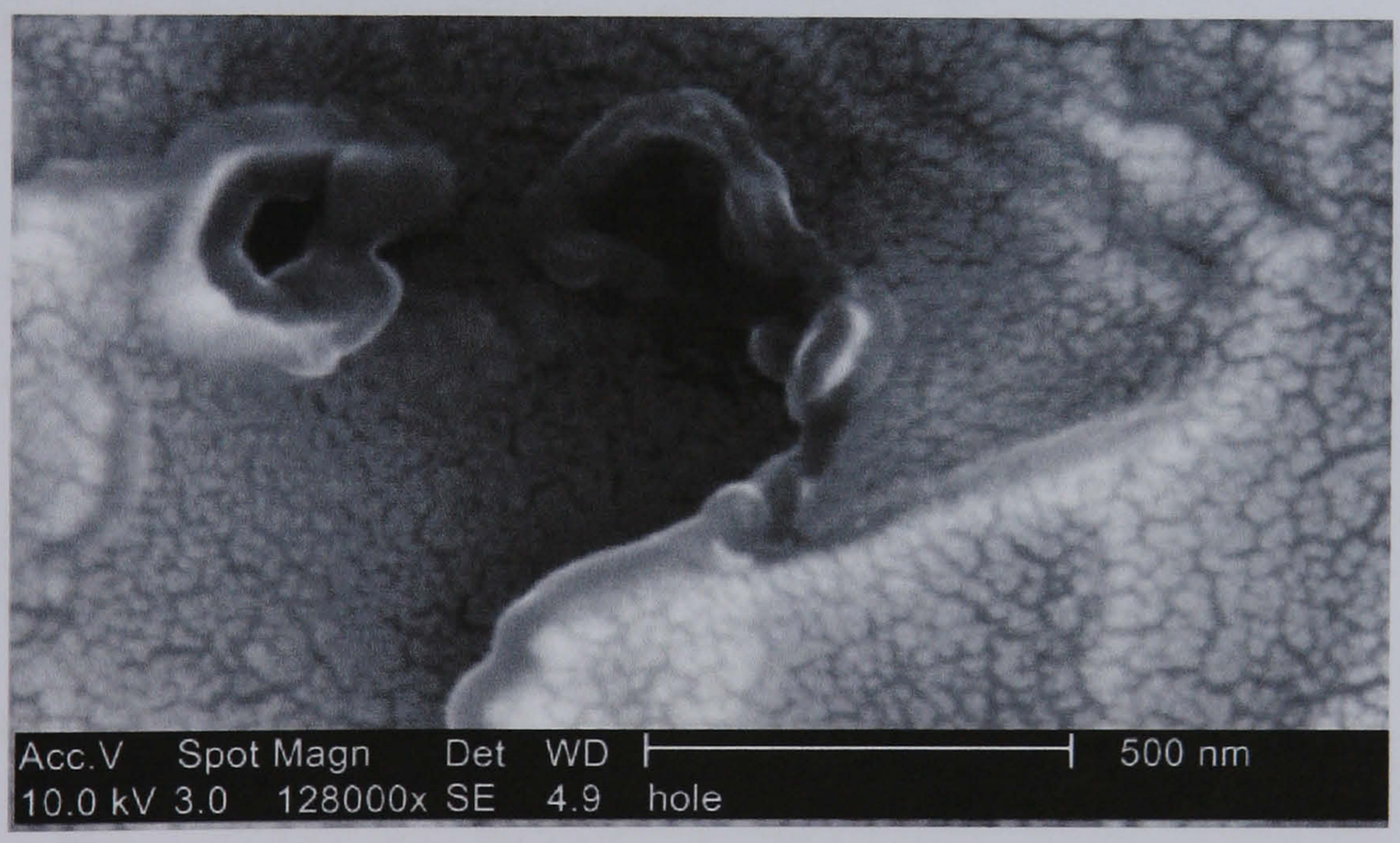

(f)

Fig. 1. (*Continued*).

sonication time as well as the reproducibility of their formation. Population density may be estimated via SEM imaging across a number of quantified cross-sectional areas. Fig. 3(a), shows that the calculated population density of the microelectrode arrays enlarges in a near linear manner as the sonication time increases from 1 through to 90 s. Coefficient of variance of the charge densities for arrays was found to be <2% (at an electrode state $E = -100$ mV versus Ag/AgCl for the reduction of 1 mM $Fe(CN)_6^{3-}$).

3.3. Convectional stir-independence of microelectrode arrays

The convectional (stir-independent behaviour) of the microelectrode arrays was investigated since this is one of the most significant advantages that arrays could offer for use within sensors.

Amperometric responses of microelectrode arrays formed via a range of differing sonication times polarised at −600 mV versus Ag/AgCl to 1 mM $Fe(CN)_6^{3-}$, were

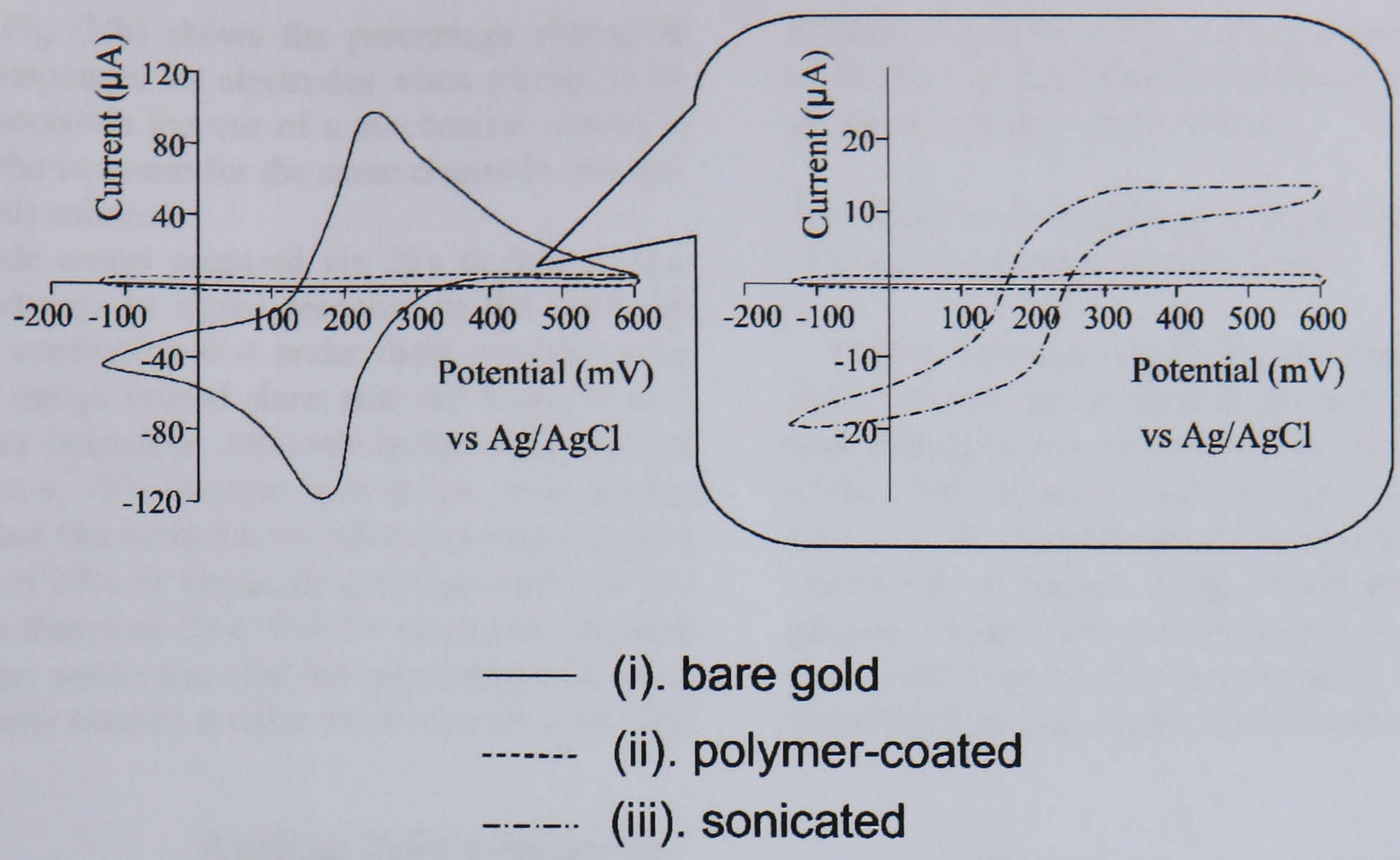

Fig. 2. Cyclic voltammetry of ferri/ferrocyanide couple at: (–) bare gold electrode, (- - -) polymer coated gold electrode and a 20 s sonochemically fabricated microelectrode array (– – –). Scan rate 50 mV s^{-1}.

recorded in both unstirred (quiescent) and stirred solutions. If the microelectrodes were to become too closely packed together, eventually hemispherical diffusion profiles would begin to overlap and ultimately all microelectrode–like behaviour would be lost.

The calculation of the percentage change in amperometric response in a quiescent and a stirred solution for a given electrode allows us to assess when microelectrode behaviour begins to be lost, as microelectrode populations increase. The performance of electrodes prepared via different son-

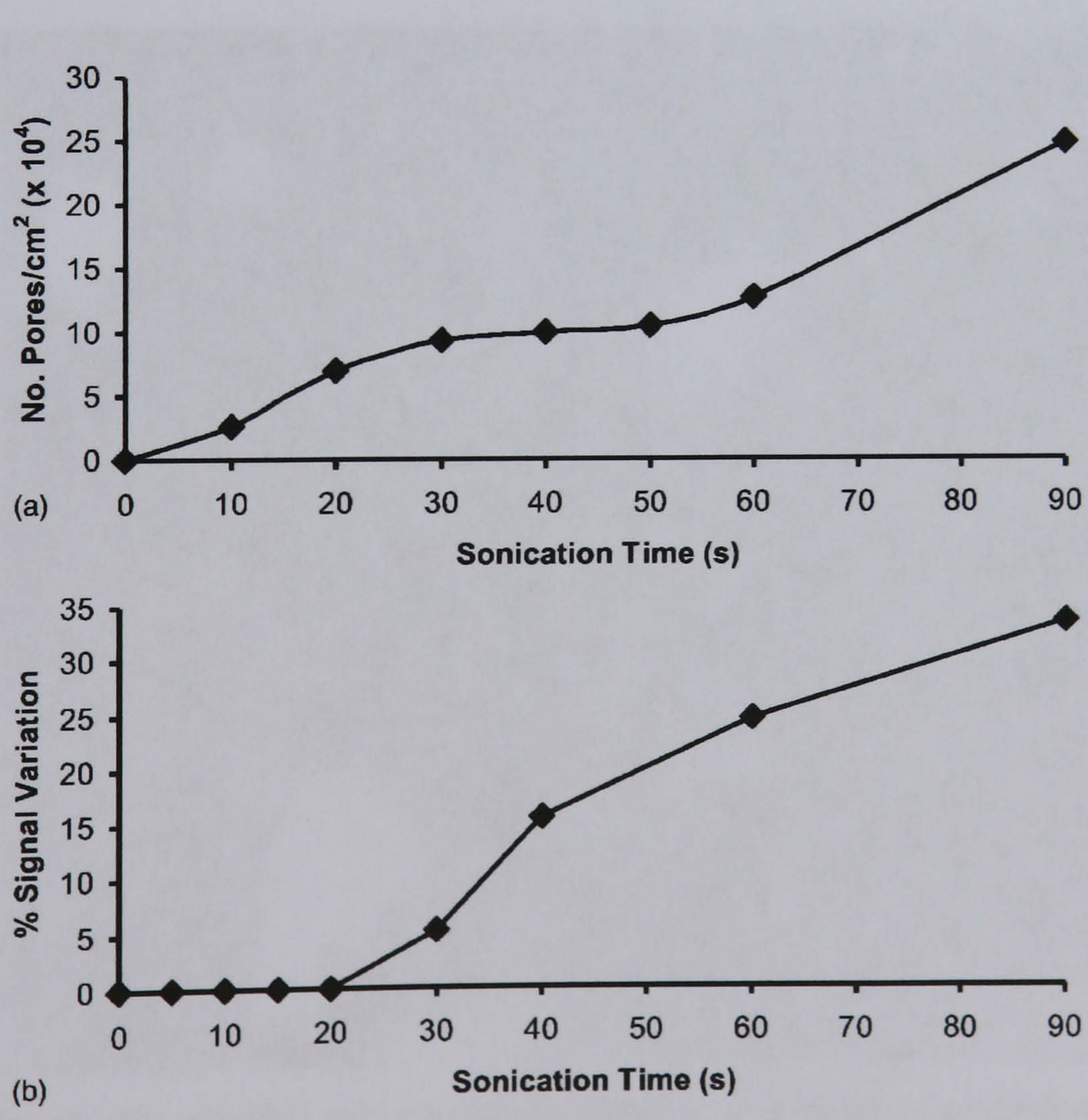

Fig. 3. (a) Population densities of sonochemically formed pores and (b) stir-dependence/independence of microelectrode arrays of these system with differing sonication times.

ication times, Fig. 3(b) shows the percentage change in amperometric responses for electrodes when stirring is introduced (in excess-via the use of a mechanical stirrer) in comparison to the response for the same electrode in a quiescent (unstirred) solution.

Microelectrode arrays prepared via 20 s or less sonication show no change in signal response to the reduction of $Fe(CN)_6^{3-}$, confirming that under these conditions the microelectrode arrays indeed show true stir independence in their response behaviour. Microelectrodes sonicated for 30 s, give rise to a ~5% increase in response upon stirring the solution—and this variation increases progressively to a value in excess of 30% for electrode arrays prepared via 90 s sonication. It is therefore clear that for electrodes prepared via 30 s or longer sonication, that the microelectrode arrays population density reaches a value where the hemispherical diffusional profiles of the individual microelectrodes begin to overlap and that this effect progressively leads to the loss of stir-independent performance.

3.4. Electropolymerisation of enzyme containing polymer protrusions in microelectrode arrays

Aniline solutions containing glucose oxidase were electropolymerised on microelectrode surfaces to form enzyme containing protrusions at each of the microelectrode cavities of the array as shown schematically, Fig. 4(a). Fig. 4(b), shows cyclic voltammograms recorded for the electropolymerisation of aniline from phosphate buffer containing glucose oxidase. The voltammogram is characteristic of an irreversible deposition with successive voltammograms progressively showing smaller peak currents (Foulds and Lowe,

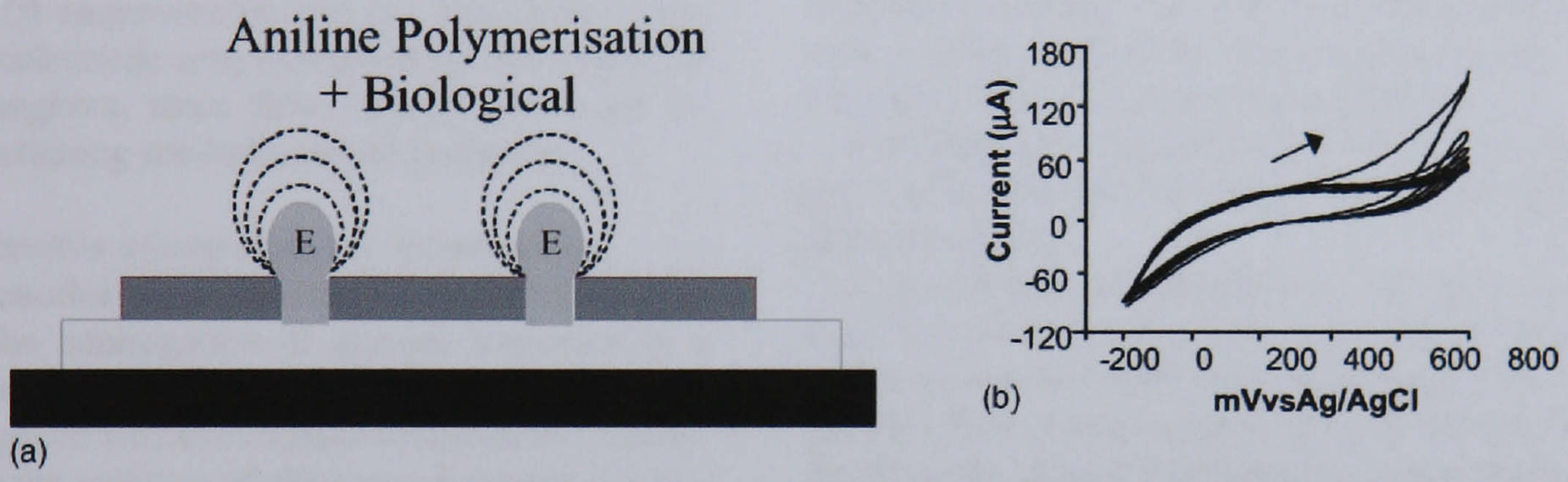

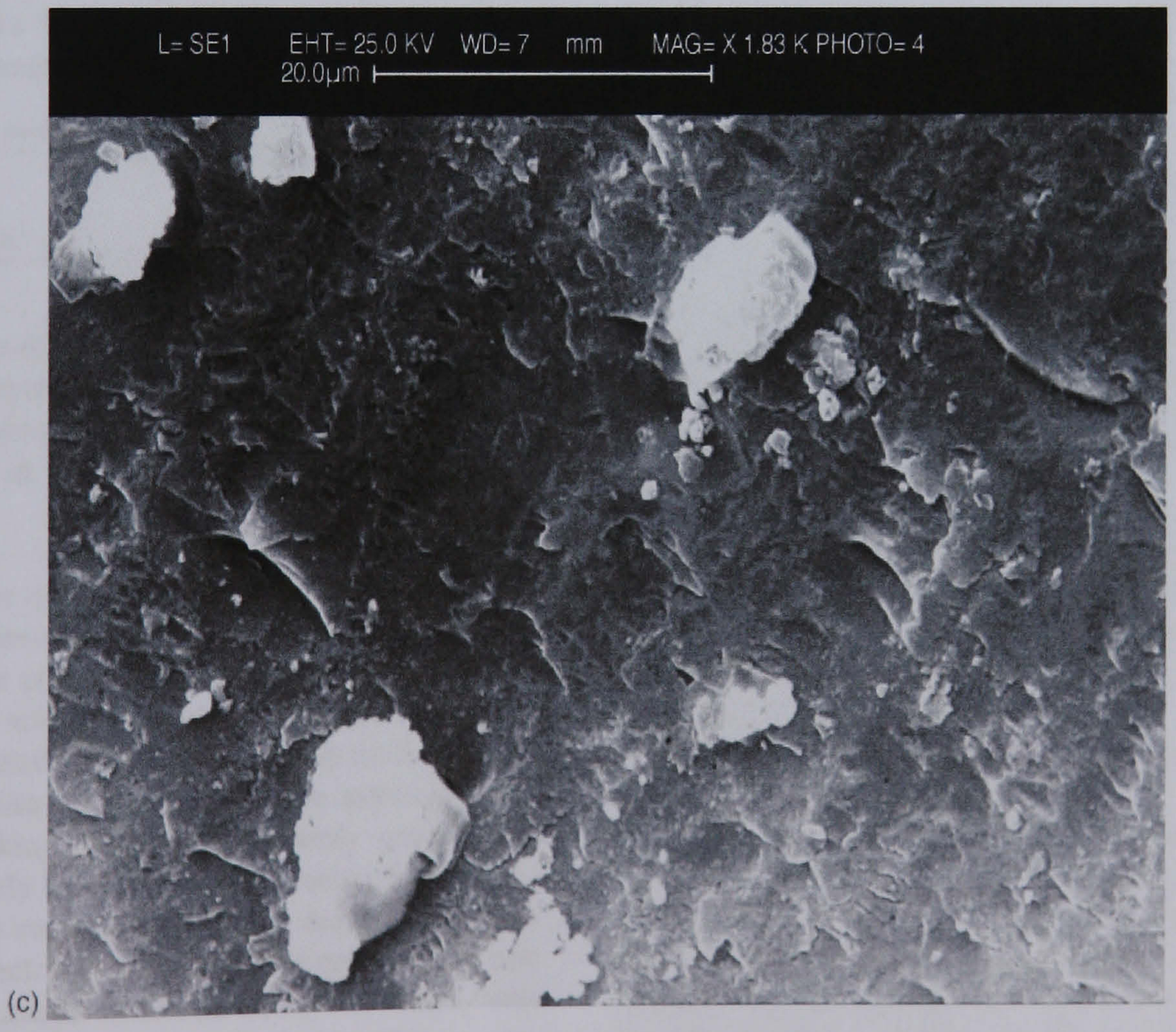

Fig. 4. Generation of enzyme containing-polyaniline protrusion microelectrode arrays. (a) Schematic of sonochemically fabricated polyaniline/enzyme microelectrode array. (b) Cyclic voltammetry (50 mV s^{-1}) for electropolymerisation of polyaniline and co-entrapment of glucose oxidase. (c) Scanning electron micrograph of sonochemically fabricated polyaniline enzyme microelectrode array.

1986, Shaolin et al., 1992). Scanning electron microscopy, Fig. 4(c), of these arrays following the electrodeposition of polyaniline shows that polymer protrusions are indeed formed via growth of the polymer from the sonochemically fabricated pores. Several interesting points should be noted from the electron micrograph of Fig. 4(c). Firstly it can be seen that all of the microelectrode cavitations appear to be filled with polyaniline, including the very smallest of the ~0.1 μm diameter pores. This shows all ablative cavitations of the insulating polymer film lead to exposure of the underlying conductive surface, since aniline could not be electropolymerised without access to the underlying conducting surface.

3.5. Sensor interrogation approaches

Enzymic microelectrode arrays of this type may interrogated by both (i) amperometric and (ii) impedimetric approaches. Microelectrode arrays prepared by 20 s sonication were used throughout, since these offered the largest response whilst retaining stir-independent properties.

3.5.1. Demonstration of amperometric interrogation

Enzyme electrodes were polarised at +650 mV versus Ag/AgCl for the interrogation of glucose responses as a first demonstration of the enzymic microelectrode array described in this paper. Glucose oxidase catalyses the production of H_2O_2 in the presence of glucose and oxygen, Eq. (1). This approach allows for the interrogation of the sensor based on the amperometric monitoring of H_2O_2, Eq. (2).

$$\text{Glucose} + O_2 \xrightarrow{\text{glucose oxidase}} \text{gluconolactone} + H_2O_2. \quad (1)$$

$$H_2O_2 \xrightarrow{+650\ \text{mV versus Ag/AgCl}} 2H^+ + O_2 + 2e^- \quad (2)$$

The calibration curve of Fig. 5(a), clearly demonstrates that an amperometric enzymatic sensor may be produced (with stir-independent responses) that could be exploited for a variety of applications in which various flow conditions may be encountered.

3.5.2. Demonstration of impedimetric interrogation

Impedimetric measurements for enzyme electrode sensors were recorded in the plane of the working microelectrode array → analyte → solution → electrode. Since the solutional impedance contribution will affect the final response of any sensor, defining and controlling the inter-electrode spacings of the working microelectrode array and counter electrode would clearly be crucial for all electrochemical investigations. A glass stage was therefore designed, to hold the working microelectrode array a fixed distance of 10 mm from the counter electrode within an analyte solution, with this assembly being designed so as to be held within a commercial Methrohm® glass cell as previously reported (Myler et al., 1997).

AC impedance spectra were first recorded for glucose oxidase/polyaniline sonochemically fabricated microelectrode arrays across a range of frequencies from 0.1 through to 10,000 Hz upon ±5 mV ac excitation (0 V bias) (Teasdale and Wallace, 1993), in order to characterise electrochemical redox behaviour and sensor performance for a range of differing concentrations of glucose within O_2 saturated conditions, Fig. 5(b). This bias potential allows monitoring of the impedance (conductivity) of the polymer without interference from, for example, the oxidation of H_2O_2 or biological interferents such as ascorbate. It is clear that *AC* Bode impedance spectra show a clear trend towards lowered impedances upon increasing concentration of glucose, with lowered impedances also occurring at higher frequencies.

Control experiments were also performed by recording impedance spectra for enzyme free polyaniline microelectrode arrays (not shown for clarity) and showed minimal impedance changes to differing concentrations of glucose, confirming that the sensor responses observed within Fig. 5(b) were indeed enzymatic in nature.

It is firstly clear that increasing concentrations of glucose give rise to lowered impedances, via the enzymic activity of glucose oxidase.

A plot of total impedance versus frequency is shown in Fig. 5(b) for a microelectrode exposed to 20 mM glucose with a corresponding Nyquist phase angle plot. For simplicity, only these plots are shown, since similar profiles are seen for all of the glucose concentration ranges studied. Fig. 5(c) shows a straight line profile of the real Z' versus the imaginary Z'' components with a slope close to unity, indicative of a diffusion controlled reversible process, where the phase angle (θ) profiles seen within Fig. 5(b) would appear to be dictated by the capacitance of the polymer film in conjunction with the double-layer contribution within the circuit.

Until now, we have only considered how recorded impedance values, or components thereof, vary under differing conditions, as opposed to how percentage changes in impedimetric behaviour vary even though the total impedance measured may be dominated by the background impedance of the circuit. Percentage changes of microelectrode array glucose sensors across a range of glucose concentrations as a function of frequency under aerobic conditions are shown within Fig. 5(d). Percentage impedances are reported relative to the corresponding impedance at 0 mM glucose at a particular frequency, as shown in Fig. 5(d). These percentage changes may be plotted with respect to the analyte concentration in the form of a calibration plot, Fig. 5(e) clearly demonstrating this approach for interrogation.

The most prominent feature of this data is that impedance minima are observed at frequencies between 10 Hz and 100 Hz. Similar responses are seen under anaerobic conditions (not shown for clarity), although the percentage changes in response are not so pronounced. We have already shown that the impedance values are modulated by enzyme catalytic behaviour, although the nature of the impedance changes have not yet been considered.

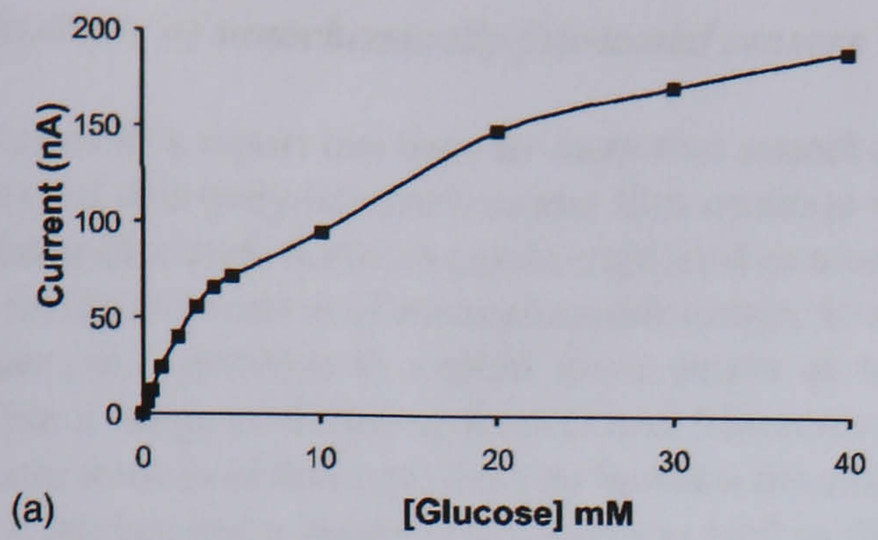

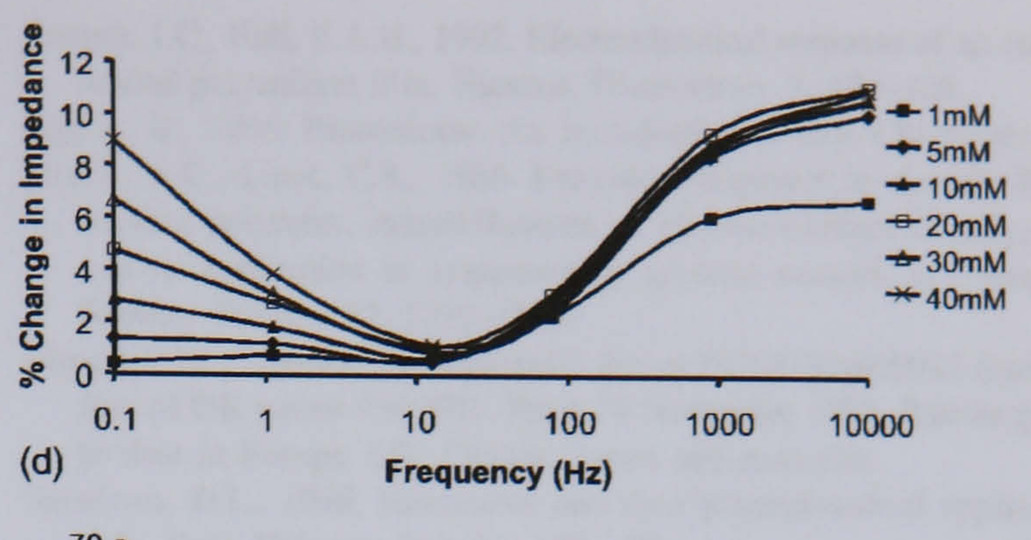

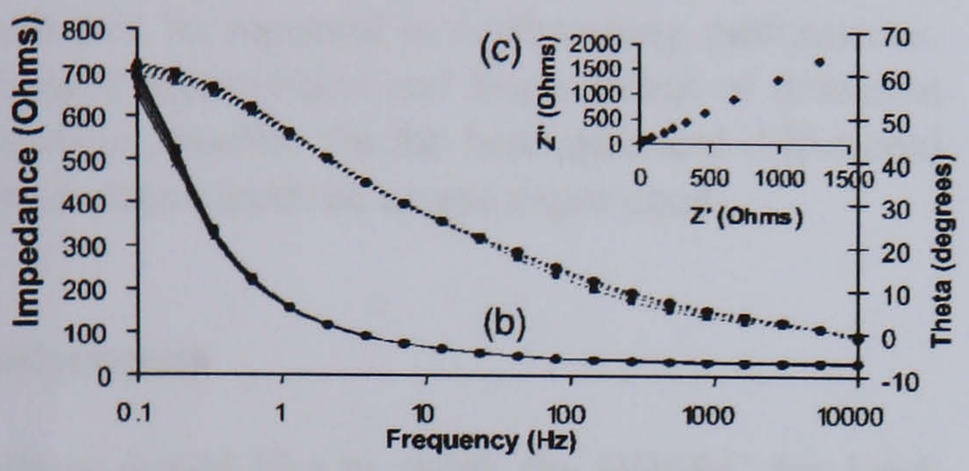

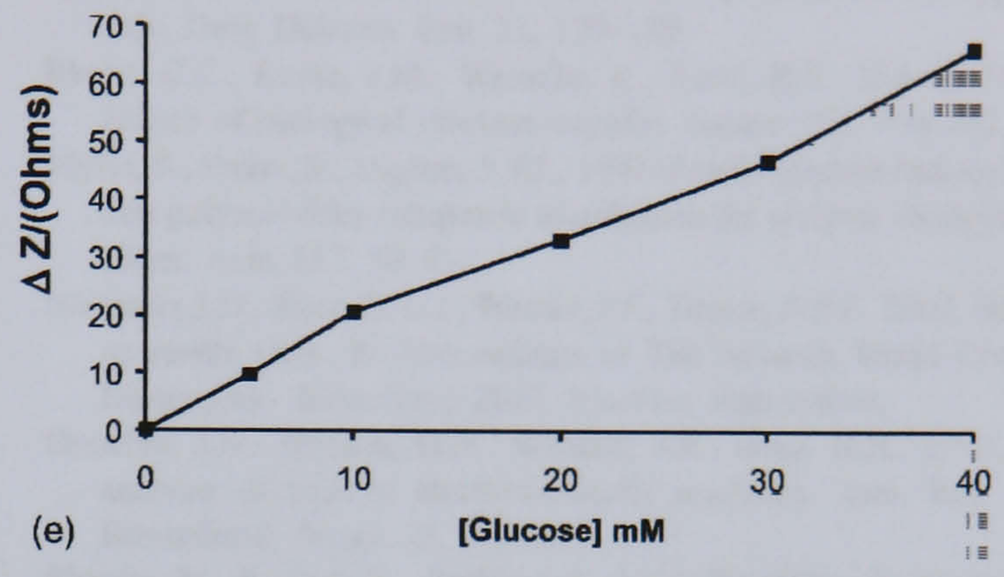

Fig. 5. (a) Amperometric glucose calibration curve for polyaniline/glucose oxidase microelectrode array. (b) Total impedance (solid line) and phase angle (dashed line) of microelectrode arrays immersed in glucose/phosphate buffer solutions. Concentration of glucose: 0 mM (■), 1 mM (◆), 5 mM (▲), 10 mM (*), 20 mM (□), 30 mM (△), 40 mM (×). (c) Complex plane plot for a microelectrode array in 20 mM glucose. (d) Percentage change in impedance for microelectrode arrays in various concentrations of glucose vs. phosphate buffer. Concentration of glucose 1 mM (■), 5 mM (◆), 10 mM (▲), 20 mM (□), 30 mM (△), 40 mM (×). (e) Calibration plot of Impedance change vs. glucose concentration for a 20 s sonicated GOD microelectrode.

At this stage the possible mechanisms by which the conductivity of the polyaniline may be modulated should be considered. Polyaniline has three differing forms (Eggins, 1996).

The first mechanism by which glucose oxidase may give rise to redox modulated conductivities within the polyaniline involves the catalysed production of H_2O_2 (Eggins, 1996). Previous workers (Cooper and Hall, 1992) have shown that in aerobic conditions, H_2O_2 would be expected to play a major role in the modulation of the impedimetric behaviour of polyaniline. The responses observed under anaerobic conditions could clearly not be accounted for by such a mechanism, since without a supply of molecular oxygen as an electron acceptor from the enzyme, H_2O_2 could not be produced. Since we have established that the impedimetric responses are due to enzyme catalytic behaviour, it follows that electron donation from the enzyme must be occurring by some other mechanism. Since the sensor responses under aerobic conditions are always greater than those observed under anaerobic conditions, it is therefore probable that the generation of H_2O_2 in aerobic conditions might contribute to this behaviour—even if additional mechanisms are involved in the overall response.

A number of other possible mechanisms to explain anaerobic glucose oxidase responses have also been proposed by other workers. One of the most controversial of these is via a possible direct electron transfer occurring between the active site of enzyme and the polymer (Cooper and Hall, 1992). The distance through which electrons would have to traverse would be in excess of 1.3 nm (http://www-biol.paisley.ac.uk, academic website containing enzyme database.) and would on first reflection appear to be prohibitive. Other workers have shown, however, that electron tunnelling can occur across distances that had previously been thought impossible via complex pathways of unsaturated and delocalised bonds together even with some saturated bonds and free space (Moser et al., 1992; Onuchic et al., 1992).

It should not be forgotten that gluconolactone may be produced under anodic conditions so long as a surrogate electron acceptor for the enzyme is provided. Gluconolactone readily hydrolyses to form gluconic acid and this may easily protonate the polymer allowing another route for altering the conductivity of the polymer.

Skinner and Hall (1997) have previously shown that gluconolactone produced under anaerobic conditions may give rise to conductivity changes within the polymer via interaction of gluconolactone with the emeraldine base to form a zwitterion complex that itself may be readily oxidised through to the perigraniline form of the polymer.

While this behaviour would account for anaerobic impedimetric responses for our sensors to glucose, it would be difficult to fully explain why the response profiles we have observed exhibit minima at frequencies of approximately 10 Hz to 100 Hz. We believe that this behaviour could be linked to the hydrogen bonding of water to the imine centre of the polymer. These effects have been extensively studied and while these findings cannot be fully described here due to space limitations, they will form the basis of a subsequent publication.

3.6. Applications of sonochemically fabricated sensors

The focus of this report has been to show that sonochemical ablation of thin-polydiaminobenzene film coatings that insulate planar electrode surfaces can be exploited as a novel approach for the fabrication of microelectrode arrays. It was, at the outset, our intention to exploit these arrays as templates within a range of differing sensors and biosensors.

Enzymatic sensors of this type have so far been developed for ethanol, oxalate and a range of pesticides as well as DNA hybridisation and affinity antibody/antigen based sensors, all of which will be reported in forthcoming publications. These enhanced sensitivities and lower limits of detection have been made possible via the hemispherical diffusional profiles these microelectrode arrays experience.

Acknowledgements

The authors would like to thank the BBSRC for funding for FD as part of the Centre for Bioarray innovation as part of the post-genomic consortium, the EPSRC for studentships for DDG and DWM and the European Community for contracts QLK3-CT-2000-000481 (SAFEGARD) for KAL, QLRT-2001-02583 (SMILE) and T505485-1 (ELISHA).

References

Clark, L.C., Lyons, I.R., 1962. Electrode systems for continuous monitoring in cardiovascular surgery. Ann. New York Acad. Sci. 102, 29.

Cooper, J.C., Hall, E.A.H., 1992. Electrochemical response of an enzyme-loaded polyaniline film. Biosens. Bioelectron. 7, 473–485.

Eggins, B., 1996. Biosensors—An Introduction. Wiley, Chichester.

Foulds, N.C., Lowe, C.R., 1986. Enzyme entrapment in electrically conducting polymers, immobilization of glucose-oxidase in polypyrrole and its application in amperometric glucose sensors. J. Chem. Soc. Faraday Trans. I 82, 1259–1264.

Higson S.P.J., "Sensor", International Patent PCT/GB96/00922 (continuation of UK patent 9507991. Filed 19 November 1996. Patents granted to date in Europe, US, Canada, Japan and Australia.

Meadows, D.L., 1996. Biosensors and their pharmaceutical applications. Adv. Drug Delivery Rev. 21, 179–189.

Moser, C.C., Keske, J.M., Warncke, K., Farid, R.S., Dutton, P.L., 1992. Nature of biological electron-transfer. Nature 355, 796–802.

Myler, S., Eaton, S., Higson, S.P.J., 1997. Poly(*o*-phenylenediamine) ultrathin polymer-film composite membranes for enzyme electrodes. Anal. Chim. Acta 357, 55–61.

Newman, J.D., Tigwell, L.J., Warner, P.J., Turner, A.P.F., 2002. Biosensors: an inside view. In: Proceedings of The Seventh World Congress on Biosensors—Biosensors 2002. Elsevier, Amsterdam.

Onuchic, J.N., Beratan, D.N., Winkler, J.R., Gray, H.B., 1992. Pathway analysis of protein electron-transfer reactions. Ann. Rev. Biophys. Biomolecul. Struct. 21, 349–377.

Shaolin, M., Jinqing, K., Jianbing, Z., 1992. Bioelectrochemical responses of the polyaniline uricase electrode. J. Electroanal. Chem. 334, 121–132.

Skinner, N.G., Hall, E.A.H., 1997. Investigation of the origin of the glucose response in a glucose oxidase polyaniline. Sys. J. Electroanal. Chem. 420, 179–188.

Southampton Electrochemistry Group, 1985. Instrumental Methods in Electrochemistry. Ellis Horwood, Chichester.

Suslick, K.S., 1990. Sonochemistry. Science 247, 1439–1445.

Taleyarkan, R.P., West, C.D., Cho, J.S., Lahey, R.T., Nigmatulin, R.I., Block, R.C., 2002. Evidence for nuclear emission during acoustic cavitation. Science 295, 1868–1873.

Teasdale, R., Wallace, G.C., 1993. Molecular recognition using conducting polymers—basis of an electrochemical sensing technology. Analyst 118, 329–334.